NORTHWEST GEOLOGY

The Journal of The Tobacco Root Geological Society

Volume 45, July–August 2016

41st Annual Field Conference

Geology of the Eastern Snake River Plain and Surrounding Highlands

July 28–August 1, 2016

Early Pleistocene basalt lava dam complex, South Fork of the Snake River, Idaho. Photo by Dan Moore.

Published by The Tobacco Root Geological Society, Inc.

P.O. Box 118
Butte, Montana 59703

http://trgs.org

Edited by: William M. Phillips (Idaho Geological Survey) and
Dan K. Moore (Brigham Young University-Idaho)

The Tobacco Root Geological Society, Inc.

P.O. Box 118
Butte, Montana 59703

Officers, 2016:

President: Jesse Mosolf, Montana Bureau of Mines and Geology, Butte, MT
Vice-President: William M. Phillips, Idaho Geological Survey, Moscow, ID
Treasurer: Katie McDonald, Montana Bureau of Mines and Geology, Butte, MT
Secretary: Emily Geraghty Ward, Rocky Mountain College, Billings, MT
Corresponding Secretary: Lara Strickland, Columbus, MT
Webmaster: Dick Gibson, Consultant, Butte, MT

Board of Directors, 2016:

Ted Antonioli, Geologist, Missoula, MT
Bruce E. Cox, Geologist (semi-retired), Missoula, MT
Larry Johnson, Consultant, Missoula, MT
Larry N. Smith, Dept. of Geological Engineering, Montana Tech, Butte, MT
Mike Stickney, Montana Bureau of Mines and Geology, Butte, MT
Robert C. Thomas, Dept. of Environmental Sciences, U. of Montana-Western, Dillon, MT
Emily Geraghty Ward, Geology Dept., Rocky Mountain College, Billings, MT

2016 Conference Organizers:

William M. Phillips (Idaho Geological Survey) and Dan K. Moore (Brigham Young University-Idaho)

Editors: William M. Phillips, Dan K. Moore, and Phyllis A. Hargrave (MBMG)

Layout and Editing: Susan Barth (MBMG)

Printed by Insty-Prints, Butte, Montana

ISSN: 0096-7769

© 2016 The Tobacco Root Geological Society, Inc.
http://trgs.org

NORTHWEST GEOLOGY

The Journal of The Tobacco Root Geological Society

Volume 45, July–August 2016

Geology of the Eastern Snake River Plain and Surrounding Highlands

TABLE OF CONTENTS

TRGS 2016 SCHOLARSHIP AWARD WINNERS

• Andrew Canada (TRGS), University of Idaho
The Tectonic Evolution of High-Elevation Lake Basins in the Cordilleran Hinterland

• Hunter Anderson (Harrison), Rocky Mountain College
Structure, emplacement and petrography of mafic Leopard Dikes in the Beartooth Range, Montana

• Nora Dwyer (Harrison), University of Montana
Petrology and geochronology of Precambrian metasedimentary rocks within the Clearwater complex, north-central Idaho

• Sarah Wright (TRGS), University of Georgia
Distinguishing sequence boundaries from other erosional surfaces: A case study from the Windy Hill Sandstone, Wyoming, USA

• Nathan Anderson (TRGS), Idaho State University
Mapping through the lens of regional geology. Correcting and reinterpreting our understanding of the southern Beaverhead Mountains

• Abram Barker (TRGS), University of Arkansas
Structural evolution of Melrose basin: Impact on Cenozoic gravel distribution

• Erin Lathrop (Harrison), Utah State University
Capturing changes in the Mesoproterozoic carbon cycle: C-isotope stratigraphy of the 1255 Ma Bass Formation, Grand Canyon Supergroup, AZ

• Shane Fussell (Foster), University of Montana
Structural Configuration of a Triangle Zone Culmination: Dearborn River, Montana

• Jordan Allen (TRGS), Montana State University
Impacts of glacial processes on nitrogen cycling in the Beartooth Mountains, Montana

• Laura Cuccio (Harrison), Utah State University
The Precambrian-sedimentary rock nonconformity: hydromechanical implications for injection-induced seismicity

• Ben Schubert (Foster), Montana Tech
Geochemistry and Mineralogy of the Heddleston Porphyry Deposit

TRGS CHARTER MEMBERS

Stanley W. Anderson
Clyde Cody
William S. Cordua
Lanny H. Fisk
Richard I. Gibson†
Thomas Hanley
Stephen W. Henderson
Thomas E. Hendrix
Mac R. Hooton
Inda Immega
Steven W. Koehler
Marian Millen Lankston†
Robert W. Lankston†
J. David Lazor
Joe J. Liteheiser, Jr.
Judson Mead*
Marvin R. Miller
Vicki M. Miller
Allen H. Nelson
Alfred H. Pekarek
Patricia Price*
Donald L. Rasmussen
Raymond M. Rene

TRGS LIFETIME MEMBERS

John Childs
Rob Foster
Joan (Mrs. Jack) Harrison*
Karen Keefer
Layaka Mann
Chris Pool

† = co-founder
* = deceased

TRGS HAMMER AWARD RECIPIENTS

Awarded for distinguished achievement in the study of the geology of the Northern Rocky Mountains

1993: Ed Ruppel*
1994: Dick Berg
2003: Don Winston
2004: Dean Kleinkopf*
2009: Betty Skipp
2010: Jim Sears
2011: John Childs
2012: J. Michael O'Neill
2013: Paul Karl Link
2014: Reed Lewis
2015: Jeff Lonn
2016: Bruce Cox

TRGS HONORARY MEMBERS

1980: Charles J. Vitaliano*
2008: Elizabeth Younggren
(also honorary Board member)
2010: Dick Berg
2010: Bruce Cox
2010: Dean Kleinkopf*
2010: Dave Lageson
2011: Marie Marshall Garsjo
2011: Paul Link
2011: Rob Thomas
2012: Jeff Lonn
2012: Mitch Reynolds
2013: Reed Lewis
2015: Don Winston

DEDICATIONS

This volume of Northwest Geology is dedicated to Dean Kleinkopf and John Whitmer, two long-time supporters of TRGS who shared a passion for geology.

Dean M. Kleinkopf (1926–2015)

Dean Kleinkopf was raised on a farm in Illinois. After an honorable discharge from West Point following World War II, he graduated from Monmouth College in Illinois with a degree in chemistry. He then went on to earn a mining engineering degree from Rolla School of Mines in Missouri, and a PhD in geology from Columbia University. Dean began his career at Chevron Oil working throughout the western U.S.

and Alaska. In 1967, he joined the U.S. Geological Survey in Denver as a geophysicist/geologist. He retired in 1999 after a distinguished 33-year career. Dean worked overseas extensively for the USGS on projects in Saudi Arabia, Bangladesh, Indonesia, and elsewhere. Much of his work in the United States was geophysical studies in Montana, Idaho, and Colorado. Dean is particularly noted for his work on the Stillwater Complex in Montana, but his many geophysical maps helped exploration geologists throughout the region. Dean could not give up geology after his formal retirement, so continued to work as a geologist emeritus in the USGS office in Tucson until he and his wife Nancy moved to Nevada.

Dean was an enthusiastic supporter of many geological societies, but he had a great love for TRGS. He faithfully attended field conferences for 40 years, served on committees, and was president in 1987–1988. Dean was appointed to the TRGS Board of Directors in 1989 and in 2004 received the TRGS Hammer Award. In 2010, he was made an honorary member of TRGS. In 2015, his family established a TRGS scholarship in his name, ensuring that his legacy will continue.

John Whitmer (1923–2016)

John Whitmer will be remembered as a Renaissance man who faithfully attended TRGS meetings wearing his yellow windbreaker and sunglasses. He was a physician by trade, but his true passion was geology and the outdoors. After retiring from medicine, John devoted his full attention to geology. He was active in the Northwest Geological Society, taught non-credit geology classes for retirees, was a member of GSA, and rarely missed a TRGS field conference. Indeed, at the age of 90, John led a field trip for the 2014 Republic, WA conference. John's motto was "Anything that takes my mind off geology is not good for me." He was an inspiration to many and proof that you are never too old to learn.

2016 HAMMER AWARD: BRUCE COX

The Tobacco Root Geologic Society is pleased to honor Bruce Cox's 40-plus years in domestic mineral exploration and mine geology with our 2016 Hammer Award!

Bruce landed in Montana at UM in the early 1970s, and did his Master's Thesis work on orbicular migmatites near Shoup. His geologic career has been centered almost entirely on domestic mineral exploration and mine geology in the Northern Rocky Mountains, particularly in Montana. He was a lead geologist on mineral exploration and engineering geology projects for industry and government with Geoplan, Inc. in the 1970s; was a founder and co-owner of Earthworks doing exploration consulting and prospect generation during the 1980s; was an independent geological consultant in the 1990s for Placer Dome and other clients; was a production geologist at Stillwater from 2001 to 2007; and a senior production geologist at Hecla's Lucky Friday mine from 2007 to 2012. From 2004 to the present he has been identifying and exploring precious metal, base metal, and industrial minerals properties with Revett Metals Associates and a variety of other partners.

Bruce's mapping skills are legendary, gracing scores of mine and prospect reports, and he is author or co-author on numerous publications for Northwest Geology, the MBMG, and GSA. These include papers and roadlogs on subjects ranging from the Stillwater and Gold Hunter mines, areal geology of the Highlands, Philipsburg, the Blackfoot watershed, and NW Montana. Bruce's contributions cover a wide range of geologic topics, from Precambrian Revett deposits to Tertiary zeolites to recent landslides.

Bruce has been involved in TRGS nearly from its inception and currently serves as the President of our Board of Directors. In addition, he has been a mainstay and officer of Western Montana mining groups such as the Missoula Chapter of the Montana Mining Association and Western Montana Exploration and Mining Association. He is currently putting together exhibits of mining equipment and history at Fort Missoula. Thanks, Bruce, for your outstanding scientific contributions to field geology and untiring service to the geologic and mining professions!

Bruce also has an artistic side and has designed several of the unique TRGS t-shirts – including the 3 shown here.

Anaconda 2010

Heise Hot Springs 1912

The Heise 1912

Heise Hot Springs

A German emigrant named Richard Camor Heise arrived in southeast Idaho around 1890. Here, he learned of medicinal hot springs on the bank the Snake River that relieved his severe rheumatism. He decided to homestead the area and develop a spa modeled after those he had observed in Europe. By 1900, he had built a store, a post office, and a large log hotel with a kitchen, dining room, parlor, and dance hall. He had also built three pools: a large outdoor swimming pool and two indoor medicinal hot pools. Elof Nelson, a neighbor, built a pipeline to supply Mr. Heise with clean, cold water from Hawley Creek. Mr. Nelson also provided a ferry service about a mile downstream from the hot springs for those who crossed the river from the south or west. (Photos courtesy of the Upper Valley Historical Society; Text summarized from Smith, Afton H., History of Heise Hot Springs).

PAPERS

Mr. Nelson's Heise Ferry, located near present day bridge

GAHNITE (ZN-FE-MG SPINEL) IN EARLY PROTEROZOIC GARNET LEUCOGNEISS OF THE SOUTHERN RUBY RANGE, SOUTHWEST MONTANA: WINDOW ON CA. 2,450 MA REGIONAL METAMORPHISM

J. Alcock,[1] P.D. Muller,[2] and R. Arenas[3]

[1]*Geoscience, Penn State Abington, Emeritus, Abington, PA 19001, USA;* [2]*Geology, SUNY Oneonta, Emeritus, 636 Burnham Road, Philadelphia, PA 19119, USA;* [3]*Departamento de Petrología y Geoquímica y Instituto de Geología Económica (UCM, CSIC), Universidad Complutense, 28040 Madrid, Spain*

Corresponding author: James Alcock, jea4118@gmail.com

ABSTRACT

A ternary spinel, gahnite (≈ $Zn_{0.47}Fe_{0.46}Mg_{0.07}Al_2O_4$), occurs with sillimanite and quartz in garnet leucogneiss and granite in the southern Ruby Range of southwest Montana. These rocks are inferred to have formed from felsic magma produced by dehydration melting of biotite during a ca. 2,450 Ma orogenic event that affected Archaean rock now exposed in the Ruby Range. Zinc released during biotite breakdown was included in gahnite and stabilized the spinel-quartz-sillimanite assemblage at temperatures ≈ 750°C. Restitic rocks rich in sillimanite and garnet with minor, ragged biotite are present throughout the area. Similar restites probably reside at somewhat deeper structural levels and so could be the actual source of the garnet leucogneiss and granite now exposed at surface.

Keywords

Gahnite, spinel-sillimanite-quartz, garnet leucogniess, Paleoproterozoic, Montana metasedimentary terrane.

INTRODUCTION

The association of spinel with sillimanite and quartz is often interpreted to be evidence of very high-temperature metamorphism. However, zinc and its incorporation as gahnite ($ZnAl_2O_4$) in solid solution with hercynite ($FeAl_2O_4$) and spinel ($MgAl_2O_4$) increases the stability of the assemblage to lower temperature and higher pressure. Zinc-rich spinel can occur in granitic rocks that experienced upper-amphibolite facies to lower-granulite facies metamorphism. In this paper we report the presence of gahnite-rich spinel (≈ $Zn_{0.47}Fe_{0.46}Mg_{0.07}Al_2O_4$, referred to as gahnite throughout the paper) with quartz ± sillimanite in an earliest Proterozoic garnet leucogneiss (Grt-LGn) that crops out in the southern Ruby Range of southwest Montana.

Archaean rocks in the Ruby Range and in the adjacent Tobacco Root Mountains experienced high-grade metamorphism during an earliest Proterozoic orogeny as evidenced by ≈ 2,450 Ma ages of zircon and monazite (Cheney and others, 2004; Jones, 2008; Alcock and Muller, 2012). They also experienced upper amphibolite facies metamorphism during the Great Falls Orogeny from ≈ 1,865 to 1,770 Ma (Cheney and others, 2004; Jones, 2008; Foster and others, 2013; Alcock and others, 2013) that has obscured effects (structure, texture, and metamorphism) produced by the earlier event. The Grt-LGn has an imprecise igneous age of ≈ 2,420 Ma (Alcock and Muller, 2012) and is inferred to have intruded during the late stages of the earliest Proterozoic orogeny. Given its age, the presence of gahnite in the Grt-LGn can be used to infer likely metamorphic reactions in metapelites that produced its precursor felsic melt and, by extension, the likely metamorphic conditions that led to crustal melting during the earliest Proterozoic orogenic event.

GEOLOGIC SETTING

The Ruby Range is one of several basement-cored Laramide uplifts in southwest Montana exposing Archaean to Early Proterozoic rocks of the Wyoming craton (fig. 1). The craton includes three subdivisions, the Beartooth–Bighorn magmatic zone, the southern accreted terranes (Mueller and Frost, 2006), and the Montana metasedimentary terrane (Mogk and others, 1992; Mueller and others, 1993). Areas within the latter terrane, including the Ruby Range, experienced a major thermo-tectonic event, the Great Falls Orogeny (Foster and others, 2013), between ≈ 1,865 and 1,770 Ma that overprints an earliest Proterozoic metamorphism at ca. 2,450 Ma (Roberts and others, 2002; Cheney and others, 2004; Mueller and others, 2004; Jones, 2008; Alcock and Muller, 2012; Alcock and others, 2013).

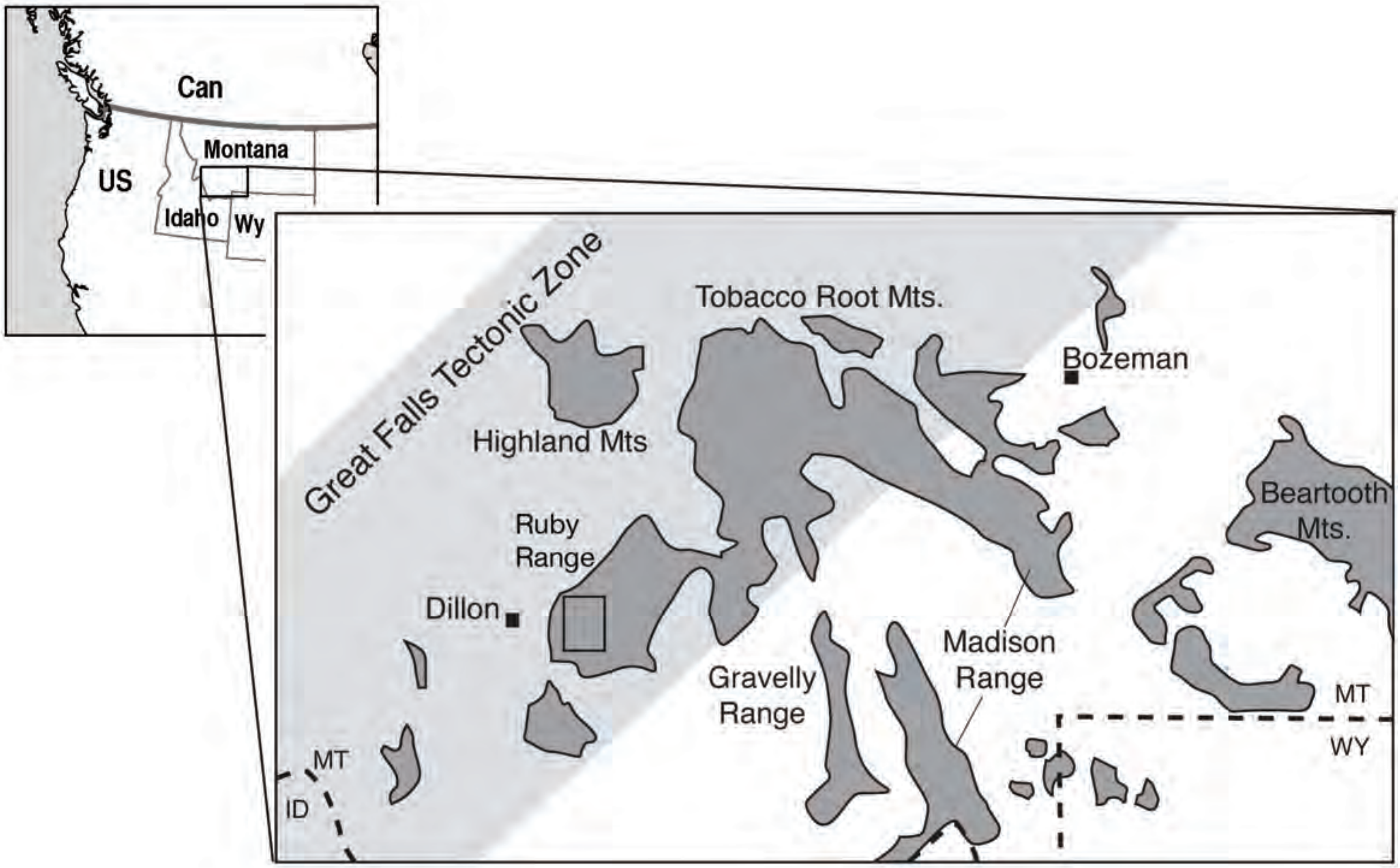

Figure 1. Regional map showing location of major uplift blocks exposing Montana metasedimentary terrane of the Wyoming Craton. Beartooth Mts. are part of the Beartooth–Bighorn magmatic terrane. The Ruby Range is the uplift east of Dillon. The square indicates the approximate location of fig. 2.

Modern geologic investigations of the Ruby Range date to the middle of the last century (Sinkler, 1942; Heinrich, 1949), with a detailed exploration of the area around the Wolf Creek ultramafic pluton (fig. 2; Heinrich, 1960). This work was followed by a series of thesis-related investigations that added considerable detail to our understanding of the distribution of rock types and their relationships (Okuma, 1971; Garihan, 1973, 1979; Karasevich and others, 1981). These efforts were compiled by James (1990) as a geologic map of the southern Ruby Range and summary paper.

Generally these workers divided the region's lithologies into three major lithotectonic units (Okuma, 1971; Garihan, 1973; James, 1990). A suite of ortho- and paragneiss with relatively minor schist and quartzite were presumed to be the oldest rocks in the range based on structural position. These were considered to be correlative with the Pre-Cherry Creek Metamorphic Suite (PCCMS) of the Madison valley to the east (Heinrich and Rabbitt, 1960; Erslev, 1983). The Dillon gneiss or Dillon quartzo-feldspathic gneiss is a second unit. James (1990) argued that rocks mapped as Dillon gneiss included orthogneiss derived from multiple protoliths, probably of different ages, and that the term should be abandoned in favor of identifying the gneiss on the basis of composition. The third unit, the Christensen Ranch Metamorphic Suite, is dominated by metasedimentary rocks including abundant marble and iron formation. This unit, largely because of the presence of marble, was interpreted to be correlative to the Cherry Creek Metamorphic Suite (CCMS), also of the Madison valley. Because the PCCMS and CCMS had been differentiated in part on the presence or absence of marble, all marble outcrops in the Ruby Range were assigned to the Christensen Ranch Metamorphic Suite.

More recently outcrop patterns, metamorphic grade, and results from geochronology have been interpreted as evidence of a more complex lithotectonic stratigraphy (Alcock and Muller, 2012; Alcock and others, 2013; fig. 2). Four lithologically distinct units are identified between the Hoffman Gulch–Sweetwater faults and the Elk Gulch fault. From the northwest and structurally highest, these are: (1) Christensen Ranch Metamorphic Suite, dominated by metasediments

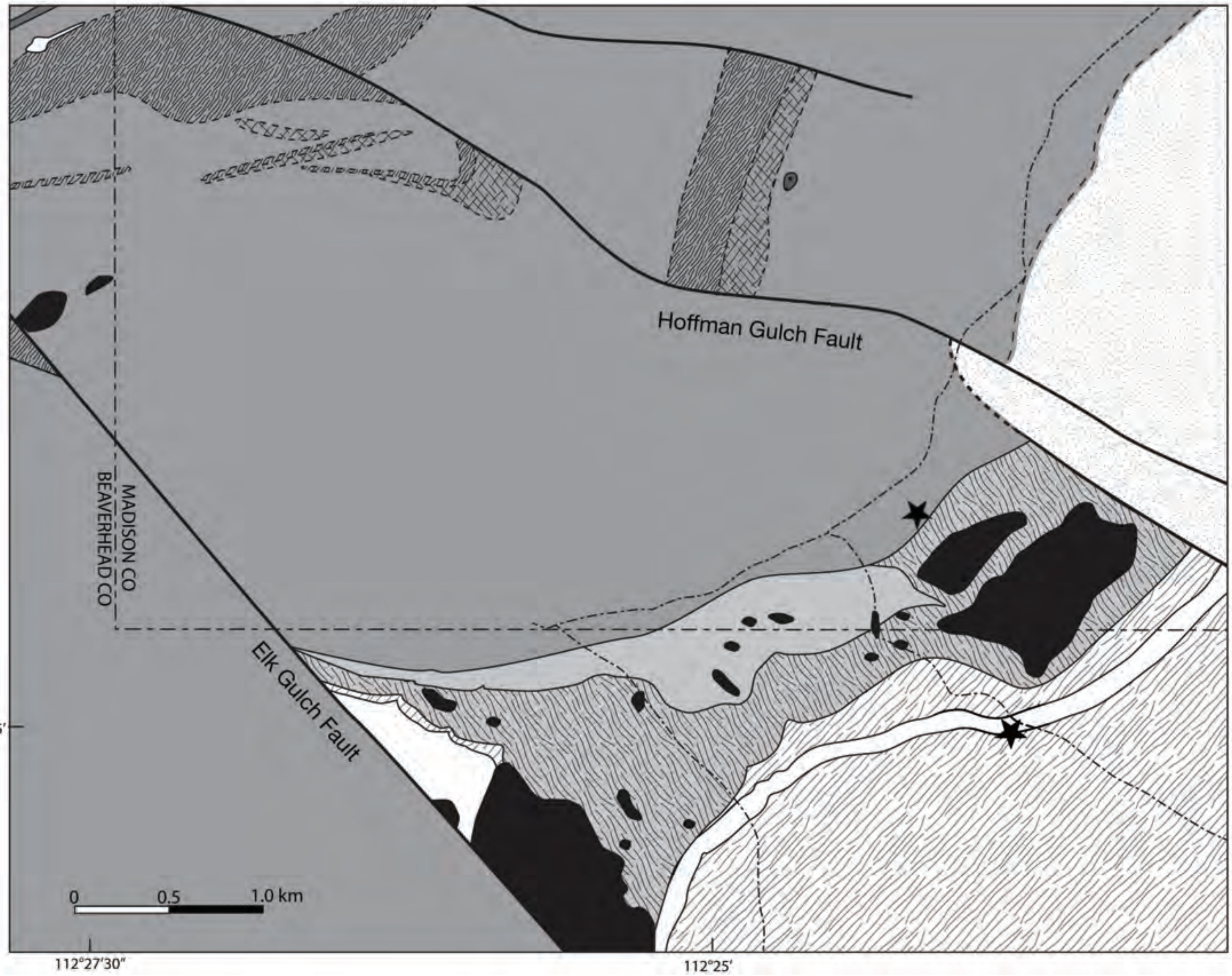

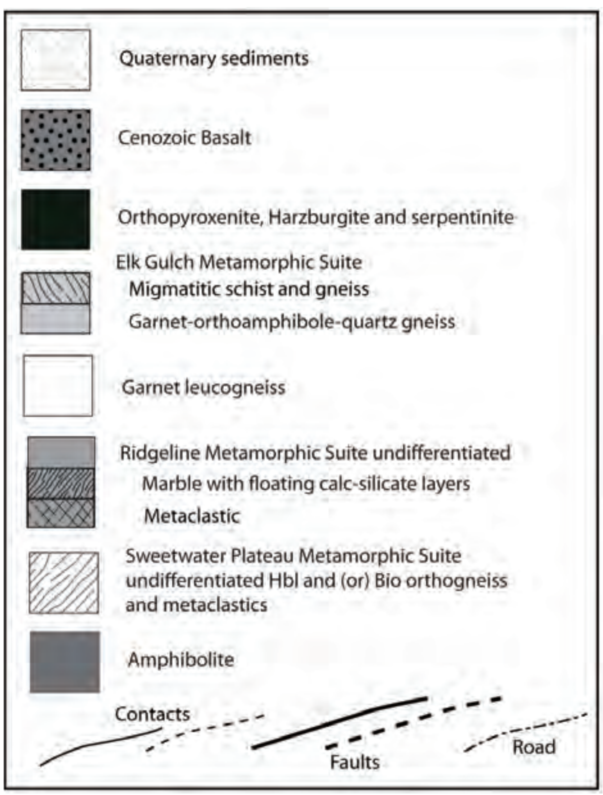

Figure 2. Detailed geologic map of the area in the southern Ruby Range. Locations where gahnite has been found are marked by stars. Included in the map area are the Ridgeline, Elk Gulch, and Sweetwater Plateau Metamorphic Suites. Width of Grt-LGn with gahnite that crosses the plateau is exaggerated to make it more visible at map scale. Legend is to the left. Grt-LGn occurs mostly as bodies too small to be shown at map scale. They are common in both the Ridgeline and Sweetwater Plateau suites.

and amphibolite with minor undeformed granite and pegmatite. (2) The Ridgeline Metamorphic Suite, dominated by hornblende-biotite quartzo-feldspathic gneiss, garnet leucogranites and garnet leucogneiss with amphibolite, marble, metapelite, and quartzite in lenses or narrow bands. (3) The Elk Gulch Metamorphic Suite, including orthoamphibole (sodic-gedrite)-garnet-quartz rock, low-calcium migmatitic metapelites, and minor amounts of other metasediments. It lies structurally below the Ridgeline Suite and only outcrops between the Elk Gulch and Hoffman Gulch faults. The suite has been intruded by the Wolf Creek ultramafic pluton (orthopyroxenite, harzburgite, and serpentinite), exposed as several large and numerous small bodies. (4) The Sweetwater Plateau Metamorphic Suite, composed of metapelite, quartzite, hornblende gneiss, and lineated hornblende ± biotite quartzo-feldspathic gneiss. The latter gneiss is lithologically and structurally distinct from gneiss of the Ridgeline Metamorphic Suite and is limited to areas south of the Sweetwater fault. The Ridgeline and Sweetwater Plateau Suites preserve extensive mylonites.

Most important to this interpretation is the recognition that a leucogranite, now mostly gneissic (Grt-LGn; fig. 3A), intruded rocks previously identified as PCCMS and Dillon quartzo-feldspathic gneiss. The Grt-LGn also intruded marbles that occur within the quartzo-feldspathic gneiss but has not been found within the area exposing only metasediments or amphibolites of the Christensen Ranch Metamorphic Suite. On this basis the marbles and metaclastics intruded by Grt-LGn were separated from the Christensen Ranch Suite and included as part of the Ridgeline Metamorphic Suite.

Zircons from one sample of the Grt-LGn that crosscuts Ridgeline Suite marble and metaclastics were analyzed and found to have an imprecise Pb-Pb age of ≈ 2,420 Ma (Alcock and Muller, 2012). This implies that the Grt-LGn protolith intruded at the end of or shortly after the ca. 2,450 Ma metamorphic event that affected Archaean rocks in the area. A pegmatitic phase of the Grt-LGn crosscuts intensely folded calc-silicate layers in marble (figs. 3B, 3C). These and similar folds observed in other outcrops of marble within the Ridgeline Suite indicate the intensity of deformation that occurred in the earliest Proterozoic.

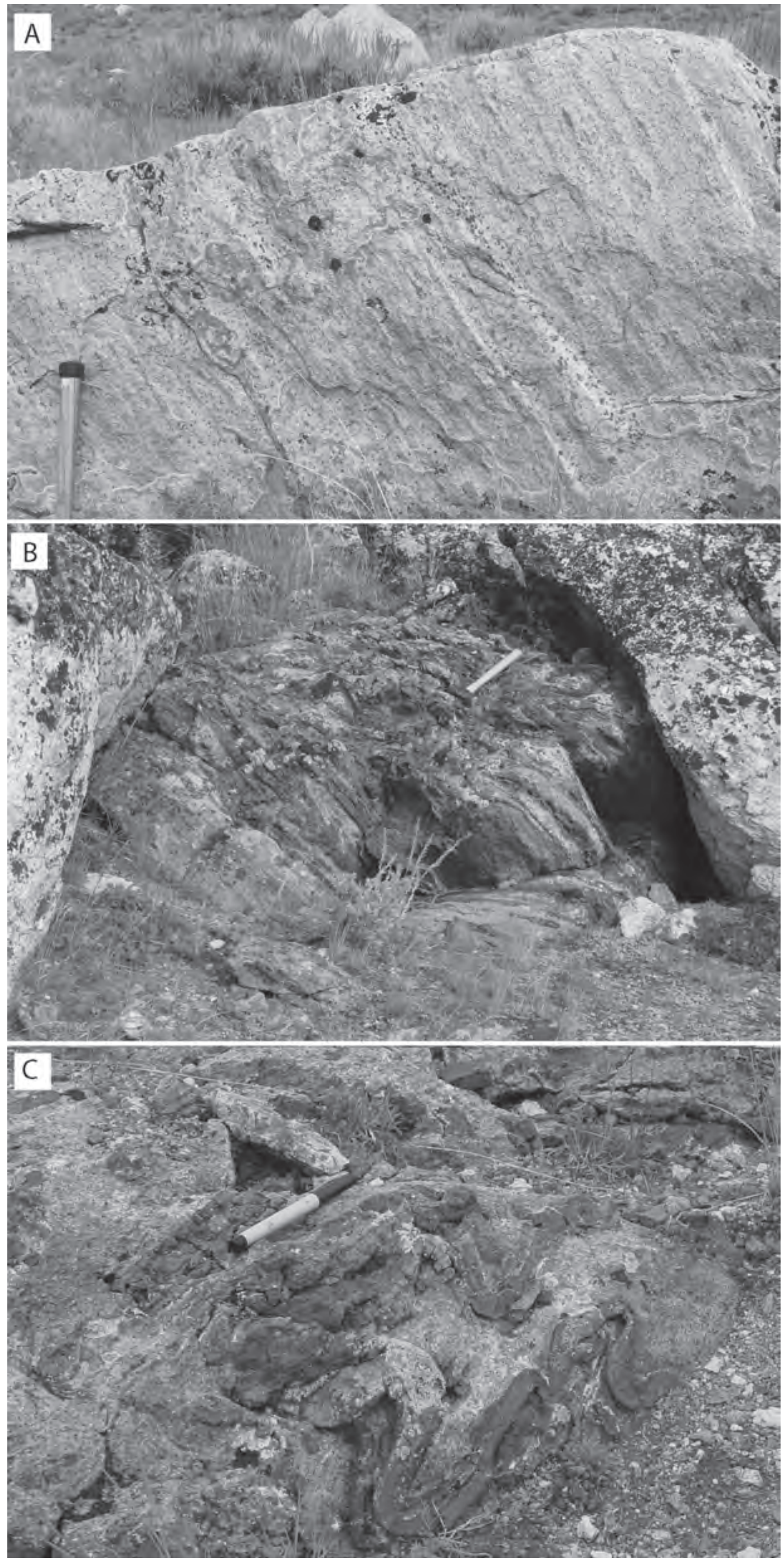

Figure 3. (A) Representative example of gneissic Grt-LGn. Garnet is the only common Fe-Mg mineral. Hammer handle is ≈ 32 cm. (B) Pegmatitic phase of Grt-LGn with large inclusion of marble with tightly folded calc-silicate layers. The hammer on the outcrop is 33 cm. (C) Closer view of folding of calc-silicate layers. The pen is 14 cm.

These marble exposures typically lie structurally above and in contact with garnet-sillimanite schist that appears to be a restite derived from partial melting of biotite. Prior investigations of peak metamorphic conditions during the Great Falls Orogeny report maximum temperatures ≈ 650°C and the occurrence of primary muscovite with sillimanite in schists of the Christensen Ranch Metamorphic Suite (Dahl, 1979). Dehydration melting of biotite that likely produced the restitic schists would imply significantly higher temperatures (≥750°C; White and others, 2007). They are interpreted, therefore, to have formed and to reflect conditions during the earliest Proterozoic metamorphism.

In the area where gahnite (fig. 2) has been observed, the Grt-LGn occurs in both the Ridgeline and Sweetwater Plateau Suites close to their contact with the Elk Gulch Suite. Electron microprobe dating of monazite in migmatites of the Elk Gulch Suite has established the timing of dehydration melting of biotite and migmatization of these rocks to be ≈ 1,780 Ma (Alcock and others, 2013). The age of the migmatites indicates that their formation is unrelated to origins of the Grt-LGn protolith.

DESCRIPTION OF GAHNITE OCCURRENCES

JA-04-32

The best-studied occurrence of gahnite is in Grt-LGn that occurs as a belt that extends for ≈ 4 km across the plateau between the Elk Gulch and Hoffman Gulch faults (fig. 2). The outcrops lie to the southeast, structurally below but near contact of the Sweetwater Plateau and Elk Gulch Suites.

Minerals present include microcline, albite, perthite and antiperthite, quartz, garnet, sillimanite, gahnite, zircon, and magnetite. Locally, the leucogneiss retains relict igneous texture with coarse (to 10 mm) perthite and antiperthite. More common are areas with finer grained quartz and feldspar, including perthite, that define a foliation. Fine prismatic sillimanite, some retrograded to sericite (fig. 4), parallels the foliation. Garnet to ≈ 5 mm is irregularly distributed, but multiple grains may follow a single plane of foliation.

Pale green to blue-green gahnite is fine-grained (<0.25 mm) and occurs in contact with sillimanite, feldspar, and quartz, with garnet and magnetite or simply in the felsic matrix of the sample. Grain shapes of the gahnite are mostly anhedral, although a few grains have a more rectangular habit. The mineral is approximately equal parts gahnite and hercynite with 7–9% spinel (table 1). There is no evidence of chemical zoning within a grain, although different grains do show chemical difference.

Table 1. Chemical composition of Zinc-spinel and garnet, sample JA-04-32

	n=5	*n*=2	*n*=2	*n*=2	*n*=1
SiO_2	0.002	0.002	0.000	0.002	0.000
TiO_2	0.000	0.000	0.000	0.000	0.000
Al_2O_3	56.387	56.323	56.498	56.416	56.759
Cr_2O_3	0.001	0.000	0.019	0.008	0.027
FeO	19.545	18.905	17.589	17.812	17.367
MnO	0.072	0.071	0.114	0.083	0.133
MgO	2.026	1.891	1.796	1.821	1.780
CaO	0.003	0.008	0.009	0.006	0.008
K_2O	0.005	0.006	0.004	0.005	0.005
NiO	0.041	0.028	0.060	0.039	0.054
ZnO	19.698	20.518	21.840	22.007	21.800
V_2O_3	0.048	0.103	0.139	0.137	0.418
CoO	0.040	0.042	0.039	0.039	0.000
P_2O_5	0.000	0.000	0.023	0.017	0.018
F	0.003	0.005	0.000	0.007	0.000
Cl	0.001	0.001	0.006	0.008	0.000
Total	97.870	97.900	98.136	98.401	98.369
Si	0.000	0.000	0.000	0.000	0.000
Al	1.982	1.986	1.986	1.977	1.991
Fe(3)	0.017	0.010	0.011	0.017	-0.004
Fe(2)	0.472	0.445	0.433	0.430	0.438
Mn	0.002	0.002	0.003	0.002	0.003
Mg	0.090	0.078	0.080	0.081	0.079
Ca	0.000	0.000	0.000	0.000	0.000
Ni	0.001	0.000	0.002	0.000	0.001
Zn	0.434	0.473	0.482	0.485	0.479
V	0.001	0.004	0.000	0.005	0.010
Co	0.001	0.001	0.001	0.001	0.000
P	0.000	0.000	0.001	0.000	0.001
F	0.000	0.001	0.000	0.001	0.000
Cl	0.000	0.000	0.000	0.000	0.000
Total	3.000	3.000	3.000	3.000	3.000
Herc	0.474	0.446	0.435	0.432	0.440
Sp	0.090	0.079	0.081	0.081	0.079
Gah	0.435	0.475	0.485	0.487	0.481

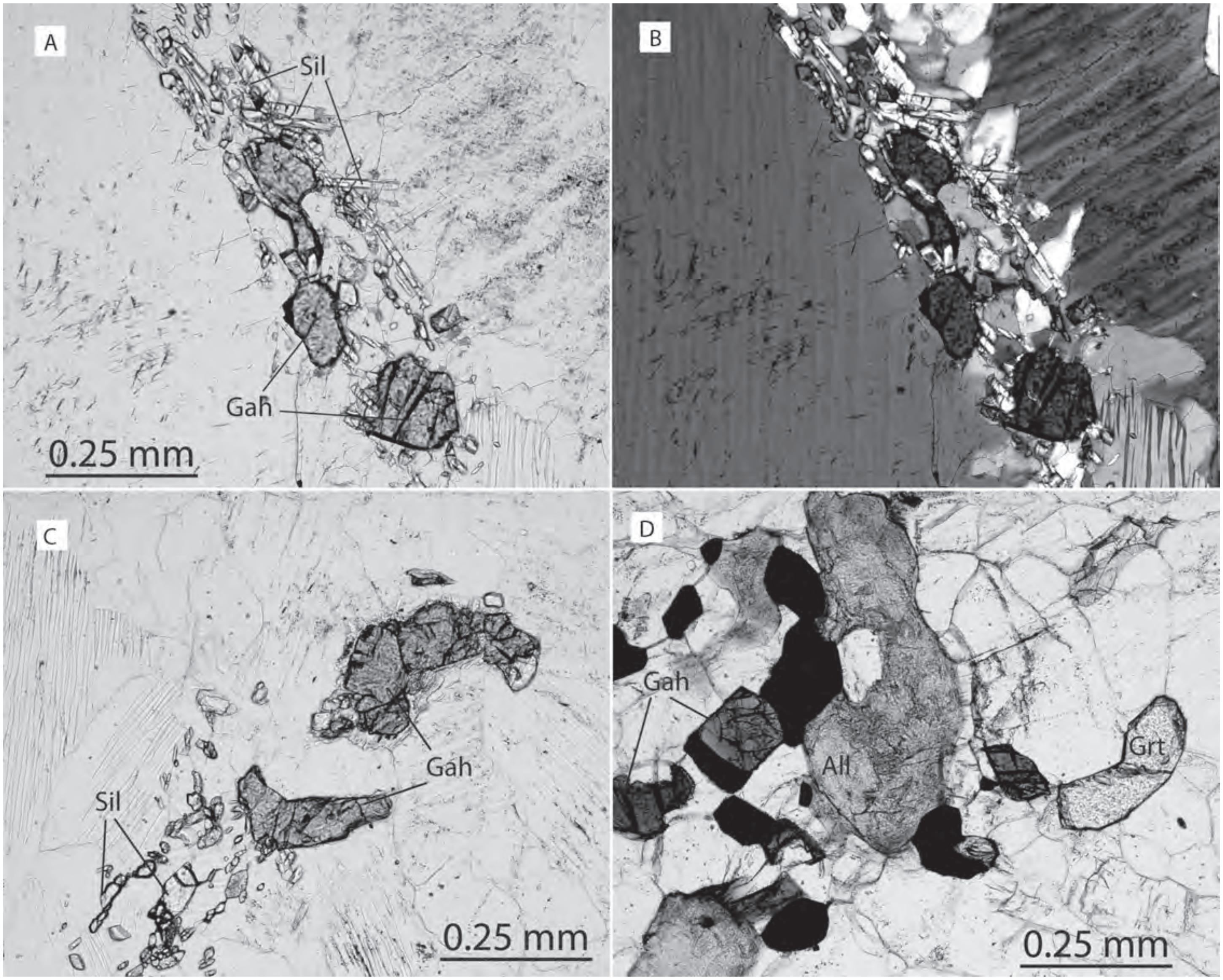

Figure 4. Photomicrographs of examples of gahnite observed in JA-04-32 and EG-04-04A. (A) Blue-green gahnite with prismatic sillimanite, perthite, antiperthite, microcline and quartz, JA-04-32. (B) Same field of view with crossed nichols. (C) Gahnite with small sillimanite prisms in perthite and microcline. (D) Gahnite in EG-04-04A with allanite, garnet, and opaque (probably ilmenite or ilmenite and magnetite) in matrix of perthite, microcline, and quartz.

Mineral analyses and BSE imaging (fig. 5) were conducted using the JEOL-Superprobe JXA-8900M microprobe equipped with five spectrometers at the ICTS-National Electronic Microscopy Centre at the Universidad Complutense of Madrid, Spain. Point analyses were conducted using 15 kV accelerating voltage and 20 nA beam current.

EG-04-04A

A second occurrence of gahnite in Grt-LGn was found in an area also close to, but structurally above, the Elk Gulch Suite. The Grt-LGn is from an area that includes amphibolite and migmatitic biotite gneiss. Minerals are predominantly microcline, quartz, and plagioclase with minor perthite. Sillimanite is not present in this sample. Discontinuous layers of fine-grained (≤0.25 mm) microcline and quartz define a gneissic fabric that is reinforced by the distribution of garnet and allanite. Besides allanite, zircon and opaques are relatively common accessory minerals. Gahnite occurs mostly in association with garnet, magnetite and (or) ilmenite, and allanite. Small amounts of probably secondary muscovite are observed.

DISCUSSION

Leucogranites may be derived from decompression and dehydration melting of muscovite and/or biotite schists at mid- to lower-crustal levels (Patiño Douce and Harris, 1998). Melting produces a leucocratic

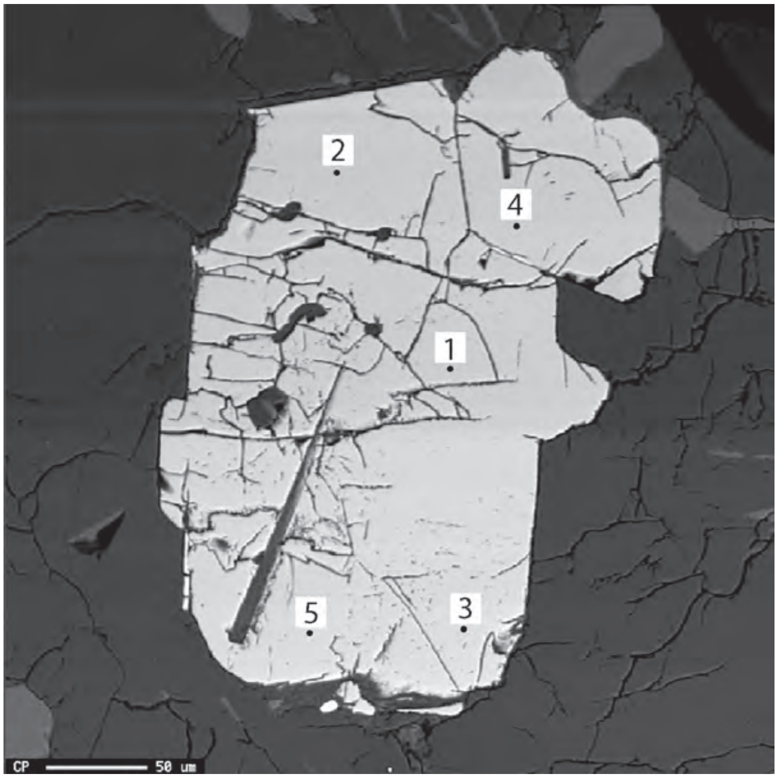

Figure 5. BSE image of gahnite grain with measured chemical composition. From an area of JA-04-32 with abundant sillimanite prisms, some retrograded to secondary muscovite. Matrix in image is predominantly quartz and feldspar. Small circles below numbers locate analyses. Scale bar is 50 µm.

magma that crystallizes to form leucogranite with garnet ± biotite ± muscovite.

The occurrence of gahnite in Grt-LGn, even as a rare accessory mineral, supports the hypothesis that the Grt-LGn is derived from biotite-melting reactions. Gahnite is observed in a wide variety of rock types including massive sulfide ore deposits, marbles, granitic rocks, and Fe-Al metasedimentary rocks (Heimann and Spry, 2005; Ghosh and others, 2011; Marino and others, 2013 and sources there-in). Heimann and Spry (2005) plotted gahnite compositions on a spinel–hercynite–gahnite ternary diagram and identified seven fields associated with gahnite from particular rock types (fig. 6). The high gahnite content of spinel in granitoids is probably caused by the release of Zn by biotite or staurolite during metamorphic reactions that consume those minerals (Stoddard, 1979; Dietvorst, 1980; Tajčmanová and others, 2009).

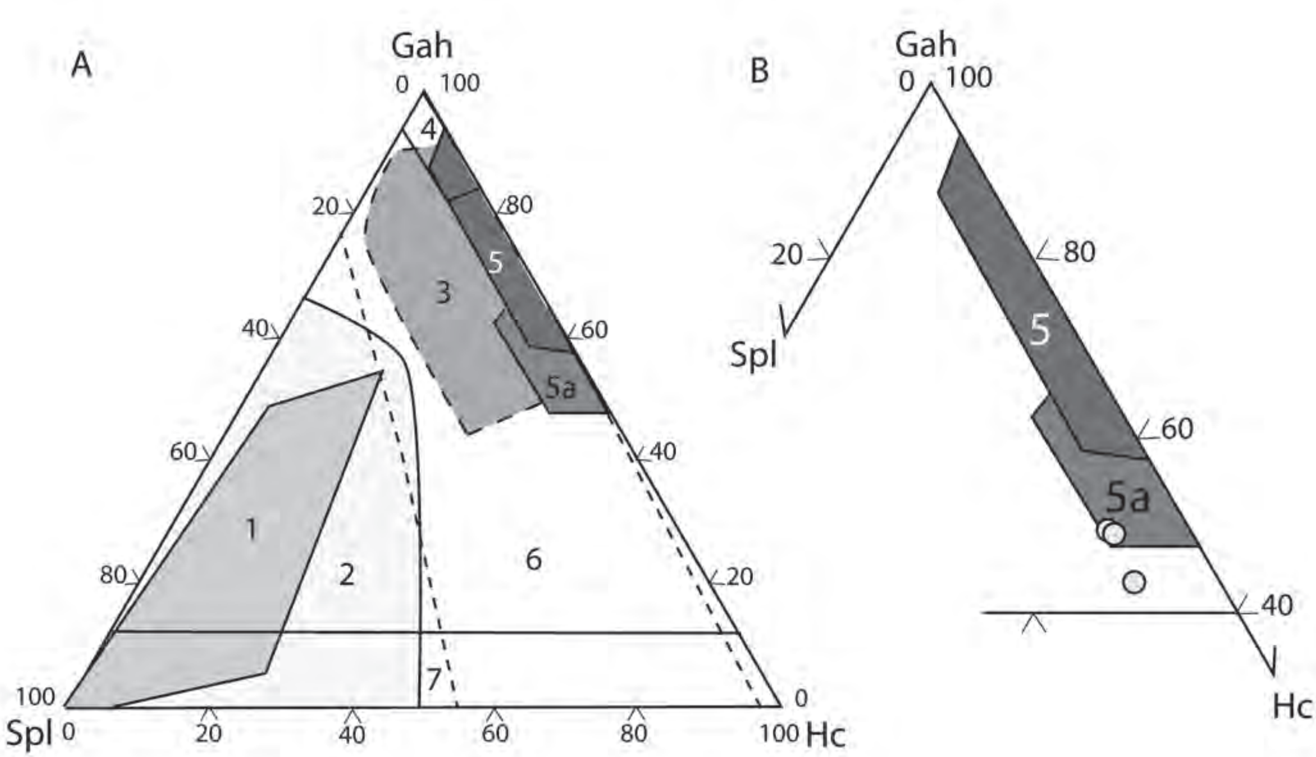

Figure 6. (A) Plot showing compositional fields of zincian spinels from different rock types after Heimann and Spry (2005) as modified by Ghosh and others (2011) and Merino and others (2013). Fields shown are: 1—marbles, 2 and 3—massive sulfide deposits, 4—metabauxites, 5 and 5a—granitic rocks including extended field by Merino and others (2013), 6—Fe-Al-rich metasedimentary and metavolcanic rocks, and 7—Al-rich granulites. (B) Enlargement of field of granitic rocks with a plot of the average compositions of the five analyzed gahnite grains. Three dots are shown as the overlap of composition hides the remaining two averaged analyses.

Spinel rich in zinc and iron and with <10% $MgAl_2O_4$ like that found in the Grt-LGn of the Ruby Range is associated with granitoids and Fe-Al metasediments. Spinels from granitic rocks are typically high in Zn-content with ≈ 50% or more gahnite like those in the Grt-LGn. One grain has a slightly lower gahnite content (≈ 43%) and falls just outside the field identified as associated with granitoid spinels. Perhaps this indicates that it formed early during the biotite melting event inferred to have released Zn and generated the Grt-LGn parent magma. Generally, the Zn-rich composition of the gahnite in the Grt-LGn is consistent with an igneous origin for the mineral from a melt derived from partial melting of an Al-rich metasedimentary rock.

Garnet-sillimanite schists with minimal biotite (fig. 7) are relatively common in the Ridgeline and Sweetwater Plateau Suites. We interpret these to be restites after biotite dehydration melting and a possible source of the Grt-LGn parent magma. It seems probable that the actual source of the Grt-LGn now exposed at the surface is similar Al-rich garnet-sillimanite schist that resided at a somewhat deeper structural level so that the melts could coalesce, move upwards, and intrude the rocks now exposed at the surface. Reactions that produced partial melting of biotite imply regional metamorphism at uppermost amphibolite to granulite facies conditions.

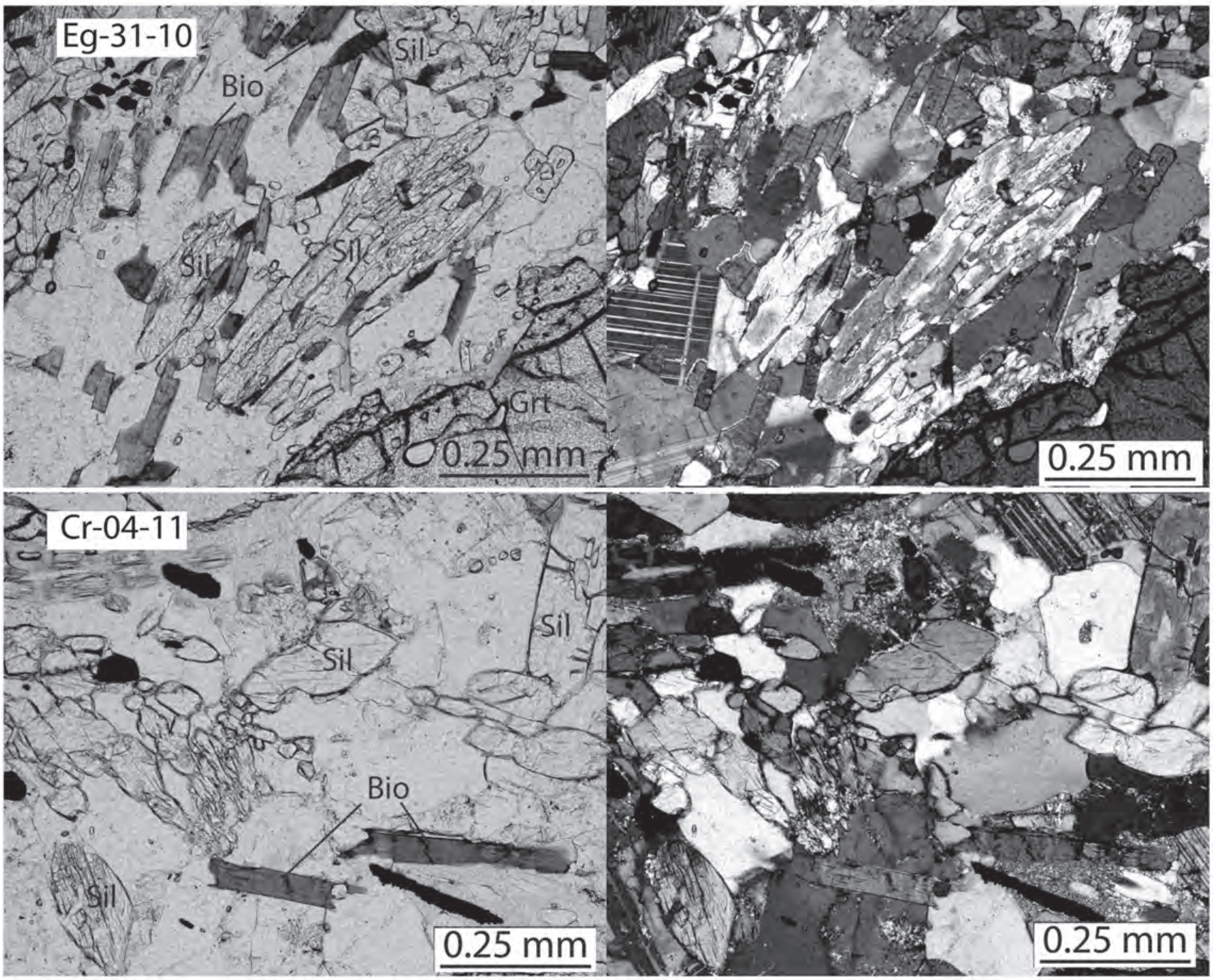

Figure 7. Photomicrographs in plane polarized light of two samples of garnet-sillimanite schist interpreted to be restite resulting from dehydration melting of biotite. Eg-31-10 minerals are Sil-Grt-Pl-Qtz-Bio and opaque, probably ilmenite or a solid solution of ilmenite + magnetite. Microcline/orthoclase is absent, presumably removed by melt transport. Cr-04-11 minerals are the same + rutile.

CONCLUSION

Gahnite-rich spinel has been observed in two samples of ca. 2,420 Ma garnet leucogneiss in the southern Ruby Range. The zinc forming the gahnite was most likely released from biotite in aluminous schists during dehydration melting reactions. This implies that regional uppermost amphibolite to granulite facies metamorphism occurred at this time and affected many of the Archaean rocks now exposed in the Ruby Range of southwest Montana.

REFERENCES CITED

Alcock, J., and Muller, P., 2012, A Paleoproterozoic sedimentary basin within the Wyoming craton exposed in the Ruby Range, SW Montana: Identified by field relations and geochronology: Northwest Geology, v. 41, p. 47–62.

Alcock, J., Muller, P.D., and Jercinovic, M.J., 2013, Monazite ages and pressure-temperature-time paths from anatectites in the southern Ruby Range, Montana, USA: evidence for delamination, ultramafic magmatism, and rapid uplift at ca. 1780 Ma: Canadian Journal of Earth Sciences, v. 50, p. 1069–1084.

Cheney, J.T., Webb, A.A., Coath, C.D., and McKeegan, K.D., 2004, In situ ion microprobe 207Pb/206Pb dating of monazite from Precambrian metamorphic suites, Tobacco Root Mountains, Montana, in Brady, J.B., Burger, H.R., Cheney, J.T., and Harms, T.A., eds., Precambrian geology of the Tobacco Root Mountains, Montana: Geological Society of America Special Paper 337, p. 151–179.

Dahl, P.S., 1979, Comparative geothermometry based on major-element and oxygen isotope distribution in Precambrian metamorphic rocks from southwestern Montana: American Mineralogist, v. 64, p. 1280–1293.

Dietvorst, E.J.L., 1980, Biotite breakdown and formation of gahnite in metapelitic rocks from Kemiö, Southwest Finland: Contributions to Mineralogy and Petrology, v. 75, p. 327–337.

Erslev, E.A., 1983. Pre-Beltian geology of the southern Madison Range, southwestern Montana: Montana Bureau of Mines and Geology Memoir 55, 26 p.

Foster, D.A., Mueller, P.A, Vogl, J.J., Gifford, J., and Mogk, D.W., 2013. The Little Belt arc of the Great Falls tectonic zone; a key component of the Belt Basin basement: Northwest Geology, v. 42, p. 107–110.

Garihan, J.M., 1973. Geology and talc deposits of the central Ruby Range, Madison County, Montana: Ph.D. dissertation, Geosciences, University Park, Pennsylvania State University, 209 p., 3 plates.

Garihan, J.M., 1979. Geology and structure of the central Ruby Range, Madison County, Montana: Geological Society of America Bulletin, Part II, v. 90, p. 695–788.

Ghosh, B., Some, S., and Thakur, A., 2011. Petrogenesis of zincian spinel from the Mamandur base metal sulphide prospect, Tamil Nadu: Journal Geological Society of India, v. 78, p. 365–369.

Heimann, A. and Spry, P.G., 2005, Zincian spinel associated with metamorphosed Proterozoic base-metal sulfide occurrences, Colorado: A re-evaluation of gahnite composition as a guide in exploration: Canadian Mineralogist, v. 43, p. 601–622.

Heinrich, E.W., 1949, Pegmatites of Montana: Economic Geology, v. 44, p. 307–335.

Heinrich, E.W., 1960, Part 2 - Geology of the Ruby Mountains and nearby areas in southwestern Montana, in Pre-Beltian geology of the Cherry Creek and Ruby Mountains areas, southwestern Montana: Montana Bureau Mines and Geology Memoir 38, p. 15–40.

Heinrich, E.W. and Rabbitt, J.C., 1960, Part 1- Geology of the Cherry Creek area, in Pre-Beltian geology of the Cherry Creek and Ruby Mountains areas, southwestern Montana: Montana Bureau Mines and Geology Memoir 38, p. 1–14.

James, H.L., 1990, Precambrian geology and bedded iron deposits of the southwestern Ruby Range, Montana: U.S. Geological Survey Professional Paper 1495, 39 p. 2 plates.

Jones, C.L., 2008, U-Pb geochronology of monazite and zircon in Precambrian metamorphic rocks from the Ruby Range, SW Montana: deciphering geological events that shaped the NW Wyoming province: M.S. thesis, Kent, OH, Kent State University.

Karasevich, L.P., Garihan, J.M., Dahl, P.S., and Okuma, A.F., 1981, Summary of Precambrian metamorphic and structural history, Ruby Range, southwest Montana, in Tucker, T.E. (ed.), Montana Geological Society Field Conference and Symposium Guidebook to Southwest Montana, Billings, MT, p. 225–237.

Marino, E., Villaseca, C., Orejana, D., and Jefferies, T., 2013, Gahnite, chrysoberyl and beryl co-occurrence as accessory minerals in a highly evolved peraluminous pluton: The Belvís de Monroy leucogranite (Cáceres, Spain): Lithos, v. 179, p. 137–156.

Mogk, D., Mueller, P., and Wooden, J., 1992, The significance of Archean terrane boundaries: evidence from the northern Wyoming Province: Precambrian Research, v. 55, p. 155–168.

Mueller, P.A., Shuster, R.D., Wooden, J.L., Erslev, E.A., and Bowes, D.R., 1993, Age and composition of Archean crystalline rocks from the southern Madison Range, Montana: implications for crustal evolution in the Wyoming Craton: Geological Society of America Bulletin, v. 105, p. 437–446.

Mueller, P.A., Burger, H.R., Wooden, J.L., Heatherington, A.L., Mogk. D.W., and D'Arcy, K., 2004, Age and evolution of the Precambrian crust of the Tobacco Root Mountains, Montana, in Brady, J.B., Burger, H.R., Cheney, J.T., and Harms, T.A., eds., Precambrian geology of the Tobacco Root Mountains, Montana: Geological Society of America Special Paper 337, p. 181–202.

Mueller, P.A. and Frost, C.D., 2006, The Wyoming Province: a distinctive Archean craton in Laurentian North America: Canadian Journal of Earth Science, v. 43, p. 1391–1397.

Okuma, A.F., 1971, Structure of the southwestern Ruby Range near Dillon, Montana: Ph.D. dissertation, , University Park, Pennsylvania State University, 122 p.

Patiño Douce, A.E. and Harris, N., 1998, Experimental constraints on Himalayan Anatexis: Journal of Petrology, v. 39, p. 689–710.

Roberts, H., Dahl, P., Kelly, S., and Frei, R. 2002, New 207Pb-206Pb and 40Ar-39Ar ages from SW Montana, USA: constraints on the Proterozoic and Archaean tectonic and depositional history of the Wyoming Province: Precambrian Research, v. 117, p. 119–143.

Sinkler, H., 1942, Geology and ore deposits of the Dillon nickel prospect, southwestern Montana: Economic Geology, v. 37, p. 136–152.

Stoddard, E.F., 1979, Zinc-rich hercynite in high-grade metamorphic rocks: a product of the dehydration of staurolite: American Mineralogist, v. 64, p. 736–741.

Tajčmanová, L., Konopásek, J., and Košler, J., 2009, Distribution of zinc and its role in the stabilization of spinel in high-grade felsic rocks of the Moldanubian domain (Bohemian Massif): European Journal of Mineralogy, v. 21, p. 407–418.

White, R.W., Powell, R., and Holland, T.J.B., 2007, Progress relating to calculation of partial melting equilibria for metapelites: Journal of Metamorphic Geology, v. 25, p. 511–527.

AGE AND ORIGIN OF THE BRIDGER GNEISSES: IMPLICATIONS FOR PROVENANCE OF THE LAHOOD FORMATION

Shane Fussell,[1]* Paul Mueller,[1] and David Mogk[2]

[1]University of Florida, Department of Geological Sciences, Gainesville, FL; [2]Montana State University, Department of Earth Sciences, Bozeman, MT

**Current address: University of Montana, Department of Geosciences, Missoula, MT*

ABSTRACT

The Bridger Range occupies a critical tectonic location in the Precambrian crystalline basement of southwest Montana, because it lies near the eastern limit of the Belt Basin and the southern limit of the Great Falls tectonic zone. Six basement samples were taken from the Bridger Range near Bozeman, MT. The range is comprised predominantly of metaigneous lithologies, mostly granitic gneisses with some amphibolites. The proximal Belt Basin is widely considered to be one of the deepest ensialic basins ever formed on the planet, but lacks the significant research on its underlying basement to allow its history to be thoroughly unraveled. This report describes the basement rocks that underlie the layers of sedimentary rocks at the eastern limit of the basin (Helena embayment). Dating of these rocks provides a greater understanding of the creation of the basin and the source of the sediments (i.e., local crystalline basement or more distal sources). These data have also helped to relate the Bridger basement (~3,300, 2,400, and 1,700 Ma) to other crystalline basements in the Wyoming province (e.g., relation to the Beartooth Mountains, ~2,800 Ma, or the Tobacco Root Mountains, ~3,200 Ma).

INTRODUCTION

The Bridger mountain range trends roughly NNW to SSE and extends for ~35 km just northeast of Bozeman, MT (fig. 1). Crystalline rocks in the range consist of mostly meta-igneous lithologies, but are overlain by Precambrian (Belt) and Phanerozoic sedimentary rocks. More specifically, the samples collected for this study are granitic gneisses and amphibolites. The range lies in a critical tectonic location along the eastern edge of the Belt Basin and the southern edge of the Great Falls tectonic zone. The Belt Basin is widely regarded to be one of the deepest ensialic basins ever formed on earth, and hosts a vast array of ore deposits. Due to the close proximity of the Bridger Range to the Belt Basin, we suggest there are implications for the provenance of the LaHood Formation, one of the oldest sedimentary units in the basin, as well as stratigraphically higher units.

METHODS

All of the samples collected are metamorphic rocks: BCW-7 is a gneiss, BCW-20 is a quartzofeldspathic gneiss, BCW-25 is a biotite-hornblende gneiss, BCW-26 is a garnet-gneiss, BCW-27 is an amphibolite, and BCW-28 is a quartzofeldspathic gneiss. The felsic gneisses are comparable to the TTG suite (tonalite-trondhjemite-granodiorite) commonly found in Archean cratons, including the nearby Beartooth and Tobacco Root Mountains (Mogk and others, 2004). BCW-7 was only analyzed for zircon ages, whereas all other samples had zircon ages as well as geochemical data. Major elemental compositions are shown in table 1.

Samples were crushed, milled, and then sifted with a #50 screen. The <50 mesh fraction was washed to remove all of the clay-sized minerals. The samples

Table 1. Major element percentages after LOI.

Major Element Analysis					
	BCW-20	BCW-25	BCW-26	BCW-27	BCW-28
SiO2	66.01	65.61	66.69	52.17	71.47
TiO2	1.06	0.41	0.46	0.80	0.39
Al2O3	13.86	13.96	13.00	19.14	15.55
Fe2O3	8.01	7.22	8.49	8.74	2.68
FeO	0.00	0.00	0.00	0.00	0.00
MnO	0.04	0.09	0.10	0.13	0.01
MgO	2.20	3.62	3.61	4.94	0.68
CaO	1.68	2.73	2.14	8.13	3.44
Na2O	2.37	2.73	2.38	3.59	4.48
K2O	3.65	2.64	2.48	1.37	1.21
P2O5	0.18	0.05	0.05	0.14	0.10
Total	99.05	99.05	99.40	99.14	100.00

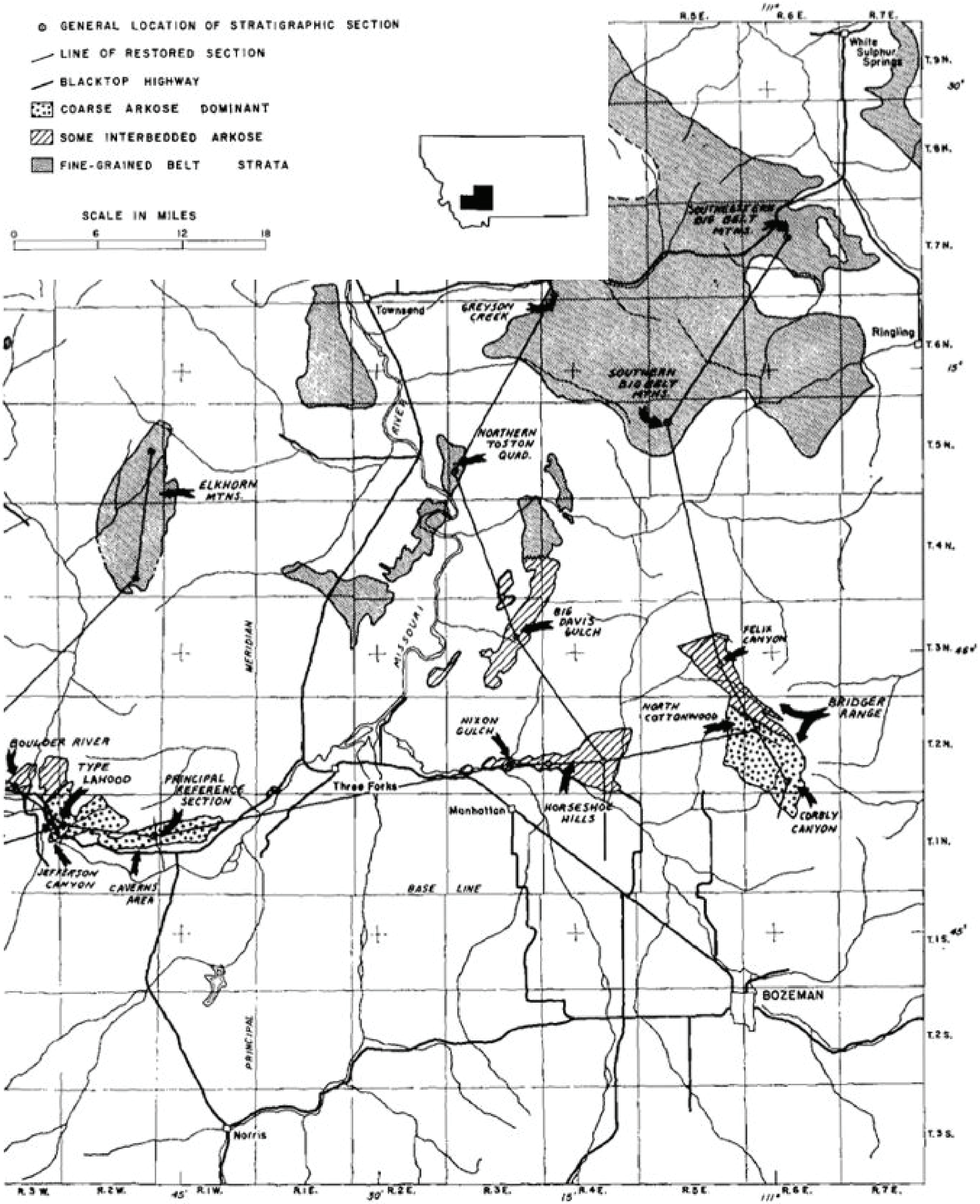

Figure 1. Geologic map showing the close proximity of the Bridger Range to Belt deposits (McMannis, 1963).

were then subjected to a hand magnet and later run through a Frantz magnetic mineral separator to remove magnetic minerals prior to density separation using tetrabromoethane. The dense fraction was then passed through the Frantz magnetic separator again to ensure that all magnetic material had been removed from the sample. Zircons were then hand-picked from the non-magnetic fraction under a binocular microscope. A minimum of 60 zircons from each sample and roughly 15 grains from the FC-1 standard sample were mounted together and a mold was placed over the grains and filled with epoxy. The epoxy mount was carefully ground until a mid-section of all the zircons could be seen. The mount was then placed into a Scanning Electron Microscope (SEM) for imaging. Back Scatter Electron Detection (BSD) was initially used to image the zircons and create maps of the samples. Then, cathodoluminescence (CL) was used to show the distribution of U in the zircons. After images were compiled, the sample was loaded into the inductively coupled plasma-mass spectrometer (ICP-MS) for laser ablation (213 nm with beam diameter of 20 μm) following methods in Mueller and others (2008).

Separately, a portion of each sample's coarsely crushed fraction was ground to a fine powder and then ~50 mg was dissolved in HF at 105°C. The dissolved sample was split into three parts: one for trace elemental analysis, one for Nd, and one for Pb isotopic analysis. Splits of the same powders were used for x-ray fluorescence (XRF) by fusion with lithium tetraborate to create glass beads for major element analysis.

RESULTS

Rare earth element (REE) abundances can be useful to constrain the source of an igneous or meta-igneous rock due to their limited mobility during metamorphism. REE analyses of the Bridger gneisses show that La is near 100 times chondritic values and Yb is 1 to 10 times chondritic values. There is a range of Eu-anomalies, both positive and negative, throughout the suite of samples (fig. 2).

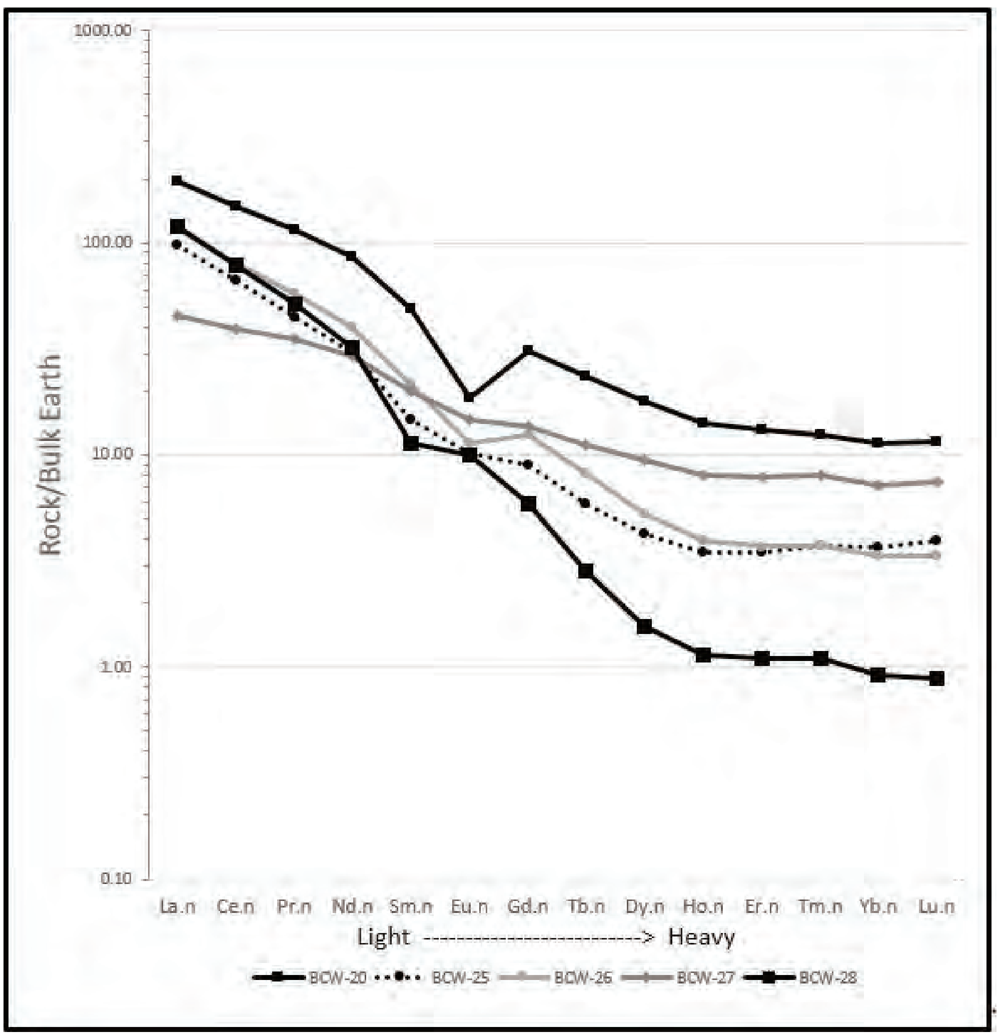

Figure 2. Rare earth elemental analyses from the Bridger gneiss samples show high values for the light rare earth elements and low values for the heavy rare earth elements. (BCW-7 was not analyzed for REE due to the state of the sample when received.)

Zircons were analyzed for their uranium and lead isotopic ratios. Uranium-238 was measured along with lead-206, lead-207, and lead-204, which cannot be distinguished from mercury-204. Consequently, no common Pb correction was made. Discordance, which expresses the percent difference between the 238/206 age and the 207/206 age, is substantial in many of these samples. Ages discussed are based on analyses with discordance between -5% and 10% and are averages if there are multiple analyses throughout a range of ages within analytical error of each other, and have low discordance. Errors are calculated by taking the standard deviation of this range of different dates and applying the Student's t multiplier to convert one sigma error into two-sigma error. Ages are shown in table 2. In general, there are three different age groupings evident in each sample, but to varying degrees and with varying coherence (figs. 3, 4). The oldest, approximately 3,300 Ma, is considered to be the crystallization of the protolith, the next oldest at approximately 2,450 Ma is thought to be a metamorphic event that is seen throughout the region, and the youngest event recorded, at around 1,700–1,800 Ma, is also thought to be the Great Falls orogeny (Mueller and others, 2016). Similar ages are seen for LaHood samples, shown in figures 5 and 6.

Table 2. $^{207}Pb/^{206}Pb$ ages and associated 2σ errors of samples.

Sample	Age (Ma)	2 σ error (Ma)	# of grains
BCW-7	2460	±115.3	7
	3205	±360.5	5
BCW-20	1790	±91.2	6
	1880	±64.5	13
	2357	±128.7	3
BCW-25	2575	N/A	1
	3289	±120.6	4
BCW-26	3532	±290.6	4
BCW-27	1775	±109.2	3
	2412	±69.5	21
BCW-28	2460	±42.3	7
	2631	±71.9	3
	3323	±126.2	13

Samarium-neodymium analyses of samples give depleted mantle model ages from 2,560 to 3,780 Ma based on comparison with the model evolution of the depleted mantle (εNd(0) of +10). This aligns well with Sm-Nd data of rocks taken from the LaHood Formation, which have ages of 2,320–3,570 Ma (fig. 7). The LaHood samples plot in a slightly younger range on this graph. In previous studies, the Belt-Purcell Supergroup, of which the LaHood is a member, gave Sm-Nd model ages averaging 2,910–3,780 Ma (Frost and Winston, 1987). This correlates with our data because the LaHood is one of the older units in the supergroup.

Zircons were also analyzed for their Lu/Hf ratios to determine ages. Figure 8 shows all of the data combined together into one kernel density plot. The ages are slightly older than dates obtained using $^{207}Pb/^{206}Pb$, with peaks showing up at 3,600, 3,250, and 2,300 Ma.

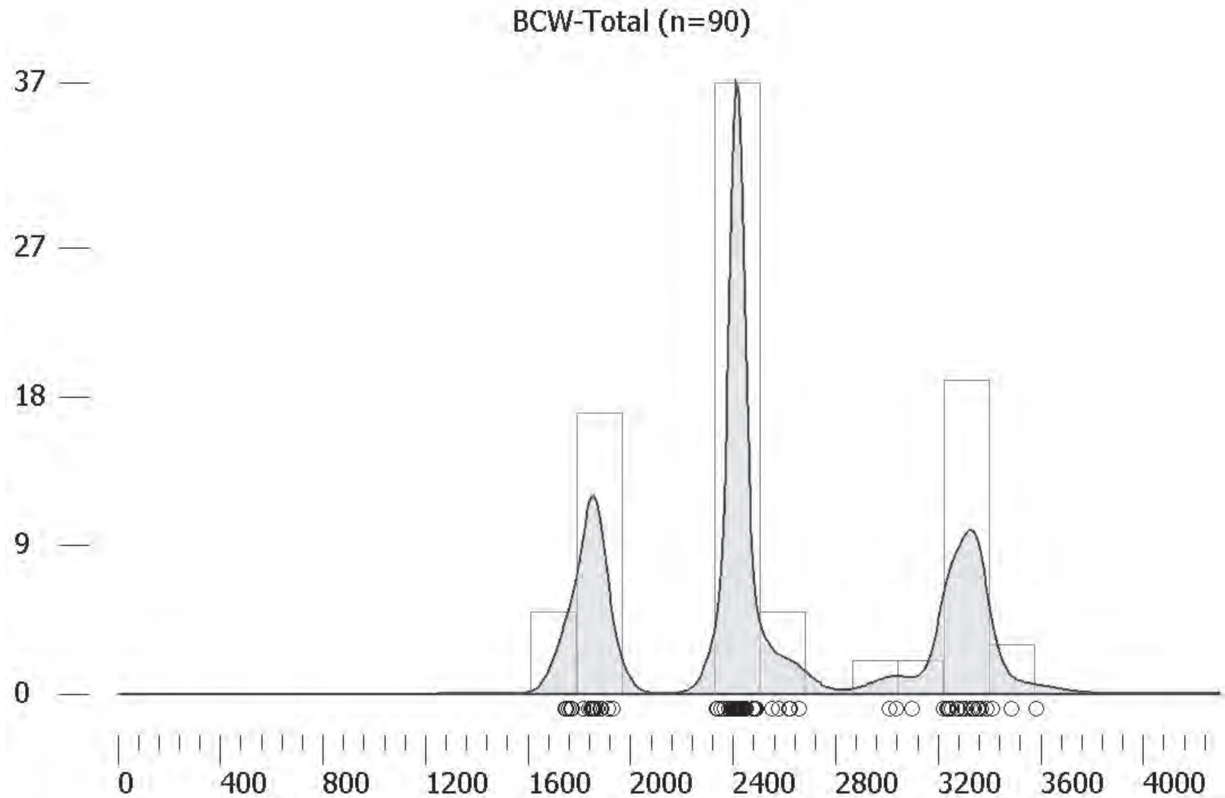

Figure 3. A composite kernel density plot (KDE, Vermeesch, 2012) of all the $^{207}Pb/^{206}Pb$ ages of -5 to 10% discordance (90 grains). Ages on x-axis are reported in millions of years. There are three clear concentrations that are present in multiple samples and considered the most reliable dates. The largest peak is present at ~2400 while other, less prominent and less well-constrained (secondary), peaks are evident at ~1800 and ~3300 Ma.

DISCUSSION AND CONCLUSIONS

Trace elements

By examining the REE diagram (fig. 2), it is evident that there are high concentrations of light REEs relative to the heavier REE. Relatively low Yb values (≤10x) suggest derivation from a garnet- or amphibole-bearing source. The "heavies" on this side of the REE diagram are highly compatible in garnet. If there were garnets present in the rock, the values would likely be much higher. Because they are so low, it can be inferred that the magma likely formed in the lower crust where garnet is stable, and many of the heavier REEs were concentrated with the garnet-retaining source. Europium in the 2+ valence state tends to be concentrated in plagioclase feldspar. Similar to the garnet, a negative anomaly suggests the plagioclase was left behind, whereas a positive anomaly shows that the plagioclase accumulated in the sample, rather than being removed by fractional crystallization. These data suggest melting in a crust sufficiently thick to have formed garnet and sufficiently mafic to generate the felsic gneisses by 3,200 Ma.

Ages

Sm-Nd depleted mantle model ages for the Bridger gneisses align well with similar ages from the overlying LaHood Formation (fig. 7). Data show that the model ages are generally older than the sedimentary units within the LaHood, which is an important indicator for a strong input from Archean sources, such as the Bridger gneisses. Crystalline basement with similar model ages is exposed in nearby uplifts such as the Madison (2,550–3,200 Ma; Mogk and others, 1992) and Tobacco Root ranges (3,200 Ma; Mueller and others, 2004; Harms and others, 2004), both of which are possible sources. Due to the fact that the LaHood model ages are slightly younger than the Bridger gneisses, it can be assumed that there must be a younger source rock involved in the provenance. Although the LaHood was not targeted in their study of the Belt-Purcell Supergroup, Frost and Winston (1987) show that average ages are much younger than the ages derived here from the Bridger gneisses (2,000 vs. 3,300 Ma). Even younger source ages for the Belt

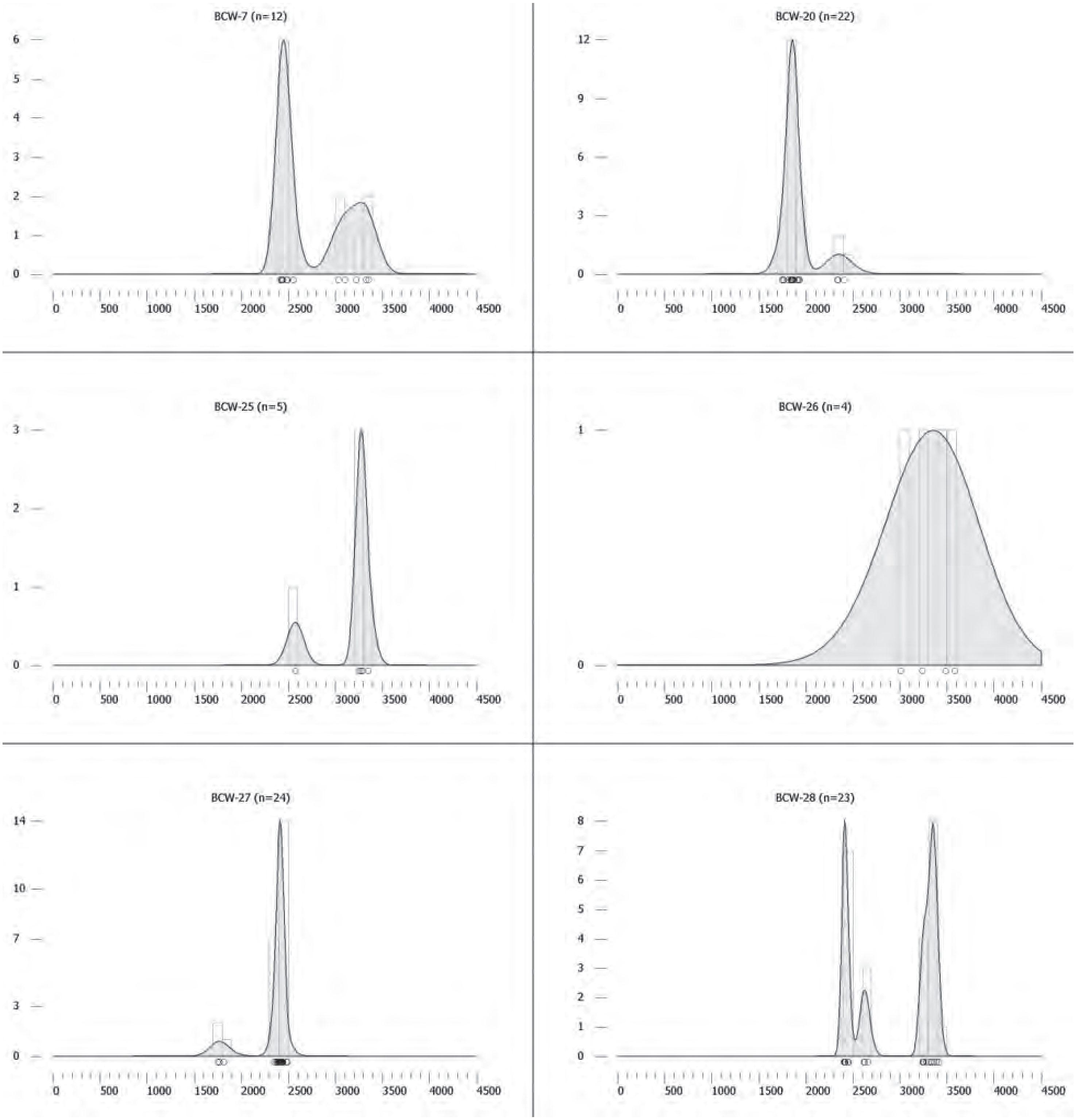

Figure 4. Kernel Density Plots of $^{207}Pb/^{206}Pb$ ages of individual Bridger Gneiss samples (-5 to 10% discordance). Ages on the x-axis are reported in millions of years.

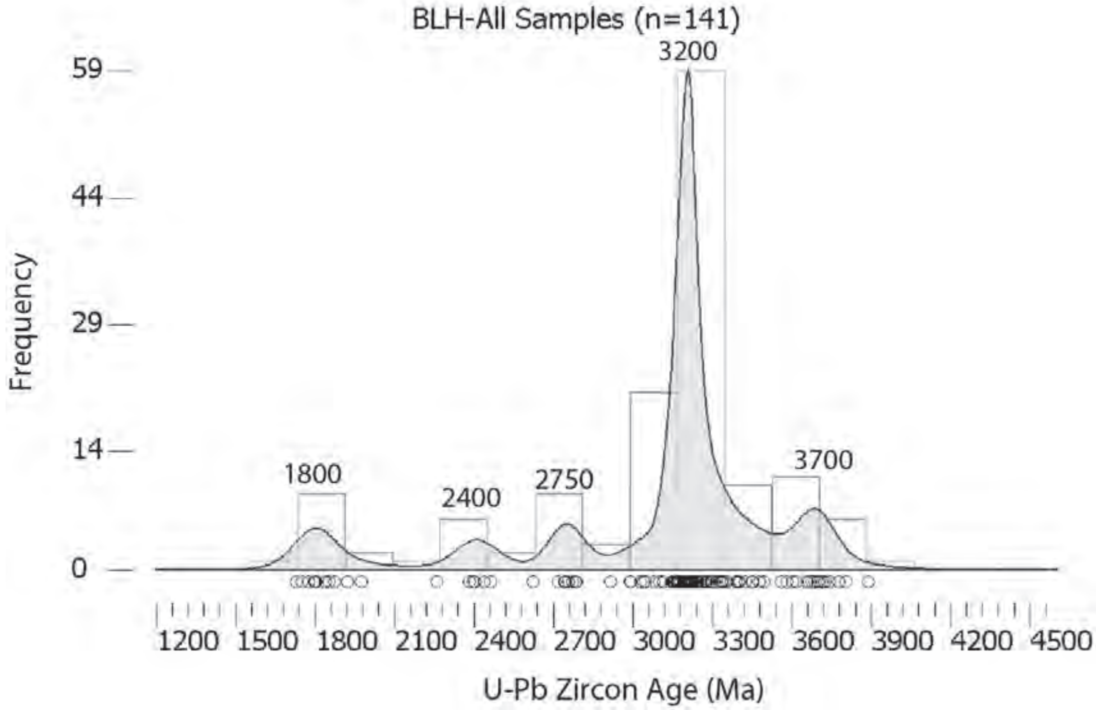

Figure 5. Kernel Density Plots of $^{207}Pb/^{206}Pb$ ages of LaHood Formation samples (-5 to 10% discordance). Ages on x-axis are reported in millions of years. Ages range from 1730 to 3890 Ma. Dominant age of ~3200 Ma is seen, with significant ages of ~1800, ~2400, ~2750, and ~3700 Ma also shown. (Guerrero and others, this issue)

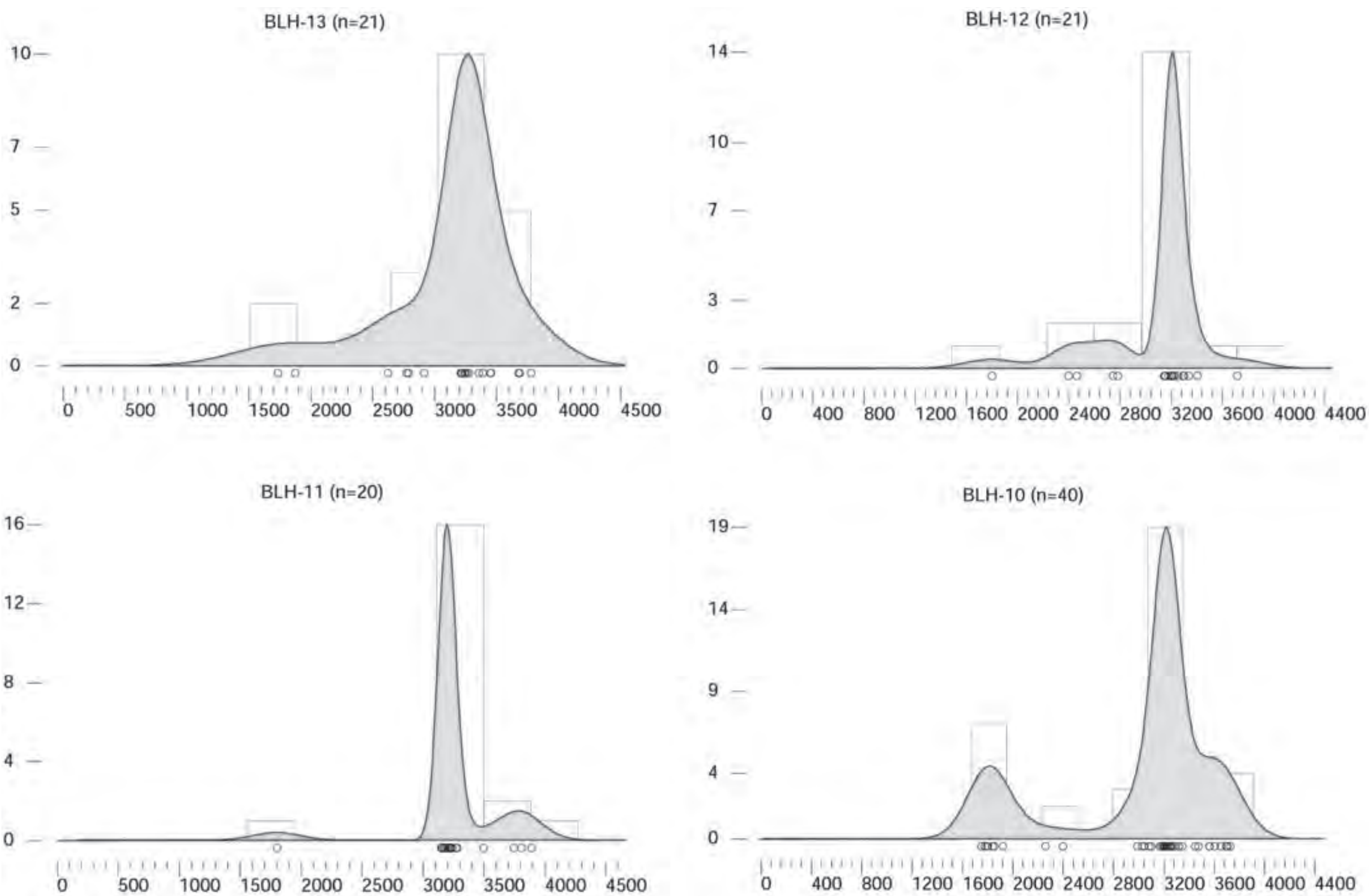

Figure 6. Kernel Density Plots of $^{207}Pb/^{206}Pb$ ages of individual LaHood Formation samples (-5 to 10% discordance). Ages on the x-axis are reported in millions of years.

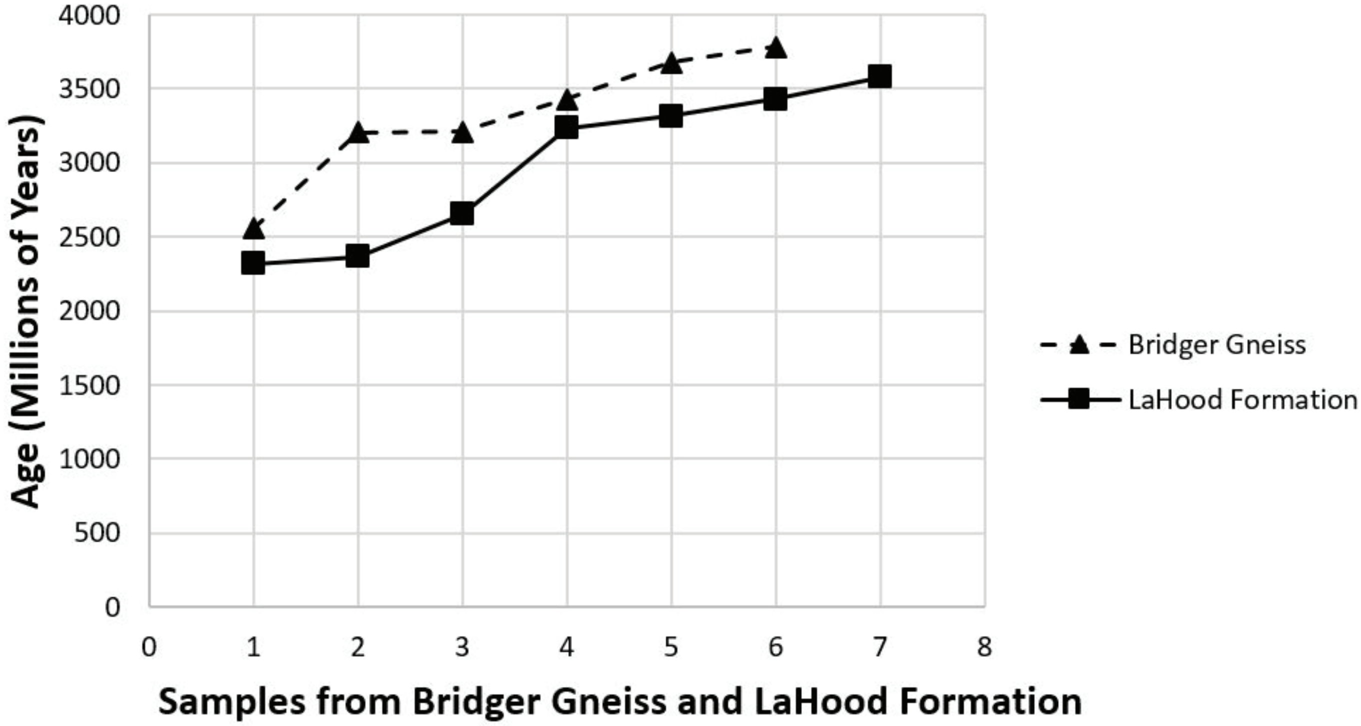

Figure 7. Sm-Nd results from the Bridger gneisses and the LaHood Formation show a definite correlation between Lu/Hf model ages (Tdm), but also imply a younger source for the LaHood.

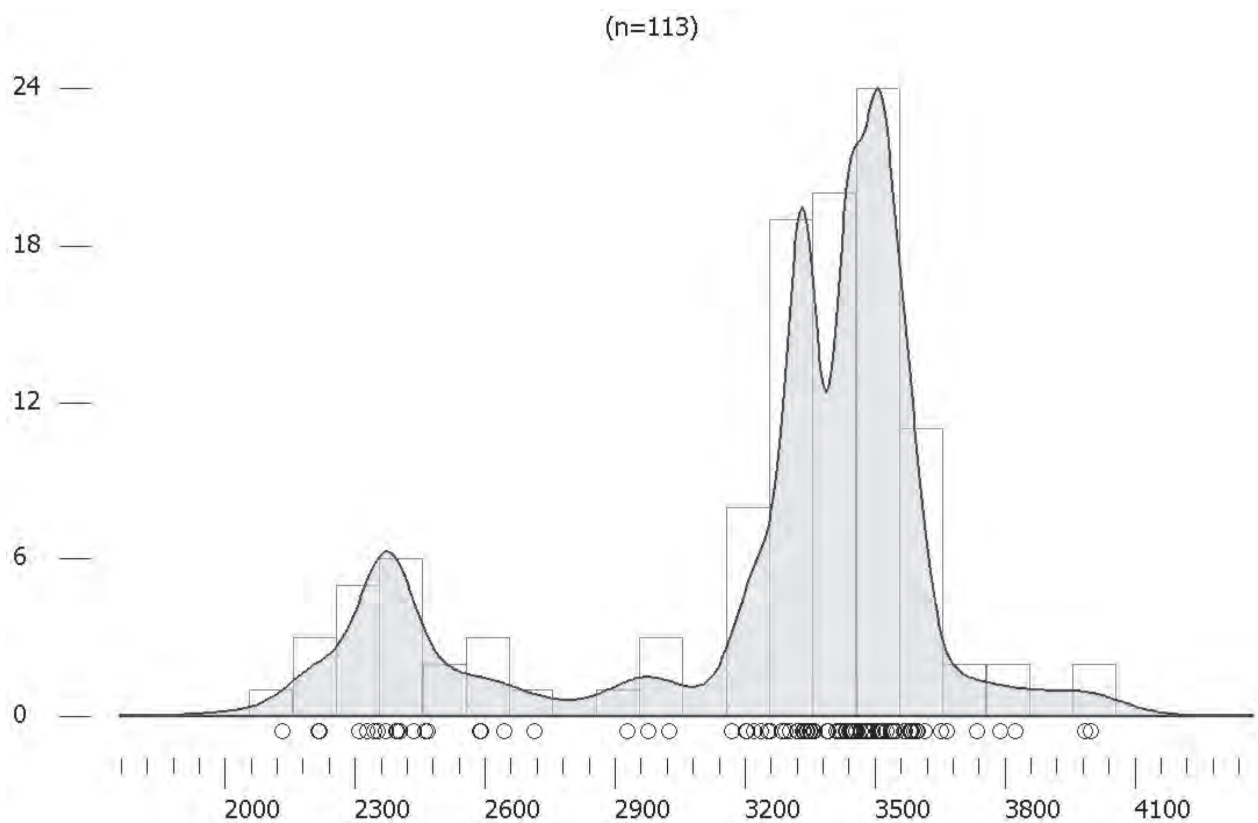

Figure 8. KDE plot for Lu/Hf model ages (Tdm) of zircons from all Bridger Gneiss samples.

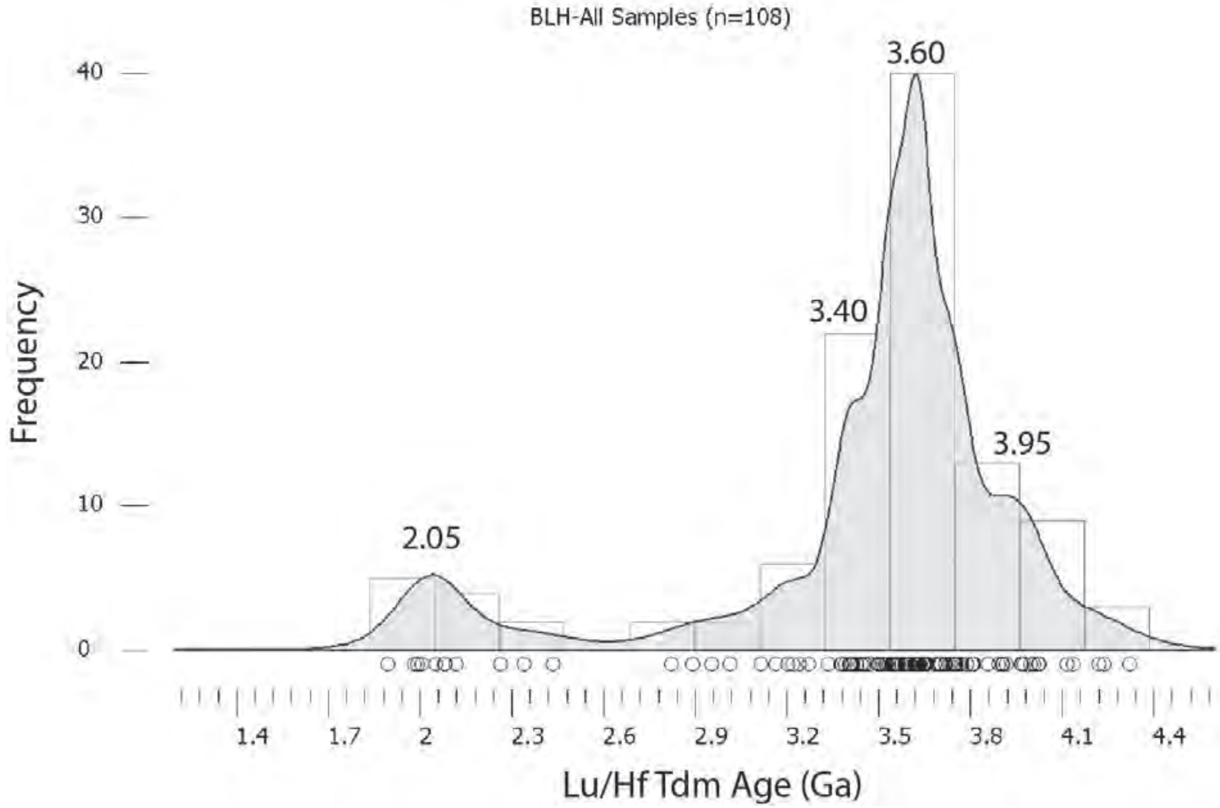

Figure 9. KDE plot for Lu/Hf model ages (Tdm) of detrital zircons from all LaHood samples. Model ages range from 1.89-4.32 Ga. Dominant age of ~3.60 Ga is seen, with another significant signal shown at ~2.05 Ga. The values suggest crustal recycling of even the oldest Archean crust in the region.

Basin range from 1,400 to 1,900 Ma (Ross and Villeneuve, 2003). Again, the LaHood was not a specific focus in this study, but some components of the provenance could be the same throughout the Belt. Figure 9 shows Lu/Hf data from the LaHood Formation that seems to align well with the data from the Bridger gneisses; however, there could possibly be an older peak present in the data set. This could imply an older source as well as a younger source for the provenance of the LaHood. Ross and Villeneuve (2003) suggested that the zircons found with ages 1,490–1,610 Ma are not Laurentian in source (North American magmatic gap), but rather from Australia or perhaps Baltica given the prominence of this age range in these localities and the lack of sources in that age range in western Mesoproterozoic Laurentia.

ACKNOWLEDGMENTS

Thank you to Dr. George Kamenov for all of his help in use of the ICP-MS instruments and with data processing; to Dr. Ann Heatherington for her help with the imaging (SEM) and XRF analyses, and to Katherine Bermudez for her help with sample preparation. This research was supported by NSF grant EAR 1145212.

REFERENCES

Frost, C.D. and Winston, D., 1987, Nd Isotope Systematics of coarse- and fine-grained sediments: Examples from the Middle Proterozoic Belt-Purcell Supergroup: The Journal of Geology, vol. 95, no. 3, p. 309–327.

Guerrero, J.C., Mueller, P.A., and Mogk, D.W., this issue, Provenance Study and Geochemical Analysis of the LaHood Formation of the Bridger Range, Montana.

Harms, T.A., Brady, J.B., Burger, H.R., Cheney, J.T., 2004, Advances in the geology of the Tobacco Root Mountains, Montana, and their implications for the history of the northern Wyoming province: Geological Society of America Special Paper 377.

McMannis, W.J., 1963, The LaHood Formation—A coarse facies of the Belt Series in southwestern Montana: Geological Society of America Bulletin 74, no. 4; 407–436, doi: 10.1130/0016-7606.

Mogk, D.W., Burger, H.R., Mueller, P.A., D'Arcy, K., Heatherington, A.L., Wooden, J.L., Abeyta, R.L., Martin, J., and Jacob, L.J., 2004, Geochemistry of quartzofeldspathic gneisses and metamorphic mafic rocks of the Indian Creek and Pony-Middle Mountain Metamorphic Suites, Tobacco Root Mountains, Montana: Geological Society of America Special Paper, v. 377, p. 15–46.

Mogk, D.W., Mueller, P.A., Wooden, J.L., and Bowes, D.R., 1992, The northern Wyoming Province: Contrasts in Archean crustal evolution, Proceedings of the International Conferences on Basement Tectonics, vol. 2, p. 283–297.

Mueller, P.A., Burger, H.R., Wooden, J.L, Heatherington, A.L., Mogk, D.W., and D'Arcy, K., 2004, Age and evolution of the Precambrian crust of the Tobacco Root Mountains, Montana: Geological Society of America Special Paper, v. 377, p. 181–202.

Mueller, P.A., Kamenov, G.D., Heatherington, A.L., and Richards, J., 2008, Crustal evolution in the southern Appalachian Orogen: Evidence from Hf Isotopes in Detrital Zircons: The Journal of Geology. v. 116, p. 414–422.

Mueller, P., Mogk, D., Wooden, J., and Spake, D., 2016, U-Pb ages of zircons from the Lower Belt Supergroup and proximal crystalline basement: Implications for the early evolution of the Belt Basin: Belt Basin: Window to Mesoproterozoic Earth: v. 522, no. 11, p.1–21, doi: 10.1130/2016.2522(11).

Ross, G.M., and Villeneuve, M., 2003, Provenance of the Mesoproterozoic (1.45 Ga) Belt Basin (western North America): Another piece in the pre-Rodinia paleogeographic puzzle: Geological Society of America Bulletin, v. 115, no. 10, p. 1191–1217.

Vermeesch, P., 2012, On the visualisation of detrital age distributions. Chemical Geology, v. 312-313, p. 190–194, doi: 10.1016/j.chemgeo.2012.04.0210

PROVENANCE STUDY AND GEOCHEMICAL ANALYSIS OF THE LAHOOD FORMATION OF THE BRIDGER RANGE, MONTANA

Juan Carlos Guerrero,[1]* Paul A. Mueller,[1] and David W. Mogk[2]

[1]Department of Geological Sciences, University of Florida, Gainesville, FL; [2]Department of Earth Sciences, Montana State University, Bozeman, MT

**Current address: Department of Geology and Geophysics, Louisiana State University, Baton Rouge, LA*

ABSTRACT

The LaHood Formation in the Bridger Range exceeds 1,000 m in thickness and is composed of alternating layers of coarse, pebbly sandstone and fine siltstone. Sandstones are mostly arkosic, typically containing more than 40% feldspar (McMannis, 1963). Exposures of the LaHood along the western flank of the Bridger Range constitute the most easterly outcrops of this formation. The significance of the LaHood to the rest of the Belt stratigraphy is not well defined. Its limited outcrop area along the southern margin of the basin (Helena embayment) makes stratigraphic relations to other "higher" Belt units difficult to define precisely. Consequently, we have undertaken a geochemical and detrital zircon study of the LaHood in the Bridger Range. Initial whole rock REE analyses show negative Eu-anomalies typical of continental crust. LREE values fall in two limited ranges, one being 80 to 50 times chondritic values and the other being 30 times chondritic values. Respectively, Yb values are 7 times chondritic values and 2 times chondritic values. Sm/Nd model ages (Tdm) range from 2.32 to 3.58 Ga, while Sm-Nd analyses yield ε-Nd(0) of from -33.9 to -21.0. These contrast with previous results from outcrops further west, which show only Archean model ages (Frost and Winston, 1987) and only Archean detrital zircons (Mueller and others, 2008). There seems to be some correlation between grain size and Tdm, with finer grained rocks generally giving younger model ages. U-Pb geochronology of detrital zircons of the LaHood Formation are useful to help define the formation's provenance and better constrain its stratigraphic position in the Belt Supergroup. The LaHood zircons gave a range of dates from 1,730 to 3,890 Ma, with a dominant age of ~3,200 Ma, and a second significant signal at ~1,800 Ma. Lu/Hf model ages (Tdm) calculated for the same zircons were also bimodal, giving two main signals at ~2.05 and ~3.60 Ga, respectively.

INTRODUCTION

The Bridger Range lies on the eastern side of the Belt Basin and south of the Great Falls Tectonic Zone (Fussell and others, 2015). The Belt Basin, located in the northwestern United States and southern Canada, holds thick layers of siliciclastic strata called the Belt Supergroup (Purcell Supergroup in Canada). The Belt Supergroup is 15–20 km thick, and divided up into the Lower Belt, Ravalli, Piegan, and Missoula groups (Stewart and others, 2010). Previous geochemical studies on the Belt Supergroup by Frost and Winston (1987) yielded crustal residence ages ranging from 1.59 to 2.14 Ga for fine-grained sediments. Coarser sediments, however, gave two different age ranges. Four of the five coarse-grained samples analyzed by Frost and Winston gave crustal residence ages ranging from 1.98 to 2.24 Ga. The fifth sample (LaHood Formation) yielded ages from 2.91 to 3.78 Ga (Frost and Winston, 1987). Proposed depositional environments for Belt strata are quite variable. Walcott (1914) and Winston (1989b) reported sedimentological observations compatible with lacustrine origin, while Schieber (1998) reported geochemical data that led him to suggest a much deeper water environment. A map of the general field area as well as a cross section showing general stratigraphic relationships are shown in figures 1 and 2.

METHODS

Geochemistry

Whole rock samples were powdered before undergoing acid dissolution and chromatographic separations. Samples were analyzed using high-resolution ICP-MS for trace elements and multi-collector ICP-MS for isotopic compositions. Methods follow those of Gifford and others (2014). Whole rock powder was also used to make glass beads to be analyzed by X-ray fluorescence (XRF). Powders were first heated over-

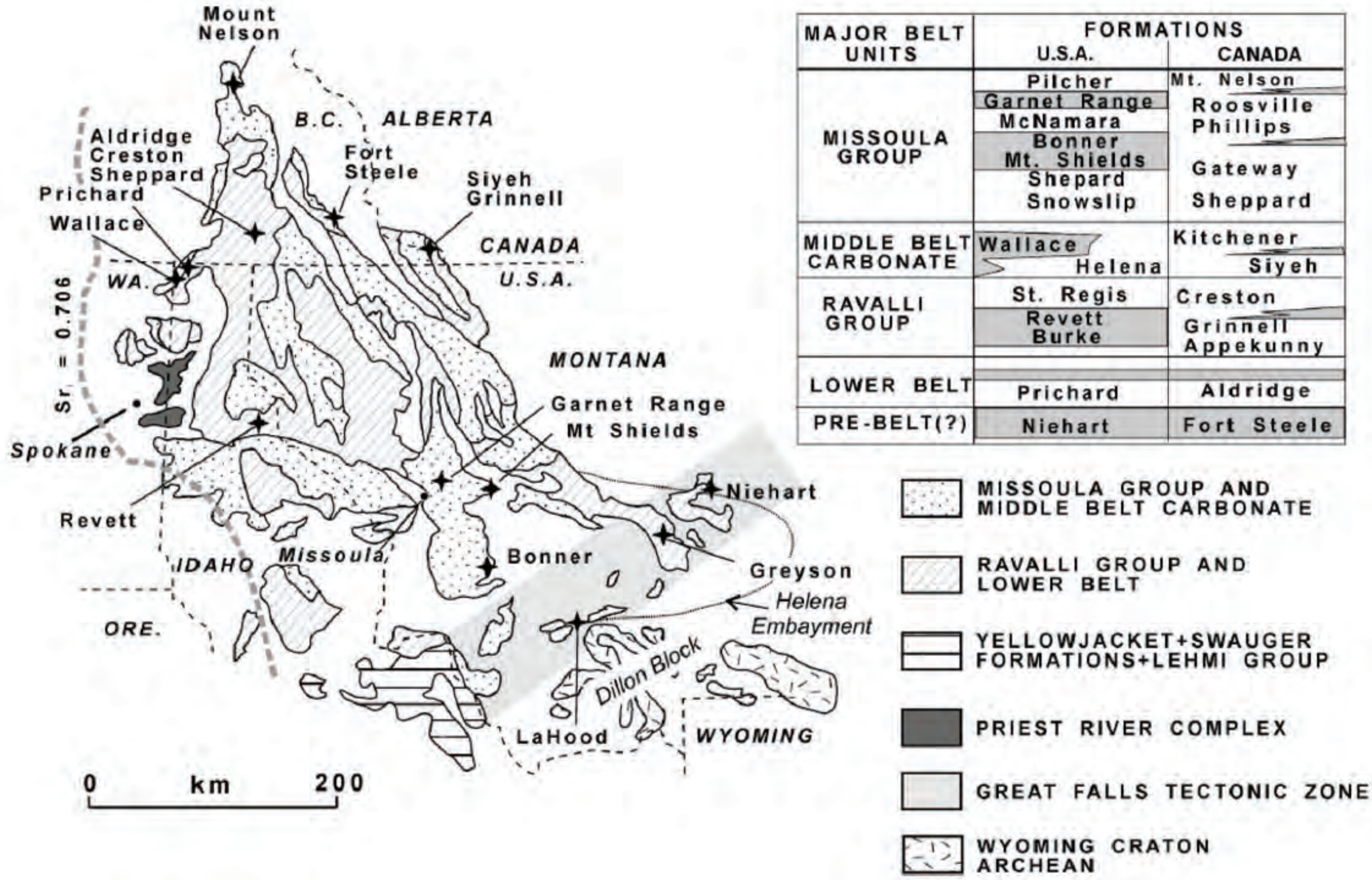

Figure 1. Geologic map and stratigraphic column for Belt–Purcell Supergroup (Ross and Villeneuve, 2003; modified from Winston, 1986a).

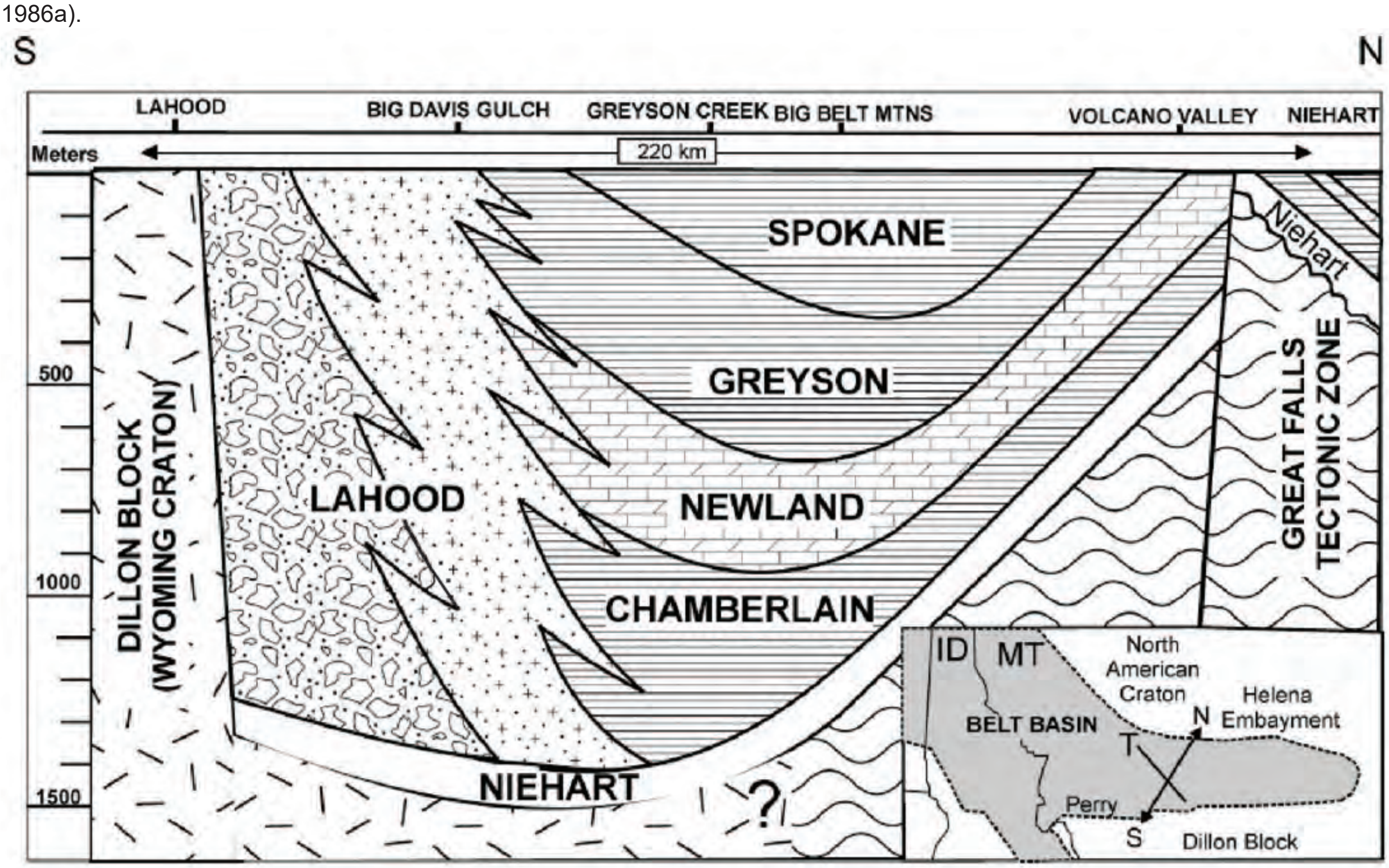

Figure 2. Cross section SW-NE through Helena Embayment showing LaHood Formation stratigraphic relationships (Ross and Villeneuve, 2003; modified from Winston and others, 1989).

night at ~100° Celsius to remove surface moisture, and then their LOI (Loss on Ignition) measured by placing them in a furnace at ~950° Celsius for an hour. Powders were then mixed with dry fusion flux and melted in a Katanax fusion machine to create glass beads. Major element data acquired by XRF were plotted on QAP and A-CN-K diagrams using the TernPlot program (Marshall, 1996). Data for QAP diagrams were converted using the CIPW Norm calculation program of Kurt Hollocher (Union College, Schenectady, New York).

Zircons

Samples were crushed and zircons separated though hydrodynamic (“Blue Bowl”), magnetic (Frantz Magnetic Separator), and density (heavy liquid separation; TBE) methods. Zircons were then picked with aid of a binocular microscope. Individual grains were mounted in epoxy, and then ground and polished to expose the inner part of the grains. Zircons were then imaged via SEM using both backscattered electrons (BSD) and cathodoluminescense (CL) methods, prior to analysis using the laser ablation ICP-MS. Data were plotted as kernel density estimator (KDE) plots using the density plotter program (Vermeesch, 2012). U-Pb data plotted are all less than 10% discordant, while Tdm data from Hf analysis plotted all had less than a 25% correction for Yb and Lu. Methods for U-Pb and Lu-Hf analyses follow those of Mueller and others (2008).

RESULTS

Geochemistry

Major element analysis yielded granite, granodiorite, and quartz-rich granitoid compositions for these samples (fig. 3). Chemical index of alteration (CIA) calculated for these samples ranged from 54.7 to 69.7, and showed normal weathering patterns (fig. 4). REE analyses showed Eu-anomalies typical of continental crust (fig. 5). La and LREE values in general defined two sets: one 80 to 50 times chondritic values and the other 30 times chondritic values. Respectively, normalized Yb values were 7 times chondritic values and 2 times chondritic values. Sm/Nd model ages (Tdm) ranged from 2.32 to 3.58 Ga (table 1), while Sm-Nd analyses yielded εNd(0) of from -33.9 to -21.0.

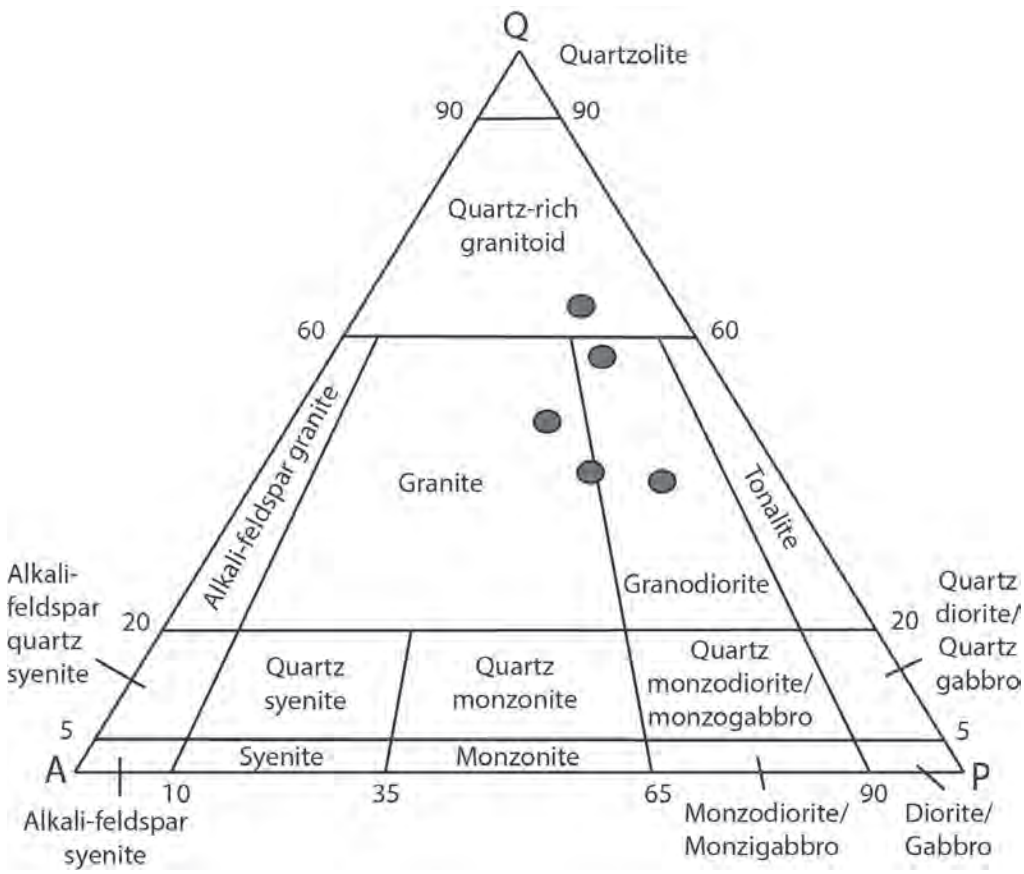

Figure 3. QAP diagram for LaHood Formation samples, yielding granite, granodiorite, and quartz-rich granitoid compositions.

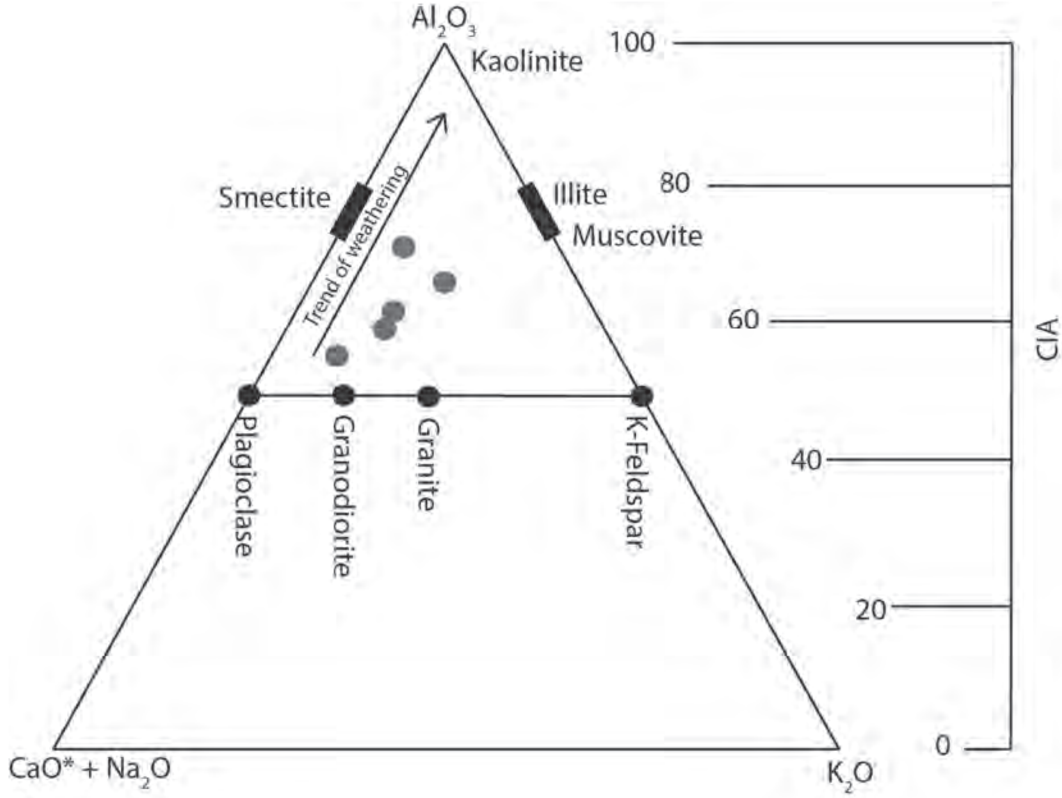

Figure 4. Al_2O_3 – CaO^* + Na_2O – K_2O (A-CN-K) diagram showing weathering patterns for LaHood Formation samples, with a CIA ranging from 54.7 to 69.7.

Detrital Zircons

U-Pb geochronology of detrital zircons of four samples (BLH-10, -11, -12, -13) of the LaHood Formation can be seen individually in figure 6. Ages ranged from 1730 to 3890 Ma for U-Pb ages and 1.89 to 4.32 Ga for Lu/Hf model ages (Tdm). These plots have been consolidated in figures 7 and 8, respectively.

DISCUSSION AND CONCLUSIONS

Major element analysis yielded granite, granodiorite, and quartz-rich granitoid compositions for the LaHood Formation samples, with a CIA ranging from 54.7 to 69.7. These compositions agree with studies by McMannis (1963) and interpretations by Schieber (1990), both of which indicate the LaHood Formation was derived from a granitoid gneiss, migmatite, and granite dominated source. Based on previous data from Nesbitt and Young (1982), granites and granodiorites have CIA values ranging from 45 to 55, while average shales range from 70 to 75. These ranges suggest the LaHood samples went through little weathering, which suggests short transport distances and/or a temperate, mild climate.

Whole rock samples gave Sm/Nd model ages ranging between 2.32 and 3.58 Ga, but mostly falling in two sets: a younger signal at an average of ~2.45 Ga, and an older signal at an average of ~3.39 Ga. Lu/Hf model ages derived from detrital zircons ranged from 1.89 to 4.32 Ga, but once again had two main signals, one at ~2.05 Ga and another at ~3.60 Ga. The presence of these Proterozoic model ages contrasts with the data reported by Frost and Winston (1987), which showed only Archean Sm/Nd model ages for the LaHood Formation.

U-Pb ages of detrital zircons show a dominant age of ~3,200 Ma for the LaHood samples, similar to Archean quartzites reported by Mueller and others (1998). This is compatible with the Lu/Hf Tdm ages of the same samples, which show a dominant ~3.60 Ga signal. However, it is also important to note a second concentration at about ~1,800 Ma for U-Pb ages and ~2.05 Ga for Lu/Hf Tdm model ages. Once again, we see both an Archean and Proterozoic signal for the LaHood Formation in both model ages and detrital zircons, contrasting with results from Mueller and others (2008), which showed only Archean detrital zircons.

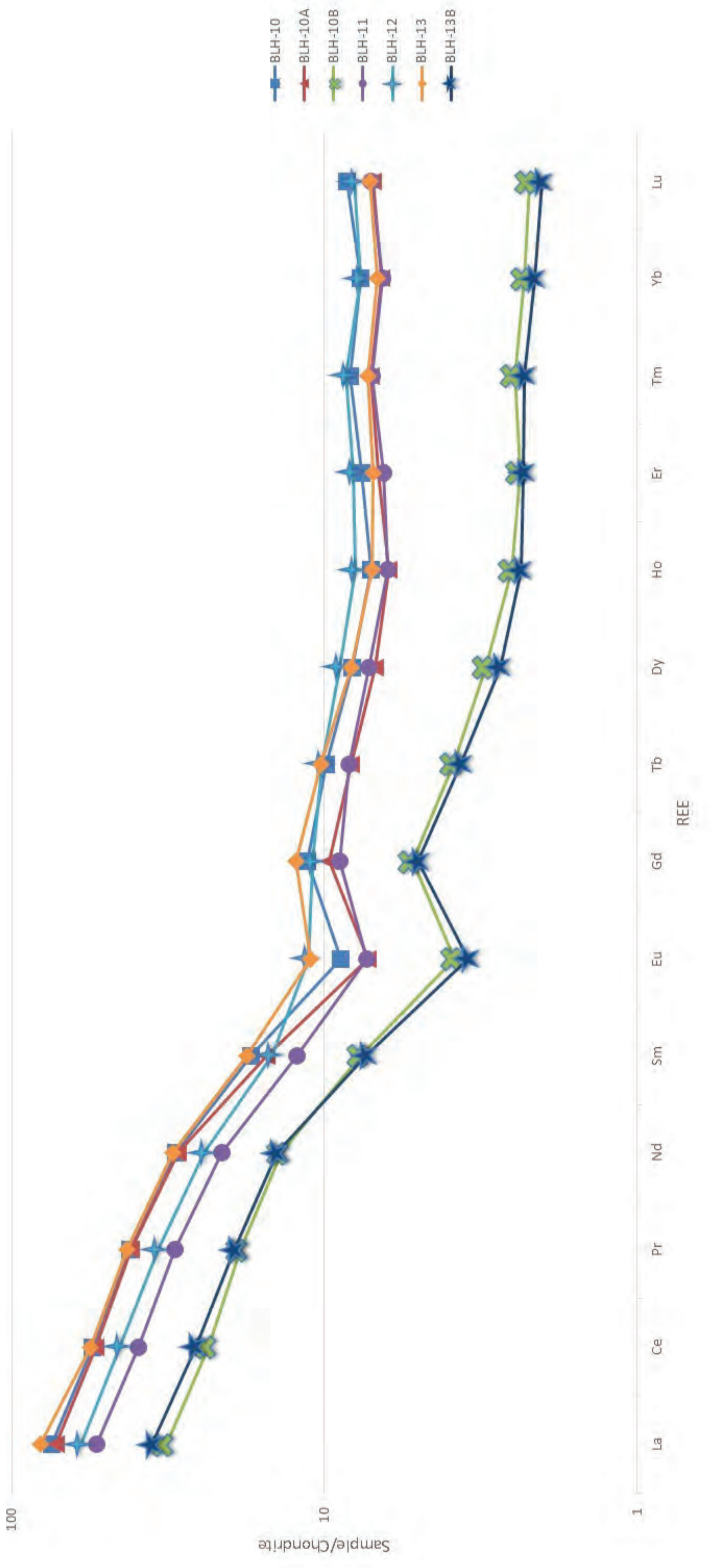

Figure 5. Rare earth element (REE) plot of all LaHood samples. REE plot shows normal crustal signatures with LREE enrichment and negative Europium anomalies.

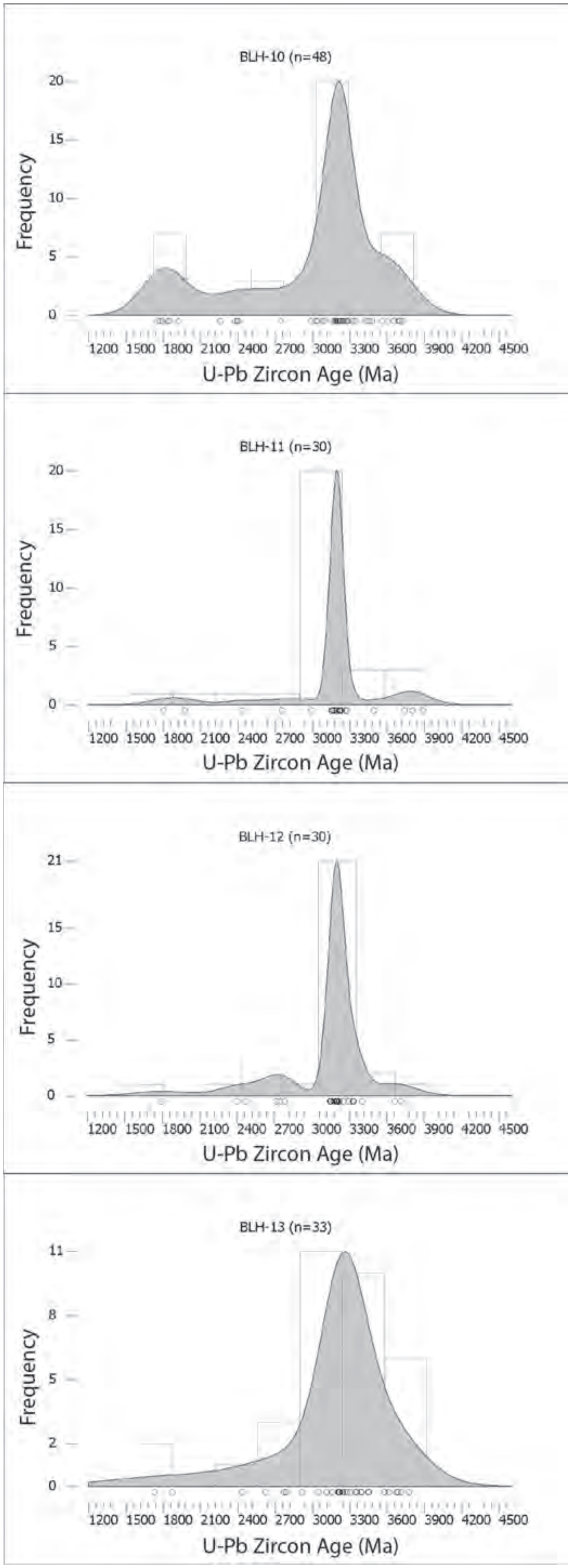

Figure 6. Kernel density estimator (KDE) plots for $^{207}Pb/^{206}Pb$ ages <10% discordant for detrital zircons from four different samples of the LaHood Formation (BLH-10, 48 grains; BLH-11, 30 grains; BLH-12, 30 grains, and BLH-13, 33 grains).

This bimodal distribution of age-related data represents at least two different sources for the LaHood Formation in the Bridger Range. The older signal is representative of ages found throughout the northern Wyoming Province (e.g., Mueller and others, 1993, 1998, 2004), while the younger signal is representative of ages seen in the Great Falls tectonic zone (e.g., Gifford and others, 2014). No western, non-Laurentian source is required, as stated by Ross and Villeneuve (2003).

In addition, given that the dominant age of ~3,200 Ma for the LaHood Formation is different from the dominant ages seen in the Niehart Quartzite (Mueller and others, 2008, 2013), the correlation between these two lowermost units in the basin is now more difficult to establish.

ACKNOWLEDGMENTS

Special thanks go to Ann Heatherington and George Kamenov for laboratory assistance in the SEM/XRF and ICP-MS labs, respectively, as well as to Katherine Bermudez for assistance with acid dissolution and chromatographic separations. We would also like to thank the National Science Foundation for funding this project (EAR-1145212).

REFERENCES

Frost, C.D., and Winston, D., 1987, Nd isotope systematics of coarse- and fine-grained sediments: Examples from the Middle Proterozoic Belt-Purcell Supergroup: Journal of Geology, v. 95, p. 309–327.

Fussell, S.S., Mueller, P.A., and Mogk, D.W., 2015, Age and origin of the Bridger gneisses: Implications for Provenance of the LaHood Formation: Geological Society of America Abstracts with Programs, v. 47, no. 6, p. 41.

Gifford, J.N., Mueller, P.A., Foster, D.A., and Mogk, D.W., 2014, Precambrian crustal evolution in the Great Falls Tectonic Zone: Insight from Xenoliths from the Montana Alkali Province: The Journal of Geology, v. 122, p. 531–548.

Table 1. Results of initial geochemical analysis of LaHood Formation samples organized based on grain size/rock type, and Sm/Nd depleted mantle model ages (Tdm).

Samples	Grain Size/Rock Type	Tdm Ages (Ga)
BLH-11	Conglomerate	3.32
BLH-10	Conglomerate	3.23
BLH-13	Sandstone	3.43
BLH-12	Siltstone	3.58
BLH-13B	Siltstone	2.65
BLH-10B	Siltstone	2.32
BLH-10A	Shale	2.37

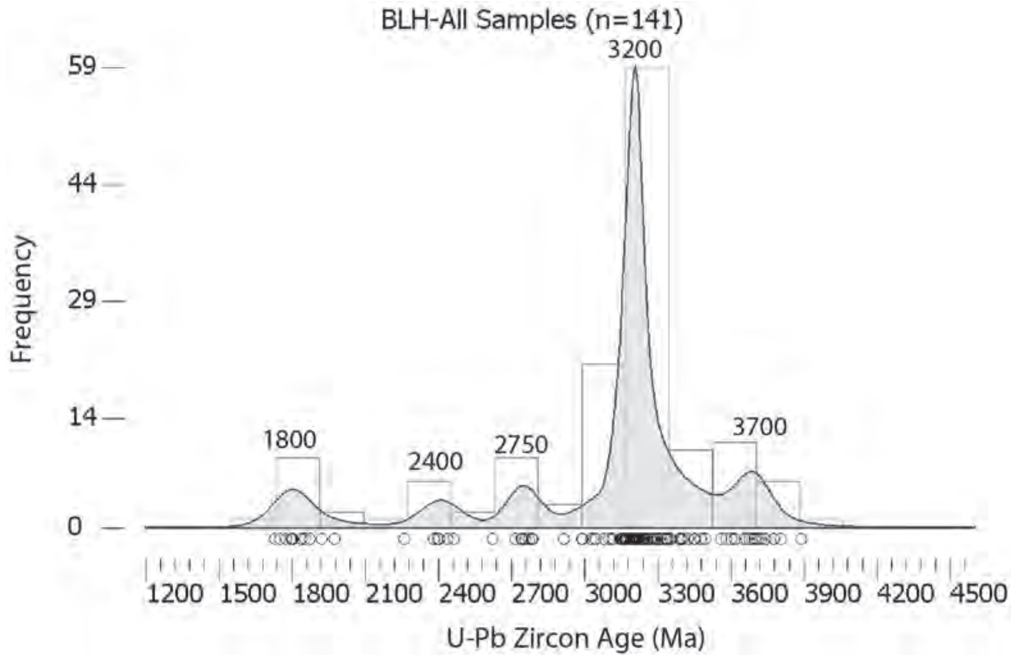

Figure 7. KDE plot for $^{207}Pb/^{206}Pb$ ages determined for detrital zircons from all LaHood samples analyzed (141 grains). Ages range from 1,730 to 3,890 Ma. Dominant age of ~3,200 Ma is seen, with significant ages of ~1,800, ~2,400, ~2,750, and ~3,700 Ma also shown.

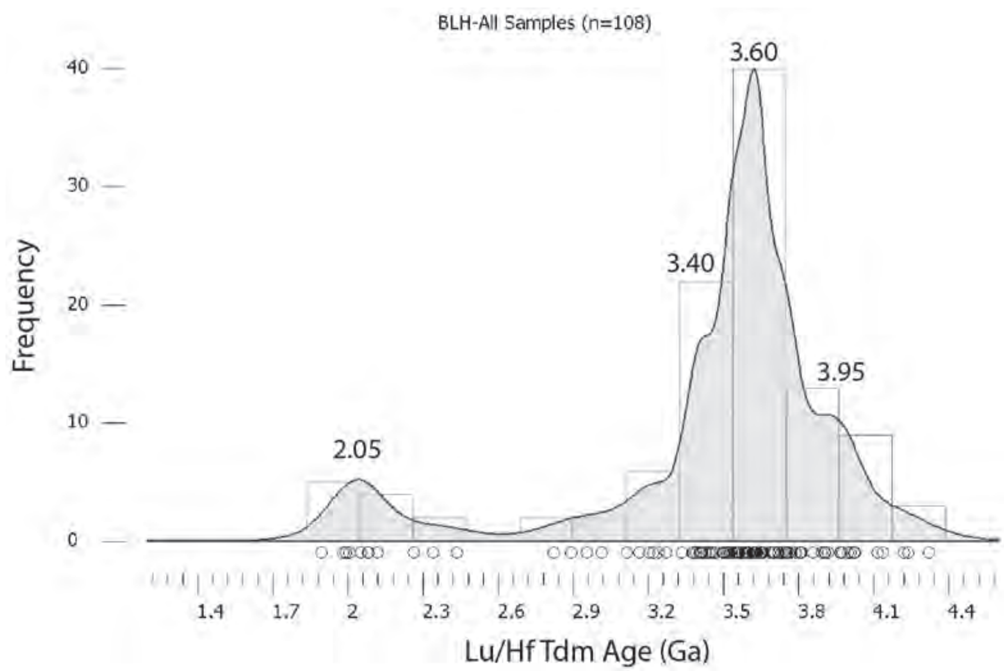

Figure 8. KDE plot for Lu/Hf model ages (Tdm) of detrital zircons from all LaHood samples. Model ages range from 1.89 to 4.32 Ga. Dominant age of ~3.60 Ga is seen, with another significant signal shown at ~2.05 Ga. The values suggest crustal recycling of even the oldest Archean crust in the region.

Marshall, D., 1996, Ternplot: An Excel spreadsheet for Ternary diagrams: Computers and Geosciences, v. 22, p. 697–699.

McMannis, W.J., 1963, LaHood Formation–A coarse facies of the Belt Series in southwestern Montana: Geological Society of America Bulletin, v. 74, p. 407–436.

Mueller, P.A., Shuster, R.D., Wooden, J.L., Erslev, E.A., and Bowes, D.R., 1993, Age and composition of Archean crystalline rocks from the southern Madison Range, Montana: Implications for crustal evolution in the Wyoming craton: Geological Society of America Bulletin, v. 105, p. 437–446.

Mueller, P.A., Wooden, J.L., Nutman, A.P., and Mogk, D.W., 1998, Early Archean crust in the northern Wyoming province Evidence from U-Pb ages of detrital zircons: Precambrian Research, v. 91, p. 295–307.

Mueller, P.A., Burger, H.R., Wooden, J.L, Heatherington, A.L., Mogk, D.W., and D'Arcy, K., 2004, Age and evolution of the Precambrian crust of the Tobacco Root Mountains, Montana: Geological Society of America Special Papers, v. 377, p. 181–202.

Mueller, P.A., Foster, D., Gifford, J., Wooden, J.L., and Mogk, D.W., 2008, Tectonic and stratigraphic implications of detrital zircon suites in Cambrian and Precambrian sandstones from the eastern margin of the Belt Basin: Northwest Geology, v. 37, p. 61–68.

Mueller, P.A., Mogk, D.W., and Wooden, J.L., 2013, Contrasts in the provenance of the LaHood Formation and Neihart Quartzite from ages of detrital zircons: Northwest Geology, v. 42, p. 79–88.

Nesbitt, H.W., and Young, G.M., 1982, Early Proterozoic climates and plate motions inferred from major element chemistry of lutites: Nature, v. 299, p. 715–717.

Ross, G.M., and Villeneuve, M., 2003, Provenance of the Mesoproterozoic (1.45 Ga) Belt Basin (western North America): Another piece in the pre-Rodinia paleogeographic puzzle: Geological Society of America Bulletin, v. 115, p. 1191–1217.

Schieber, J., 1990, Distribution of REE in the Eastern Belt Supergroup (Montana, U.S.A.): Implications for stratigraphic correlations and basin evolution: Chemical Geology, v. 81, p. 83–98.

Schieber, J., 1998, Sedimentologic, geochemical, and mineralogical features of the Belt Supergroup and their bearing on the lacustrine versus marine debate: Proceedings of Belt Symposium III, Montana Bureau of Mines and Geology Special Publication 112, p. 177–189.

Stewart, E.D., Link, P.K., Fanning, C.M., Frost, C.D., and McCurry, M., 2010, Paleogeographic implications of non-North American sediment in the Mesoproterozoic upper Belt Supergroup and Lemhi Group, Idaho and Montana, USA: Geology, v. 38, p. 927–930.

Vermeesch, P., 2012, On the visualisation of detrital age distributions: Chemical Geology, v. 312-313, p. 190–194.

Walcott, C.D., 1914, Pre-Cambrian Algonkian algal flora, in Cambrian geology and paleontology III: Smithsonian Miscellaneous Collections, v.64, p. 77–156.

Winston, D., 1986a, Middle Proterozoic tectonics of the Belt basin, western Montana and northern Idaho, in Roberts, S., ed., Belt Supergroup: A guide to the Proterozoic rocks of western Montana and adjacent areas: Montana Bureau of Mines and Geology Special Publication 94, p. 245–257.

Winston, D., 1986b, Sedimentology and stratigraphy of the Ravalli Group, Middle Belt Carbonate and Missoula Group, Middle Proterozoic Belt Supergroup, in Belt Supergroup: A Guide to Proterozoic rocks of western Montana and adjacent areas, S.M. Roberts: Montana Bureau of Mines and Geology Special Publication 94, p. 85–124.

Winston, D., Horodyski, R.J., and Whipple, J.W., 1989, Middle Proterozoic Belt Supergroup, western Montana: Washington, D.C., American Geophysical Union, 28th International Geological Congress, Field Trip Guidebook T334, p. 102.

EARLY CRETACEOUS (APTIAN–ALBIAN) ECOSYSTEM REVOLUTION—THE FIRST FLOWERING PLANTS IN THE NORTHERN ROCKIES

Kevin Lielke

Independent Geologist, Ennis, MT 59729

INTRODUCTION

The early Cretaceous witnessed one of the most important revolutions in the history of life on Earth—the evolution, diversification, and migration of the flowering plants (angiosperms). This angiosperm revolution drastically altered the global ecosystem and ultimately led to the replacement of the fern- and gymnosperm-dominant vegetation of the early Mesozoic (Saward, 1992; Vakhrameev, 2010). However, this transition did not occur suddenly; rather the older flora was replaced discontinuously over an extended period of time (Doyle and Hickey, 1976; Wing and Sues, 1992). During the late early Cretaceous, angiosperms, which originated in the tropical Tethian region, migrated north along the western margin of the Cretaceous interior seaway (Brenner, 1976; Retallack and Dilcher, 1986; Tidwell and others, 2007). During this timeframe a transition flora, still dominated by early Mesozoic ferns and conifers but now containing a secondary angiosperm component, served as a bridge to the essentially modern, angiosperm-dominated floras of the late Cretaceous (Retallack and Dilcher, 1986; Crane, 1987; Tidwell and others, 2007). The purpose of this paper is to examine the ecosystem dynamics of this transition flora in southwestern Montana in its stratigraphic and sedimentological context. In addition to previously documented paleofloras, this paper incorporates recent field work and new fossil material from the early Cretaceous rocks of the western Gravelly Range.

EARLY CRETACEOUS GEOLOGIC CONTEXT

The western flank of the Gravelly Range in southwestern Montana (fig. 1) contains an extensive record of early Cretaceous sedimentary rocks (Hadley, 1980; Gibson, 2007). Of particular interest here is the section from the Aptian/Albian upper Kootenai Formation through the upper Albian/lower Cenomanian Vaughn Member of the Mowry (Blackleaf) Formation. This interval covers the initial transgression of the Cretaceous interior seaway and its subsequent regression (Vuke, 1984; Hallam, 1992). Volcaniclastic sediments of the Vaughn Member contain the earliest known megafossil record of flowering plants in this area. Despite the importance of this event for the evolution of regional ecosystems, these early angiosperms are little studied. Also poorly understood is the role of sea level change and volcanism along the margin of the Cretaceous epeiric sea in the development of vegetation of modern aspect. Knowledge of the geological context of fossil vegetation is essential for its proper interpretation, so a brief review of lower Cretaceous stratigraphy and sedimentology is presented below.

Lower Cretaceous rocks in southwest Montana (fig. 2) were deposited in the nonmarine portion of the foreland of the fold and thrust belt in the west and in a marine shelf facies of the foreland to the east (Tysdal and others, 1989; Vuke, 1984). Stratigraphic nomenclature tracks sedimentary facies changes from east to west with the axis of the Ruby River valley serving as a rough dividing line. At the base of the section of interest is the nonmarine Kootenai Formation, whose upper unit in this area is the informally named lacustrine “gastropod limestone.” Separated from the Kootenai by an unconformity is a transgressive sandstone–shale sequence that represents the earliest marine deposition along the western margin of the Cretaceous interior seaway. In the Gravelly Range, these units are assigned to the Thermopolis shale and correspond to the Flood Member of the Blackleaf Formation further to the west. Above this is a regressive sequence comprising the shallow marine Muddy sandstone and the volcaniclastic Vaughn Member. The Vaughn, as currently defined, is a member of both the Mowry and Blackleaf Formations and correlates with the informal Albino Member in the Madison Range to the east (Tysdal and others, 1989).

The late Albian/early Cenomanian Vaughn Member is characterized by its high content of volcanic material, sourced from subduction-related volcanoes whose substructure formed the present-day Idaho

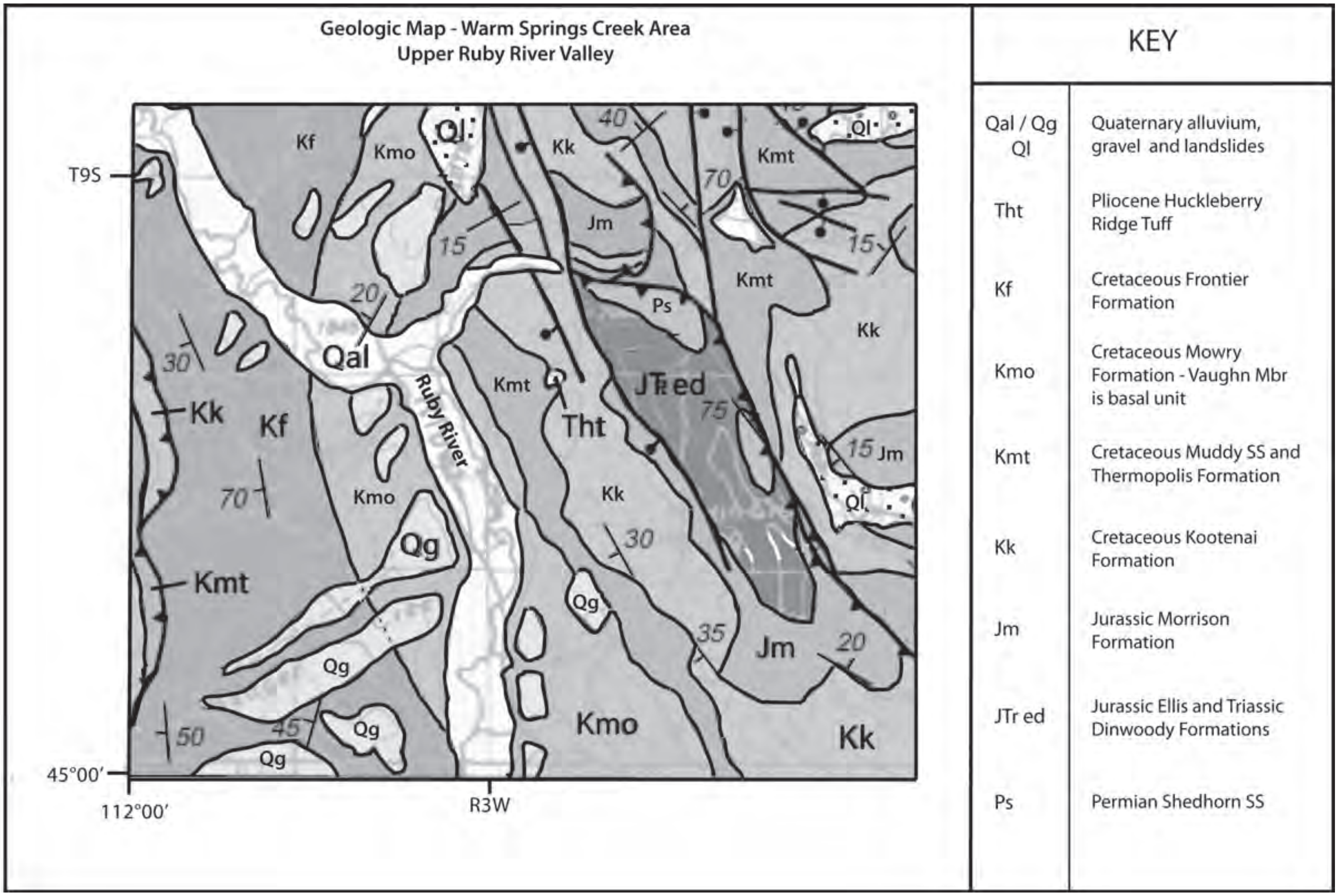

Figure 1. Geologic map of the Warm Springs Creek area in the Upper Ruby River Valley. The primary geologic structure in this area is the Warm Springs anticline. Fossil localities occur along the flanks of this structure in the lower part of the Mowry Formation (Vaughn Member - Kmo). Modified from Kellogg and Williams (2006).

batholith. Associated plant fossils represent vegetation growing on a coastal plain near the western shores of the Cretaceous interior seaway. The sedimentary depositional environments represented in the Vaughn are primarily fine-grained, low-energy nonmarine environments influenced by proximity to the open ocean. Brackish and tidally influenced conditions interacted with fluvial systems sourced from high volcanic topography to the west (Hadley, 1980; Vuke, 1984). Large fluvial channels are not exposed in the western Gravelly Range; this area is characterized by interfluvial mudflats, marshes, and other low-energy coastal plain environments. However, small-scale fluvial channels and lacustrine facies, including thinly layered or varved mudstones, are present and may have afforded early angiosperms a diversity of habitats to exploit within the dominant fern/gymnosperm community.

THE VIGILANTE FLORA

Plant macrofossils and palynomorphs have been documented from early Cretaceous sediments in southwestern Montana and adjacent areas (Bell, 1956; Rushforth, 1971; Vuke, 1984; Crabtree, 1987; Tidwell, 1998). However, in southwestern Montana, paleobotanical discoveries have generally been incidental to studies primarily concerned with mapping or sedimentology/stratigraphy research. Only a few dedicated paleobotany studies have been undertaken. Prior studies have examined the taxonomy of fossil ferns (Crabtree, 1988) and the regional associations of late early Cretaceous angiosperms (Crabtree, 1987). A few studies have also described fossil pollen and spores as part of larger research projects (Hadley, 1980; Tysdal and others, 1989). A new megafossil locality, the Vigilante paleoflora, provides a more detailed picture of early Cretaceous plant dynamics. The Vigilante paleoflora is contained within fine-grained volcaniclastic sediments

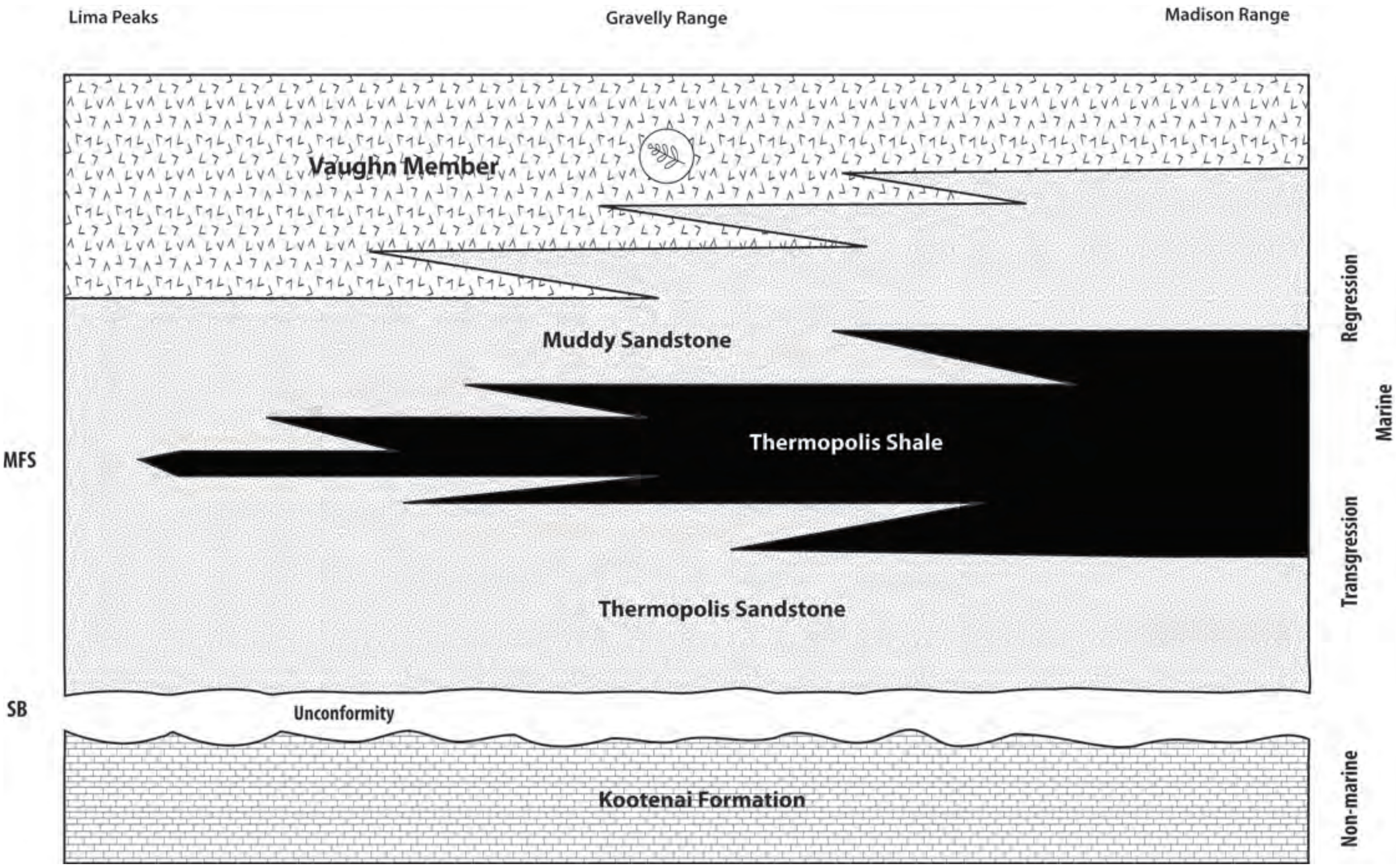

Figure 2. Generalized stratigraphic relationships of lower Cretaceous units in southwestern Montana. Circle with fern frond shows position of Vigilante paleoflora in relation to stratigraphy. SB, sequence boundary; MFS, maximum flooding surface of late early Cretaceous marine transgression.

of the Vaughn Member (fig. 2). As these sediments show no sign of extensive transport, it is believed the associated fossils represent a largely autochthonous community of plants—that is, plants that grew near each other within a low-lying coastal plain environment.

The Vigilante paleoflora consists of three components. Numerically, it is dominated by ferns belonging to the families Gleicheniaceae, Schizaeaceae, Dicksoniaceae, and possibly the Matoniaceae (fig. 3). Only a single species of gymnosperm, similar to specimens previously identified as *Sequoiadendron*, or less likely, *Araucarites* (Bell, 1956; Hadley, 1980; Miller and LaPasha, 1985; Taylor and others, 2009), appears to be present. However, its remains are present in almost every fossiliferous sample. Angiosperms are numerically the least common element; however, they are represented by five to eight different morphotypes (fig. 4)—incomplete specimens in some cases make exact determination of morphotype difficult. Given the probability that most early angiosperms represent extinct lineages, their remains will be referred to with morphotypes rather than identified with extant taxa (Crabtree, 1987; Taylor and others, 2009). The composition of the Vigilante paleoflora suggests an extensive "fern savanna" where herbaceous members of the Gleicheniaceae and Schizaeaceae formed the Mesozoic equivalent of a coastal grassland or marsh. Large stems up to several centimeters in diameter suggest that some ferns attained shrubby stature. An alternative interpretation is that these represent fronds of tree ferns. These large stems are usually associated with fern pinnules similar to those assigned by Crabtree (1987) to the Dicksoniaceae genus *Coniopteris* in the Madison Range. However, a lack of fertile pinnules makes definitive identification difficult.

Angiosperms likely inhabited micro-habitats within this fern savanna. Small fluvial channels and lakes in this shifting, dynamic environment would have provided excellent habitat for invasive weedy opportunists—the favored interpretation for the environmental preferences of early angiosperms (Taylor and others, 2009). (However, see Feild and others (2004) for an alternative interpretation.) The single conifer species present, attested by the common occurrence of *Sequoiadendron* type foliage (fig. 4), likely formed

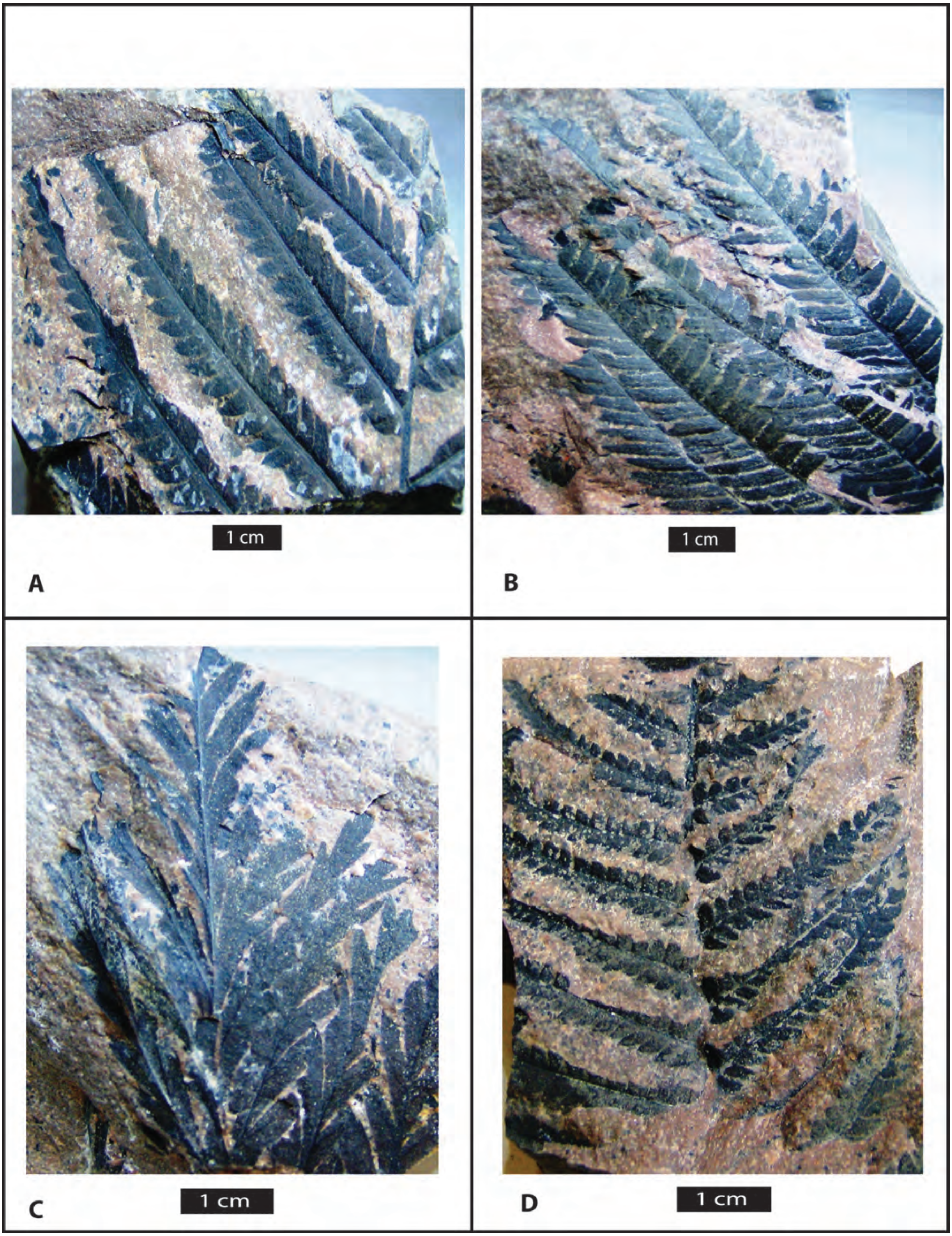

Figure 3. Representative fern taxa from the Vigilante paleoflora. (A and B) Fern fronds likely belonging to the families Dicksoniaceae or Schizaeaceae. Specimen in (A) similar to genus *Coniopteris* described by Crabtree (1988) from Madison Range; (C) Fern frond likely belonging to genus *Anemia* (family Schizaeaceae); (D) Fern frond likely belonging to *Gleichenia* (family Gleicheniaceae).

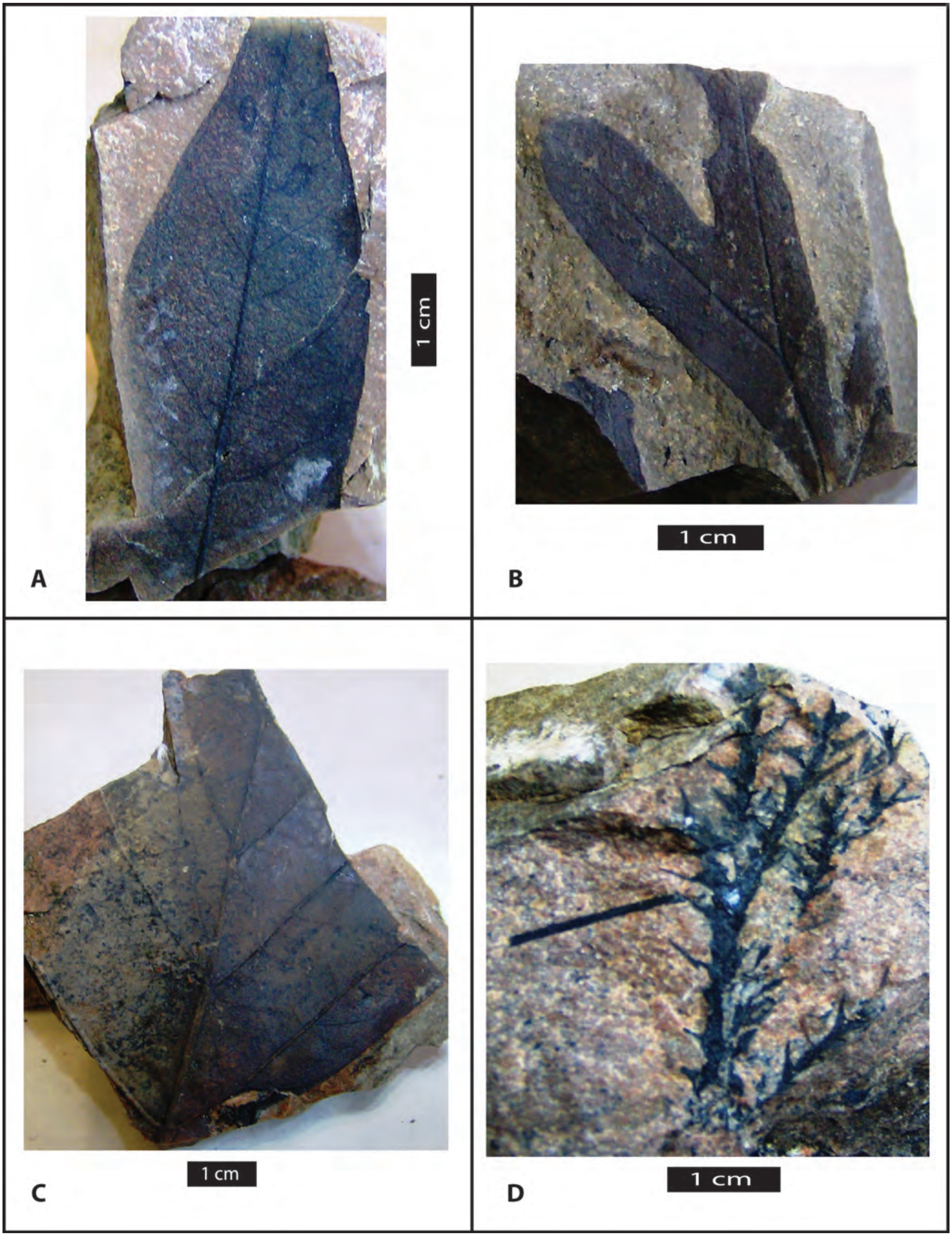

Figure 4. Representative angiosperm and gymnosperm taxa from the Vigilante paleoflora (leaf morphotypes following Crabtree, 1987.) (A) Leaf belonging to Sapindophyll morphotype—possibly ancestral to Rosidae (note circular damage at top of leaf likely due to insect activity); (B) Leaf belonging to Pentalobaphyll morphotype—possibly ancestral to Magnoliidae; (C) Leaf belonging to Platanophyll morphotype—possibly ancestral to Hamamelididae; (D) Gymnosperm foliage similar to *Sequoiadendron*.

discrete groves on higher ground within the fern savanna or were a constituent of the riparian vegetation along streams draining the western highlands. Extensive delta deposits in the Madison Range suggest that these fern savannas functioned as marshland in the interfluvial areas of a major eastward-flowing river system.

RECONSTRUCTION OF AN EARLY CRETACEOUS PLANT COMMUNITY

Combining the ecological and geological information obtained from the Vigilante paleoflora with paleobotanical data from correlative strata allows a preliminary reconstruction of the regional vegetation during this important transition period. Unfortunately, early Cretaceous paleobotany data are scarce; however, plant macrofossils have been described from marine deltaic deposits in the Madison Range, and microfossil material has been reported from several contemporary localities. Seen in this context, the Vigilante flora represents a vegetation type that grew in a lowland coastal plain between the open ocean to the east and highlands to the west.

In this area of fluctuating marine influence and high influx of volcanic material, stress-tolerant and early successional plants likely predominated. The single conifer present is likely either a marsh-adapted species similar in habitat to modern bald cypress, or an inhabitant of stream banks and other higher ground. The large number of conifer shoots of similar size, none found still attached to stems, may indicate deciduousness. Moving eastward, gymnosperms are absent in the deltaic deposits of the Albino Member (Crabtree, 1988). Angiosperms also disappear in the more distal portions of the delta, replaced by a high-density and low-diversity fern flora dominated by the families Gleicheniaceae and Schizaeaceae (Crabtree, 1988).

Palynomorph data from the Vaughn Member further to the west (Tysdal and others, 1989) confirm and expand upon the conclusions drawn from leaf fossils. The fern families Gleicheniaceae, Schizaeaceae, Dicksoniaceae, and Polypoidaceae are represented. Gymnosperm pollen (including *Pityosporites* and *Taxodiaceaepollenites*) suggests the presence of multiple conifers in addition to the one attested by leaf remains. These additional conifer species likely inhabited upland, better drained habitats. *Tricolpites* pollen confirms the presence of angiosperms, although it isn't diagnostic as to number and type of taxa. Equally noteworthy is the absence from both micro- and macrofloras of several important taxa well-represented in the late Jurassic to early Cretaceous Great Falls coal field (LaPasha and Miller, 1982, 1985; Miller and LaPasha, 1985).

Cycads, gingkoes, and cheirolepideceous conifers appear to be absent from the latest Albian vegetation in southwestern Montana. Their absence could be an artifact of preservation, or it could reflect particularly harsh growth conditions in the brackish, volcanic mire along this sector of the Cretaceous seaway. The presence of palynomorphs of these missing taxa in both overlying and underlying Cretaceous sediments suggests the latter, as does the lithological similarity of the fossil leaf-bearing rocks to typical Vaughn volcaniclastic sediments. There is no geologic evidence to suggest the Vigilante paleoflora is atypical for this area.

CONCLUSIONS

The first occurrence of angiosperm megafossils in sediments associated with marine regression following deposition of the Thermopolis black shale is likely not a coincidence. This initial marine inundation disrupted the fern/gymnosperm plant community that had dominated global terrestrial ecosystems since the late Triassic. Ecosystem perturbation due to major sea level fluctuations was enhanced in late Albian time by a massive influx of volcanic material from the subduction arc to the west. It is theorized here that these events in tandem massively disrupted the preexisting vegetation and provided opportunistic weedy angiosperms the means to successfully colonize the northern Rocky Mountain region. Starting as early successional species or colonizers of unstable substrates, flowering plants quickly diversified into niches previously occupied by ferns, cycads, ginkgos, and various conifers (Retallack and Dilcher, 1986; Saward, 1992). So successful was this transformation that coal seams in the overlying Cenomanian Frontier Formation are almost entirely derived from angiosperm remains (Hadley, 1980). However, this angiosperm invasion was episodic in nature and only occurred following the initial massive disruption of the preexisting, and highly successful, early Mesozoic vegetation. The "superior" biological traits of flowering plants accomplished little prior to these events.

RECOMMENDATIONS FOR FUTURE RESEARCH

The volcaniclastic rocks of the Vaughn Member have demonstrated a high potential for the preservation of fossil plant material. A dedicated search for fossil material should be undertaken in order to establish: (1) the habitat preferences of early Cretaceous angiosperms by examination of the fossil content of different sedimentological depositional environments; (2) ecosystem composition changes from the uplands bordering high volcanic terrain to the west to the margin of the Cretaceous interior seaway to the east; and (3) the role that changing sea level and input of volcanic material played in the migration and establishment of early angiosperms. This last goal would require acquisition of fossil material from different horizons, preferentially within a relatively small area in order to document floral changes over time. The published literature suggests that certain sections of the underlying Thermopolis and Kootenai Formations and overlying Frontier Formation may be prospective for macrofossil plant remains. Microfossil remains are generally more widely distributed.

REFERENCES

Bell, W.A., 1956, Lower Cretaceous floras of western Canada: Geological Survey of Canada Memoir 285, 331 p.

Brenner, G., 1976, Middle Cretaceous floral provinces and early migrations of angiosperms: Origin and early evolution of angiosperms: Columbia University Press, p. 23–47.

Crabtree, D., 1987, Angiosperms of the northern Rocky Mountains: Albian to Campanian (Cretaceous) Megafossil floras: Annals of the Missouri Botanical Garden, v. 74, no. 4, p. 707–747.

Crabtree, D., 1988, Mid-Cretaceous ferns in situ from the Albino member of the Mowry shale, southwestern Montana: Palaeontographica Abteilung B, 209, Lfg. 1–3, p. 135.

Crane, P., 1987, Vegetational consequences of angiosperm diversification: The origins of angiosperms and their biological consequences, Cambridge University Press, p. 107–144.

Doyle, J., and Hickey, L., 1976, Pollen and leaves from the Mid-Cretaceous Potomac Group and their bearing on early angiosperm evolution: Origin and early evolution of angiosperms: Columbia University Press, p. 139–206.

Feild, T., Arens, N., Doyle, J., Dawson, T., and Donoghue, M., 2004, Dark and disturbed: a new image of early angiosperm ecology: Paleobiology, v. 30, no. 1, p. 82–107.

Gibson, R., 2007, Mesozoic sedimentation in southwest Montana: Northwestern Geology, v. 36, p. 57–66.

Hadley, J., 1980, Geology of the Varney and Cameron quadrangles, Madison County, Montana: USGS Bulletin 1459, 108 p.

Hallam, A., 1992, Phanerozoic sea-level changes: Perspectives in paleobiology and earth history series; Columbia University Press, 266 p.

Kellogg, K. and Williams, V., 2006, Geologic map of the Ennis 30’ X 60’ quadrangle, Madison and Gallatin Counties, Montana and Park County, Wyoming: Montana Bureau of Mines and Geology Open-File Report 529, 27 p, 1 sheet, scale 1:100,000.

LaPasha, C., and Miller, C., 1982, The lower Cretaceous Kootenai Fm. flora in Montana – Floristics and paleoecology: Third North American Paleontology Conference Proceedings, v. 2, p. 319–322.

LaPasha, C., and Miller, C., 1985, Flora of the early Cretaceous Kootenai Formation in Montana, bryophytes and tracheophytes excluding conifers: Palaeontographica Abteilung B, 196, Lfg 4-6, p. 111–145.

Miller, C., and LaPasha, C., 1985, Flora of the early Cretaceous Kootenai Formation in Montana, conifers: Palaeontographica Abteilung B, 193, Lfg 1-4, p. 1–17.

Retallack, G., and Dilcher, D., 1986, Cretaceous angiosperm invasion of North America: Cretaceous Research, v. 7, p. 227–252.

Rushforth, S., 1971, A flora from the Dakota sandstone formation (Cenomanian) near Westwater, Grand County, Utah: Brigham Young University Science Bulletin, v. 14, no. 3, 44 p.

Saward, S.A., 1992, A global view of Cretaceous vegetation patterns, in McCabe, P.J. and Parrish J.T., eds, Controls on the distribution and quality of Cretaceous coals: Geological Society of America Special Paper 267, p. 17–35.

Taylor, T., Taylor, E., and Krings, M., 2009, Paleobotany – The biology and evolution of fossil plants, (2nd ed): Academic Press, 1,230 p.

Tidwell, W., 1998, Common fossil plants of western North America, second edition: Smithsonian Institution Press, 299 p.

Tidwell, W., Britt, B., and Tidwell, L., 2007, A review of the Cretaceous floras of east-central Utah and western Colorado: Utah Geological Association Publication 36, p. 467–482.

Tysdal, R., Dyman, T., and Nichols, D., 1989, Correlation chart of lower Cretaceous rocks, Madison Range to Lima Peaks area, southwestern Montana: U.S. Geological Survey Miscellaneous Field Studies Map MF-2067, 16 p., 1 sheet.

Wing, S.L, and Sues, H-D. and others, 1992, Mesozoic and early Cenozoic terrestrial ecosystems, in Behrensmeyer, A.K., Damuth, J. D., DiMichele, W.A., Potts, R.; Sues, H-D., and Wing, S. L., eds., Terrestrial ecosystems through time – Evolutionary paleoecology of terrestrial plants and animals: University of Chicago Press, p. 327–416.

Vakhrameev, V., 2010, Jurassic and Cretaceous floras and climates of the Earth: Cambridge University Press, 318 p.

Vuke, S.M, 1984, Depositional environments of the early Cretaceous western interior seaway in southwestern Montana and the northern United States, in The Mesozoic of middle North America, Stott, D.F, and Glass, D.J., eds., Canadian Society of Petroleum Geologists v. 9, p. 127–144.

RANGES OF LIGHT HYDROCARBON CONCENTRATIONS IN THE SOILS OF THE MONTANA OVERTHRUST BELT

D.H. Vice

Pennsylvania State Hazleton, 76 University Drive, Hazleton, PA 18202

ABSTRACT

Surface geochemistry refers to a group of soil sampling methods that are used as “pathfinders” in oil and natural gas exploration. These methods have been used to reduce exploration costs by screening a group of prospects to pick those that have the best potential to contain oil or natural gas. These methods can also be used as a reconnaissance tool to narrow the exploration focus in large blocks of land. Although surface geochemistry is not used for “fracking” (hydraulic fracturing) wells, surface geochemistry is still used for conventional exploration, and that type of petroleum exploration is still being done (Bob Merrill, written communication, 2016). Surface geochemical surveys can also be useful in helping to establish a baseline of light hydrocarbon concentrations in the soil environment in an area before any petroleum exploration is done, including fracking.

A series of reconnaissance surface geochemical surveys were conducted in the Overthrust Belt in southwestern Montana and over the Devils Fence prospect near Townsend in west-central Montana in the early and mid-1980s. The purpose of this paper is to show the range of concentrations for the individual light hydrocarbon species (i.e., methane, ethane, propane, butane, and pentane) in the soil environment that can then be compared with areas that are being investigated for hydrocarbon potential such as southwestern Idaho. Another reason to publish the concentrations of the light hydrocarbons is that the type of survey method used also can cause variations in these concentrations, so anyone planning a survey will need to be aware of these variations.

Methane concentrations in the southwestern Montana surveys and the Devils Fence survey generally ranged from 0 to 20 ppm, but concentrations up to 8,600 ppm were obtained. Ethane and propane concentrations generally ranged from 0 to 20 ppm, but some concentrations up to 96 ppm were obtained. Butane concentrations ranged between 0 and 100 ppm, but isolated concentrations as high as 317 ppm were detected. Isolated pentane concentrations as high 477 ppm were obtained.

INTRODUCTION

This paper discusses 18 surface geochemical profile line surveys, with a total of 314 samples in the Montana Overthrust Belt, that were conducted in southwestern Montana by the author (Vice, 1983) and compares them to two surface geochemical surveys conducted in the Townsend area of Montana in 1985 (Vice, 1985; Landrum and others, 1989) (figs. 1, 2). The results from these surveys can provide background ranges for the light hydrocarbons of methane, ethane, propane, butane, and pentane in the soil environment in other areas of the Rocky Mountain states. Rose and others (1979) indicate that this information is useful in helping other geologists and geochemists plan a surface geochemistry survey, because there are a wide variety of different surface geochemical survey techniques (Klusman, 1993; Tedesco, 1995) that give widely varying values depending on the depth that the sample was collected, the type of method used, and the type of soil, as well as other surface environmental conditions.

The different surface geochemical survey techniques can be placed into two basic groups depending on whether the method: (1) measures the light hydrocarbon concentration directly from the gas that has been extracted from the soil; or (2) uses some indirect method to determine the presence of hydrocarbons in the subsurface, such as the formation of carbonate cement in the soil, the formation of pyrite in the subsurface, or the presence of certain types of microbes in the soil (Tedesco, 1995). The use of isotopes is a third group of survey methods that is discussed elsewhere (Sofer, 1991; Tedesco, 1995). The wide variety of survey techniques has introduced variation into the data, which has made it more difficult to interpret. The sample depth can also introduce variability into the data.

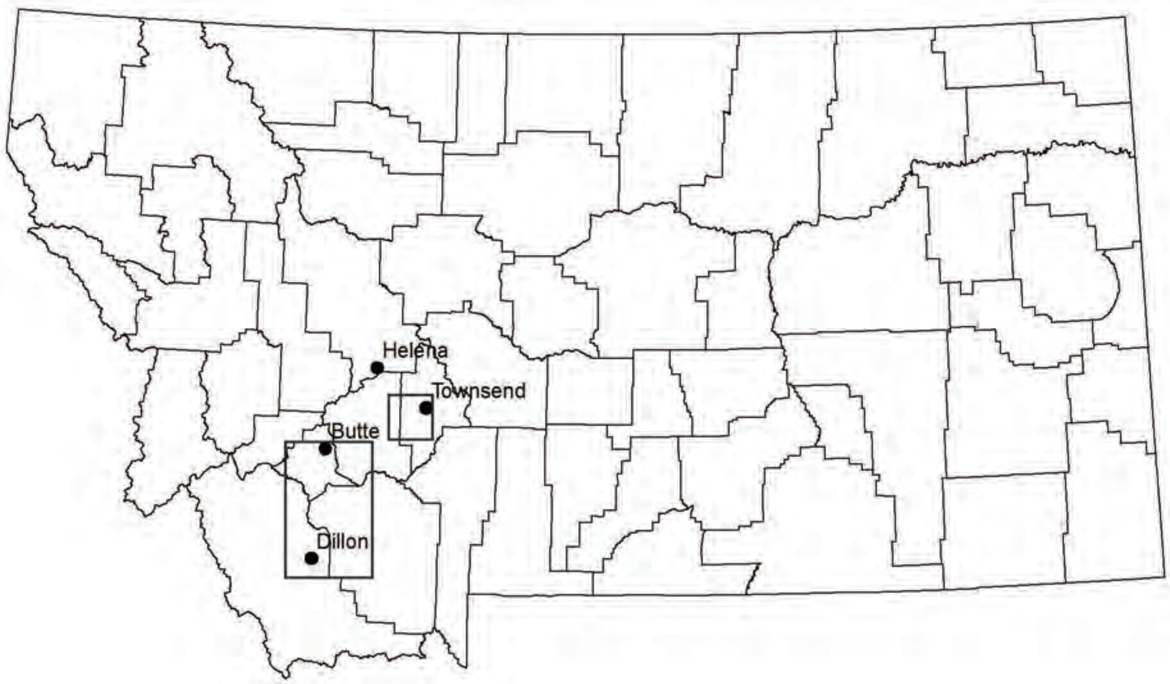

Figure 1. Index map of study areas.

The surveys conducted by the author and by Landrum and others (1989) were conducted at a time when there was considerable interest in the Montana Overthrust Belt as a frontier petroleum province due to oil and gas production in the Overthrust Belt in Wyoming and also in Alberta, Canada. The SW Montana surveys and the Townsend Valley survey were designed to look for areas of anomalous concentrations and provide a starting point for more detailed exploration.

AN OVERVIEW OF TYPES OF SURVEYS USED IN THE 1980S

Surface geochemical surveys are unconventional methods used for oil and gas exploration because they can detect concentrations of light hydrocarbons in the soil environment that may represent leakage from a subsurface reservoir. Some of the surface geochemical methods involve the collection and analysis of soil gases, which are analyzed for light hydrocarbons that have leaked from a subsurface reservoir, while others look for secondary indicators of these gases, e.g., the formation of calcite or iron deposits in the subsurface (Tedesco, 1995; Saunders and others, 1999). Some of the direct methods collect soil samples near the surface while others collect from a depth of 3 to 10 ft (Landrum and others, 1989). The indirect methods usually look for indicators on or near the surface.

These surface geochemical methods are considered "pathfinders" or preliminary exploration methods (B.W. Roberts, 1983, verbal communication) and have been used since 1930 (Tedesco, 1995). For example, a paper by Ransone (1958) describes the early use of surface geochemistry to find the Sojourner oil field in Texas. Potter and others (1996) give an example of how surface geochemistry can be used to select prospects that show the best hydrocarbon potential and thus reduce the total cost of exploration by limiting the amount of seismic lines that needed to be conducted and also by reducing the number of dry holes that were drilled.

The development and widespread use of fracking technology has reduced the use of surface geochemical surveys. However, some conventional wells are still being drilled, so surface geochemical surveys are still being used (Bob Merrill, written communication, 2016).

LIGHT HYDROCARBON OCCURRENCE IN SOILS

The light hydrocarbons of methane, ethane, propane, butane, and pentane occur in soils either through the activity of anaerobic bacteria or through migration from the subsurface (Dickinson and Matthews, 1993; Vice, 1996). Methane is formed in the surface environment when anaerobic bacteria break down organic

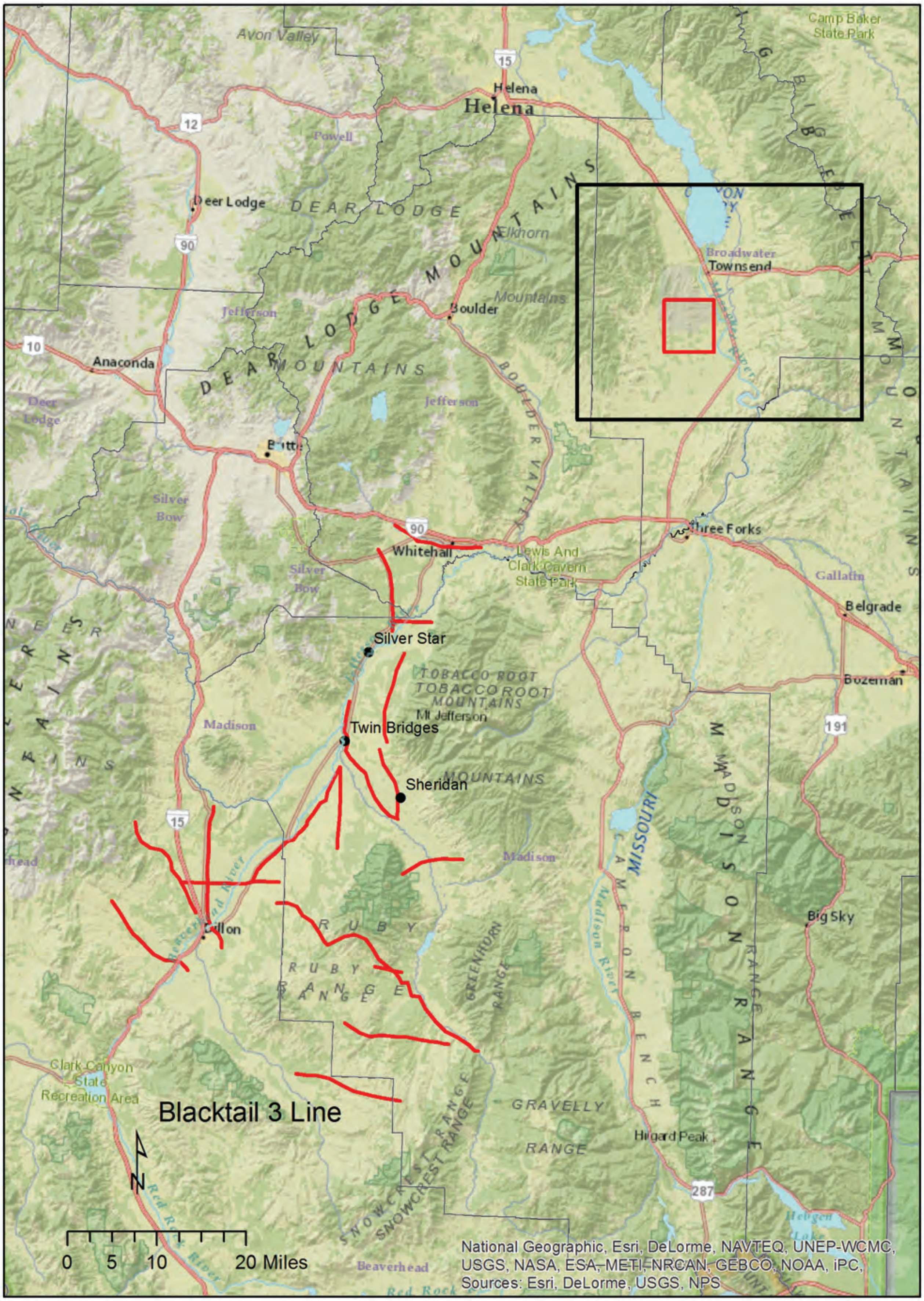

Figure 2. Location map showing approximate locations of surface geochemical surveys. Red lines are southwestern Montana surveys (Vice, 1983). Black box is the Townsend study area (Landrum and others, 1989). Red box is the Devils Fence survey area (Vice, 1985).

Table 1. Light hydrocarbon data showing possible surface generation of methane (Vice, 1996).

Sample Nos.	Methane in ppm	Ethane in ppm	Propane/H_20 in ppm	Butane in ppm	Pentane (Backflush)
F 283	200	0	18	7.8	34
F 284	6000	0	16	4.7	20

matter in an environment that has limited oxygen. This situation can result in methane being present in much larger concentrations than ethane, propane, butane, and pentane (table 1). Dickinson and Matthews (1993) suggest that the heavier light hydrocarbons (i.e., ethane, propane, butane, and pentane) occur in the surface environment either due to migration from a subsurface reservoir or from contamination. However, the author has observed widespread, low-level concentrations of these light hydrocarbons in many surveys (Vice, 1996; Vice, 1986), which suggests that small amounts of the heavier light hydrocarbons can occur in soil environments by biological activity. An alternative explanation is that the heavier light hydrocarbons of ethane, propane, butane, and pentane migrate to the atmosphere at a slower rate than methane does. The author conducted a study over a leak in a natural gas pipeline in the Snowshoe gas field in Centre Co., Pennsylvania and found that while the natural gas leaking from the pipeline was 95 per cent methane, after 3 months, the relative concentrations of the light hydrocarbons were similar to the methane concentrations (table 1; Vice, 1996).

The migration of the light hydrocarbons from a subsurface hydrocarbon reservoir to the surface soil environment is not fully understood, but appears to occur as buoyant, colloidal-sized microbubbles. The microbubbles appear to ascend rapidly through a water-filled network of fractures, joints, and bedding planes (Saunders and others, 1999; Nunn and Meulbroek, 2002). Saunders and others (1999) suggest this migration could be intermittent, which may be one reason for a lack of repeatability of surface geochemical surveys. Dickinson and Matthews (1993) suggest that the migration of the light hydrocarbons occurs along relatively narrow pathways.

A study over a gas leak in the Snowshoe gas field in Centre County, Pennsylvania, suggests that the light hydrocarbons are temporarily adsorbed onto clay and organic particles (Vice, 1996) once they reach the soil and then migrate to the atmosphere over a 3-month period (Vice, 1996). During this 3-month period, the total light hydrocarbon concentration in the soil decreased but the proportions of ethane, propane, butane, and pentane increased to be similar in concentration to methane, which initially made up more than 95 percent of the gas leaking into the soil (Vice, 1996).

SURVEY AND ANALYTICAL PROCEDURES

The author used a modified headspace sample procedure for the surface geochemical surveys he conducted in southwestern Montana and at the Devils Fence area, which is a direct method that involved using a standard hand probe (Soil Division Staff, 1993, p. 250) to extract gas and light hydrocarbons adsorbed on clay and organic particles within the soil. Approximately 50 grams of soil was collected from depths of 6 to 18 inches below the surface. Each sample was placed in a 40-ml glass vial and sealed with a Teflon septum and a plastic cap. The surveys consisted of lines of samples rather than a grid pattern. The individual lines were sampled in 1 day to provide more uniform weather conditions during sampling, because limited research suggests that an overnight rain could lead to increased soil moisture that would displace some of the light hydrocarbons in the soil (Hinkle and Ryder, 1987; Bandeira de Mello and others, 2007) and thus change the concentrations of the light hydrocarbons in the soil environment.

The analytical procedure for the soil samples involved heating each sample (with the lid and septum on) in an oven for 1 hour at approximately 70˚C to drive the weakly adsorbed hydrocarbon atoms off from clay or organic particles within the soil sample. Five hundred microliters (µl) of gas was collected from under the cap of the sample bottle using a precision syringe (i.e., a syringe with a side port in the needle to prevent plugging) and immediately injected into a flame ionization gas chromatograph (GC) for analysis. A Carle Basic Gas Chromatograph (model 9500) with a 10-ft Poropak-P column was used for the analyses. The Poropak-P column was a packed column that can handle larger volumes of gas and still detect low concentrations of light hydrocarbon species (Vice, 1996).

The methane, ethane, propane, butane, and pentane plus data from the southwestern Montana surveys and the Devils Fence survey were analyzed statistically as separate data sets for each line using simple descriptive statistics of the arithmetic mean and the Student's t-test. Concentrations that exceeded one standard deviation from the mean were considered anomalous and so might represent leakage from a subsurface hydrocarbon reservoir. This is a low threshold, but the choice between anomalous and not-anomalous is a trade-off between the risk of making a type II error (i.e., accepting the anomaly when it is false) with the lower threshold and a type I error (i.e., rejecting the anomaly when it is real) with the higher threshold (van Belle, 2008). The author chose the lower threshold because of the reconnaissance character of these surveys because of the greater concern about making a type II error than a type I error.

SOUTHWESTERN MONTANA SURVEYS

Southwestern Montana extends from the Lewis and Clark Line southward to the Idaho border and has a complex geology. The geologic history of the area consists of sediments deposited in a shallow marine shelf during the late Paleozoic and Mesozoic, followed by the formation of a series of thrust faults (i.e., the Overthrust Belt), which formed when exotic terrains collided with the western margin of North America in what is now eastern Washington. Southwestern Montana is now being broken into a series of isolated mountains separated by basins (Orr and Orr, 2002) and is part of the Basin and Range structural province (Pardee, 1950; Orr and Orr, 2002).

The author conducted a group of 18 surface geochemical surveys totaling 314 samples in southwestern Montana in 1983 that consisted of single lines with 1-mile spacing between individual sample sites (Vice, 1983), which was the industry practice for reconnaissance surveys at the time (Landrum and others, 1989; Dickinson and Matthews, 1993). The surface geochemical surveys were concentrated in the Jefferson Intermontane Basin, which has a north–south trend and is asymmetric (Rasmussen and Fields, 1985; Vuke and others, 2009). A steep, west-dipping fault occurs on the east side of the basin adjacent to the Tobacco Root Mountains, with shallower sloping, east-dipping faults on the west side of the basin near the Highland Mountains. Rasmussen and Fields (1985) suggest that the Tertiary sediments exceed 9,000 ft in the basin in the deepest parts near Twin Bridges and Silver Star. Most of the surface geochemical surveys were conducted in the Alder, Dillon, Twin Bridges, and Whitehall valleys.

A wide variety of soil conditions are present in southwestern Montana due to rapid changes of bedrock, elevation, slope, and local climate. Most of the soils within the survey areas were mollisols, inceptisols, or aridisols (Soil Conservation Service, 1978). Inceptisols are brownish soils that have weakly developed horizons (Rose and others, 1979); however, the critical feature was that these soils contained some clay and organic matter, so sites were available for the light hydrocarbon molecules to adsorb to (Vice, 1996). Aridisols and mollisols are brownish to gray soils that have high base saturation (Rose and others, 1979). The aridisols may have calcic, gypsic, argillic, or natric B horizons; in other words, they may have layers of calcite, clay, or other mineral deposition within the soil. However, as with the inceptisols, both the aridisols and mollisols have clay and organic matter sites that could absorb the light hydrocarbons (Vice, 1996).

The methane (C1) concentrations within the southwestern Montana surveys generally ranged from 0 to 20 ppm (table 2), but higher concentrations were detected; e.g., one sample (F278) had a concentration of 8,600 ppm. This latter sample appeared to be from a river bottom environment that had a moist, brown to gray-brown, sandy clay soil that was actively generating methane. The evidence for this is the presence of high concentrations of methane but very low concentrations of the heavier light hydrocarbons (see example in table 1).

Table 2. Light hydrocarbon data for some samples from the Blacktail Three line (fig. 2; Vice, 1983) showing the relative proportions ethane, propane, butane, and pentane to methane.

Sample Nos.	Methane in ppm	Ethane in ppm	Propane/H_2O in ppm	Butane in ppm	Pentane (Backflush)
F 349	14	4.5	34	25	69
F 350	11	16	38	41	170
F 351	23	31	18	28	160
F 352	3.8	3.6	13	17	85
F 353	28	85	44	160	640

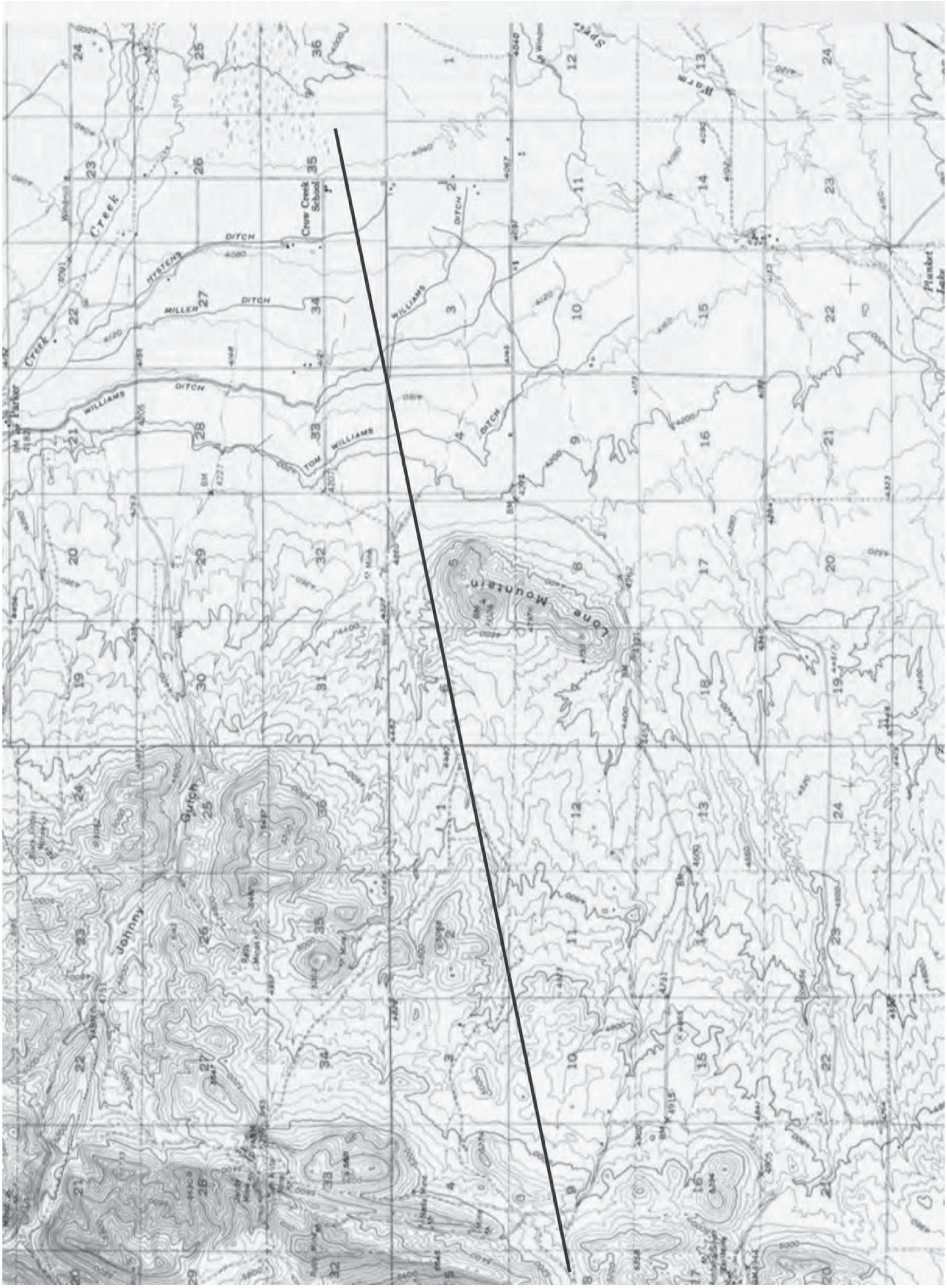

Figure 3. North half of the U.S. Geological Survey Radersburg 15' topographic map quadrangle showing the approximate trace of the Devils Fence surface geochemical survey.

Ethane (C2) and propane (C3) concentrations in the southwestern Montana surveys ranged between 0 and 30 ppm, but concentrations up to 96 ppm were detected. Butane (C4) concentrations ranged from 0 to 100 ppm, but concentrations as high as 317 ppm were detected. Pentane (C5) concentrations as high as 477 ppm were obtained.

DEVILS FENCE AND TOWNSEND VALLEY SURVEYS

The Devils Fence survey (fig. 3) is a small (43 samples) branched profile line with a sample spacing of approximately 1/4 mile that was conducted over the Devils Fence anticline in early April, 1985 (fig. 2; Vice, 1985). The survey area is on the Lombard plate (Ballard and others, 1993) in the west-central part of the Overthrust Belt of Montana and contained Proterozoic, Paleozoic, and Mesozoic sediments in the upper plate and Cretaceous Kootenai Formation sediments in the lower plate (Ballard and others, 1993). The soils of this survey area are alluvium that has been classified as aridisols and mollisols (Soil Conservation Service, 1978). As with the soils of southwestern Montana, these soils contain some clay and organic matter, so sites are present for the light hydrocarbons to attach to.

The Devils Fence survey followed the standard industry practice of 1/4-mile spacing or greater between sample sites at the time that the survey was conducted in the 1980s (Leaver and Thomasson, 2002; Webster and Van Arsdale, 1995). This survey used a modified headspace sampling procedure (see description above) and was sampled in 1 day to provide uniform weather conditions during sampling.

The methane concentrations in the Devils Fence Survey ranged from 0 to 10 ppm, the concentrations of ethane ranged from 1 to 3 ppm, the propane concentrations ranged from 1 to 5 ppm, and the pentane plus concentrations ranged from 0 to 20 ppm (Vice, 1985). The butane concentrations were very low and showed very little variability, so very little information was in the data (Borg and Gall, 1989). Therefore, the butane data were not analyzed (Vice, 1985).

A large reconnaissance surface geochemical survey (231 samples) was conducted in the Townsend Valley north of the Devils Fence survey area during the summers of 1980 and 1982 by Landrum and others (1989). The purpose of the Townsend Valley survey was to detect indications of hydrocarbons on a regional basis and so covered all or portions of 19 townships in a loose grid pattern that had a sample spacing of 1.5 to 2 miles. The samples were analyzed for adsorbed methane, ethane, propane, butane, and pentane (i.e., light hydrocarbons that were loosely absorbed on clay and /or organic particles).

Landrum and others (1989) indicated that the majority of their samples in the Townsend Valley survey had low concentrations of light hydrocarbons, although the concentrations were higher than those in the southwestern Montana and Devils Fence surveys, which may be due to a greater depth for sampling (approximately 3.5 ft). Methane had the highest concentrations (180 ppm average), ethane averaged around 8 ppm, and both propane and butane were below detection limits in nearly all samples (Landrum and others, 1989).

POTENTIAL CAUSES OF VARIATION

Variability in light hydrocarbon concentrations occurs both within and between the southwestern Montana and Devils Fence surveys and the Townsend Valley survey because of differences in the depth of sample collection and in analytical procedures. Different soil types and the amount of soil moisture in the soil at the time of the survey also can introduce variation in the data by causing differences in the amount of light hydrocarbons present (Vice, 1996; Blanchette, 1989; Tedesco, 1995).

Surface geochemical soil sampling has the advantage of helping to focus exploration at a relative low cost, but has the disadvantage of having a great deal of data variability, which can affect interpretation. One way that this variability can adversely affect interpretation of the data is that too wide a sample spacing can miss an anomaly or give an incomplete picture. On the other hand, too many samples can increase the cost. In other words, the design of a surface geochemical survey is a trade-off between cost and risk of missing the target. Another way of stating the problem is that it is a trade-off between type I errors and type II errors.

A separate problem of surface geochemical surveys is a lack of repeatability of the surveys. The author did not study this problem (Vice, 1996), but it appears to be due to the migration of the light hydrocarbons from the soil environment to the atmosphere on a slow, gradual but steady basis ,while the movement of the light hydrocarbons from the subsurface to the soil environment is discontinuous.

SUMMARY AND CONCLUSIONS

Surface geochemical surveys are a "pathfinder" method of oil and natural gas exploration that has been used since about 1930 to reduce the cost of exploration using conventional technology. The author conducted surface geochemical surveys in the southwestern Montana and central Montana Overthrust Belt during the early 1980s as part of a reconnaissance survey to locate indications of hydrocarbon accumulations. The geochemical data from these 1980 surveys can be used now to help establish a baseline of light hydrocarbon concentrations in soil environments of other parts of Montana and Idaho. Methane ranged from 0 to 20 ppm in the southwestern Montana survey, but had concentrations up to 8,600 ppm, and from 0 to 10 ppm in the Devils Fence survey with concentrations up to 18 ppm. Ethane concentrations in the southwestern Montana survey ranged from 0 to 20 ppm, with the highest concentration being 96 ppm, while propane concentrations ranged from 0 to 30 ppm in the same survey, with the highest being 71 ppm. Butane concentrations in the southwestern Montana survey ranged from 0 to 317 ppm and pentane concentrations ranged up to 477 ppm. The ethane and propane concentrations were low in the Devils Fence survey (1 to 3 ppm for C2; 1 to 5 ppm for C3) and showed little variation.

Differences in concentration levels of the light hydrocarbon species of methane, ethane, and pentane that occurs between the Devils Fence and southwestern Montana surveys and the Townsend Valley survey can have a couple of potential explanations. One could be due to sampling procedure; i.e., the Townsend Valley samples were collected from greater depths. The greater sampling depth should result in the higher concentrations of light hydrocarbons present in the soil because fewer hydrocarbons could escape to the atmosphere.

ACKNOWLEDGMENTS

The author wishes to thank Jack Viviano for his assistance in sampling the Southwestern Montana surveys, and Mari Vice for her assistance in preparing the southwestern Montana and Devils Fence reports. Bob Merrill has very generously reviewed earlier drafts of a paper on these surveys and suggested many useful corrections. Irv Kranzler has graciously given me permission to publish the Devils Fence surface geochemical survey. I wish to thank Phil Halleck of Penn State University for help and direction on the use of surface geochemistry to detect the Sabinsville gas storage field and the residence time of gas in the soil environment as part of my dissertation. I wish to thank Bill Phillips for his help and direction on this paper. I also wish to thank the technical staffs at both Penn State Hazleton and Penn State Schuylkill campuses for help. In particular, I wish to thank Jackie Rtizko for help in scanning and inserting figure 1 into the paper. I wish to thank my wife, Beth, for her patience while I worked on different versions of this paper.

REFERENCES

Ballard, D.W., Burton, B.R., Lageson, D.R., and Warne, J.R., 1993, Drilling experiences at Devils Fence Anticline, Jefferson County, Montana: Baseline data for future activity in a promising Overthrust province, in L.D. Hunter, Old Timers' Rendezvous, Energy and Mineral Resources of Central Montana: 1993 Montana Geological Society Field Conference Guidebook, p. 159–168.

Blanchette, P.L., 1989, Effects of soil characteristics on adsorbed hydrocarbon data: Bulletin of Association of Petroleum Geochemical Explorationists, v. 6, no. 1, p. 116–138.

Bandeira de Mello, C.S., Cordeiro, J.L.R., Miller, D.J. Goncalves, R.C.S. Polinanov, H. and Barroso, V.E., 2007, Experimental data on light hydrocarbon contents in different clays and their contribution to headspace, blender, probe, and adsorbed sample interpretation in surface geochemistry survey: The 23rd International Meeting on Organic Geochemistry, Abstracts of Reports, v. 23, p. 323–324.

Borg, W.R., and Gall, M.D., 1989, Educational Research: An Introduction (5th ed.): New York and London, Longman, p. 939.

Dickinson, R.G., and Matthews, M.D., 1993, Regional microseep survey of part of the productive Wyoming-Utah thrust belt: American Association of Petroleum Geologists Bulletin, v. 77, no. 10, p. 1710–1722.

Hinkle, M.E., and Ryder, J.L. 1987, Effect of moisture and carbon dioxide on concentrations of helium in soils and soil gases: Journal of Geophysical Research, v. 92, no. B12, (November 10), p. 12,587–12,594.

Klusman, R.W., 1993, Soil gas and related methods for natural resource exploration: John Wiley & Sons, 483 p.

Landrum, J.H., Richers, D.M., Maxwell, L.E. and Fallgatter, W., 1989, A comparative hydrocarbon soil-gas study of the Flathead Valley and Townsend Valley areas, Montana: Journal of Geochemical Exploration, v. 34, p. 303–335.

Leaver, J.S., and Thomasson, M.R., 2002, Case studies relating soil-iodine geochemistry to subsequent drilling results, in D. Schumacher and L.A. LeSchack, eds., Surface exploration case histories: Applications of geochemistry, magnetics, and remote sensing, American Association of Petroleum Geologists Studies in Geology and SEG Geophysical Reference Series, no. 11, p. 41–57.

Matthews, M.D., 1996, Importance of sampling design and density in target recognition, in D. Schumacher and M.A. Abrams, eds., Hydrocarbon migration and its near-surface expression: American Association of Petroleum Geologists Memoir 66, p. 243–253.

Nunn, J. A., and Meulbroek, P., 2002, Kilometer-scale upward migration of hydrocarbons in geopressured sediments by buoyancy-driven propagation of methane-filled fractures: American Association of Petroleum Geologists Bulletin, v. 86, no. 5, p. 907–918.

Orr, W.N., and Orr, E.L., 2002, Geology of the Pacific Northwest (2nd ed.): Long Grove, Illinois, Waveland Press, 337 p.

Pardee, J.T., 1950, Late Cenozoic block faulting in Western Montana: Geological Society of America Bulletin, v. 61, p. 359–406.

Potter, R.W., III, Harrington, P.A., Silliman, A.H. and Viellenave, J.H., 1996, Significance of geochemical anomalies in hydrocarbon exploration, in D. Schumacher and J.H. Abrams, eds., Hydrocarbon migration and its near-surface expression: American Association of Petroleum Geologists Memoir 66, p. 431–439.

Ransone, W.R., 1958, Case history of the Sojourner oil field, Haskell County, Texas, a geochemical confirmation: Geophysics, v. 23, no. 3, p. 574–578.

Rasmussen, D.L., and R.W. Fields, 1985, Cenozoic structure and depositional history, Jefferson and Madison intermontane basins, southwestern Montana, in P. Beaver, ed., Geology and Mineral Resources of the Tobacco Root Mountains and Adjacent Region: 10th Annual Field Conference, Tobacco Root Geological Society, Aug. 7th -10th, Bozeman, Montana, p. 14.

Rose, A.W., Hawkes, H.E., and Webb, J.S., 1979, Geochemistry in mineral exploration (2nd ed.): New York, Academic Press, 657 p.

Saunders, D.F., Burson, K.R., and Thompson, C.K., 1999, Model for hydrocarbon microseepage and related near-surface alterations: American Association of Petroleum Geologists Bulletin, v. 83, no. 1, p. 170–185.

Sofer, Zvi, 1991, Stable isotopes in petroleum exploration, in Merrill, R.K. (ed.), Treatise of Source and Migration Processes and Evaluation Techniques: American Association of Petroleum Geologists Handbook of Petroleum Geology, p. 103–106.

Soil Conservation Service Staff, 1993, Soil survey manual: United States Department of Agriculture Handbook, no. 18, 437 p.

Soil Conservation Service, 1978, General soil map: Montana: United States Department of Agriculture, Soil Conservation Service, in cooperation with U.S. Forest Service, Montana Agricultural Experiment Station, Montana State University, Extension Miscellaneous Publication no. 16.

Tedesco, S.A., 1995, Surface geochemistry in petroleum exploration: Chapman & Hall, 206 p.

van Belle, Gerald, 2008, Statistical rules of thumb (2nd ed.): Wiley, 272 p.

Vice, D.H., 1996, The effect of surface factors on light hydrocarbon concentrations in the environment: The Pennsylvania State University, D. Ed. thesis, University Park, PA, 187 p.

Vice, D.H., 1986, Geochemical soil surveys in the Golden Dome and Mosser Dome areas, Carbon and Yellowstone Counties, Montana, in P.B. Garrison, Geology of the Beartooth uplift and adjacent basins, Montana Geological Society and Yellowstone Bighorn Research Association Joint Field Conference and Symposium, YBRA 50th Anniversary edition, p. 233–238.

Vice, D. H., 1985, The Devils Fence geochemical soil survey, Broadwater and Jefferson Counties, Montana: Unpublished report prepared for Irv Kranzler and J.R. Warne, Independent Geologists in Billings, Montana, 5 p., plus 2 figures.

Vice, D.H., 1983, Unpublished report to Mr. B.W. Roberts, Exploration Manager, North American Resources Company, 24 p.

Vuke, S.M., Porter, K.W., Lonn, J.D., and Lopez, D.A., 2009, Geologic map of Montana field notebook: Montana Bureau of Mines and Geology Geologic Map 62-E, scale 1:500,000.

Webster, M., and Van Arsdale, T., 1995, Geochemical microseep survey of the Plaza and Wabek productive trends, Mountail and Ward Counties, North Dakota, in L.D. Vern Hunter and Robert Schalla (eds.), Seventh International Williston Basin Symposium, 1995 Guidebook, Montana Geological Society, p. 57–65.

NEOTECTONICS AND POLYCYCLIC QUARTZITE-CLAST CONGLOMERATES OF THE NORTHERN BASIN AND RANGE PROVINCE

Stuart D. Parker and James W. Sears

University of Montana, Missoula, Montana, 59812

ABSTRACT

Depositional characteristics of the "Divide unit" of the Cretaceous Beaverhead Group within the southern Beaverhead Mountains challenge previous interpretations. This study reassigns the "Divide" unit to the Neogene. This revised age assignment highlights a major influx of immature sediment at the onset of Basin and Range normal faulting. Syntectonic deposition in an active half-graben continued from Middle Miocene to the Pliocene, attaining a thickness of 800 m. Local clasts of carbonate, orthoquartzite, and siliciclastic sedimentary lithologies entered the channel from the immediate west through large mass-wasting events. Dacitic fluvial cobbles dated herein to 98 Ma were recycled from the underlying Beaverhead Group. Clasts of the Ordovician Kinnikinic or Swan Peak Quartzite of Idaho experienced multiple phases of recycling from regional Cretaceous conglomerates such as the Beaverhead Group. Preliminary detrital zircon analysis of a feldspathic quartzite cobble identifies the Brigham Group of the Pocatello area as a source. Detrital zircons of anomalous ages suggest long-distance transport from the southern Basin and Range. This major drainage, analogous and likely continuous with that of the Sixmile Creek Formation in SW Montana, was long-lived until uplift associated with passage of the Yellowstone volcanic system (aka Yellowstone hotspot) halted deposition between 4.5 and 4.1 Ma. A broad volcanic plain persisted until movement along the Middle Creek Butte fault exposed the deposit around 0.365 Ma. Progressive recycling of resistant quartzite cobbles creates a subtle record of sedimentation in the northern Basin and Range, which has long been misidentified or overlooked. A revised interpretation for the Divide deposit allows for investigation of Neogene tectonics in the northern Basin and Range.

INTRODUCTION

An extensive gravel deposit known as the "Divide unit" of the Beaverhead Group occurs in the southern Beaverhead Mountains of southwest Montana and Idaho (fig. 1). Scholten (1955) and Ryder and Scholten (1973) described and named the informal Divide unit, but its source and age remain poorly constrained (Nichols and others, 1985). This study reevaluates the Divide deposit, investigating possible sources for exotic cobbles and providing a timeline for deposition. Resistant quartzite cobbles are common among conglomerates and gravel deposits of the Basin and Range, throughout Cretaceous and Cenozoic time (Lindsey, 1972; Janecke and Snee, 1993). Researchers often cite recycling of such clasts, yet local stratigraphy typically fails to highlight episodes of such reworking (Lindsey, 1972; Ryder and Scholten, 1973). Constraining age and source among recycled quartzite-clast conglomerates, such as the Divide, is crucial to understanding the tectonic evolution of the northern Basin and Range province.

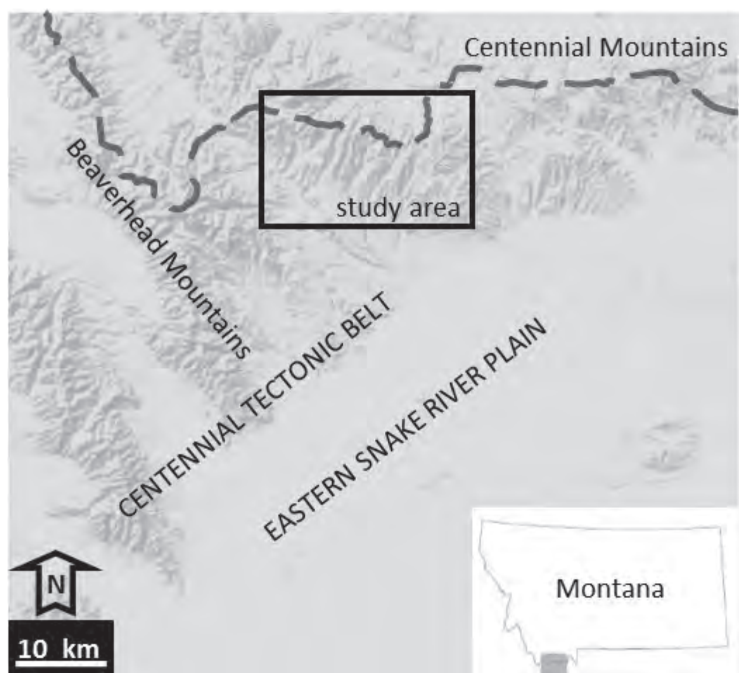

Figure 1. Map of the study area within the southern Beaverhead Mountains, bounding the Centennial tectonic belt and the ESRP.

GEOLOGIC FRAMEWORK

Lowell and Klepper (1953) defined and mapped the Beaverhead Formation across the Beaverhead Mountains near the southern Montana/Idaho border. The Beaverhead was later raised to Group status by Nichols and others (1985). Oxidized alluvial conglomerates of predominantly quartzite to limestone cobbles and boulders typify the Beaverhead Group. Ryder and Scholten (1973) and Nichols and others (1985) dated several units to Late Cretaceous. Forming the Continental Divide in the southern Beaverhead Mountains, the Divide quartzite-conglomerate unit has not been dated, due to lack of fossil specimens (Nichols and others, 1985).

Lowell and Klepper (1953) and Ryder and Scholten (1973) cited the Belt Supergroup as the primary source of abundant feldspathic quartzite cobbles within the Beaverhead Group, while orthoquartzite clasts were assigned to the nearby Ordovician Kinnikinic Quartzite. The Kidd conglomerate unit of the Beaverhead Group contains numerous clasts of green siliceous argillites, typical of the Belt Supergroup, while the Divide unit does not (Ryder and Scholten, 1973). Ryder and Scholten (1973) highlighted the abundance of quartz-veined black chert, chert-breccia, and dacite clasts, but failed to constrain their sources. While the presence of these unique clasts led to the distinction between the Divide and Kidd units, deposition was considered synchronous.

Curiously, the Divide unit displays a consistent northerly transport direction, inconsistent with interpreted sources that lie west and northwest of the Divide unit (Ryder and Scholten, 1973). Love (1956) explained this discrepancy in paleoflow by invoking the hypothetical "Targhee uplift," which later conveniently sank beneath the eastern Snake River Plain (ESRP). This hypothesis claimed that a large uplift just south of the Beaverhead Mountains exposed stratigraphic units down to the Belt Supergroup in Late Cretaceous time, providing the source for the Divide unit. While stratigraphic, structural, and geophysical data have since disproven this hypothesis, the source of the Divide unit remains poorly constrained and largely ignored (Schmitt and Steidtmann, 1990).

Field observations indicate a much younger age than proposed by Ryder and Scholten (1973). Abundant dacite cobbles contain bipyramidal smoky quartz crystals, a common characteristic of the Eocene Challis volcanic field (Janecke and Snee, 1993). High in the Divide section, the 4.5 Ma Kilgore Tuff rests conformably within the gravel deposit (Morgan and McIntosh, 2005). Abundant lithophysae are a unique characteristic of the Kilgore Tuff, which allow for easy field identification and differentiation from other tuffs of the ESRP region (Morgan and McIntosh, 2005). Overlying the deposit is the 4.1 Ma rhyolite of Indian Creek Butte (Morgan and McIntosh, 2005).

These observations indicate that at least the upper part of the Divide unit has been incorrectly assigned to the Cretaceous Beaverhead Group. Several questions need to be addressed in order to identify its origin. Clast sources must be identified and a timeline for deposition must be established. Once these questions are satisfied, interpretations can be formulated regarding post-depositional deformation within the unit. The expansive and homogenous nature of the Neogene gravel deposit make it an ideal candidate for studying the complex crustal dynamics at play between the actively extending terranes of the northern Basin and Range and the ESRP.

The southern Beaverhead Mountains lie within the Cordilleran fold-and-thrust belt, which formed during the Jurassic through Paleocene Sevier and Laramide orogenies. Following the compressional phases of the Laramide orogeny, widespread extension characterized the region (Link and others, 2005). At 17 Ma, Basin and Range extension and northeasterly migration of the Yellowstone volcanic system began (Pierce and Morgan, 2009). Regional NW–SE-directed crustal extension took place in the Middle Miocene, followed by a hiatus, before initiation of NE–SW-directed crustal extension in the later Neogene (Sears and Fritz, 1998). By roughly 6 Ma, the active caldera was adjacent to the southern Beaverhead Mountains. The Middle Creek Butte fault strikes roughly N115°E, bounding the study area to the south, and crosscuts the 4.1 Ma Indian Creek Butte Tuff (Link and others, 2005). No river gravel has been observed on top of the Indian Creek Butte Tuff. Movement along the Middle Creek Butte fault lifted the Divide unit to its present location along the Continental Divide at roughly 7,880–9,190 ft (2,400-2,800 m). Erosion of its footwall has exposed the river gravel deposit in numerous deep and steep valleys of the southern Beaverhead Mountains. The Middle Creek Butte fault projects toward 0.365 Ma to 15 ka volcanic fissures of the Spencer-High Point trend, suggesting continued movement in the Pleistocene (Kuntz and others, 1992).

A measured section from the basal contact near Paul Reservoir to the Kilgore Tuff along Forest Service road 323 indicates a thickness of roughly 800 m. An additional ~100 m of gravel overlies the Kilgore Tuff. This section lies in the half-graben, just west of the Miocene normal fault. Given the geometry of half-graben valleys, this is likely the thickest portion of the deposit. A measured section just west of I-15 to the Kilgore Tuff records a thickness of roughly 700 m. A measured section from the basal contact on the Divide unit east of the Red Conglomerate peaks, to the Middle Creek Butte fault, suggests a thickness of over 2,000 m. However, this transect, originally used by Ryder and Scholten (1973), crosses countless high-angle faults that greatly inflate the thickness of the Divide unit. The best estimate for maximum thickness is thus the roughly 700–800 m measured in the east.

METHODS

I conducted pebble counts to assess compositional changes throughout the Divide deposit. I catalogued lithologies within 1 m^2 plots or 0.25 m^2 plots, depending on outcrop size, and classified clasts as quartzite (feldspathic, orthoquartzite, and other), volcanic, carbonate, metamorphic, chert, and other. Key lithologies included quartz-veined black chert, lithic chert arenite, andesite, dacite (containing bi-pyramidal smoky quartz phenocrysts), Ordovician quartzite (containing pock marks resulting from incomplete silica cementation), and silicified crinoidal packstone/wackestone (assigned to the Mississippian Scott Peak Formation). Imbricated cobbles recorded paleoflow direction. A, B, and C axis lengths of clasts classified shape and size distribution. At each outcrop, I measured the length of the C axis of the largest cobble, recorded the degree of cementation (poorly/well), and classified the matrix with regard to composition, size, shape, and degree of sorting. Due to weak cementation within the deposit and scarcity of outcrops, not all attributes were measurable at each outcrop. Measurements taken at individual sites (M1-M99) were grouped into areas (MA-MS). Bedding and fault geometries were measured when possible.

Thin sections of key cobble lithologies, possible bedrock sources, and sandstone lenses within the deposit were investigated. Radiometric U/Pb dating of zircons was conducted in order to match possible sources and constrain age. A cobble sample of dacite containing bi-pyramidal smoky quartz phenocrysts was U-Pb dated in order to assess the hypothesis of post Cretaceous deposition and constrain source. A cobble of feldspathic quartzite was U-Pb dated to constrain source. Detrital zircon grains intermixed with the conglomerate matrix were U-Pb dated to further constrain age and possible sources. Zircon grains were separated using standard techniques and annealed at 900°C for 60 hours in a muffle furnace. Grains were mounted in epoxy and polished until their centers were exposed. Zircons were analyzed by laser ablation-inductively coupled plasma-mass spectrometry (LA-ICP-MS). Technicians at the Boise State University Isotope Geology Laboratory conducted all lab analyses.

RESULTS

Clast Lithologies

The Divide deposit was found to be a remarkably homogeneous conglomerate, containing local <1-m-thick sandstone lenses. Quartzite-cobble conglomerates contain crude beds with highly imbricated clasts. Armored bedding was often observed. The average clast size of 8.6 cm ± 2.8 cm indicates a fine cobble-size fraction. Commonly boulders exhibit C axis lengths as great as 68 cm. Slide blocks with C axis exceeding several meters also occur. Clasts are well-rounded, regardless of lithology. Shape analysis of 187 cobbles across the deposit revealed a distribution of 50% spheroid, 34% disk, 13% roller, and 3% blade. Pebble counts across the deposit revealed an average composition of 71% quartzite, 7% volcanics, 7% carbonate, 0% metamorphic, 8% chert, and 7% other. Feldspathic quartzites account for 33% of the total assemblage, orthoquartzites 20%, and other quartzites 18%. Measurements of 536 imbricated cobble sets revealed a mean transport direction towards N 22.4° ± 1.3°E (fig. 2). All areas display this mean vector with the exception of the easternmost (MA), which displays a mean transport direction of N 92.3° ± 14.8°E (N=13).

Partially silicified crinoidal pack/wackestone clasts displaying disharmonic folds are common throughout the deposit. The Middle Canyon and Scott Peak Formations of the Mississippian Madison Group are likely sources. An outcrop of the Scott Peak Formation in the hanging wall of the Middle Creek Butte

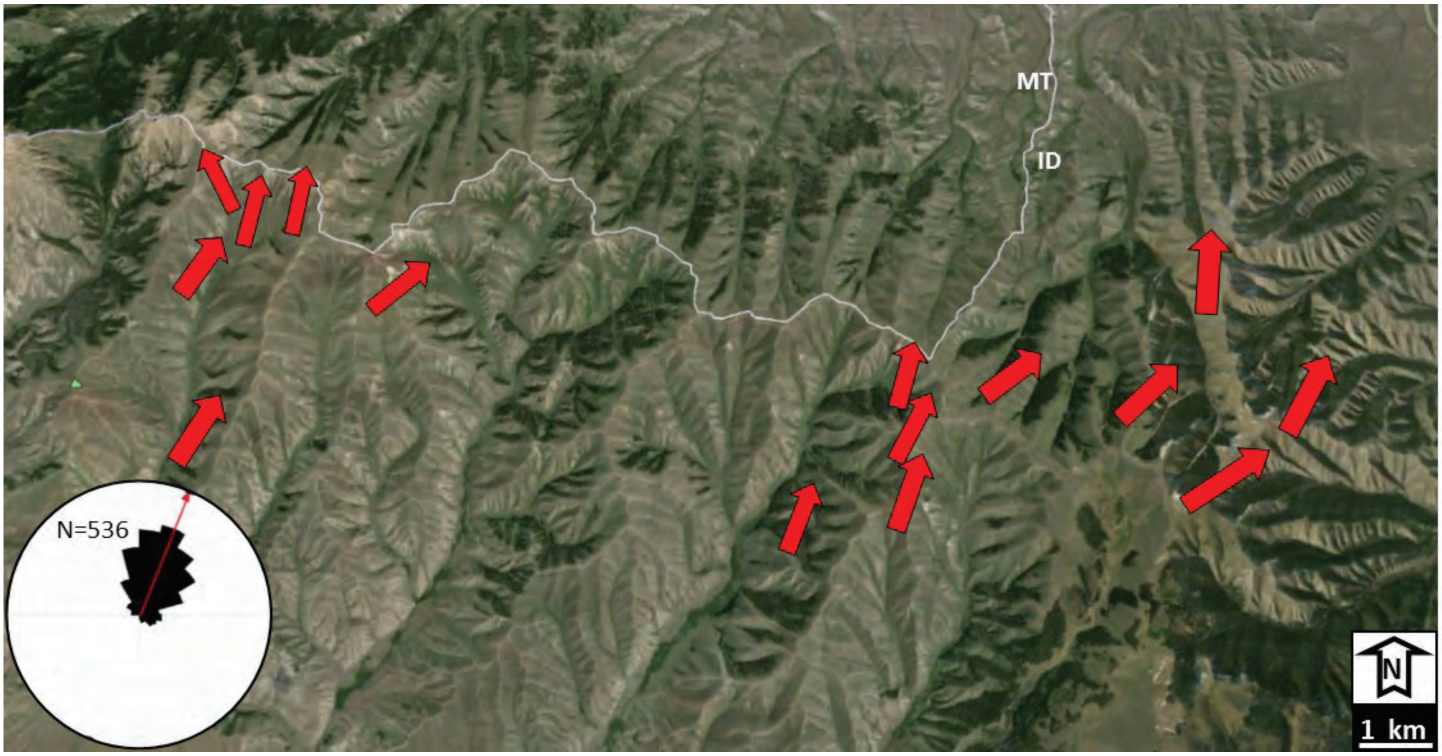

Figure 2. Map showing averaged paleoflow directions, interpreted from cobble imbrications. Inset shows rose diagram of paleoflow directions based on 536 imbrication sets. Mean flow is highlighted.

fault in Middle Creek displays similar disharmonic folds of alternating bands of chert and carbonate in hand sample and thin section. The outcrop of the Scott Peak Formation lies within alluvium and below the 4.1 Ma Indian Creek Butte Tuff. This spatial relationship suggests that the outcrop marks an erosional surface which is overlain by gravel of the Divide deposit. At the same outcrop, minor amounts of black chert with quartz veins were found. This clast lithology in the Divide unit was previously thought to be exotic to the region, with the most likely source being the Valmy Formation of Nevada (Sears and others, 2014). This outcrop identifies the Middle Canyon and Scott Peak Formation as the most suitable sources and provides a local source for some quartz-veined black chert clasts within the gravel deposit.

Several large slide blocks of orthoquartzite and carbonate were found throughout the deposit. The slide blocks form a tight ESE/WNW trend across the map area. The slide blocks occur above and below the Kilgore Tuff, in various stratigraphic positions. Contoured measurements of the maximum observed C axis (long axis) lengths of each outcrop correlate with the slide block distribution, with highest values oriented to the NW-SE (fig. 3). Slide blocks of quartzite match the Cambrian Flathead and the Ordovician Kinnikinic Formations, which occur just west of the field site (Ryder and Scholten, 1973). No slide blocks of the Proterozoic Belt Supergroup lithologies were observed.

Contoured maximum clast measurements and distribution of slide blocks shows westerly provenance. Occurrence throughout the stratigraphic column shows that mass wasting events (possibly rockslides) were characteristic of this deposit, occupying a consistent spatial domain. Average clast size loosely correlates with this trend.

The apparent debris path, highlighted by slide block distribution and contoured clast size measurements, appears to occupy a fixed band through time and splits compositional data into two categories: slide influenced and non-slide influenced. This classification allows for separate investigation of the two drastically different transport mechanisms; along-channel fluvial transport vs. gravitational transport from the west. Clast-composition plots demonstrate spatial and temporal trends. Composition data derived from individual outcrops were averaged when outcrops were in high proximity (less than a few hundred meters) and of similar stratigraphic position. These average compositions were plotted with respect to longitudinal and latitudinal position to assess spatial trends in composition. Compositions were also plotted against relative age, as interpreted by position in the stratigraphic

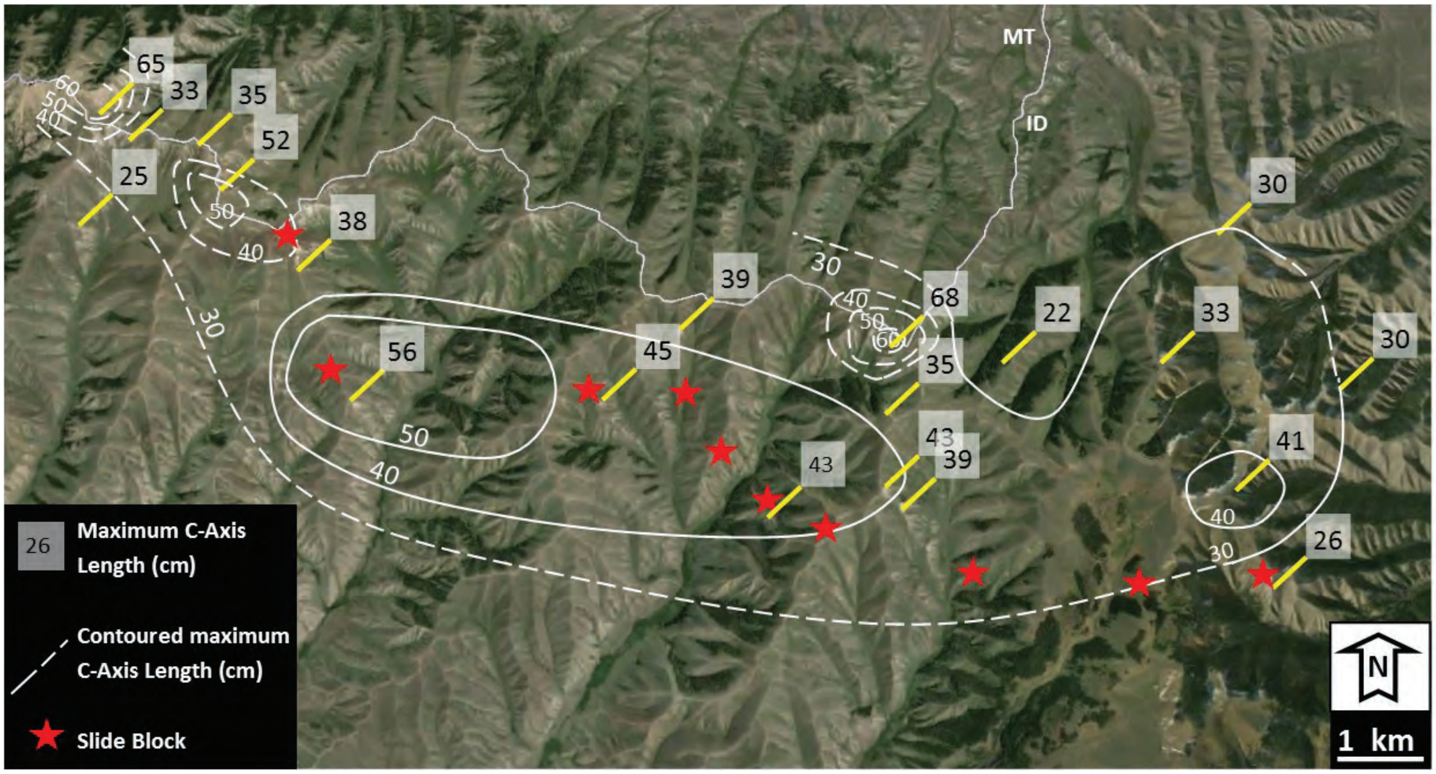

Figure 3. Map showing contoured maximum C-axis measurements of clasts and slide block distributions. These trends reveal that mass wasting events persisted through time, occupying a consistent spatial domain and were a major sediment transport mechanism.

column, to assess temporal trends.

Longitudinal trends were identified within the slide-influenced sites (fig. 4). A strong decrease from W to E was found for the "other" category. Throughout this study, the other category was almost entirely comprised of siliciclastic sedimentary rocks, hence it will be referred to as "sedimentary" rather than "other." Sedimentary percentages decrease from 30% to 0%, from W to E, in slide-influenced sites with a loose best fit ($R^2 = 0.51$). This decreasing trend is compensated by quartzite-clasts that increase from W to E to a varying degree, best defined for the feldspathic quartzite-clast category ($R^2 = 0.50$). Volcanic clast percentages also increase to the east ($R^2 = 0.63$). Carbonate

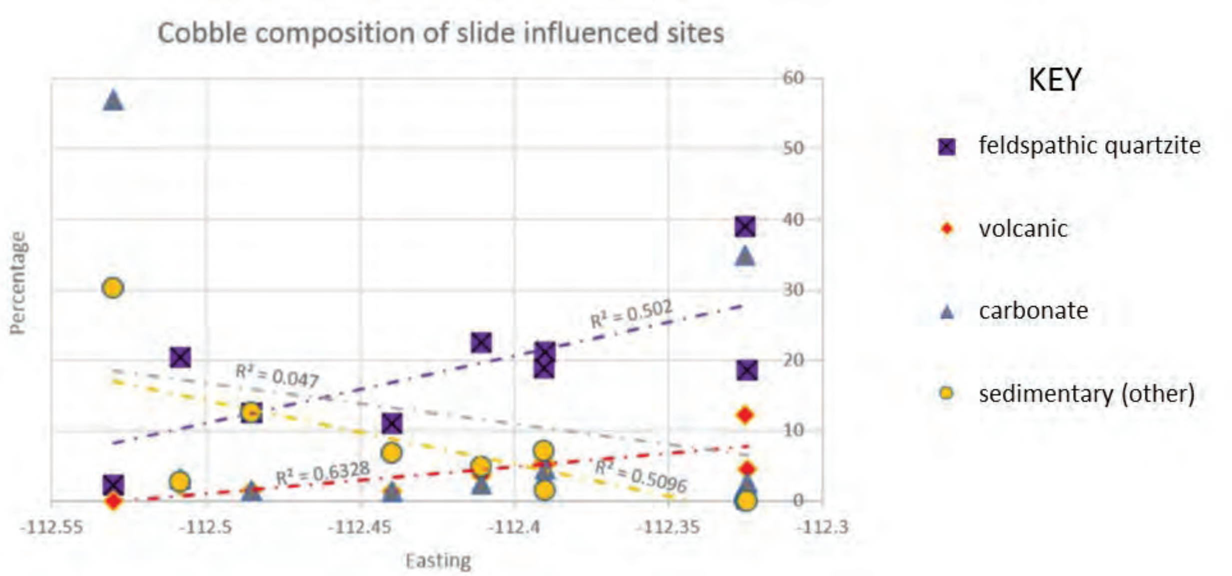

Figure 4. Plot of measured clast composition in slide-influenced sites relative to longitudinal position. Sedimentary and carbonate clasts are more abundant in the west, where mass wasting events introduce such lithologies. Feldspathic quartzite and volcanic clasts compensate for this trend, with a higher abundance in the east. This illustrates that sedimentary and carbonate lithologies are primarily added to the river channel through large mass wasting events sourced from the west, while feldspathic quartzites and volcanic lithologies are not.

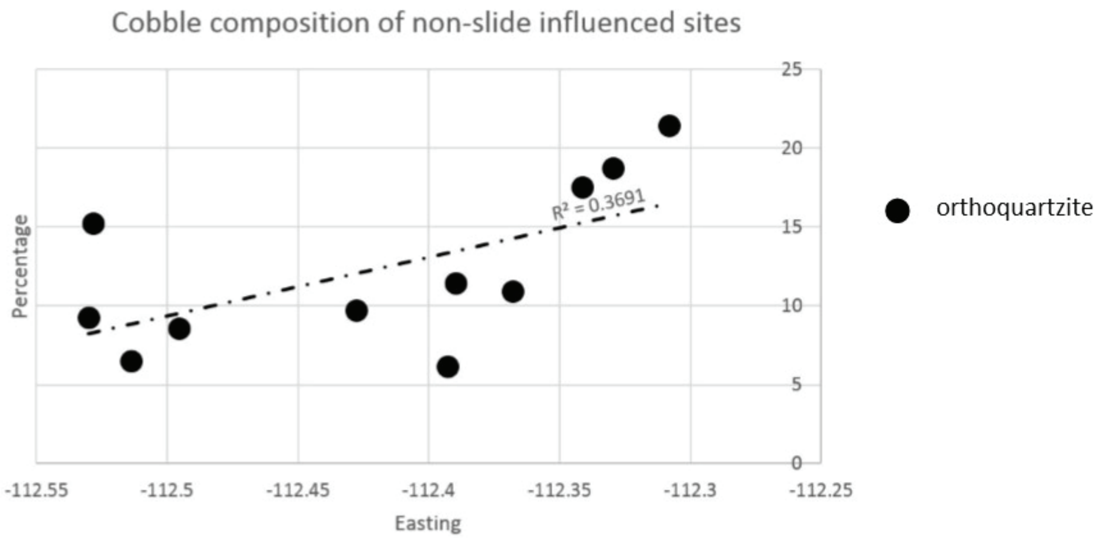

Figure 5. Plot of orthoquartzite abundance in non-slide-influenced sites relative to longitudinal position. A surprising increase to the east exists. Such a trend is not expected such a short distance across a braided river gravel deposit. This trend may represent an eastern source such as a tributary or recycling from the basal Beaverhead Group.

clasts spike in the west, in basal carbonate conglomerates. No trend in chert-clast occurrence was found.

Along-channel trends in non-slide-influenced sites show a minor downstream (to the NE) increase from roughly 3% to 7% in volcanic clasts ($R^2 = 0.35$). Carbonate clasts also increase downstream, from roughly 3% to 8% ($R^2 = 0.40$). A surprising W to E cross-sectional trend occurs for orthoquartzite clasts, from ~ 10% to ~ 20% ($R^2 = 0.37$) (fig. 5). No other lithologies, including the dominant feldpathic quartzites, display a strong trend complimentary to this.

To address temporal trends, sites were arranged in descending relative age, based on observed stratigraphic relationships. A high degree of uncertainty exists for these relative age relations. It is assumed that sites in the footwall of the syndepositional normal fault predate all syntectonic deposits within the half-graben. In the plots, this boundary has been plotted in order to address changes between these two distinct facies.

In slide-influenced sites, abundance of volcanics displays a slight bimodal and positive trend (fig. 6).

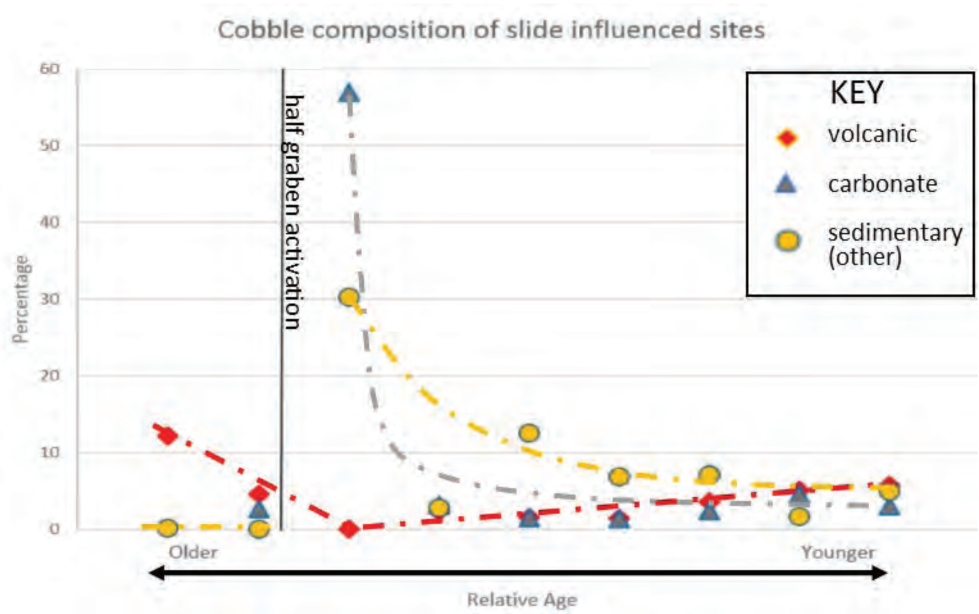

Figure 6. Plot of measured clast composition in slide-influenced sites against relative age. It should be noted that age is approximate and relative; therefore the x-axis is not to scale. Vertical boundary signifies approximate timing of activation of the half graben. Carbonate clasts are high around the onset of movement on the fault and quickly decrease through time. This observed trend may be the result of the previously mentioned spatial trend. The oldest carbonate data point was discounted due to technician error. Volcanic clasts are more abundant before normal faulting, suggesting they are not sourced through mass wasting events. Sedimentary units are highest near onset of normal faulting, suggesting that mass wasting events are the primary transport mechanism for sedimentary lithologies.

Volcanics suddenly disappear in the base of the syntectonic deposit before increasing. Values range from 0 to ~6 %. Carbonates also display a bimodal trend, with a spike in the basal sytectonic unit, which quickly falls towards 0%. The oldest data point reflects an error in the classification scheme and was thus discounted. Sedimentary clast abundance shows a bimodal distribution as well. They are initially absent, but spike in the basal syntectonic deposit. The trend then falls from 30% to 5% and approaches an asymptote. Due to a lack of scale on the x-axis, the strength of these trends is difficult to assess.

In non-slide-influenced sites, feldspathic quartzite abundance falls from ~40% to ~15% and approaches an asymptote (fig. 7). This trend shows no relation to activation of the half-graben within which sedimentation occurred. Due to the fact that feldspathic quartzites are the dominant lithology, this may also be viewed as an increase in diversity which reaches an asymptote. Sedimentary abundance declines slightly up section from <10 % to nearly absent. This trend is continuous across the fault as well.

Matrix Lithology

Thin sections of key lithologies and the interstitial sandstone matrix were analyzed. Matrix samples were taken from pre-fault and syntectonic deposits (M1 and M14, M16, M97, M88 respectively) (fig. 8). Sample M88 represents the matrix of the basal limestone conglomerate. This is likely a lithosome to the deposit at M93, which contains a cliff-forming exposure of fluvial conglomerate several hundred feet thick. The fluvial gravel at M93 grades upward from quartzite-clast- to limestone-clast-dominated. The unit is slightly folded into a syncline with a plunge of 10^{o} to the SE. This fold represents the only visible fold of this study. This structure may be part of the Laramide orogeny, predating the main body of the Divide unit.

The basal limestone conglomerate (M88) contains sub-angular to sub-rounded quartz grains of the fine sand size fraction (fig. 9). This arenite sample is the most compositionally and texturally mature of the study, consisting of tightly packed quartz sand grains in calcite cement. Moving up section, M97 is a transitional conglomerate, containing both quartzite and carbonate cobbles. Sample M97 contains sub-rounded fine sand sized quartz grains in calcite cement. The sample is well sorted in size and shape. It contains minor inter-grown feldspar and quartz grains with graphic texture and little to no chert or carbonate lithics. Farther up section, M1 (within the footwall of the syndepositional fault) consists of medium sand grains

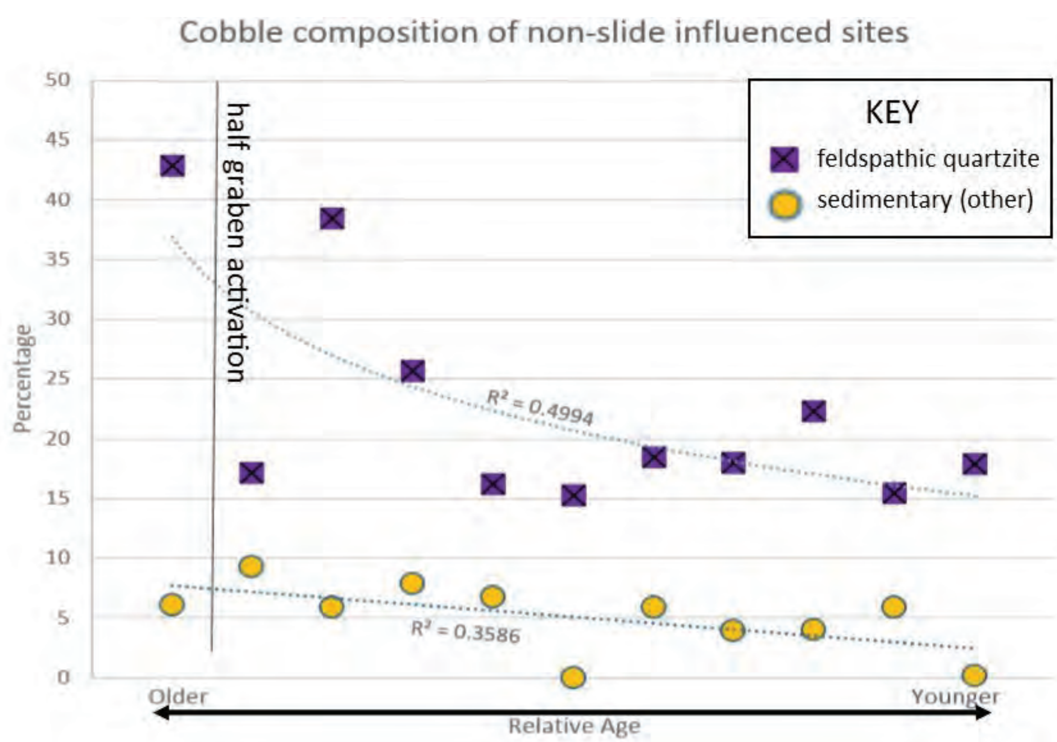

Figure 7. Plot of measured clast composition in non-slide-influenced sites against relative age. It should be noted that age is approximate and relative; therefore the x-axis is not to scale. Vertical boundary signifies approximate timing of activation of the half graben. Feldspathic and sedimentary lithologies decrease in abundance through time, signifying that transportation/weathering outpaces sedimentation. Activation of the half graben does not affect either lithology.

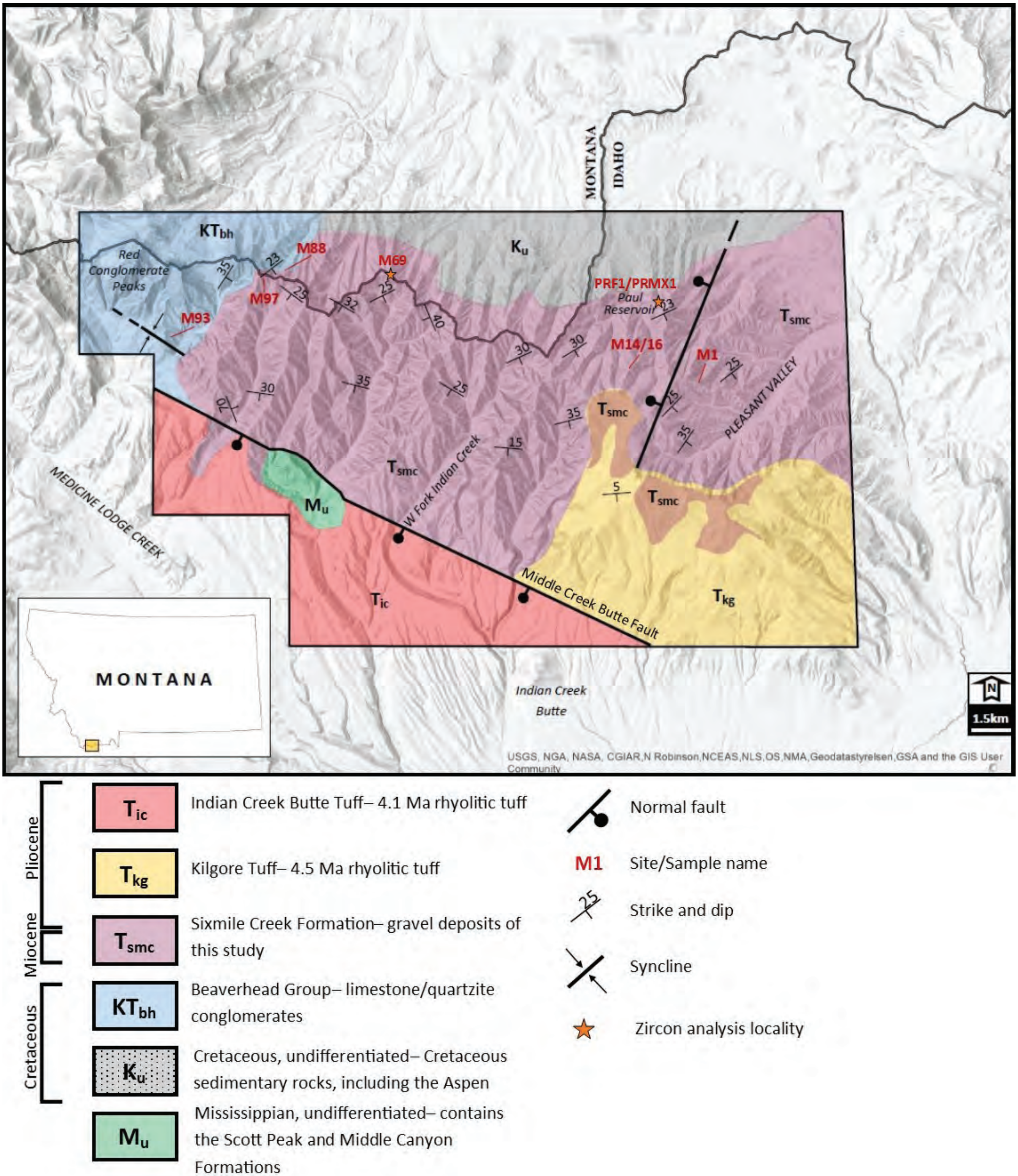

Figure 8. Preliminary bedrock geologic map of the study area, assigning the Divide deposit to the Neogene Sixmile Creek Formation. Unit boundaries are loosely defined and should be viewed as approximate.

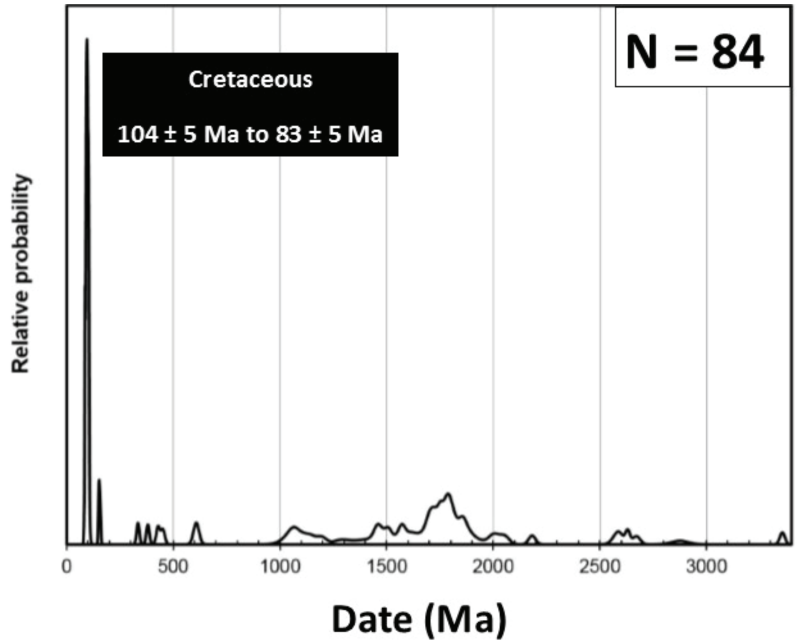

Figure 9. Probability distribution plots of LA-ICPMS analysis of detrital zircons within sample PRMX1, extracted from *in situ* matrix sand near Paul Reservoir, ID.

of angular feldspar and quartz with a calcite cement (fig. 9). Grains are poorly sorted and compositionally and texturally immature. Grains of sedimentary chert, sedimentary lithics, graphic granite, and quartz-veined chert are present. Highest in the section (M14 and M16), angular grains of the fine sand size fraction dominate. Sub-rounded quartz and angular grains of feldspar with graphic texture, carbonate lithics, volcanic lithics, and chert are common. Graphic feldspar grains are common within dacitic cobbles containing bi-pyramidal smoky quartz crystals. This texture is also common in the neighboring Idaho Batholith and Challis volcanic field (Janecke and Snee, 1993). In the outcrop, degraded, white petrified wood is common. Samples M1, M14, and M16 are drastically less mature than samples M88 and M97.

U-Pb Dating of Zircon

Radiometric dating (U-Pb zircon) of a dacite cobble containing bi-pyramidal smoky quartz crystals (M69; $N = 8$) revealed an eruptive age of 98.3 ± 1.7 Ma. Fluid inclusions of elongate and colorless apatite limited the sample size to 8 grains. The same sample contains high total rare earth element (ΣREE) concentrations (1,000–6,000 ppm) and large Eu anomalies (Eu/Eu* = 0.1). Cathode luminescence images, consistent chemical compositions, and concordant dates do not suggest inheritance of zircons.

Matrix sand grains sampled from Paul Reservoir (PRMX1; $N = 84$) revealed ages ranging from 3357 ± 24 Ma to 83 ± 5 Ma (fig. 10). Largest peaks are at ~100; 1,110; 1,800; and 2,600 Ma. The 24 youngest dates (29%) are Cretaceous in age (104 ± 5 to 83 ± 5 Ma).

Detrital zircons from a feldspathic quartzite cobble within an outcrop at Paul Reservoir (PRF1; $N = 28$) revealed dates ranging from 3325 ± 24 Ma to 1303 ± 65 Ma. Two zircons postdate the 1.45 Ga Belt basin within uncertainty (1303 ± 65 Ma, 1314 ± 49 Ma) and a third straddles the boundary within uncertainty (1399 ± 79 Ma) (Ross and Villeneuve, 2003). 17 grains (61%) correspond to Paleoproterozoic peak between 1,600 and 1,900 Ma. Another strong peak occurs (7 grains, 25%) around the Archean/Proterozoic boundary around 2,500 Ma.

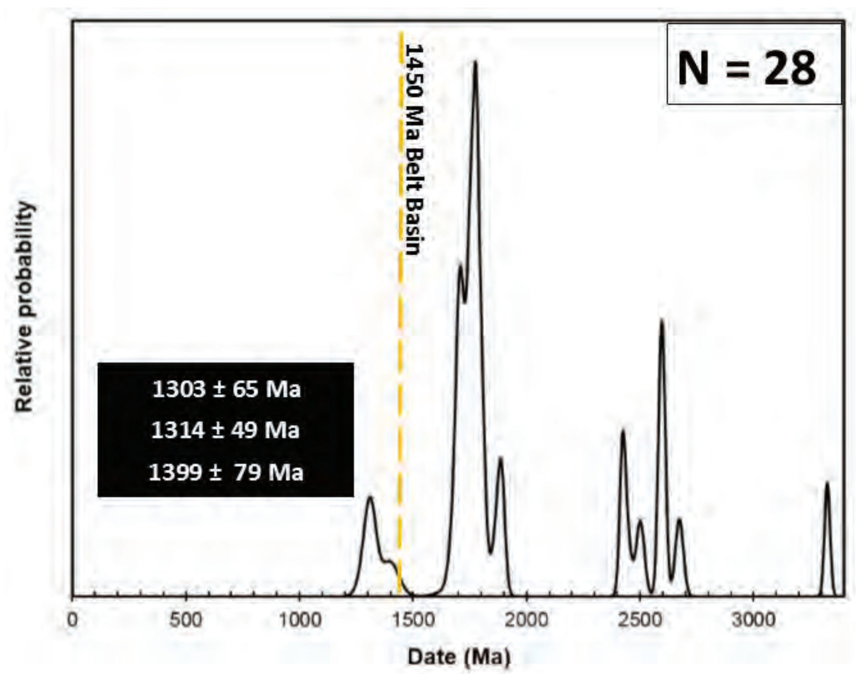

Figure 10. Stacked probability distribution plots of LA-ICPMS analysis of detrital zircons within sample PRF1, Brigham Group (Yonkee and others, 2014) and Belt Supergroup (Jones and others, 2015). Approximate initiation of Belt Basin highlighted.

DISCUSSION

Justification of Categorizing Compositional Data

Compositional data were split into the categories of "slide-influenced" and "non-slide-influenced" on the basis of several observations that highlight mass wasting events and fluvial transport as the two dominant sediment transport mechanisms. Distribution of slide blocks and contoured clast measurements reveal that addition of local lithologies to the river channel persisted through stratigraphic time and occupied a discrete area. Bedding geometry and sub-perpendicular joint sets indicate tilting (~10^{o}) prior to lithification, supporting the hypothesis of syntectonic deposition in an actively subsiding half-graben of likely Mid-Miocene age. Imbrication measurements suggest a mean flow towards N 22.4° ± 1.3° E, coincident with strike of the Miocene normal fault, suggesting that half-graben geometry controlled the flow direction. The interpretation of gravitational addition of material from high topography in the west and deposition in a subsiding NNE striking normal fault was the justification for splitting compositional data into two distinct categories of "slide-influenced" and "non-slide-influenced."

Without this delineation (slide- vs. non-slide-influenced) no trends are observed, with associated R^2 values averaging 0.08 and not exceeding 0.28. With this split of the data spatial and temporal trends become observable but slight ,with associated R^2 values averaging 0.20 and reaching a maximum of 0.63. It is important to note that such trends are poorly defined and it could be argued that the associated increase in R^2 values could merely reflect a reduction in sample size. Such low R^2 values illustrate the highly variable nature of the deposit. For this reason only general trends can be suggested. Interpretations gathered from such compositional trends must be strongly supported by field observations and more reliable data sets.

Slide-Influenced Sites

Slight E–W trends are observed within the slide-influenced sites, while N–S trends were not. Slide blocks and contoured clast measurements strongly suggest sediment input from the west during mass wasting events, which likely highlights a regional trend of mass wasting events given the immaturity of observed sand grains throughout the deposit. For these reasons along-channel variations in composition are not expected to dominate within slide-influenced sites.

A trend favoring abundance of sedimentary clasts in the west was observed. Being the dominant lithology, quartzite responds to this trend, evident as a westward decrease in abundance. Presence of orthoquartzite slide blocks suggests a proximal western source, yet a decrease in abundance to the west is observed, suggesting that orthoquartzite is not a simple first cycle sediment. Throughout the deposit quartzite is most abundant, with the exception of a few basal deposits. Therefore, trends in quartzite abundance are attributed to compensation for other declining trends in lithologies, unless the quartzite trend was anomalous. It is important to note that while sparse outcrops of Belt Supergroup occur roughly 15 km to the west, no evidence of gravitational transportation of Belt blocks was found, and while some feldspathic boulders were observed, all clasts were well rounded. Abundance of volcanic cobbles also increases to the east, suggesting that mass wasting events added little to no volcanic material to the river channel.

The spike in carbonates occurs within the basal transitional conglomerate, thus providing little insight to source, although a proximal source to the immediate west is most obvious and consistent with observations. Thin sections show an abundance of lithics derived from carbonates, while at the outcrop scale low occurrences of carbonate clasts are observed. Given the abundance of carbonates in the region, it is likely a major sediment input to the system but is quickly weathered away before lithification. The E–W trends in slide-influenced deposits suggest that siliclastic, carbonate, and orthoquartzite lithologies were proximally sourced from the west through mass-wasting events, while feldspathic quartzite and volcanic lithologies were not. This interpretation is consistent with field observations and local bedrock geology.

Non-Slide-Influenced Sites

For non-slide-influenced sites, NE-oriented along-channel trends are apparent but slight. A weak and minimal downstream (to NE) increase is observed for volcanic and sedimentary cobbles. This may highlight constant addition to the channel, which would slowly increase abundance downstream. An eastward increase in orthoquartzites is accommodated by a westward decrease in other lithologies. This trend was carefully examined and could not be discounted. This may highlight the addition of orthoquartzite from an eastern tributary. More likely, it may reflect recycling of clasts of the Beaverhead Group, which forms the basal contact to the deposit in the west but is absent in the east. In the east, the deposit rests on Cretaceous shales, which underlie the Beaverhead Group. This relationship seems to suggest that increased incision in the half-graben axis has eroded through the Beaverhead Group, reincorporating quartzite clasts into the system.

Cobbles are commonly well-rounded and irregular in shape, resembling half-cobbles, suggesting reworking of previously deposited stream-rounded cobbles. Many samples display percussion marks, with a less common occurrence on faces which appear to be fracture planes. Quartzite clasts are abundant to the east of the study areas, in the Harebell and Pinyon Formations of NW Wyoming (Lindsey, 1972). Recycled quartzite clasts have been found within a Pliocene river gravel deposit on Signal Mountain in Jackson Hole (Parker, 2015). Several stratigraphic relationships in the area suggest reworking of the Harebell and Pinyon Formations since the Late Cretaceous (Love and others, 1992; Lindsey, 1972). It is possible that reworking of such a deposit to the east could explain the observable trend in abundance of quartzite clasts. Local reworking of the Beaverhead Group is more plausible; however, investigations into the relationship to the Pinyon and Harebell Formations deserves consideration and further attention.

Assessing Temporal Trends in Composition

Temporal trends are difficult to assess due to the sparse nature of outcrops and the lack of time markers within much of the Divide unit. Sites were ranked in ascending relative age in order to investigate changes through time. Simple bed geometry within the syntectonic deposit allows for fairly reliable ranking of age. However, the pre-fault and basal conglomerates are difficult to assess due to the lack of any visible field relationships.

The basal conglomerate appears to conformably underlie the syntectonic deposit, showing no change in bed geometry between the two. It is inferred that the basal conglomerate marks the initial deposition in the subsiding half-graben, and is thereby younger than the pre-faulted deposit. Given the lack of evidence needed to properly assess this critical age relation, data points of the basal conglomerate (M98, M98 low, and M96) could be viewed as being younger or older than pre-fault data points (M3, M6, and M23). Interpretations were made with this uncertainty in mind. It is also important to note that the x-axis is not to scale; therefore, the rate of change (slope) of any compositional trend cannot be identified. With this consideration in mind, these trends should be viewed with skepticism as the fit and slope are indeterminable. Best fit lines were used to visually identify broad trends, but it should be kept in mind that the habit of such trends are indistinguishable due to lack of scale about the x-axis.

Temporal Trends of Slide-Influenced Sites

A bimodal trend in abundance of volcanic cobbles among slide-influenced sites shows higher values in the pre-faulted deposit and lower values in the syntectonic deposit which may increase through time thereafter. The majority of volcanic cobbles were dacitic, containing bi-pyramidal smoky quartz crystals, which were dated at 98.3 ± 1.7 Ma. This result is inconsistent with the hypothesis of an Eocene (Challis Group) source, as is the detrital zircon sample of sand grains within the matrix (PRMX1). An increase to the east is also observable for volcanic cobbles in slide-influenced locations. This spatial trend is likely the dominant trend due to the uncertainty associated with temporal plots.

A similar trend is observed in carbonate abundance through time. A spike occurs in the basal limestone conglomerate, and values are low elsewhere. The data point M6 reflects an early flaw in the classification scheme and was therefore discounted. This trend shows that the basal conglomerate is extremely enriched in carbonates. More information is needed in order to determine if this trend is the result of adjacent high topography which provides sediment through mass wasting events, or a change in depositional environment at the base. The same trend is observable for siliciclastic sedimentary lithologies, which are absent prior to activation of the fault and are most abundant immediately after. In each case the strength of such temporal trends is difficult to assess. Regardless, these data along with field observations agree with the interpretation that carbonate and siliciclastic sedimentary material is primarily sourced to the immediate west and was transported in a mass wasting event which is related to activation of the syndepositional half-graben. Volcanic material is not a first cycle sediment sourced from the proximal west.

Temporal Trends in Non-Slide-Influenced Sites and Source of Feldspathic Quartzite

In non-slide-influenced sites, a decrease (from ~40% to ~15%) in feldspathic quartzite clasts is observable through time. Feldspathic quartzite clasts also decrease in abundance to the west, as mass wasting adds diversity to the deposit. The temporal trend in non-slide sites is not easily explained spatially. This likely highlights either a decrease in total feldspathic quartzite clast content or an increase in diversity over time. Burial and erosion cycles render feldspathic quartzites clasts unstable and readily weatherable due to feldspar hydrolysis in groundwater. It is possible that preexisting feldspathic quartzite cobbles (derived from the basal Beaverhead Group) were exhumed, re-transported, and gradually weathered out of the system. However, a first cycle Belt Supergroup source cannot be satisfied given the observed paleoflow.

Preliminary LA-ICPMS results of sample PRF1 match the Brigham Group, on the basis of the three youngest grains (1,303 ± 65 Ma, 1,314 ± 49 Ma, 1,399 ± 79 Ma), which lie outside of the typical minimum age extent of the Belt Supergroup. While it could be argued that such grains could be hosted within the Belt Supergroup, as grains of ~1,370 Ma have rarely been documented within the belt (Evans and Zartman, 1990), this peak is slight to absent in typical Belt Supergroup signatures. In a sample of this size, the probability of three grains of such ages is extremely low. With these observations in mind, a Brigham Group source is favored over a Belt Supergroup source.

Field observations are consistent with the interpretation of at least a partial Brigham Group source of cobbles. The Brigham Group occurs nearly 200 km to the south, beyond the ESRP. The time progressive decrease of feldspathic quartzite clasts, from ~40% to ~15%, may reflect termination of the southern provenance (containing the Brigham Group) of the fluvial system due to uplift across the ESRP. The asymptote of ~ 5 % may represent the abundance of locally reworked Belt Supergroup clasts, recycled from the Beaverhead Group. This interpretation supports tectonic alteration of the long-lived and major drainage that deposited the Divide unit, and suggests that long-distance transportation of clasts derived from the Brigham Group provided a considerable amount of coarse sediment.

Constraining Age and Source Using Feldspathic Quartzite

Compositional data suggest that feldspathic quartzite was not added to the stream channel through mass-wasting events. The dated feldspathic quartzite cobble from Paul Reservoir may constrain source and time of deposition. The two likely sources for this lithology are the Belt Supergroup and the Brigham Group. Most noticeably, two grains slightly post-date the Belt Supergroup (1,314 ± 49 Ma; 1,303 ± 65 Ma). A third grain straddles the end of deposition in the Belt Basin (1,399 ± 79 Ma). As mentioned previously, it could be argued that this lies within the measured age range of the Belt, although such an age range is rarely observed. Grains around 1.45 Ga are common within the Belt Supergroup, less so in the upper Belt, which includes the Lemhi sub-basin (Jones and others, 2015; Ross and Villenevue, 2003). Only one grain satisfies this peak (1,399 ± 79 Ma).

The largest peak falls within 1,600 Ma–1,900 Ma, containing 17 grains (61%). This peak is correlative with the Yavapai Mazatzal, which is a shared Laurentian source to the upper Belt and the Brigham (Jones and others, 2015; Yonkee and others, 2014). While sample size is small ($N = 28$), a Belt Supergroup source is not favored by the two youngest grains, while a Brigham Group source satisfies the observed peaks (Yonkee and others, 2014). Detrital signatures of the Brigham Group typically contain a major peak corresponding to the 1,600 Ma–1,800 Ma Yavapai–Mazatzal Province, which often dominates (Yonkee and others, 2014). The presence of young ~1,300 Ma grains, near lack of ~1,450 Ma grains, and dominant peak corresponding to the Yavapai–Mazatzal Province match the Brigham Group (fig. 11).

The absence of argillite clasts, which are common within the Belt Supergroup but generally less durable, is consistent with a Brigham Group source or a recycled Belt Supergroup Source. The cobble analyzed was well rounded and roughly 10 cm in diameter. The nearest Brigham Group source occurs beneath the Miocene Bannock Detachment in the Pocatello area, ~200 km upstream (Carney and Janecke, 2005). A Brigham Group source constrains time of deposition to the Miocene, when the group was exposed beneath the Bannock detachment, and necessitates long-distance transport of coarse clasts (Carney and Janecke, 2005).

The large quantities of feldspathic quartzite add

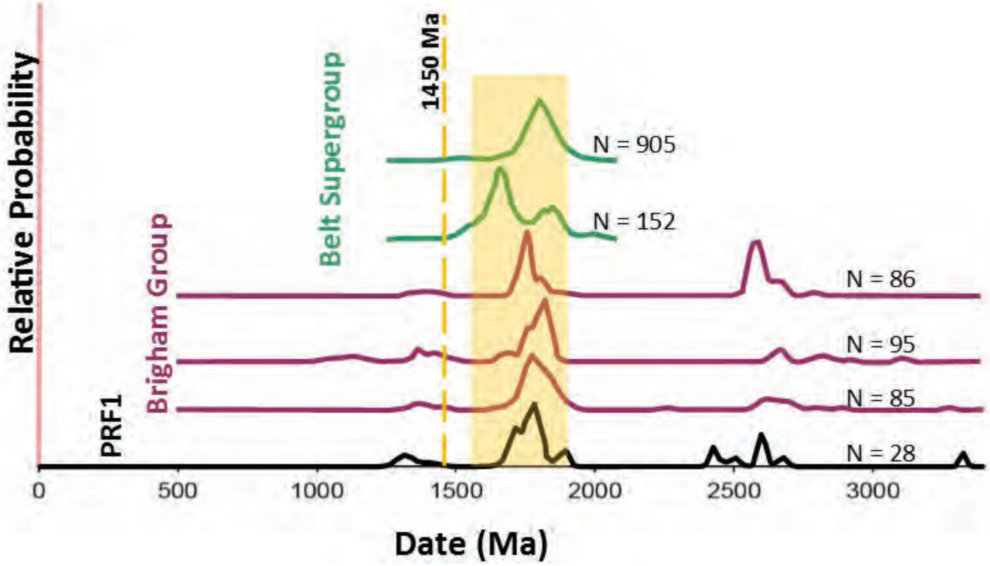

Figure 11. Stacked probability distribution plots of LA-ICPMS analysis of detrital zircons within sample PRF1, Brigham Group (Yonkee and others, 2014) and Belt Supergroup (Jones and others, 2015). Initiation of Belt Basin highlighted

further constraints on source. Feldspathic quartzite is also the dominant lithology within the Kidd Quartzite conglomerate unit of the Beaverhead Group, which has been successfully dated to the late Cretaceous (Ryder and Scholten, 1973). The Kidd is comparable to the Divide deposit in quartzite abundance (Ryder and Scholten, 1973). Although the abundance of feldspathic quartzite in the Kidd was not measured, it appears to be comparable to the Divide. The extent of the Divide and Kidd are comparable, while the Divide exceeds the thickness of the Kidd (Ryder and Scholten, 1973).

Given the weatherability of feldspathic quartzite clasts that have experienced multiple burial/exhumation cycles, it would be expected that such reworking would noticeably reduce the overall volume of material. Such a decrease in abundance within the Divide as compared to the Kidd is not observed. This observation further supports a first cycle Brigham Group source. While a Brigham Group source is hypothesized, reworking of Belt Supergroup clasts cannot be discounted. Given the basal contact relationship of the Divide deposit, the Beaverhead Group has likely provided reworked material, including clasts of Belt Supergroup. However, the results of this study do not support such recycling as being the primary or sole source of feldspathic quartzite.

Progressive Recycling of Laramide Conglomerates

Large feldspathic quartzite boulders within the Divide deposit are likely sourced from the Belt Supergroup, reworked from proximal conglomerates of the basal Beaverhead Group. Orthoquartzite was also added to the channel, at least in part, through slide blocks from bedrock sources to the immediate west. Reworking the basal Beaverhead Group likely provided orthoquartzite and volcanic clasts to the channel. High topography in the west triggered mass wasting events which added siliciclastics and carbonates to the channel. These highly weatherable lithologies were quickly removed from the competent, quartzite cobble-dominated system.

These relationships suggest a long history of progressive recycling punctuated by progressive tectonic pulses. Initial thrusting during the Laramide orogeny transported large volumes of coarse quartzite sediment to the east. These alluvial fans and fluvial systems achieved incredible thickness and extended far beyond the thrust belt (Lindsey, 1972). Competent rivers flowing to the east distributed resistant quartzite cobbles to what would become the Harebell and Pinyon Formations, among others (Lindsey, 1972). This widespread dispersal set the stage for subsequent recycling of resistant quartzite clasts. As the Laramide orogeny waned, broad erosional plains developed until extension in the Late Eocene initiated large volcanic systems such as the Challis volcanic field (Link and others, 2005; Janecke and Snee, 1993). Minor extension in the Oligocene likely transported and recycled coarse conglomerates over broad arid planes (Janecke and Snee, 1993). Basin and Range extension initiated around 17 Ma, providing large volumes of coarse sediment and transporting material far to the north within active grabens. Basin and Range extension has dominated the western U.S. since the Miocene, with pulses of extension rerouting drainages and recycling previous fill.

These relationships between recycling and tectonic activity are evident at the field site. To the immediate west towers the folded and oxidized Beaverhead Group. The alluvial deposits of the Beaverhead Group achieve great thicknesses (up to ~2,000 m) in the southern Beaverhead Mountains (Ryder and Scholten, 1973). Above the Beaverhead Group, separated by a major sequence boundary, lies an extensive river gravel deposit, assigned to the Divide unit (Ryder and Scholten, 1973). The deposit is well cemented and slightly folded, grading up section from quartzite- to limestone-rich. This deposit also contains the dated dacite cobbles, bracketing its age at <98 Ma. While this deposit was not investigated thoroughly, folded strata suggests it was affected by the Laramide orogeny.

At the western boundary of the Divide deposit, a well-cemented limestone conglomerate with highly mature sandstone lenses marks the base. This sequence, from the Beaverhead Group up to the basal limestone conglomerate, highlights a hiatus after the Laramide orogeny, which allowed for progressive reworking to remove immature sediment. The oldest sites of the deposit, pre-fault and transitional conglomerates stratigraphically above the basal limestone conglomerate, show a sudden and drastic decrease in maturity corresponding with addition of new sources (fig. 9). The apparent gradation from the basal limestone conglomerate with highly mature sandstone lenses into a quartzite conglomerate with immature sandstone lenses likely highlights the addition of new sources that mark the onset of a tectonic pulse.

A NNE-striking normal fault became activated after onset of deposition, coinciding with lithification of the oldest units, uplifting units in the footwall to their present location. Units within the footwall are no more lithified than the overlying parts of the deposit, yet evidence of a normal fault is visible. Minimal lithification appears to have occurred before faulting, suggesting pre- and post-fault deposits are comparable. However, after onset of faulting, the coarse clast composition became highly diverse. This is interpreted as coinciding with the onset of the addition of proximal sedimentary lithologies through large mass wasting events. The river system seemed to have been well established prior to movement on this fault, with more mature sediment being transported from more distal sources such as the Bannock Detachment. Initiation of movement on the west-dipping normal fault resulted in mass wasting events from the actively uplifting high topography to the immediate west.

The compositional trends observed and the absence of an un-roofing sequence imply that a majority of the coarse clastic material was recycled from previous gravels or transported great distances rather than being sourced from mass wasting events from the west. Matrix composition shows dominance of chert, carbonate, and siliclastic grains sourced from the immediate west. Presence of the Scott Peak Formation and quartz-veined black chert predates activation of the half-graben. A prominent outcrop of the Scott Peak Formation was found within the river valley, showing that while recycling dominated, first cycle sedimentation was not limited to gravity slides from the west.

In regards to regional tectonics, the transition between the mature basal conglomerate (M88) and the immature gravel deposit (M1, M97, M14, M16) likely highlights onset of extensional Basin and Range deformation in the region. This onset of active faulting added volumes of immature material from bedrock sources in uplifting footwalls far to the south. The presence of other western assemblages that were not shown to be added to the system through mass wasting events were previously transported eastward and then recycled as was the case with reworking of the Beaverhead Group.

Provenance of the Divide Unit Fluvial Deposits

Cobble sources can all be satisfied within the stratigraphy of central Idaho but require multiple stages of transport (Janecke and Snee, 1993). Exotic cobbles, such as the lithic chert arenite, quartz-veined black chert, and feldspathic quartzite have suitable sources in the southern Basin and Range as well that can be satisfied with first cycle sedimentation (Sears and others, 2014). A local source of black chert with quartz veins was found along the paleochannel, bounding the Scott Peak Formation. Lithic chert arenite cobbles match the Diamond Peak Formation of Nevada and the Copper Basin Group of Idaho (Brew and Gordon, 1971; Link and others, 1996). The Copper Basin Group occurs roughly 150 km to the SW.

Thin section analysis did not reveal a tight correlation between cobbles of the field site and the Diamond Peak Formation. The Copper Basin Group is the closest, and therefore most likely, source although it is poorly constrained. Both suitable sources of lithic chert arenite lie a considerable distance from the field site (>150 km), yet cobbles greater than 10 cm were observed within the deposit. While transport of large feldspathic quartzites is contentious, distribution of lithic chert arenites necessitates long-distance transport of large cobbles.

Within the deposit, clasts of orthoquartzite containing small red specks were fairly common (Ryder and Scholten, 1973). These cobbles contain deep pockmarks, resulting from rapid weathering of calcite-cemented zones that occur irregularly within the quartzite. This feature is characteristic of Ordovician orthoquartzites such as the Kinnikinic Quartzite in Idaho, the Swan Peak Quartzite in central/southeastern Idaho, and the Eureka Quartzite, which is found across much of the Great Basin and extends into SE Idaho (McBride, 2012). Photographs and documentations of these distinct red spots were found in several reports regarding the Eureka Quartzite (McBride, 2012; Reber, 1952). They have also been observed in the Swan Peak (Paul Link, personal communication). However, no mentions of this texture were found in reference to the Kinnikinic. Thus, the possibility of long-distance transport from the Eureka and Swan Peak Formations (~250 km to the south) cannot be ruled out. It is important to note that this distinct lithology was found by the author during reconnaissance on Mt. Leidy within the Gros Ventre Range and within a deposit 4.5–2 Ma river gravel on Signal Mountain. Both of these locations are within Jackson Hole, Wyoming, roughly 180 km SE of the Divide deposit. The associated deposits are mapped as the Late Cretaceous-Paleocene Pinyon Formation and as Pliocene glacial till (Love and others, 1992). The "glacial till" deposit contained no observable clay or silt sized grains, only sand and well sorted and rounded quartzite cobbles. These two occurrences highlight the long transport distances that can be achieved by resistant quartzite clasts, considering that the Eureka/Swan Peak Formations and Brigham Group are possible sources.

Speculation on Southern Extent of Paleodrainage

Matrix composition offers support for the north-flowing Paleogene Colorado River hypothesis of Sears (2013). A long lived continental-scale drainage, associated with the Divide unit, would likely be discernible using detrital zircon analyses. Extensive geochronological studies have been conducted for the Snake River Plain (Link and others, 2005). Detrital zircons within modern Medicine Lodge Creek of Idaho provide strong evidence for the Colorado River hypothesis, which proposes a major river drainage that flowed through SW Montana was linked to the early Grand Canyon (Sears, 2013).

Medicine Lodge Creek drains the Divide deposit, among other lithologies. Within the age signature of the Medicine Lodge Creek sands, several anomalies are present, including a Middle Miocene-aged grain (fig. 12). This has previously been attributed to the Yellowstone hotspot system, which spans from 17 Ma to the present (Link and others, 2005). Other distinct spikes are present around 500 Ma and 1,000 Ma, corresponding to grains of the Antler and Grenville Orogeny. Also observable are spikes attributed to the Idaho Batholith and the Challis volcanics. The Antler and recycled Grenville grains are not common throughout the region, but are occasionally observed, typically around central and SE Idaho (Link and others, 2005). Mid Miocene grains are present to the SW but were only observed at four sites (~15%) within the upper ESRP, including Crooked Creek, Medicine Lodge Creek, and Beaver Creek, all of which drain the Divide deposit. The ancestral (Pleistocene) Henry's Fork also contained a Mid Miocene-aged grain, but it is unclear whether this Pleistocene drainage reached the Divide deposit.

When the modern Medicine Lodge Creek detrital signature is compared with the signature taken from the Pliocene Medicine Lodge Creek (3.0–2.5 Ma), the distinct signatures of the Mid Miocene, Antler, and recycled Grenville become absent in the Pliocene. Idaho Batholith and Belt Supergroup/ Brigham Group signatures persist. These sources (with the exclusion of the Brigham) have been identified in the Medicine Lodge beds themselves, which were exposed in Pliocene time

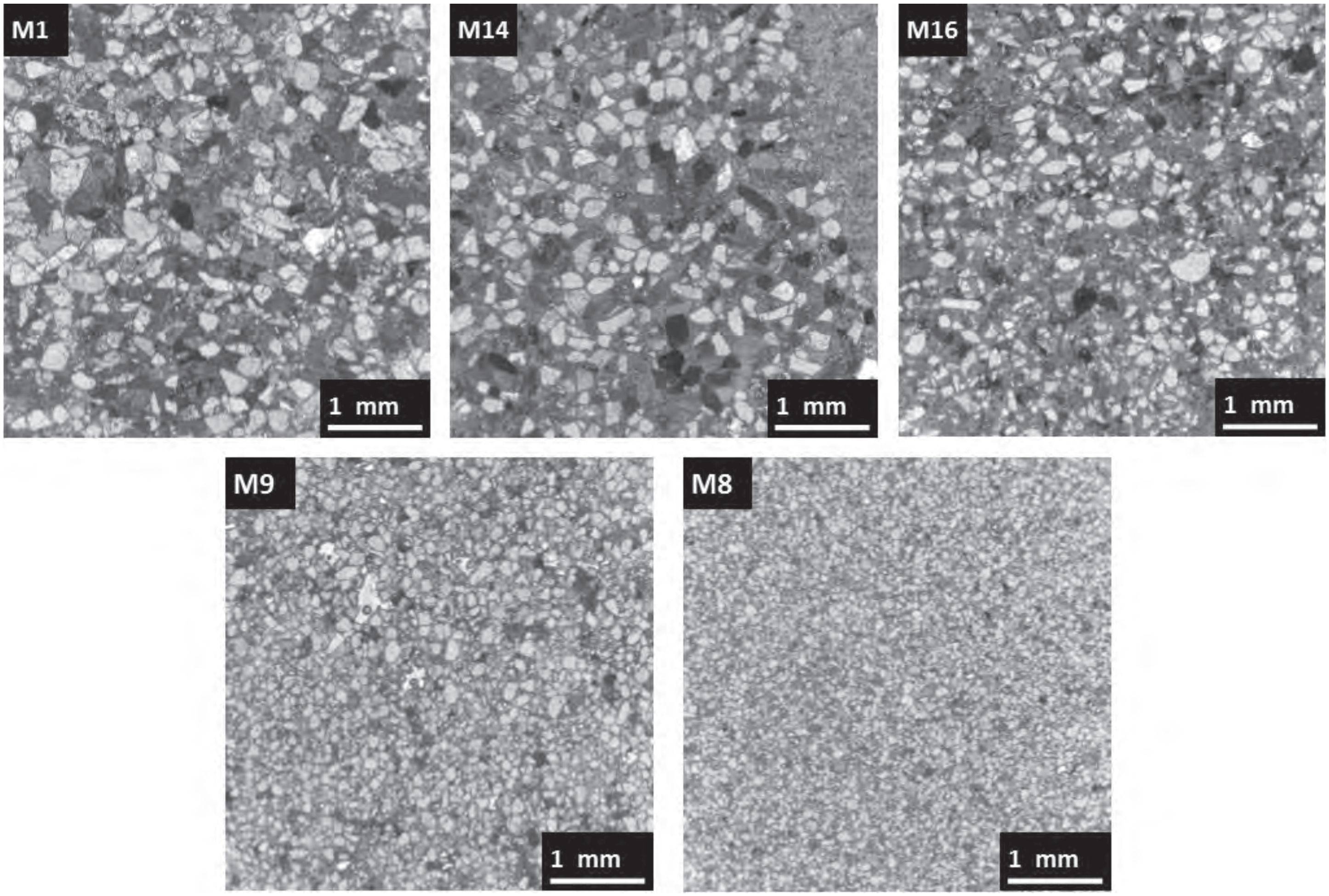

Figure 12. Thin sections of sandstone lenses within various sites. Textural and compositional maturity is drastically different between the two rows of samples. Mature units (M97 and M88) occur in the west, near the basal contact. Immature units (M1, M14, and M16) occur in the east, in both blocks of the syndepositional fault.

(Stroup and others, 2008a).

Evidence from this study suggests the Divide deposit was uplifted and exhumed around 0.365 Ma (Kuntz and others, 1992). Therefore, the Pliocene (3.0–2.5 Ma) Medicine Lodge drainage received no sediment input from the Divide deposit. This suggests that the unique signatures of the Mid Miocene, Antler, and recycled Grenville are unique to the Divide deposit. This hypothesis of uniqueness of detrital zircons within the Divide explains the limited spatial extent of Mid Miocene grains and the temporal change in signature from the Pliocene to the modern Medicine Lodge Creek.

Mid Miocene grains, unique to the Divide deposit, may constrain age and source of the depositional system. Mid Miocene-aged grains dominate northern Nevada, where extensive ignimbrites characterized the Miocene (Link and others, 2005). Such extensive Miocene volcanics are scarce in Idaho, with the exception of the early Yellowstone eruptions. A northern Nevada source is consistent with paleoflow, structural geometry and age interpretations within the Divide unit.

Antler-aged grains occur to the west along the Antler fold-and-thrust belt in central Idaho and in the Great Basin (Link and others, 2005). Antler-aged grains are not present within the Medicine Lodge Beds, which display the best evidence of easterly transport in the Oligocene (Stroup and others, 2008a). This evidence supports a Great Basin source, consistent with observations of the field site.

Recycled Grenville grains are also present in central Idaho, although this trend is once again not observed in the Medicine Lodge Beds (Stroup and others, 2008a). The Brigham Group contains peaks of 1.2–1.0 Ga, corresponding with the Grenville, as well as 1.3–1.5 Ga and 2.7–2.6 Ga (Keeley and others, 2009). These unique peaks are all present within the modern Medicine Lodge Creek, but not the Pliocene

Medicine Lodge Creek sediment (Link and others, 2005). This makes the Brigham Group a strong source candidate for the Divide deposit (Keeley and others, 2009). These temporal and spatial trends are consistent with the Colorado River hypothesis, and support a linkage between the Divide deposit and the Great Basin in the Middle Miocene (Sears, 2013).

Within the matrix sample taken from Paul Reservoir (PRMX1), a major spike occurs around 100 Ma (fig. 10). Detrital grains ranging from 104 ± 5.3 Ma to 83 ± 4.8 Ma account for 29% of the total population (N = 84). No grains younger than Late Cretaceous were identified. The Divide deposit sits on the Late Cretaceous Aspen shale near Paul Reservoir. A local tuff of Late Cretaceous age occurs just below the contact. Ash and tuff layers of ~98 Ma have been identified in the Mowry, Aspen, and Blackleaf shale (Mudge and Sheppard, 1968; Rothfuss and others, 2012; Scott, 2007). Detrital zircon dating within the modern Upper Snake River drainage and the Oligocene Renova Formation locally sourced from the Blackleaf shale show a strong peak around 100 Ma (Link and others, 2005; Stroup and others, 2008a). This relationship shows that reworking of tuffaceous shale of the Late Cretaceous flooded local sediment with Late Cretaceous-aged grains. In the Divide unit, Late Cretaceous grains are attributed to recycling of the basal Aspen shale. This fluvial system shows no connection to the Idaho batholith or Challis volcanics. The detrital signature of matrix-derived zircons shows several other prominent peaks (fig. 10).

An observed Jurassic peak (2 grains) is unique to the ESRP (Link and others, 2005). Jurassic intrusions of northern Nevada are the largest single point source in the region (Miller and Hoisch, 1995; Link and others, 2005). Probability curves from northern Nevada show that only Miocene and Jurassic grains are common (Link and others, 2005). Paleoflow data are consistent with interpretation of a northern Nevada source. It is important to recognize that the Cypress Hill and Wood Mountain Formations of southern Alberta have been hypothesized as being analogous to the Renova and Sixmile Creek Formation (Sears, 2013; Leier and others, 2016). Within these analogous gravels, Jurassic grains are also observed (Leier and others, 2016).

While detrital zircon analyses of these deposits contain larger sample sizes, the distribution and intensity of peaks are comparable to results of this study (Leier and others, 2016).

Within the PRMX1 sample, other observed peaks (12 grains) correspond with the Antler and Grenville orogenies. Grains of these ages are fairly sporadic across the ESRP, generally sourced along the Cordilleran fold-and-thrust belt, which locally occurs to the W and SW of the field site (Link and others, 2005). Two Neoproterozoic grains are observed within the matrix. The nearest point sources occur in the Pioneer Core Complex of Central Idaho and within the Brigham Group near Pocatello (Yonkee and others, 2014; Link and others, 2005). The Miocene Bannock detachment exposes large volumes of Brigham Group and is consistent with paleoflow (Carney and Janecke, 2005). Recycling from the Pioneer Core Complex is also possible, but less likely.

Mesoproterozoic peaks (32 grains) likely correspond to the local Belt Supergroup, but can also be satisfied by the Brigham Group (Ross and Villeneuve, 2003; Yonkee and others, 2014). Archean grains (3) are also observed, likely derived from the Wyoming Province ,which becomes more common to the southeast, particularly in the Upper Snake River drainage, but are also present in many quartzites across the ESRP (Link and others, 2005). These observations are largely speculative given the small populations at hand. The mere existence of such grains is the basis of such source constraints. It should be emphasized that while these data sets are small, they are consistent with several lines of field observations. The sparse presence of grains of the mentioned age ranges illustrates that such sources must exist, yet they likely represent only minor contributions of sediment and are therefore inherently difficult to assess.

Preliminary Constraints on Maximum Age

The detrital matrix sample (PRMX1) contains no Cenozoic-aged grains. The comparable data set of Leier and others (2016) also displays a sparse to absent Cenozoic population in analogous beds of gravel which have been successfully dated to Oliocene–Miocene. Data of Link and others (2005) suggest that Miocene grains are unique to the Divide deposit as discussed previously. The oldest Miocene grain sampled from the Divide drainage was ~18 Ma (Link and others, 2005). Most grains were Mid Miocene in age, around 10 Ma (Link and others, 2005).

The analyzed sample at Paul Reservoir occurs very low in the section and is dominated by Cretaceous-aged grains, locally recycled from the basal Cretaceous Aspen Shale. The base of the gravel deposit may predate extensive volcanism in the southern Basin and Range. The probability of Miocene-aged grains may also be increasingly low near the basal contact where Cretaceous grains dominate.

Unique lithologies such as disharmonically folded crinoidal packstone/wackestones of the Mississippian Scott Peak and Middle Canyon Formations can be found to the northeast within the Miocene–Pliocene Sixmile Creek Formation of the Bozeman Group (Sears and others, 2009). Numerous volcanic time markers constrain age to Miocene within the Sixmile Creek Formation (Sears and others, 2009). Detrital signatures of the Sixmile Creek Formation show similar probability peaks with a near absence of grains between ~15 Ma and 300 Ma, suggesting that Paleogene sources, such as the Challis, are not tightly linked to this fluvial system (Stroup and others, 2008b). Similar results were found in the Oligocene Renova Formation, but locally the Blackleaf Formation adds Cretaceous zircons to the system (Stroup and others, 2008a). Therefore, while the observed absence of Tertiary grains in the analyzed matrix sample of the Divide deposit may suggest that deposition preceded extensive volcanism to the south, it does not falsify a Cenozoic age. Additional detrital zircon analyses are desired to further constrain source and test the hypothesis of linkage to the southern Basin and Range.

Evidence for Volcanic Cover to the Idaho Batholith

Surprising, the dacite cobble (M69) originally hypothesized as belonging to the Eocene Challis Group was found to be Late Cretaceous in age (98 ± 1.7 Ma). No regional volcanic source of this age has been documented (Vuke and others, 2007; Lewis and others, 2012). This age coincides with the Atlanta Lobe of the Idaho Batholith; however, no volcanic cover to the Idaho Batholith has been found (Gaschnig and others, 2010). High ΣREE concentrations and large Eu anomalies observed in sample M69 are consistent with compositional trends of the Idaho Batholith (van Middlesworth and Wood, 1998).

Ash and tuff layers of coincident age are found throughout Late Cretaceous shale units along the Cretaceous Interior Seaway (Mudge and Sheppard, 1968; Rothfuss and others, 2012; Zartman and others, 1995). One such Late Cretaceous porcellanite tuff layer occurs in the Aspen shale, just below the basal contact near Paul Reservoir. Grain size of this ash fall tuff layer indicates the distil relationship between the source. Superposition of well-rounded cobbles to this distal tuff deposit suggest that dacite volcanism was not contemporaneous with gravel deposition and that transportation distance of the ash fall tuff and dacite cobbles is comparable. Compositional trends of volcanic abundance show that the downstream transportation dominated. Large amounts of volcanic material (calculated at ~15 km^3) appear to have either been transported moderate distances from the SW or reworked from existing deposits.

It should be noted that dacite cobbles comparable to the analyzed sample were observed in the folded strata of site M93, which is interpreted as being true Beaverhead Group. Additionally, dacite cobbles are absent in the Kidd quartzite conglomerate unit of the Beaverhead Group (Ryder and Scholten, 1973). Paleoflow (SSE) of the Kidd unit loosely constrains the position of the possible volcanic source to the W or SW of the present-day location of the Divide deposit.

Stratigraphic relationships between the Idaho Batholith and the Challis Group offer further insight into this perplexing issue. The Challis Group in part lies unconformably atop the Atlanta Lobe of the Idaho Batholith (Gashnig and others, 2010).

It is important to recognize that no evidence for sediment derived from the Challis or the intrusive rocks of the Atlanta Lobe of the Idaho Batholith was found in this study. This presents a difficult problem: how could a volcanic layer provide sediment to the system without also sampling the over and underlying lithologies? This question cannot be easily explained under the assumption of a first cycle sediment. However, a recycling scenario can easily explain this relationship.

The preferred interpretation is that Cretaceous volcanic material was transported east in the Late Cretaceous and deposited in the Beaverhead Group, such as is observable at site M93. Heavy erosion during the Larmide and emplacement of the Challis Group likely facilitated in removal of the Cretaceous volcanics. Local recycling of the Beaverhead Group remobilized the dacitic cobbles and incorporated them into the fluvial system of the Divide deposit, which at this time was not coupled to the original source, which was at this time dominated by Challis Group. This interpretation of recycling is consistent with compositional data and field observations of this study, such as the poor level of preservation typically associated with volcanic cobbles. Further investigation is needed to assess the validity of this hypothesis. It is likely that volcanic cover to the Idaho Batholith is confined to the study area, providing the only opportunity to study this topic.

Assignation to the Six Mile Creek Formation

Based on the evidence presented in this study, I propose the Divide deposit be reassigned to the Neogene Sixmile Creek Formation of the Bozeman Group (fig. 8) (Sears and others, 2009). Based on detrital zircon analysis of Link and others (2005), it is hypothesized that additional detrital zircon analysis taken from higher in the section may reveal Miocene-aged grains. Such samples are required to constrain age and assess the hypothesis of a Basin and Range source. It is likely that other units assigned to the Beaverhead Group contain recycled deposits of post-Cretaceous age. Continued work is required to differentiate such deposits.

Throughout this study, similarities between the Harebell and Pinyon Formations of NW Wyoming were recognized. There is likely a connection between the Divide and conglomerates of Jackson Hole, possibly more than just an initial shared source. Results of this study are consistent with much of the pre-Pliocene Colorado River hypothesis of Sears (2013), as are results of Leier and others (2016). Continued investigations of recycled quartzite conglomerates throughout the western US deserve attention in that they are a useful tool in improving our understanding of the tectonic evolution of the region.

CONCLUSION

This field study of the gravel deposits of the southern Beaverhead Mountains supports a Neogene (Mid Miocene–Pliocene) rather than Cretaceous age for the Divide unit. It is suggested that the deposit be reassigned to the Sixmile Creek Formation of the Bozeman Group. Bedrock sources lie predominantly to the west, but most lack evidence of first order transport in a north-flowing river. Preliminary detrital zircon analysis suggests that cobbles of the Brigham Group have been fluvially transported from nearly 200 km to the south. Resistant quartzite clasts belonging to the Belt Supergroup and the Ordovician Kinnikinic were likely recycled from the Late Cretaceous Beaverhead Group but do not reflect the only source of such lithologies. Large volumes of intermediate to felsic volcanic material were likely recycled from the local Beaverhead Group. This 98 Ma volcanic source, hypothesized as cover to the Idaho Batholith, predated deposition and has since been eroded.

Syntectonic deposition associated with a major and long-lived, northerly flowing river system occurred within an active NNE-striking half-graben of probable Middle Miocene age. Locally, tuffaceous volcanic material was recycled from the Cretaceous Aspen shale or an equivalent. Large mass-wasting events added local carbonate, siliciclastic, and quartzite units from proximal sources in the west. High competence and a coarse quartzite clast bed load removed much of the coarse sediment sourced from local carbonate and siliciclastic units. Long-lived, long-distance transport of fine sediments from what is now the Great Basin is hypothesized but poorly constrained. Progressive recycling of quartzite clasts persisted through time. Deposition ceased between 4.5 and 4.1 Ma as a result of Basin and Range tectonics and volcanism associated with the Yellowstone volcanic system, which shifted the Continental Divide eastward and established a drainage divide within the ESRP. Movement along the Middle Creek Butte fault exhumed the gravel deposit around 0.365 Ma.

REFERENCES

Brew, D.A., and Gordon Jr, M., 1971, Mississippian stratigraphy of the Diamond Peak area, Eureka County, Nevada, with a section on the biostratigraphy and age of the Carboniferous formations: U.S. Geological Survey Professional Paper 661, 84 p.

Carney, S.M., and Janecke, S.U., 2005, Excision and the original low dip of the Miocene-Pliocene Bannock detachment system, SE Idaho: Northern cousin of the Sevier Desert detachment: Geological Society of America Bulletin, v. 117, no. 3–4, p. 334–353.

Evans, K.V., and Zartman, R.E. 1990, U-Th-Pb and Rb-Sr geochronology of middle Proterozoic granite and augen gneiss, Salmon River Mountains, east-central Idaho: Geological Society of America Bulletin v. 102, no. 1, p. 63–73.

Gaschnig, R.M., Vervoort, J.D., Lewis, R.S., and McClelland, W.C., 2010, Migrating magmatism in the northern US Cordillera: In situ U-Pb geochronology of the Idaho batholiths: Contributions to Mineralogy and Petrology, v. 159, no. 6, p. 86 –883.

Leier, A., Leckie, D.A., Ames, C. and Chesley, J., 2016, Detrital zircon data from Paleogene-Neogene fluvial conglomerates on the Canadian plains: Geological Society of America Abstracts with Programs, v. 48, no. 6.

Link, P.K., Fanning, C.M. and Beranek, L.P., 2005, Reliability and longitudinal change of detrital-zircon age spectra in the Snake River system, Idaho and Wyoming: An example of reproducing the bumpy barcode: Sedimentary Geology, v. 182, no. 1, p. 101–142.

Lewis, R.S., Link, P.K., Stanford, L.R., and Long, S.P., 2012. Geologic map of Idaho: Idaho Geological Survey M-9, scale 1:750,000, 18 p.

Janecke, S.U. and Snee, L.W., 1993. Timing and episodicity of middle Eocene volcanism and onset of conglomerate deposition, Idaho: Journal of Geology, v. 101, no. 5, p. 603–621.

Jones, J.V., Daniel, C.G., and Doe, M.F., 2015. Tectonic and sedimentary linkages between the Belt-Purcell basin and southwestern Laurentia during the Mesoproterozoic, ca. 1.60–1.40 Ga.: Lithosphere, vol. 7, no. 4, p. 465–472.

Kuntz, M.A., Covington, H.R., and Schorr, L.J., 1992, An overview of basaltic volcanism of the eastern Snake River Plain, Idaho, in Link, P.K, Kuntz, M.A., Platt, L.B., Regional geology of eastern Idaho and western Wyoming: Geological Society of America Memoir 179, p. 227–267.

Keeley, J.A., Link, P.K. and Dehler, C.M., 2009, Detrital zircon analysis of the Neoproterozoic to Cambrian Brigham Group in the southern Portneuf Range, southeast Idaho: Geological Society of America Abstracts with Programs, vol. 41, no. 6, p. 45.

Lindsey, D.A., 1972, Sedimentary petrology and paleocurrents of the Harebell Formation, Pinyon Conglomerate, and associated coarse clastic deposits, northwestern Wyoming. U.S. Geological Survey Professional Paper 734-B, 67 p.

Link, P.K., Warren, E., Preacher, J.M., and Skipp, B., 1996, Stratigraphic analysis and interpretation of the Mississippian Copper Basin Group, McGowan Creek Formation, and White Knob Limestone, south-central Idaho, in Longman, M.W., and Sonnenfeld, M.D., eds., Paleozoic Systems of the Rocky Mountain Region: Denver, Rocky Mountain Section, SEPM (Society for Sedimentary Geology), p. 117–144.

Link, P.K., Fanning, C.M. and Beranek, L.P., 2005, Reliability and longitudinal change of detrital-zircon age spectra in the Snake River system, Idaho and Wyoming: An example of reproducing the bumpy barcode: Sedimentary Geology, vol. 182, no. 1, p. 101–142.

Link, P.K., Warren, I., Preacher, J.M. and Skipp, B., 1996. Stratigraphic analysis and interpretation of the Mississippian Copper Basin Group, McGowan Creek Formation, and White Knob Limestone, south-central Idaho, in Longman, M.W. and Sonnenfeld, M.D., Paleozoic systems of the Rocky Mountain region: Rocky Mountain Section, Society for Sedimentary Geology (SEPM), p. 117–144.

Love, J.D., 1956, Cretaceous and Tertiary stratigraphy of the Jackson Hole area, northwestern Wyoming: Wyoming Geological Association Guidebook 11th Annual Conference, p. 76–93.

Love, J.D., Reed, J.C., Jr, and Christiansen, A.C., 1992, Geologic map of Grand Teton National Park, Wyoming: U.S. Geological Survey Miscellaneous Investigations Series Map I-2031, scale 1:62,500.

Lowell, W.R., and Klepper, M.R., 1953, Beaverhead Formation, a Laramide deposit in Beaverhead County, Montana; Geological Society of America Bulletin, vol. 64, n. ?, p. 235–243.

McBride, E.F., 2012, Petrology of the Eureka Quartzite (Middle and Late Ordovician), Utah and Nevada, USA: Rocky Mountain Geology, vol. 47, no. 2, p. 81–111.

Miller, D.M. and Hoisch, T.D., 1995, Jurassic tectonics of northeastern Nevada and northwestern Utah from the perspective of barometric studies: Geological Society of America Special Paper 299, p. 267–294.

Morgan, L.A., and McIntosh, W.C., 2005, Timing and development of the Heise volcanic field, Snake River Plain, Idaho, western USA: Geological Society of America Bulletin, v. 117, no. 3-4, p. 288–306.

Mudge, M.R., and Sheppard, R.A., 1968, Provenance of igneous rocks in Cretaceous conglomerates in northwestern Montana: U.S. Geological Survey Research, p. D137–D146.

Nichols, D.J., Perry, W.J., and Johns, J.H., 1985, Reinterpretation of the palynology and age of Laramide syntectonic deposits, southwestern Montana, and revision of the Beaverhead Group: Geology, vol. 13, no. 2, p. 149–153.

Parker, S., 2015, Deformed river gravels of the southern Beaverhead Mountains; Neotectonic implications. Rocky Mountain Section, 67th annual Meeting. Geological Society of America Abstracts with Programs, vol. 47, no. 6, p. 4.

Pierce, K.L., and Morgan, L.A., 2009, Is the track of the Yellowstone hotspot driven by a deep mantle plume? Review of volcanism, faulting, and uplift in light of new data: Journal of Volcanology and Geothermal Research, vol. 188, no. 1, p. 1–25.

Reber, S.J., 1952,Stratigraphy and structure of the south-central and northern Beaver Dam Mountains, Utah, in Geological Society of Utah, Guidebook to the Geology of Utah,. p. 101–108.

Ross, G.M. and Villeneuve, M., 2003, Provenance of the Mesoproterozoic (1.45 Ga) Belt basin (western North America): Another piece in the pre-Rodinia paleogeographic puzzle: Geological Society of America Bulletin, vol. 115, no.10, p. 1191–1217.

Rothfuss, J.L., Lielke, K., and Weislogel, A.L., 2012, Application of detrital zircon provenance in paleogeographic reconstruction of an intermontane basin system, Paleogene Renova Formation, southwest Montana: Geological Society of America Special Paper 487, p. 63–95.

Ryder, R.T., and Scholten, R., 1973, Syntectonic conglomerates in southwestern Montana: Their nature, origin, and tectonic significance: Geological Society of America Bulletin, vol. 84, no. 3, p. 773–796.

Scholten, R., Keenmon, K.A., and Kupsch, W.O., 1955, Geology of the Lima region, southwestern Montana and adjacent Idaho: Geological Society of America Bulletin, vol. 66, no. 4, p. 345–404.

Schmitt, J.G., and Steidtmann, J.R., 1990, Interior ramp-supported uplifts: Implications for sediment provenance in foreland basins: Geological Society of America Bulletin, vol. 102, no. 4, p. 494–501.

Scott, R.W., 2007, Calibration of the Albian/Cenomanian boundary by ammonite biostratigraphy: US Western Interior: Acta Geologica Sinica (English Edition), vol. 81, no. 6, p. 940– 948.

Sears, J.W., and Fritz, W.J., 1998, Cenozoic tilt domains in southwestern Montana; interference among three generations of extensional fault systems, in Faulds, J.E., and Stewart, J.H., eds., Accommodation zones and transfer zones; the regional segmentation of the Basin and Range Province, Geological Society of America Special Paper 323, p. 241–247.

Sears, J.W., Hendrix, M.S., Thomas, R.C., and Fritz, W.J., 2009, Stratigraphic record of the Yellowstone hotspot track, Neogene Sixmile Creek Formation grabens, southwest Montana: Journal of Volcanology and Geothermal Research, vol.188, no.1, p. 250–259.

Sears, J.W., 2013, Late Oligocene–early Miocene Grand Canyon: A Canadian connection? GSA Today, vol. 23, no.11, p. 4–10.

Sears, J.W., Link, P.K., and Karlstrom, K.E., 2014, Amazon-scale, Mid-Cenozoic “Bell River” drainage basin of North America: Implications for Tectonics of the Western Interior: GSA Abstracts with Programs, vol. 46, no. 5, p. 20.

Stroup, C.N., Link, P.K., Janecke, S.U., Fanning, C.M. and Yaxley, G.M., 2008a, Eocene to Oligocene provenance and drainage in extensional basins of southwest Montana and east-central Idaho:Arizona Geological Society Digest, vol. 22, p. 529–546.

Stroup, C. N., Link, P. K., and Fanning, C. M., 2008b, Provenance of late Miocene fluvial strata of the Sixmile Creek Formation, southwest Montana: evidence from detrital zircon: Northwest Geology, v. 37, p. 69–84.

van Middlesworth, P.E., and Wood, S.A., 1998, The aqueous geochemistry of the rare earth elements and yttrium; Part 7, REE, Th and U contents in thermal springs associated with the Idaho batholith: Applied Geochemistry, vol. 13, no. 7, p. 861–884.

Vuke, S.M., Porter, K.W., Lonn, J.D., and Lopez, D.A., 2007, Geologic map of Montana: Montana Bureau of Mines and Geology Geologic Map 62, scale 1:500,000.

Yonkee, W.A., Dehler, C.D., Link, P.K., Balgord, E.A., Keeley, J.A., Hayes, D.S., Wells, M.L., Fanning, C.M. and Johnston, S. M., 2014, Tectono-stratigraphic framework of Neoproterozoic to Cambrian strata, west-central US: Protracted rifting, glaciation, and evolution of the North American Cordilleran margin: Earth-Science Reviews: vol. 136, p. 59–95.

Zartman R.E., Smith J.V., 1995, Mineralogy and U-Th-Pb ages of a uranium bearing jasperoid vein from the Sunshine mine, Coeur d'Alene district, Idaho, in Leon T. Silver Symposium: Pasadena, California Institute of Technology, p. 37–41.

VOLUMES OF RECENTLY ERUPTED RHYOLITE LAVA FLOWS IN THE YELLOWSTONE PLATEAU VOLCANIC FIELD

D.K. Moore, Cameron Taylor,* and Schuyler Robinson*

Brigham Young University, Rexburg, Idaho

*Undergraduate students
Corresponding author: Dan K. Moore, moored@byu.edu

INTRODUCTION

The Yellowstone–Snake River Plain magmatic province encompasses the Yellowstone Plateau volcanic field in the northeast, the Eastern Snake River Plain in the southwest, and the area near the Idaho–Nevada–Oregon border. The province consists of voluminous eruptions of rhyolite and basalt. Rhyolite magmatism began in the early Miocene and migrated northeast, as the North American plate moved southwest over the Yellowstone hotspot. Rhyolite is abundant on the Yellowstone plateau. In the Island Park area, basaltic lava flows have begun burying the rhyolite, and in the southwestern Snake River Plain, up to several thousands of feet of basalt cover the rhyolite.

The Yellowstone Plateau volcanic field is an upland containing abundant rhyolite. It includes the Yellowstone III caldera and surrounding area (fig. 1). The plateau transitions into Basin and Range mountains and valleys to the north and south and the Absaroka Mountains to the east. Island Park and the Snake River Plain bound the plateau to the west and southwest. Christiansen (2001) reports three cycles of rhyolite magmatism. These cycles began with rhyolite lava eruptions along the ring fracture zone and a climactic eruption; they were followed by smaller rhyolite eruptions during periods of relative quiescence. The climactic eruptions consist of the voluminous (2,450 km^3) Huckleberry Ridge Tuff at 2.1 Ma, which formed the Yellowstone I caldera; the smaller (280 km^3) Mesa Falls Tuff at 1.3 Ma, which produced the Yellowstone II caldera; and the Lava Creek Tuff (1,000 km^3) at 0.64 Ma, which generated the Yellowstone III caldera (fig. 1). Eruptions of rhyolite lava and subordinate tuff followed the third climactic eruption. Together, these flows mostly filled the Yellowstone III caldera and overflowed its western boundary (fig. 1). The spatial and temporal distribution, volume of these eruptions, and the composition of the rocks they produced inform our understanding of Yellowstone magmatic cycles and of the likely nature of future volcanism. This short descriptive paper reports estimated volumes of the rhyolite lava flows and tuffs that erupted in the Yellowstone Plateau volcanic field after the Lava Creek Tuff.

METHODS

We calculated minimum volumes for lava flows (and tuffs) using conservative estimates of unit areas and thicknesses. We measured the surface areas of flows in ArcGIS, using the unit distributions of Christiansen (2001; fig. 1). We estimated thicknesses using the average elevation of the flow, measured in ArcGIS, and conservative inferred estimates of the average elevation of the pre-flow surface. For young flows, accurate estimates of the elevation of the pre-flow surface are straightforward. On the plateau, flows and tuffs erupted on a relatively flat surface (fig. 1). Some lava flows that erupted near the western margin of the caldera moved west, down the flank of the plateau and onto the floor of Island Park (e.g., the West Yellowstone flow; 35 in fig. 1). We calculated the volume of these flows in three portions—the relatively flat-lying areas on the plateau and in Island Park and the dipping zones on the flank of the plateau. The length and width yielded the surface area for the flank zones.

The accuracy of our measurements decreases with age: the uncertainties of area and thickness estimates are low for young flows that are well exposed and relatively uneroded, and most of this uncertainty lies in the estimates of thickness.

We used the Ar and relative ages of Christiansen (2001) to analyze the temporal patterns of erupted lava volumes. There are inconsistencies between reported absolute and relative ages for a few units; e.g., field relations indicate one unit is older than another, whereas the Ar ages indicate the opposite relation. We use Ar ages to sequence dated flows and relative ages and age inferences to sequence undated flows.

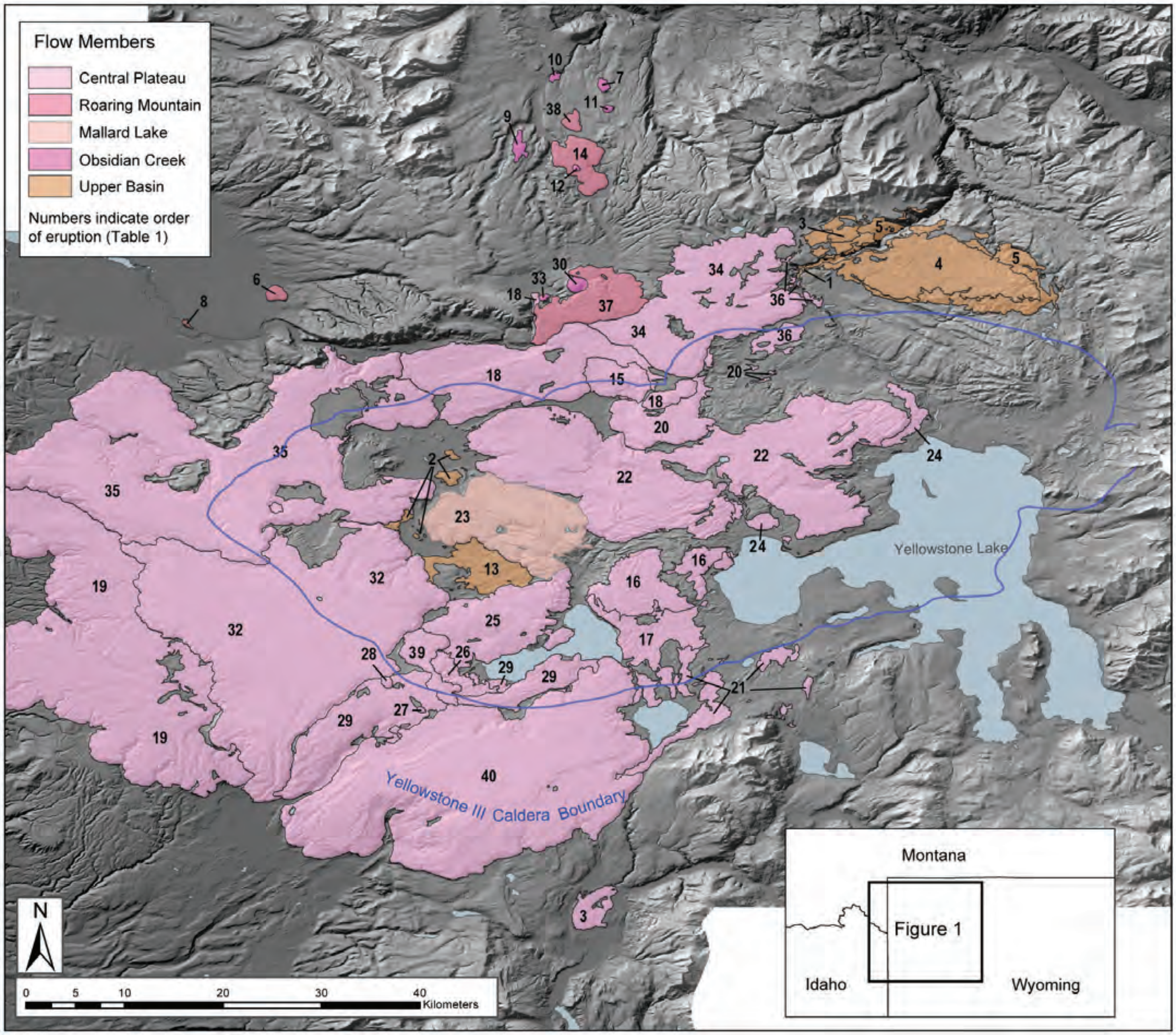

Figure 1. Shaded relief map showing the exposed distribution of rhyolite units that erupted after the Lava Creek Tuff (after Christiansen, 2001). Rhyolite unit numbers are the sequence numbers of table 1. This table provides the name and age of each unit.

RESULTS AND DISCUSSION

Table 1 lists the ages and volume estimates of volcanic units erupted since 640 ka; figure 2 displays these data. During this period, at least 40 eruptions produced ~650 km^3 of rhyolite magma. This volume is more than twice that erupted in the smallest of the Yellowstone climactic eruptions (Mesa Falls Tuff, ~280 km^3) and ~10% of the total volume of rhyolite (~6,500 km^3) that Christiansen (2001) suggested erupted in the Yellowstone Plateau volcanic field.

About 100 ky passed between emplacement of the Lava Creek Tuff and the first eruption (table 1; fig. 2). In the subsequent ~35 ka, there were at least 4 more small eruptions, followed by a ~240 ky period in which as few as 7 tiny eruptions occurred. Volcanic activity increased between 200 and 70 ka, a period in which at least 28 eruptions generated most of the post-Lava-Creek magma. Several large, mostly recent eruptions produced most of magma (fig. 2): 64% of the magma erupted in the 5 largest flows, all of which are younger than 160 ka; 90% erupted in the 13 largest units, all of which are younger than 162 ka; and 99% of the magma erupted in the 22 largest units, all but three of which are younger than 198 ka. Since nearly all of the magma erupted recently, the larger uncertainties in volume estimates that are associated with older units have little effect on the estimated total volume.

Figure 3 shows the temporal distribution of erupt-

Table 1. Rhyolite lava flows and tuffs erupted after the Lava Creek Tuff (640 ka), in or near the Yellowstone III caldera. Total erupted volume is 654 km^3. Sequence numbers indicate the order of eruption and identify units in figure 1. Map symbols are from Christiansen (2001), for use with his maps. Double lines separate units into four temporal groups; dark lines separate temporal subgroups (fig. 3). Italicized dates indicate units with only relative ages; we infer ages and uncertainties using the field relations and age inferences reported by Christiansen (2001).

Eruption Sequence	Age (ka)	Estimated Volume (km^3)	Unit Name	Map Symbol
40	70 ± 2	98	Pitchstone Plateau Flow	Qpcp
39	72 ± 3	4	Grants Pass Flow	Qpcg
38	80 ± 2	0.2	Crystal Spring	Qprs
37	90 ± 2	4	Gibbon River Flow	Qprg
36	102 ± 4	5	Hayden Valley Flow	Qpch
35	108 ± 1	76	West Yellowstone Flow	Qpcy
34	110 ± 3	28	Solfatara Plateau Flow	Qpcf
33	*110 ± 20*	0.04	Paintpot Hill Dome	Qpop
32	112 ± 2	100	Summit Lake Flow	Qpcs
31	*115 ± 45*	1	Moose Falls Flow	Qpcmf
30	116 ± 8	0.3	Gibbon Hill Dome	Qpoh
29	117 ± 2	21	Bechler River Flow	Qpcr
28	*135 ± 20*	0.3	Trischman Knob Dome	Qpct
27	*135 ± 20*	1	Douglass Knob Dome	Qpck
26	*135 ± 20*	1	Tuff of Cold Mountain Creek	Qpco
25	*135 ± 20*	17	Spring Creek Flow	Qpcc
24	147 ± 4	13	West Thumb Flow	Qpcw
23	151 ± 4	10	Mallard Lake Flow	Qpm
22	153 ± 2	73	Elephant Back Flow	Qpce
21	155 ± 3	30	Aster Creek Flow	Qpca
20	*157 ± 6*	15	Spruce Creek Flow	Qpcu
19	160 ± 3	74	Buffalo Lake Flow	Qpcb
18	160 ± 2	9	Nez Perce Creek Flow	Qpcn
17	162 ± 2	6	Tuff of Bluff Point	Qpcl
16	162 ± 2.5	35	Dry Creek Flow	Qpcd
15	165 ± 4	2	Mary Lake Flow	Qpcm
14	183 ± 3	1	Obsidian Cliff Flow	Qpro
13	198 ± 8	7	Scaup Lake Flow	Qpul
12	*290 ± 110*	0.1	Landmark Dome	Qpol
11	*290 ± 110*	0.04	Apollinaris Spring Dome	Qpoa
10	*290 ± 110*	0.1	Mixed lavas of Gardner River	Qpog
9	*290 ± 110*	0.1	Mixed lavas of Grizzly Lake	Qpoz
8	*290 ± 110*	0.02	Riverside Flow	Qprr
7	316 ± 5	0.1	Willow Park Dome	Qpow
6	399 ± 3	0.1	Cougar Creek Dome	Qprc
5	479 ± 10	8	Tuff of Sulphur Creek	Qpus
4	484 ± 15	7	Canyon Flow	Qpuc
3	489 ± 42	1	Dunraven Road Flow	Qpud
2	516 ± 7	5	Biscuit Basin Flow	Qpub
1	533.5 ± 54.5	0.004	Tuff of Uncle Tom's Trail	Qput

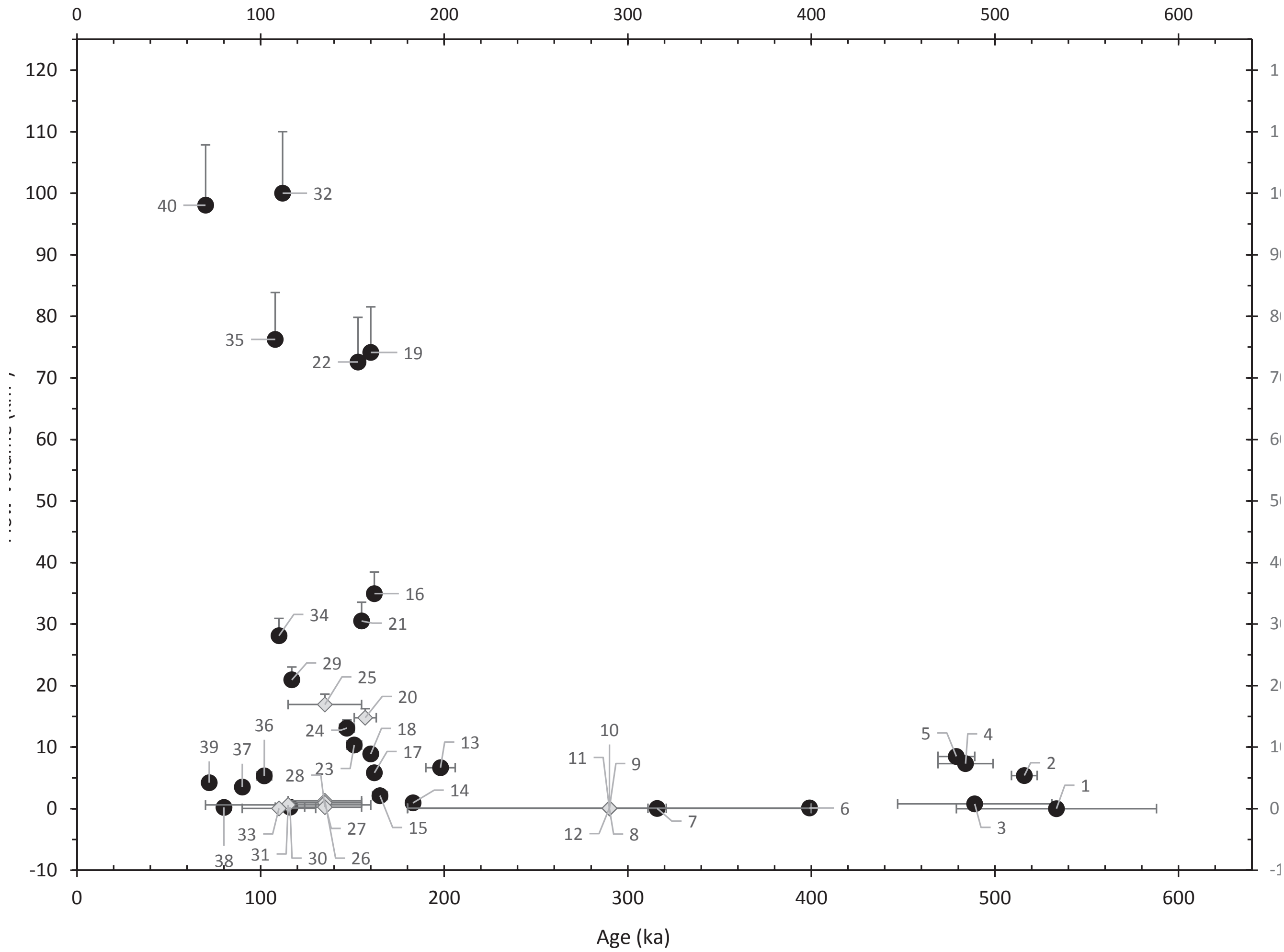

Figure 2. Graph of age and volume of rhyolite units that erupted after the Lava Creek Tuff. Circles show units with absolute ages; diamonds show units with relative ages. Horizontal lines show uncertainty in age. The volumes are minimum estimates; vertical lines show +10% error in volume. Data point (unit) numbers correspond to the sequence numbers in table 1.

ed magma volume. The gray line shows cumulative volume through time; the dashed line is a +10% error line. The black line shows the time-averaged distribution of volume. We produced this line by summing the volume of magma erupted in each 20-ky interval, assigning this value to the midpoint of the interval, and smoothing the line. The line shows the general character of erupted volume through time.

Post-Lava-Creek eruptions occurred in four temporal groups (fig. 3; table 1). The first group extends from 640 to about 520 ka and includes at least one small rhyolite unit. The second group (520–480 ka) consists of at least 4 flows that erupted 22 km^3 of magma, 3% of the post-Lava-Creek cycle III total. At least 7 small eruptions (<0.5 km^3) constitute the third group (480–200 ka). The fourth group (200–70 ka) produced over 95% of the magma (624 km^3), in at least 28 eruptions. This group contains three subgroups: the first (200–130 ka) produced 294 km^3 (45% of the post-Lava-Creek magma) in at least 16 eruptions; the second (130–90 ka) generated 235 km^3 (36%) in at least 8 eruptions; and the third (90–70 ka) formed 102 km^3 (16%) in at least 4 eruptions.

The rate of magma production varied through time (fig. 3): during the first and third groups it was negligible; during the second group it was 0.6 km^3/ka ; and during the fourth group it was ~5 km^3/ka. The three subgroups of the fourth group also produced magma at different rates (fig. 3): ~4 km^3/ka from 200 to 130 ka; ~16 km^3/ka from 117 to 102 ka; and ~5 km^3/ka from 90 to 70 ka. The background production rate since the beginning of cycle I volcanism is ~3 km^3/ka (6,500 km^3 in 2,100 ka) if climactic eruptions are included and ~1 km^3/ka (2,770 km^3 in 2,100 ka) for the periods between climactic eruptions. The post-Lava-Creek production rate is ~1 km^3/ka (654 km^3 in 640 ka), consistent with that from other periods.

Does group four magmatism represent a climactic

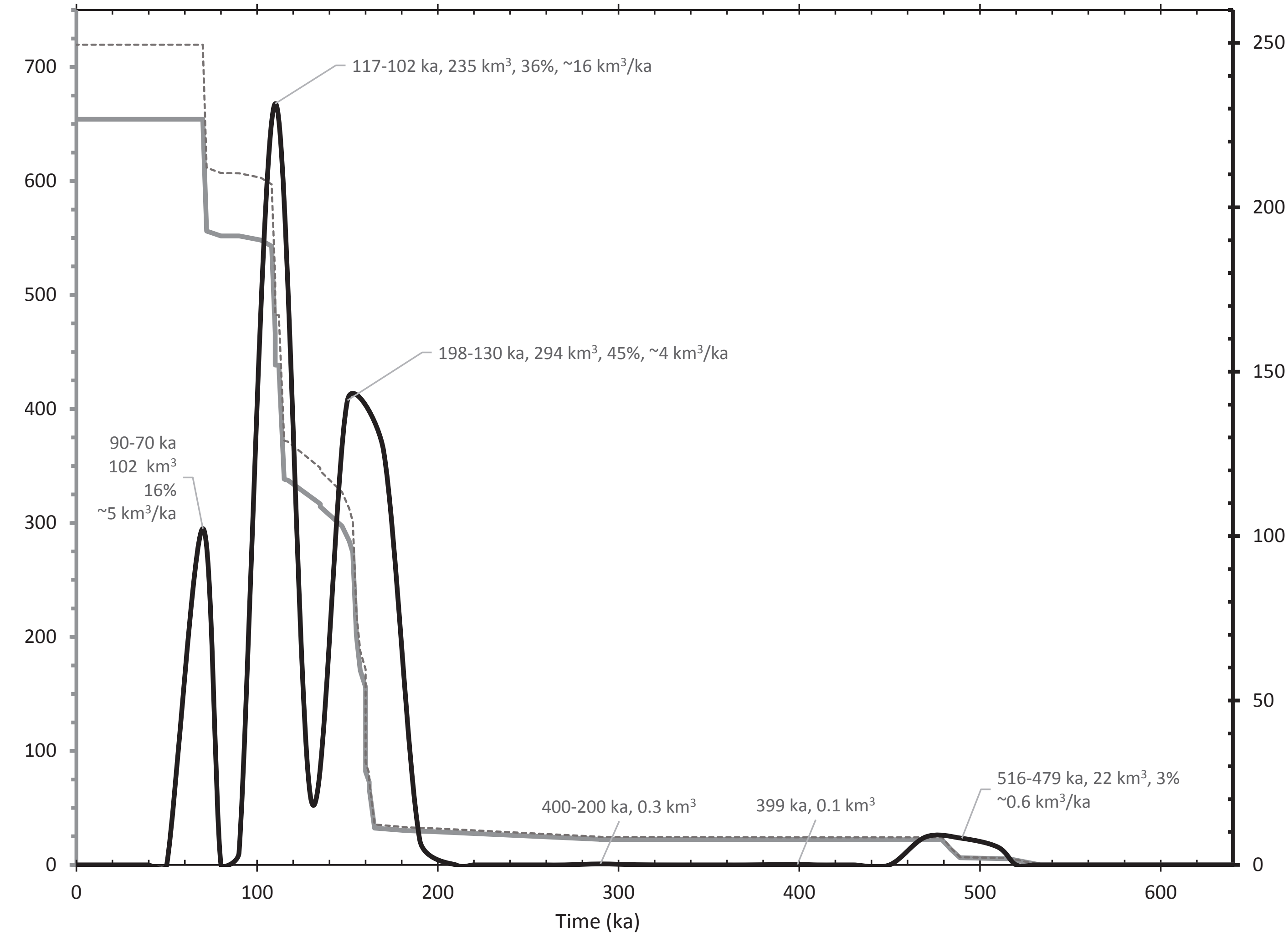

Figure 3. Temporal distribution of erupted magma volume. The black line, which uses the right axis, shows the time-averaged distribution of volume. We produced this line by summing the volume of magma erupted in each 20-ky interval, assigning this value to the midpoint of the interval, and smoothing the line. The gray line, which uses the left axis, shows cumulative volume through time; the dashed line is a +10% error line.

phase that instead erupted effusively, or does it represent a period of voluminous volcanism between climactic eruptions? Unfortunately, there are insufficient data to answer this question definitely. The volume of magma erupted in group four (624 km^3; fig. 3) is more than twice that in the Mesa Falls Tuff and more than half that in the Lava Creek Tuff, suggesting that group four represents magma that could have produced a super-eruption. However, eruption rates suggest the opposite. The post-Lava-Creek production rate is consistent with the average rate of eruption for periods between climactic eruptions (both ~1 km^3/ka). Even so, the eruption of group four magma was voluminous and rapid—particularly for the second subgroup, which generated magma more than five times faster than the overall production rate (16 vs. 3 km^3/ka) and 16 times the inter-climactic rate.

FUTURE WORK

The temporal distribution of erupted volumes (fig. 3) presents interesting opportunities for further study. For example, was the magma erupted during group four produced deep in the crust or was it produced by remelting of the shallow Lava Creek batholith? If the latter, is this part of the waning stages of a Yellowstone–Snake River Plain rhyolite volcanic field? I.e.,in between the stages where basalt does and does not erupt inside the caldera, does basalt rise into the shallow subsurface to remelt a preexisting granitic intrusion? Another interesting line of inquiry: was there a rise in heat flux associated with the group four pulses of volcanism, and did this affect uplift rates in the area?

REFERENCES

Christiansen, R.L., 2001, The Quaternary and Pliocene Yellowstone Plateau volcanic field of Wyoming, Idaho, and Montana: United States Geological

Bowman School in Newdale: This one-room schoolhouse is made of blocks of Huckleberry Ridge Tuff and is located near Newdale, Idaho. (Photo courtesy of the Upper Valley Historical Society)

VERTICAL DENSITY VARIATIONS IN CLIMACTIC TUFFS OF THE YELLOWSTONE PLATEAU VOLCANIC FIELD, SOUTHEAST IDAHO

D.K. Moore, Blake Rothlisberger,* Braden Hartmann,* and Greg L. Melton

Brigham Young University, Rexburg, Idaho

**Undergraduate students*
Corresponding author: Dan K. Moore, moored@byui.edu

INTRODUCTION

The Yellowstone–Snake River Plain magmatic province encompasses the Yellowstone Plateau Volcanic Field in the northeast, the Eastern Snake River Plain in the southwest, and the area near the Idaho–Nevada–Oregon border. The province consists of voluminous deposits of rhyolite and basalt. Rhyolite magmatism began in the early Miocene and migrated northeast, as the North American plate moved southwest over the Yellowstone hotspot. Although rhyolite is abundant on the Yellowstone plateau, the Island Park area contains basalt flows that have begun burying the rhyolite. In the southwestern Snake River Plain, up to thousands of feet of basalt cover the rhyolite.

Christiansen (2001) reports three cycles of rhyolite magmatism. These cycles began with rhyolite lava eruptions along a ring fracture zone and a climactic eruption and were followed by smaller rhyolite eruptions during periods of relative quiescence. The climactic eruptions consist of the voluminous (2450 km^3) Huckleberry Ridge Tuff at 2.1 Ma, which formed the Yellowstone I caldera; the smaller (280 km^3) Mesa Falls Tuff at 1.3 Ma, which produced the Yellowstone II caldera; and the Lava Creek Tuff (1000 km^3) at 0.64 Ma, which generated the Yellowstone III caldera (fig. 1).

Pyroclastic flows from the Yellowstone climactic eruptions deposited hot ash that compacted and welded under its own weight, which increased the density of the resultant tuffs. Vertical density variations in the tuffs result from, among other variables, the temperature, thickness, and rate of cooling of the ash deposits (Riehle and others, 1995). The density of a rhyolite ash-flow tuff is a proxy for the degree of post-depositional welding. Riehle and others (1995, 2010) modeled the welding/density profiles of rhyolite ignimbrite sheets. Their modeling indicates correlations between maximum density (welding) and temperature of emplacement and between density reversals and the durations of intervals between eruptions.

This short, descriptive paper reports vertical density variations in exposed portions of the Huckleberry Ridge, Mesa Falls, and Lava Creek Tuffs, and uses qualitative correlations of density—temperature and density reversal—eruption timing to infer the relative emplacement temperatures and eruption histories of these tuffs.

METHODS

We determined the vertical density variations of each ignimbrite by collecting samples at intervals throughout the exposed thickness at each location, measuring the mass and volume of specimens, and calculating densities. Accessible vertical exposures of thick tuffs are rare. Our sampling strategy assumes that the density profile of an ignimbrite is laterally continuous at the outcrop scale, i.e., that elevation and stratigraphic/depositional position correlate well across closely spaced outcrops. We sampled exposures of thin tuffs vertically. We sampled thick tuffs in a stepwise fashion, across nearby outcrops, then assembled a psuedovertical. The pattern coherence of a specific density profile suggests whether the validity of the approach at that location.

We calculated the density of each sample (ρs) using the formula $\rho s = ma / (ma - mw)$, where ma is the mass of the sample in air and mw is the mass when suspended in water. The denominator in the equation is the mass of the water displaced by the sample and, by extension, the volume of the sample. We used cylindrical and rectangular samples with masses of about 50 g. We coated samples with a layer of spray adhesive covered by a layer of concrete sealant. (Both coatings were necessary to seal most samples effectively,

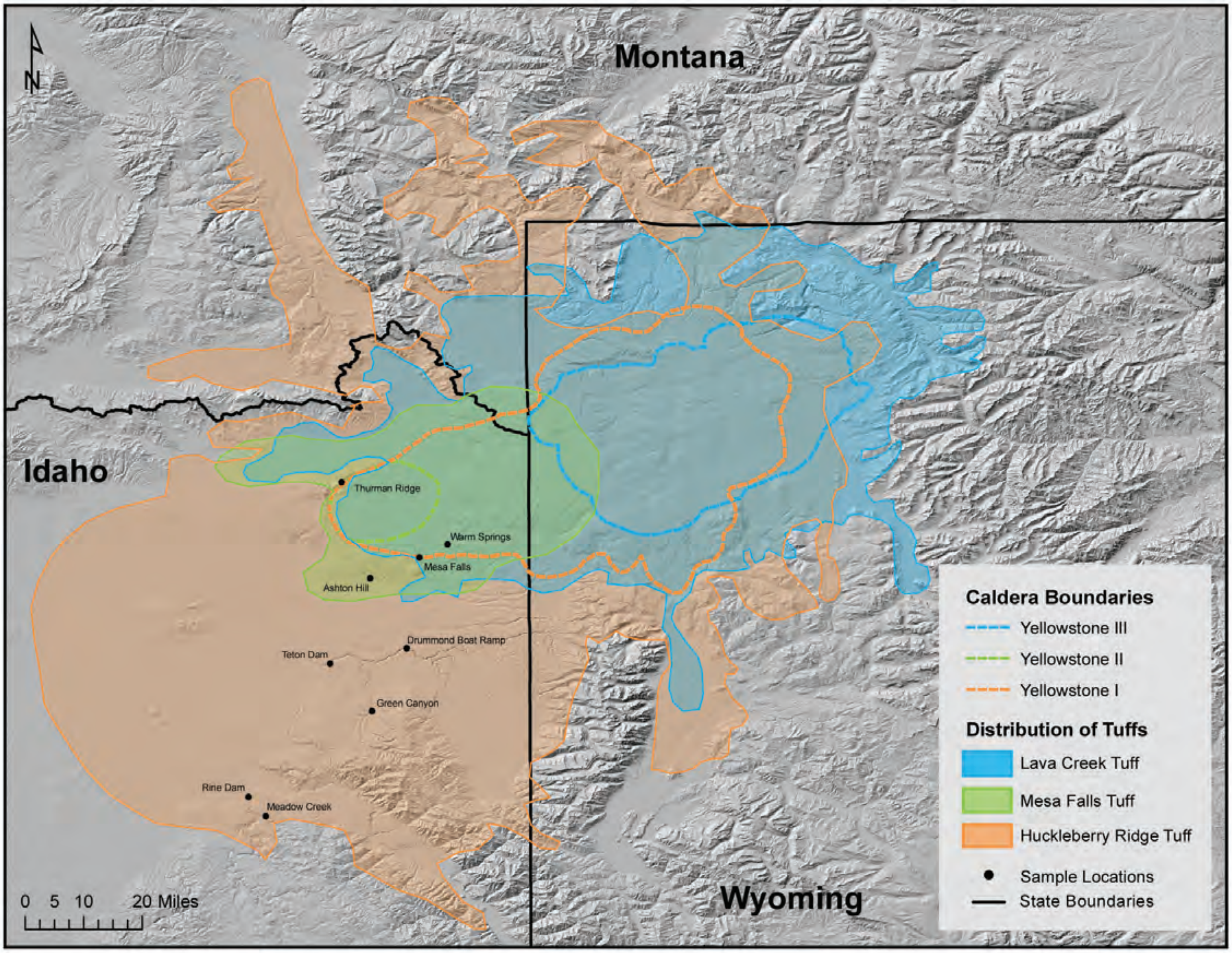

Figure 1. Map showing approximate distribution of climactic tuffs, caldera boundaries, and sample locations. Distribution of tuffs and Yellowstone I and III caldera boundaries after Christiansen (2001). Yellowstone II caldera boundary after Kuntz and others (accepted) and Moore and others (this volume).

and this technique produced density measurements with the highest precision. Attempts to seal samples with heated plastic wrap were difficult and ultimately unsuccessful.) The coatings added ~2% to the weight of the specimens.

Repeated measurements on the same sample and on different samples from the same location indicate the precision of our measurements was ± 0.02 g/cm^3 (1-sigma standard deviation, 1σSD). Density measurements on the densest samples—with and without sealant—showed that coating the samples as we did reduced measured densities by 0.07 ± 0.02 g/cm^3 (1σSD). (The densest samples lack significant porosity, so we could measure the density of these samples directly, without a coating; as such, comparing the densities of coated and uncoated specimens showed how coating affects density.) We added 0.07 g/cm^3 to measured densities to adjust for the effects of coating. We also tested accuracy by collecting two profiles collected within 5 m of each other at Meadow Creek. We compared the densities of these profiles to each other and to measurements made by Riehle and others (2010) in the same area (fig. 2A). Our profiles lie within within 0.13 g/cm^3 (1σSD) of Riehle and others (2010). As such, we estimate the accuracy of our measurements as ± 0.07 g/cm^3 (1σSD).

RESULTS AND DISCUSSION

Figures 2, 3, and 4 display vertical density variations in outcrops of, respectively, the 2.1 Ma Huckleberry Ridge Tuff, the 1.2 Ma Mesa Falls Tuff, and the 0.64 Ma Lava Creek Tuff. Table 1 lists and Figure 1 shows where we sampled the tuffs. The density profiles yield information about the relative temperature

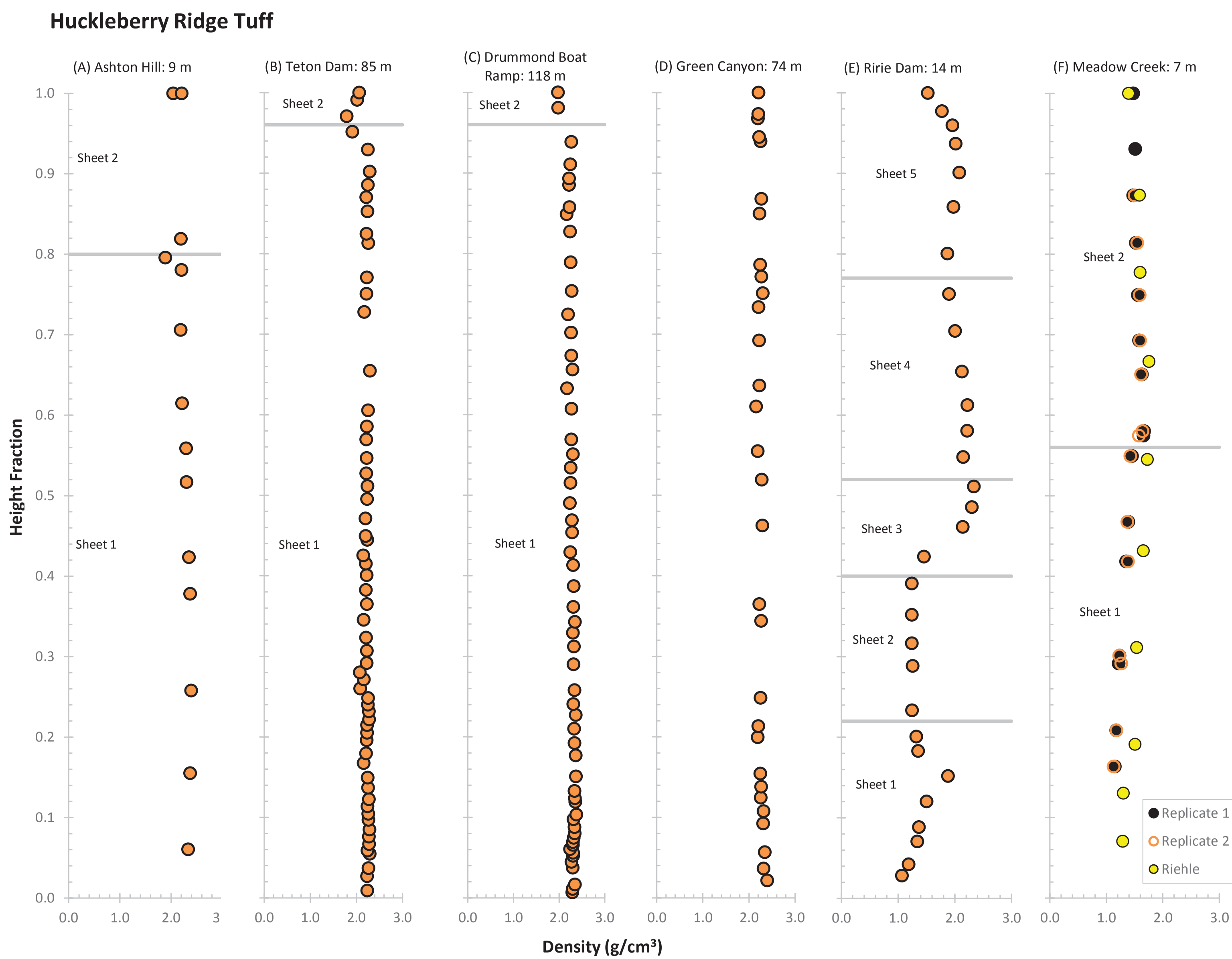

Figure 2. Vertical density variations in outcrops of member B of the 2.1 Ma Huckleberry Ridge Tuff at Ashton Hill (A), Teton Dam (B), Drummond Boat Ramp (C), Green Canyon (D), Ririe Dam (E), and Meadow Creek (F). Profiles lie in order of increasing distance from the Yellowstone I caldera. Figure 2A shows profiles collected near each other to estimate the precision and accuracy of our density measurements—Replicate 1 and 2 are our profiles; the 'Riehle' profile is from Riehle and others (2010). We present height in the density profiles of Figures 2-4 as height fraction (hf) and give total height above each plot, next to the title. The width of data points (circles) in Figures 2-4 approximates our estimate of the accuracy of our density measurements, i.e., ± 0.07 g/cm3.

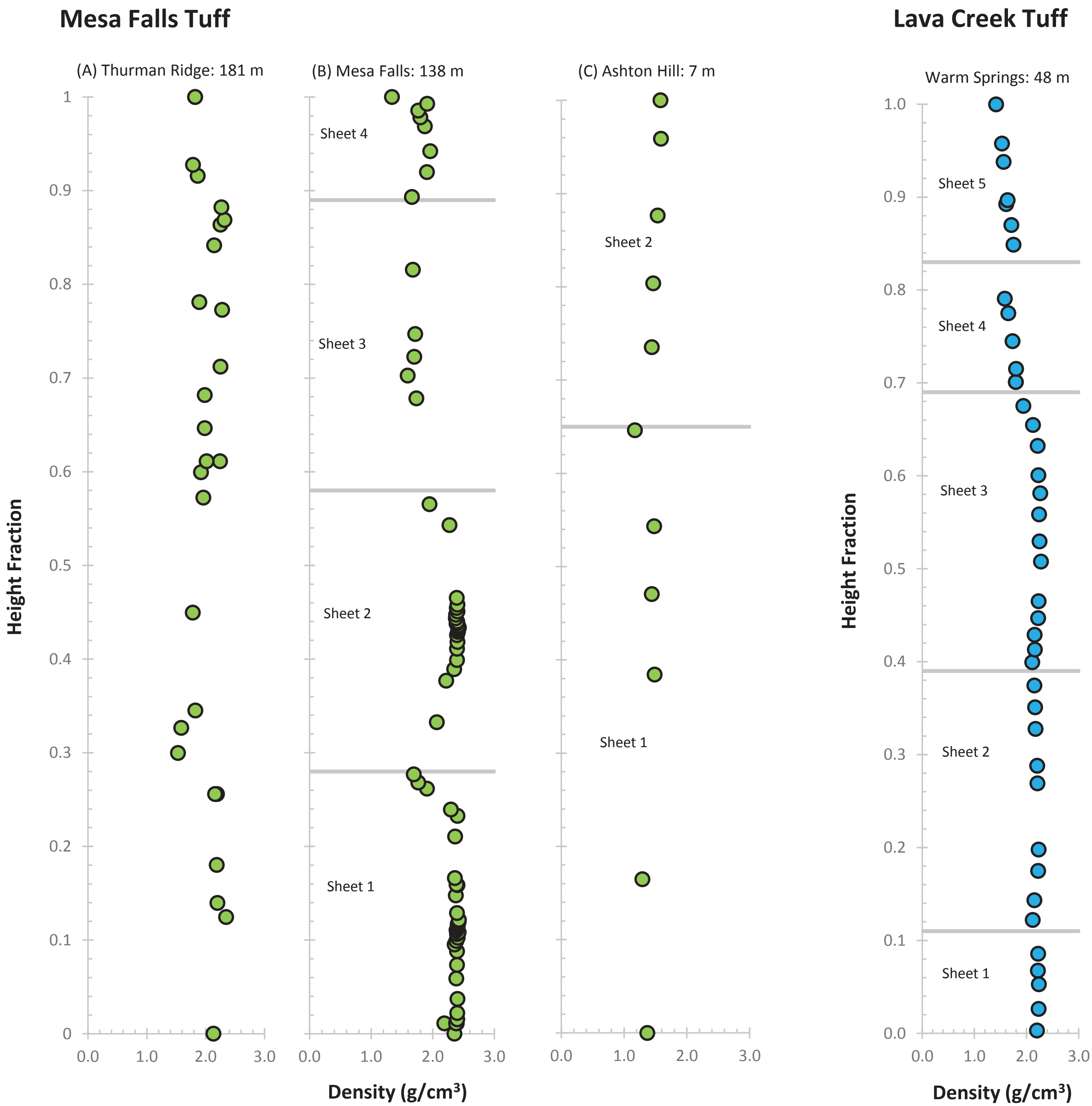

Figure 3. Vertical density variations in outcrops of the 1.3 Ma Mesa Falls Tuff at Ashton Hill (A), Thurman Ridge (B), and Mesa Falls (C). Profiles lie in order of increasing distance from the Yellowstone I caldera. Far right profile is the vertical density variations in outcrops of member B of the 0.64 Ma Lava Creek Tuff at Warm Springs.

Table 1. Locations of measured profiles

Location	Latitude	Longitude	Unit(s) Sampled
Warm Springs	44.20533	-111.25089	Lava Creek Tuff
Mesa Falls	44.18119	-111.3227	Mesa Falls Tuff
Thurmon Ridge	44.36191	111.50642	Mesa Falls Tuff
Ashton Hill	44.12148	-111.44208	Huckleberry Ridge & Mesa Falls Tuff
Teton Dam	43.91043	-111.54108	Huckleberry Ridge Tuff
Green Canyon	43.79323	-111.43713	Huckleberry Ridge Tuff
Drummond Boat Ramp	43.94762	-111.35181	Huckleberry Ridge Tuff
Ririe Dam	43.58053	-111.74348	Huckleberry Ridge Tuff
Meadow Creek	43.53305	-111.70001	Huckleberry Ridge Tuff

and emplacement history of the successive ash-flow units that built each tuff (Riehle and others, 1995; 2010).

Huckleberry Ridge Tuff

Christiansen (2001) identifies three members of the Huckleberry Ridge Tuff, based on density and abundance of phenocrysts. Members A and B are petrographically similar, although member A has a higher proportion of plagioclase to quartz phenocrysts. Member C has smaller phenocrysts and the lowest proportion of plagioclase to quartz. Density breaks separate the three members. Christiansen (2001) indicates that members A and C lie mostly in the northeast part of the Yellowstone I caldera and that member B lies mostly in the southwest portion of the caldera. Wilson (2009) proposes that most exposures south and west of the Yellowstone 1 caldera consist of member A, with thin deposits of member B locally present and thinning rapidly to the south. We measured vertical density variations in the Huckleberry Ridge Tuff at sites south and west of the Yellowstone I caldera—at Ashton Hill (figs. 1, 2A), Teton Dam (figs.1, 2D), and Drummond Boat Ramp (figs. 1, 2E), Green Canyon (figs.1, 2D), Ririe Dam (figs.1, 2E), and Meadow Creek (figs.1, 2F). Member A likely comprises these sites, with a thin section of member B locally present (Wilson, 2009).

The profile at Ashton Hill (fig. 2A) shows high densities, with a break at 0.8 hf (7 m). These two sheets were emplaced hot and were separated by short breaks (less than months). The lower sheet may be member A and the upper sheet may be member B (Phillips, pers. comm., 2016).

The density profiles at several Huckleberry Ridge Tuff sites show that deposit thickness and emplacement temperature influence the depositional information an ignimbrite can record. The thickest deposits—Teton Dam, Drummond Boat Ramp, and Green Canyon (figs. 2B-D)—welded so intensely that information about the tuff's depositional history was mostly erased. Teton Dam and Drummond Boat Ramp profiles only retained the transition to the last sheet (both at 0.96 hf; 82 m and 113 m, respectively); this uppermost sheet may be member B (Phillips, pers. comm., 2016; Wilson, 2009). No record of this sheet remains in the Green Canyon profile—the sheet either never reached the Green Canyon site, was removed by erosion, or is covered.

The Meadow Creek site lies on a paleotopographic high four miles to the northwest of the Ririe Dam site, which was deposited in the paleocanyon of Willow Creek. These depositional environments formed different records. Not surprisingly, the tuff deposited in the ancient canyon (fig. 2E) is thicker and captured more ash than the tuff deposited on an ancient hill (fig. 2F). The Meadow Creek profile (fig. 2F) shows a density break across a distinct color change in the tuff, at 0.56 height fraction (hf; 4.1 m). We interpret this profile to represent at least two sheets of ash, with the upper sheet emplaced at somewhat higher temperature. The Ririe Dam profile (fig. 2E) shows density breaks at 0.22 hf (3 m), 0.4 hf (5.7 m), 0.52 hf (7.5 m), and 0.77 hf (11 m)—suggesting that the tuff at this location formed from at least five sheets of ash. The higher density between 0.13–0.17 hf (1.5–2.5 m) in sheet 1 may indicate that this is a separate sheet, formed by hotter ash. Sheets 1 and 2 were emplaced at relatively low temperature, followed by hotter sheets of ash. We tentatively correlate the density break at Meadow Creek with the break at Ririe Dam between sheet 2 and one of the hotter overlying sheets. The modeling of Riehle and others (1995 and 2010) suggests that the density inversions in the profiles from both sites result from short periods (hours to weeks) between eruptions.

Generally, profiles from sites near the source record less information about the depositional history of a tuff, because the ash there is hot and welds intensely.

Mesa Falls Tuff

Christiansen (2001) reports that the Mesa Falls Tuff formed as a single cooling unit. We measured vertical density variations in this tuff at Thurman Ridge (fig. 1 and 3A), Mesa Falls (fig. 1 and 3B), and Ashton Hill (fig. 1 and 3C). The Thurman Ridge profile (fig. 3A) is difficult to interpret, perhaps because elevation and stratigraphic position in the tuff correlate poorly in this area, where the tuff was deposited against a preexisting topographic high. Still, profile densities are uniformly high, indicating emplacement at relatively high temperatures. The density profile near Mesa Falls has density breaks at 0.28 hf (39 m), 0.58 hf (80 m), and 0.89 hf (122 m)—suggesting the presence of at least four individual ash sheets (fig. 3B). Using the modeling of Riehle et al (1995 and 2010), we infer the following depositional history for the tuff at this location: sheet 1 was emplaced hot; after months to years, sheet 2 was emplaced at about the same temperature; after at least a few days, sheet 3 was emplaced at relatively low temperature; and, after days to months, sheet 4 was emplaced at an intermediate temperature.

The Ashton Hill profile (fig. 3C) shows a density inversion at 0.65 hf (4.5 m), which suggests the tuff at this location was emplaced as (at least) two relatively cool sheets, with only a short period (hours to days) between eruptions. The sheets apparent at Ashton Hill may be components of one of the sheets apparent at Mesa Falls (but were not preserved as distinct sheets at Mesa Falls), because the inferred interval between the eruptions recorded at Ashton Hill is short compared to any at Mesa Falls. The pattern of decreasing average density with distance from the caldera observed for the Huckleberry Ridge Tuff also applies to the Mesa Falls Tuff.

Lava Creek Tuff Member B

Christiansen (2001) identifies two members of the Lava Creek Tuff, based on density and abundance of phenocrysts. The entire unit cooled as one; contacts between members represent significant, but partial cooling breaks (Christiansen, 2001). The upper portion of member A is densely-welded, devitrified, and contains ~30% phenocrysts. Above it, member B consists of an unwelded to poorly welded deposit that contains ~10% phenocrysts and grades upward into a densely-welded, devitrified tuff that contains ~30% phenocrysts. Member A lies mostly inside and north of the Yellowstone III caldera; member B is distributed more broadly, extending throughout the Yellowstone I caldera (Christiansen, 2001). We measured vertical density variations in member B of the Lava Creek Tuff at Warm Springs. Figure 3 (far right profile) shows density breaks at 0.11 hf (5 m), 0.39 hf (19 m), 0.69 hf (33 m), and 0.83 hf (40 m)—suggesting it was emplaced as at least five individual sheets. The modeling of Riehle and others (1995 and 2010) suggests the first three sheets were emplaced relatively hot, followed by two cooler sheets, and the eruptions were separated by short periods (hours to weeks).

CONCLUSIONS AND FUTURE WORK

Our vertical density profiles of Yellowstone climactic tuffs suggest that individual members of tuffs were built from distinct eruptions separated by short intervals between eruptions—most commonly hours to days, but in one case months to a few years. Our work also indicates that profiles collected at sites near the source or on paleotopographic highs are less likely to preserve information about the depositional architecture of a tuff.

Collecting additional density profiles of each member of each tuff at carefully chosen sites could yield the fine-scale eruption history and flow paths of eruption sheets. In addition, numerical modeling of density profiles could quantify emplacement temperatures of individual eruption sheets, progressively lower emplacement temperatures with individual eruption sheets with distance from the source, cooling histories of cooling units, and the durations between eruptions—including between members of the Huckleberry Ridge and Lava Creek Tuffs.

REFERENCES

Christiansen, R.L., 2001, The Quaternary and Pliocene Yellowstone Plateau Volcanic Field of Wyoming, Idaho, and Montana: United States Geological Survey Professional paper 729G, 145 p.

Kuntz, M.A., Turrin, B.D., Champion, D.E., and Moore, D.K., in press, The Pleistocene volcanic and alluvial history of the Henrys Fork Caldera area, Fremont County, Idaho, in Kuntz, M.A., DeRito, J., and Van Kirk, R., eds., 2016, Geological, hydrological, and ecological studies of the Henrys Fork of the Snake River, eastern Idaho, U.S. Geological Survey Professional Paper, U.S. Geological Survey.

Moore, D.K., Embree, G.F., Champion, D.E., and Kuntz, M.A., this volume, Field guide to lava benches in Henrys Fork and Warm River Canyons and to the origin of Upper and Lower Mesa Falls, Island Park, Idaho: Northwest Geology, v. 45.

Riehle, J.R., Miller, T.F., and Bailey, R.A., 1995, Cooling, degassing and compaction of rhyolitic ash flow tuffs: a computational model: Bulletin of Volcanology, v. 57, no. 5, p. 319–336.

Riehle, J.R., Miller, T.F., and Paquereau-Lebti, P., 2010, Compaction profiles of ash-flow tuffs: Modeling versus reality: Journal of Volcanology and Geothermal Research, v. 195, no. 2-4, p. 106–120.

Wilson, C.J.N., 2009, Physical volcanology of the Huckleberry Ridge Tuff: EOS, Transactions of the American Geophysical Union, v. 90(52), Fall Meeting Supplement, Abstract V23C-2085.

Earliest Stone House in Rexburg: John Smalley and Tamera Ricks built this home in 1892 from blocks of Huckleberry Ridge Tuff. Today it lies at at 112 N 1st E Street in Rexburg. Like most local stone buildings, the 24-inch-thick exterior walls withstood the Teton Flood waters far better than modern frame and brick houses. (Photo courtesy of Glenn Embree.)

FIELD TRIP GUIDES

GEOLOGIC FIELD GUIDE TO THE HOLOCENE NORTHEASTERN ST. ANTHONY DUNE FIELD AND MID-LATE PLEISTOCENE GHOST DUNES, EASTERN SNAKE RIVER PLAIN, IDAHO

David R. Gaylord,[1] Paul K. Link,[2] and Tammy M. Rittenour[3]

[1]School of the Environment, Washington State University, Pullman, WA 99164-2812, gaylordd@wsu.edu; [2]Department of Geosciences, Idaho State University, Pocatello, ID 83209, linkpaul@isu.edu; [3]Department of Geology, Utah State University, Logan, UT 84322, tammy.rittenour@usu.edu

INTRODUCTION

This half-day field trip provides the opportunity to explore the geomorphology and sedimentology of a variety of Quaternary eolian sand dune, loess, and sand sheet deposits, to observe and consider the evolution of a mid-Late Pleistocene ghost dune between St. Anthony and Ashton, Idaho. The trip guide begins at the junction of Sand Creek Road and old U.S. Highway 20 (Yellowstone Highway) east of St. Anthony, Idaho and involves about 37 mi (60 km) of driving and a moderate to challenging ~1 mi (1.6 km) hike over uneven vegetated sand sheet as well as stabilized and active sand dunes. Surface elevations average 5,200 ft (1,585 m) asl, there is little shade, and air temperatures are commonly at upper 80°s F to low 90°s F (upper 27°s C to low 32°s C) in late July and August. There are no service facilities and no water is available. The gravel road used for access to the St. Anthony dunes is located on public-access, Bureau of Land Management (BLM) land. Travel on this road generally requires a four-wheel drive vehicle because the loose, dry dune sand frequently reduces traction. Vehicles should be equipped with tow ropes, planks, and a hydraulic jack. Also, even though this is an arid region, strong thunderstorms with heavy rains are possible, making travel difficult where the road crosses playa and loess surfaces.

NOTE: The ghost dunes are located on private land; thus, prior permission is absolutely required to access these features directly. However, this field guide provides the background necessary to appreciate the genesis of a ghost dune from a public-access road.

GEOLOGIC SETTING

The eastern Snake River Plain (ESRP) of eastern Idaho is a northeasterly trending lowland of contrasting volcanic and sedimentary deposits that intersects the largely north–south trending tectonic fabric of the northern Basin and Range Province. The late Miocene to Pleistocene silicic and basaltic volcanic rocks that characterize much of the ESRP were generated as the North American plate moved over the Yellowstone hotspot or mantle plume during the late Cenozoic (Kuntz and others, 1992; Pierce and Morgan, 1992; Christiansen, 2001; Champion and others, 2002; Morgan and McIntosh, 2005). Post-eruptive subsidence of these volcanic centers provided accommodation space for shallow lacustrine, alluvial, and deltaic deposits during the late Pliocene and early Pleistocene when the climate was episodically moist (Bestland and others, 2002; Geslin and others, 2002). From mid-Pleistocene time to present, persistently arid to sub-arid climatic conditions promoted deposition and preservation of eolian, glaciofluvial, alluvial, and shallow lacustrine deposits (Scott, 1982; Bestland and others, 2002; Geslin and others, 2002).

The two stops for this field trip are shown on the surficial geologic map adapted from Scott (1982) (fig. 1). The Quaternary units depicted on the Explanation are roughly coeval; in general, however, the oldest deposits (lower right) consist of largely Pleistocene silicic and basaltic rocks and colluvium derived from volcanic centers; the next oldest deposits consist of Pleistocene to Holocene lacustrine glaciofluvial outwash, ghost dune hollows, sand sheet, alluvial, stabilized sand dune, loess, and active sand dune deposits. The ghost dunes are mid-Late Pleistocene (Gaylord and others, 2015, 2016), whereas the stabilized and active sand dune deposits are inferred to have accumulated largely during the Holocene (Gaylord and others, 2000; Coughlin, 2000; Coleman, 2002; Rich and others, 2015).

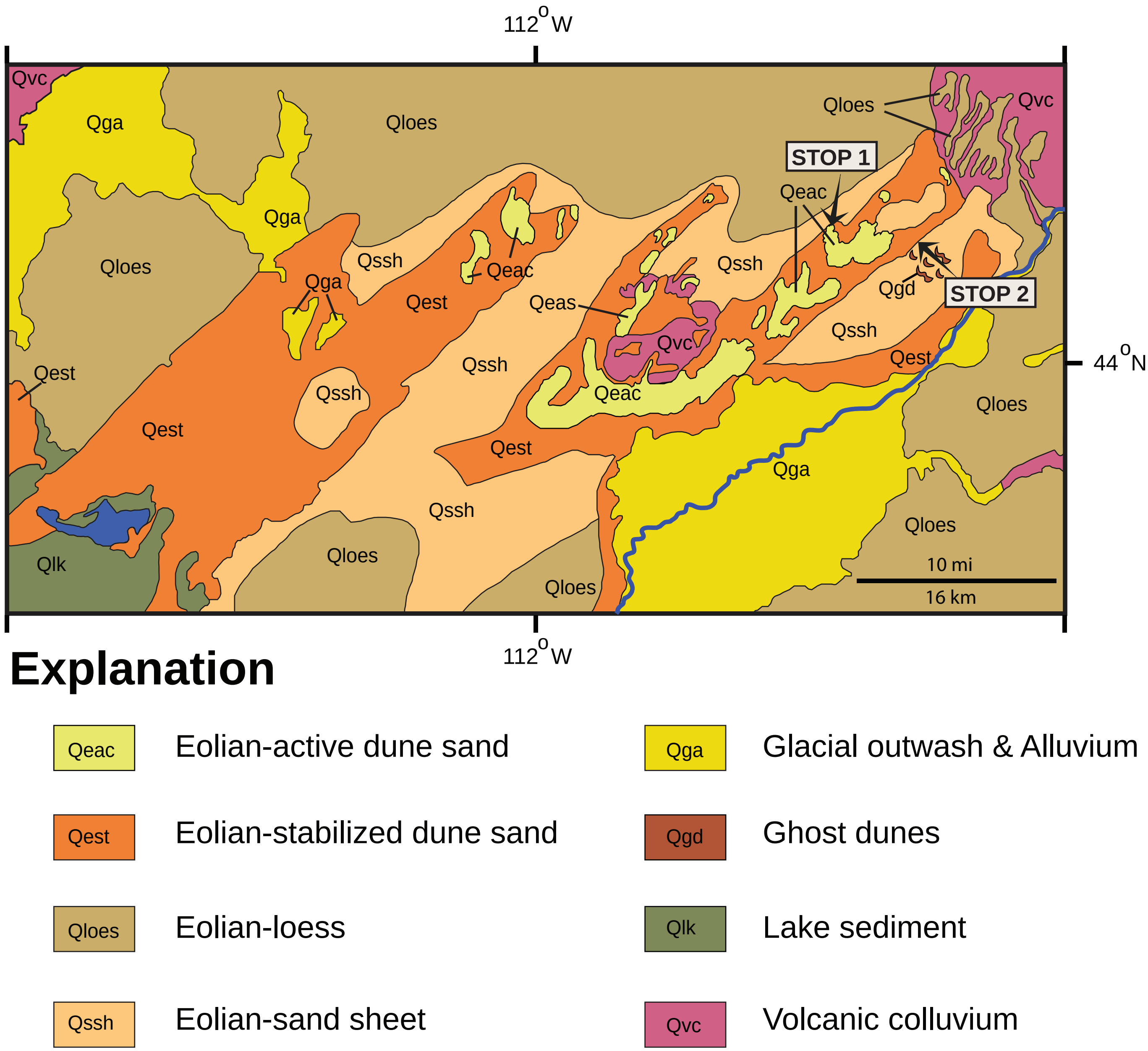

Figure 1. Surficial geologic map with field trip stops. Henrys Fork of Snake River depicted as blue line. Modified from Scott (1982).

ROAD LOG

The field trip begins at the junction of Sand Creek Road and old U.S. Highway 20 (the Yellowstone Highway) just east of St. Anthony. Reset odometers. This junction is 0.25 mi west of the old U.S. 20 bridge over the Henrys Fork of the Snake River (fig. 2).

0.0 Sand Creek Road. Drive north and east on pavement across Pleistocene glaciofluvial and Pleistocene and Holocene alluvial deposits of the Henrys Fork of the Snake River. These deposits consist of discontinuous, silt- and clay-enriched, pebble to cobble gravel and pebbly very-coarse to very-fine sand. Clastic particles include a variety of metamorphic, igneous, and sedimentary lithologies derived from tributaries that drain diverse geologic terrains, including the southwestern Yellowstone Plateau and northern Teton Range.

1.2 Junction with E 700 N. Sand Creek Road turns north at this intersection.

1.4 Leave paved road. Stabilized dune sand consisting of low-relief (<1.5 m high), SW–NE-oriented linear ridges that grade northward into lower-relief sand- and loess-mantled sand sheet deposits. These vegetated and largely stabilized sand sheet deposits consist of poorly to moderately sorted, horizontally laminated and locally cross-laminated silty, coarse to

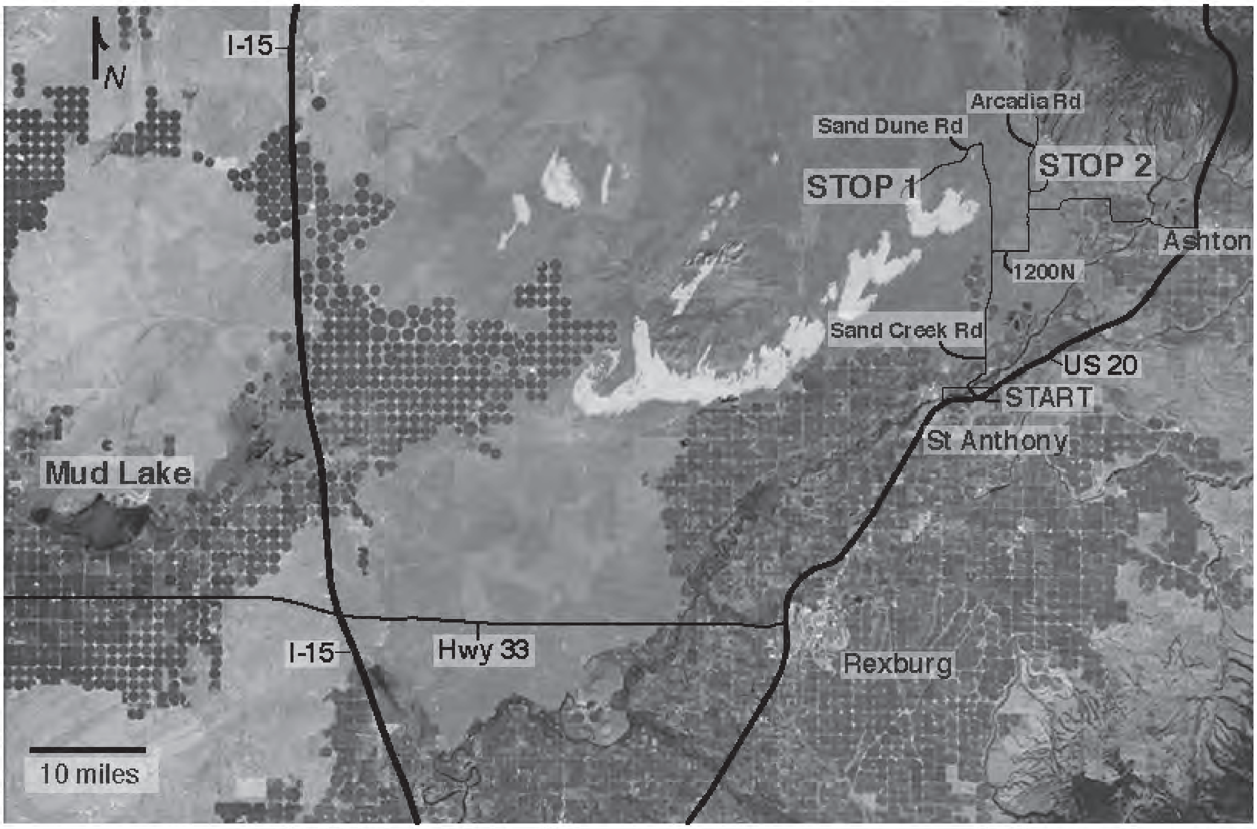

Figure 2. Location map showing primary roads and field trip stops. Underlying image from Google Earth.

fine granule and pebbly very-fine to coarse sand.

4.9 Intersection with 1200 N. At this location Sand Creek Road has climbed over 40 m above the glaciofluvial and alluvial deposits that are proximal to the Henrys Fork. Mark this intersection; you will return to it later when you drive to view a ghost dune hollow (Stop 2). The surface to either side of Sand Creek Road at this location is dominated by mixed loess and sand sheet deposits that discontinuously mantle the low-relief basaltic bedrock topography typical of Pleistocene and Holocene lava flows on the ESRP (Kuntz and others, 1992, 2003).

6.3 Cross the contact from loess-covered sand sheet deposits to thin, low-relief, <6.6 ft high (<2 m) stabilized parabolic dunes that are marginal to the main concentration of NE-migrating active dunes in the St. Anthony dune field. The leeward slopes and slip faces of these active sand dunes are visible to the west of Sand Creek Road, which here is ~213 ft (~65 m) above the Henrys Fork. The discontinuously stabilized sand dune cover adjacent to Sand Creek Road is interrupted by prominent and jagged basaltic lava flows and hollows spaced tens to hundreds of meters apart, including those exposed immediately to the east. The >16 ft deep (>5 m) hollows in these basalt flows are interpreted to have resulted from the collapse of lava tubes and blister-like domes generated during basalt extrusion.

7.7 Contact between stabilized parabolic dune sand to granule and small-pebble-rich, loess-covered sand sheet deposits.

8.6 Contact between sand sheet and stabilized parabolic dune sand. Actively migrating, N50°E-trending parabolic dune limbs are part of a series of nested parabolic dunes that are visible immediately to the west (fig. 3).

9.7 Junction of Sand Creek Road with BLM ‘Sand Dune Road.’ Turn left onto ‘Sand Dune Road,’ which is only occasionally identified by road signs. The surficial geology at this junction is dominated by low-relief (<10 ft, <3 m) stabilized parabolic dunes. Drive 0.7 mi (1.1 km) to the SW where you can pull off the road and park in order to hike 0.1 mi (0.16 km) to a small cluster of actively migrating parabolic dunes; there you can also examine the geomorphology, sedimentology, and ecology of these features. These active sand dunes are located at the downwind end of a 2-mi-long by <1-mi-wide (3.2-km-long by 1.6-km-wide), lobate-shaped concentration of nested, largely stabilized parabolic dunes that are oriented to N50°E (fig. 3). This nesting of similarly oriented sand dunes over a lobate area is highlighted by the dashed lines in fig. 3. Note that actively migrating barchan and barchanoid-ridge dunes currently are migrating towards and encroaching upon this lobate concentration of nested dunes.

11.2 Sand Dune Road. The road climbs across the limb of a weakly stabilized parabolic dune that is in sharp contact with sand sheet deposits to the north. This portion of the road commonly is mantled with loose dune sand that can make travel challenging.

12.9 Junction with an unnamed E–W-oriented dirt road that commonly is overgrown with vegetation, making it difficult to see from Sand Dune Road. For the ambitious, a 1.5-mi (2.4-km) hike east along this primitive road will take you to the downwind margin of the northeastern complex of the St. Anthony dune field (fig. 3) as named by Coughlin (2000). Bare, wind-swept, slightly up-domed and locally columnar-jointed basalt flows are common on this part of the road.

13.4 Abandoned corrals and an old water tank were constructed on discontinuously loess-covered and locally pebble- and granule-rich sand sheet deposits. Basalt flows are mantled by up to a meter of mixed sand sheet and loess deposits.

14.2 **STOP 1**

(44° 05' 36.6" N, 111° 42' 34.5" W) This stop provides the opportunity to explore the northwestern margin of the northeastern dune complex (figs. 3, 4).

Stop 1 Background

The northeastern dune complex of the St. Anthony dunes consists dominantly of ~1.9 mi^2 (~5 km^2) of actively migrating 10–33 ft (3–10-m) high, partially stabilized barchanoid-ridge and barchan dunes; many of these dunes, however, are currently in transition to parabolic dunes. Prevailing sand-moving winds in this area are to the NE. Investigated by Coughlin (2000) and Hoover (2014), the NE dune complex contains two concentrations of active dunes: a primary, downwind concentration that covers ~1.2 mi^2 (~3 km^2) and a secondary concentration covering ~0.8 mi^2 (~2 km^2) (fig. 3). The primary concentration of active dunes is migrating to N40-45°E, whereas the secondary active-dune concentration is migrating to ~N35°E. The secondary active-dune concentration appears in the recent geologic past to have both partially overridden and attached itself to the primary active-dune concentration. Differences in sand dune migration directions are attributed to the differential influence of the local topography on the prevailing airflow. The secondary active-dune concentration where you will hike consists of well-sorted fine sand with a mean grain size of 0.18 mm (Hoover, 2015). These dune deposits are slightly finer grained

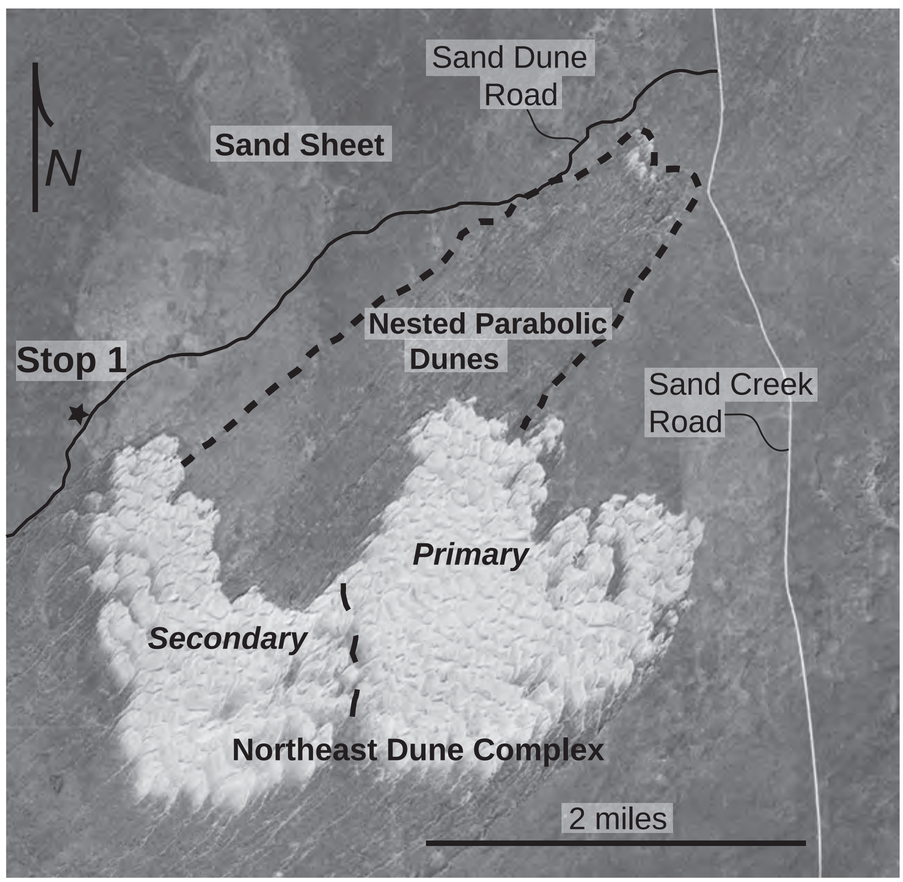

Figure 3. Overview map highlighting active sand dunes of the northeastern complex of the St. Anthony dune field as described by Coughlin (2000) and Gaylord and others (2000). Active sand dunes in the complex consist of barchanoid-ridge and barchan dunes in transition to parabolic dunes. Dunes within the 'Secondary' portion of the northeastern complex are migrating more northwardly than are dunes within the 'Primary' portion and are separated here by a dashed line. A lobe of dominantly stabilized 'nested' parabolic dunes are delineated with a dashed line; these nested dunes overprint sand-sheet deposits and are being overridden by actively migrating dunes from the northeastern complex. Stop 1 is located along BLM 'Sand Dune Road' and is accessible via Sand Creek Road. Photo from Google Earth.

and better sorted than the St. Anthony dune field as a whole (Coughlin, 2000; 0.23 mm mean grain size). However, these dunes also are slightly finer-grained than the dunes at the downwind margin of the dune field near Sand Creek (Coleman, 2002; 0.19 mm).

The provenance of these dune sands is under continuing investigation. Preliminary results from thin-section point counts and XRF bulk chemical analyses suggest these sands were derived primarily from Snake River sources. Sediment sources include the headwater regions of the Henrys Fork, Teton, the main fork of the Snake River, the western Big and Little Lost River, and glacial Lake Terreton (Coughlin, 2000; Gaylord and others, 2000; Hoover, 2014). More recently U/Pb detrital-zircon geochronology of a limited number of eolian and alluvial sources, including those immediately north of Mud Lake (fig. 1), suggest that dune sands from the NE complex of the St. Anthony dunes were derived primarily from the Henrys Fork of the Snake River. In contrast, dune sands in the western St. Anthony dune field appear to have been derived primarily from Pleistocene glacial Lake Terreton and from Big Lost Trough alluvial sources (Gaylord and others, 2015).

A sand sample collected from the distal side of the dune field (near Stop 1) contains abundant Eocene grains (26% of total; peak at 48 Ma), as well as Heise volcanic field (8% of total; peaks at 4.0 and 6.6 Ma) and recycled Idaho batholith grains (17% of total; dispersed ages from 80 to 104 Ma with a peak at 98 Ma). This sample is in distinct contrast with dune sands analyzed from the upwind, western side of the St. Anthony dunes, which contains no Yellowstone Plateau grains, abundant Eocene grains (60% of the grains, peak at 49 Ma), and no 80–100 Ma grains, which is consistent with its derivation from the Lake Terreton area and the Big Lost Trough (Gaylord and others, 2015). Pleistocene Henrys Fork alluvium (as mapped by Scott, 1982) is exposed near Camas National Wildlife Refuge and contains all three Mesozoic to Tertiary grain groups. The Snake River Plain–Yellowstone grains in this alluvium are largely >5 Ma (peaks at 6.7 and 8.3 Ma). This sample contains more than 50% pre-Mesozoic grains that are interpreted to have been transported by the Henrys Fork from sources in the Montana–Wyoming thrust belt.

Hike

Park your vehicle on the loess-covered pebble- and granule-rich sand sheet on Sand Dunes Road and hike ~0.25 mi (0.40 km) to the SE towards the nearby active dunes (fig. 4). A walking stick will facilitate travel.

This hike provides an opportunity to traverse both stabilized and active dunes. You will first walk along and around a vegetated ~15 ft high (~3 m) limb of a largely stabilized parabolic dune that marks the boundary between sand dune and sand sheet deposits. The hiking path on figure 4 traverses a series of weakly stabilized to active linear parabolic dune limbs and the broad windward (stoss) sides of barchanoid-ridge and barchan dunes that currently appear to be changing into parabolic dunes. Take the opportunity to hike up to the top of a crescent-shaped, ~30 ft high (~10 m) barchan dune that is migrating towards N35°–40°E. Along the way stop to notice that the coarser sand grains are concentrated on the tops of the ripples. Continued migration and aggradation of these ripples

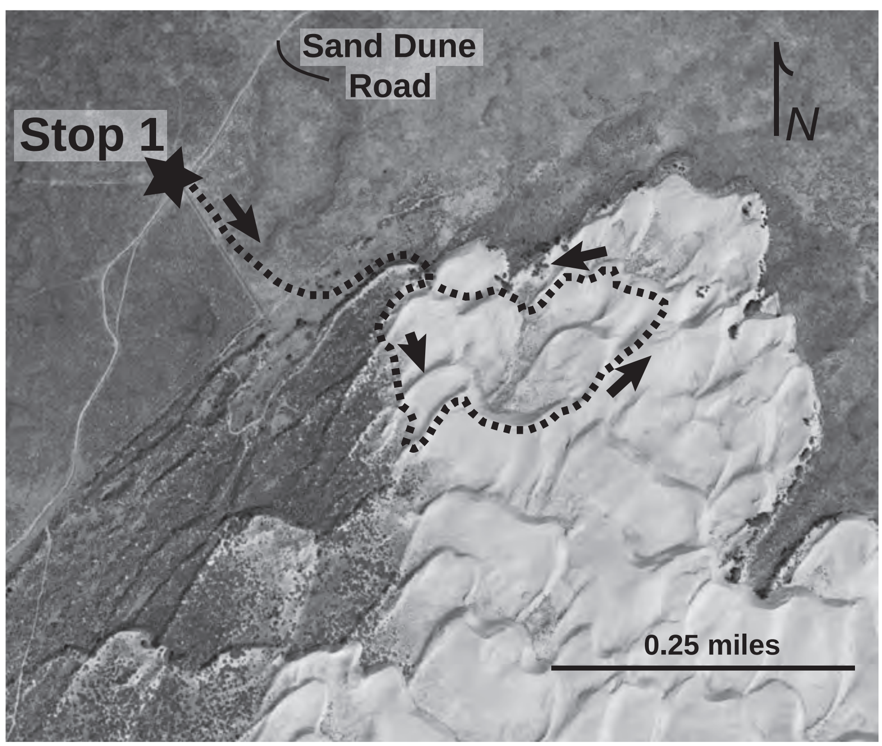

Figure 4. Air photo showing Stop 1 and path of hike across a portion of stabilized and active sand dunes. Entry to Stop 1 is via Sand Dune Road (see fig. 3). Photo from Google Earth.

at angles of climb that are less than the stoss side of the ripple produces inversely graded laminations that Hunter (1977) termed subcritically climbing translatent strata. While walking along the stoss side of this dune you also will find concentrations of granules and coarse sand in granule ripples. The granule ripples and granule-ripple trains are evidence for the preferential removal of finer-grained particles in deflation-dominated parts of the dune. You also will be able to trigger and observe grainflow avalanches down the ~30° angle-of-repose slipfaces. Short grasses, leguminous plants, and occasional shrubs baffle the wind, induce deposition, and promote dune stabilization. The shingle-like appearance of the migrating dune forms on this hike is easily discerned from air photos (fig. 4) and reflects the relative abundance of sediment that has led to these closely spaced and aggrading dunes. The remainder of the hike provides an opportunity to examine surface sedimentary and geomorphic features and observe the influence of the vegetation on surface features and dune morphology.

Drive to the Ghost Dunes

18.7 Junction with Sand Creek Road. Turn right.

23.5 Intersection with Rd 1200 N. Turn left to east.

25.1 Drive to intersection with Arcadia Road. Turn left and drive north 2.6 miles to Stop 2.

27.7 **STOP 2**

(44° 05’ 33.2” N, 111° 36’ 06.9” W) This stop provides an excellent opportunity to observe a ghost dune hollow and consider its depositional history and paleoclimatic implications.

Ghost Dune Background

This and other ghost dune hollows were generated by an inversion of the topography following partial encasement of the active sand dune by a basaltic lava flow. Originally recognized as dune molds by USGS geologists M.A. Kuntz and Robin Holcomb in the early 1970s, over 30, ~16 to 49 ft deep (~5 to 15 m) ghost dune hollows are distributed over ~40 km^2 (s. 1 and 2). The barchan-shaped ghost dune hollow at QS1 (fig. 5) was hand-augered and sampled to determine stratigraphic relations as well as grain-size ranges and sand composition (Gaylord and others, 2016). The stratigraphy reconstructed from auger cuttings is summarized in the QS1 stratigraphic column (fig. 6).

The depositional history of the basalt-rich sediment in ghost dune hollow QS1 (figs. 5, 6) preserves a paleoclimatically sensitive record from the time immediately preceding and then following encasement of the original barchan dune by the Split Butte basaltic lava (ca. 62 ± 3 ka; Kuntz and others, 2016). The ~60 cm of remnant barchan dune sand from the base of the QS1 stratigraphic section consists of very-fine and fine-grained, moderately sorted, laminated to massive sand that unconformably overlies a basaltic lava flow. The orientation of the original barchan dune was to ~N50°E, a direction that is ~10–15° more easterly than the orientations of most modern active and stabilized sand dunes in the St. Anthony dune field. Columnar joints that formed the perpendicular top of the Split Butte basalt flow also formed perpendicular to the steep face of this flow as it advanced towards the dune. As a result, the columnar cooling joints that formed in the contact zone between the basalt flow and the slip face of this ghost dune are oriented down and away from the ghost dune slip face (Gaylord and others, 2016).

Following its encasement in a <16 ft thick (<5 m) basalt, the majority of the original barchan dune was deflated and transported downwind towards the flanks of the Henrys Fork Caldera (Christiansen, 2001) and Sand Creek. The remnant dune sands were stabilized by vegetation. Evidence for stabilization and pedogenesis includes the dominantly massive nature of the remnant deposits, the orange-red color and a few granular soil aggregates, or peds. Since this ghost dune hollow is surrounded and underlain by relatively low-permeability basalt, subsequent runoff and precipitation has long been concentrated in it, thus promoting plant growth, soil formation, and ponding. Episodes of regional drought also likely promoted the accumulation of remobilized eolian sand that was transported into the relatively moist hollow. Slope-wash processes contributed fine-grained sediment to the hollow as well as locally derived gravel-sized basalt clasts from weathered lava margins (note large colluvial clasts at ~100 cm depth of section QS1; fig. 6). The dune sands at the top of the QS1 stratigraphic section are interpreted as deposits that are largely coeval with the stabilized parabolic dune sands that lie immediately north of QS1, and which may bury other ghost dunes to the

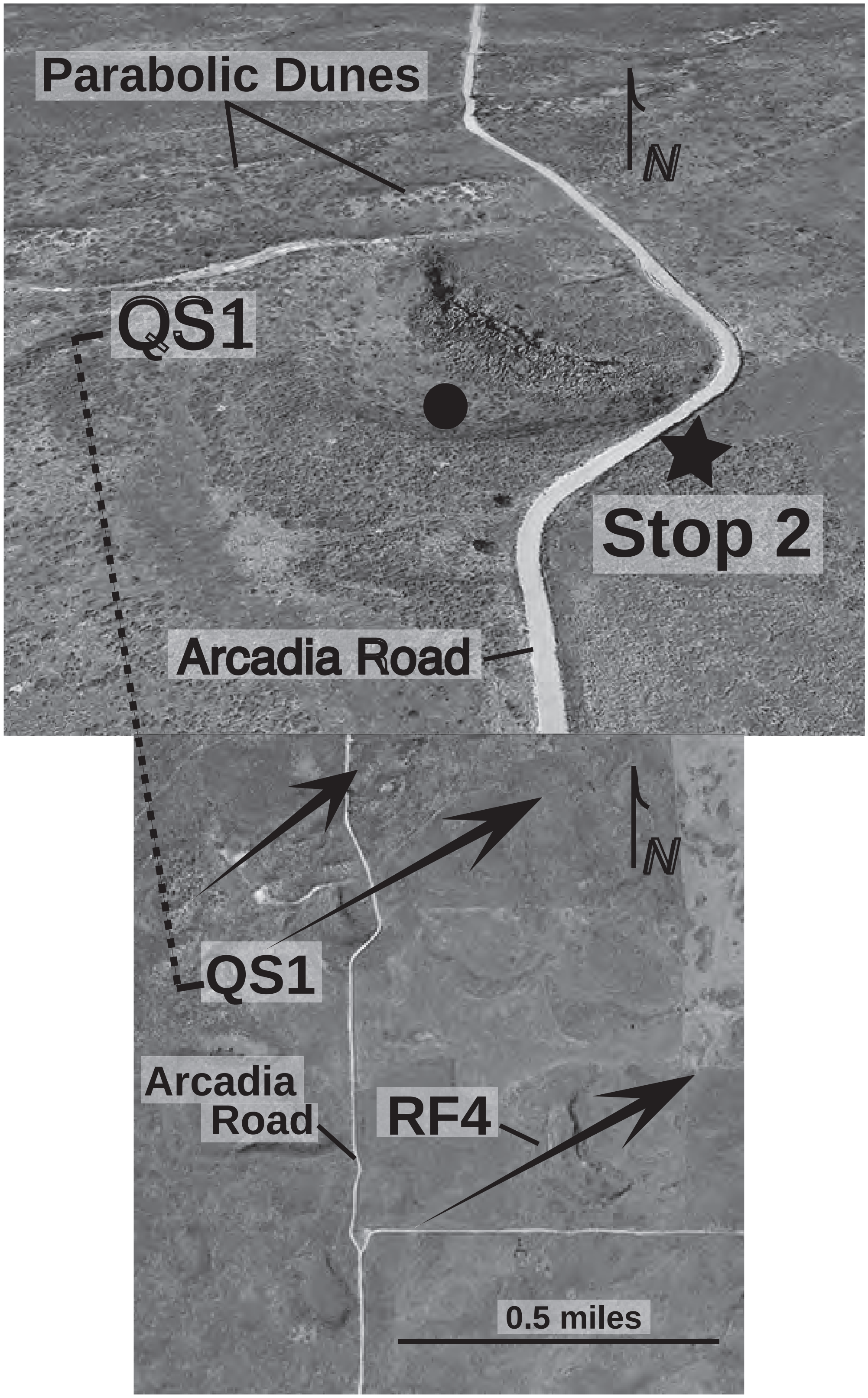

Figure 5. Oblique (top) and vertical (bottom) air-photo maps showing location of Stop 2, ghost dune hollow QS1, and relation to ghost dune hollow RF4. Large black dot denotes hand-auger hole from which QS1 stratigraphic column in figure 6 constructed. Photos from Google Earth.

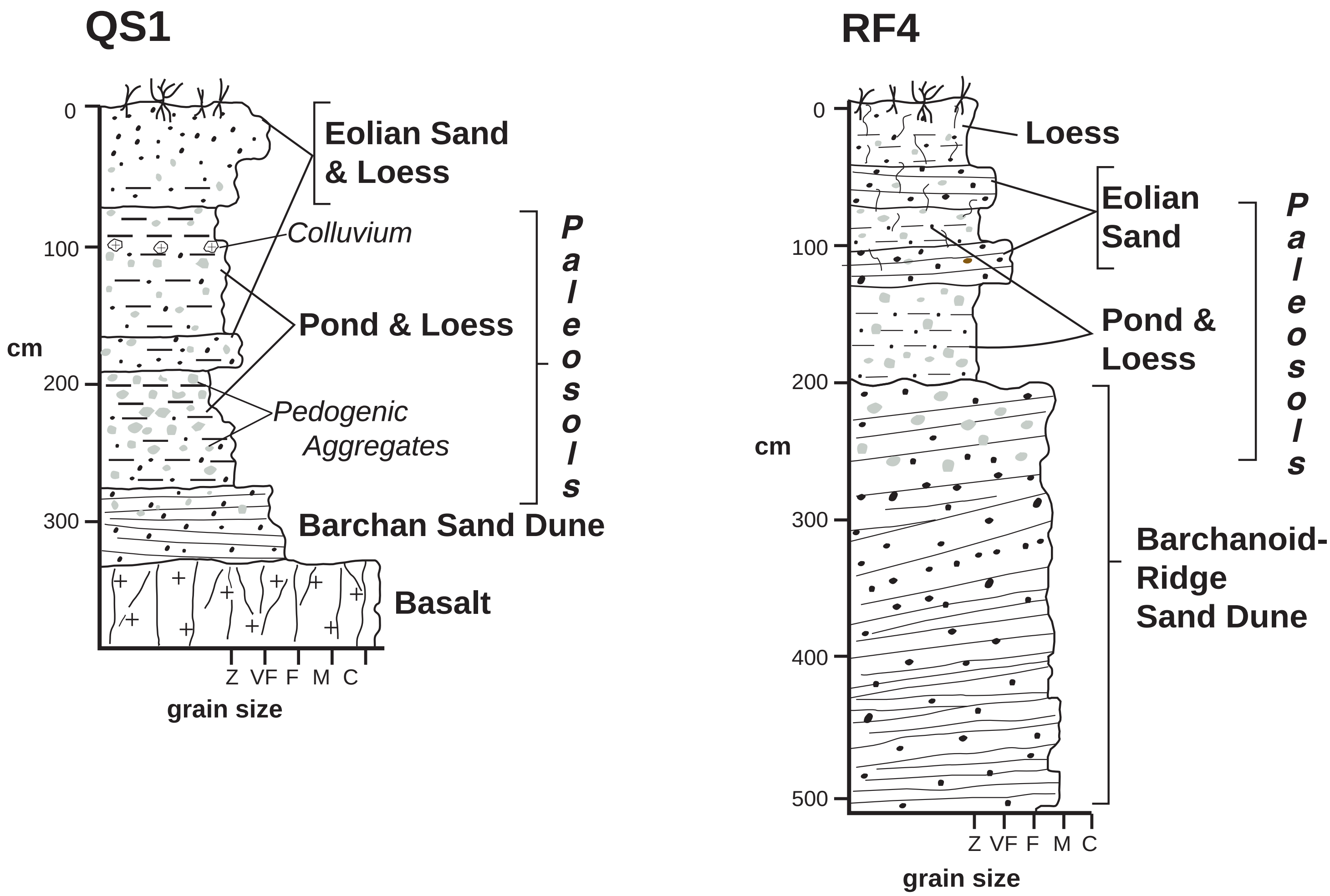

Figure 6. Ghost dune hollow stratigraphy constructed from field descriptions and textural and compositional analyses of hand-augered samples. QS1 is located ~0.5 mi (0.8 km) NW of ghost dune hollow RF4 (see fig. 5). Large clasts with + symbol at ~100 cm depth in QS1 are colluvial basaltic gravel clasts derived from weathered margins of the surrounding Split Butte basalt flow. Gray-colored clasts in both sections denote concentrations of granular and blocky peds (i.e., soil aggregates). Grain size symbols: Z = silt; VF = very fine sand; F = fine sand; M = medium sand; C = coarse sand.

north of this site. Based on preliminary compositional analysis of the mineralogy and lithology of sand-rich sedimentary deposits preserved in QS1, the bulk of the basalt lithic-rich dune sands at this site are inferred to have been derived primarily from reworked sediment from Henrys Fork alluvial deposits that include detrital zircons from the Yellowstone Plateau (Gaylord and others, 2015, 2016).

Ghost dune hollow RF4 shares a broadly similar depositional history to ghost dune hollow QS1 (figs. 5, 6), but in contrast to QS1 contains a much thicker (>10 ft thick, >3 m) succession of barchanoid-rich dune sand characterized by grainflow and grainfall cross strata and subcritically climbing translatent laminations (Hunter, 1977). The barchanoid-ridge identity of this dune is based on the barchanoid-ridge shape of the hollow. Unlike QS1, however, no basalt flow was reached beneath the dune sands in RF4; this was likely due to the 17 ft (5.2 m) limit of hand-augering. Like in ghost dune hollow QS1, following initial truncation and vegetational stabilization of the original barchanoid-ridge sand dune, the RF4 ghost hollow was subjected to episodes of loess deposition, pond sedimentation, eolian sand accumulation, and pedogenesis. Dating via optically stimulated luminescence (OSL) and assessment of the paleoclimatic record of the deposits in RF4 is ongoing.

The mineralogy and lithology of the basalt lithic-rich dune sands preserved in RF4 reveal they were primarily derived from reworked alluvial material from Henrys Fork alluvium. However, in contrast to QS1, the detrital zircons geochronology of RF4 dune sands also reveal a significant contribution of zircon grains from the Yellowstone Plateau (24% of total, peaks at 0.6 and 2.0 Ma; Gaylord and others, 2015). This ghost dune detrital zircon sample also contains a secondary Eocene grain peak representing Challis magmatic grains (9% of total, peak at 49 Ma).

Drive 0.4 mi west to Arcadia Road and drive south 2 mi to 1200 N. Turn right and drive 1.6 mi to Sand Creek Road. Drive 4.9 mi south to Yellowstone Highway and Sand Creek Junction.

36.7 END OF TRIP

ACKNOWLEDGMENTS

The authors gratefully acknowledge the access to private lands given by Q. Saurey and R. and K. Frederickson, the generous logistical support of Paul and Donna Hopperdietzel of St. Anthony, Idaho, laboratory analyses provided by Caleb A. Grant, and the helpful coordination of manuscript reviews and critical feedback provided by William M. Phillips of the Idaho Geological Survey. Financial support from the E. Meyers Grant Research Fund, College of Arts and Sciences at Washington State University, and the College of Sciences at Idaho State University is greatly appreciated.

REFERENCES CITED

Bestland, E.A., Link, P.K., Lanphere, M.A., and Champion, D.E., 2002, Paleoenvironments of sedimentary interbeds in the Pliocene and Quaternary Big Lost Trough, eastern Snake River Plain, Idaho, in Link, P.K., and Mink, L.L., eds., Geology, Hydrogeology, and Environmental Remediation: Idaho National Engineering and Environmental Laboratory, Eastern Snake River Plain, Idaho: Boulder Colorado, Geological Society of America Special Paper 353, p. 27–44.

Champion, D.E., Lanphere, M.A., Anderson, S.R., and Kuntz, M.A., 2002, Accumulation and subsidence of late Pleistocene basaltic flava flows of the eastern Snake River Plain, Idaho, in Link, P.K., and Mink, L.L., eds., Geology, Hydrogeology, and Environmental Remediation: Idaho National Engineering and Environmental Laboratory, Eastern Snake River Plain, Idaho: Boulder Colorado, Geological Society of America Special Paper 353, p. 175–192.

Christiansen, R.L., 2001, The Quaternary and Pliocene Yellowstone Plateau Volcanic Field of Wyoming, Idaho, and Montana: U.S. Geological Survey Professional Paper 729G, 145 p.

Coleman, A.J., 2002, Mid-to-late Holocene eolian, alluvial and lacustrine deposits and paleoclimate fluctuations from the eastern St. Anthony dune field, southeastern Idaho: Washington State University, unpublished M.S. thesis, 103 p.

Coughlin, J., 2000, Sedimentary and geomorphic development and climatic implications of the St. Anthony dune field, Fremont County, southeastern Idaho: Washington State University, unpublished M.S. thesis, 83 p.

Gaylord, D.R., Coughlin, J., Coleman, A., Sweeney, M., and Rutford, R.H., 2000, Holocene sand dune activity and paleoclimate from Sand Creek, St. Anthony dune field, Idaho: Geological Society of America, Abstracts with Programs, Rocky Mountain Section Meeting, (April 17-19), University of Montana, Missoula, Montana, v. 32, no 5, p.10.

Gaylord, D.R., Link, P.K., and McKoon, J.T., 2015, Provenance of the Pleistocene and Holocene St. Anthony dune field, eastern Snake River Plain, Idaho: insights from U/Pb detrital zircon geochronology: Northwest Geology, v. 44, p. 89–100.

Gaylord, D.R., Link, P.K., Rittenour, T.M., Grant, C.A., and Coleman, A.J., 2016, Sedimentology, stratigraphy, geomorphology and paleoclimate in mid-Late Pleistocene ghost dune hollows, eastern Snake River Plain, Idaho: Abstracts with Programs, Rocky Mountain Section Meeting, (May 18-19), University of Idaho, Moscow, Idaho.

Geslin, J.K., Link, P.K., Riesterer, J.W., Kuntz, M.A., and Fanning, C.M., 2002, Pliocene and Quaternary stratigraphic architecture and drainage systems of the Big Lost Trough, northeastern Snake River Plain, Idaho, in Link, P.K., and Mink, L.L., eds., Geology, Hydrogeology, and Environmental Remediation: Idaho National Engineering and Environmental Laboratory, Eastern Snake River Plain, Idaho: Boulder Colorado, Geological Society of America Special Paper 353, p. 11–26.

Hoover, R.H., 2014, Investigation of the influences of meteorology and topographic features on the mobility of the NE portion of the St. Anthony dune field, Idaho: Washington State University, unpublished M.S. thesis, 98 p.

Hunter, R.E., 1977, Basic types of stratification in small eolian dunes: Sedimentology, v. 24, p.

361–387.

Kuntz, M.A., Covington, H.R., and Schorr, L.J., 1992, An overview of basaltic volcanism of the eastern Snake River Plain, in Link, P.K., Kuntz, M.A., and Platt, L.B., eds., Regional Geology of Eastern Idaho and Western Wyoming: Geological Society of America Memoir 179, p. 227–267.

Kuntz, M.A., Geslin, J.K., Mark, L.E, Hodges, M.K.V., Kauffman, M.E., Champion, D.E., Lanphere, M.R., Rodgers, D.W., Anders, M.H., Link, P.K., and Boyack, D.L., 2003, Geologic map of the northern and central parts of the Idaho National Engineering and Environmental Laboratory, Eastern Idaho: Idaho Geological Survey Geologic Map 35, scale 1:50,000.

Kuntz, M.A., Christiansen, D.P., Van Sistine, D.E. Champion, K.L., Pierce, K.L., Moore, D.K., and Turrin, B.D., in press, Geologic map of the Henrys Fork Caldera and the eastern part of the Spencer-High Point Volcanic Rift Zone, eastern Idaho, Henrys Fork Foundation: U.S. Geological Survey Miscellaneous Map Series, scale 1:50,000.

Morgan, L.A. and McIntosh, W.C., 2005, Timing and development of the Heise volcanic field: Geological Society of America Bulletin, v. 117, p. 288–306.

Pierce, K.L., and Morgan, L.A., 1992, The track of the Yellowstone hot spot : Volcanism, faulting, and uplift, in Link, P.K., Kuntz, M.A., and Platt, L.B., (eds.), Regional Geology of Eastern Idaho and Western Wyoming: Geological Society of America Memoir 179, p. 1–54.

Rich, J., Rittenour, T.M., Nelson, M.S., and Owen, J., 2015, OSL chronology of middle to late Holocene aeolian activity in the St. Anthony dune field, southeastern Idaho, USA: Quaternary International, v. 362, p. 1–10.

Scott, W.D., 1982, Surficial geologic map of the eastern Snake River Plain and adjacent areas, 111°–115°W. Idaho and Wyoming: U.S. Geological Survey Miscellaneous Series Map I-1372, scale 1:250,000.

FIELD GUIDE TO THE RECENT VOLCANIC HISTORY OF THE SOUTH FORK AREA BETWEEN SWAN VALLEY AND RIRIE, IDAHO

D.K. Moore and G.F. Embree

Brigham Young University, Rexburg, Idaho

INTRODUCTION

From Alpine, WY to Ririe, ID, the South Fork of the Snake River flows northwest within the Swan Valley graben. The river enters the Heise volcanic field just before it emerges onto the Snake River Plain, near Ririe, ID. Figure 1 shows the geography of the area and the field trip route. The Big Hole Mountains and Caribou Range that bound the Swan Valley graben are Basin and Range horsts composed of folded and faulted Paleozoic and Mesozoic sedimentary rocks. These rocks underlie Miocene to Pliocene (~6.6–4.4 Ma) rhyolites of the Heise volcanic field and Pliocene to Pleistocene (~4–2 Ma) Snake River Plain basalt lava fields. The graben fill consists of Miocene through Pleistocene volcanic rocks and intercalated fluvial, alluvial, and lacustrine sediments. This field guide summarizes the recent volcanic history of the area and its effect on the course of the South Fork River. Moore and others (2014) divided this recent history into four periods, summarized below and illustrated in figure 2.

Stage 1: ~7 to after 4 Ma. The Yellowstone–Snake River Plain volcanic field began at ~17 Ma near the Idaho–Nevada–Oregon border and reached the Yellowstone National Park area by 2 Ma. It consist of rhyolite overlain by basalt. These volcanic patterns result from movement of North America over the Yellowstone hotspot, which produced topographic highs and rhyolitic volcanism. Subsidence and basaltic volcanism followed, as North America carried the volcanic centers off the hotspot. When the Heise volcanic field lay above the hotspot, the ancient Snake River flowed to the south, away from the hotspot bulge through the active Swan Valley graben (fig 2A).

Stage 2: ~4 to 2 Ma. As the North American plate carried the Heise volcanic field southwest off the hotspot, the area subsided. Around 4 Ma, the basalt of Swan Valley erupted near the center of the graben, forming a broad constructive edifice. Eventually, the South Fork drainage reversed course and began flowing north. At this time, deposits from the ~4 Ma basalt eruption diverted Pine Creek to the north, causing Pine Creek to join the South Fork farther downstream, near present day Table Rock (fig 2B).

Stage 3: ~2 Ma. Shortly after emplacement of the Huckleberry Ridge Tuff, basaltic lava erupted on Antelope Flats. Flows from this eruption filled and dammed South Fork canyon, forming a large reservoir that Moore and others (2014) named Swan Lake. Figure 3 shows the maximum extent of this lake. Lava flows also partially filled Pine Creek canyon, damming Pine and Table Rock Creeks. Figure 2C shows basalt flowing into both canyons and damming the South Fork River. When Swan Lake filled, water flowed east into the partially lava-filled Pine Creek canyon, over the volcanic deposits that separated the two canyons.

Stage 4: ~2 Ma to present. Swan Lake persisted, at ever-shallower depths, as water flowing from the lake into Pine Creek canyon cut the current course of the South Fork between Conant Valley and the mouth of Pine Creek. Figure 2D shows the current course of the South Fork River.

FIELD TRIP

Figure 1 shows the field trip route, stops (table 1), and other notable locations (table 1). The Dossett and others (2012) map shows the distribution of geologic units in the area of the field guide; the Heise (Phillips and others, 2016a) and Poplar (Phillips and others, 2016b) quadrangle geologic maps may also be helpful. Table 2 gives the ages of local volcanic units.

Before beginning the trip, enter the coordinates from table 1 into a global positioning system (GPS) instrument. Use these coordinates to navigate to each spot. (We also provide road directions below.) The field guide begins at the intersection of Highway 26 and 48, 1 mi south of Ririe, Idaho.

Drive southeast on Highway 26 for 21.4 mi into Conant Valley, then turn right onto a gravel road and park.

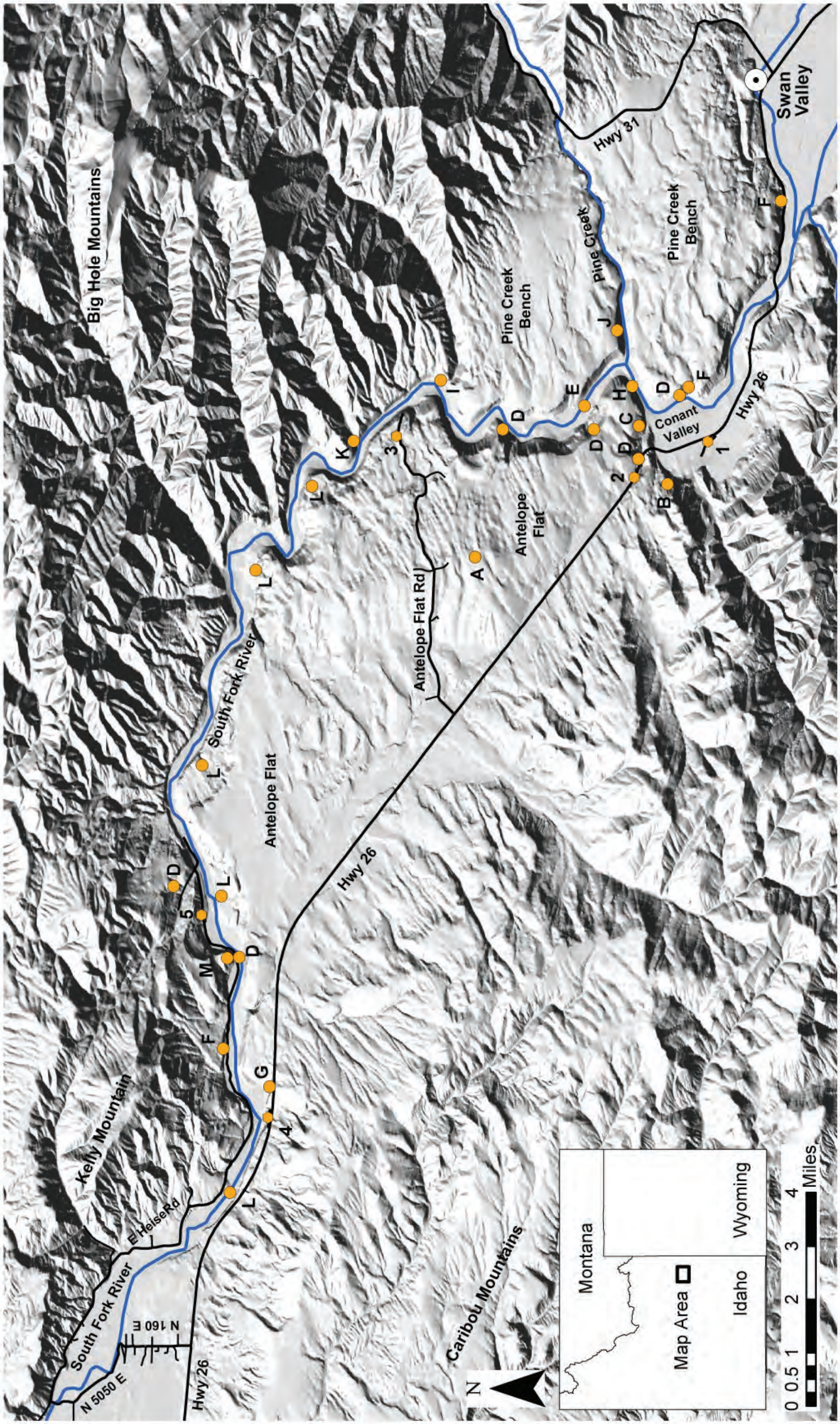

Figure 1. Local geography and field trip route and locations. Numbered locations are field trip stops; locations marked by letters are additional areas of interest. Table 1 lists location coordinates. We show roads that cross the field trip route as stubs—to aid in navigation.

Table 1. Field trip coordinates. Numbered locations are field trip stops; locations marked by letters are additional areas of interest. Datum: WGS84.

Location	Name	Latitude	Longitude
1	Overview	43.4692	111.4398
2	The dam	43.4891	111.4494
3	Canyon overlook	43.5535	111.4383
4	Hwy 26 0verlook	43.5883	111.6230
5	Table Rock	43.6064	111.5680
A	Vent area	43.5322	111.4711
B	Western paleocanyon wall	43.4800	111.4513
C	Eastern paleocanyon wall	43.4878	111.4356
D	Hyaloclastite	43.4768	111.4273
		43.4879	111.4445
		43.5000	111.4364
		43.5247	111.4365
		43.6139	111.5603
		43.5961	111.5795
E	Pine Creek lava dam	43.5025	111.4301
F	Pillow Basalt	43.4744	111.4249
		43.6004	111.6044
		43.4493	111.3745
G	South Fork paleocanyon	43.5879	111.6146
H	Paleogeographic high	43.4895	111.4247
I	Dry Canyon	43.5415	111.4231
J	Pine Creek Canyon	43.4937	111.4096
K	Gomer Canyon	43.5651	111.4396
L	Late stage lava bench	43.5990	111.6439
		43.6010	111.5629
		43.6062	111.5274
		43.5916	111.4746
		43.5764	111.4518
M	Table Mountain Dam	43.5994	111.5798

Table 2. Ages of local volcanic units.

Unit	Age (Ma)	Reference
Basalt of Sommer's Butte	2.08 ± 0.08 (Ar-Ar)	Embree and others, 2016a
Basalt of Antelope Flat	1.5 ± 0.8 (K-Ar) ~2 Ma (correlation)	Anders and others, 1989 Moore and others, this volume
Huckleberry Ridge Tuff	2.059 ± 0.004 (Ar-Ar)	Lanphere and others, 2002
Rexburg Basalt	3.59 ± 1.36	Embree and others, 2016b
Basalt of Swan Valley	4.0 ± 1.0 (K-Ar)	Anders and others, 1989

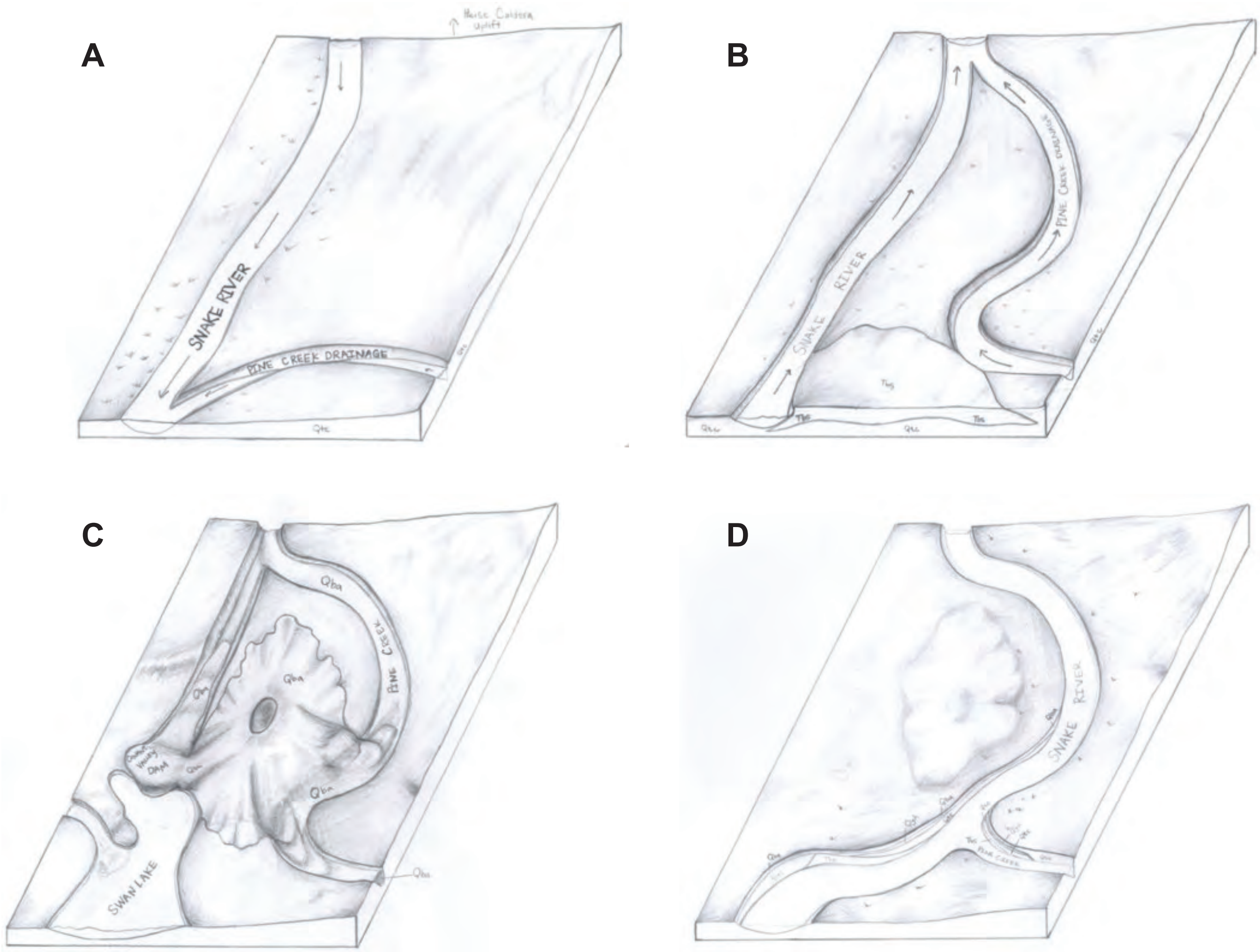

Figure 2. Inferred history of interactions between the South Fork, Pine Creek, and basalt lava flows (Moore and others, 2014). A. Between ~7 and 4 Ma, the South Fork and its tributaries flowed southward from the topographic high of the Heise volcanic field, which produced the rhyolite units of the Heise group. B. Between ~4 and 2 Ma, this area subsided—after migrating off the Yellowstone hotspot high—and the South Fork River drainage reversed course and began flowing north. During this time, the basalt of Swan Valley erupted near present-day Swan Valley bridge, forming a topographic high that separated South Fork and Pine Creek canyons. C. Around 2 Ma, the Antelope Flat flow field erupted, shortly after emplacement of the Huckleberry Ridge Tuff. The resulting lava flows dammed and filled the ancient South Fork River canyon, dammed and partially filled the ancient canyons of Pine and Table Rock Creeks, and formed Swan Lake. D. Not long after forming, Swan Lake overflowed, cut a canyon through the topographic high that had separated South Fork and Pine Creek canyons, and formed the current courses and canyons of the these rivers.

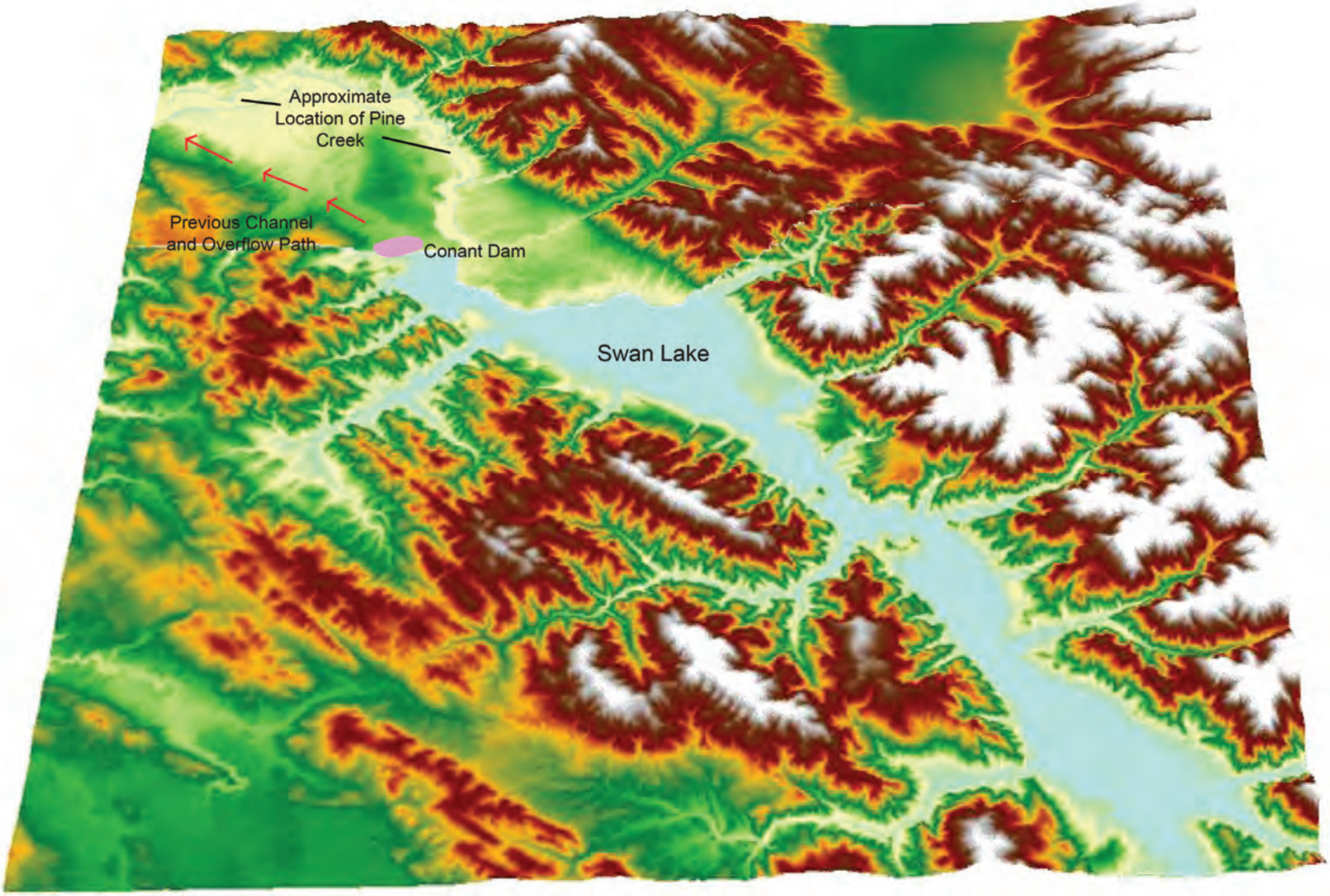

Figure 3. Image showing the maximum extent of Swan Lake, which formed when a lava dam filled the ancient South Fork canyon. The top of the lava dam is at about the same elevation as Palisades dam. Swan Lake, which extended as much as 30 mi south, created a reservoir that covered about twice as large an area as Palisades Reservoir.

STOP 1

Overview of basalt–river interactions. Shortly after 2 Ma, basalt erupted from a vent on Antelope Flat. Location A (fig. 1, table 1) marks the vent area for this eruption. Lava from the vent covered Antelope Flat and flowed west into the South Fork paleocanyon, east into the Pine Creek paleocanyon, and onto the northern part of Pine Creek Bench. To the south, it flowed across the basalt of Swan Valley deposits onto the southern part of Pine Creek Bench. These flows dammed the canyons they entered. The basalt formed thin deposits (usually less than 100 ft) on Antelope Flat and Pine Creek Bench and thick deposits (up to ~400 ft) in paleocanyons (Dossett and others, 2012).

Figure 4 is an annotated image of the Conant Valley lava dam, which formed in the South Fork paleocanyon and lies in front of you to the north. The dam deposits in this escarpment consist of more than 200 ft of hyaloclastite, overlain by several subaerial basalt flows with pillow bases and thin, intercalated hyaloclastite deposits. These flow packages record interactions between the deepening lake and the growing dam. Location B marks the western paleocanyon wall, made mostly of Heise volcanic field units, and location C marks the eastern paleocanyon wall, made of the basalt of Swan Valley (fig. 1; Dossett and others, 2012). At the base of Pine Creek Bench to the east lies a laminated to thin-bedded hyaloclastite deposit composed of silt to course sand. Abundant graded bedding suggests that much of this deposit resulted from turbidity currents flowing down the hyaloclastite delta and onto the bottom of Swan Lake.

The interactions of basalt and water produced abundant hyaloclastite and some pillow basalt. Locations marked by D in figure 1 contain hyaloclastite deposits. These deposits record at least three lava dams: the largest—the Conant Valley lava dam—lies at location 2; two additional dams in ancient Pine Creek canyon lie at locations marked by E (the Pine Creek lava dam) and K (the Table Rock lava dam) in

Figure 4. Annotated image of the Conant Valley lava dam. Map unit symbols show rock type (Dossett and others, 2012). Qbah and Qbar are the basalt of Antelope Flat: Qbah is the hyaloclastite facies and Qbar is the plateau facies. Tbs is the basalt of Swan Valley.

figure 1. These lava dam remnants consist of variably-palagonitized hyaloclastite, angular basalt fragments, spatter, and intercalated basaltic lava flows. Locations marked by F in figure 1 contain pillow basalts. At the southernmost location F, just east of the Swan Valley bridge, basalt from Antelope Flat that had flowed south over Pine Creek Bench entered the reservoir (Swan Lake) it had created.

Today, the South Fork turns east at the northern end of Conant Valley. At 2 Ma, it flowed straight to the north. The lava that dammed the canyon filled it from the dam north to location G (fig. 1)—where ancient Pine Creek joined the South Fork. At that time, a paleotopographic high extended north and south from location H (fig. 1). The paleotopographic high consisted mostly of older basalt.

Return to Highway 26. Drive north for 1.8 mi, out of Conant Valley, to Stop 2.

STOP 2

Conant Valley lava dam. Figure 5 shows the interior structure of the upper part of the dam complex. As seen from the last stop, the dam consists of hyaloclastite, overlain by several subaerial basalt flows with pillow bases and thin, intercalated hyaloclastite deposits. The hyaloclastite consists of angular basalt sands cemented by palagonite and contains angular blocks, spatter, and bombs. Depositional contacts and slump faults separate cohesive blocks of hyaloclastite. The hyaloclastite records subaerial basalt that flowed into water near the shore. The subaerial flows with pillow bases likewise record interactions between the deepening lake and the growing dam. A short, strenuous hike to the east leads to a well-exposed portion of the paleocanyon wall at location E (fig. 1). Thick sections of basalt (and hyaloclastite) in wells located to the north identify the course of ancient South Fork and Pine Creek canyons (fig. 6). Today, the straight section of highway to the north follows the basalt-filled paleocanyon of the South Fork River.

Drive north on Highway 26 for 4.7 mi. Turn right on Antelope Flat Road. This road leads through private land. Obtain permission before entering. (Contact the property manager at South Fork Lodge; 208-483-2112; 40 Conant Valley Loop Rd, Swan Valley, ID 83449. Ask for access to Antelope Flat Road at the canyon rim.) Use GPS to drive 4.5 mi to a cabin near the canyon rim. From the cabin, follow the path east to the rim.

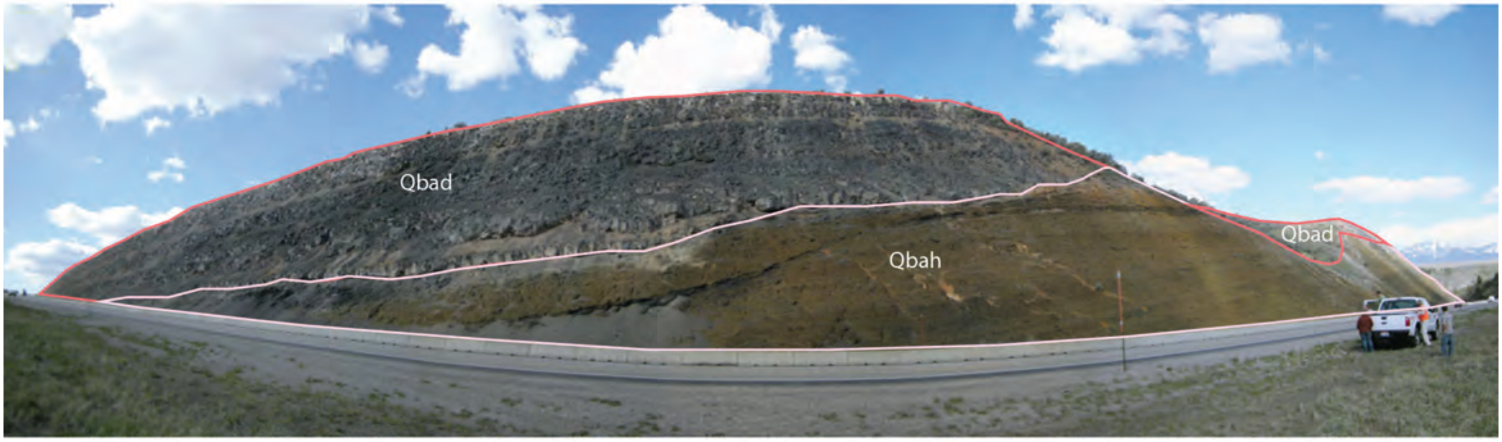

Figure 5. Annotated image of road cut through Conant Valley lava dam. The lower part of the dam (Qbah) is hyaloclastite with some basalt fragments and splatter. The upper portion (Qbad) consists of several lava flow packages: subaerial lava flows with pillow bases on hyaloclastite. These packages record interactions between the deepening lake and growing dam.

STOP 3

Paleocanyon-fill basalt. This stop shows the distribution of canyon-fill basalt. In the present South Fork canyon, thick paleocanyon-fill lava provides the false impression that the thick basalt extends laterally into the canyon walls. Instead, the basalt thins rapidly up the edges of the paleocanyon and into its tributaries. Figure 7 shows annotated images of paleocanyon walls and tributary canyons—upstream at Dry Canyon (fig. 7A; location I in fig. 1) and Pine Creek Canyon (fig. 7B; location J in fig. 1) and downstream at Gomer Canyon (fig. 7C; location K in fig. 1).

Return to Highway 26. Turn right (north) on the highway and drive 6.8 mi to the rest stop on the right. Follow the walkway down to a good overlook of the canyon.

STOP 4

Highway overlook. This stop shows where ancient Pine Creek flowed into the South Fork (fig. 6A). Location G (fig. 1), to the right, marks the cliff wall that exposes lava flows that filled the ancient South Fork River canyon. To the east, the modern South Fork River follows the ancient course of Pine Creek. The Table Rock lava dam lies in this canyon at location M. In the foreground near the bend of the river lies a slump block of basalt. To the northeast, Kelly Mountain and the Heise cliffs expose volcanic rocks of the Heise volcanic field (~6.6–4.4 Ma).

Orientations of remanent magnetization indicate that complex interactions between the river and Antelope Flat lava produced basalt flows at several elevations in paleocanyons near this stop (Dossett and others, 2012). Flows from the vent covered Antelope Flat, forming thin basalt deposits seen on the canyon rim to the east and south. Flows that entered and filled the South Fork paleocanyon produced the thick basalt deposits seen to the south. Basalt that flowed from the South Fork paleocanyon and over the rim dammed ancient Pine Creek near Table Rock, to the east. At times, the basalt flowed into water, producing hyaloclastite and pillows. At other times, it flowed across the exposed top of the dam to form subaerial lava flows. As the dam grew, hyaloclastite and basalt flows formed at successively higher levels. Eventually, rising water flowed over the dam and cut through it. Shortly thereafter, basalt entered the Pine Creek paleocanyon west of the vent and flowed downstream through the breach in the Table Rock dam. Later, the river cut a new channel along the margins of these flows. Today, remnants of these flows form the lava benches seen near the canyon bottom to the east and north. The terminus of this late stage flow lies nearly 2.5 mi downstream, to the north.

Turn right onto US-26 and use your GPS unit to drive to the Heise Bridge, cross the river, and drive to stop 5. (Drive for 5.1 mi on the highway, and then turn right onto N 160 E. Drive north 0.9 mi, and then continue north on N 4950 E. Drive north 1.1 mi, and then turn right onto E 100 N/Heise Road/Poplar Loop. Drive east 0.8 mi, and then continue left on N 5050 E for 0.4 mi, across the bridge. Turn right onto E Heise Road for 2.3 mi, and then turn right to stay on E Heise Road. Drive 6.8 mi, past Table Rock, to stop 5.)

A

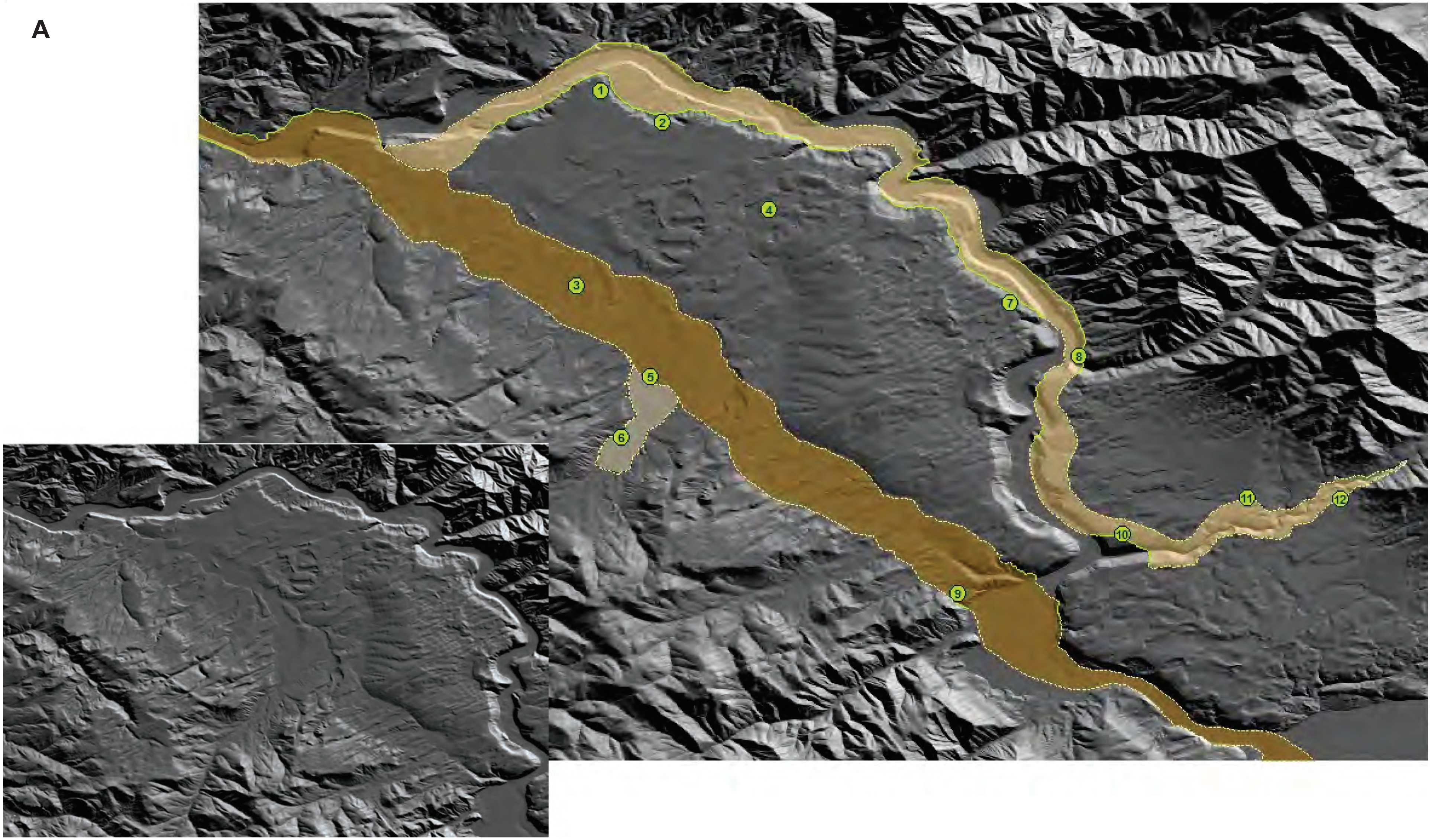

Figure 6. Locations of paleocanyons. A. Shaded relief map showing the locations of well logs and ancient South Fork (darker) and Pine Creek (lighter) canyons. The basalt is thin where it flowed across plateaus and thick where it flowed into canyons. B. Well logs showing thin basalt on Antelope Flat and Pine Creek Bench (in wells 1, 2, 4, 7, and 8) and thick basalt/hyaloclastite in South Fork and Pine Creek paleocanyons (in wells 3, 5, 9, 10, 11, and 12).

B

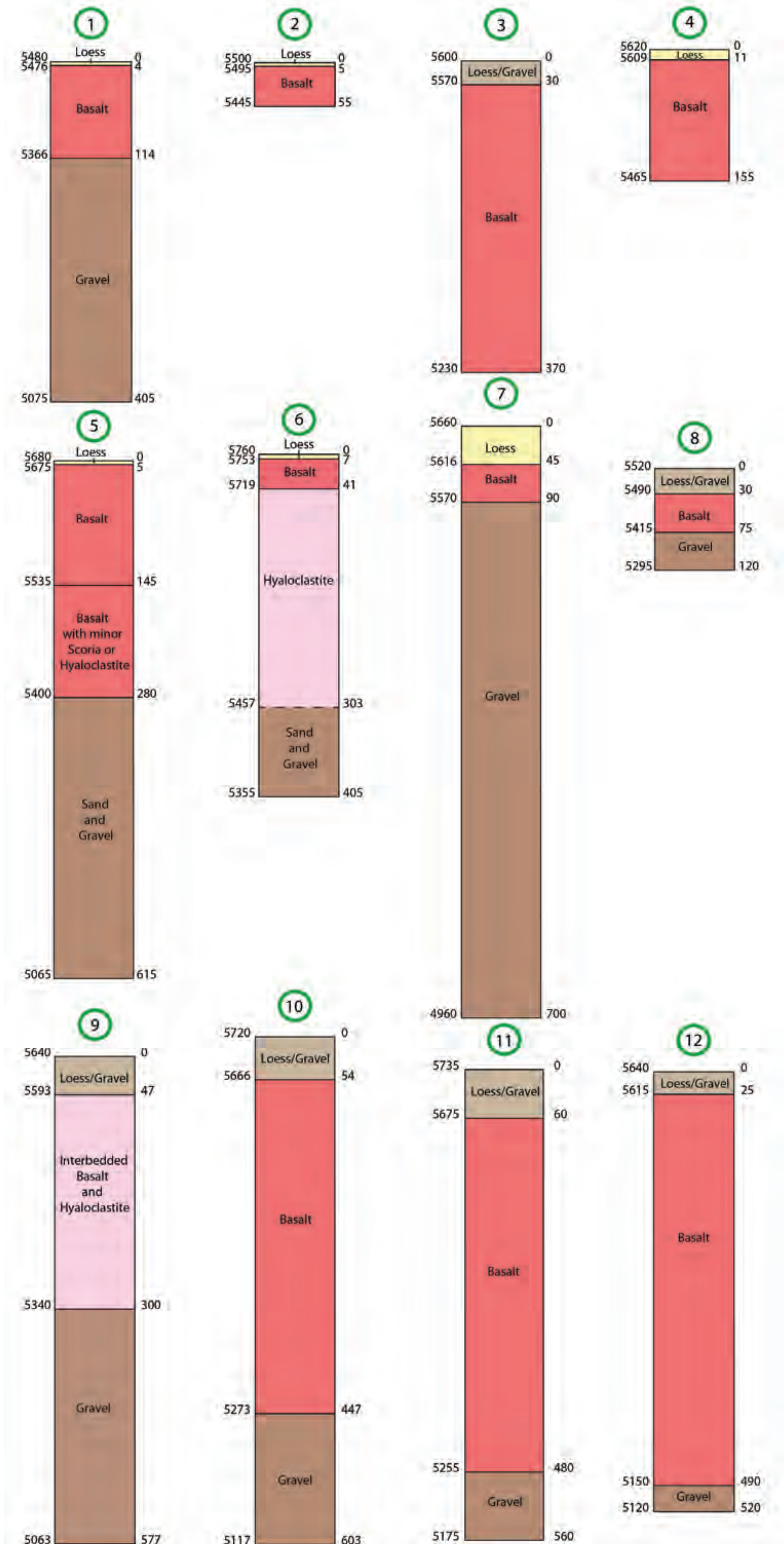
1
5480
5476
Loess
0
4
Basalt
5366
114
Gravel
5075
405
2
5500
5495
Loess
0
5
Basalt
5445
55
3
5600
0
Loess/Gravel
5570
30
Basalt
5230
370
4
5620
5609
Loess
0
11
Basalt
5465
155
5
5680
5675
Loess
0
5
Basalt
5535
145
Basalt with minor Scoria or Hyaloclastite
5400
280
Sand and Gravel
5065
615
6
5760
5753
Loess
0
7
Basalt
5719
41
Hyaloclastite
5457
303
Sand and Gravel
5355
405
7
5660
0
Loess
5616
45
Basalt
5570
90
Gravel
4960
700
8
5520
0
Loess/Gravel
5490
30
Basalt
5415
75
Gravel
5295
120
9
5640
0
Loess/Gravel
5593
47
Interbedded Basalt and Hyaloclastite
5340
300
Gravel
5063
577
10
5720
0
Loess/Gravel
5666
54
Basalt
5273
447
Gravel
5117
603
11
5735
0
Loess/Gravel
5675
60
Basalt
5255
480
Gravel
5175
560
12
5640
0
Loess/Gravel
5615
25
Basalt
5150
490
Gravel
5120
520

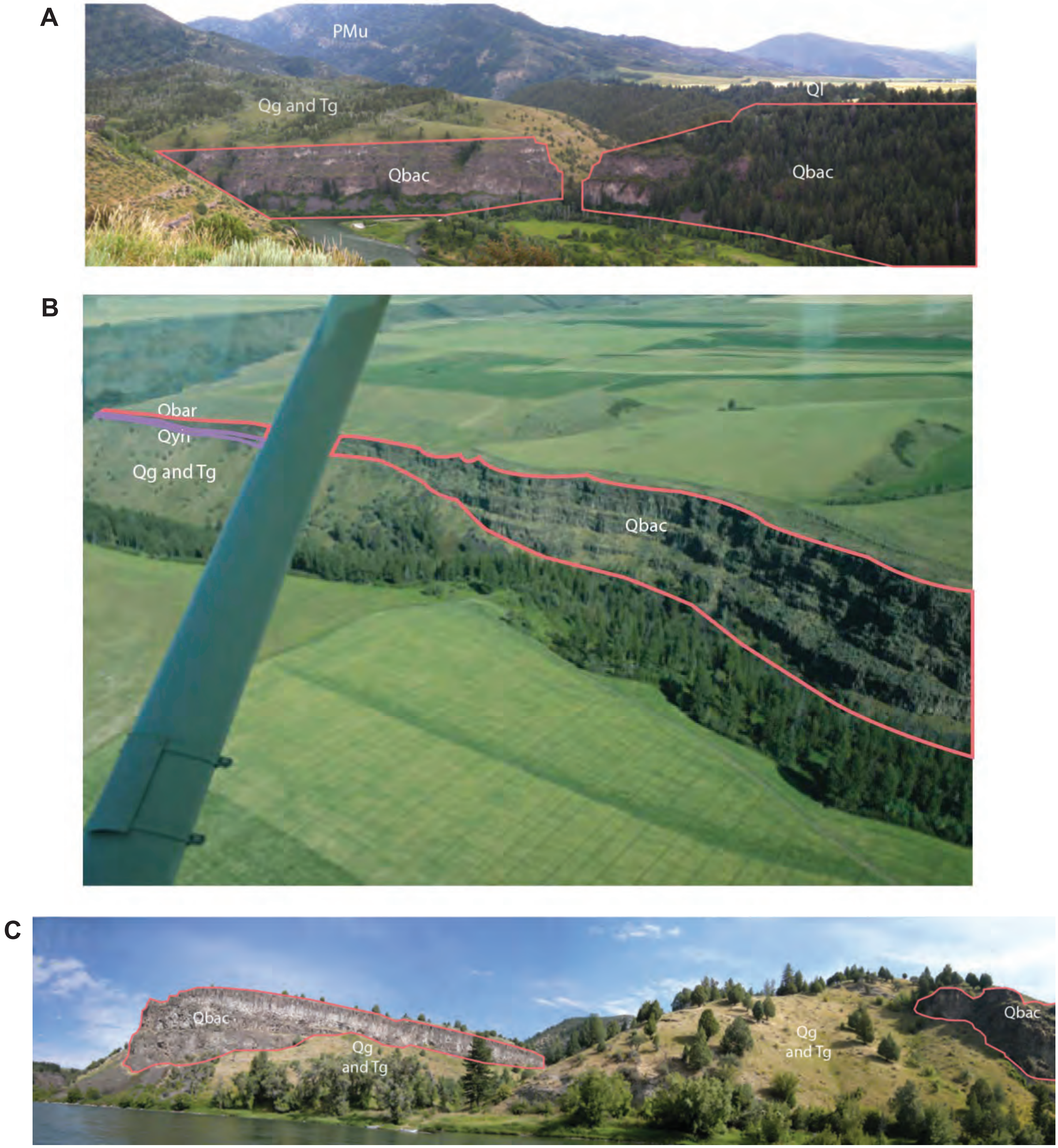

Figure 7. Ancient canyon walls. A-C. Annotated images showing the distribution of the paleocanyon-fill facies of the basalt of Antelope Flat (Qbac) at Dry Canyon (A; Location I in fig. 1), Pine Creek Canyon (B; Location J in fig. 1), and Gomer Canyon (C; location K in fig. 1); Qbar is the plateau facies; Qyh is the Huckleberry Ridge Tuff; Qg and Tg are gravel; PMu are Paleozoic sedimentary rock units. The basalt is thick where it flowed into and partially filled the canyons and thins rapidly up canyon walls and into tributary canyons.

Figure 8. Annotated image of the Table Rock lava dam. The line drawn from the northern edge of the Huckleberry Ridge Tuff (Qyh) beneath the hyaloclastite (Qbah) and lowest subaerial flow (Qbad) marks the northern edge of the paleocanyon. (Note: the hyaloclastite that appears to lie beneath the Huckleberry Ridge Tuff in the image does not; instead, the hyaloclastite lies next to rocks that underlie the Huckleberry Ridge Tuff, along the paleocanyon wall.) The lava dam consists of hyaloclastite facies (Qbah) and subaerial basalt facies (Qbad). The relationships between facies records the formation of the dam and rising of water in the intracanyon reservoir upstream of Table Rock.

STOP 5

Table Rock lava dam. Figure 8 shows the internal structure of the lava dam to the west, at Table Rock. The dam, which lies on river gravel, consists of hyaloclastite and intercalated subaerial lava flows. The hyaloclastite contains angular basalt blocks and vesicular spatter. The subaerial lava flow that caps the dam entered the canyon from the south rim and flowed north across the dam. The northern paleocanyon wall begins at the southern extent of the Huckleberry Ridge Tuff (fig. 8) and extends vertically down and then laterally to where hyaloclastite overlies gravel, near the river. Hyaloclastite that was once part of the dam lies at the base of the cliff across the river.

Shortly after the Table Rock lava dam formed and before the Antelope Flat eruption ended, water from the intracanyon reservoir overtopped the dam and cut through it, allowing ancient Pine Creek to follow its pre-dam course. Then, late-stage lava from the Antelope Flat vent flowed into and down ancient Pine Creek, through the breached Table Rock dam, and down South Fork canyon to where it ends nearly 5 mi downstream from the dam. This lava formed the lava bench that lies across the river. At this stop, subaerial Antelope Flat flows lie at four elevations—at the lava bench to the south, at the canyon rim to the south, and inside and atop the dam to the west.

Remnants of the Table Rock lava dam lie to the southeast up Table Rock Creek canyon. Here, up-to-the-north normal faults lifted the hyaloclastite deposits to nearly the same elevation as the Antelope Flat vent (Dossett and others, 2012).

REFERENCES

Anders, M.H., Geissman, J.W., Piety, L.A., and Sullivan, J. T., 1989, Parabolic distribution of circum-eastern Snake River Plain seismicity, and latest Quaternary faulting: Migratory pattern and association with the Yellowstone hotspot: Journal of Geophysical Research, v. 94, p. 1589-1621.

Dossett, T.S., Reed, T.H., McIlrath, S.L., Moore, D.K., and Embree, G.F., 2012, Geologic Map of the South Fork of the Snake River between Swan Valley and Ririe, Idaho: Idaho Geological Survey Technical Report T-12-5.

Embree, G.F., Moore, D.K., Phillips, W.M., and Prostka, H.J., 2016a, Geologic Maps of the Moody, White Owl Butte, and Wright Creek Quadrangles, Madison and Teton Counties, Idaho: Idaho Geological Survey Technical Report T-16-2.

Embree, G.F., Phillips, W.M., and Welhan, J.A., 2016b, Geologic map of the Rexburg quadrangle, Madison County, Idaho: Idaho Geological Survey Digital Web Map 178.

Lanphere, M.A., Champion, D.E., Christiansen, R.L., Izett, G.A., Obradovich, J.D., 2002, Revised ages for tuffs of the Yellowstone Plateau volcanic field: Assignment of the Huckleberry Ridge Tuff to a new geomagnetic polarity event, GSA Bulletin, v. 114, p. 559-568.

Moore, D.K., Embree, G.F., Dossett, T.S., Reed, T.H., and McIlrath, S.L., 2014, Plio-Pleistocene Interactions Involving Basalt Flows and the South Fork of the Snake River between Swan Valley and

Ririe, Idaho, Conference on the Late Cenozoic to Recent Geologic and Biotic History of the Snake River, Idaho State University, Pocatello, Idaho.

Phillips, W.M., Moore, D.K., Feeney, D.M., and Embree, G.F., 2016a, Geologic Map of the Heise Quadrangle, Bonneville, Jefferson, and Madison Counties, Idaho: Idaho Geological Survey Digital Web Map 176.

Phillips, W.M., Moore, D.K., and Feeney, D.M., 2016b, Geologic Map of the Poplar Quadrangle, Bonneville County, Idaho: Idaho Geological Survey Digital Web Map 175.

FIELD GUIDE TO THE REXBURG BENCH, IDAHO

G.F. Embree,[1] D.K. Moore,[1] and W.M. Phillips[2]

[1]Department of Geology, Brigham Young University, Rexburg, Idaho; [2]Idaho Geological Survey, University of Idaho, Moscow, Idaho

INTRODUCTION

The southern margin of the Eastern Snake River Plain near Rexburg, Idaho consists of a gently rolling, incised plateau known locally as the Rexburg Bench. This plateau extends west and northwest to the Rexburg Fault and floodplains of the Snake and Teton Rivers, north to the Teton River, east to Canyon Creek, and south and southeast to the Big Hole Mountains. Figure 1 shows the geography of the area. Thick loess deposits cover most of the bedrock on the Rexburg Bench. Table 1 lists the ages of local volcanic units.

The foundations of the Rexburg Bench and surrounding area developed in the Archean and Proterozoic when the Wyoming crustal province formed and developed. Paleozoic and Mesozoic sedimentary rocks deposited on this crystalline basement were thrust eastward during the Sevier Orogeny. Later, slab rollback following the Laramide Orogeny produced the Absaroka volcanic field to the northeast and the Challis volcanic field to the northwest. Block-faulted mountains and valleys developed in the area during Miocene-to-recent extension. The area rose in the Pliocene as North America overrode the Yellowstone hotspot. Volcanism above the hotspot produced the rocks of the Heise volcanic field, including the Blacktail and Kilgore rhyolite tuffs and the rhyolite of Long Hollow lava flow (table 1). These and other volcanic eruptions eliminated the surface expression of Basin-and-Range features in the area. The region subsided and extensional structures, including the Rexburg and Grand Valley faults, redeveloped as the North American plate carried the area off the Yellowstone hotspot.

The Rexburg Bench, which lies at the transition between the Yellowstone–Snake River Plain volcanic province to the north and the Basin and Range extensional province to the south, developed as the area was covered by locally erupted rhyolite and basalt, rhyolite from Yellowstone, and loess. The basalt of Rexburg formed a shield volcano atop Heise volcanic rocks and was later covered by the Huckleberry Ridge Tuff (which erupted from the Yellowstone I caldera). A small volcanic complex consisting of five lava fields developed atop the Huckleberry Ridge Tuff. Over time, loess—derived from the Snake River floodplain—mantled the area. Subsidence of the Snake

Table 1. Ages of local volcanic units.

Unit	Age (Ma)	Reference
Basalt of Aard Farms	1.79-1.95 (stratigraphy)	Embree and others, 2016a
Basalt of White Owl Butte Basalt of Canyon Creek Butte Basalt of Bitter's Butte Basalt of Moody Creek Basalt of Antelope Flat	1.79-2.05 (stratigraphy)	Embree and others, 2016a
Basalt of Sommer's Butte	2.08 ± 0.08 ($^{40}Ar/^{39}Ar$)	Embree and others, 2016a
Huckleberry Ridge Tuff	2.059 ± 0.004 ($^{40}Ar/^{39}Ar$)	Lanphere and others, 2002
Rexburg Basalt	3.59 ± 1.36 (K-Ar)	Embree and others, 2016b
Long Hollow Rhyolite	3.5 ± 0.4 (K-Ar) 4.28 ± 0.18 Ma (U-Pb on zircons)	Morgan and McIntosh, 2005 Bindeman, 2007
Kilgore Tuff	4.45 ± 0.05 ($^{40}Ar/^{39}Ar$)	Bindeman, 2007
Blacktail Tuff	6.62 ± 0.03 ($^{40}Ar/^{39}Ar$)	Bindeman, 2007

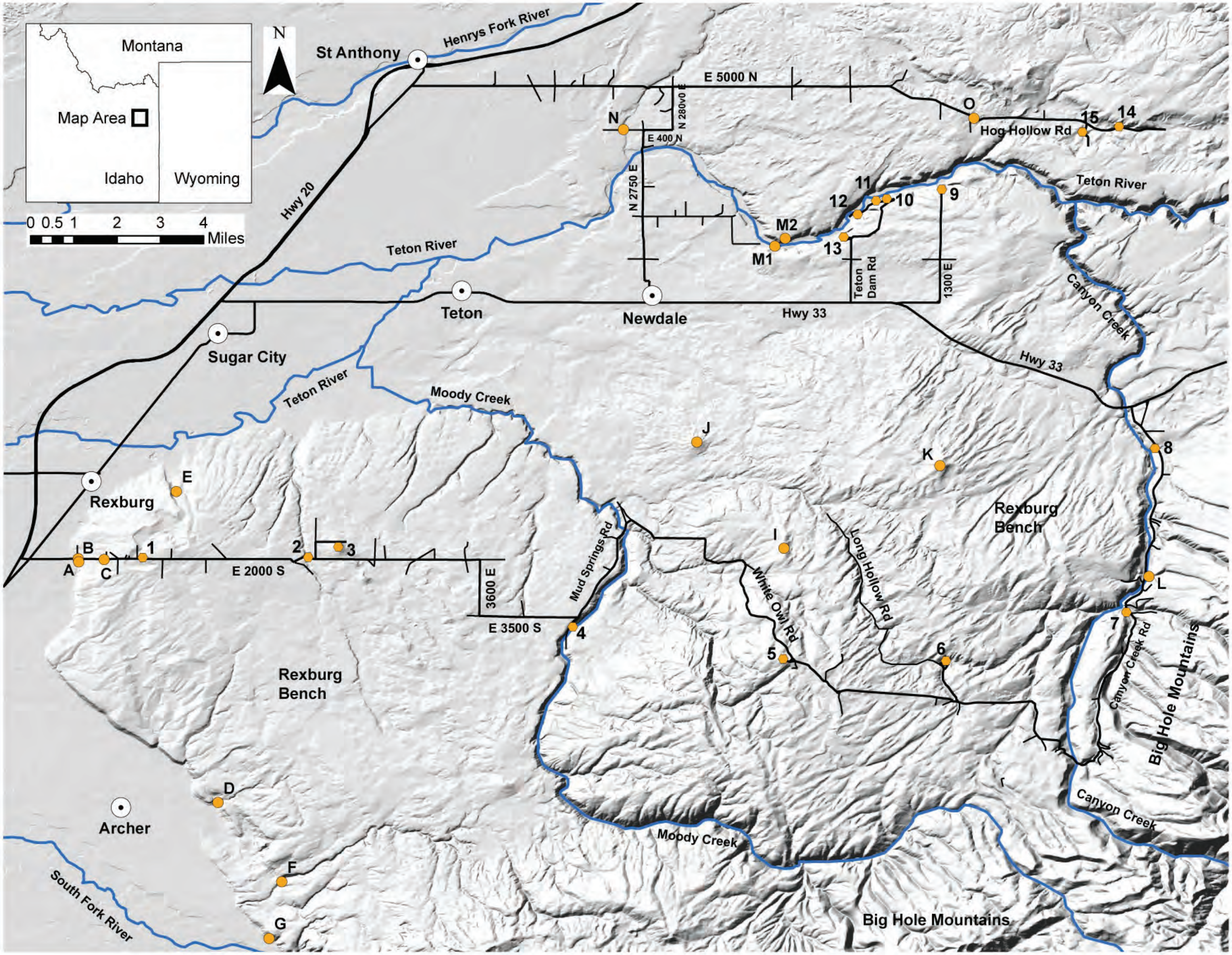

Figure 1. Location map of the field trip route. Numbered locations are field trip stops; locations marked by letters are additional areas of interest. Table 2 lists the latitude and longitude coordinates of the stops and points of interest. Roads that cross the field trip route show as stubs in order to aid in navigation.

River Plain and movement on the Rexburg Fault produced the Rexburg Bench.

FIELD GUIDE

Figure 1 shows the field trip route, stops, and other notable locations. Geologic maps of the following quadrangles show the distribution of geologic units in the area of the field guide: Newdale (Embree and others, 2011), Linderman Dam (Embree and Phillips, 2011), Rexburg (Embree and others, 2016b), Moody (Embree and others, 2016a), White Owl Butte (Embree and others, 2016a), Wright Creek (Embree and others, 2016a), Ririe (Phillips and others, 2014), and Heise (Phillips and others, 2016).

Before beginning the trip, enter the coordinates from table 2 into a global positioning system (GPS) instrument. Use these coordinates to navigate to each spot. (We also provide road directions below.) The field guide begins at the intersection of Old Yellowstone Highway (S Highway 191) and Poleline Road (W 2000 S), ~1 mi south of the intersection of Highway 20 and University Boulevard.

The topographic high that starts nearly a mile east is the Rexburg Bench. Movement along the Rexburg and subsidiary faults elevated the Rexburg Bench. The Rexburg Fault produced the escarpment that defines the western boundary of the Rexburg Bench. The displacement of this normal fault increases to the south where it merges with the Heise Fault, a step-over segment of the Grand Valley Fault system (Dossett and others, 2012).

Drive east along Poleline Road for 1.9 mi.

Location A lies on the Rexburg Fault scarp and marks an outcrop of the Rexburg Basalt. Location B is where Ricks College (BYU-Idaho) geology faculty trenched the Rexburg Fault in 1978 (Williams and Embree, 1980a,b) (fig. 2). The fault zone is about 13 ft (4 m) across and consists of a normal fault with strike N 5º W dip 85º W. The upper 1.3 ft (0.4 m) of sediment was unfaulted. An unconformity separates these sediments from underlying, faulted sediments with about 5.2 ft (1.6 m) of displacement. Location C marks the offset associated with one of the subsidiary faults that forms the margin of the Rexburg Bench.

Table 2. Field trip coordinates. Numbered locations are field trip stops; locations marked by letters are additional areas of interest. Datum: WGS84.

Location	Name	N. Latitude	W. Longitude
1	Rexburg Basalt	43.7978	111.7754
2	Basalt over tuff	43.7980	111.7200
3	Sommer's Butte volcanic rift	43.8015	111.7098
4	Moody Creek	43.7747	111.6313
5	White Owl Butte	43.7639	111.5608
6	Long Hollow Rhyolite	43.7633	111.5061
7	Canyon Creek	43.7795	111.4456
8	Basalt of Ard Farms	43.8344	111.4361
9	Huckleberry antiforms	43.9212	111.5076
10	Upper Huckleberry Ridge Tuff	43.9180	111.5260
11	Middle Huckleberry Ridge Tuff	43.9175	111.5295
12	Huckleberry antiform	43.9128	111.5357
13	Teton Dam overlook	43.9053	111.5404
14	Northern edge of Hog Hollow	43.9423	111.4481
15	Pre-Huckleberry lava flow	43.9405	111.4605
A	Rexburg Basalt outcrop	43.7974	111.7971
B	Rexburg Fault trench	43.7964	111.7970
C	Subsidiary fault	43.7972	111.7884
D	Basalt Quarry	43.7157	111.7502
E	Hidden Valley Graben	43.8200	111.7642
F	Mouth of Lyons Creek	43.6892	111.7288
G	Sommer's Butte hyaloclastite	43.6702	111.7331
H	Sommer's Butte hyaloclastite	43.6633	111.7249
I	Basalt of Moody vent	43.8010	111.5605
J	Bitters Butte vent	43.8365	111.5898
K	Canyon Creek Butte vent	43.8286	111.5081
L	Green Canyon Hot Springs	43.7915	111.4382
M1	Basalt of Moody pillow lavas	43.9021	111.5636
M2	Vantage point for M1	43.9048	111.5601
N	Edge of Chester flow field	43.9413	111.6143
O	Southern rim of Hog Hollow	43.9449	111.4968

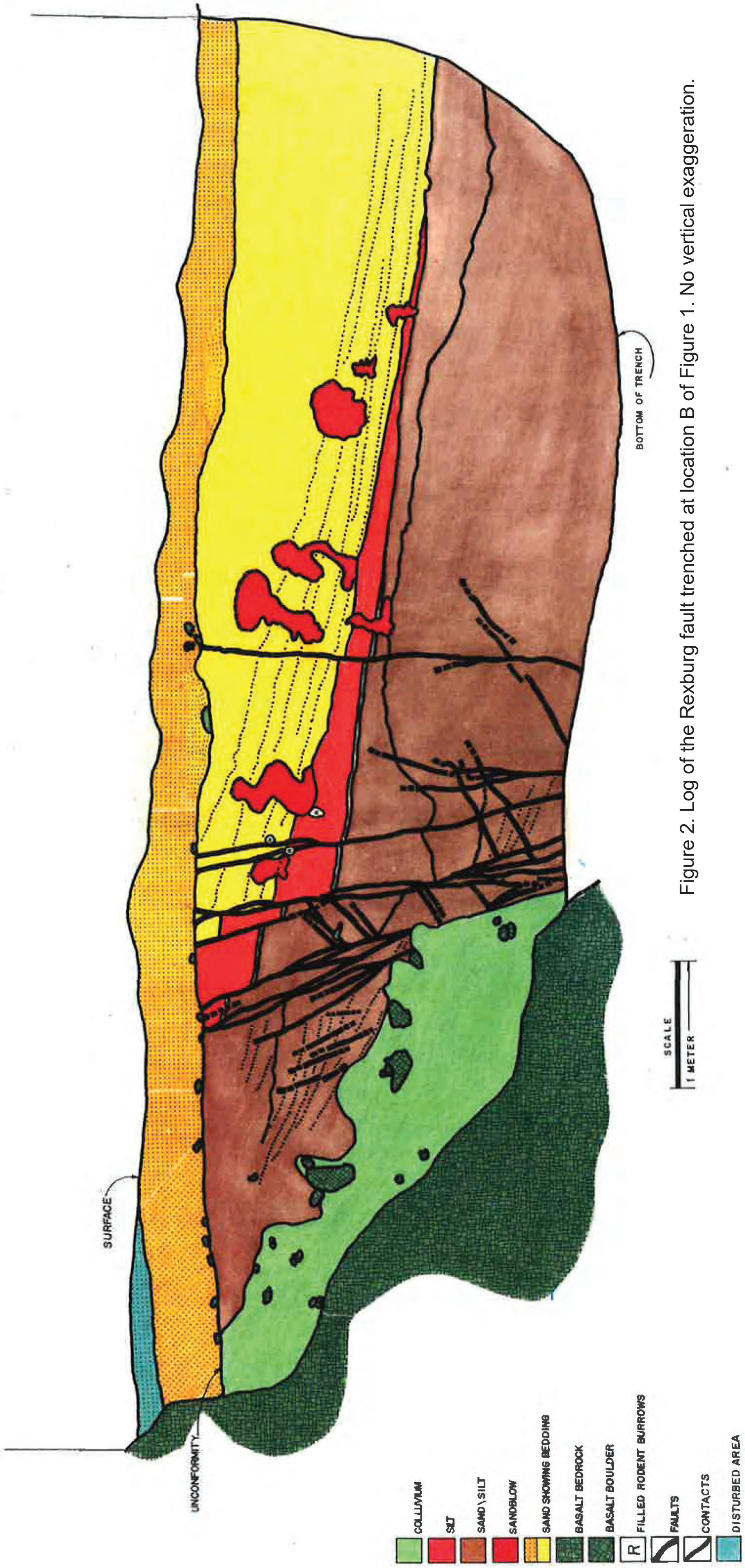

Figure 2. Log of the Rexburg fault trenched at location B of Figure 1. No vertical exaggeration.

Turn left on Ridge View Drive and park where the road intersects Wind Song Drive.

STOP 1

Basalt of Rexburg. A trench to the east exposes fresh outcrop of the basalt of Rexburg, a coarse-grained, diktytaxitic olivine tholeiite. Location D marks a large quarry in this unit, about 6 mi to the south along the Rexburg Fault scarp. Loess conceals nearly all the rock units on the Rexburg Bench. Scattered surface outcrops, several deep gullies, excavations, and well data show the distribution of rock units. Recently, Embree and others (2016a) used digital shaded relief maps to identify flow fronts and vent locations (fig. 3). Well data and topography indicate that the basalt of Rexburg forms a shield volcano that extends beyond the Rexburg Fault to the west and to Moody Creek to the east (fig. 1). The vent area for this shield volcano lies near this stop; it consists of several pit craters and lies concealed beneath Huckleberry Ridge Tuff and loess (Embree and others, 2016b).

Location E marks Hidden Valley, a graben on the northern edge of the Rexburg Bench. The basalt of Rexburg composes the graben walls and floor. The Huckleberry Ridge Tuff caps the basalt in the northernmost part of the graben.

The basalt of Rexburg lies on volcanic rocks of the Heise volcanic field (table 1; Phillips and others, 2016; Embree and others, 1978). In the eastern portion of the Rexburg Bench, the rhyolite of Long Hollow overlies the Kilgore Tuff. The Heise Cliffs, Ririe Reservoir, and Ammon areas provide the best exposures of Heise volcanic field units.

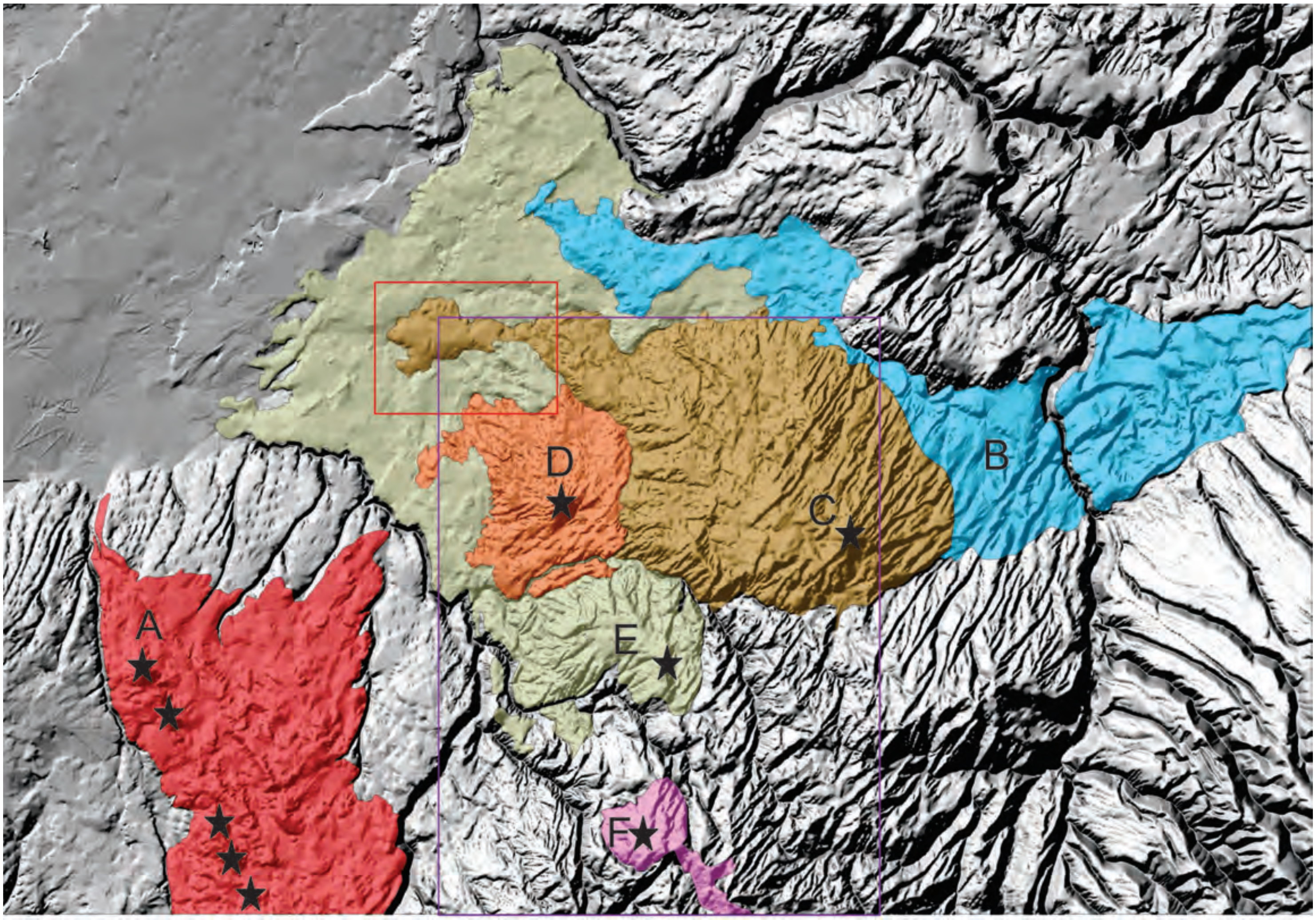

Figure 3. Geologic map showing lava flows of the Rexburg Bench on a 10 m digital hillshade base (after Moore and Embree, 2014). Stars indicate vents. Units A–F are listed in order of youngest to oldest. A. Sommers Butte volcanic rift zone. Note NW–SE alignment of vents. The rift zone appears to be the northern extension of the Basin and Range Grand Valley Fault. B. Basalt of Ards Farm. Vent lies to east of the figure. C. Basalt of Canyon Creek Butte. D. Basalt of Bitters Butte. E. Basalt of Moody. F. Basalt of White Owl Butte. Prominent NE-trending lineaments on the hillshade are parallel to dominant present-day ~N45°E wind direction. Many vents have asymmetrical SW–NE profiles, indicating wind-influenced deposition of cinder during eruptions and/or preferential deposition of loess on the lee side of vent edifices.

Drive east on Poleline Road for 2.5 mi, and then turn left on E 2000 S. Drive for 0.3 mi, and then turn left and park on the dirt road near the bottom of the gully.

STOP 2

Basalt and rhyolite. This small canyon runs along the western edge of the Sommers Butte volcanic rift zone. On the east side of the gully, the basalt of Sommers Butte overlies the Huckleberry Ridge Tuff. The exposures of the Huckleberry Ridge Tuff on the west side of the gully are typical of those found on the Rexburg Bench.

Continue to drive east on E 2000 S for 0.1 mi. At the top of the hill, turn left on S 3000 E (Sommers Road). Drive 0.5 mi, and then turn right on E 1496 S. After 0.4 mi, stop at the farm headquarters on the right to obtain permission to proceed to the top of the butte. If you do not have permission, return to the intersection of E 2000 S and S 3000 E. With permission, continue to the top of the butte.

STOP 3

Summit of Sommers Butte. This is the northernmost and largest of about a dozen cinder and spatter cones in the Sommers Butte volcanic rift zone, a graben that is 13 mi (21 km long and up to 2 mi, 3.2 km, wide). This rift zone trends NW–SE and represents an extension of the Grand Valley Fault (Embree and others, 2016) (fig. 4). No soil horizon lies between this unit and the underlying Huckleberry Ridge Tuff, which is consistent with similar $^{40}Ar/^{39}Ar$ dates for

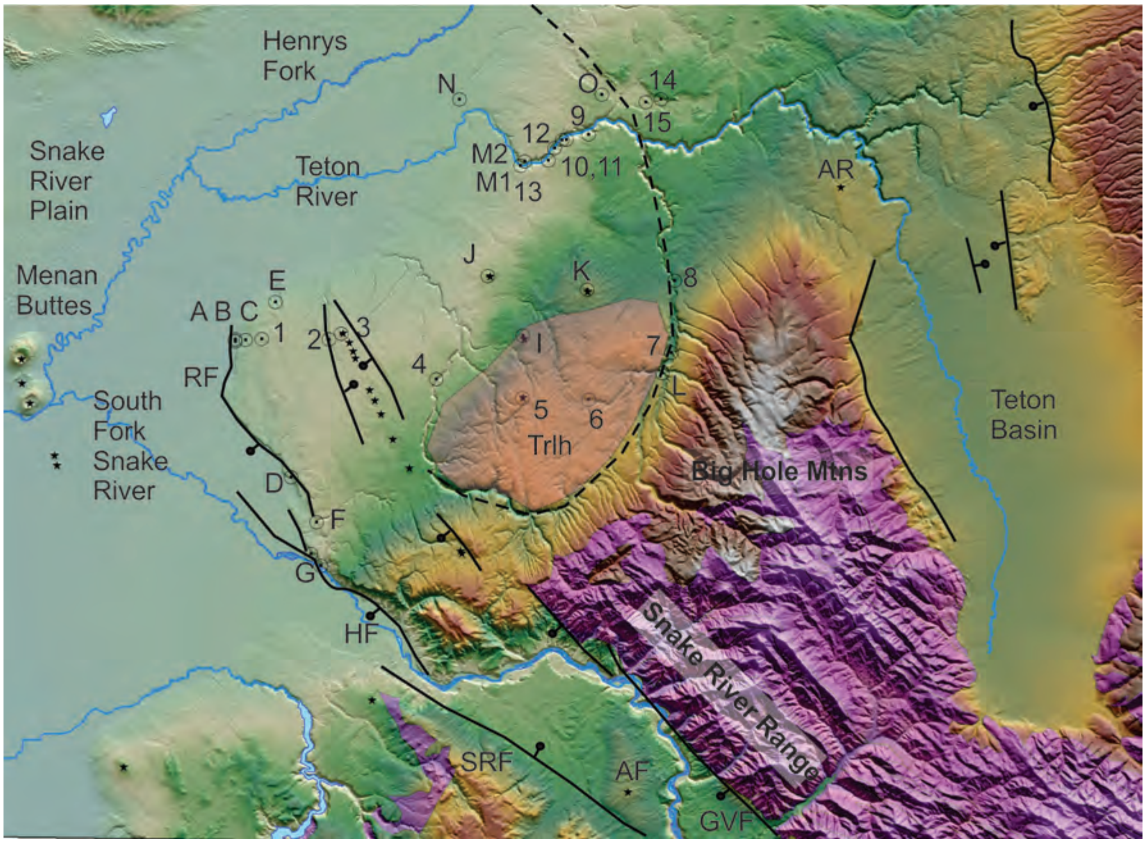

Figure 4. Shaded relief map of the Rexburg Bench area showing rhyolite of Long Hollow (Trlh) and the inferred location of the eastern Kilgore caldera boundary (dashed line). Note the truncation of the Big Hole Mountains and Snake River Range (shown in purple where underlain by Paleozoic and Mesozoic sedimentary rocks) by the inferred caldera boundary. Open circles are field stops and locations of interest (fig. 1; table 2). Black lines are normal faults with mostly early Pleistocene movement. Stars are basaltic vents; AF is vent for basalt of Antelope Flat; AR is vent for basalt of Aard Farms. Major faults are GVF–Grand Valley Fault, SRF–Snake River Fault, RF–Rexburg Fault, HF–Heise Fault.

these units (table 1). The vent for the basalt of Antelope Flat lies along strike, 16 mi (26 km) to the south (fig. 4, location AF). This lava field likewise lies directly on the Huckleberry Ridge Tuff, suggesting that the Sommers Butte and Antelope Flat eruptions were nearly contemporaneous (Dossett and others, 2012; Moore and others, this volume).

Lava flows filled the Sommers Butte rift graben and overflowed to the east and west. In this graben, basalt is up to 320 ft (98 m) thick; outside the graben, basalt is less than 70 ft (21 m) thick (Embree and others, 2016). Location F marks the mouth of Lyons Creek, and Locations G and H mark hyaloclastite deposits formed as lava from the rift zone flowed southwest down Lyons Creek and into the South Fork River (Phillips and others, 2016).

Return to E 2000 S and drive east for 2.7 mi, and then turn right (south) on 3600 E. After 1.3 mi, turn left (east) on E 3500 S. Continue for 1.7 mi, until the road forks at the rim of Moody Creek canyon. Take the left (north) fork, along the canyon rim, then turn right (south) on Mud Springs Road, down into the canyon. Park at Stop 4.

STOP 4

Moody Creek. Moody Creek cut this canyon into the Huckleberry Ridge Tuff. Later, basalt from the Sommers Butte rift zone reached the west canyon rim, flowed into the canyon, and partially filled it. Today, remnants of this basalt form the west canyon rim to the south and lie in the bottom of the canyon at your feet, upstream to the south, and downstream on the west canyon wall to the north. Additional canyon-fill remnants exist at other locations downstream.

Turn around. Drive north for 2.1 mi on Mud Springs Road along the canyon rim, until you reach the junction with E 2000 S. Stay right and drive into Moody Creek Canyon. Near the top of the east rim, turn right to where the road ends. Turn right (southeast) onto White Owl Road. Use your GPS unit to continue on White Owl Road for 4.8 mi, to stop 5 at the top of White Owl Butte. (The narrow road to the summit leaves White Owl Road just southeast of the butte and winds west and north to stop 5.)

STOP 5

Overview. White Owl Butte provides a productive vantage point for observing the area. North and west of White Owl Butte, the Rexburg Bench consists of gently rolling hills, dips to the north, and contains a number of conical features, locally called buttes. The flat character results from deposition of the Huckleberry Ridge Tuff and loess. Loess dunes and prevalent, underlying lava flows produce the small hills. The buttes are small basalt vents, including cinder cones and lava cones.

Explore the area clockwise, from west to east (see figs. 1, 3, and 4). The high point between 9 and 10 o'clock is the vent area of the Rexburg Basalt. Well data and topography indicate that this shield volcano extends east to Moody Creek—which traces the eastern and northeastern boundaries of the volcano—and south beyond Lyons Creek (Phillips and others, 2016). The Sommers Butte volcanic rift, seen from here as aligned cinder cones, extends from about 7 to 10 o'clock.

The other small shield volcanoes on the Rexburg Bench may have formed at about the same time as the Sommers Butte lava field. The vents for these shield volcanoes, in order of decreasing relative age, are White Owl Butte, an unnamed butte that produced the Moody flow field, Bitter's Butte, and Canyon Creek Butte (Loc. 5, fig. 4; table 2; Embree and others, 2016b). The White Owl Butte vent on which you stand produced a small flow field that is not in contact with the other basalt flows. The unnamed butte that produced the basalt of Moody lies ~2.5 mi directly north (Loc. I, fig. 4). The Moody flow field extends north and west from the vent; it entered and dammed Teton Canyon just downstream of the failed Teton dam at location M1 (figs. 1, 4; Embree and others, 2016b). Bitter's Butte lies ~5.3 mi northwest at 11:30 o'clock (Loc. J, fig. 4). Canyon Creek Butte lies ~5.2 mi northeast at 1 o'clock (Loc. K, fig. 4). A younger basalt flow, the basalt of Ards Farm, erupted several miles to the northeast, flowing west into and across Canyon Creek, along the northern flank of the Canyon Creek flow field, and onto the Moody flow field (Loc. AR, fig. 4; Embree and others, 2016b; Feeney and others, 2014; Phillips and others, 2013).

The rhyolite of Long Hollow, the youngest known unit of the Heise volcanic field, extends from the upper reaches of Moody Creek (which traces the western boundary of the flow) on the south and west to the upper reaches of Canyon Creek (north of stop 7) on the east (fig. 4). This flow covers ~60 mi^2. The older units of the Heise volcanic field are best exposed to the southwest near the Heise Cliffs and Kelly Canyon. To the east, Canyon Creek marks the eastern edge of a Heise caldera (fig. 4).

East of Canyon Creek, the Big Hole Mountains and the Snake River Range consist of folded and faulted Paleozoic and Mesozoic sedimentary rocks overlain by ~6.6 Ma dacitic lava flows and tuffs that underlie the Blacktail Tuff (Price and Rodgers, 2010). Compositions suggest these rocks may be transitional between Basin and Range and Snake River Plain magmatism (Price, 2009).

Return to White Owl Road, and then turn right (southeast). Use your GPS unit to navigate to stop 6, which lies just off Long Hollow Road about 2.75 mi due east of White Owl Butte. Take the second left hand turn after leaving White Owl Butte. After 2 mi, this road intersects Long Hollow Road. Turn left on Long Hollow Road. Stop 6 lies ~1 mi ahead, on the right (east).

STOP 6

Rhyolite of Long Hollow. Here, the Huckleberry Ridge Tuff overlies the type locality for the rhyolite of Long Hollow. Here and on surrounding hillsides, this unit displays characteristic lithologies, including perlitic vitrophyre, red and black vitrophyre flow breccia, and devitrified rhyolite. Assuming an average thickness of 500 ft (150 m), the rhyolite of Long Hollow has an erupted volume of ~20 mi^3 (~84 km^3).

Return to Long Hollow Road. Use your GPS unit to reach stop 7. Turn left (south) and drive south on Long Hollow Road for ~1 mi, and then turn left on Canyon Creek Road. Stay on this road until you reach stop 7. (The road will head south, then east, then north into the Canyon Creek canyon. You should travel ~8.5 mi.)

STOP 7

Canyon Creek. This canyon marks the eastern edge of the rhyolite of Long Hollow, which is exposed along the cliff between 10 and 11 o'clock. The Huckleberry Ridge Tuff is relatively thin where it overlies this rhyolite lava flow, but composes the entire canyon wall downstream. The truncation of the northwestern Big Hole Mountains and the Snake River Range, eastward abrupt thinning of Heise volcanic units and the Huckleberry Ridge Tuff, and the presence of hot springs along the eastern margin of the canyon indicate that Canyon Creek marks the eastern edge of a Heise caldera (fig. 4).

Drive north on Canyon Creek Road for ~4 mi. To your right, on the hill above the Green Canyon hot springs resort, Location L marks a travertine deposit associated with the hot spring the resort uses. Continue north on Canyon Creek Road until you reach stop 8.

STOP 8

Basalt of Ards Farm in Canyon Creek. The vent for the basalt of Ards Farm lies several miles to the northeast (Feeney and others, 2014; Phillips and others, 2013). This lava field flowed west into and filled Canyon Creek, and then continued west to where it covered the Canyon Creek and Moody lava fields (Embree and others, 2016). Here, the basalt of Ards Farm lies 1.5 mi upstream from where it flowed into Canyon Creek.

Drive north on Canyon Creek Road for 0.3 mi, and then turn left (west) on Highway 33. Stay on the highway for ~4.5 mi to where it turns directly west. At this point, turn right (east) onto 1300 E (Reed–Parkinson Road). Continue on this road and use your GPS unit to reach stop 9, which lies just west of a farm road along the canyon rim.

STOP 9

Antiforms in the Huckleberry Ridge Tuff (fig. 5). Two large antiforms in the Huckleberry Ridge Tuff lie on the opposite side of the canyon, about 0.25 mi apart. Antiforms such as these occur at several places along Teton River Canyon (e.g., at stop 12). They are abundant, though less well exposed, north to Big Bend Ridge, the southern rim of the Yellowstone I caldera (Christiansen, 2001; Embree and Hoggan, 1999). Above the antiforms, the Huckleberry Ridge Tuff is as little as 30 ft thick; elsewhere in the canyon, the Huckleberry Ridge Tuff is 300-400 ft thick. A prominent basal vitrophyre and adjacent columnar jointing outline the antiforms. The cores of the antiforms consist of unconsolidated fluvial and lacustrine

Figure 5. Large overturned antiform within the Huckleberry Ridge Tuff (Qyh) and underlying Tertiary gravels and sediments (Ts) exposed on the north side of the Teton River canyon (from Embree and Hoggan, 1999, p. 186). The basal vitrophyre (Qyhv) is outlined.

sediments and minor basalt flows. These easily eroded pre-Huckleberry materials form prominent alcoves in the canyon wall. Note how the eastern antiform is overturned (verges to the southwest, left).

The antiforms in Teton Canyon are load structures resulting from rapid deposition of the thick Huckleberry ignimbrite on water-saturated, unconsolidated sediments. In this area, pre-ignimbrite topography sloped gently to the southwest. Remobilized rhyolite in the ignimbrite flowed down this slope, causing some antiforms to overturn. Field observations indicate several zones of deformation within the sheet: a lower zone that deformed plastically, a transition zone, and an uppermost zone of brittle deformation (Embree and Hoggan, 1999). Differential, subhorizontal shear produced different structures in each zone, e.g., widening of spaces between cooling columns in the brittle zone (see stop 10), horizontal shear structures in the transition zone (see stop 11), and recumbent isoclinal folds in the ductile zone. Paleomagnetic data are consistent with field observations and indicate that the antiforms developed shortly after deposition, while still hot (above 580 °C) (Geissman and others, 2010). Differential down-slope movement produced tear faults within the remobilized sheet (Embree and Hoggan, 1999). Tributary canyons developed along these shear zones. The pair of antiforms on the north canyon wall match a pair of antiforms located upstream along the south canyon wall. These structures are offset by 0.5 mi across a tear fault. Embree and Hoggan (1999) explain the nature, origin, and geographic distribution of these remobilized structures in detail.

Return to the vehicle and retrace your path, to Highway 33. Turn right (west) on the highway, and then turn right at the next road (Teton Dam Road) and drive north. Use your GPS unit to navigate to stop 10, at the top of the boat ramp along the edge of the canyon. (Turn right just before reaching the Teton Dam Overlook parking lot. Follow the road near the canyon rim to stop 10.)

STOP 10

Huckleberry Ridge Tuff at top of boat ramp. This stop shows the brittle zone in the remobilized Huckleberry Ridge Tuff (fig. 6). Columnar joints formed in this zone. Then, as movement continued in the underlying transition and ductile zones, these joints opened (creating spaces up to 3 ft wide). Some joint faces cooled quickly and preserved glassy textures; the remaining tuff devitrified (fig. 7). Tuffaceous sediments from the surface filled some open joints.

Continue down the boat ramp to where the concrete ends.

STOP 11

Huckleberry Ridge Tuff where the concrete ramp ends. This stop shows the transition zone in the remobilized Huckleberry Ridge Tuff (fig. 8). This zone contains abundant subhorizontal shear structures and en échelon extension fractures. Vapor phase deposits formed in and highlight these structures.

Continue down the boat ramp to stop 12, at the bottom of the canyon.

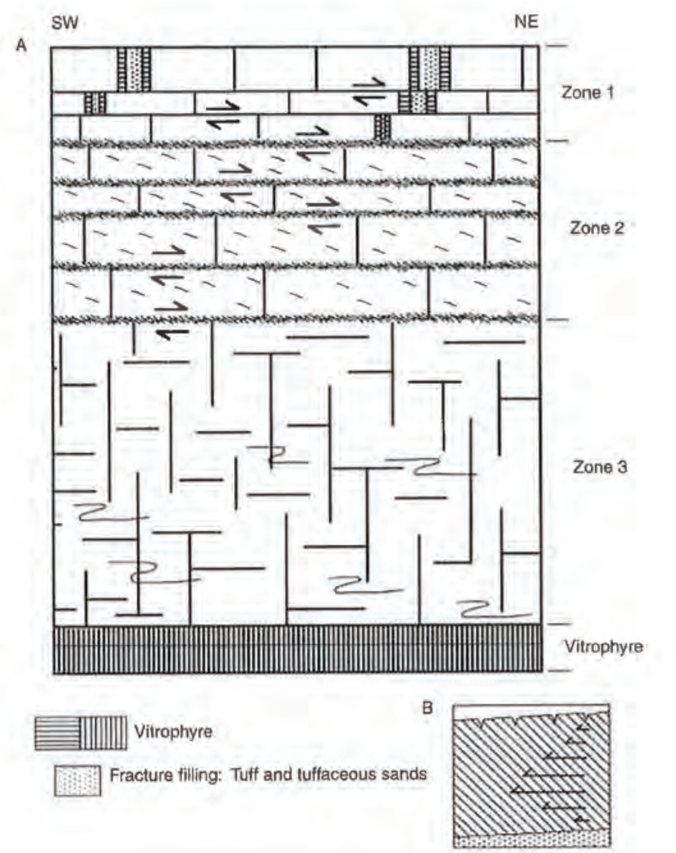

Figure 6. Schematic cross section of the Huckleberry Ridge Tuff in the Teton River canyon area. Secondary flow within the sheet is expressed by different behavior at different levels within the unit. The lower part of the unit, Zone 3, deformed by viscous flow and contains small-scale recumbent isoclinal folds. Zone 2 was dominated by shear and contains numerous brecciated, subhorizontal shear zones with relative movement indicated by the arrows. This zone also contains numerous tension fractures which dip northeast at low angles. Zone 1 was cool and brittle; columnar joints in this zone were pulled apart and filled with ash and sediments from above.

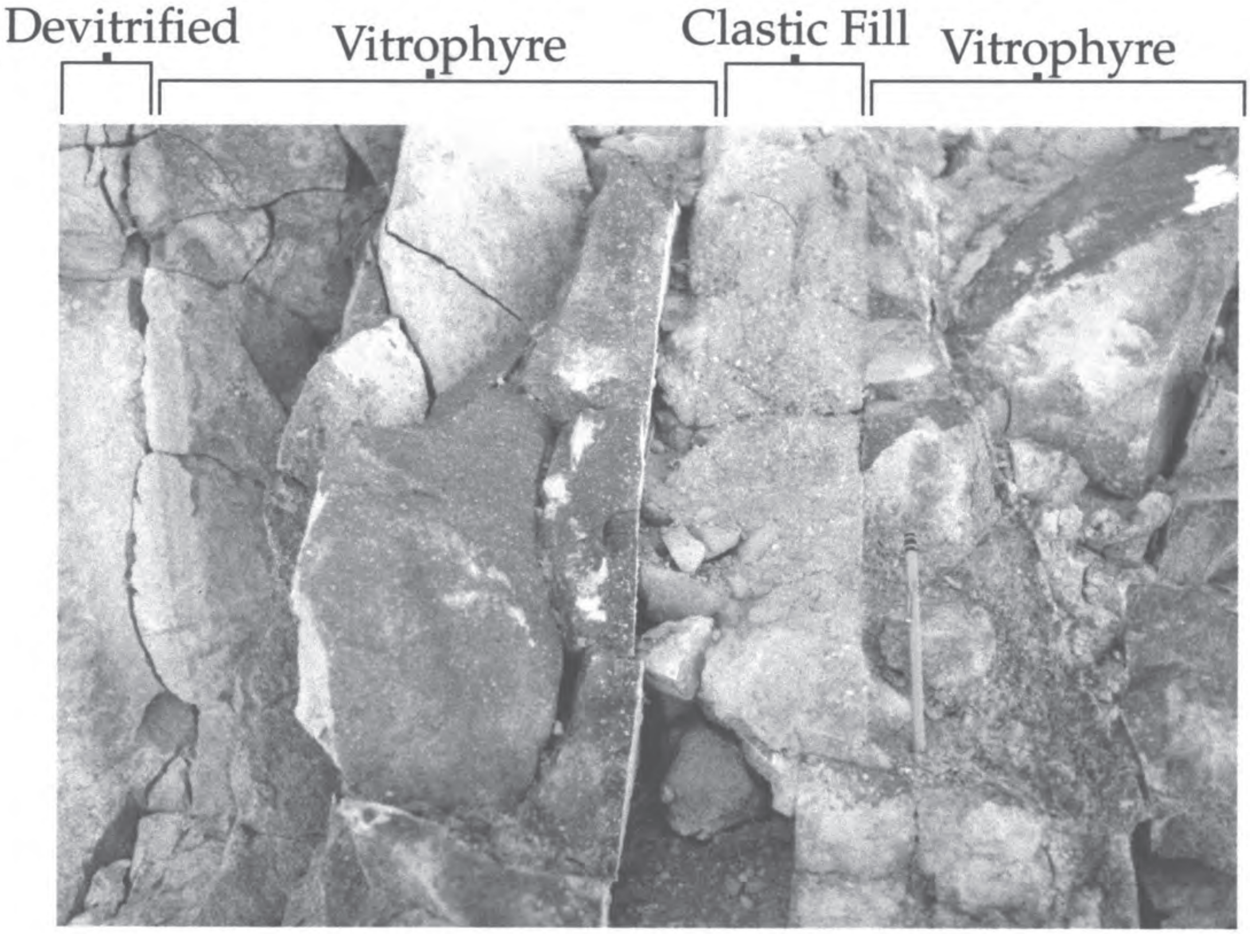

Figure 7. Section view of lateral zonation in devitrification adjacent to an open joint filled with reworked ash from above. This and several other similar joints are located at Stop 10 near the top of the boat ramp (from Embree and Hoggan, 1999, p. 188).

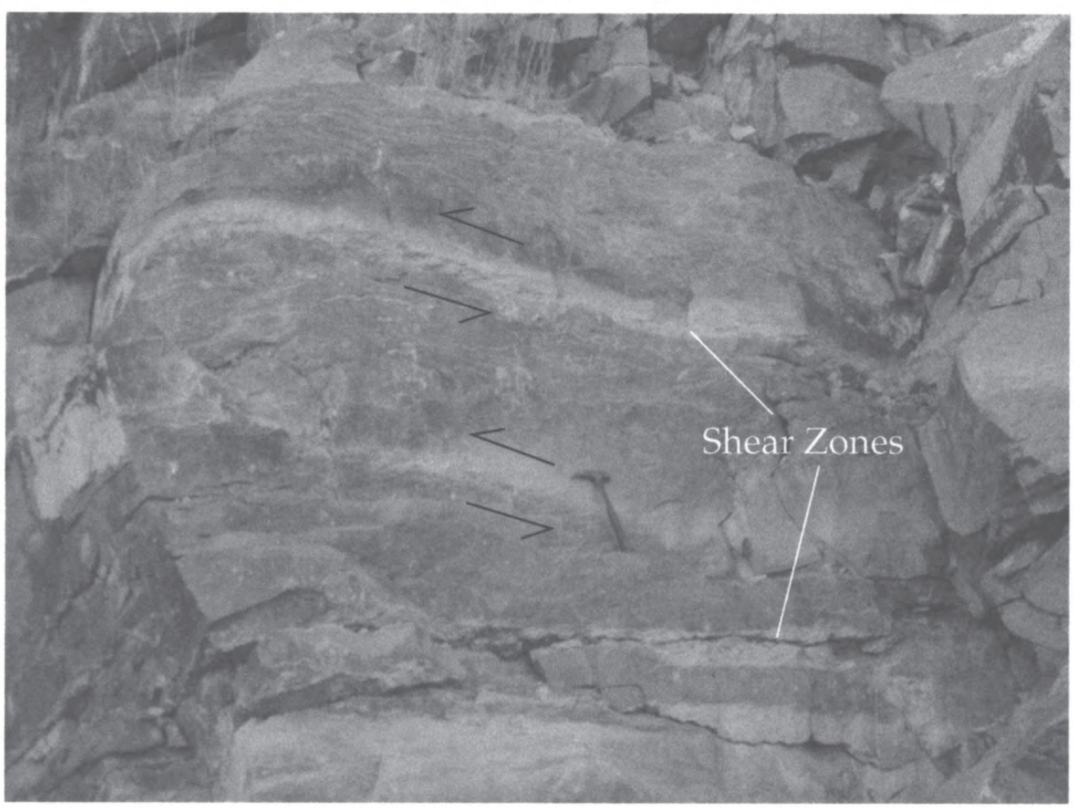

Figure 8. Vapor-phase filled en échelon extensional fractures in massive gray tuff, separated by white vapor phase filled and open shear zones (from Embree and Hoggan, 1999, p. 188). Location is at Stop 11 near the bottom of the boat ramp.

STOP 12

Basal vitrophyre in an antiform. Another Huckleberry antiform lies to the left along the east canyon wall. This stop presents an opportunity to observe the basal vitrophyre in detail. A separate, less conspicuous antiform, without exposed pre-Huckleberry materials, lies across the river along the west canyon wall.

Drive back up the boat ramp and return to the Teton Dam overlook, at stop 13.

STOP 13

Teton Dam Overlook. Embree and others (2011) describe the Teton Dam disaster. On June 5, 1976, the Teton Dam failed catastrophically, killing 14 people and causing $400 million to $1 billion dollars (1976 dollars) in flooding damage. The causes of the disaster have been extensively studied (e.g. Seed and Duncan, 1987) and show that poor understanding of the geologic conditions at the dam site directly contributed to the disaster.

The Huckleberry Ridge Tuff near the dam site contains numerous joints and shear zones; these features (observed at stops 10 and 11) form an extensive interconnecting system of fractures that make the tuff extremely permeable and difficult to seal (fig. 9). During dam construction, engineers recognized the potential for seepage problems through the joints. To try to solve these problems, they removed 70 ft (21 m) of jointed tuff along both sides of the dam and along the base, pumped grout (mixtures of sand and cement) into fractures using vertical drill holes spaced 10 ft (3 m) apart, and filled the excavated areas with compacted loess.

Reservoir filling began in November 1975 with an intended filling rate of 1 ft per day. Late spring snowfall created a heavier runoff than expected. This caused rapid filling rates of about 4 ft per day in late May. Completion of the river outlet works (used to control reservoir elevation below that of the spillway) was delayed. By the day of failure (June 5), the water level stood at elevation 5,301.7 ft (1,616.0 m) 3 ft (1 m) below spillway crest elevation and 30 ft (9 m) be-

Figure 9. Open vertical to steeply dipping cooling fractures in Huckleberry Ridge Tuff offset by horizontal shear zones in the north key trench of the Teton Dam. Both sets of open joints allowed piping of water from the reservoir, which eroded the core of the dam and caused its failure. Arrows indicate relative motion along shear zones (from Embree and Hoggan, 1999, p. 188).

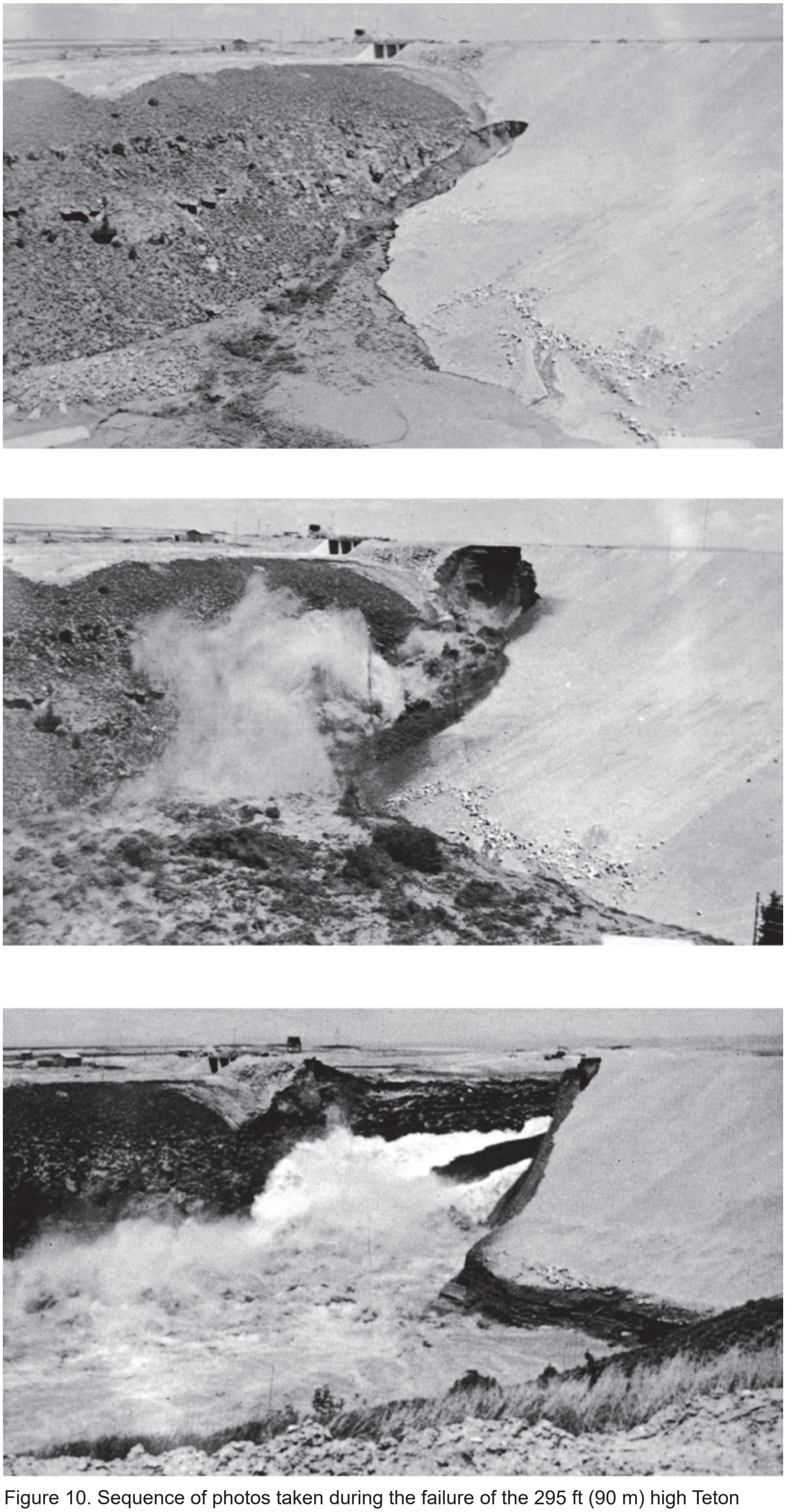

Figure 10. Sequence of photos taken during the failure of the 295 ft (90 m) high Teton Dam on June 5, 1976. These three photos were taken at 11:20 a.m., 11:50 a.m., and in the early afternoon (from Embree and Hoggan, 1999, p. 198).

low the top of the dam. When indications of seepage through the dam first appeared late on June 4, there was no means to reduce the water level. By 7:00 am on June 5, other springs appeared on the dam and on the canyon wall downstream from the dam. Efforts to reduce the leaks were futile and at 11:57 am the dam crest was breached, spilling 240,000 acre-ft (0.3 km^3) of water down the Teton River to the Snake River Plain over a period of 6–8 hours (fig. 10). Property damage was highest in Sugar City and Rexburg.

The remains of the dam lie to the right, in the center of the canyon. The dam failed on the far side of the canyon. Engineers excavated the dam on the near side of the canyon to study how it failed. The excavated wall exposes the internal structure of the dam. Reconstruction of the failure indicates that movement of reservoir water along open joints and within loess at the base of dam was the major contributing cause. The grout barrier was ineffective at preventing leakage. Engineers used loess to build the core of the dam because there are no large clay deposits in the area (but loess is abundant). The use of loess was a poor engineering decision because loess is erodible by flowing water and can be fractured under some conditions.

The dam break had many geomorphic effects (Scott, 1977). Rapid drawdown of the reservoir caused numerous small landslides (Schuster and Embree, 1980; figs. 11, 12). A peak discharge of 2.3 x 106 ft^3/s (65,000 m^3/s) and average velocity of 40 ft/s (12 m/s) produced features in the Teton River canyon such as scoured bedrock

Figure 11. Landslides in the Teton River canyon produced by the rapid drawdown of the reservoir following catastrophic failure of the Teton Dam.

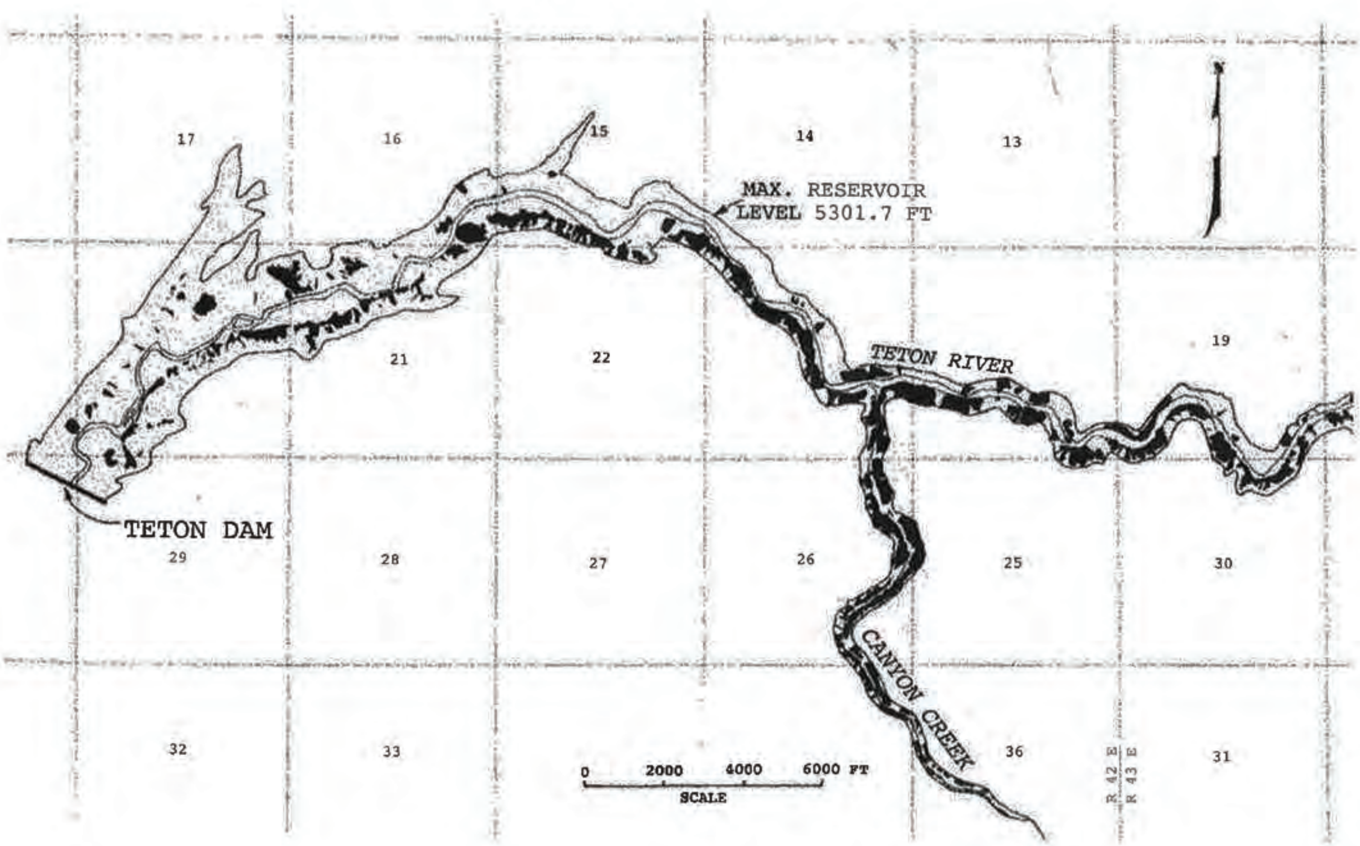

Figure 12. Map showing landslides (black polygons) in the Teton River canyon produced by reservoir drawdown (from Schuster and Embree, 1980).

and large pendent bars similar to those of prehistoric catastrophic floods such as the Missoula and Bonneville floods. Flood discharge in the canyon was roughly equivalent to the flow of the Mississippi River at flood stage. Flood deposits consist of approximately equal volumes of wall rock and dam fill.

Location M1, located downstream near where the canyon turns, marks the ancient lava dam produced when the basalt of Moody entered and partly filled the canyon. The dam consists of three subaerial basalt flows (fig. 13). At the base of each flow lies a layer of pillow basalt surrounded by hyaloclastite. These alternating lithologies record the interaction between deepening water and a rising dam. (These rocks lie on private land. Ask permission at the nearby farmhouse before visiting.) If you would prefer, an excellent vantage point lies on the north rim at location M2.

Return to Highway 33. Turn right onto the highway and drive west for 3.4 mi, to Newdale, Idaho. Turn right on Main Street (N 2750 E) and drive north for 4.1 mi. At the bridge over the Teton River, notice the large gravel bars deposited by the Teton Dam flood described above. Stop at the intersection with E 400 N.

Location N, to the west, marks the eastern edge of the basalt of Chester, which flowed down an ancient drainage from the northeast ($^{40}Ar/^{39}Ar$ age of 256 ± 44 ka; Embree and others, 2011). The current drainage follows the contact between the basalt and the Huckleberry Ridge Tuff.

Drive east on E 400 N for 0.5 mi, and then turn left (north) on N 2800 E. After 1 mi, turn right (east) on Hog Hollow Road and drive for 5.3 mi. Location O marks the rim of Hog Hollow, a pull-apart basin in the Huckleberry Ridge Tuff. Shortly after deposition of the Huckleberry ignimbrite, downslope movement of this sheet formed a tear, which widened to create this basin. Rapid cooling along the edges of the basin formed subvertical/lateral vitrophyres. Continue east on Hog Hollow Road for 2.5 mi, to stop 14.

STOP 14

North wall of Hog Hollow (fig. 14). This stop shows the subvertical vitrophyre that formed when Hog Hollow opened. The gullies show that devitrified

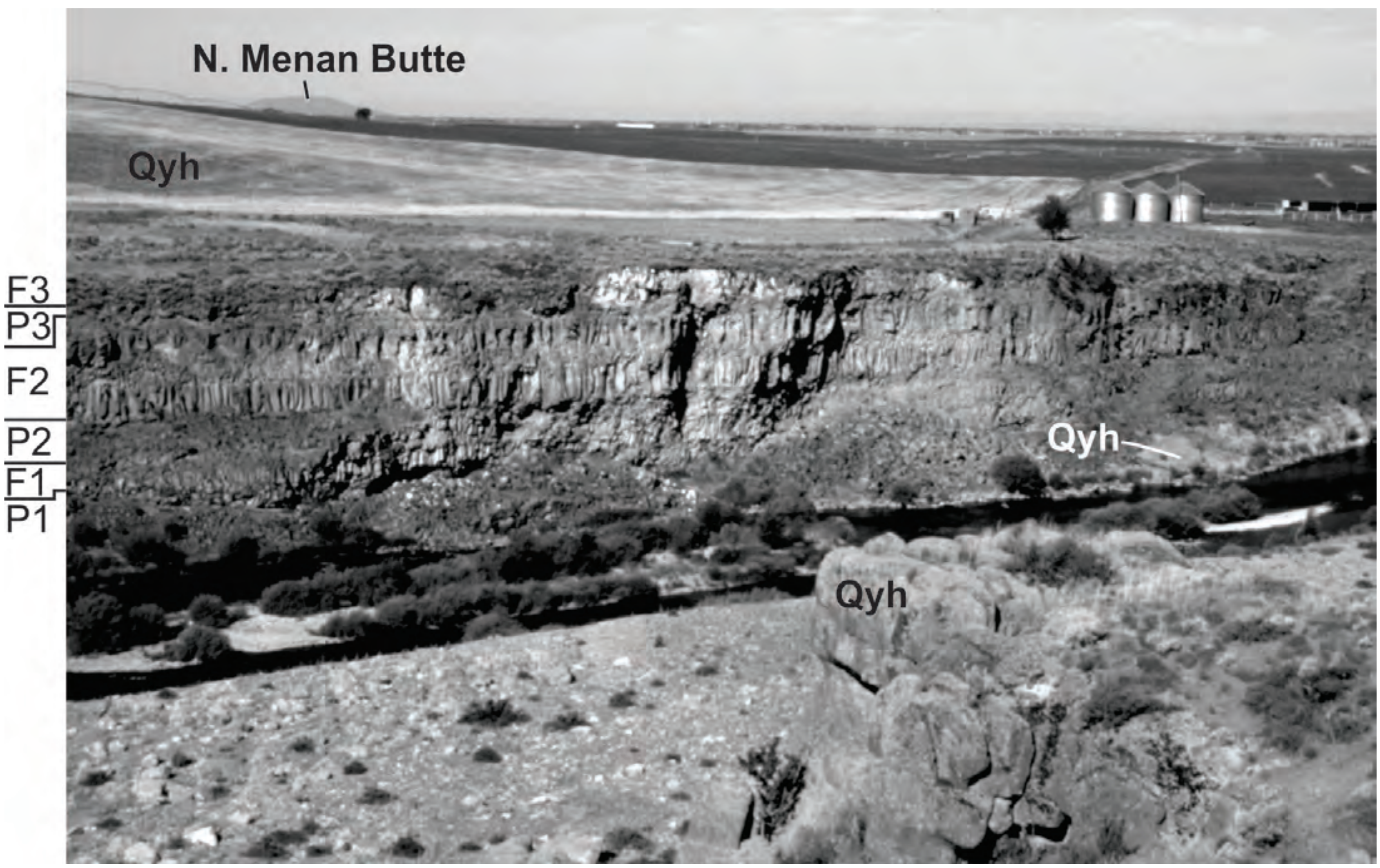

Figure 13. Three basalt flows (F1-F3) of the Moody basalt lava dam on the south side of the Teton River canyon near its mouth, 1.2 mi (2 km) downstream form the Teton Dam site (after Embree and Hoggan, 1999). Each flow has a pillow zone at its base (P1-P3). Image was taken from the north rim at location M2 (fig. 1).

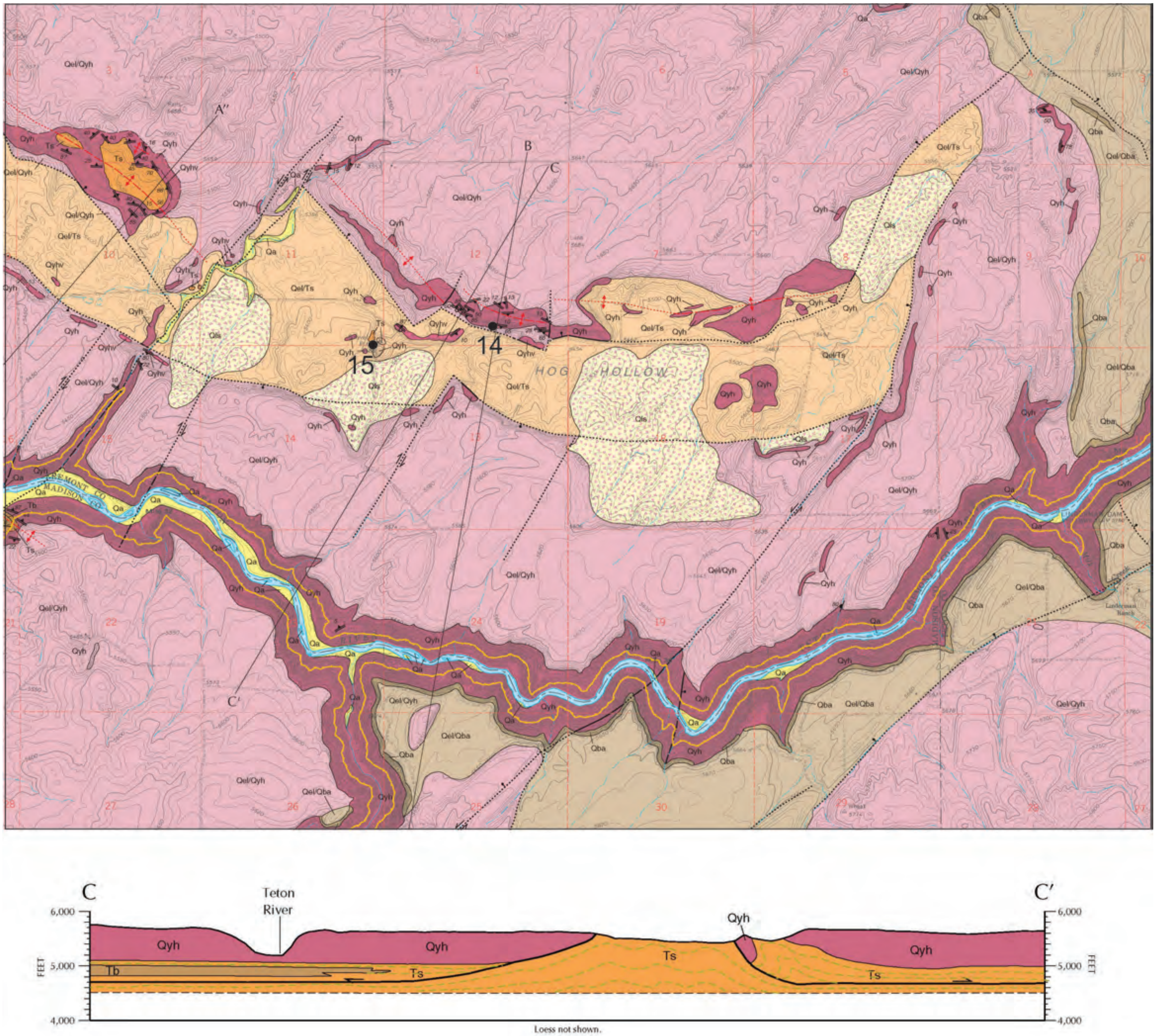

Figure 14. Geologic map and cross section of the eastern portion of Hog Hollow showing antiforms and tear faults (from Embree and others, 2011a). Locations of Stops 14 and 15 are shown. Map units are Qa (alluvium); Qyh (Huckleberry Ridge Tuff); Qyhv (vitrophyre of Huckleberry Ridge Tuff); Qba (basalt of Ards Farm); Ts (Tertiary sediments). Units covered with loess are given prefix "Qel/".

rhyolite lies behind the vitrophyric face. The foliation at the hilltop dips 20° south; at the base of the hill, behind the vitrophyre, the foliation dips approximately 80° south. This monocline-like structure formed as the separating edges of the ductile Huckleberry Ridge Tuff thinned and separated (fig. 14).

Turn around, drive 0.5 mi back up the road, and turn left on the farm road. This is a private road. The landowner allows geologists to visit the outcrop 300 yards to the south. Do not go beyond the outcrop.

STOP 15

Pre-Huckleberry rhyolite lava flow and sediments. This stop shows a mélange block left behind when the Huckleberry Ridge Tuff separated to form Hog Hollow. It consists of a chaotic mixture of pre-Huckleberry rhyolite lava flow (located near the base), tuffaceous fluvial and lacustrine sediments (throughout), and Huckleberry Ridge Tuff (which caps the hill). Sediments include clay, silt, sand, gravel, and diatomite. Sedimentary layers are discontinuous. The block contains clastic dikes that cut both sediments and rhyolite.

Return to Highway 20 by following the Hog Hollow Road west into Saint Anthony. When the road ends, turn right (north) onto S 3rd E. This road turns left (west) and becomes E 6th S. Turn right at S Yellowstone Highway, which leads to Highway 20.

REFERENCES

Bindeman, I.N., Watts, K.E., Schmitt, A.K., Morgan, L.A., and Shanks, P.W.C., 2007, Voluminous low delta18O magmas in the late Miocene Heise volcanic field, Idaho: Implications for the fate of Yellowstone hotspot calderas: Geology, v. 35, p. 1019–1022, doi: 10.1130/g24141a.1.

Christiansen, R.L., 2001, The Quaternary and Pliocene Yellowstone Plateau Volcanic Field of Wyoming, Idaho, and Montana: United States Geological Survey Professional paper 729G, 145 p.

Dossett, T.S., Reed, T.H., McIlrath, S.L., Moore, D.K., and Embree, G.F., 2012, Geologic Map of the South Fork of the Snake River between Swan Valley and Ririe, Idaho: Idaho Geological Survey Technical Report T-12-5, scale 1:24,000.

Embree, G.F., Moore, D.K., Phillips, W.M., and Prostka, H.J., 2016a, Geologic Maps of the Moody, White Owl Butte, and Wright Creek Quadrangles, Madison and Teton Counties, Idaho: Idaho Geological Survey Technical Report T-16-2, scale 1:24,000.

Embree, G.F., Phillips, W.M., and Welhan, J.A., 2016b, Geologic map of the Rexburg quadrangle, Madison County, Idaho: Idaho Geological Survey Digital Web Map 178, scale 1:24,000.

Embree, G.F., and Phillips, W.M., 2011a, Geologic map of the Linderman Dam quadrangle, Fremont, Madison, and Teton Counties, Idaho: Idaho Geological Survey Digital Web Map 133, scale 1:24,000.

Embree, G.F., Phillips, W.M., and Welhan, J.A., 2011b, Geologic map of the Newdale quadrangle, Fremont and Madison Counties, Idaho: Idaho Geological Survey Digital Web Map 122, scale 1:24,000.

Embree, G.F., and Hoggan, R.D., 1999, Secondary deformation within the Huckleberry Ridge Tuff and subjacent Pliocene units near the Teton Dam; road log to the regional geology of the eastern margin of the Snake River plain, Idaho, in Hughes, S.S. and Thackray, G.D. eds., Guidebook to the Geology of Eastern Idaho, Idaho Museum of Natural History, Pocatello, ID, United States, p. 181–202.

Embree, G.F., M.D. Lovell, and D.J. Doherty, 1978, Drilling data from Sugar City exploration well, Madison County, Idaho. U.S. Geological Survey Open-File Report 78-1095.

Feeney, D.M., Garwood, D.L., and Phillips, W.M., 2014, Geologic Map of the Drummond Quadrangle, Fremont and Teton Counties, Idaho: Idaho Geological Survey Digital Web Map 167, scale 1:24,000.

Geissman, J.W., Holm, D., Harlan, S.S., and Embree, G.F., 2010, Rapid, high-temperature formation of large-scale rheomorphic structures in the 2.06 Ma Huckleberry Ridge Tuff, Idaho, USA: Geology, v. 38, no. 3, p. 263–266.

Lanphere, M.A., Champion, D.E., Christiansen, R.L., Izett, G.A., Obradovich, J.D., 2002, Revised ages for tuffs of the Yellowstone Plateau volcanic field: Assignment of the Huckleberry Ridge Tuff to a new geomagnetic polarity event, GSA Bulletin, v. 114, p. 559-568.

Moore, D.K., and Embree, G.F., this volume, Field guide to interactions Involving basalt flows and the South Fork of the Snake River between Swan Valley and Ririe, Idaho: Northwest Geology, v. 45.

Moore, D.K. and G.F. Embree, 2014, Looking through loess; unraveling the volcanic history at the transition to the Snake River plain near Rexburg, Idaho: Geological Society of America Abstracts with Programs, v. 46, no. 5, p. 88.

Morgan, L.A., and McIntosh, W.C., 2005, Timing and development of the Heise volcanic field, Snake River plain, Idaho, western USA: Geological Society of America Bulletin, v. 117, p. 288.

Phillips, W.M., In Press, Geologic map of the Hawley Gulch quadrangle, Madison and Bonneville counties, Idaho: Idaho Geological Survey Digital Web Map, scale 1:24,000.

Phillips, W.M., Moore, D.K., Feeney, D.M., and Embree, G.F., 2016, Geologic map of the Heise quadrangle, Bonneville, Jefferson, and Madison counties, Idaho: Idaho Geological Survey Digital Web Map 176, scale 1:24,000.

Phillips, W.M., Embree, G.F., Welhan, J.F., and Garwood, D.L., 2014, Geologic map of the Ririe quadrangle, Madison, Jefferson, and Bonneville counties, Idaho: Idaho Geological Survey Digital Web Map 165, scale 1:24,000.

Phillips, W.M., Garwood, D.L., Embree, G.F., 2013, Geologic Map of the Packsaddle Lake Quadrangle, Teton County, Idaho: Idaho Geological Survey Digital Web Map 155, scale 1:24,000.

Pierce, K.L., and Scott, W.E., 1978, personal communication.

Price, K.B. and Rodgers, D.W., 2010, Geologic map of the North End of the Big Hole Mountains, Madison and Teton counties, Idaho: Idaho Geological Survey T-10-2, scale 1:24,000.

Price, K.B., 2009, Geology of the northern end of the Big Hole Mountains, Madison and Teton County, Idaho [M.Sc. Thesis], Idaho State University, Pocatello, Idaho, 130 p.

Scott, W.E., 1977, Geologic effects of flooding from Teton Dam failure, southeastern Idaho: U.S. Geological Survey Open-File Report 77-507, 11 p., scale 1:48,000.

Seed, H.B., and J.M. Duncan, 1987, The failure of Teton Dam: Engineering Geology, v. 24, p. 173-205.

Schuster, R.L. and Embree, G.F., 1980, Landslides caused by rapid draining of Teton Reservoir, Idaho in Proceedings or 17th Annual Symposium of Engineering Geology and Soils Engineering, Boise, Idaho. p. 1-14.

Williams, E.J. and Embree, G.F, 1980a, Seismic risk on the Rexburg fault, Idaho: U.S. Geological Survey Professional Paper 1175, Geological Survey Research, p. 76.

Williams, E.J. and Embree, G.F., 1980b, Pleistocene movement on Rexburg fault, eastern Idaho: Geological Society of America Abstracts with Programs, v. 12, no. 6, p. 308.

Homes and buildings damaged during Teton Dam failure

VOLCANIC GEOLOGY, HYDROGEOLOGY, AND GEOTHERMAL POTENTIAL OF THE EASTERN SNAKE RIVER PLAIN

Michael McCurry,[1] Roy C. Bartholomay,[2] Mary K.V. Hodges,[2] and Robert Podgorney[3]

[1]Department of Geosciences, Idaho State University, Pocatello, ID 83209; [2]U.S. Geological Survey, Idaho National Laboratory Project Office, Idaho Falls, ID 83415; [3]Idaho National Laboratory, PO Box 1625, Idaho Falls, ID 83415

INTRODUCTION

This paper presents an overview of selected geologic, volcanic, and hydrogeological features of, and a potential geothermal exploration initiative in. the Eastern Snake River Plain. We focus on six road-accessible field sites in the vicinity of the Idaho National Laboratory (INL). The sites are selected to demonstrate specific salient features of the regional geology, volcanology, and hydrogeology, and to provide context for descriptions and discussions of their origin and broader significance. Stops 1-4 focus on the Quaternary volcanic development and magma genesis of the ESRP. Stop 5 provides an overview of the regional hydrogeology and related monitoring, characterization, and modeling activities by the USGS, as well as the ongoing Snake River Geothermal Consortium DOE FORGE (Frontier Observatory for Research in Geothermal Energy) initiative within INL's Geothermal Resources Research Area (GRRA). Stop 6 focuses on Miocene hot spot track-related volcanism and Miocene to Recent regional tectonic activity. The locations of field stops are shown in figure 4.

Regional Geology and Tectonics (McCurry)

The focus area is located on the northern margin of the Yellowstone–Snake River Plain (YSRP) volcanic track, the world's largest active continental hot spot system (e.g., Smith and others, 2009). The hot spot is widely interpreted to result from interaction of a stationary near-vertical mantle plume with overlying lithosphere that is drifting to the southeast at ~2 cm/yr (fig. 1). Activity began at ~17 Ma with formation of the flood-basalt dominated Columbia River and Steens basalts, and additional magmatic and extension-dominated tectonic activity that extended into Nevada (fig. 1). The focus of activity shifted incrementally to the northeast, mirroring the southwest motion of the North American tectonic plate. Volcanic activity shifted from basalt- to rhyolite-dominated as the hot spot traversed the boundary between denser accreted terrains, and less dense Paleoproterozoic to Archean craton (dashed line in fig. 1). Mafic magmas interacted with the craton by intraplating into low-density mid and upper crust. Densification of and heat transfer into the crust via mixing, assimilation, and homogenization processes led to development of voluminous felsic magmas and concomitant formation of a system of felsic comagmatic batholithic and volcanic rocks (e.g., Christiansen and McCurry, 2008; Szymanowski and others, 2015).

Volcanic fields produced numerous rhyolite "super eruptions" (≥ ~100 km^3) and cogenetic calderas as well as voluminous rhyolite lava flows. Rhyolites and calderas within the central and eastern Snake River Plain are almost entirely buried by up to 2 km of basalt lavas. Locations and shapes of the "cryptic" calderas and volcanic vent systems are therefore uncertain. Their existence and locations are inferred mainly from outflow facies of ignimbrites that extend in regions surrounding the plain (fig. 2), and from deep borehole and geophysical information. Ages of the inception of formation of the volcanic fields is illustrated in Figure 1. Major rhyolitic volcanic activity associated with individual fields lasted 2–3 m.y., and have cumulative eruptive volumes of ~104 km^3 (e.g., Bonnichsen and others, 2008).

Dynamic and thermal interactions between the mantle plume and regionally extending lithosphere produced uplift and a parabolic-shaped band of seismicity in surrounding cold felsic crust, and enhanced the magnitude of regional extension and concomitant basin development in areas north and south of the hot spot (Pierce and Morgan, 2009; Rodgers and others, 2002). Loading of the crust with dense, mantle-derived magma, equivalent to a layer of gabbro ~14 km thick (McCurry and Rodgers, 2009; Leeman and others

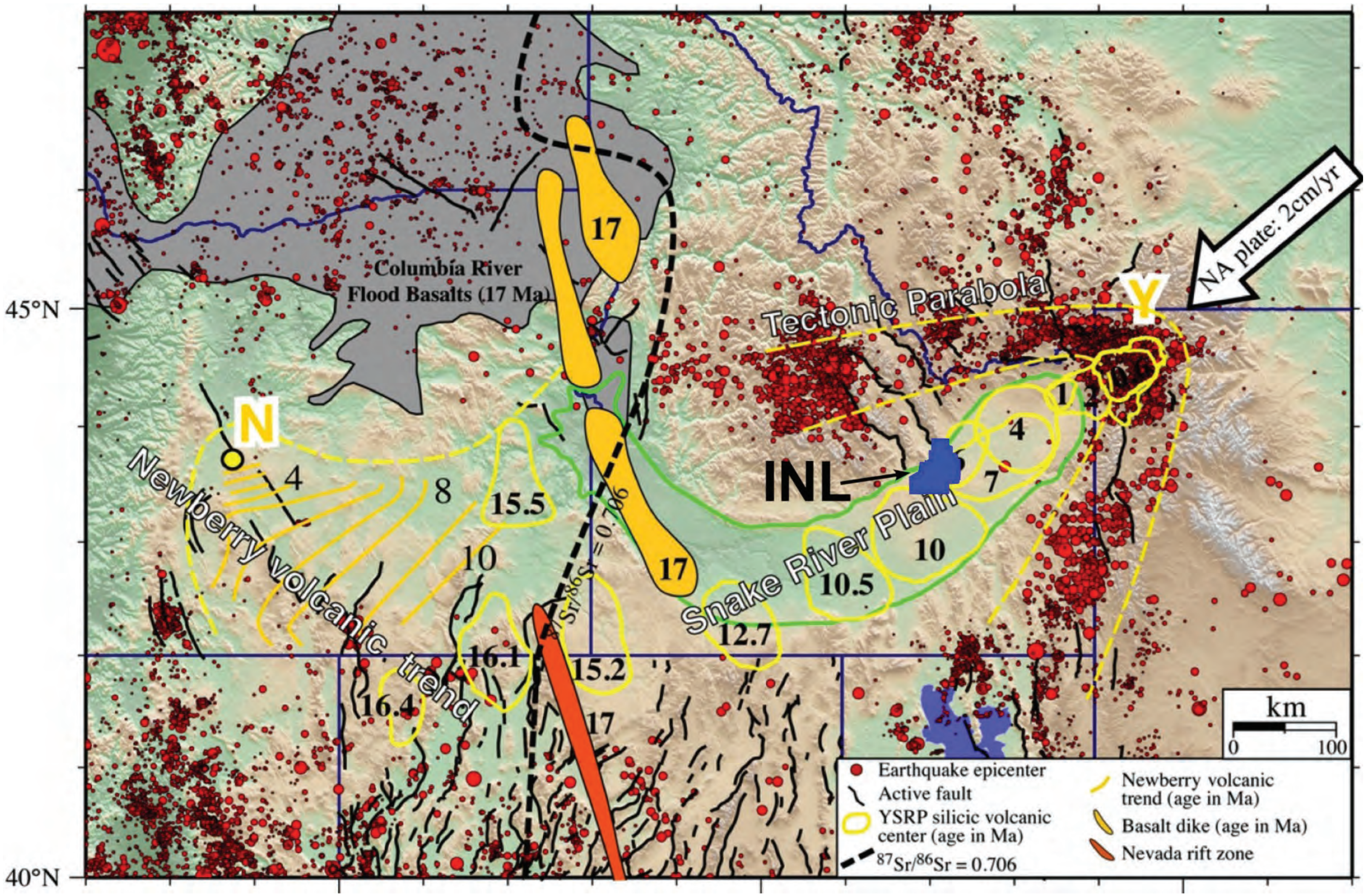

Figure 1. The location and regional geologic and tectonic setting of the Yellowstone–Snake River Plain hot spot track (YSRP) (after Smith and others, 2009, their fig. 2). The focus area is located on the northwest margin of the eastern Snake River plain, in the vicinity of the Idaho National Laboratory (shown in dark blue). The map emphasizes major Neogene to Recent volcanic and tectonic features related to development and evolution of the Nevada–Columbia magmatic belt (Camp and others, 2015) and the YSRP system. Most lines and symbols are explained on the inset explanation. Ages of initiation of major silicic volcanism are indicated for rhyolite volcanic fields (yellow lines). The green line encompasses Quaternary to Pliocene basalt lavas that postdate local rhyolite volcanism. Modified from McCurry and others (2016).

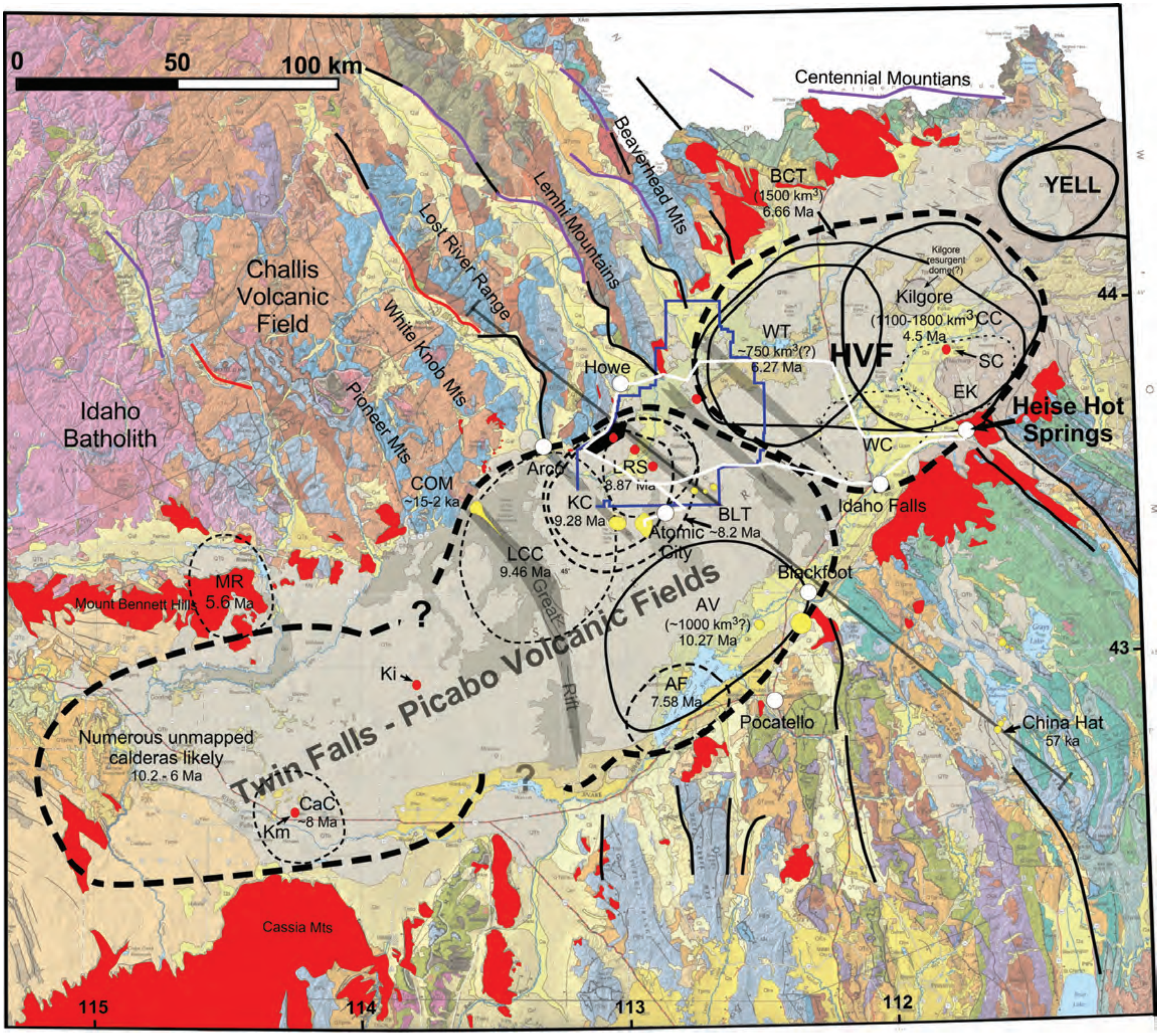

Figure 2. Geologic map of the Eastern Snake River Plain (ESRP) and its surroundings, emphasizing salient volcanic and tectonic features. The INL is outlined in blue with a black inset showing the location of the FORGE/GRRA. The field trip route is shown with a white line originating at Heise Hot Springs. A more detailed route map, including stop locations, is shown in fig. 4. The geologic base map is from Lewis and others (2012). Shades of green, blue, and purple illustrate late Precambrian to Paleozoic sedimentary rocks exposed in Basin and Range horst blocks north and south of the plain. Faults having late Neogene to Recent activity are shown in bold lines (after Anders and others, 2014). Pale shades of gray on the Snake River Plain indicate Quaternary basalt lavas (Holocene in darker shade); pale yellow indicates Quaternary sediment. Yellow = Quaternary cryptodomes, lava domes, and volcanic fields consisting of geochemically evolved mafic to rhyolitic composition (e.g., McCurry and Welhan, 2012). Bold red colors indicate exposures of rhyolites (mostly ignimbrites) exposed along the margins of the plain. Major rhyolite volcanic fields are illustrated with bold dashed lines; HVF = Heise volcanic field (~7.6–4.5 Ma); YELL=Yellowstone volcanic field (~2.1 Ma–active). Twin Falls and Picabo fields overlap in age (~10.5 to 7 Ma) and are therefore combined. Deep boreholes are shown as red dots (Km=Kimberly; Ki=Kimama; SC=Sugar City; after Shervais and others, 2013). Boreholes located within the boundaries of INL are distinguished in figs. 4, 12, and 13. Inferred caldera locations and ages are illustrated with solid (better defined location) and dashed (less well defined location) black lines. CaC=Castleford Crossing ignimbrite and Twin Falls caldera, after Knott and others, 2016 and Shervais and others, 2013; MR=Magic Reservoir, after Leeman, 1982b; AF=American Falls, LCC=Little Chokecherry Canyon, KC=Kyle Canyon, LRS=Lost River Sinks, are after Anders and others, 2014; AV=Arbon Valley (or Taber), after Kellogg and others, 1994; Kuntz, Covington, and Schorr, 1992; McCurry, 2009; WT=Walcott, BCT=Blacktail Creek, Kilgore, and CC=Conant Creek, are after Morgan and McIntosh, 2005, modified by Anders and others, 2014; WC=Wolverine Creek, Ek=Elkhorn Spring, are after Anders and others, 2014. The line extending northwest to southeast across the ESRP corresponds to the cross-section in fig. 3.

2009), led to coeval or subsequent downwarping of the surface by at least 5 km in some areas (fig. 3) (e.g., Rodgers and others, 2002).

Regional crustal architecture consists mainly of early Precambrian crystalline rocks (Foster and others, 2006) that are overlain by late Precambrian to Mesozoic age sedimentary rocks of the Cordilleran fold and thrust belt (Dickinson, 2004; DeCelles 2004; Yonkee and others, 2014). Regional magmatic activity produced the late Cretaceous Idaho Batholith and Eocene Challis volcanic province (e.g., Gaschnig and others, 2011) and Oligocene intrusions of the Albion Mountains region (Konstantinou and others, 2012; Konstantinou, 2013). But with the exception of distal sedimentary facies of the Challis system, none of these appear to have extended to the GRRA area (fig. 2). Strong extension occurred in Eocene to early Oligocene, exposing mid-crustal rocks in isolated metamorphic core complexes of the Pioneer and Albion-Raft River Mountain areas, northwest and southwest of GRRA (Strickland and others, 2011; Strickland, Miller, and Wooden, 2011). Coeval, less intense extension produced half graben basins over a wider region, including formation of the Arco Pass Basin located just north of the GRRA in the Arco Hills (e.g., Link and Janecke, 1999). Another, later phase of late Miocene extension and uplift occurred during proximal volcanism along the YSRP (Vogel and others, 2014; Konstantinou and others, 2012, Konstantinou and others, 2013). Figure 3 illustrates a conceptual model of the large-scale regional crustal architecture.

Cessation of voluminous hot spot track-related rhyolite volcanism was followed soon after by eruption of basalt lavas, beginning at ~6 Ma in the CSRP and ~4.2 Ma in the ESRP (Shervais and others, 2013; Potter, 2014; Champion and others, 2002). The basalt eruptions produced a widely distributed basalt-dominated field consisting of hundreds of coalescing shield volcanoes (e.g., Greeley and King 1977; Kuntz and others, 1992; Hughes and others, 2002), having a cumulative volume of over 10,000 km^3 (e.g., McCurry and others, 2008). Basalt lavas are commonly interlayered with clastic sediment derived from drainage off ranges bounding the plain (e.g., Bestland and others, 2002; Geslin and others, 2002). Accumulation of the basalts and concomitant subsidence of ESRP produced a basalt-dominated basin up to ~2 km deep (Shervais and others, 2013; Potter, 2014).

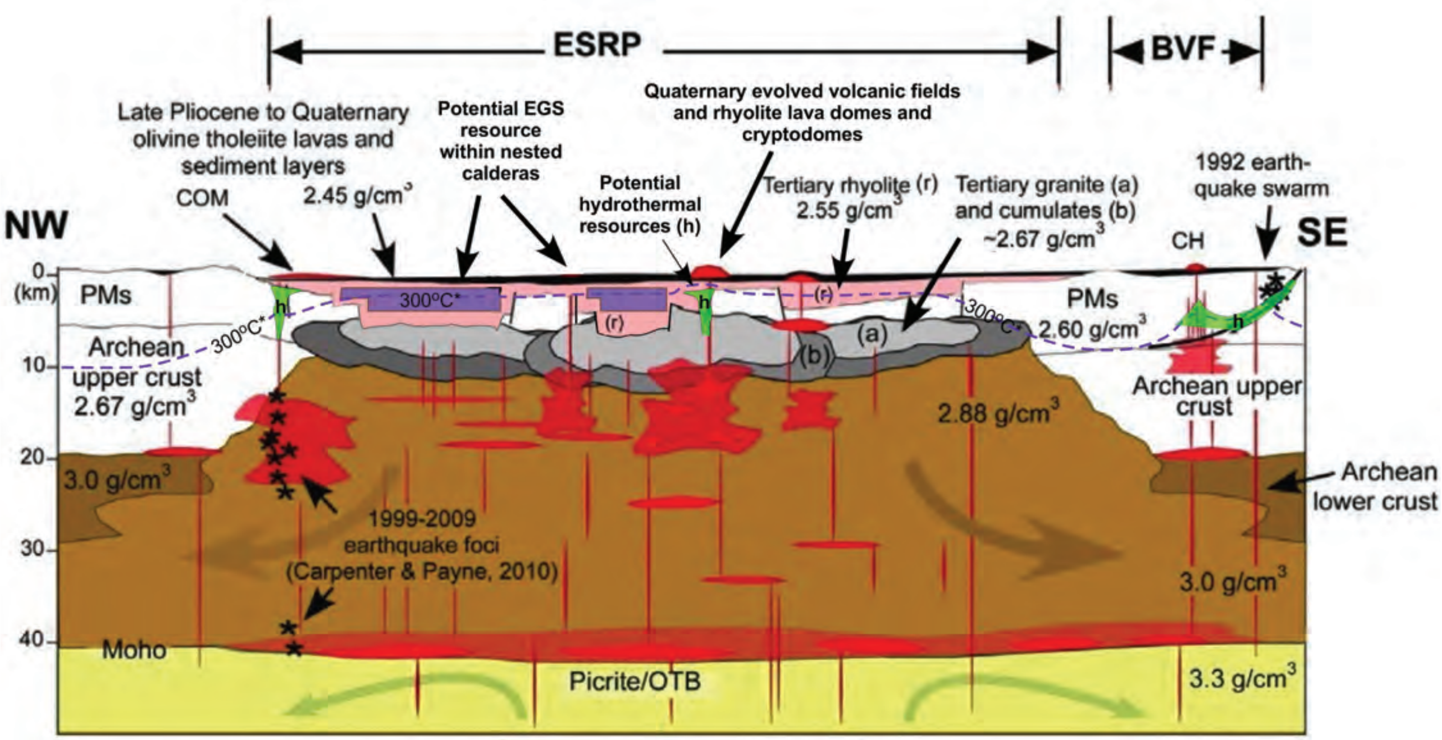

Figure 3. A cross-section model of the crust and upper mantle (modified from McCurry and others, 2016; and from Peng and Humphreys, 1998). The cross-section extends southeast from the southern end of the Lost River Range to China Hat (shown in fig. 2). ESRP = Eastern Snake River Plain; COM = Craters of the Moon volcanic field; BVF = Blackfoot Volcanic Field; PMs = late Precambrian to Paleozoic miogeoclinal sedimentary rocks. A hypothetical 300oC isotherm illustrates possible regional and more localized variation in geotherms. Arrows in the crust represent inferred patterns of mid- and lower-crustal flow (McCurry and Rodgers, 2009; Rodgers and McCurry, 2009).

A number of spatially systematic patterns occur within the ESRP basalt field (e.g., Kuntz and others, 2002, Kuntz and others, 1992; Hackett and Smith, 1992; Hughes and others, 2002; Wetmore and others, 2009) (fig. 2). Many linear vents, alignments of vents, and fracture systems trend to the northwest across parts of the ESRP, and west–northwest in the Spencer-Kilgore region south of the Centennial Range (e.g., Kuntz and others, 1992). Some of these vent features cluster into diffuse linear, northwest-trending zones, and are identified as volcanic rift zones (e.g., Kuntz and others, 1992, Kuntz and others, 2002; Rodgers and others, 2002). Some volcanic rift zones appear to merge into range bounding normal faults (e.g., Arco-Big Southern Butte Rift Zone, figs. 2, 14), and may be dominantly tectonic in origin. Others may root into robust dike swarms (e.g., Parsons and others, 1998; Kuntz and others, 2002; Rodgers and others, 2002; Rodgers and others, 1990). The "Great Rift" is the youngest and most prominent of these (e.g., Holmes and others, 2008). Interestingly, the Great Rift exhibits a systematic change in trend from northwest to northerly (fig. 2), likely reflecting a northward change in the direction of regional strain (e.g., Payne and others, 2012). Other patterns in the distribution of volcanic vents have produced diffuse linear and curvilinear constructional topographic highs (e.g., "Axial Volcanic Zone"; figs. 4 and 5).

In the ESRP eruptions of primitive basalts overlap in time and space with eruptions of comagmatic, highly geochemically evolved rocks, varying from Fe-enhanced and alkaline basalt to rhyolite (McCurry and others, 2008; Shervais and others, 2006; Leeman, 1982a). These have produced a number of domes and cryptodomes across the ESRP such as Big Southern Butte and Middle Butte, and evolved lava fields (e.g., Craters of the Moon, Cedar Butte, Unnamed Butte). Unlike the primitive basalt, parental magmas to these rocks underwent strong intracrustal fractional crystallization (e.g., Putirka and others, 2009; Whitaker and others, 2008) and remelting (e.g., Shervais and others, 2006; Bindeman and others, 2014). Hot cumulates associated with the long-lived active COM system (e.g., Kuntz and others, 1986), and voluminous young BSB system (e.g., McCurry and others, 2008), or possibly other cryptic (blind) systems across the ESRP, may be associated with localized thermal anomalies that are masked by the shallow active ESRP aquifer (fig. 3) (e.g., McCurry and Welhan, 2012).

Hydrogeology (Roy Bartholomay and Mary Hodges, USGS)

The ESRP aquifer is recharged primarily from infiltration of applied irrigation water, infiltration of streamflow, groundwater inflow from adjoining mountain drainage basins, and infiltration of precipitation (Ackerman and others, 2006). Discharge from the aquifer is primarily by pumping for irrigation and flow from springs to the Snake River (Mann and Knobel, 1990). Spring discharge fluctuates as a result of changes in water use, irrigation practices, and precipitation (Kjelstrom, 1992). For water year 2011, 3.13 million acre-ft/yr of groundwater was discharged from springs along the Snake River downstream from Twin Falls (Davis and others, 2013). Recharge to the ESRP aquifer at the INL is influenced by local surface drainage. The Big Lost River drains more than 1390 mi^2 of mountainous area that includes parts of the Lost River and Pioneer Ranges west of the INL (fig. 5). The average stream flow in the Big Lost River below the Mackay Reservoir for the 99-yr period of record (water years 1905, 1913–1914, and 1920–2014) was 217,600 acre-ft/yr (Bartholomay and Twining, 2015). Flow in the Big Lost River infiltrates to the Snake River Plain aquifer along its channel and at sinks and playas at the river's terminus in the Big Lost River sinks, in the central Big Lost Trough. To avoid flooding at the INL facilities, excess runoff has been diverted since 1965 to spreading areas in the southwestern part of the INL, where much of the water rapidly infiltrates.

The ESRP aquifer is one of the most productive aquifers in the United States (U.S. Geological Survey, 1985). Groundwater generally moves from northeast to southwest and discharges to springs along the Snake River downstream of Twin Falls, Idaho, about 100 mi southwest of the INL (fig. 5). Groundwater moves horizontally through basalt interflow zones and vertically through joints and interfingering edges of basalt flows. Infiltration of surface water, heavy pumpage, geohydrologic conditions, and seasonal fluxes of recharge and discharge locally affect the movement of groundwater (Garabedian, 1986).

At the INL, depth to water in wells completed in the ESRP aquifer ranges from about 200 ft below land surface in the northern part of the INL to more than 900 ft below land surface in the southeastern part of

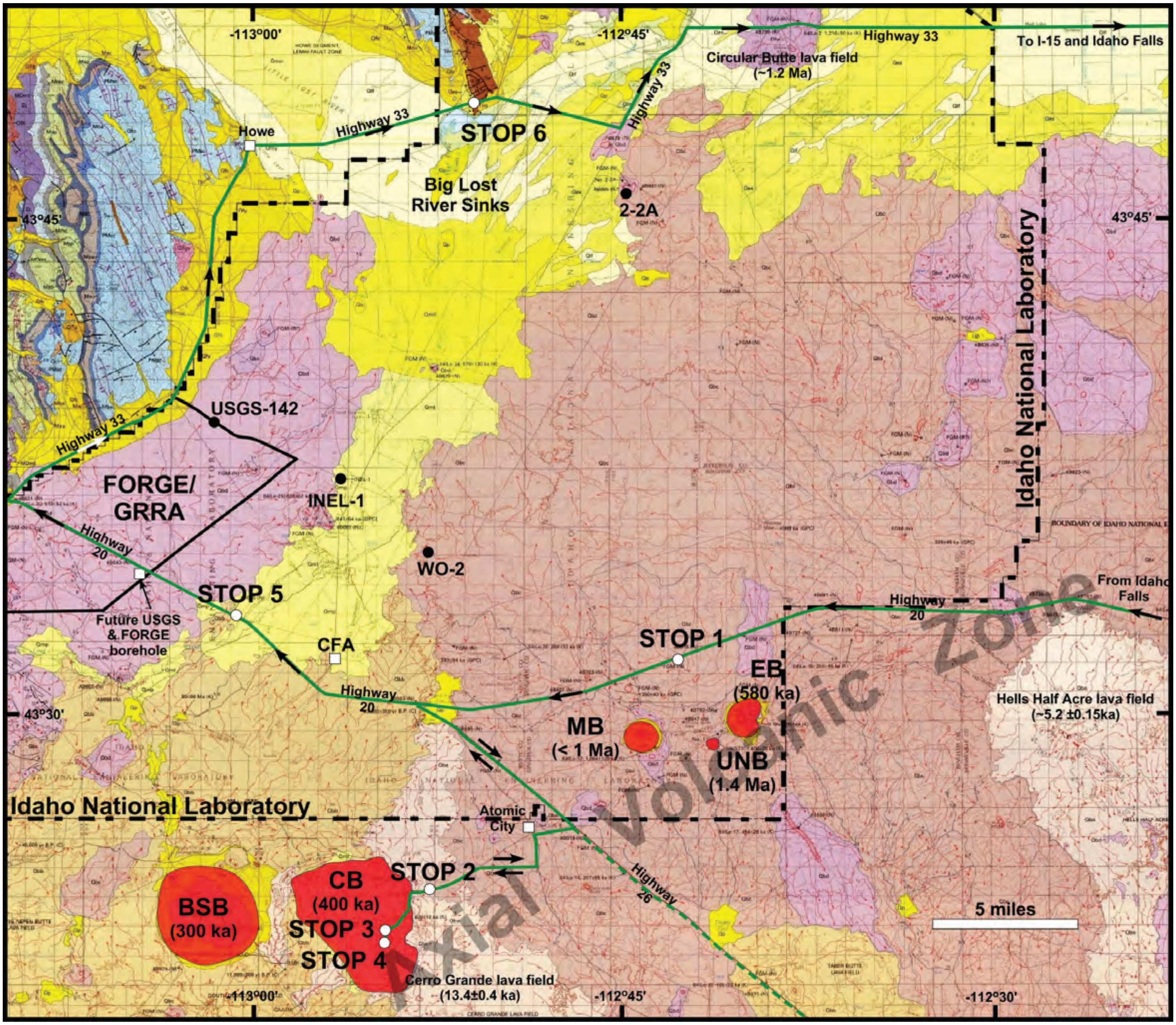

Figure 4. Geologic setting and field trip route. Base geologic map is from Kuntz and others (1994). Buttes are highlighted in red color: BSB = Big Southern Butte; CB = Cedar Butte; MB = Middle Butte; EB = East Butte. Approximate boundaries are also shown for FORGE = proposed INL Frontier Observatory for Research in Geothermal Energy site; GRRA = Geothermal Research Resource Area.

the INL. A significant proportion of the groundwater moves through the upper 200–800 ft of basaltic rock (Mann, 1986, p. 21). Ackerman (1991, p. 30) and Bartholomay and others (1997) reported transmissivity values for basalt in the upper part of the aquifer ranging from 1.1 to 760,000 ft^2/day. The hydraulic gradient at the INL ranges from 2 to 10 ft/mi, with an average of 4 ft/mi (Davis and others, 2013). Horizontal flow velocities of 2 to 26 ft/day have been calculated based on the movement of various constituents in different areas of the aquifer at and near the INL (Robertson and others, 1974; Mann and Beasley, 1994; Cecil and others, 2000; Plummer and others, 2000; and Busenberg and others, 2001). These flow rates equate to a travel time of about 50–700 years for water beneath the INL to travel to springs that discharge at the terminus of the ESRP groundwater-flow system near Twin Falls, Idaho. Localized tracer tests at the INL have shown that vertical- and horizontal-transport rates are as high as 60–150 ft/day (Nimmo and others, 2002; Duke and others, 2007).

Recent trend studies (Bartholomay and others, 2012; Davis and others, 2015) done at the INL to determine long-term changes in constituent concentrations indicate tritium and strontium-90 show mostly

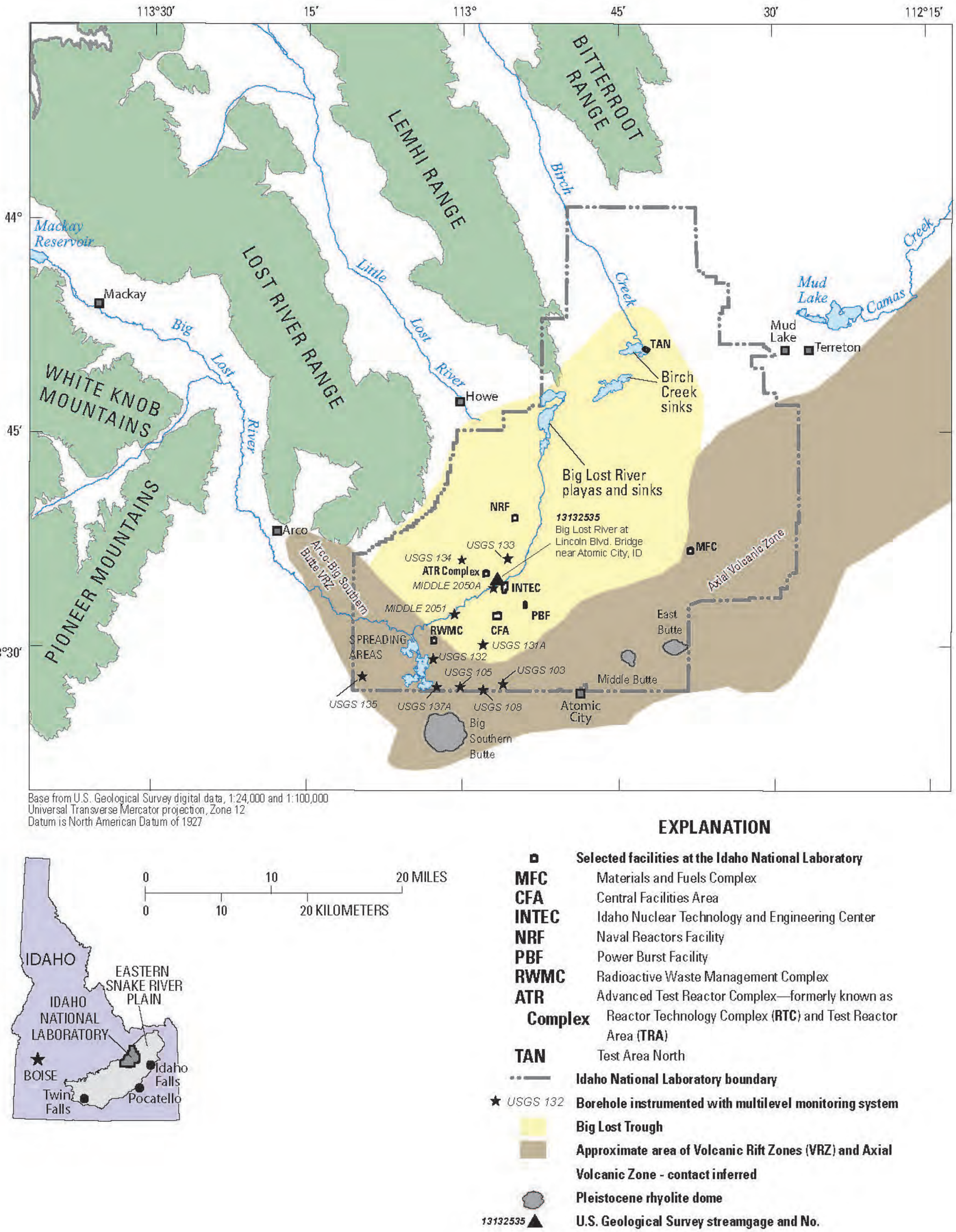

Figure 5. Location map for features of the Idaho National Laboratory and surrounding area.

decreasing or no trend in the data because of discontinued disposal, dilution, and dispersion in the aquifer and because of radioactive decay. Trend test results for chloride, sodium, sulfate, nitrate, and chromium from wells in the southwestern area of the INL near their areas of disposal also indicated decreasing or no trend. Some wells further downgradient from disposal areas show increasing trends for sodium and chloride indicating the mass of higher concentration water is still moving downgradient. Chemical concentrations in some wells show fluctuating increasing chloride, sodium, sulfate, and nitrate concentrations with wet and dry cycles of recharge with concentrations decreasing during wet periods (presumably from dilution) and increasing during drier periods. Trend test results for chloride, sodium, sulfate, and nitrate in the eastern part of the INL show mostly increasing or no trends and the increases are attributed to agricultural or other anthropogenic influences on the aquifer upgradient of the INL.

The FORGE Initiative (Rob Podgorney)

The Snake River Geothermal Consortium (SRGC) is competing nationally to host and operate an enhanced geothermal systems (EGS) field laboratory test site for the U.S. Department of Energy (DOE; Podgorney and others, 2016, 2013). Led by Idaho National Laboratory (INL), the SRGC was one of five teams selected by DOE's Office of Energy Efficiency and Renewable Energy to participate in the first phase of the Frontier Observatory for Research in Geothermal Energy (FORGE) initiative.

The consortium is proposing to locate the nation's first EGS test site on the western edge of DOE's 890-mi^2 Idaho desert site, in an area that is home to the lab's Geothermal Resource Research Area.

The goal of FORGE is to prove the necessary technologies to bring EGS into the mainstream and provide industry with the confidence to adopt the technologies. EGS has the potential to revolutionize the geothermal and renewable energy industries and greatly expand this source of clean, carbon-free baseload (continuous) power.

ROAD LOG

The Road Log begins in west Idaho Falls where N Bellin Rd/Old Hwy 91 intersects with Hwy 20. From Idaho Falls proceed west on Highway 20 for ~53 km (33 mi) to the Three Buttes roadside stop (fig. 4).

STOP 1

Three Buttes roadside stop. Latitude 43°31'42" N, Longitude 112°42'51" W.

Purpose: Overview of ESRP Axial Volcanic Zone and Quaternary volcanic evolution of ESRP.

Stop 1 is located on the ESRP Axial Volcanic Zone (AVZ) of the Eastern Snake River Plain (fig. 4). Figure 6 illustrates a vista view to the south of our location.

AVZ is a volcanic constructional high that consists mainly of numerous overlapping basaltic shield volcanoes. Many of these have erupted from northwest trending vents, high concentrations of which are referred to as volcanic rift systems (e.g., Kuntz and others, 1992, 2002). We are standing within the Howe-East Butte rift zone (H-EB of fig. 14).

Physiographic development of the broad, northeast-trending AVZ has had the important hydrogeolog-

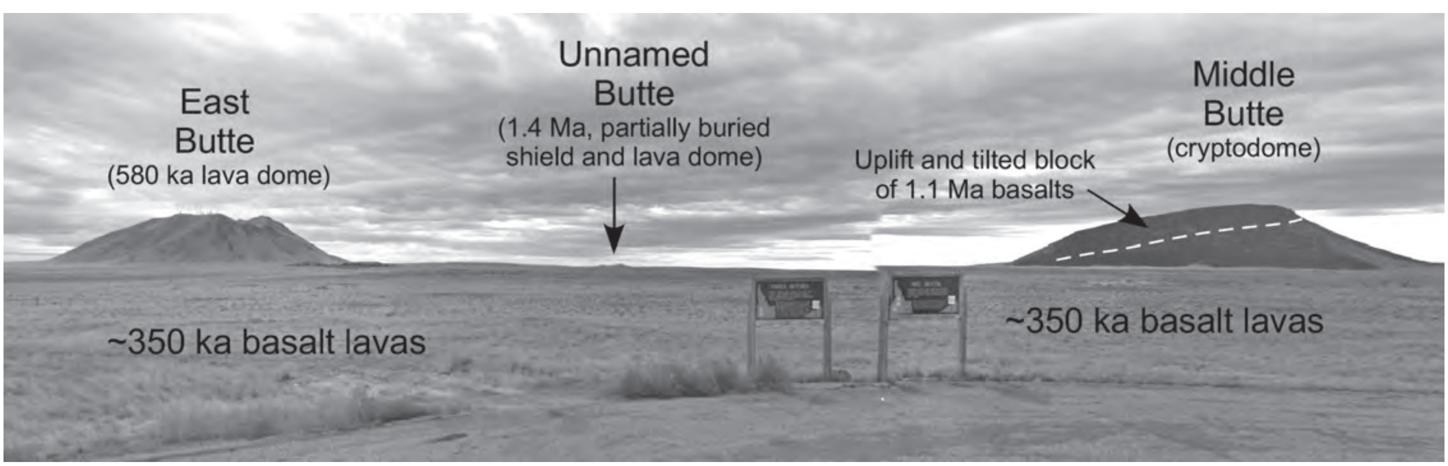

Figure 6. View looking to the south from Stop 1 (Google Maps vista image). Feature labels and dates are from Kuntz and others (1994).

ical effect of blocking or diverting drainage systems flowing to the southeast from valleys northwest of the ESRP (e.g., Allison, 2001), and feeding water into recharge systems for the Eastern Snake River Plain aquifer system (e.g., Lost River Sinks) (Ackerman and others, 2006). This will be more fully discussed at STOP 5.

Relatively primitive (i.e. mantle-derived) olivine tholeiite basalt (OTB) volcanism has dominated the ESRP following cessation of voluminous hot spot track-related volcanism which at this site began about 4.2 Ma (Kuntz and others, 1992; Champion and others, 2002). Basalt lavas have accumulated at a nearly constant rate, producing an elongated bowel-like basin that is up to 2 km deep along its axis, and a volume of basaltic lavas that is > 10,000 km^3 (McCurry and others 2008).

The buttes that are so prominent to the south and southwest of us are a product of magmatism that is compositionally distinct from, but genetically linked to, the OTB. We'll refer to this as the COM-CB suite (for representative volcanic fields at Craters of the Moon and Cedar Butte; after McCurry and others, 2008).

The COM-CB suite is distinguished from the primitive and relatively homogeneous OTB by a wide and continuous range of geochemically evolved compositions extending from "evolved basalt" to intermediate compositions (andesite- and dacite-like) to high-silica rhyolites (e.g., fig. 10c). The latter have produced the prominent lava domes and cryptodomes in front of us. Evidence for shallow storage and interactions of compositionally diverse types of magma are indicated in the common occurrence of magmatic enclaves in the lava domes (fig. 7).

Stop 1 to Stop 2: Drive 9 km (5.6 mi) west on Hwy 20; turn south onto Hwy 26. Drive ~9 km (5.6 mi) south on Hwy 26; turn west on road to Atomic City. In Atomic City, turn south on Taber Road. Drive 4.5 km (2.8 mi) south on Taber Road, then turn west onto W1600N (toward Cedar Butte and Big Southern Butte). Drive 7 km (4.3 mi) west on W1600N to train tracks and park off side of road. Walk along the train track to the northwest 450 m (0.3 mi).

STOP 2

Cerro Grande lava flow at railroad crossing. Latitude 43°24'51" N; Longitude 112°53'2" W.

Purpose: Examine an inflated pahoehoe basalt lava flow.

Discuss characteristics and origin of ESRP tholeiite (primitive basalt) lavas.

Discuss implications of basalt stratigraphic and subsurface architecture for the regional hydrogeology.

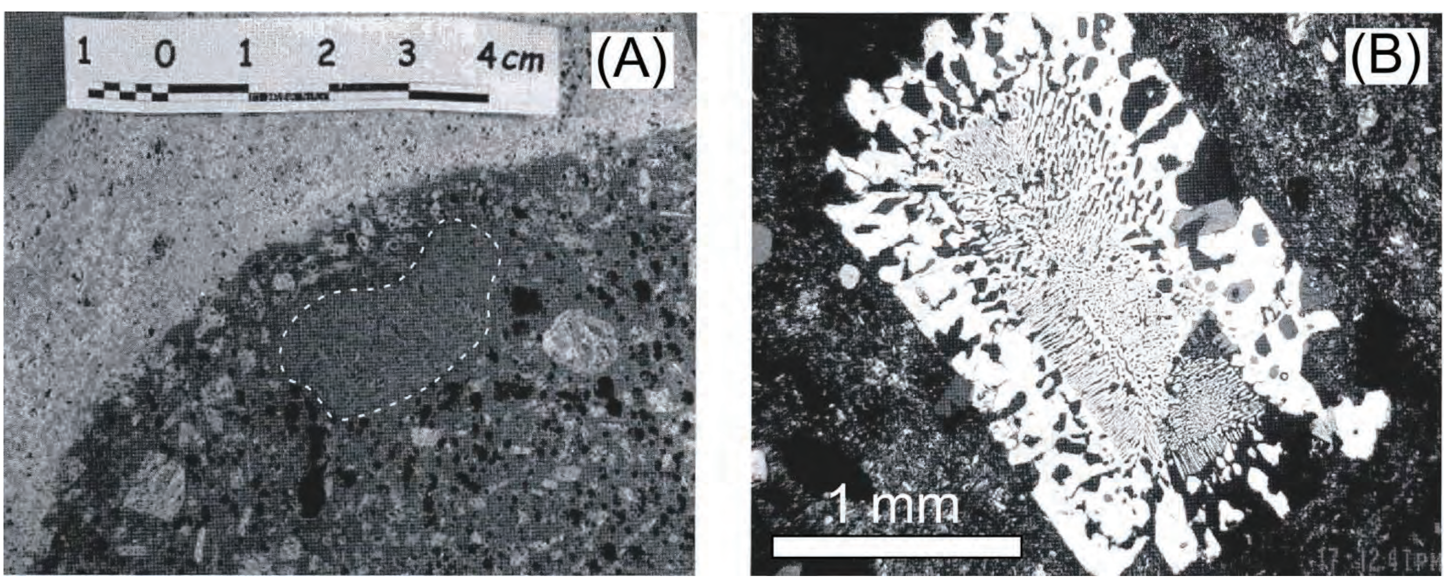

Figure 7. (A) Intermingling of diverse magma types is a common feature of Quaternary evolved volcanoes in the ESRP. This figure illustrates occurrence of a basaltic magmatic enclave (dashed line) enclosed in an andesitic host (dark colored with large plagioclase phenocrysts), that is in turn engulfed in high-silica rhyolite (light gray color). (B). A splendid example of a granophyric alkali feldspar phenocryst in the rhyolite of East Butte. Such features may be produced by loss of volatiles during the ascent of rhyolite magma. Both (A) and (B) are after Ganske and McCurry (2007).

At this stop we will examine a part of the 13.4 ka Cerro Grande lava flow, a typical example of ESRP OTB. Eruption of the Cerro Grande lavas occurred from northwest-trending vents just southeast of Cedar Butte. Eruptions occurred on the crest of AVZ, producing large lobes of pahoehoe lavas that extended downhill up to ~7 mi to the north and 10 mi to the southeast. We are standing on the northern lobe.

Figure 9 illustrates the complex nature of the basalt lavas. Although sheet-like on a large scale, the "sheets" actually consist of numerous, complex anastomosing and overlapping lobes. These evolve through a process called inflation, in which the leading front advancing fluidal lavas cool, producing back pressure, and subsequent inflation of following parts of the lava flow (Self and others, 1998; Hughes and others, 1999). Sustained back-pressure can lead to development of huge mounds up to 10 m high and 100s of meters long (fig. 9).

Break-outs from the margins of developing inflated lobes result in decompression within still liquid parts of the lobe, commonly causing vesiculation ("vesicle zones") and collapse of the solidified roof of the lava flow (see "collapse pits" in fig. 9).

Stretching and cracking of solidified surficial parts of inflated lobes led to formation of large fissures (fig. 9 and inset). Welhan and Reed (1997) demonstrated that when buried by subsequent lavas, many of the fractures may remain partially open, creating regions of high permeability and a high degree of hydrologic anisotropy. Aligned fissures, collapsed lava tubes, and interflow basalt rubble play key roles in the basalt-hosted parts of the Eastern Snake River Plain aquifer system (e.g., Johnson and others, 2000).

Stop 2 to Stop 3: From the train tracks, drive 900 m west on W1600N, then turn south off of W1600N on a dirt road. Drive south on the dirt road ~ 1 km (0.6

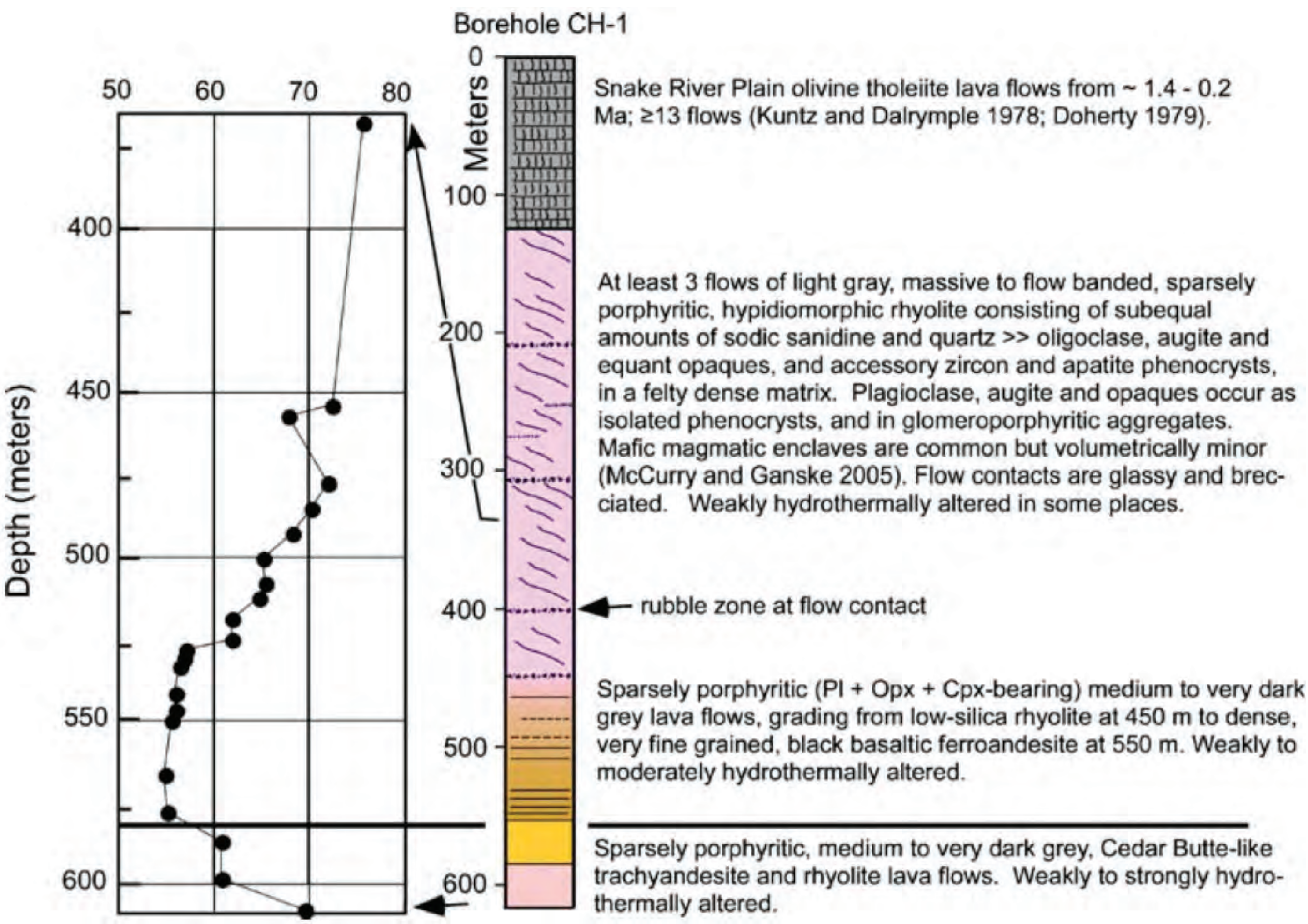

Figure 8. A simplified log of borehole CH-1, located near the northwest margin of Unnamed Butte. The borehole log indicates that the butte is the iceberg-like tip of a large composite volcano that has been largely buried by younger primitive basalt lavas. The exposed part of the butte is high silica rhyolite. Deeper parts of the volcano are intermediate to mafic in composition (after McCurry and others, 2008).

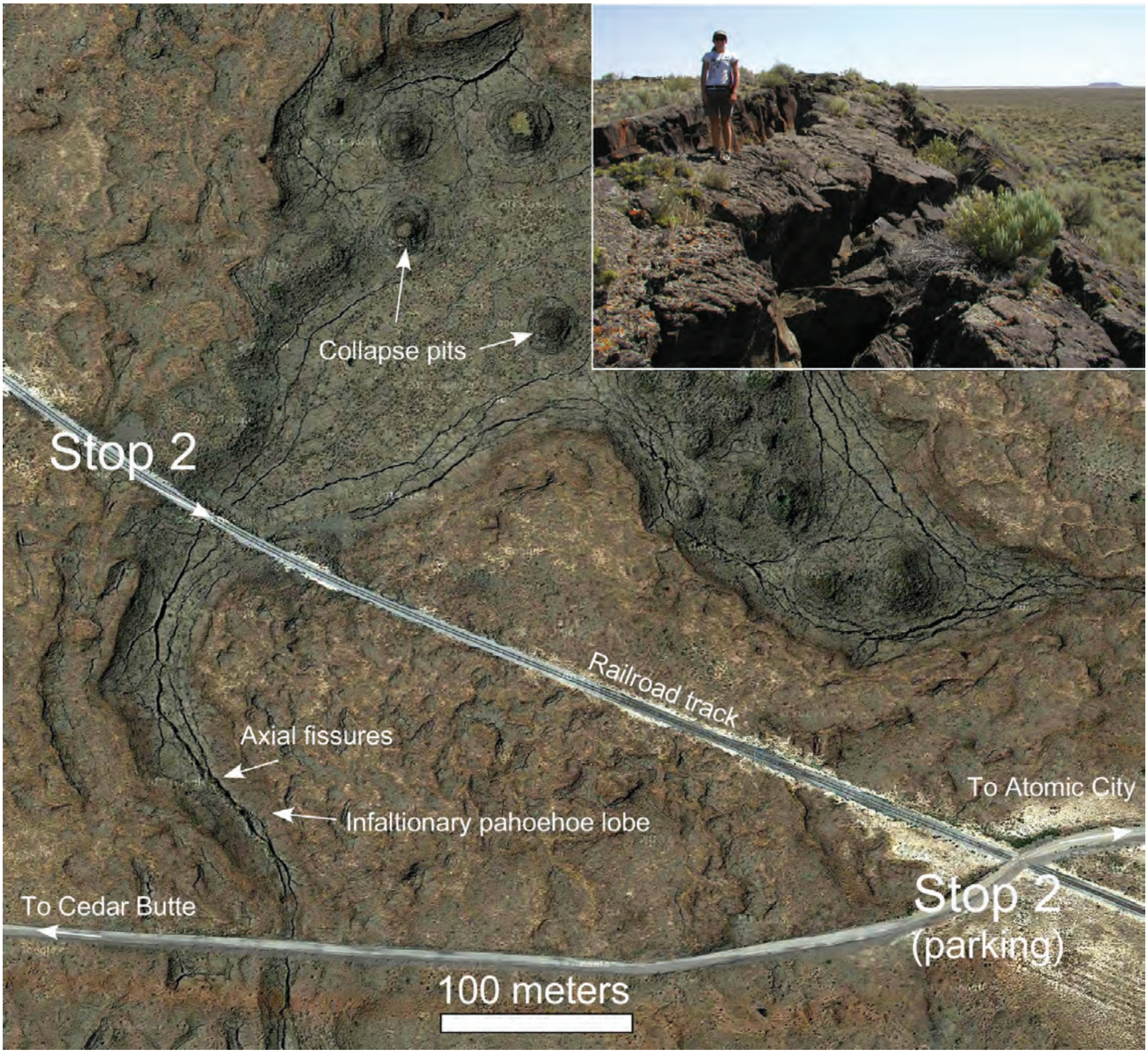

Figure 9. Aerial view (from GoogleMaps) of inflated pahoehoe lobes of the 13.4 ka Cerro Grande lava flow (north is towards the top of the photo). The inset photo is taken from near the crest of lava flow at Stop 2 (courtesy of Scott Hughes).

mi) to intersection with another dirt road; turn right (to the southwest) and proceed ~2 km (1.2 mi) on a rough, unimproved road toward the northern flank of an erosionally breached tephra cone near the center of Cedar Butte. Take a left fork in the road, due south. Proceed south ~900 m (0.6 mi) to the southern rim of the Cedar Butte tephra cone.

STOP 3

Cedar Butte volcano-summit. Latitude 42°23’13” N. Longitude 112°54’34” W

Purpose: Examine compositionally diverse pyroclastic deposits of Cedar Butte volcano.

Discuss characteristics and evolution of evolved, polygenetic Quaternary volcanoes of the ESRP (e.g., Cedar Butte, Unnamed Butte, Craters of the Moon)

From a distance of 400 ka Cedar Butte appears similar to other shield volcanoes on the Eastern Snake River Plain, with the exception of being capped by a large tephra cone on which we are now standing (fig. 10b). However, the Cedar Butte shield differs from typical shields constructed of OTB, in that it consists entirely of evolved mafic to intermediate and silicic volcanic rocks (fig. 10c). More mafic lavas were erupted first, followed by sequentially more felsic compositions, and ending with eruptions of a high-silica rhyolite lava flow and explosive eruptions that produced the tephra cone. All of these appear to have occurred within a few hundred years (McCurry and others 2008; D. Champion, personal commun., USGS).

The view from the top of Cedar Butte provides a sweeping vista of the ESRP. The Big Lost River and Lemhi Ranges can be observed in the distance to the northwest and north, respectively. Middle, Unnamed, and East Buttes can be seen to the northeast. Prominently, ~5 mi to the west, is ~300 ka Big Southern Butte.

Big Southern Butte is the largest of the ESRP Buttes, rising ~760 m above the surrounding plain. It is one of the largest and most geochemically evolved rhyolitic lava domes on Earth. The volcano evolved initially from a cryptodome, akin to Middle Butte. Cryptodomes are formed by shallow laccolith-like intrusions that domally uplift overlying country rocks. In the case of Big Southern Butte the laccolith magma body continued to inflate, growing to the point that the rocks overlying roof rocks collapsed into it, and the rhyolitic magma extruded onto the surface as a lava dome. A hinge-like mass of a part of the roof that did not collapse makes up much of the northern flank of Big Southern Butte.

Walk along the rim of Cedar Butte to observe diverse types of pyroclastic rocks. Erosionally resistant parts of the rim are volcanic agglutinate. Agglutinate, small rootless lava flows, and unconsolidated parts of the tephra cone contain pyroclasts that vary from dense and massive to highly pumiceous. Compositions vary from intermediate (reddish to black) to silicic (white), and in some cases include complexly intermingled compositions.

The diverse and continuous range of compositions of lavas and pyroclasts at Cedar Butte overlap remarkably with those of Craters of the Moon (fig. 10c). Similar compositions also occur in many borehole and surface samples from other parts of the ESRP. We refer to this as the COM-CB association. More mafic and intermediate compositions dominate over silicic compositions, and phenocryst assemblages and compositions reflect near-equilibrium crystallization conditions. McCurry and others (2008) and Whitaker and others (2008) suggest that the COM-CB suite is mainly a product of extreme mid- to upper-crustal fractional crystallization of primitive OTB, with or without minor crustal assimilation (e.g., Putirka and others, 2009). Mixing and homogenization are common but subordinate processes (except at Unnamed Butte, fig. 8; McCurry and others, 2008).

Stop 3 to Stop 4: Return to the north to the intersection on the northern breached margin of the tephra cone.

STOP 4

Cedar Butte volcano-dike. Latitude 43°23’33” N. Longitude 112°54’33” W

Purpose: Examine a spectacular example of a compositionally zoned dike.

Discuss magma plumbing systems and connec-

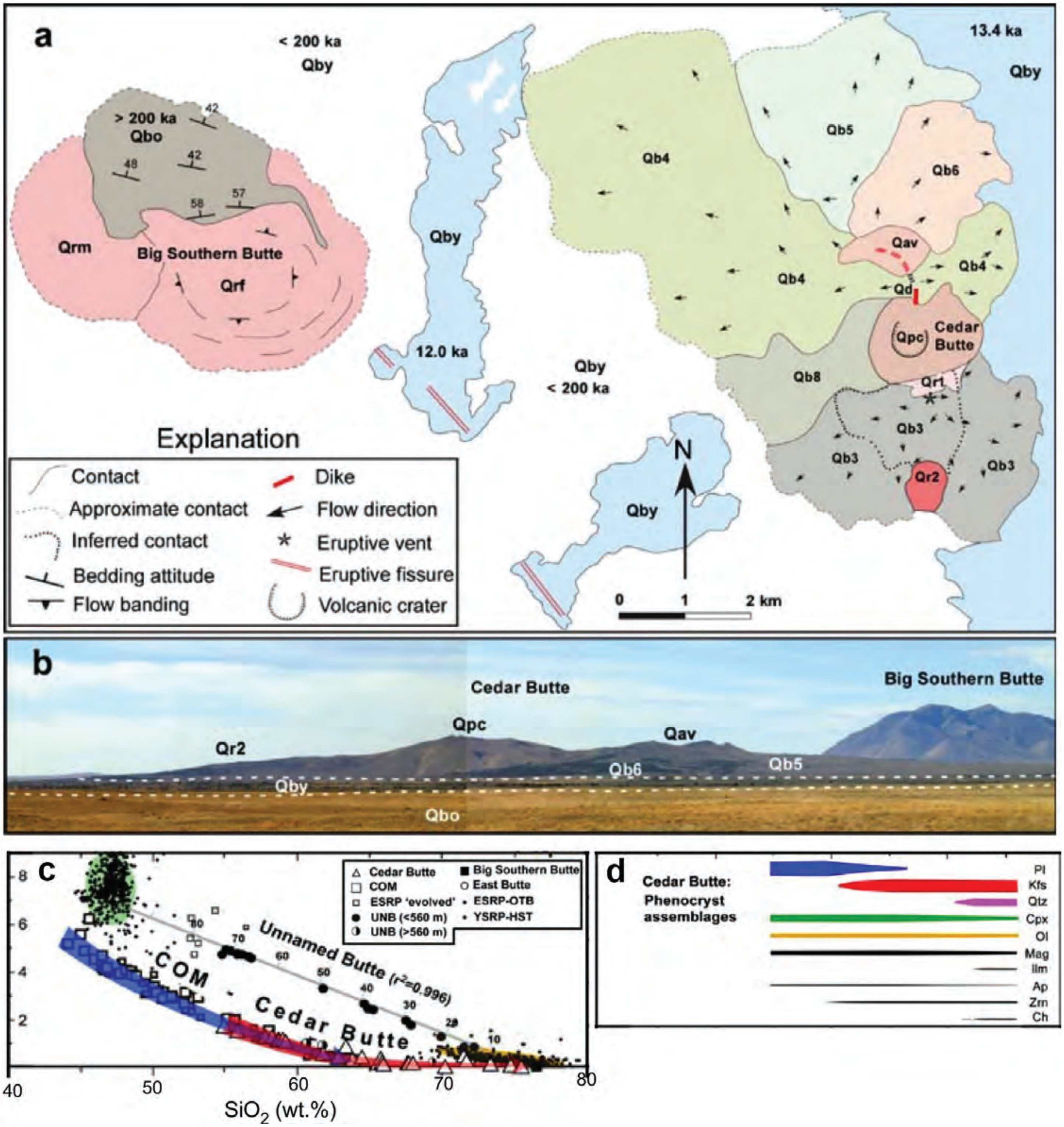

Figure 10. (a) A simplified geologic map of Big Southern and Cedar Butte. (b) A view to the southwest of Cedar Butte and Big Southern Butte from near Atomic City. (c) A plot of silica vs MgO illustrating the wide range of composition and curvilinear patterns of most evolved Quaternary volcanic rocks in ESRP. Shallower parts of Unnamed Butte volcano exhibit strikingly linear pattern typical of magma mixing and homogenization. (d) Phenocryst abundance (width of line) and assemblages correlate systematically with bulk composition of Cedar Butte volcanic rocks (from McCurry and others, 2008).

tions between Quaternary volcanoes and mid- to upper-crustal magma storage regions.

At this site several en echelon dike segments have been erosionally exhumed. These are parts of a system of dikes that fed into eruption vents beneath the Cedar Butte tephra cone to the south and a curvilinear spatter rampart and vent zone to the north of this site. Two of these exhibit cross-sectional views of the dikes that reveal a strong internal compositional zonation from mafic margins to felsic interiors (fig. 11).

Processes by which mafic magmas tend to migrate toward conduit walls, when in contact with more silicic magma, are referred to by Carrigan (1994) as "viscous segregation" and "encapsulation." Carrigan describes experimental and theoretical bases for the segregation process, indicating that it is primarily the result of the highly contrasting viscosities of magma types. More fluid mafic melts tend to migrate into the zones of high shear (i.e., margin) within the conduits. Carrigan demonstrates that it is possible to produce such a dike geometry even though the original source reservoir was continuously zoned, with rhyolitic melts on the top—as seems possible beneath Cedar Butte. The dikes are a part of a nearly continuous curvilinear system of vents and intrusions extending for ~2 km, including the tephra cone to the south, and curvilinear vent zone to the north, and circumscribing a near circular 150° arc (fig. 10a). The arc has a radius of curvature of about 0.8 km, and may have originated by incipient formation of ring fractures above a shallow, compositionally zone magma reservoir system (McCurry and others, 1999).

Stop 4 to Stop 5: Retrace route back to the intersection of Highways 20 and 26. Proceed west on Hwy 20 for ~12 km (7.5 mi) to the highway rest stop.

STOP 5

Big Lost River roadside rest stop. Latitude 42°31'42" N; 112°42'51" W

Purpose: Overview of the hydrogeology and subsurface architecture of the INL and ESRP.

Discuss USGS activities for understanding and monitoring regional and INL hydrogeology and the USGS/INL core library.

Discuss the SRGC and FORGE initiative for research and development of renewable, clean geothermal energy.

This site is adjacent to the Big Lost River (usually a dry wash). It is one of the principal sources of surface and ground water recharge to the INL Lost River Sinks and Eastern Snake River Plain aquifer system. The Big Lost River originates in the Pioneer Mountains. It flows to the south through the Big Lost River valley. Southward drainage is blocked and diverted in the ESRP, first to the east and then to the northeast by constructional volcanic features of the Axial Volcanic Zone (Hodges and others, 2009). This pattern of flow has existed since the mid to late Pliocene (Hodges and others, 2009) producing the "Big Lost Trough" (Geslin and others, 2002).

The Idaho National Laboratory (INL), operated by the U.S. Department of Energy (DOE), encompasses about 890 mi^2 of the eastern Snake River Plain in southeastern Idaho (fig. 12). The INL was established in 1949 to develop atomic energy, nuclear safety research, defense programs, environmental research, and advanced energy concepts. More recent work has focused on spent nuclear fuel management; hazardous and mixed waste management and minimization; national security; cultural resources preservation; and environmental engineering, protection, and remediation. Wastewater disposal sites at the Test Area North (TAN), the Naval Reactors Facility (NRF), the Advanced Test Reactor Complex (ATR Complex), and the Idaho Nuclear Technology and Engineering Center (INTEC) have contributed radioactive- and chemical-waste contaminants to the ESRP aquifer. These sites incorporated various wastewater disposal methods, including lined evaporation ponds, unlined percolation (infiltration) ponds and ditches, drain fields, and injection wells. Waste material buried in shallow pits and trenches within the Subsurface Disposal Area at the Radioactive Waste Management Complex (RWMC) have also contributed contaminants to groundwater.

The U.S. Geological Survey (USGS) has undertaken systematic research at the INL since 1949. This work initially characterized water resources before nuclear-reactor testing facilities (Walker, 1964; Barraclough and others, 1967; Barraclough and others, 1976; Robertson and others, 1974; Nace and others, 1975). Since then, the USGS has operated a ground-

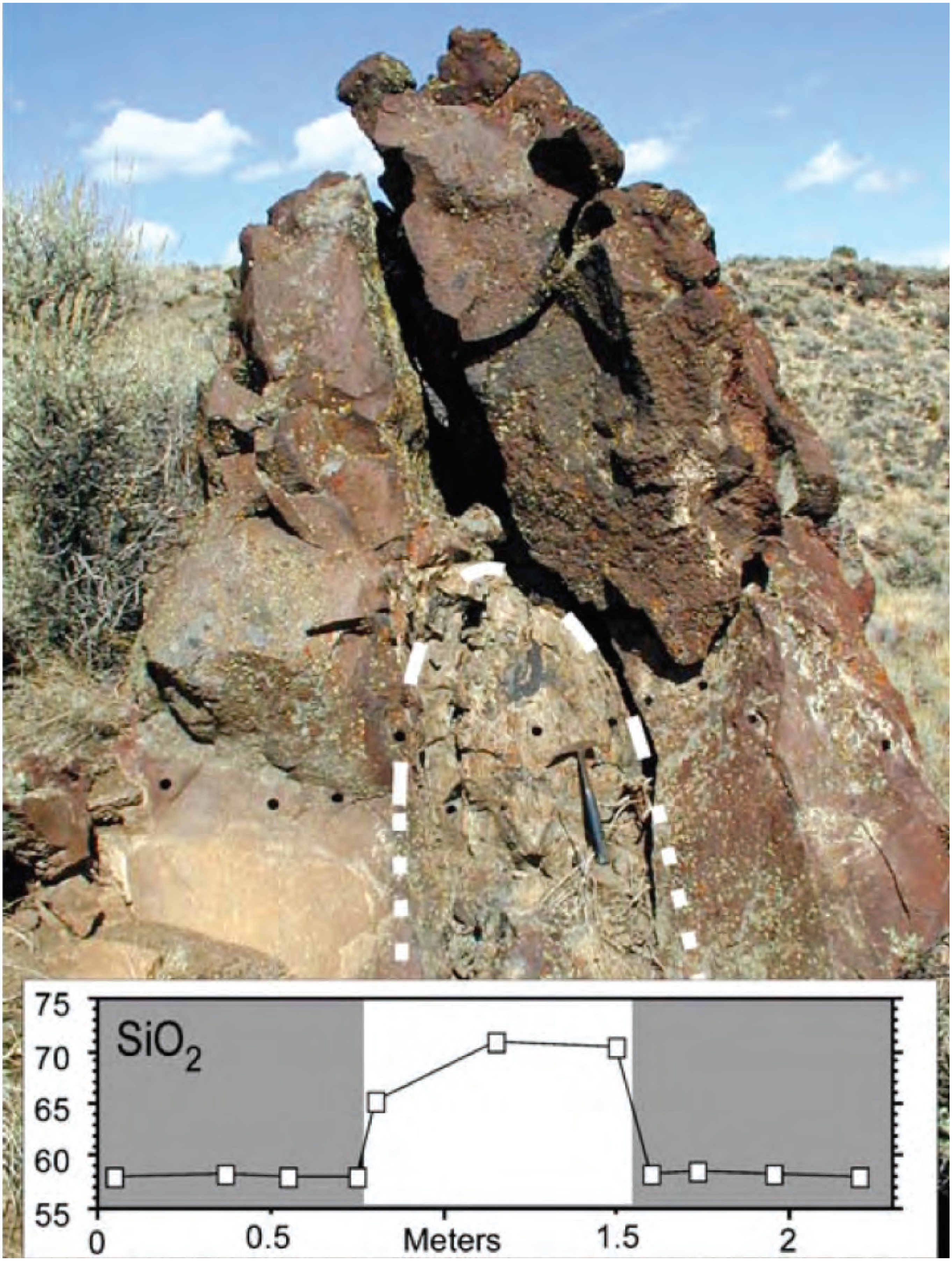

Figure 11. A spectacular cross-sectional exposure of a dike emplaced into and erosionally exhumed from within the northern margin of the tephra cone capping Cedar Butte. The blade-like dike is almost perfectly preserved. The inset figure illustrates extreme compositional zoning within the dike.

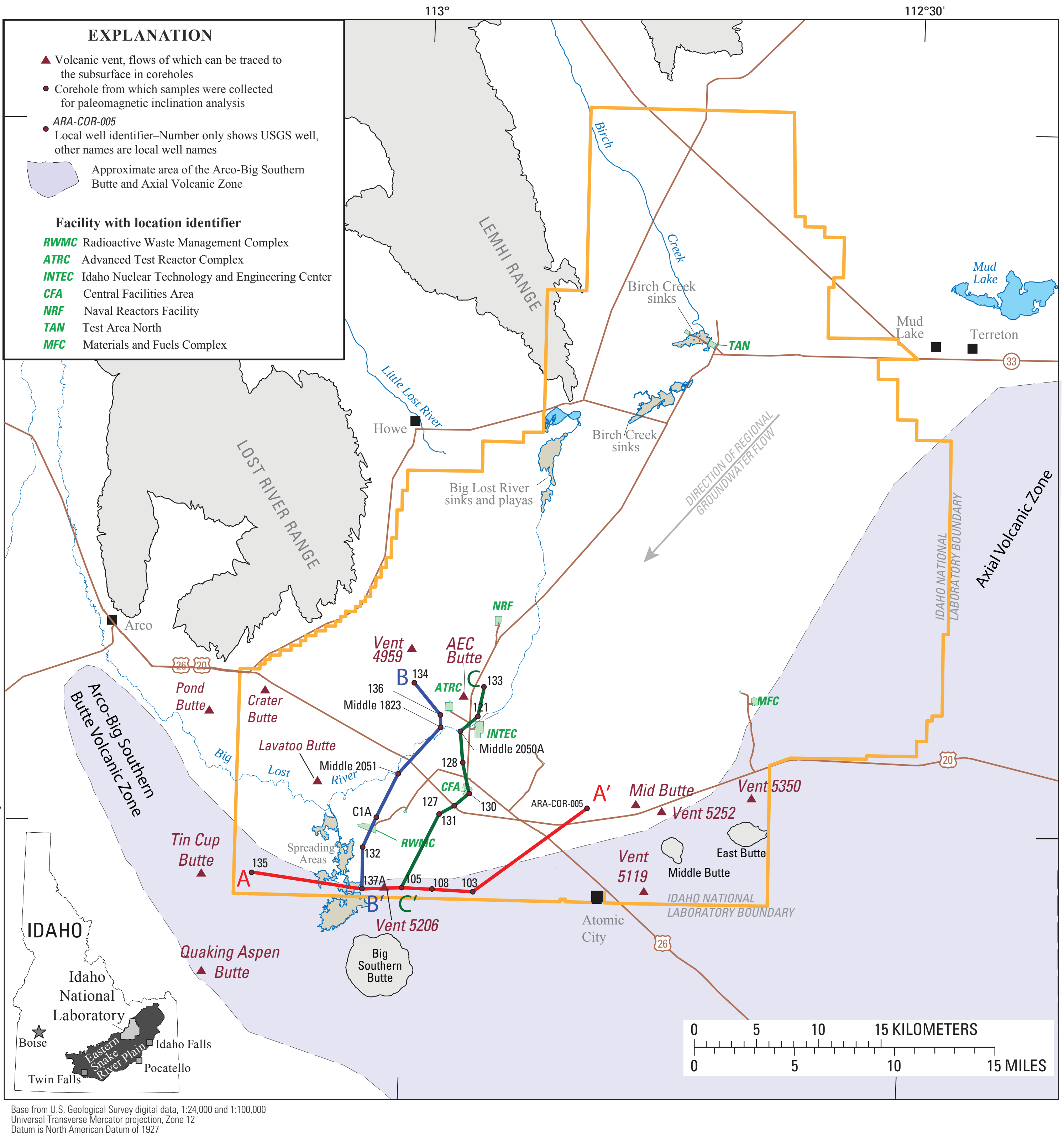

Figure 12. Location of wells and cross-sections of geologic flow units at the Idaho National Laboratory.

water quality and water-level measurement network to provide data for research on hydrologic trends and to delineate the movement of facility-related radiochemical and chemical wastes in the ESRP aquifer. Additionally, work is ongoing to better understand the stratigraphic deposition of basalts and sediment below the INL to support groundwater-flow models.

Subsurface Geology and Paleomagnetic Studies

Building on earlier studies, especially Champion and others (2011), a recent study using paleomagnetic inclination and polarity, done in cooperation with DOE, on paleomagnetic data from subsurface drill cores and surface outcrops provides valuable data that can help constrain the age and areal extent of basalt flows in the subsurface at and near the southern INL. Knowledge of the subsurface horizontal and vertical distribution of basalt flows and sediment layers is needed to construct numerical models of groundwater movement and contaminant transport.

Data from paleomagnetic studies were used to refine Pleistocene and Holocene stratigraphy at and near the southern part of the INL (fig. 12). Samples from 18 coreholes in the southern INL were analyzed for mean paleomagnetic inclination. Paleomagnetic samples were collected from coreholes with total depths from a few hundred feet (USGS 127, total depth, 598 ft), to more than 1,800 ft (C1A, total depth 1,805 ft). Paleomagnetic inclination data were used to correlate surface and subsurface basalt stratigraphy, determine relative ages, and, in conjunction with other studies, to determine the absolute age of some basalt flows.

Basalt shield volcanoes erupt a wide range of lava flow volumes, filling the topography present at the time of eruption. The cross-sections presented at this field trip stop show this in several flows.

Correlative lava flows found in drill cores may be found at different depths. Large lava flow groups may be intersected by numerous coreholes; small lava flows may be found in only one corehole. Correlation of lava flows and flow groups was established using subsurface cross sections through different areas of the INL. One cross section represents the deep sections in the southern part of the INL, showing the stratigraphic sequences of the lava flows near and below the approximate Brunhes-Matuyama polarity boundary. Results demonstrate that coreholes a few miles apart have stratigraphic successions that correlate over tens to hundreds of feet of depth. Correlations between coreholes separated by greater distances are less consistent because some stratigraphic sequences may be missing, added, or are at different depths. Possible vent locations of buried basalt flows were identified by determining the location of the maximum thickness of flows.

Possible subsurface vent locations in this study area include:

- The D3 flow is thickest in ARA-COR-005, thins westward, and may have come from the Axial Volcanic Zone. The D3 flow is much larger than previously reported; it now includes the flow previously labeled South Central Facilities Area buried vent (lower).
- The Big Lost flow vent probably lies beneath RWMC.
- The G flow thickens to the south and its vent is probably south of USGS 135.
- The CFA buried vent flow is probably located in the subsurface below CFA.
- The North INTEC buried vent is thickest beneath USGS 121 and, as the name implies, probably originates somewhere north of INTEC.
- The South Late Matuyama flow thickens towards the southwest; it is likely that its vent is south and west of USGS 135.
- The Matuyama flow is thickest in the subsurface between coreholes C1A and USGS 132, so its vent is probably near RWMC.
- The Jaramillo flow is thickest in the subsurface at USGS 131, so the Jaramillo vent is probably underground near USGS 131.

INL Lithologic Core Storage Library

In 1990, the USGS, in cooperation with DOE, established the Core Storage Library at the INL. The facility was established to consolidate, catalog, and permanently store nonradioactive drill cores and cuttings from investigations of the subsurface conducted at and near the INL and to provide a location for researchers to examine, sample, and test these materials. Core samples are used for site-wide and site-specific characterization of the subsurface in support of the USGS and INL contractor groundwater-flow and contaminant-transport modeling and the construction of new facilities. By examining and/or analyzing core samples, a 3-D representation of basalts and sediments in the subsurface can be developed. Modelers use this information to refine model input of the geologic framework, to improve the conceptual model of groundwater flow and contaminant transport, and to improve the numerical model output simulations. Additionally, detailed subsurface information will support future facility-scale 2-D and 3-D groundwater-flow and contaminant-transport modeling. Cores are also used by the scientific community (including university faculty and students, researchers from state agencies, and other national laboratories) to investigate geologic, seismic, and hydrologic aspects of the evolution of the ESRP.

Approximately 130,000 ft of drill core and 9,000 ft of drill cuttings are stored in the Core Library and at additional core storage space at a warehouse at the Central Facilities Area at the INL. A description of the facility, procedures for use, and core and cuttings available for research can be found in Davis and others (1997).

Since the 1950s, greater than 500 test holes, auger holes, and wells have been drilled at and near the INL to characterize hydrologic and geologic conditions in the subsurface and to supply water to facilities. Data derived from drill cores, such as petrographic analyses, paleomagnetic properties, $^{40}Ar/^{39}Ar$ age dates, geochemistry, and natural-gamma geophysical logs from boreholes at the INL have been used to determine the subsurface stratigraphy.

SRGC and FORGE Initiative

Geothermal energy generation occurs almost exclusively in hydrothermal systems, whereas approximately 90% of the potential geothermal power resource in the United States has been estimated to reside in Enhanced Geothermal System (EGS) settings. Enabling EGS development could provide 10 to 100+ GWe or more, and make geothermal energy a significant component of the nation's renewable energy portfolio. To enable development and deployment of EGS technologies, the U.S. Department of Energy Geothermal Technologies Office (GTO) has solicited teams to bring multidisciplinary, world-class researchers together with industry to find innovative solutions and creative, transformational paths via a new Frontier Observatory for Research in Geothermal Energy (FORGE) Laboratory.

To meet the challenges and drive the solutions for EGS, the Snake River Geothermal Consortium (SRGC), a research partnership focused on advancing geothermal energy, was established. The SRGC is comprised of national laboratories, academic institutions, federal/state agencies, and private industry partners. National laboratory partners include Idaho National Laboratory (INL), the National Renewable Energy Laboratory, and Lawrence Livermore National Laboratory, which support the full spectrum RD&D on energy technologies. In addition to the national laboratories, six academic institutions are SRGC partners, including the Center for Advanced Energy Studies (University of Idaho, Idaho State University, Boise State University, University of Wyoming), University of Utah, and University of Oklahoma; they add diversity of research innovation and network to the broader STEM educational functions and outreach that will be instrumental in helping secure the long-term goals for EGS. Also, six private partners participate as SRGC members and bring key perspectives to the research team and provide a context for commercializing the research outcomes; they include Mink GeoHydro, Baker Hughes, Geothermal Resource Group, Chena Power, Campbell Scientific, and US Geothermal. The team also has participants from federal and state agencies, including the USGS, Idaho Department of Water Resources, and the Idaho Geological Survey.

The INL, one of DOE's largest laboratories [2,300 km^2 (890 mi^2)], intends to host the FORGE Laboratory within its site on the Eastern Snake River Plain, providing the central physical location for the research. It has dedicated 100 km^2 (39 mi^2) of land as a Geothermal Resource Research Area (GRRA), and has an established permitting framework for projects such as FORGE. The INL is located on the track of the Yellowstone Hotspot, and deep well data indicate that the GRRA occupies an area of high subsurface temperature, with regional stress conditions and rock mechanical properties favorable for reservoir stimulation. The GRRA also has abundant groundwater resources and water rights for geothermal research, development, and deployment.

Stop 5 to Stop 6: Proceed northwest on Hwy 26 for 9.5 mi (15 km) to the intersection with Hwy 33. Turn right (to the northeast) on Hwy 33 towards Howe, ID. Proceed ~14 mi (22 km) to Howe, ID. In the town of Howe, continue due east on Hwy 33 for 8 mi (13 km) to Howe Point.

STOP 6

Howe Point. Latitude 42°31'42" N; Longitude 112°42'51" W.

Purpose: Examine ignimbrites of the Heise and Picabo volcanic fields.

Overviews and discussion of:

1. Hydrogeology focusing on aquifer recharge and Lost River Sinks area;
2. Ignimbrite supereruptions, and related ignimbrite stratigraphy and cryptic and nested caldera systems; implications of caldera systems for potential EGS exploration and development; and
3. Regional structure and tectonics.

Park in the large roadside pull-out area on the south side of the road. A high-grade, rheomorphic ignimbrite exposed adjacent to the north and south sides of the highway is the 8.87 Ma tuff of Lost River Sinks (fig. 13a,b). Sequentially uphill to the north are east tilted exposures of the Heise volcanic field-related Blacktail Creek Tuff (6.66 Ma) and Walcott Tuff (6.27 Ma) ignimbrites. Anders and others (2014) also describe a second thin ignimbrite beneath the thick exposure of Walcott Tuff. They suggest a correlation exists between these two ignimbrites and similar ignimbrites samples in INL borehole WO-2. The two yield indistinguishable $^{40}Ar/^{39}Ar$ dates, and are referred to by Anders and others (2014) as Walcott A (lower) and Walcott B (upper).

Older Picabo-age ignimbrites are exposed in more northern parts of the southern Lemhi Mountains (Anders and others, 2014; Kuntz and others, 2009). The oldest and most compositional and mineralogically distinctive is the Arbon Valley Tuff (AVT; Kellogg and others, 1994). It is a rare biotite-bearing deposit, and it has therefore been used extensively in regional tephrochronology studies (e.g., Perkins and Nash, 2002). Anders and others (2014, 2009) have defined two age populations of sanidine phenocrysts in various parts of the deposit (Arbon Valley Tuff A = 10.41 ± 0.1 Ma and Arbon Valley Tuff B = 10.22 ± 0.01 Ma), indicating that it was produced in two major eruptions. At least one of those is strongly compositionally zoned from nonwelded, crystal-poor (<5% Sa> Q>Pl>Bt>Hbl) high silica rhyolite at the base to crystal-rich (~40% Sa>Q>P>Bt+Opx) lower-silica rhyolite at the top (McCurry, 2009).

The AVT is exposed in many locations both on the northern and southern sides of the ESRP, including ~1 mi north of us (fig. 13A), and is likely to have an original volume comparable to some of the largest ignimbrites erupted in the ESRP (perhaps ~1,000 km^3). It may have been derived from a large cryptic caldera located near Blackfoot, ID, named the Taber Caldera by Kuntz and others (1992) and Kellogg and others (1994), and the Arbon Valley Tuff caldera by Anders and others (2014).

The AVT was erupted at about the same time as the first voluminous rhyolite eruptions occurred in the Twin Falls area, leading to some complication of the time-space pattern of hot spot track migration (figs. 1, 2). Petrogenetic implications of AVT are also discussed in recent work by Drew and others (2016).

A fault that roughly parallels the highway has downdropped rocks on the south side of the road by at least 50 m (Morgan and others, 2008). Morgan and others (2008) infer that this fault is faulted topographic boundary of a caldera. Anders and others (2014) argue that the fault is related to flexure and tectonic subsidence of the Snake River Plain.

After examining ignimbrites along and north of the highway, proceed south ~200 m over downdropped rocks of the densely welded Walcott Tuff on a rough trail to the top of the small hill (Howe Point overview). The overview offers a superb view of the ESRP, Lost River Sinks, and Big Lost and Beaverhead ranges. Figure 14 illustrates the regional geology. The Big Lost, Lemhi, and Beaverhead Mountains are east-tilted, horst blocks bounded on the west by large Quaternary normal faults. Older normal faults, and related extension, produced a late Eocene or Oligocene half graben in the southern Lost River Range and Arco

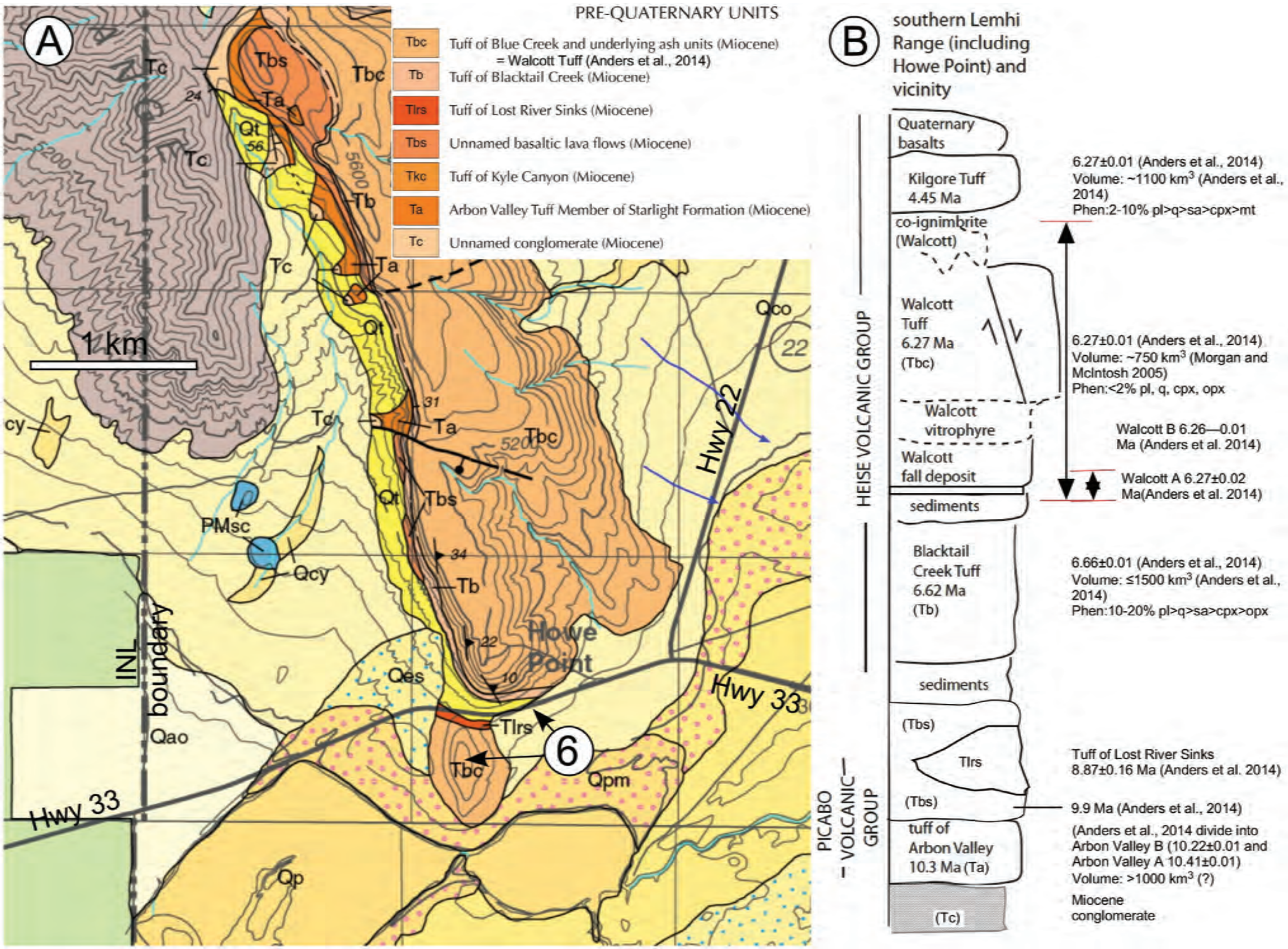

Figure 13. (A) Stop 6 is overlain on a geologic map of the Howe Point area (modified after Kuntz and others, 2003). (B) Stratigraphy of the Howe Point area (modified after Morgan and others, 2008).

Hills (Arco Pass Graben) (Link and Janecke, 1999).

Red lines on Figure 14 illustrate patterns of Miocene and younger tilting of originally horizontal features (e.g., Laramide fold axes) into the ESRP. Rodgers and others (2002, and references therein) suggest that tilting was an elastic response to loading of the mid-crust with dense mafic intrusions associated with Yellowstone hot spot magmatism. Their modeling indicates that the original Miocene surface has been downwarped by at least 5 km beneath the ESRP (inset to fig. 14).

Complex patterns of faulting occur in the south ends of the ESRP-bounding mountain ranges, where they dip into the Snake River Plain. Bruhn and others (1992) indicate that those in the southern Lemhi Mountains are a product of complex fault tip evolution of the Lemhi fault. Morgan and others (1984) suggested that some of the small faults could be related

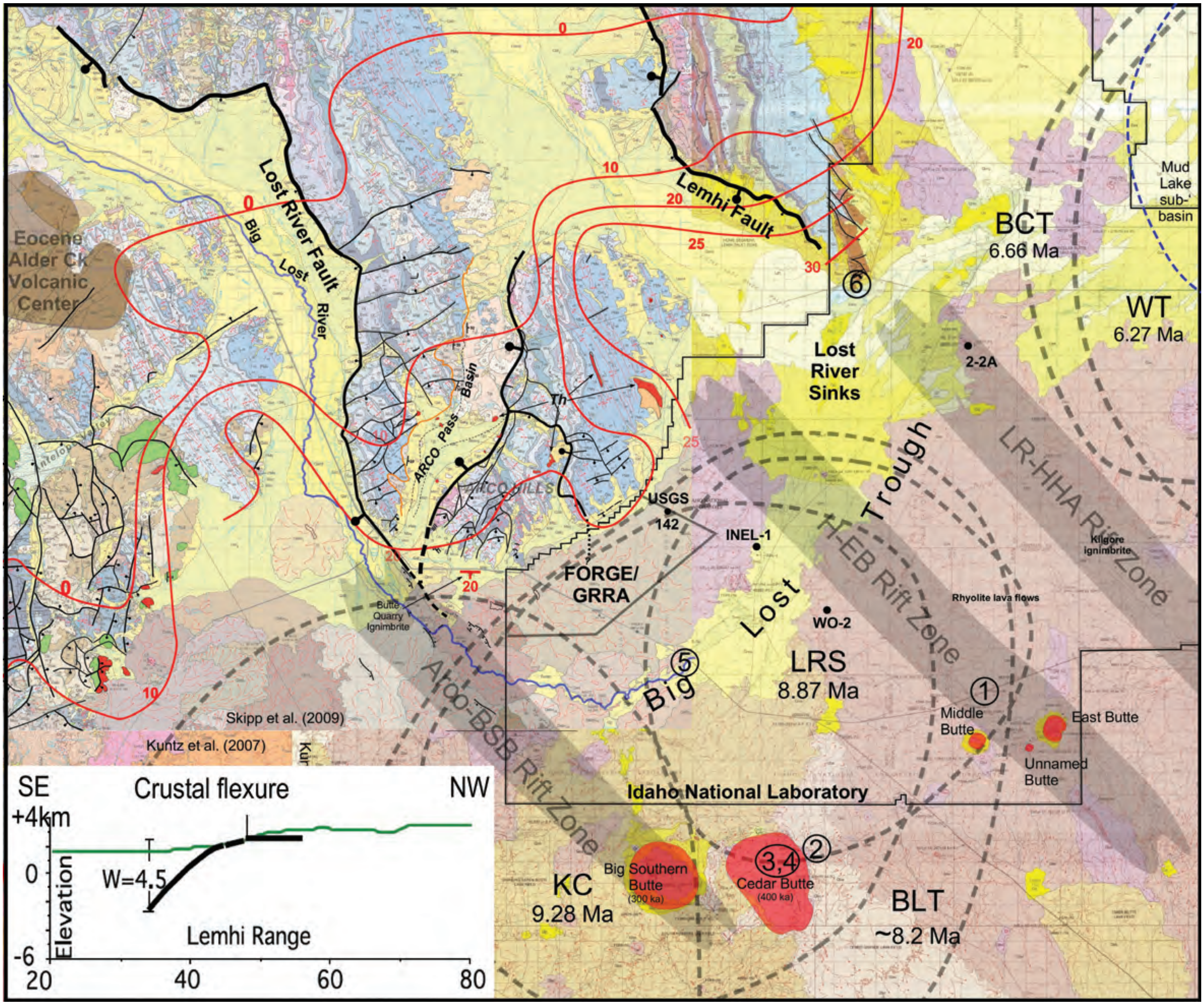

Figure 14. An intermediate scale geologic map of the field trip focus area emphasizing the regional geology and tectonics. Field trip localities are circled 1 through 6. Three base geologic maps are tiled together in the figure (Skipp and others, 2009; Kuntz and others, 2007, 1994). Neogene and Quaternary faults are highlighted in black; Quaternary rhyolite lava domes and cryptodomes in red shade. Picabo age and Heise age ignimbrites are also highlighted (in green and red colors, respectively). The geology base map is overlain by inferred calderas (bold dashed lines); outlines of the Big Lost Trough basin and Mud Lake sub-basin are shown in thin dashed lines; red lines (red dots are measurement locations) that contour the tilt of Laramide fold axes into the plain (after Rodgers and others, 2002; McQuarrie and Rodgers, 1998); shaded regions illustrate volcanic rift zones; locations of deep borehole (USGS142, INEL-1, WO-2, and 2-2A). Inset diagram illustrates inferred crust flexure and subsidence into the ESRP (from Rodgers and others 2002).

to normal fault ring fracture zones bordering calderas that may reside a short distance to the south of the ranges. Very few or no tectonic faults extend into and across the ESRP. Regional extension in the ESRP may be accommodated by dike injection (e.g., Parsons and others, 1998; Rodgers and others, 1990). Interestingly high-resolution GPS and seismicity studies by Payne and others (2012, 2013) indicates that extension rates are higher in regions north of ESRP than within the ESRP, producing a complex zone of shear accommodation between the regions.

The view to the south is across the basalt-dominated lava fields of the ESRP. However, the (usually) dry lake beds immediately south of Howe Point, the Lost River Sinks (fig. 14), are the youngest part of a long-lived region of sediment deposition referred to as the Big Lost Trough (Geslin and others, 2002).

The nearly flat-lying surface of the ESRP, so prominent from this point, veils a Miocene to Pliocene age system of enormous cryptic, likely overlapping and nested calderas (Anders and others, 2014; Morgan and McIntosh, 2005; McCurry and others, 2016, and references therein). These are inferred from ignimbrite and ash fall remnants marginal to the Snake River Plain, from borehole and geophysical studies, and by analogy with the ongoing formation of the Yellowstone volcanic field (fig. 15).

Figure 16 illustrates a cross-section interpretation extending southeast from the southern Big Lost River Range and Arco Hills into the ESRP (after McCurry and others, 2016). At least three nested calderas are tilted toward the southeast. Although uncertainties in the locations and sizes of the calderas are large, figures 15 and 16 (cross-section A–A') may be the most constrained interpretation of local caldera structures and upper crustal structure now possible (McCurry and others, 2016).

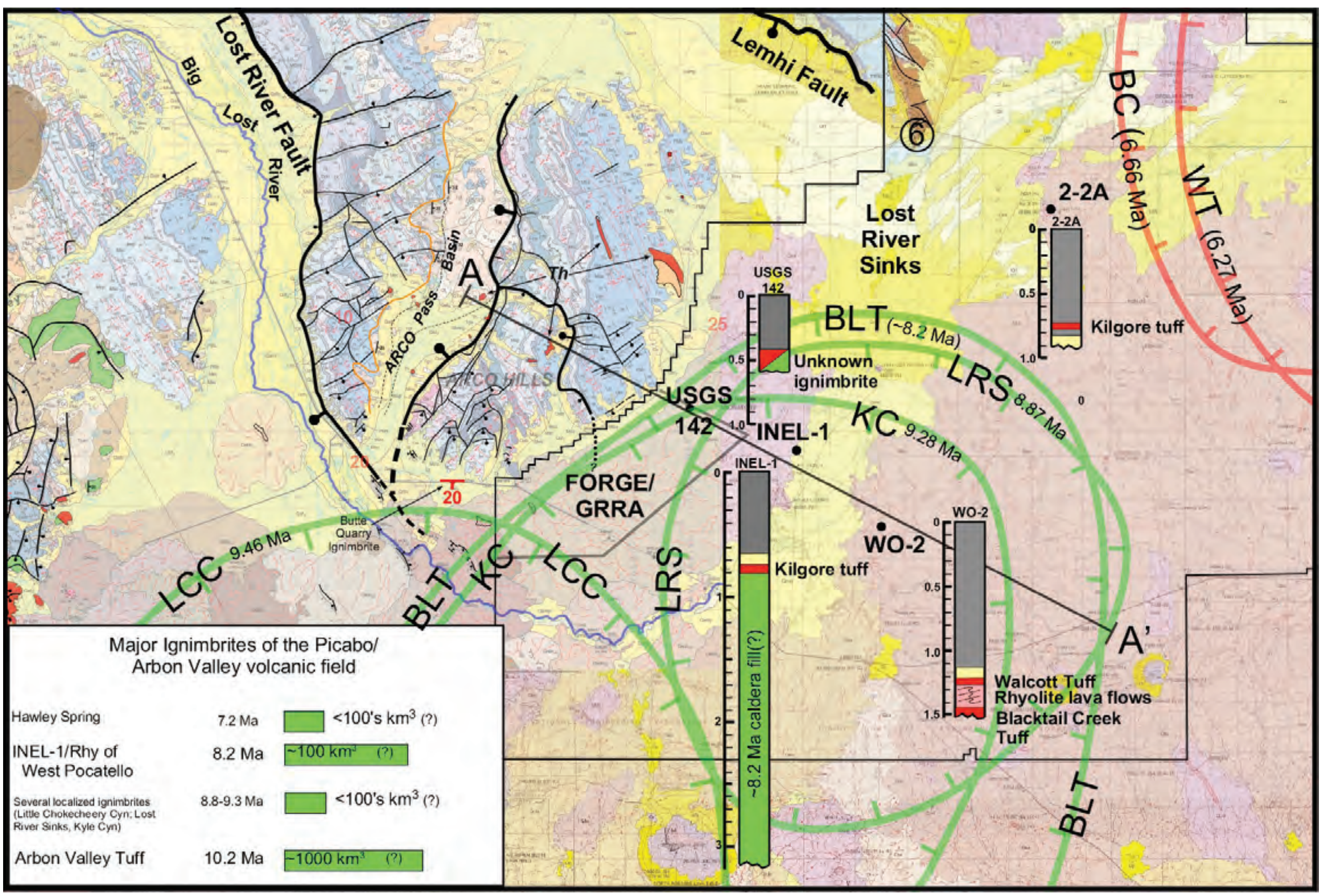

Figure 15. Summary map illustrating volcanic rock stratigraphy observed in boreholes INEL-1, 2-2A, WO-2, and USGS 142. Green: rhyolite correlated with the Picabo volcanic field; red: rhyolite correlated with the Heise volcanic field. Inferred caldera margins are after Anders and others (2014) and McCurry and others (2016).

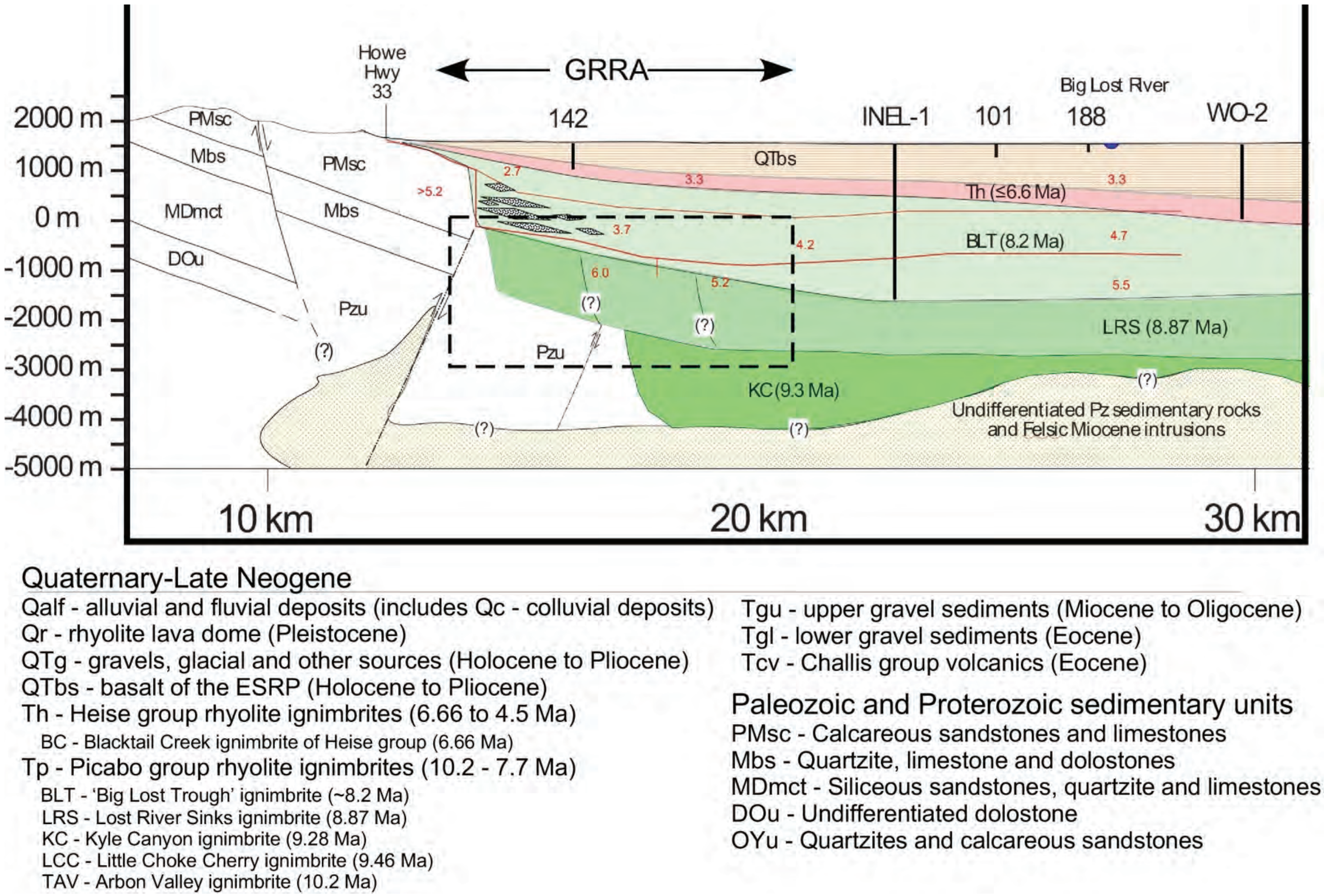

Figure 16. Blow-up view of the part of cross-section A–A' (fig. 3) near the GRRA. Numbers across the top of the figure indicate boreholes located close to the cross-section (mostly with USGS prefix). Faint red lines and numbers are model boundaries and seismic velocities from Pankhurst and Ackermann (1982). The dashed box illustrates the potential GRRA reservoir target zone (assumed to be 1.5–4 km depth). Stippled regions near caldera boundaries represent likely mega- and mesobreccia-rich regions. Question marks indicate uncertainty in location of the deeper nested Picabo-age caldera boundaries. The diagram illustrates that USGS 142 penetrates into Th (Heise volcanics, undifferentiated). New geochemical data suggest that it is either an unknown Heise unit, or a Picabo-age unit.

Return to Heise Hot Springs: Continue east on Hwy 33 to I-15 (50 mi). Turn south onto I-15; proceed south toward Idaho Falls for 15 mi. Take exit 128 and then proceed east on County Line Road (W145N) for 21 mi to Heise Hot Springs.

REFERENCES CITED

Ackerman, D.J., Rattray, G.W., Rousseau, J.P., Davis, L.C., and Orr, B.R., 2006, A conceptual model of ground-water flow in the eastern Snake River Plan aquifer at the Idaho National Laboratory and vicinity with implications for contaminant transport: U.S. Geological Survey Scientific Investigations Report 2006–5122, 62 p.

Ackerman, D.J., 1991, Transmissivity of the Snake River Plain aquifer at the Idaho National Engineering Laboratory, Idaho: U.S. Geological Survey Water-Resources Investigations Report 91–4058 (DOE/ID–22097), 35 p.

Allison, R. R., 2001, Climatic, volcanic, and tectonic influences on late Pleistocene sedimentation along the Snake River and in Market Lake, Bonneville, Jefferson, and Madison counties, Idaho: Idaho State University M.S. thesis, 153 p.

Anders, M.H., Rodgers, D.W., Hemming, S.R., Saltzman, J., Divenere, V.J., Hagstrum, J.T., Embree, G.F., and Walter, R.C., 2014, A fixed sublithospheric source for the late Neogene track of the Yellowstone hotspot: Implications of the Heise and Picabo volcanic fields: Journal of Geophysical Research: Solid Earth, v. 119, p. 2871–2906.

Anders, M.H., Saltzman, J., and Hemming, S.R., 2009, Neogene tephra correlations in eastern Idaho and

Wyoming: Implications for Yellowstone hotspot-related volcanism and tectonic activity: Bulletin of the Geological Society of America, v. 121, p. 837–856.

Barraclough, J.T., Robertson, J.B., and Janzer, V.J., 1976, Hydrology of the solid waste burial ground, as related to the potential migration of radionuclides, Idaho National Engineering Laboratory: U.S. Geological Survey Open-File Report 76-471, 183 p.

Barraclough, J.T., Teasdale, W.E., and Jensen, R.G., 1967, Hydrology of the National Reactor Testing Station, Idaho, 1965: U.S. Geological Survey Open-File Report, 107 p.

Bartholomay, R.C., and Twining, B.V., 2015, Hydrologic influences on water-level changes in the eastern Snake River Plain aquifer at and near the Idaho National Laboratory, Idaho 1949-2014: U.S. Geological Survey Scientific Investigations Report 2015-5085 (DOE/ID-22236), 36 p.

Bartholomay, R.C., Davis, L.C., Fisher, J.C., Tucker, B.J., and Raben, F.A., 2012, Water-quality characteristics and trends for selected sites at and near the Idaho National Laboratory, Idaho, 1949-2009: U.S. Geological Survey Scientific Investigations Report 2012-5169 (DOE/ID 22219), 68 p.

Bartholomay, R.C., Tucker, B.J., Ackerman, D.J., and Liszewski, M.J., 1997, Hydrologic conditions and distribution of selected radiochemical and chemical constituents in water, Snake River Plain aquifer, Idaho National Engineering Laboratory, Idaho, 1992 through 1995: U.S. Geological Survey Water-Resources Investigations Report 97-4086 (DOE/ID-22137), 57 p.

Bestland, E.A., Link, P.K., Lanphere, M.A., and Champion, D.E., 2002, Paleoenvironments of sedimentary interbeds in the Pliocene and Quaternary Big Lost Trough (eastern Snake River Plain, Idaho): Geological Society of America Special Paper, v. 353, p. 27–44.

Bindeman, I.N., and Simakin, A.G., 2014, Rhyolites — Hard to produce, but easy to recycle and sequester: Integrating microgeochemical observations and numerical models: Geosphere, v. 10, p. 930–957.

Bonnichsen, B., Leeman, W.P., Honjo, N., McIntosh, W.C., and Godchaux, M.M., 2008, Miocene silicic volcanism in southwestern Idaho: geochronology, geochemistry, and evolution of the central Snake River Plain: Bulletin of Volcanology, v. 70, p. 315–342.

Bruhn, R.L., Wu, D., and Lee, J.-J., 1992, Final report on structure of the southern Lemhi and Arco Fault Zone, Idaho. Prepared for U.S. Department of Energy Office of New Production Reactors under DOE, Idaho Field Office, Contract No. DE-AC07-761001570.

Busenberg, E., Plummer, L.N., and Bartholomay, R.C., 2001, Estimated age and source of the young fraction of ground water at the Idaho National Engineering and Environmental Laboratory: U.S. Geological Survey Water-Resources Investigations Report 2001–4265 (DOE/ID-22177), 144 p.

Camp, V. E., Pierce, K.L., and Morgan, L.A., 2015, Yellowstone plume trigger for Basin and Range extension, and coeval emplacement of the Nevada–Columbia Basin magmatic belt: Geosphere, v. 11, no. 2, p. 203–225.

Carrigan, C. R. (1994). Two-component magma transport and the origin of composite intrusions and lava flows. International Geophysics Series, v. 57, p. 319-319.

Cecil, L.D., Welhan, J.A., Green, J.R., Frape, S.K., and Sudicky, E.R., 2000, Use of chlorine-36 to determine regional-scale aquifer dispersivity, eastern Snake River Plain aquifer, Idaho/USA: Nuclear Instruments and Methods in Physics Research, section B, v. 172, no. 1–4, p. 679–687.

Champion, D.E., Hodges, M.K.V., Davis, L.C., and Lanphere, M.A., 2011, Paleomagnetic correlation of surface and subsurface basaltic lava flows and flow groups in the southern part of the Idaho National Laboratory, Idaho, with paleomagnetic data tables for drill cores: U.S. Geological Survey Scientific Investigations Report 2011-5049, (DOE/ID 22214) 34 p., 1 pl.

Champion, D.E., Lanphere, M.A., and Kuntz, M.A., 2002, Accumulation and subsidence of late Pleistocene basaltic lava flows of the eastern Snake River Plain, Idaho, in Link, P.K. and Mink, L.L. eds., Geological Society of America Special Paper, Geological Society of America, p. 175–192.

Christiansen, E.H., and McCurry, M., 2008, Contrasting origins of Cenozoic silicic volcanic rocks from the western Cordillera of the United States: Bulletin of Volcanology, v. 70, p. 251–267.

Davis, L.C., Bartholomay, R.C., Fisher, J.C., and Maimer, N.V., 2015, Water-quality characteristics and trends for selected wells possibly influenced by wastewater disposal at the Idaho National Laboratory, Idaho, 1981-2012: U.S. Geological Survey Scientific Investigations Report 2015-5003, 106 p.

Davis, L.C., Bartholomay, R.C., Rattray, G.W., 2013, An update of hydrologic conditions and distribution of selected constituents in water, eastern Snake River Plain aquifer and perched groundwater zones, Idaho National Laboratory, Idaho, emphasis 2009–11: U.S. Geological Survey Scientific Investigations Report 2013-5214, 89 p.

Davis, L.C., Hannula, S.R., and Bowers, B., 1997, Procedures for use of, and drill cores and cuttings available for study at, the Lithologic Core Storage Library, Idaho National Engineering Laboratory, Idaho: U.S. Geological Survey Open-File Report 97 124, 34 p.

DeCelles, P.G., 2004, Late Jurassic to Eocene evolution of the Cordilleran Thrust Belt and Foreland Basin System, Western U.S.A.: American Journal of Science, v. 304, p. 105–168.

Dickinson, W.R., 2004, Evolution of the North American Cordillera: Annual Review of Earth and Planetary Sciences, v. 32, p. 13–45.

Drew, D.L., Bindeman, I.N., Loewen, M.W., and Wallace, P.J., 2016, Initiation of large-volume silicic centers in the Yellowstone hotspot track: insights from H2O- and F-rich quartz-hosted rhyolitic melt inclusions in the Arbon Valley Tuff of the Snake River Plain: Contributions to Mineralogy and Petrology, v. 171, p. 1–20.

Duke, C.L., Roback, R.C., Reimus, P.W., Bowman, R.S., McLing, T.L., Baker, K.E., and Hull, L.C., 2007, Elucidation of flow and transport processes in a variably saturated system of interlayered sediment and fractured rock using tracer tests: Vadose Zone Journal, v. 6, no. 4, p. 855–867.

Ganske, R., and McCurry, M., 2006, Petrogenesis of A-type Quaternary rhyolite and cogenetic mafic magmatic enclaves at East Butte volcanic dome, Eastern Snake River Plain, Idaho, in S.S. Hughes, ed., Proceedings of the 2005 Great Rift Science Symposium: Idaho Museum of Natural History, p. 49-55.

Garabedian, S.P., 1986, Application of a parameter-estimation technique to modeling the regional aquifer underlying the eastern Snake River Plain, Idaho: U.S. Geological Survey Water Supply Paper 2278, 60 p.

Gaschnig, R.M., Vervoort, J.D., Lewis, R.S., and Tikoff, B., 2011, Isotopic Evolution of the Idaho Batholith and Challis Intrusive Province, Northern US Cordillera: Journal of Petrology, v. 52, p. 2397–2429.

Geslin, J.K., Link, P.K., Riesterer, J.W., Kuntz, M.A., and Fanning, C.M., 2002, Pliocene and Quaternary stratigraphic architecture and drainage systems of the Big Lost Trough, northeastern Snake River Plain, Idaho: Geological Society of America Special Paper, v. 353, p. 11–26.

Greely, R. and King, J.S. eds., 1977, Volcanism of the Eastern Snake River Plain, Idaho: A comparative planetary geology guidebook: Office of Planetary Geology, National Aeronautics and Space Administration, 308 p.

Hackett, W.R., and Smith, R.P., 1992, Quaternary volcanism, tectonics, and sedimentation in the Idaho National Engineering Laboratory area, in Wilson, J.R. ed., Field Guide to Geological Excursions in Utah and Adjacent Areas of Nevada, Idaho, and Wyoming, Utah Geological Survey Miscellaneous Publication 92-3, p. 1–18.

Hodges, M.K. V, Link, P.K., and Fanning, C.M., 2009, The Pliocene Lost River found to west: Detrital zircon evidence of drainage disruption along a subsiding hotspot track: Journal of Volcanology and Geothermal Research, v. 188, p. 237–249.

Holmes, A. A. J., Rodgers, D.W., and Hughes, S.S., 2008, Kinematic analysis of fractures in the Great Rift, Idaho: Implications for subsurface dike geometry, crustal extension, and magma dynamics: Journal of Geophysical Research, v. 113, p. 1–15.

Hughes, S.S., Wetmore, P.H., and Casper, J.L., 2002, Evolution of Quaternary tholeiitic tasalt eruptive centers on the Eastern Snake River Plain , Idaho, in Bonnichsen, B., White, C.M. and McCurry, M., eds., Tectonic and Magmatic Evolution of the Snake River Plain Volcanic Province: Idaho Geological Survey Bulletin 30, p. 363-385.

Hughes, S.S., Smith, R.P., Hackett, W.R., and Anderson, S.R., 1999, Mafic volcanism and environmental geology of the eastern Snake River Plain, in Hughes, S.S., and Thackray, G.D., eds., Guidebook to the geology of eastern Idaho: Idaho Museum of Natural History, p. 143-168.

Johnson, T. M., Roback, R. C., McLing, T. L., Bullen, T. D., DePaolo, D. J., Doughty, C., and Murrell, M. T., 2000, Groundwater "fast paths" in the Snake River Plain aquifer: Radiogenic isotope ratios as natural groundwater tracers: Geology, v. 28, no. 10, p. 871-874.

Kellogg, K.S., Harlan, S.S., Mehnert, H.H., Snee, L.W., Pierce, K.L., Hackett, W.R., and Rodgers, D.W., 1994, Major 10.2-Ma Rhyolitic Volcanism in the Eastern Snake River Plain , Idaho: Isotopic age and stratigraphic setting of the Arbon Valley Tuff Member of the Starlight Formation. U. S. Geological Survey Bulletin 2091, 18 p.

Kjelstrom, L.C., 1992, Assessment of spring discharge to the Snake River, Milner Dam to King Hill, Idaho: Water Fact Sheet, U.S. Geological Survey Open-File Report 92-142, 2 p.

Konstantinou, A., Miller, E.L., and Wooden, J.P., 2012, Multistage Cenozoic extension of the Albion-Raft River-Grouse Creek metamorphic core complex: Geochronologic and stratigraphic constraints: Geosphere, v. 8, p. 1429–1466.

Konstantinou, A., Strickland, A., Miller, E., Vervoort, J., Fisher, C.M., Wooden, J., and Valley, J., 2013, Syn-extensional magmatism leading to crustal flow in the Albion – Raft River – Grouse Creek metamorphic core complex , northeastern Basin and Range: Tectonics, v. 32, p. 1–20.

Konstantinou, A., Valley, J.W., Strickland, A., Miller, E.L., Fisher, C., Vervoort, J., and Wooden, J.L., 2013, Geochemistry and geochronology of the Jim Sage volcanic suite, southern Idaho: Implications for Snake River Plain magmatism and its role in the history of Basin and Range extension: Geosphere, v. 9, p. 1681–1703.

Kuntz, M.A., Skipp, B., Champion, D.E., Gans, P.B., Van Sistine, D.P. and Snyders, S.R., 2007. Geologic map of the Craters of the Moon 30'x 60'quadrangle. Idaho: US Geological Survey Scientific Investigations Map 2969, 64 p., 1 plate, scale 1:100,000.

Kuntz, M.A., Geslin, J.K., Mark, L.E., Hodges, M.K.V., Kauffman, M.E., Champion, D.E., Lanphere, M.R., Rodgers, D.W., Anders, M.H., Link, P.K., Boyack, D.L., 2003. Geologic map of the northern and central parts of the Idaho National Engineering and Environmental Laboratory, eastern Idaho. Idaho Geological Survey Geologic Map 35, 14 p., scale 1:50,000.

Kuntz, M.A., Anderson, S.R., Champion, D.E., Lanphere, M.A., and Grunwald, D.J., 2002, Tension cracks, eruptive fissures, dikes, and faults related to late Pleistocene-Holocene basaltic volcanism and implications for the distribution of hydraulic conductivity in the eastern Snake River Plain, Idaho: Geological Society of America Special Paper, v. 353, p. 111–133.

Kuntz, M.A., Skipp, B.A., Lanphere, M.A., Scott, W.E., Pierce, K.L., Dalrymple, G. B. Champion, D.E., Embree, G.F., Page, W.R., Morgan, L.A., Smith, R.P., Hackett, W.R., and Rodgers, D.W., 1994, Geologic map of the Idaho National Engineering Laboratory and adjoining areas, eastern Idaho: U. S. Geological Survey Miscellaneous Investigations Series I-2330, scale 1:100,000.

Kuntz, M.A., Champion, D.E., Spiker, E.C., and Lefebvre, R.H., 1986, Contrasting magma types and steady-state, volume-predictable, basaltic volcanism along the Great Rift, Idaho: Geological Society of America Bulletin, v. 97, no. 5, p. 579–594.

Kuntz, M.A., Covington, H.R., and Schorr, L.J., 1992, An overview of basaltic volcanism of the eastern Snake River Plain, Idaho, in Link, P.K., Kuntz, M.A., and Platt, L.B. eds., Geological Society of America Memoir 179, p. 227–267.

Leeman, W.P., 1982a, Evolved and Hybrid Lavas from the Snake River Plain, Idaho, in Bonnichsen, B. and Breckenridge, R.M. eds., Cenozoic Geology of Idaho, Idaho Bureau of Mines and Geology Bulletin 26, p. 193–202.

Leeman, W.P., 1982b, Geology of the Magic Reservoir area, Snake River Plain, Idaho, in Bonnichsen, B. and Breckenridge, R.M. eds., Cenozoic geology of Idaho: Idaho Bureau of Mines and Geology Bulletin 26, p. 369-376.

Leeman, W.P., Schutt, D.L., and Hughes, S.S., 2009, Thermal structure beneath the Snake River Plain: Implications for the Yellowstone hotspot: Journal of Volcanology and Geothermal Research, v. 188, p. 57–67.

Lewis, R. S., P. K. Link, L. R. Stanford, and S.L. Long, 2012, Geologic map of Idaho: Idaho Geological Survey Geologic Map 9, 18 p., scale 1:750,000.

Link, P.K., and Janecke, S.U., 1999, Geology of East-Central Idaho: Geologic Roadlogs for the Big and Little Lost River, Lemhi, and Salmon River Valleys, in Hughes, S.S. and Thackray, G.D. eds., Guidebook to the Geology of Eastern Idaho, Idaho Museum of Natural History, p. 295–334.

Mann, L.J., 1986, Hydraulic properties of rock units and chemical quality of water for INEL-1: A 10,365-foot deep test hole drilled at the Idaho National Engineering Laboratory, Idaho: U.S. Geological Survey Water-Resources Investigations Report 86–4020, 23 p.

Mann, L.J., and Beasley, T.M., 1994, Iodine-129 in the Snake River Plain aquifer at and near the Idaho National Engineering Laboratory, Idaho, 1990–1991: U.S. Geological Survey Water-Resources Investigations Report 94–4053, 27 p.

Mann, L.J., and Knobel, L.L., 1990, Radionuclides, metals, and organic compounds in water, eastern part of A & B Irrigation District, Minidoka County, Idaho: U.S. Geological Survey Open-File Report 90-191, 36 p.

McCurry, M., 2009, The Arbon Valley Tuff: A new look at a highly anomalous ignimbrite from the Yellowstone–Snake River Plain track: Geological Society of America Abstracts with Programs, v. 41, p. 43.

McCurry, M., Hackett, W.R., and Hayden, K., 1999, Cedar Butte and cogenetic Quaternary rhyolite domes of the eastern Snake River Plain, in Scott S. Hughes and Thackray, G.D. eds., Guidebook to the Geology of Eastern Idaho, Idaho Museum of Natural History, p. 169–179.

McCurry, M., Hayden, K.P., Morse, L.H., and Mertzman, S., 2008, Genesis of post-hotspot, A-type rhyolite of the Eastern Snake River Plain volcanic field by extreme fractional crystallization of olivine tholeiite: Bulletin of Volcanology, v. 70, p. 361–383.

McCurry, M., Mcling, T., Smith, R.P., Hackett, W.R., Goldsby, R., Lochridge, W., Wood, T., Pearson, D., Welhan, J., and Plummer, M., 2016, Geologic Setting of the Idaho National Laboratory Geothermal Resource Research Area: Proceedings, 41st Workshop on Geothermal Reservoir Engineering, Stanford University, v. SGP-TR-209, p. 1–20.

McCurry, M., and Rodgers, D.W., 2009, Mass transfer along the Yellowstone hotspot track I: Petrologic constraints on the volume of mantle-derived magma: Journal of Volcanology and Geothermal Research, v. 188, p. 86–98.

McCurry, M., and Welhan, J., 2012, Do Magmatic-Related Geothermal Energy Resources Exist in Southeast Idaho? GRC Transactions, v. 36, p. 699–707.

McQuarrie, N., and Rodgers, D.W., 1998, Subsidence of a volcanic basin by flexure and lower crustal flow: The eastern Snake River Plain, Idaho: Tectonics, v. 17, no. 2, p. 203-220.

Morgan, L.A., Doherty, D.J., and Leeman, W.P., 1984, Ignimbrites of the Eastern Snake River Plain: Evidence for major caldera-forming eruptions: Journal of Geophysical Research, v. 89, p. 8665-8678.

Morgan, L. A., and McIntosh, W.C., 2005, Timing and development of the Heise volcanic field, Snake River Plain, Idaho, western USA: Geological Society of America Bulletin, v. 117, p. 288-306.

Morgan, L.A., Pierce, K.L., and Shanks, W.C.P., 2008, Track of the Yellowstone hotspot: Young and ongoing geologic processes from the Snake River Plain to the Yellowstone Plateau and Tetons, in Roaming the Rocky Mountains and Environs: Geological Field Trips: Geological Society of America Field Guide, p. 1–35.

Nace, R.L., Voegeli, P.T., Jones, J.R., and Deutsch, M., 1975, Generalized geologic framework of the National Testing Reactor Station, Idaho: U.S. Geological Survey Professional Paper 725-B, 49 p.

Nimmo, J.R., Perkins, K.S., Rose, P.A., Rousseau, J.P., Orr, B.R., Twining, B.V., and Anderson, S.R., 2002, Kilometer-scale rapid transport of naphthalene sulfonate tracer in the unsaturated zone at the Idaho National Engineering and Environmental Laboratory: Vadose Zone Journal, v. 1, no. 1, p. 89–101.

Parsons, T., Thompson, G. A., and Smith, R.P., 1998, More than one way to stretch: a tectonic model for extension along the plume track of the Yellowstone hotspot and adjacent Basin and Range Province: Tectonics, v. 17, p. 221-234.

Payne, S.J., McCaffrey, R., King, R.W., and Kattenhorn, S.A., 2012, A new interpretation of deformation rates in the Snake River Plain and adjacent basin and range regions based on GPS measurements: Geophysical Journal International, v. 189, p. 101–122.

Payne, S., McCaffrey, R., and Kattenhorn, S.A., 2013, Extension-driven right-lateral shear in the Centennial shear zone adjacent to the eastern Snake River Plain, Idaho: Lithosphere, v. 5, p. 407–419.

Perkins, M.E., and Nash, B.P., 2002, Explosive silicic volcanism of the Yellowstone hotspot: The ash fall tuff record: Geological Society of America Bulletin, v. 114, p. 367–381.

Pierce, K.L., and Morgan, L. A., 2009, Is the track of the Yellowstone hotspot driven by a deep mantle plume? Review of volcanism, faulting, and uplift in light of new data: Journal of Volcanology and Geothermal Research, v. 188, p. 1–25.

Plummer, L.N., Rupert, M.G., Busenberg, Eurybiades, and Schlosser, P., 2000, Age of irrigation water in ground water from the eastern Snake River Plain aquifer, south-central Idaho: Ground Water, v. 38, no. 2, p. 264–283.

Podgorney, R.K., Snyder, N., Mink, L.R., and Mcling, T., 2016, A Snake River Plain Field Laboratory for Enhanced Geothermal Systems : An Overview of the Snake River Geothermal Consortium's proposed FORGE Site: Proceedings, 41st Workshop on Geothermal Reservoir Engineering Stanford University, Stanford, California, v. SGP-TR-209, p. 1–13.

Podgorney, R., McCurry, M., Wood, T., Mcling, T., Ghassemi, A., Welhan, J., Mines, G., Plummer, M., Moore, J., Fairley, J., and Wood, R., 2013, Enhanced Geothermal System Potential for Sites on the Eastern Snake River Plain, Idaho: GRC Transactions, v. 37, p. 191–197.

Potter, K.E., 2014, The Kimama Core: A 6.4 Ma record of volcanism, sedimentation, and magma petrogenesis on the axial volcanic high, Snake River Plain , ID: M.S. thesis, Utah State University, 174 p.

Putirka, K.D., Kuntz, M. A., Unruh, D.M., and Vaid, N., 2009, Magma Evolution and Ascent at the Craters of the Moon and Neighboring Volcanic Fields, Southern Idaho, USA: Implications for the Evolution of Polygenetic and Monogenetic Volcanic Fields: Journal of Petrology, v. 50, p. 1639–1665.

Robertson, J.B., Schoen, Robert, and Barraclough, J.T., 1974, The influence of liquid waste disposal on the geochemistry of water at the National Reactor Testing Station, Idaho, 1952–1970: U.S. Geological Survey Open-File Report 73–238, 231 p.

Rodgers, D.W., and McCurry, M., 2009, Mass transfer along the Yellowstone hotspot track II: Kinematic constraints on the volume of mantle-derived magma: Journal of Volcanology and Geothermal Research, v. 188, no. 1-3, p. 99–107.

Rodgers, D.W., Ore, H.T., and Bobo, R.T., 2002, Extension and subsidence of the eastern Snake River Plain, Idaho, in Bonnichsen, B., White, C.M. and McCurry, M., eds., Tectonic and Magmatic Evolution of the Snake River Plain Volcanic Province: Idaho Geological Survey Bulletin 30, p. 121–155.

Rodgers, D.W., Hackett, W.R., and Ore, H.T., 1990, Extension of the Yellowstone plateau, eastern Snake River Plain, and Owyhee plateau: Geology, v. 18, no. 11, p. 1138–1141.

Self, S., Keszthelyi, L., and Thordarson, T., 1998, The importance of pahoehoe: Annual Review of Earth and Planetary Sciences, v. 26, p. 81-110.

Shervais, J.W., Schmitt, D.R., Nielson, D., Evans, J.P., Christiansen, E.H., Morgan, L., Pat Shanks, W.C., Prokopenko, A. A., Lachmar, T., Liberty, L.M., Blackwell, D.D., Glen, J.M., Champion, D., Potter, K.E., and others., 2013, First results from HOTSPOT: The Snake River Plain scientific drilling project, Idaho, U.S.A.: Scientific Drilling, p. 36–45.

Shervais, J.W., Vetter, S.K., and Hanan, B.B., 2006, Layered mafic sill complex beneath the eastern Snake River Plain: Evidence from cyclic geochemical variations in basalt: Geology, v. 34, p. 365–368.

Skipp, B., Snider, L.G., Janecke, S.U., and Kuntz, M.A., 2009, Geologic map of the Arco 30 x 60 minute quadrangle, Idaho: Idaho Geological Survey Geologic Map 47, 42 p., scale 1:100,000.

Smith, R.B., Jordan, M., Steinberger, B., Puskas, C.M., Farrell, J., Waite, G.P., Husen, S., Chang, W.-L., and O'Connell, R., 2009, Geodynamics of the Yellowstone hotspot and mantle plume: Seismic and GPS imaging, kinematics, and mantle flow: Journal of Volcanology and Geothermal Research, v. 188, p. 26–56.

Strickland, A., Miller, E.L., Wooden, J.L., Kozdon, R., and Valley, J.W., 2011, Syn-extensional plutonism and peak metamorphism in the Albion-Raft River-Grouse Creek metamorphic core complex: American Journal of Science, v. 311, no. 4, p. 261–314.

Strickland, A., Miller, E.L., and Wooden, J.L., 2011, The Timing of Tertiary Metamorphism and Deformation in the Albion–Raft River–Grouse Creek Metamorphic Core Complex, Utah and Idaho: Journal of Geology, v. 119, no. 2, p. 185–206.

Szymanowski, D., Ellis, B.S., Bachmann, O., Guillong, M., and Phillips, W.M., 2015, Bridging basalts and rhyolites in the Yellowstone–Snake River Plain volcanic province: The elusive intermediate step: Earth and Planetary Science Letters, v. 415, p. 80–89.

U.S. Geological Survey, 1985, National water summary, 1984—Hydrologic events, selected water-quality trends, and ground-water resources: U.S. Geological Survey Water-Supply Paper 2275, 467 p.

Vogel, J.J., Min, K., Carmenate, A., Foster, D.A., and Marsellos, A., 2014, Miocene regional hotspot-related uplift, exhumation, and extension north of the Snake River Plain: Evidence from apatite (U-Th)/He thermochronology: Lithosphere, v. 6, p. 108–123.

Welhan, J.A., and Reed, M.F., 1997, Geostatistical analysis of regional hydraulic conductivity variations in the Snake River Plain aquifer, eastern Idaho: Geological Society of America Bulletin, v. 109, no.7, p.855-868.

Wetmore, P.H., Hughes, S.S., Connor, L., and Caplinger, M., 2009, Spatial distribution of eruptive centers about the Idaho National Laboratory, in Connor, C.B., Chapman, N.A., and Connor, L.J. eds., Volcanic and Tectonic Assessment for Nuclear Facilities, Cambridge, UK, Cambridge University Press, 385-405.

Walker, E.H., 1964, Subsurface geology of the National Reactor Testing Station, Idaho: U.S. Geological Survey Bulletin 1133-E, 22 p.

Whitaker, M.L., Nekvasil, H., Lindsley, D.H., and McCurry, M., 2008, Can crystallization of olivine tholeiite give rise to potassic rhyolites? An experimental investigation: Bulletin of Volcanology, v. 70, p. 417–434.

Yonkee, W.A., Dehler, C.D., Link, P.K., Balgord, E.A., Keeley, J.A, Hayes, D.S., Wells, M.L., Fanning, C.M., and Johnston, S.M., 2014, Tectono-stratigraphic framework of Neoproterozoic to Cambrian strata, west-central U.S.: Protracted rifting, glaciation, and evolution of the North American Cordilleran margin: Earth-Science Reviews, v. 136, p. 59–95.

Rigby Church. This early Presbyterian Church building was dedicated in 1923 and lies at 111 1st N Street in Rigby. It is made of the tuff from the Menan Buttes with Huckleberry Ridge Tuff accents. (Photo courtesy of Glenn Embree.)

GEOLOGIC FIELD GUIDE TO THE HEISE VOLCANIC FIELD, EASTERN SNAKE RIVER PLAIN, IDAHO

William M. Phillips,[1] Daniel K. Moore,[2] and Glenn F. Embree[2]

[1]Idaho Geological Survey, University of Idaho, Moscow, Idaho 83844-3014; [2]Department of Geology, Brigham Young University, Rexburg, Idaho 83460-0510

INTRODUCTION AND GEOLOGIC SETTING

This field guide focuses on stratigraphic and volcanic features of the Heise volcanic field (HVF). The HVF is the second youngest of the rhyolitic eruptive centers along the Snake River Plain–Yellowstone hotspot trend. The HVF rhyolites consist of large-volume, generally densely welded ignimbrites erupted from overlapping, nested calderas (fig. 1). Four caldera cycles are recognized, each erupting a large volume regional ignimbrite. Rhyolite flows and domes are associated with each of the cycles.

The locations of HVF calderas within the Eastern Snake River Plain (ESRP) have been inferred from sparse outcrop and deep well data because of cover by younger basalts. As a result, locations are uncertain, and the calderas are sometimes referred to as "crypto-calderas" (McCurry and others, this volume). The best exposures of HVF units are in the uplands surrounding the ESRP. This field trip examines localities in the southwest margin of the ESRP. Points of interest on the northwest margin are also noted.

The major HFV welded ignimbrite units are assigned to the Heise Group (table 1). They consist of the Blacktail Creek Tuff, Walcott Tuff, Conant Creek Tuff, and Kilgore Tuff. The field trip examines exposures of each ignimbrite together with associated units of more restricted occurrence including unwelded tuffs and lava flows. Emphasis is placed upon noting characteristic features that permit identification of each Heise Group unit in the field.

History of Geologic Studies in the Heise Volcanic Field

Systematic studies of rhyolites in the southwest margin of the ESRP began with Mansfield and Ross (1935). Their work in the Ammon area was important in documenting the then-novel hypothesis of post-depositional welding of tuffs. Over the next half-century, stratigraphic relationships, paleomagnetism, geochemistry, and isotopic ages were established for the rhyolitic section of the southeast margin of the ESRP by Stearns and others (1938), Mansfield (1952), Carr and Trimble (1963), Staaz and Albee (1966), Prostka and Hackman (1974), Albee and others (1975), Armstrong and others (1975), Doherty (1976), unpublished mapping compiled by Barney and others, in press, and by Phillips and others (2016a,b), Christiansen and Love (1978), Prostka and Embree (1978), McBroome (1981), McBroome and others (1981), Embree and others (1982), Morgan and others (1984), Morgan (1988), Allmendinger (1980), Armstrong and others (1980), Hladky and others (1992), Morgan (1992), Kellogg and others (1994), and Anders and others (2009, 2014).

In 2005, the Heise Group was formally defined (Morgan and McIntosh, 2005; table 1). In general, this nomenclature addressed inconsistencies resulting from incorrect or redundant correlations of units on the southeast margin of the Eastern Snake River Plain with units on the northwest margin. Thick cover by Pleistocene basalt lava flows separates the two regions, leading to confusion. High precision ages from $^{40}Ar/^{39}Ar$ dating of single sanidine crystals from regional ignimbrites were crucial in establishing firm correlations for most units. This nomenclature is in general usage at present. Revisions for the Conant Creek Tuff (involving separation of the tuff of Elkhorn Springs from the main Conant Creek Tuff), and Walcott Tuff (involving recognition of two members) have been proposed (Anders and others, 2009, 2014).

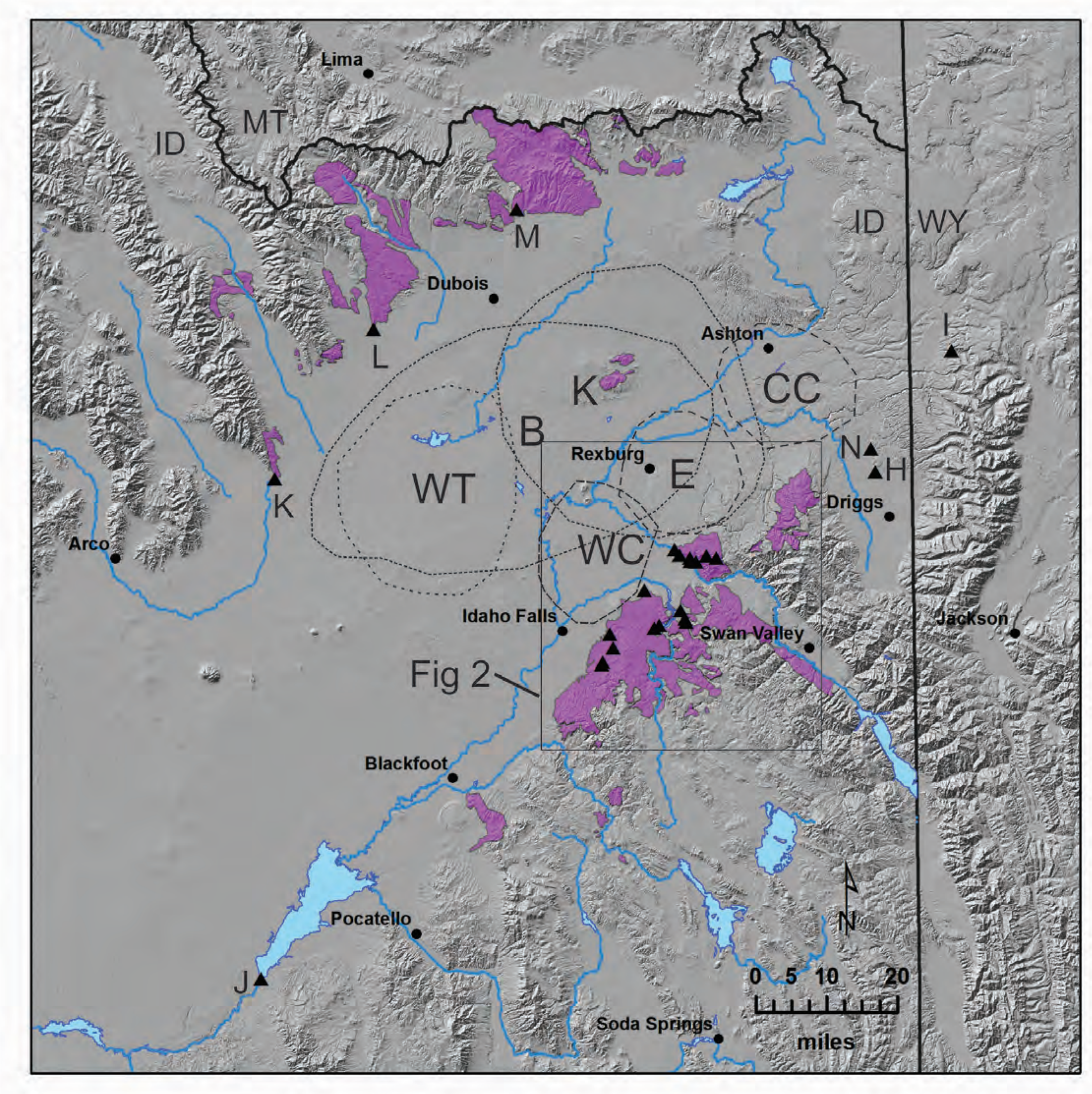

Figure 1. Location of the Heise volcanic field. Heise Group deposits are indicated in purple (modified from Lewis and others, 2012). Approximate locations of "crypto-calderas" for Heise caldera cycles I-IV are shown with dotted lines (modified from Anders and others, 2014); B = Blacktail Creek Tuff (Heise I); WT = Walcott Tuff (Heise II); WC = tuff of Wolverine Creek (Heise III); E= tuff of Elkhorn Springs (Heise III); CC = Conant Creek Tuff (Heise III); K = Kilgore Tuff (Heise IV).

Table 1. Stratigraphy of the Heise Group and associated units (after Morgan and McIntosh, 2005; caldera cycles after Watts and others, 2011). Formal units are large-volume welded ignimbrites with regional extent. Local units (italics) are rhyolite lava flows/domes and unwelded tuffs. Ages are $^{40}Ar/^{39}Ar$ (sanidine) except where marked * K-Ar and $^{\$}$U-Pb (zircon; from Watts and others, 2011).

Caldera Cycle	Unit Name	Map Symbol	Age (Ma)	Volume (km^3)
IV	Kilgore Tuff	Thk	4.45 ± 0.05	1,800
	tuff of Hawley Gulch	*Thh*	—	—
	pre-Kilgore tuff	—	4.87 ± 0.20$^{\&}$	—
	rhyolite of Indian Creek	*Tri*	4.1 ± 0.1*	—
	rhyolite of Juniper Buttes	*Trj*	4.29 ± 0.15$^{\&}$	—
	rhyolite of Long Hollow	*Trl*	3.25 ± 0.4* 4.28 ± 0.18$^{\&}$	—
III	Conant Creek Tuff	Thcc	5.51 ± 0.13	300
	tuff of Elkhorn Springs	*The*	5.48 ± 0.13	—
	tuff of Wolverine Creek	*Thw*	5.59 ± 0.05	—
	rhyolite of Kelly Canyon	*Trk*	5.7 ± 0.04	—
II	Walcott Tuff	Thwt	6.27 ± 0.04	750
	Neeley Formation	Thnf	—	—
	rhyolite of Liddy Hot Springs	*Trlhs*	6.20 ±0.05	—
I	Blacktail Creek Tuff	Thb	6.62 ± 0.03	1,200
	rhyolite of Milo Dry Farm	*Trm*	—	—
Pre-Heise	*rhyolite of Hawley Springs*	Trhs	7.50 ± 0.04	—
	tuff of Newby Ranch	*Ttnb*	8.6 ± 0.5*	—
	Arbon Valley Tuff	*Tav*	10.21 ± 0.03	—

Understanding of the petrogenesis and geochronology of the Heise Group has progressed in recent years with increasingly precise single- and sub-crystal isotopic and elemental analyses. Besides Morgan and McIntosh (2005), these studies include Bindeman and others (2007), Anders and others (2009, 2014), Watts and others (2010, 2011), Westgate and others (2011), Drew and others (2013), Bolte and others (2015), Wotzlaw and others (2014), and Szymanowski and others (2015). Besides providing powerful tools for correlation of units, this body of work has resulted in new models for generation of large-volume silicic magma and "super-eruptions."

Previous field guides covering portions of the HVF area include McBroome and others (1981), Hackett and Morgan (1988), Bonnichson and others (1989), Morgan and Hackett (1989), Morgan (1989), and Morgan and others (2008).

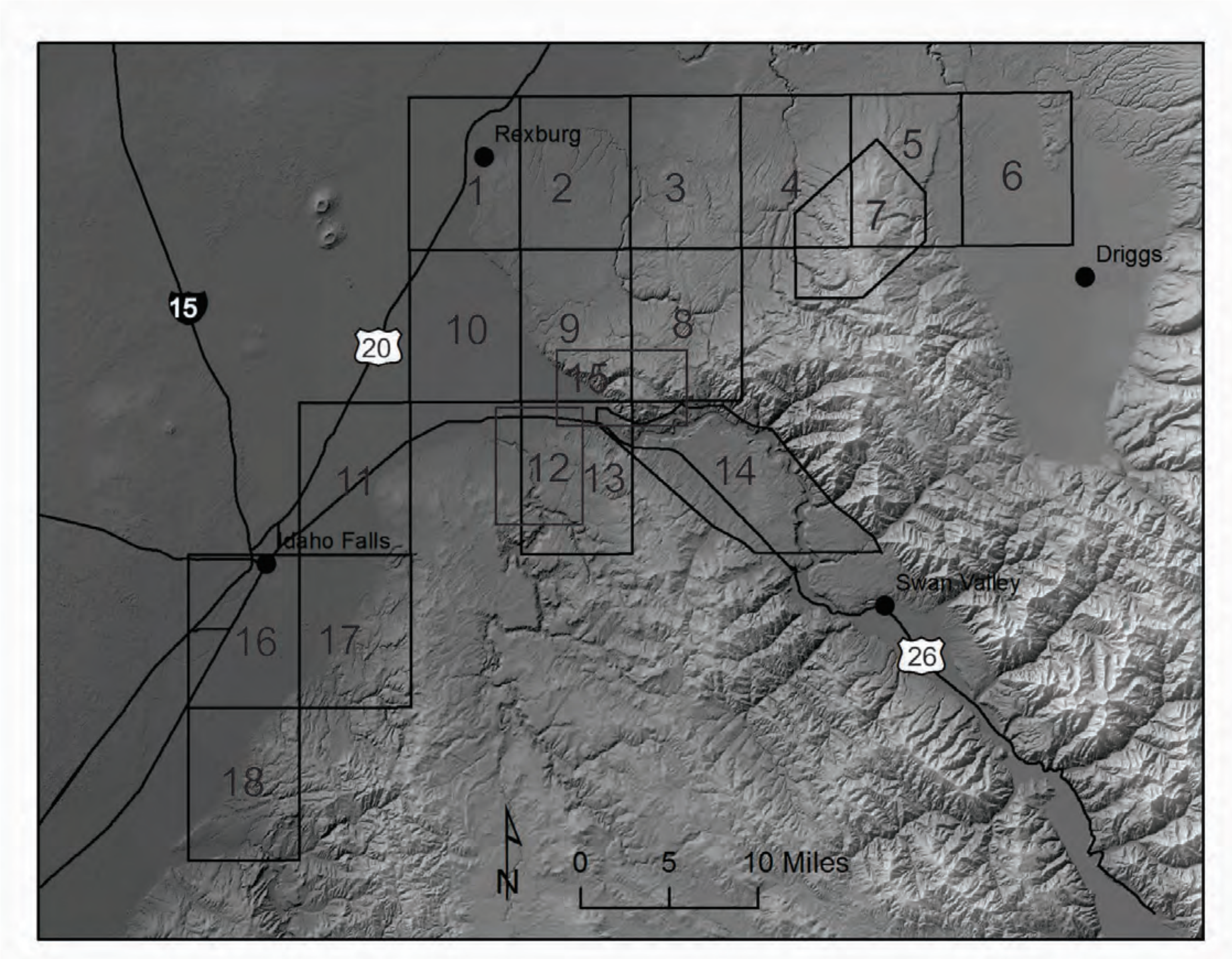

Map ID	Quadrangle or Area	Reference
1	Rexburg	Phillips and others (2016c)
2	Moody	Embree and others (2016)
3	White Owl Butte	Embree and others (2016)
4	Wright Creek (part)	Embree and others (2016)
5	Packsaddle Lake	Phillips and others (2013a)
6	Tetonia	Phillips and others (2013b)
7	Big Hole Mountains	Price and Rodgers (2010)
8	Hawley Gulch	Phillips and others (In Press)
9	Heise	Phillips and others (2016a)
10	Ririe	Phillips and others (2014)
11	Ucon	Phillips and Welhan (2012)
12	Ririe Reservoir	Engleman and others (2012)
13	Poplar	Phillips and others (2016b)
14	South Fork	Dossett and others (2012)
15	Heise Area	Barney and others (In Press)
16	Idaho Falls South	Phillips and Welhan (2011)
17	Goshen	Phillips and Welhan (2013)
18	Ammon	Phillips and Welhan (In Preparation)

Figure 2. Geologic mapping in the HVF area published or in preparation by the Idaho Geological Survey (2010-2016).

Geologic mapping at scales sufficient to accurately depict details of unit distribution, thickness, and stratigraphic relationships has lagged behind the petrological and geochronologic progress. Mapping and compilation by the Idaho Geological Survey with additional support by the U.S. Geological Survey Cooperative Mapping Program (STATEMAP and EDMAP) has begun to remedy this problem (fig. 2).

FIELD TRIP ROAD LOG

The field trip begins at Little Rock Campground at Heise Hot Springs Resort on the South Fork of the Snake River (figs. 1, 3). Field trip stops and additional points of interest are referenced to GPS coordinates (decimal degrees with WGS84 datum), and also to geographic locations and road names (table 2). Symbols used on geologic maps are defined at first usage in text and also referred to a Caldera Cycle (i.e., Heise I-IV; table 1).

Start of Field Trip

(43.63594°, -111.67387°)

Little Rock Campground, Heise Hot Springs Resort.

Reset car odometer. Turn northwest onto E Heise Rd. The Heise cliffs to the north expose units of the Heise volcanic field. Normal displacement along the Heise Fault, a splay of the major Grand Valley fault zone, has uplifted and tilted the units to the north (figs. 3, 4, 5).

1.2 mi Heise Hot Springs. The road passes over a travertine hot springs mound exposed along the Snake River. The hot springs lie over the approximate trace of the Heise Fault. Temperature of the springs is reported (U.S. Geological Survey, 1970) as 47.8°C (118°F). The springs are named after Richard Camor Heise, a German immigrant who came to the area in about 1890.

1.7 mi Intersection of N 5050 E with E Heise Rd at the Heise Bridge over South Fork of the Snake River. Continue west on E Heise Road.

3.0 mi Park at Cress Creek Nature Trail.

Table 2. Field trip stops (numbers) and points of interest (letters). Coordinates are decimal degrees (datum WGS84).

	Latitude N.	Longitude W.	Locality
0	43.63594	-111.67387	Little Rock Campground – Beginning of field trip
1	43.65921	-111.71829	Cress Creek Nature Trail
2	43.64898	-111.70342	Climb to Top of Heise Cliffs
3	43.64654	-111.62872	Kelly Canyon Ski Area
4	43.53443	-111.70142	Top of Call Dugway
5	43.51079	-111.68623	Upper Meadow Creek
6	43.49868	-111.77603	Blacktail Recreation Area View Point
7	43.50428	-111.76290	Blacktail Recreation Area Boat Ramp
8	43.42385	-111.92488	Rock Ledge Canyon - Parking for walk to Walcott Tuff
9	43.42907	-111.92194	Rock Ledge Canyon - Pumice Pit
10	43.40188	-111.91336	ESRP View Point - Summary and Overview of Field Trip
A	43.64292	-111.67480	Heise cliffs - tuff of Newby Ranch
B	43.63439	-111.65708	Kelly Canyon - Contact Jurassic rocks with Heise Group
C	43.59200	-111.60070	Hawley Gulch - dated tuff of Elkhorn Springs
D	43.51810	-111.69003	Deep Creek - intracaldera outcrops of Blacktail Tuff
E	43.57640	-111.80372	Milo Dry Farm - rhyolite of Milo Dry Farm
F	43.48700	-111.90230	Ammon - welded rhyolites of Mansfield & Ross (1935)
G	43.45833	-111.89322	Walcott Tuff cliff exposure and measured section
H	43.81625	-111.14801	Tetonia - Wolverine Creek tuff in pumice pit
I	44.06265	-120.92681	Conant Creek Tuff type section (Christiansen and Love, 1978)
J	42.77660	-112.87650	American Falls Dam - Walcott Tuff type section (Carr and Trimble, 1963)
K	43.80393	-112.84971	Howe Point and Big Lost River Sinks - Walcott Tuff and other units
L	44.11229	-112.57301	Lidy Hot Springs - rhyolite of Liddy Hot Springs - Kilgore Tuff reference section
M	44.35926	-112.16421	Spencer - Kilgore Tuff reference section
N	43.86340	-111.16011	Badger Creek - Conant Creek Tuff

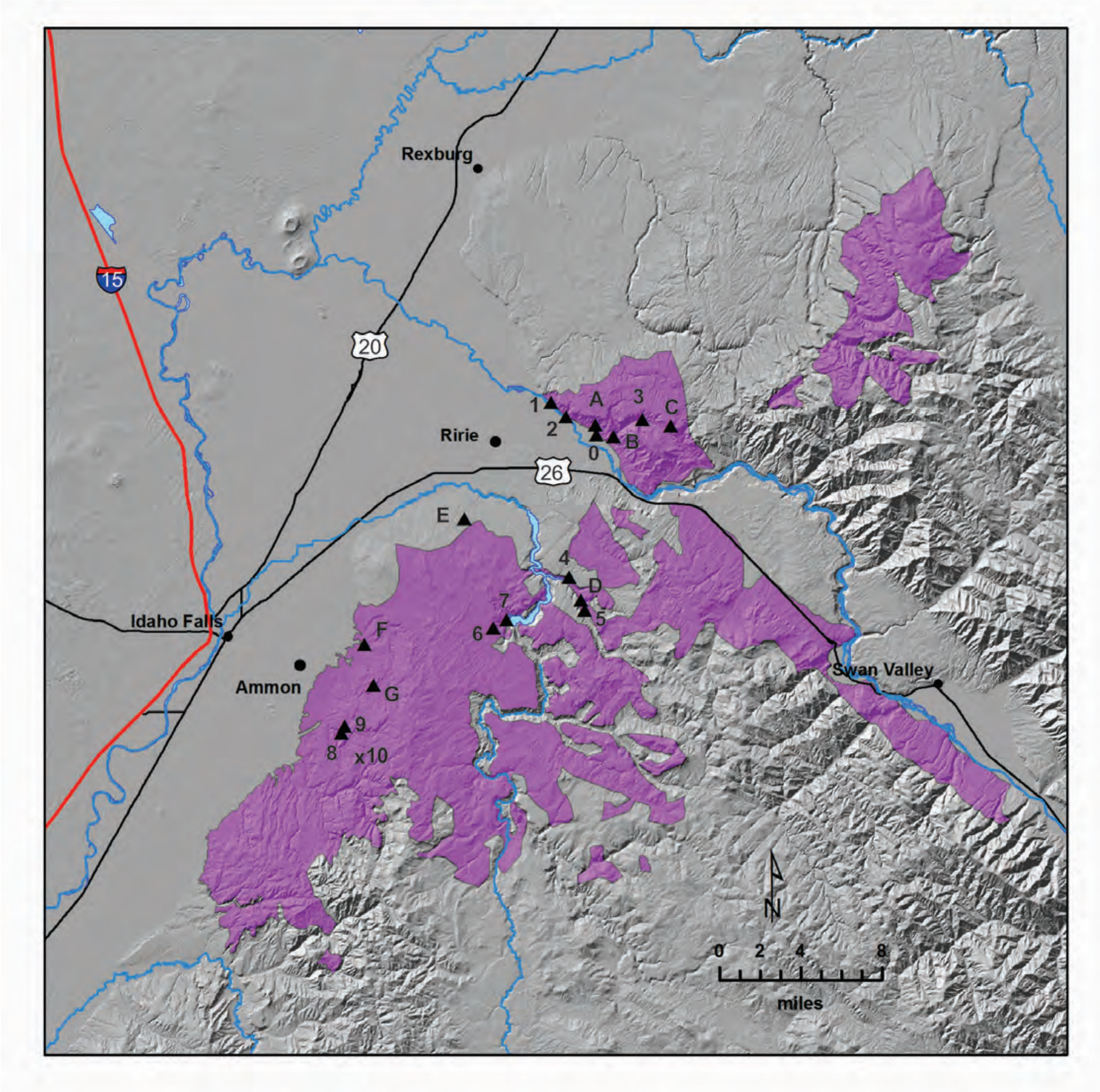

Figure 3. Location map of the field trip area showing stops (numbers) and points of interest (letters). See figure 1 for additional points of interest.

STOP 1

(43.65921°, -111.71829°)

Cress Nature Trail. Examine units below and in the lower to middle part of the Heise Group. These units are cut by a normal fault locally associated with minor hydrothermal alteration.

STOP 1A

Walk to outcrops of the rhyolite of Hawley Spring (Trhs; pre-Heise) on south side of parking lot at the level of road.

Rhyolite of Hawley Spring is a pre-HVF rhyolite lying unconformably at the base of the HVF stratigraphic column (Prostka and Embree, 1978). It underlies tuffaceous deposits of the tuff of Newby Ranch (see Point of Interest A). Trhs is yellow-brown to reddish, locally altered, with abundant (>20 percent) phenocrysts of plagioclase, quartz, and sanidine (1-3

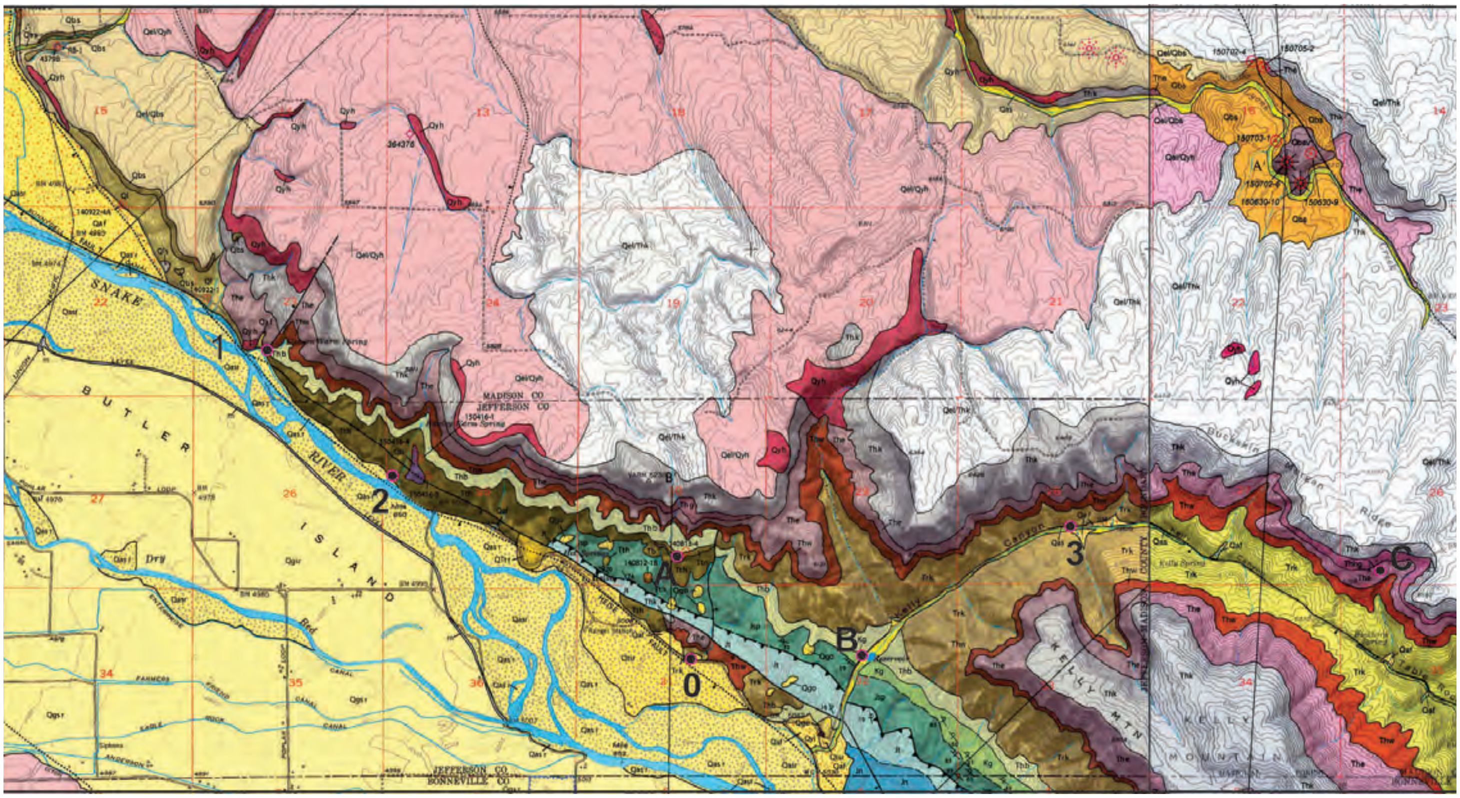

Figure 4. Detail from geologic map of the Heise quadrangle showing field stops 0–3 and points of interest A–C (after Phillips and others, 2016a; Phillips and others, in press). See text for definition of unit symbols.

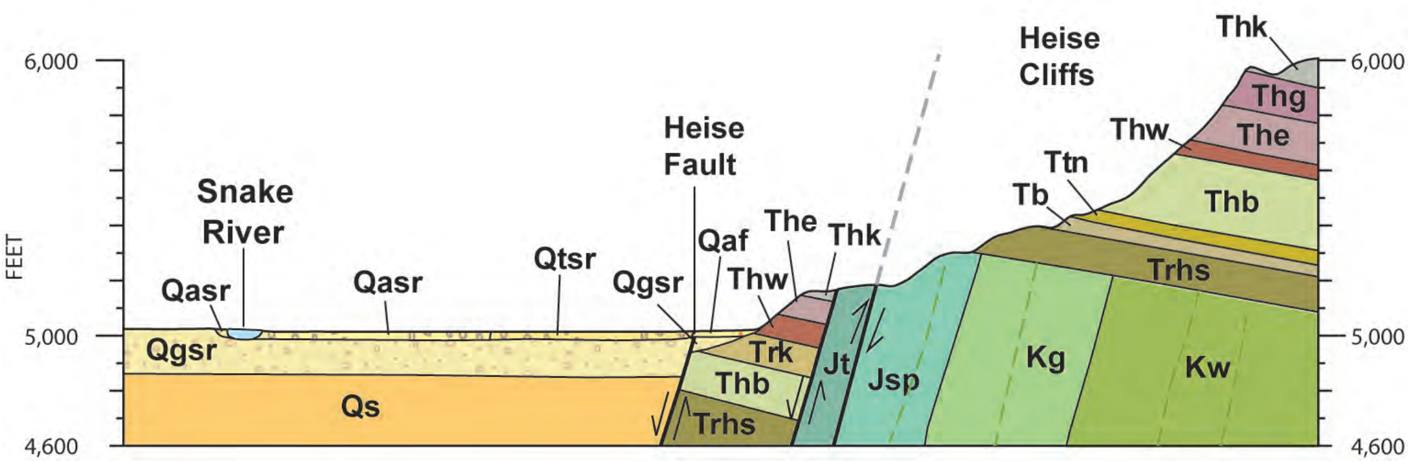

Figure 5. Cross section of the Heise cliffs in the area of Little Rock Campground (from Phillips and others, 2016).

mm). Sparse black biotite (0.5 to 1 mm) is characteristic and separates this unit from all HVF units. Locally, quartz is milky gray and bipyramidal. Most outcrops form cliffs and expose devitrified rhyolite with well-developed eutaxitic foliation. Mean single-crystal laser-fusion $^{40}Ar/^{39}Ar$ age from locality along E Heise Rd (43.6469°, -111.6975°), is 7.50 ± 0.04 Ma (Morgan and McIntosh, 2005). This age falls outside the generally accepted range of the HVF. Some workers consider the unit a rhyolite lava flow, noting undulating upper surface, limited extent, vertical and folded columnar joints, flow margins, and crumble breccia (Prostka and Embree, 1978; Bonnichsen and others, 1989, p. 156; Morgan and McIntosh, 2005). However, the unit displays some features (e.g., eutaxitic foliation) compatible with a rheomorphic welded ignimbrite. Drew and others (2013; sample PC-76, p. 66–67) consider the unit to be an ignimbrite and correlate it with Arbon Valley Tuff of the Picabo volcanic field (Kellogg and others, 1994; Hladky and others, 1992) on the basis of mineralogy (presence of biotite), geochemistry, and stratigraphic position. However, $^{40}Ar/^{39}Ar$ sanidine ages and U-Pb zircon ages for the Arbon Valley Tuff range from about 10.2 to 10.4 Ma (Morgan and McIntosh, 2005; Anders and others, 2014; Drew and others, 2013).

STOP 1B

Tuff of Elkhorn Springs (The; Heise III). Walk to exposures behind the toilet and fence at level of parking lot (fig. 6).

Tuff of Elkhorn Springs is stratigraphically near the middle of the Heise Group section. It has been dropped to this level by the down-to-north normal fault, which here is nearly vertical. Tuff of Elkhorn Springs is a densely welded rhyolitic ignimbrite, crystal-poor with <1 percent small (<2 mm) plagioclase, quartz, sanidine, and augite. The eutaxitic, devitrified lithology outcropping here is characteristic of much of the unit. Note the grayish-brown, grayish-pink, and pale purple colors, and the tendency to form abundant platy talus. The unit grades from a basal, nearly aphyric, black vitrophyre up to 2 m (6.5 ft) thick to the eutaxitic devitrified zone, then to a lithophysal zone. Forms prominent cliffs. Maximum thickness in map area is about 100 m (330 ft). First named tuff of Elkhorn Spring by Prostka and Embree (1978). Correlated with the Conant Creek Tuff of the western Teton Range (Christiansen and Love, 1978) by Morgan and McIntosh (2005). This correlation was questioned by Anders and others (2014), who suggested that the tuff of Elkhorn Springs is slightly younger than Conant Creek Tuff (ages 5.57–5.65 Ma). Sanidine laser-fusion single-crystal $^{40}Ar/^{39}Ar$ ages for tuff of Elkhorn Springs are 5.52 ± 0.03 Ma (1σ error, Anders and others, 2014) and 5.48 ± 0.13 Ma (2σ error; Morgan and McIntosh, 2005). Feldspar crystals and glass from tuff of Elkhorn Spring, Conant Creek Tuff, and Wolverine Creek Tuff are nearly identical in their major and trace element concentrations (Szymanowski and others, 2015), suggesting that they are closely spaced events from the same caldera (Anders and others, 2014).

Figure 6. Annotated photograph of trailhead for Cress Nature Trail. Symbols are defined in text.

STOP 1C

(43.65943, -111.71696)

Wolverine Creek tuff (Thw; Heise III). Ascend the nature trail to point where a small spring crosses the main trail. Take moderately difficult, unmaintained trail and cross to top of bench cut into bedrock. Falling Hazard. Be careful not to dislodge rocks on people or cars below.

The bedrock bench is composed of altered, crystal-rich, lithophysal rhyolite with small black pyroxene but little or no biotite. Based on this, it is provisionally assigned to Blacktail Creek Tuff (cf. Stop 1D). Overlying it is Wolverine Creek tuff.

Thw is an unwelded, crystal-poor, pumaceous rhyolitic tuff (Prostka and Embree, 1978; Morgan and McIntosh, 2005; Szymanowski and others, 2015). It is dominated by angular to sub-rounded, black obsidian fragments 2 to 10 mm, and black and white bubble wall shards. Pale yellowish-brown pumice 0.5 to 3 cm with elongated bubble walls, and very sparse (<1 percent) crystals of plagioclase, augite, and sanidine are also present. General color is light gray becoming medium dark gray toward top because of increase in crushed obsidian glass. Stratification ranges from massive and planar to cross-bedded, consistent with airfall and pyroclastic surge deposits (Doherty, 1976). Elutriation pipes produced by escaping gas are present in many exposures. Generally poorly exposed but outcrops can be spotted by light-colored soil colors. Thickness about 18 to 60 m (60 to 300 ft) in the Heise cliffs area. Laser-fusion single-crystal $^{40}Ar/^{39}Ar$ ages from sanidine yielded an age of 5.59 ± 0.05 Ma (Morgan and McIntosh, 2005).

Return to main nature trail and continue uphill.

STOP 1D

(43.658205°, -111.716890º)

Basal vitrophyre and lithophyssal zone of Blacktail Creek Tuff (Thb; Heise I).

Blacktail Creek Tuff is the oldest regional ignimbrite of the HVF. It is readily identified by the most abundant phenocrysts (10–20%) of any Heise ignimbrite. Phenocrysts are plagioclase, quartz, sanidine, augite, opaque oxides (magnetite and ilmenite), and pigeonite (Bolte and others, 2015). Rare biotite is sometimes reported but is not typical. Plagioclase and quartz are 1 to 2 mm; sanidine about 1 to 0.5 mm; and pyroxenes <0.5 mm. Most exposures in the Heise cliffs are cliff forming, columnar jointed, medium gray, devitrified, intensely welded, and locally with lithophysal cavities 5 to 10 cm in diameter (Thb at this stop is unusually thin). A black basal vitrophyre with distinctive "spotted" appearance from high crystal content is also typical. The unit as a whole tends to weather into crumbly gray float. Mean age from single-crystal laser-fusion $^{40}Ar/^{39}Ar$ analyses is 6.62 ± 0.03 Ma (Morgan and McIntosh, 2005).

Continue up the nature trail to where reddish soils are present.

STOP 1E

(43.65782°, -111.71643°)

Reddish soils mark a paleosol zone between the base of Thb and top of Trhs. The paleosol represents a time interval between units of about ~0.8 Ma based on $^{40}Ar/^{39}Ar$ ages. Note the white, biotite-bearing, unwelded tuff, interpreted here as a local pyroclastic deposit related to Trhs. Alternatively, it could be associated with tuff of Newby Ranch (Ttn; pre-Heise; Point of Interest A).

Continue up the nature trail.

STOP 1F

(43.65677°, -111.71496°)

Good exposure of Trhs with biotite and bipyromidal quartz. Note ridge-forming welded tuff cropping out to east and uphill; this is Thb. Poorly exposed interval between the two exposures is unwelded, biotite-bearing tuff and paleosol zone.

Proceed on main trail to overlook.

STOP 1G

(43.65520°, -111.71336°)

Snake River Overlook. Views north of the South Fork alluvial fan and Menan Buttes tuff cones. Both features are broadly linked to Pleistocene extension and mafic magmatism along the Grand Valley fault zone. The South Fork fan is the thickest depocenter for glacial outwash in the upper Snake River drainage.

Accommodation space for the outwash was provided by extension at the junction of the Grand Valley fault zone and the ESRP. Basaltic magmatism also occurred here, as evidenced by late Pleistocene Menan Buttes, where magma was injected into the aquifer hosted by the thick outwash deposits. Splays of Grand Valley faults parallel the ~N5° trend of the Menan Buttes rift zone. A similar-trending feature (Sommers Butte volcanic rift zone) is present on Rexburg Bench (Embree and others, Field Trip Guide to the Rexburg Bench, this volume).

Views uphill are of cliffs of tuff of Elkhorn Springs and Kilgore Tuff. Note break in slope between The and Thk (see Stop 2). This is the interval containing unwelded tuff of Hawley Gulch (Thhg). Reddish colors at top of The mark a paleosol zone.

Return to parking lot.

Turn east on E Heise Rd and drive 1.3 mi to Heise Bridge (junction N 5050 E. and E Heise Rd) and park on south side of bridge (43.64585°, -111.70114°). Re-trace route on foot 0.3 mi to head gate of irrigation canal on the South Fork of Snake River (43.64897°, -111.704487°). Trail to the top of Heise cliffs begins here. Optionally, drop off people at Stop 2 before parking cars at Heise Bridge. Small groups (1–2 cars) can also park along the road at the head gate. Do not block head gate road—it is a popular access point for fishermen.

4.3 mi

STOP 2

(43.64894°, -111.70449°)

Hill climb to top of Heise cliffs. Trail to top of Heise cliffs begins on north side of road. The trail is not formally marked or maintained, and has limited shade. Difficulty ranges from easy to moderate but there are several short, steep intervals and some walking on talus. Elevation gain is 753 ft.

STOP 2A

(43.65365°, - 111.70404°)

The trail climbs along ridges covered with colluvium underlain by rhyolite of Hawley Spring (Trhs) to the poorly exposed contact with Blacktail Creek tuff (Thb) at about 5,320 ft. Thb is much thinner than normal in this portion of the Heise cliffs, possibly because of emplacement over a lava dome or flow of Trhs. Thw is poorly exposed.

Continue uphill through the break in slope that marks approximate contact between Thw and The. Leave trail at this point (43.65393, -111.70303) and scramble south for ~200 ft along contour over talus to base of nearby cliffs.

STOP 2B

(43.65375°, -111.70337°)

Vitrophyre of tuff of Elkhorn Springs (The, Heise III). Prominent cliffs with platy talus and a dark vitrophyric base is characteristic of tuff of Elkhorn Springs. Here, the unit consists of monotonous, white to lavender, crystal-poor, devitrified, welded tuff with well-developed eutaxitic foliation and lithophysal zones with oval centers 2–0.5 cm. Flattened pumice 0.5–<0.1 cm in length is locally abundant. At base of exposure is prominent, reddish-brown to dark gray vitrophyre. Exposure with Thw is not exposed.

Return to trail and continue upward

STOP 2C

(43.65495°, -111.70367°)

Paleosol zone developed between The and tuff of Hawley Gulch (Thhg; Heise IV?) (fig. 7). Dark brown to reddish brown, clay-rich soils mark the paleosol zone. The paleosol is responsible for staining part of the top of The cliffs. It represents a time break between eruptions of ~0.9 Ma based on $^{40}Ar/^{39}Ar$ ages (table 1). The paleosol zone is visible on air photos and Google Earth images along much of the Heise cliffs. Soils, sediments and unwelded tuffs in a similar stratigraphic horizon are traceable approximately 8.7 mi (14 km) south to Meadow Creek (Stops 4 and 5) and 22.5 mi (36 km) to the Ammon area (Stop 6). To the north, paleosol development at a similar stratigraphic horizon is also present at Point of Interest H (Tetonia pumice pit; fig. 1).

Continue up the trail to elevation 5,655 ft where gray-white, crudely bedded unwelded tuffs are exposed.

Figure 7. Annotated photograph of the Heise cliffs in vicinity of Stop 2C-2F.

STOP 2D

(43.65561°, -111.70312°)

Tuff of Hawley Gulch (Thhg; Heise IV?). This poorly exposed (and poorly documented) unit consists here of light gray, unwelded tuff with sand- to granule-sized glass shards, rounded crystal-poor pumice and rhyolite gravels, and local concentrations of quartz and feldspar crystals with dark lithic fragments. Thickly bedded to massive with several thin ash beds. Locally slightly welded or cemented, with concretions. Note the lack of black obsidian and the presence of crystals that distinguish it from the underlying Wolverine Creek tuff. This unit is not well exposed along Heise Cliffs, making it easy to miss how thick it is [minimum thickness is ~100 ft (~30 m)]. The unit thickens toward the Hawley Gulch type area near Kelly Canyon ski area (Stop 3) to >460 ft (>140 m). Probable correlatives are also present in Meadow Creek (Stop 4) and near Ammon (Stop 6).

Walk to NE along the trail to a large landslide block of welded tuff with prominent lithophysae (43.65603, -111.70099). This block is Kilgore Tuff (discussed at stop 2F). Leave trail and hike NW and directly uphill through trees to position on the mid-slope.

STOP 2E

(43.65639°, -111.70206°)

Tuffaceous, clay-rich sediments of Thhg. Yellowish to brownish clay-rich soils indicate a poorly exposed interval of sediments and reworked tuffs with one or more paleosols. These clay-rich deposits promote slope instability. This interval is an aquitard in water wells on the Rexburg Bench. Kilgore Tuff float (brown lithophysal blocks and reddish-orange pieces of vitric tuff) are scattered over the soil.

Continue uphill to the summit on the Rexburg Bench geomorphic surface. Walk along the eastern side of a large landslide head scarp (“amphitheater”) to a point near the NW corner of the headscarp.

STOP 2F

(43.65922°, -111.70151°)

Ledges of Kilgore Tuff (Thk, Heise IV). Cap rock forming the resistant ledge of the amphitheater is a reddish-brown devitrified welded tuff, with spherical lithophasae, about 0.5–1.5 cm in diameter. Some outcrops display cavernous weathering. This very resistant, ledge-forming lithophysal zone is characteristic of the Kilgore Tuff and is much used in landscaping in the Idaho Falls area. Also present are scattered erosional remnants of orange to brown vitric tuff—part of the upper vitrophyre of Thk. The base of Kilgore Tuff typically has a black obsidian vitrophyre and well-developed eutaxitic foliation with flattened purplish (“maroon”) pumice (see Stop 4).

Note the general dip of the Rexburg Bench northward, caused by its position on the footwall of the normal Heise fault (see cross section in fig. 5). The Rexburg Bench is underlain by Kilgore Tuff (Thk), Huckleberry Ridge Tuff (Qyh), basalt flows of the Sommers Butte volcanic rift zone (Qbs), and loess (fig. 4; Embree and others, Field Guide to the Rexburg Bench, this volume)

Return to parked vehicles. **Reset odometers.**

Return to E Heise Rd and continue east until approaching Little Rock Campground (Stop 0).

Point of Interest A

(43.64292°, -111.67480°)

Visible near the base of the Heise cliffs are white thinly bedded ash layers with local plant fossils (tuff of Newby Ranch, Ttn; pre-Heise), and a dark basaltic andesite flow (Tb; pre-Heise; see geochemical analysis in Phillips and others, 2016a). Ttn has been dated by K-Ar at ~8.6 Ma (Morgan and McIntosh, 2005). This age suggests that Ttn is older than Trhs (dated by ^{40}Ar/^{39}Ar at ~7.5 Ma) while in fact it overlies Trhs. The K-Ar age is probably too imprecise to reliably date the unit. These outcrops can be reached on a short hike from Little Rock Campground (crosses private property; please ask for permission at Heise Hot Springs Resort).

Continue to junction with Kelly Canyon Rd at 2.4 mi. Continue NE (left) onto Kelly Canyon Rd.

2.6 mi Exposure of white Lava Creek B tephra above fluvial gravels and alluvial fan deposits (M. Anders, personal commun. to G.F. Embree, 2014). Lava Creek Member B was erupted at ~0.640 ka from the Yellowstone III caldera. Continue on Kelly Canyon Rd.

3.2 mi

Point of Interest B

(43.63439, -111.65708)

Contact of Jurassic rocks with Miocene rhyolite of Kelly Canyon. Slow to observe general features, or pull safely off the road if time and interest permit. The Jurassic rocks (light yellow-gray Twin Creek Limestone, reddish and olive-brown Stump and Preuss Sandstones, and white lithographic limestone of the Gannett Group) are some of the “basement rocks” of the Heise cliffs area (see cross section in fig. 5). They form the truncated edge of the Snake River Range, part of the Idaho–Wyoming fold-and-thrust belt. The HVF units lie unconformably over thrust faulted and locally overturned Jurassic strata. The Jurassic units indicate that HVF units here are extracaldera (outflow) facies. Constraints on the locations of HVF calderas can be inferred from outcrops of basement units.

4.5 mi

STOP 3

(43.64623°, -111.62890°)

Kelly Canyon Ski Area and rhyolite of Kelly Canyon (Trk; Heise III). Rhyolite of Kelly Canyon consists of thick lava flows with a range of textures and colors. Most exposures are cliff forming and massive, composed of brown, devitrified, very crystal-poor rhyolite with closely spaced joints and flow banding, some of which conform to regional bedding and others which are highly eccentric. Abrecciation is common in some outcrops (i.e., at Little Rock Campground, Stop 0). Less common is the gray perlite with black and orange obsidian fragments exposed in road cuts across from the ski area and along Kelly Canyon Rd. Contacts between units are somewhat enigmatic here. Other diagnostic features are purplish, flow-deformed chips and blocks contained in an aphyric groundmass. The K-Ar age for the rhyolite of Kelly Canyon is ~5.7 Ma (Morgan and McIntosh, 2005). This age and the general aphyric character of the unit suggest a relationship with Heise III eruptions (tuff of Elkhorn Springs, Conant Creek tuff, and tuff of Wolverine Creek). If so, then the rhyolite may mark the approximate location of a Heise III caldera margin.

Retrace route to E Heise Rd unless visiting Point of Interest C below. In that case, continue uphill on Kelly Canyon Road to Forest Rd 218. Proceed to Point of Interest C using GPS coordinates.

Point of Interest C

(43.6417°, -111.6007°)

Dated locality of tuff of Elkhorn Springs at roadcut on Forest Rd 218 (Morgan and McIntosh, 2005, Supplement Appendix 4, sample ESRP-95-2013). Reported age is 5.48 ± 0.13 Ma. This is considered to be the age of tuff of Elkhorn Springs, and directly correlative with outcrops visited on Stops 1 and 2. Anders and others (2014) argue that this unit is separate from the Conant Creek Tuff, which has a type section on NW slope of the Teton Range and exposures in the Teton Basin (fig. 1; Points of Interest I and N).

Return to E Heise Rd and continue westbound past Little Rock Campground and Heise Resort to the junction with N 5050 E. **Reset odometers.**

Cross the South Fork of the Snake River at Heise Bridge.

Continue south on N 5050 E for 0.4 mi, then west on E 100 N for 0.8 mi. Turn south onto N 4950 E and proceed for 2.1 mi to junction with US 26.

3.3 mi Turn west on US 26 and proceed for 1.5 mi.

4.8 mi Turn south onto Meadow Creek Rd. Continue past Ririe Dam, Juniper Campground, and Ririe Reservoir. Proceed 6.1 mi to overlook of Meadow Creek.

10.9 mi

STOP 4

(43.53367°, -111.70118°)

Meadow Creek Overlook with exposures of Heise IV-III units (fig. 8). "Call Dugway" (as this steep gravel road is labeled on the USGS Poplar 7.5-minute topographic map) is among the best known of HVF localities (e.g., Bonnichson and others, 1989). The site is a Reference Section for Kilgore Tuff (Morgan and McIntosh, 2005, Data Repository item 2005059). Many samples for dating and geochemical/petrological studies have been taken here (e.g., Watts and others, 2011; Wotzlaw and others, 2014; Szymanowski and others, 2015).

From top to bottom, the sequence is Huckleberry Ridge Tuff (Yellowstone I), Kilgore Tuff (Heise IV), "colluvium" consisting of gravel of Jurassic (?) sandstone, stacked paleosols developed on reworked airfall deposits and floodplain sediments, "pre-Kilgore tuff" (dated at 4.87 Ma; Watts and others, 2011), and the crystal-poor, unwelded pumice-obsidian tuffs of Wolverine Creek tuff (Heise III).

The sequence stratigraphically below Kilgore Tuff resembles the section observed at Stops 2E and 2F (i.e., tuff of Hawley Gulch and associated sediments and paleosols). Note that tuff of Elkhorn Springs, which formed impressive cliffs at Heise cliffs, is missing here. The Wolverine Creek and Elkhorn Springs units are similar in terms of low crystal content, statistically overlapping eruption ages, and geochemical properties (Szymanowski and others, 2015; Anders and others, 2014). Could the time represented by Elkhorn Springs tuff at the Heise cliffs be represented at Meadow Creek by a portion of the unwelded Wolverine Creek section? Perhaps tuff of Elkhorn Springs (The) was too thin to weld here?

If time and interest permit, walk down the road from the overlook to Meadow Creek observing excellent exposures of gas/fluid release features, bed forms, folds, channels, enigmatic "colluvial deposits" in channels, and minor normal faults (Doherty, 1976).

Proceed south into Meadow Creek.

11.1 mi Cross Mud Spring Creek. Concealed normal fault separates the upper HVF section (Heise III-IV) from the lowest ignimbrite (Blacktail Creek Tuff; Heise I).

12.4 mi

Point of Interest D

(43.51810°, -111.69003°)

Junction with Deep Creek; good outcrops of Blacktail Creek Tuff (Thb, Heise I). Note gray color, abundant crystals, and vertical joints. Miminum thickness of Thb here is ~200 ft (~60 m), suggesting that this is an "intracaldera facies." Intercaldera facies are much thicker than outflow (extracaldera) facies due to ponding within the caldera as well as proximity to vents. Here, the thickness of Thb could also be the result of filling of a canyon or other depression by outflow Thb.

Continue south Meadow Creek Rd.

14.3 mi

STOP 5

(43.51049°, -111.68761°)

Contact of Heise Group with Cretaceous Wayan Formation. Ledges of Kilgore Tuff form the NE horizon with white unwelded tuffs outcropping below. The unwelded tuff section contains a paleosol horizon, similar to that observed at Stop 2 and Stop 4. Walk to the north and uphill across a concealed normal fault to exposures of Blacktail Creek Tuff underlain by sticky reddish clay-rich soils. Note that Thk appears to be involved in the faulting (figs. 8, 9). While landslides and colluvium obscure relationships here, the clay-rich soils are indicative of the lower Cretaceous Wayan Formation, well-exposed along Willow Creek to the west (visible when Ririe Reservoir is at low levels). The Wayan Formation (Kw) is weakly consolidated with bentonitic tuffs and shales prone to landslides. The presence of "basement" units such as the Wayan Formation can be used to constrain locations of caldera margins (see Point of Interest B for a similar setting). Here, Heise Group units to the SE including both Thk and Thb are shown to be relatively thin extracaldera facies lying unconformably over Kw.

Return to Highway 26 by retracing route northward along Meadow Creek Rd.

Reset odometers at junction of Meadow Creek Rd with Highway 26.

Turn west (left) on Highway 26 and proceed 3.0 mi to N 115 E.

3.0 mi Turn south (left) on N 115 E and proceed 2.2 mi to 89th Rd N.

5.2 mi Junction with 89th Rd N.

Point of Interest E

(43.57640, -111.80372)

Rhyolite of Milo Dry Farm (Trmd; Heise I). To the east is the poorly exposed and poorly documented rhyolite of Milo Dry Farm (Morgan and McIntosh, 2005; Watts and others, 2011). This rhyolite appears to be a dome or flow associated with Blacktail Creek Tuff.

Continue south on N 115 E 4.6 mi to E Lincoln Rd.

9.8 mi Turn east (left) on E Lincoln Rd and proceed 1.9 mi.

11.7 mi

STOP 6

(43.49867°, -111.77603°)

Overview of volcanic rocks exposed at Blacktail Creek Reservoir.

The rugged cliffs rising above the reservoir are Blacktail Creek Tuff (Heise I). Unwelded Wolverine Creek tuff (Heise III) is exposed along the road down to the reservoir. Kilgore Tuff (Heise IV) crops out near this vantage point and is also visible in the distance. Huckleberry Ridge Tuff (Yellowstone I) forms the surface of this stop and also forms the uppermost inclined surface in the distance above the reservoir. Pleistocene intercanyon basalt flows (Qbw; basalt of Willow Creek; Phillips and others, 2016b) partially fill the canyon in middle distance.

If time and interest permit, walk 1.1 mi down the road to Blacktail Creek Recreation Area, passing outcrops of Huckleberry Ridge Tuff followed by excellent exposures of Wolverine Creek tuff showing diverse bed forms and elution pipes. Parking along the road is limited and traffic is heavy in summer months. Otherwise, continue by vehicle to day use area parking lot (parking fee may be required in summer months). Walk to boat ramp.

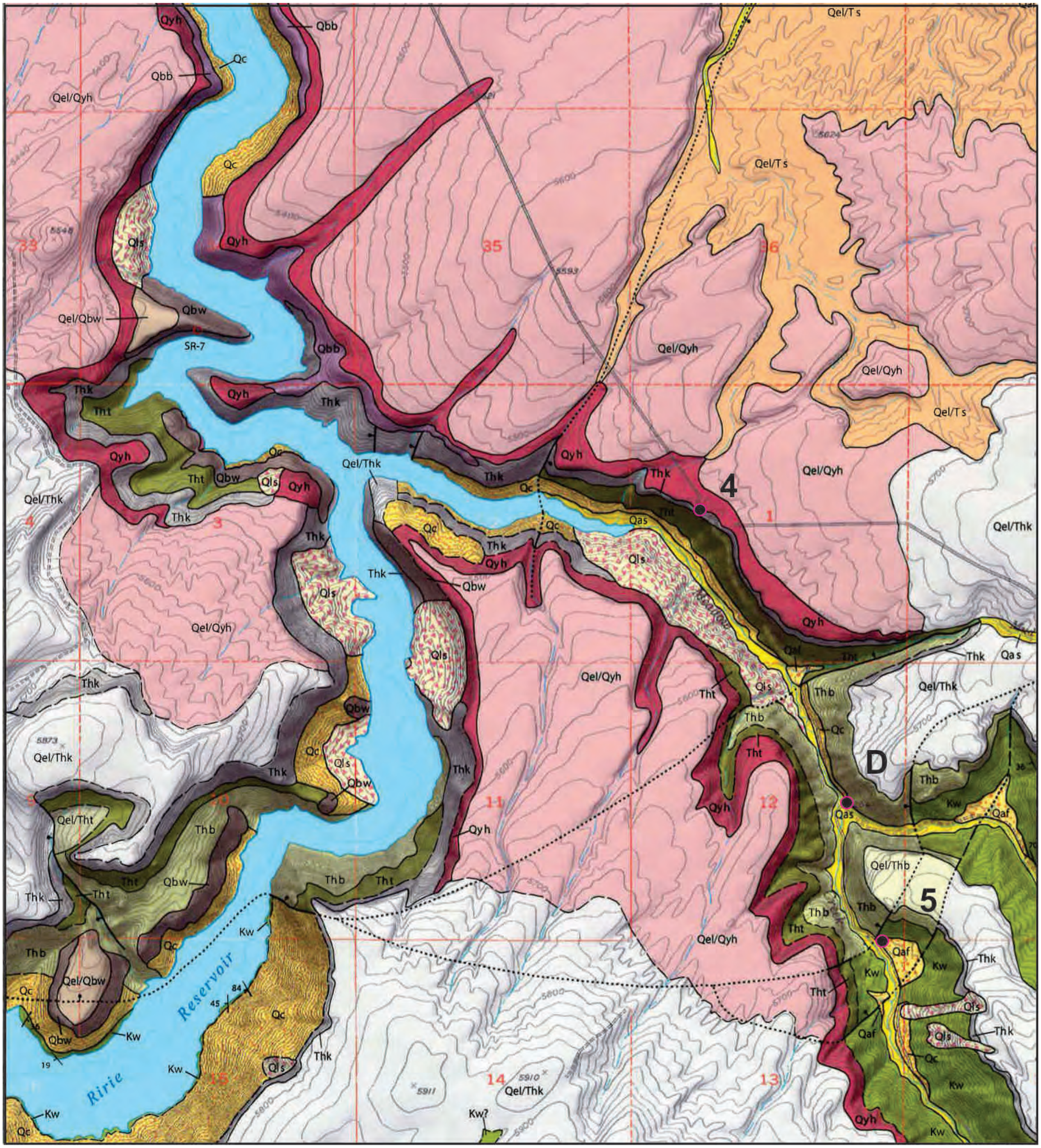

Figure 8. Detail of geologic map of Poplar quadrangle (from Phillips and others, 2016b) showing stops 4–5 and point of interest D.

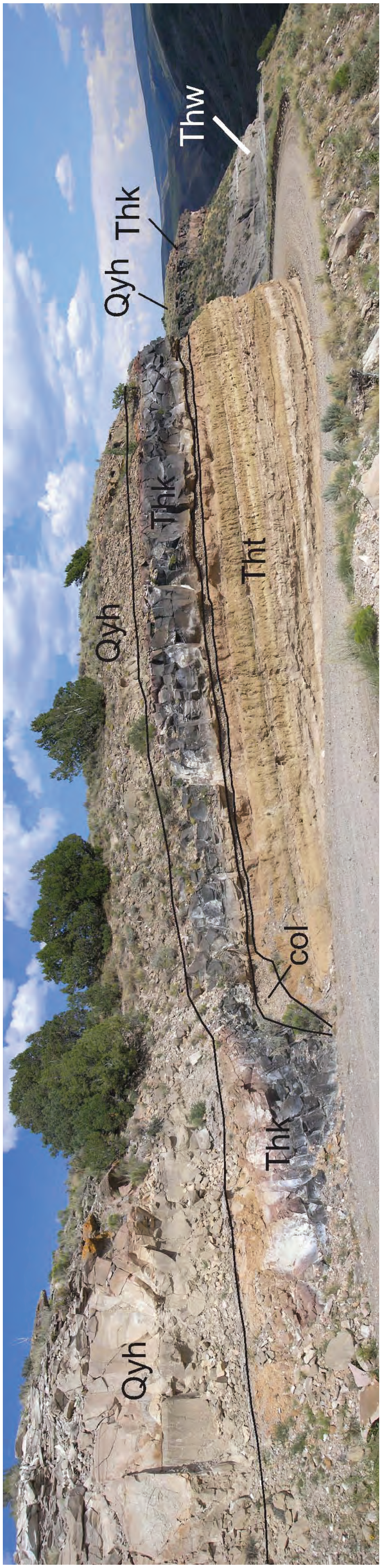

Figure 9. Annotated photograph showing geologic units from Meadow Creek Overlook (from Phillips and others, 2016b).

12.8 mi

STOP 7

(43.504920°, -111.761540°)

Type section of Blacktail Creek Tuff (Thb; Heise I). This is the type section of Blackfoot Creek Tuff (Morgan and McIntosh, 2005, Data Repository item 2005059). Prior to formal definition of the Heise Group, this unit was called “tuff of Spring Creek” on the SE margin of the ESRP (Prostka and Embree, 1978), and “tuff of Edie Ranch” on the NW margin (Skipp and others, 1979).

The section along the boat ramp/reservoir shoreline is about 25 ft (7.5 m) thick. It thickens to >300 ft (>150 m) to the north where it is silicified and has tight flow folds. Bonnichsen and others (1989) and Morgan and McIntosh (2005) inferred a caldera margin to be present at this locality, with the thick exposures consisting of ponded intracaldera facies and the thin section consisting of extracaldera (outflow) facies.

Retrace route to Stop 6 and continue west 6.8 mi on Lincoln Rd to junction with Foothill Rd.

The route passes to the south of an early Pleistocene shield volcano (unnamed on USGS topographic maps; called “Iona Butte” by Phillips and Welhan, 2012). Flows from this ediface contain plagioclase megacrysts. The road passes over a Pliocene (?) basalt flow overlying the Kilgore Tuff. The flow has the same stratigraphic position as the ~3.3 Ma basalt of Rexburg (Phillips and others, 2016c). The basalt flow dips gently into the Snake River Plain, as do underlying HVF units. Basalts are absent within the Heise Group, as currently defined. This basalt and the basalt of Rexburg may represent early mafic magmatism that followed the rhyolitic Heise Group.

19.6 mi Turn south (left) on Foothill Rd.

If visiting Point of Interest F, proceed 1.7 mi to intersection with Valverde Street and park.

Point of Interest F

(43.4870, -111.9023)

Welded rhyolites of Mansfield and Ross (1935).

Rhyolitic welded tuffs (later assigned to the Heise

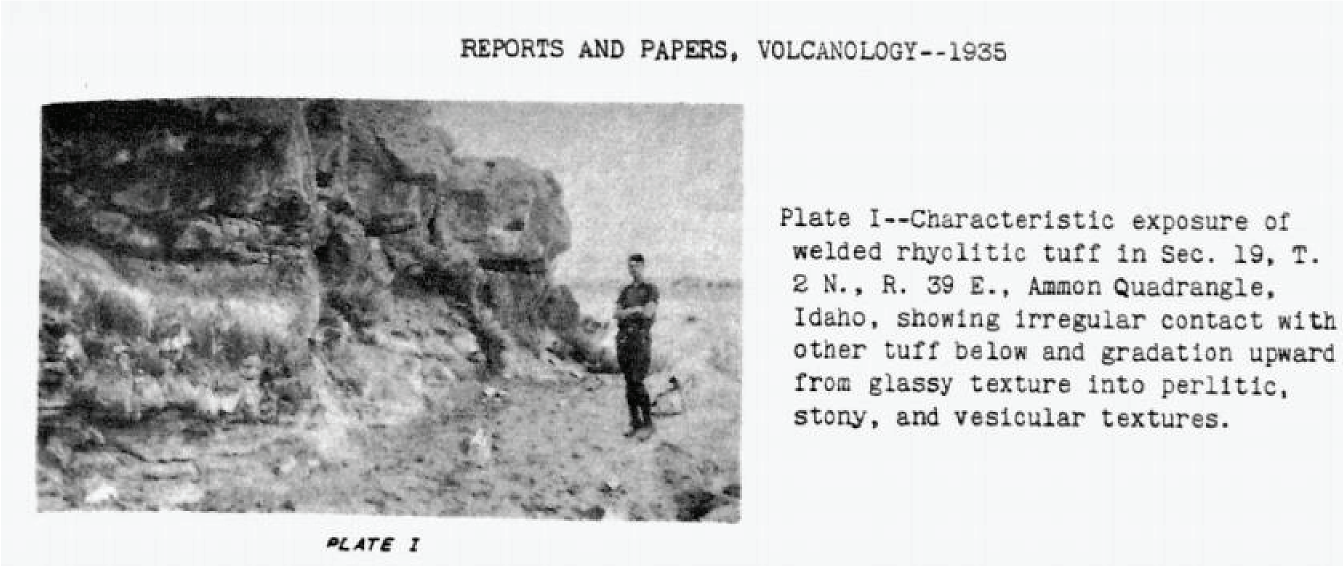
REPORTS AND PAPERS, VOLCANOLOGY--1935

Plate I--Characteristic exposure of welded rhyolitic tuff in Sec. 19, T. 2 N., R. 39 E., Ammon Quadrangle, Idaho, showing irregular contact with other tuff below and gradation upward from glassy texture into perlitic, stony, and vesicular textures.

PLATE I

Figure 10. Reproduction of Plate 1 from Mansfield and Ross (1935) showing “welded rhyolitic tuff” from the approximate location of Point of Interest F.

Group) were reported by Mansfield and Ross (1935) from this approximate locality (fig. 10). This report was among the first in the world to describe welded textures in pyroclastic rocks. Petrographic descriptions and thin section photographs of specimens from Ammon were important in supporting the hypothesis of post-emplacement welding of pyroclastic rocks. The pumice mine here exposes Kilgore Tuff overlying unwelded pumice deposits of Wolverine Creek tuff. Walcott Tuff (Heise II) is poorly exposed in Black Canyon Creek to south of pumice mine.

Continue 0.6 mi south on Foothill Rd to intersection with E 21st S.

19.6 mi Turn west on E 21st S and proceed 1.9 mi to intersection with S 45 E/Crowley Rd.

Turn south on S 45th E and proceed 3.0 mi to S Ledge Rock Dr.

26.7 mi Continue on S Ledge Rock Dr into canyon containing pumice mines. Note the ridge-capping ledges of lithophysal rhyolite (Kilgore Tuff) over unwelded pumice deposits (Wolverine Creek tuff).

STOP 8A

(43.42385°, -111.92488°)

Parking for walk to Walcott Tuff outcrops.

Walk ~0.8 mi on easy to moderate route through pumice pits to Stop 8B (Walcott Tuff outcrops). Note changes in color and size of pumice and obsidian clasts. Blocks up to 6 in (15 cm) are present, suggesting proximity to vents. The presence of large broken obsidian clasts may indicate explosion of a lava dome capped by a vitrophyre.

STOP 8B

(43.41982°, -111.91950°)

Outcrops of Walcott Tuff (Thwt; Heise II) in Rock Hollow. Explore outcrops for ~1,000 ft (300 m) SW to vitrophyre of Thwt (43.41763°, -111.92077°).

The type section of Walcott Tuff lies far to the south, near American Falls Reservoir (Carr and Trimble, 1963; Point of Interest J; fig. 1). Characteristic features are very sparse crystals, a basal vitrophyre with obsidian that is locally of “artifact” quality, large spherical lithophysae (2 to 4 in, 5 to 10 cm) that weather bluish-gray, and a capping reddish-orange vitric tuff. At this locality and at the type section, Walcott Tuff is underlain by unwelded, partially reworked pumiceous tuffs, locally with paleosols (Neeley Formation of Carr and Trimble, 1963). Walcott Tuff has not been recognized to the northeast in the Heise cliffs or Meadow Creek areas. Thick deposits of Walcott Tuff are present on the northwest side of the Eastern Snake River Plain at Howe Point (e.g., Point of Interest J; McCurry and others, this volume; Hackett and Morgan, 1988, Morgan, 1989). Based on dating of units in deep core holes on the ESRP, Anders and others (2014) suggested that there are two ignimbrites contained in the Walcott Tuff interval.

STOP 8C

(43.42596, -111.906289)

Cliff exposures of Walcott Tuff (fig. 11). Walk NE ~0.5 mi (~0.8 km) to view cliff exposures of Walcott Tuff. Thwt thickens locally here and for several miles to north before disappearing. It is absent at Blacktail Recreation Area, Meadow Creek, and Heise cliffs, as well as in the west side of Teton Range.

If time and interest permit, continue north along cliff line to Point of Interest G.

Point of Interest G

(43.45833, -111.89322)

Measured section of Walcott Tuff (fig. 11). Alternate access (private property) to this site is from E. Sunnyside Rd (road entrance at 43.436365°, -111.875201°).

Return to vehicles.

Continue NE ~0.5 mi (~0.8 km) to end of road in pumice pit.

STOP 9

(43.42834°, -111.92095°)

Pumice Pit exposures of Kilgore Tuff and unconformity with underlying sediments and tuffs.

Explore views of contacts exposed in high walls of pumice mine. Caution: do not climb or stand close to high walls as they could collapse. This locality displays contacts between Wolverine Creek tuff, a reddish paleosol zone, “pre-Kilgore tuff and sediments,” and Kilgore Tuff. While these contacts are planar in many exposures, cut-and-fill channels are relatively common. These channels cut pumice deposits, and are filled with tuffs and tuffaceous sediments and topped

Figure 11. Annotated photograph showing Walcott Tuff (Thwt) at point of interest G. A: orange vitric tuff; B: black devitrified welded tuff; C: lithophyssal zone; D: black basal vitrophyre; E: concealed unwelded airfall and reworked pumiceous tuff and ash.

Figure 12. Pumice pit highwall showing fissure filled with semi-rounded boulders of Kilgore Tuff and poorly sorted matrix. The fissure cuts poorly sorted reworked tuffs and tuffaceous sediments. Location is (43.42933°, -111.92225).

by undeformed Kilgore Tuff. Rarely, near-vertical fissures are present. These enigmatic features are filled from above with Kilgore Tuff vitrophyre (fig. 12).

Return to vehicles and retrace route to S Ledge Rock Rd. and S 45th E.

Proceed south on S 45 E (Henry Canyon Rd) and follow 3.9 mi uphill to viewpoint.

STOP 10

(43.40188, -111.91336)

Summary of Heise Group stratigraphy (fig. 13) and overview of the Ammon foothills area and ESRP.

From this vantage point, localities containing all major Heise Group units can be seen in the near distance to north and northeast. These include Blacktail Creek Tuff (Thb; Heise I), Walcott Tuff (Thwt, Heise II), pumice mines containing the Wolverine Creek tuff (Thw, Heise III), and Kilgore Tuff (Thk, Heise IV). To the northwest and west are views of alluvial Snake River deposits, and Pleistocene basalt lava flows and shield volcanoes of the ESRP. On a clear day, Basin and Range mountains of the Lost River and Lemhi ranges on the northwest margin of the ESRP can be seen. Heise Group units are exposed on the edges of these ranges (see Points of Interest K (Howe Point); L (Lidy Hot Springs); and M (Spencer); table 2). Several deep drill holes penetrate the basalts (Anders and others, 2009; McCurry and others, this volume) and provide valuable insights into the Heise “crypto-calderas” (fig. 1).

End of Trip.

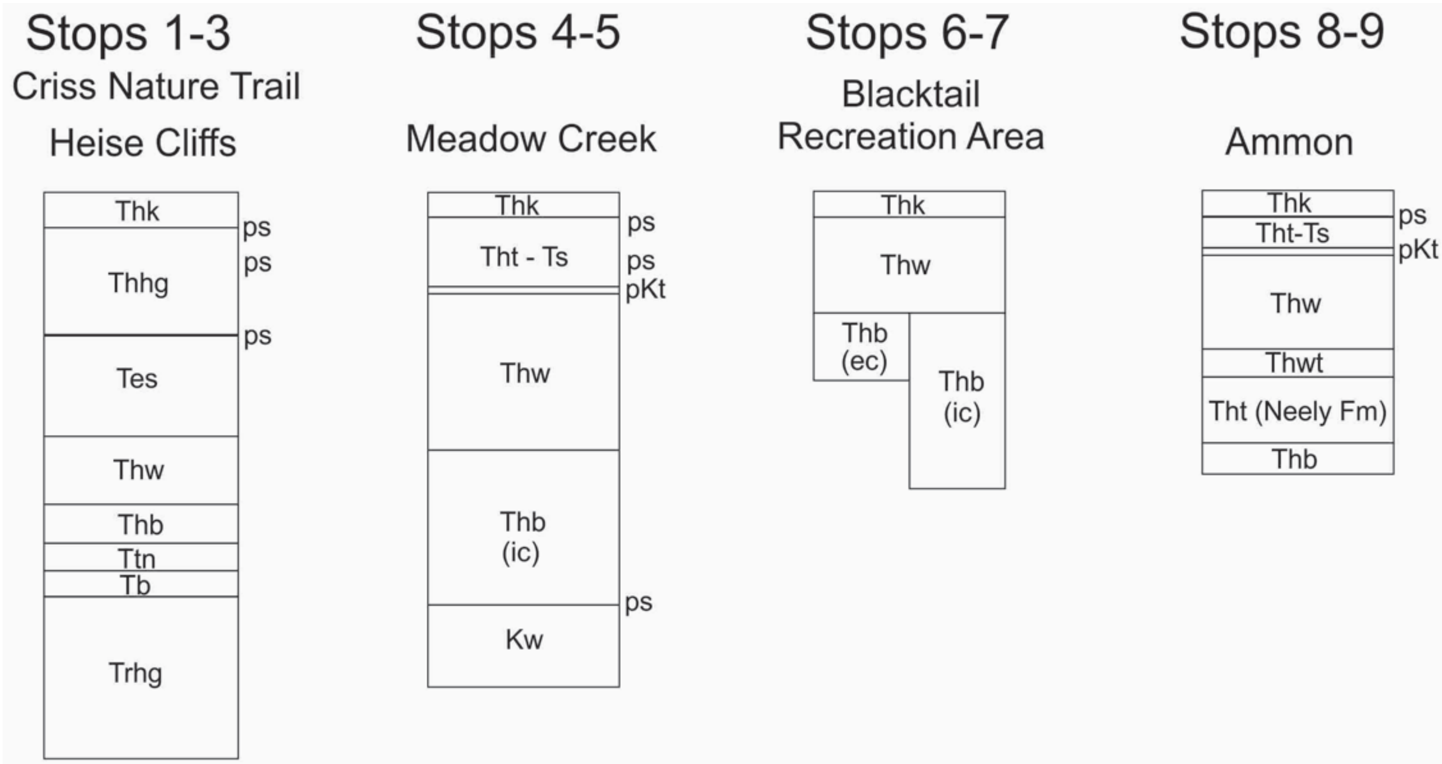

Figure 13. Summary of Heise Group sections visited on the field trip; Tht – Ts: reworked tuffs and tuffaceous sediments; pKt: pre-Kilgore Tuff; ps: paleosol; ec: extracaldera facies; ic: intracaldera facies.

REFERENCES

Albee, H.F., Prostka, H.J., Jobin, D.A., and Love, J.D., 1975, Field trip guide to the Idaho-Wyoming thrust-fault zone: Geological Society of America, Rocky Mountain Section, twenty-eighth annual meeting, Boise, Idaho, field trip 4.

Anders, D.W., Rodgers, M.H., Hemming, S.R., Saltzman, Janet, DiVenere, V.J., Hagstrum, J.T., Embree, G.F. and Walter, R.C., 2014, A fixed sublithospheric source for the late Neogene track of the Yellowstone hotspot: Implications of the Heise and Picabo volcanic fields: Journal of Geophysical Research Solid Earth, v. 119, p. 2871–2906.

Anders, M.H., Saltzman, J., and Hemming, S.R., 2009, Neogene tephra correlations in eastern Idaho and Wyoming: Implications for Yellowstone hotspot-related volcanism and tectonic activity: Bulletin of the Geological Society of America, v. 121, p. 837–856.

Allmendinger, R.W., 1980, Geologic map of the south half of the Ammon quadrangle, Bingham and Bonneville Counties, Idaho: U.S. Geological Survey Miscellaneous Field Studies Map, MF-1259, scale 1:24,000.

Armstrong, R.L., Leeman, W.P., and Malde, H.E., 1975, K-Ar dating, Quaternary and Neogene volcanic rocks of the Snake River Plain, Idaho: American Journal of Science, v. 275, p. 225-251.

Armstrong, R.L., Harakel, J.E., and Neill, W.M., 1980, K-Ar dating of Snake River Plain (Idaho) volcanic rocks—new results: Isochron West, no. 27, p. 5-10.

Barney, B., Jernigan, AJ, Doherty, D., Moore, D., and Embree, G., In Press, Bedrock geology of the Heise area, Idaho: Idaho Geological Survey Technical Report, scale 1:24,000.

Bindeman, I.N., Watts, K.E., Schmitt, A.K., Morgan, L.A., and Shanks, P.W.C., 2007, Voluminous low ¬δ^{18}O magmas in the late Miocene Heise volcanic field, Idaho—Implications for the fate of the Yellowstone hotspot calderas: Geology v. 35, p. 1019-1023.

Bolte, Torsten, Holtz, Francois, Almeev, Renat, and Nash, Barbara, 2015, The Blacktail Creek Tuff: an analytical and experimental study of rhyolites from the Heise volcanic field, Yellowstone hotspot system: Contributions to Mineralogy and Petrology, v. 169, p. 1-24.

Bonnichsen, Bill, Christiansen, R.L., Morgan, L.A., Moye, F.J., Hackett, W.R., Leeman, W.P., Honjo, Norio, Jenks, M.D. and Godchaux, M.M., 1989, Excursion 4A—Silicic volcanic rocks in the Snake River Plain—Yellowstone Plateau province, in C.E. Chapin and J. Zidek, eds., Field excursions to volcanic terranes in the western United States, Volume II—Cascades and Intermountain West: New Mexico Bureau of Mines and Mineral Resources Memoir 47, p. 135-182.

Carr, W.J. and Trimble, D.E., 1963, Geology of the American Falls quadrangle, Idaho: U.S. Geological Survey Bulletin 1121-G, 44 p.

Christiansen, R.L. and J.D. Love, 1978, The Pliocene Conant Creek Tuff in the northern part of the Teton Range and Jackson Hole, Wyoming: U.S. Geological Survey Bulletin 1435-C, 9 p.

Doherty, D.J., 1976, Ground surge deposits in eastern Idaho: Master's thesis, Wayne State University, 114 p.

Dossett, T.S., Reed, T.H., McIlrath, S.L, Moore, D.K. and Embree, G.F., 2012, Geologic map of the South Fork of the Snake River between Swan Valley and Ririe, Idaho: Idaho Geological Survey Technical Report 12-5, scale 1:24,000.

Drew, D.L., Bindeman, I.N., Watts, K.E., Schmitt, A.K., Fu, Bin, and McCurry, Michael, 2013, Crustal-scale recycling in caldera complexes and rift zones along the Yellowstone hotspot track—O and Hf isotopic evidence in diverse zircons from voluminous rhyolites of the Picabo volcanic field, Idaho: Earth and Planetary Science Letters, v. 381, p. 63-77.

Embree, G.F., McBroome, L.A., and Doherty, D.J., 1982, Preliminary stratigraphic framework of the Pliocene and Miocene rhyolite, Eastern Snake River Plain, Idaho, in Bonnichsen, Bill, and Breckenridge, R.M., eds., Cenozoic Geology of Idaho: Idaho Bureau of Mines and Geology Bulletin 26, p. 333-343.

Embree, G. F., Moore, D.K., Phillips, W.M., and Prostka, H.J., 2016, Geologic maps of the Moody, White Owl Butte, and Wright Creek quadrangles, Madison and Teton counties, Idaho: Idaho Geological Survey Digital Web Map 122, scale: 1:24,000.

Engleman, B., Atkinson, T. Thornton, V. Doherty, D. Moore, D. Embree, G. and Tracy, R., 2013, Geologic Map of Ririe Reservoir, Ririe, Idaho: Idaho Geological Survey Technical Report 13-2, scale 1:24,000.

Hackett, W.R. and Morgan, L.A., 1988, Explosive basaltic and rhyolitic volcanism of the Eastern Snake River Plain, Idaho, in P.K. Link and W.R. Hackett, Guidebook to the Geology of Central and Southern Idaho: Idaho Geological Survey Bulletin 27, p. 283-301.

Hladky, F.R., Kellog, K.S. , Oriel, S.S., Link, P.K., Nielson, J.W., and Amerman, R.E., 1992, Geologic map of the eastern part of the Fort Hall Indian Reservation, Bannock, Bingham, and Caribou Counties, Idaho: U.S. Geological Survey Miscellaneous Investigations Map I-2006, scale 1:150,000.

Kellogg, K.S., Harlan, S.S., Mehnert, H.H., Snee, L.W., Pierce, K.L., Hackett, W.R., and Rodgers, D.W., 1994, Major 10.2-Ma rhyolitic volcanism in the eastern Snake River Plain, Idaho−Isotopic age and stratigraphic setting of the Arbon Valley Tuff Member of the Starlight Formation: U.S. Geological Survey Bulletin 2091, 18 p.

Lewis, R.S, Link, P.K., Stanford, L.R., and Long, S.P., 2012, Geologic map of Idaho: Idaho Geological Survey Map 9, scale 1:750,000, booklet, 18 p.

Mansfield, G.R. and Ross, C.S., 1935, Welded rhyolite tuffs in southeastern Idaho: Transactions, American Geophysical Union, Reports and Papers, Volcanology, p. 308-320.

Mansfield, G.R., 1952, Geography, geology, and mineral resources of the Ammon and Paradise Valley quadrangles, Idaho: U.S. Geological Survey Professional Paper 238, 92 p. scale 1:62,500.

McBroome, L.A. 1981, Stratigraphy and origin of Neogene ash-flow tuffs on the north-central margin of the eastern Snake River plain, Idaho: Master's Thesis, University of Colorado at Boulder, 74 p.

McBroome, L.A., Doherty, D.J., and Embree, G.F., 1981, Correlation of major Pliocene and Miocene rhyolites, eastern Snake River Plain, Idaho: Geological Society of Montana Guidebook, Southwest Montana Field Conference, p. 323–330.

Morgan, L.A., Doherty, D.J., and Leeman, W.P., 1984, Ignimbrites of the Eastern Snake River Plain: Evidence for major caldera-forming eruptions: Journal of Geophysical Research, v. 89, p. 8665-8678.

Morgan, L.A., 1988, Explosive rhyolitic volcanism on the eastern Snake River plain: University of Hawaii, PhD Dissertation, 191 p.

Morgan, L.A., and Hackett, W.R., 1989, Chapter Three, Explosive basaltic and rhyolitic volcanism of the eastern Snake River Plain, in Ruebelmann, K.L., Smith, R.P., Downs, W.F., Christiansen, R.L., Hacket, W.R., Morgan, L.A., Leeman, W.P., Wood, S.H., Malde, H.E., and Kuntz, M.A., eds., Volume 2, Snake River plain-Yellowstone volcanic province, Jackson, Wyoming to Boise, Idaho July 21-29, 1989, Volcanism and plutonism of western North America: American Geophysical Union, Field trips for the 28th international geological congress, p. 39-47. Available at: http://onlinelibrary.wiley.com/doi/10.1029/FT305p0038/pdf.

Morgan, L.A., 1989, Howe Point, in Ruebelmann, K.L., Smith, R.P., Downs, W.F., Christiansen, R.L., Hacket, W.R., Morgan, L.A., Leeman, W.P., Wood, S.H., Malde, H.E., and Kuntz, M.A., eds., Volume 2, Snake River plain-Yellowstone volcanic province, Jackson, Wyoming to Boise, Idaho July 21-29, 1989, Volcanism and plutonism of western North America: American Geophysical Union, Field trips for the 28th international geological congress, p. 50. Available at: http://onlinelibrary.wiley.com/doi/10.1029/FT305p0050/pdf.

Morgan, L.A., 1992, Stratigraphic relations and paleomagnetic and geochemical correlations of ignimbrites of the Heise volcanic field, eastern Snake River plain, eastern Idaho and western Wyoming, in Link, P.K., Kuntz, M.A., Platt, L.B., eds., Regional geology of eastern Idaho and western Wyoming: Geological Society of America Memoir 179, p. 215-226.

Morgan, L.A., and W.C. McIntosh, 2005, Timing and development of the Heise volcanic field, Snake River Plain, Idaho, western USA: Geological Society of America Bulletin v. 117, p. 288-306.

Morgan, L.A., Pierce, K.L., and Shanks, W.C.P., 2008, Track of the Yellowstone hotspot: Young and ongoing geologic processes from the Snake River Plain to the Yellowstone Plateau and Tetons, in Roaming the Rocky Mountains and Environs: Geological Field Trips: Geological Society of America Field Guide, p. 1–35.

Phillips, W.M., and Welhan, J.A., 2011, Geologic map of the Idaho Falls South quadrangle, Bonneville and Bingham counties, Idaho: Idaho Geological Survey Digital Web Map 78, scale 1:24,000.

Phillips, W.M., and Welhan, J.A., 2012, Geologic map of the Ucon quadrangle, Bonneville County, Idaho: Idaho Geological Survey Digital Web Map 147, scale 1:24,000.

Phillips, W.M., Garwood, D.L., and Embree, G.F., 2013a, Geologic map of the Packsaddle Lake quadrangle, Teton County, Idaho: Idaho Geological Survey Digital Web Map 155, scale 1:24,000.

Phillips, W.M., Embree, G.F., and Garwood, D.L., 2013b, Geologic map of the Tetonia quadrangle, Teton County, Idaho: Idaho Geological Survey Digital Web Map 157, scale 1:24,000.

Phillips, W.M., and Welhan, J.A., 2013c, Geologic map of the Goshen quadrangle, Teton County, Idaho: Idaho Geological Survey Digital Web Map 156, scale 1:24,000.

Phillips, W.M., Embree, G.F., Welhan, J.A., and Garwood D.L., 2014, Geologic map of the Ririe quadrangle, Madison, Jefferson, and Bonneville, counties, Idaho: Idaho Geological Survey Digital Web Map 165, scale 1:24,000.

Phillips, W.M., Moore, D.K., Feeney, D.M., and Embree, G.F., 2016a, Geologic map of the Heise quadrangle, Bonneville, Jefferson, and Madison counties, Idaho: Idaho Geological Survey Digital Web Map 176, scale 1:24,000.

Phillips, W.M., Moore, D.K., and Feeney, D.M., 2016b, Geologic map of the Poplar quadrangle, Bonneville county, Idaho: Idaho Geological Survey Digital Web Map 175, scale 1:24,000.

Phillips, W.M., Embree., G.F., and Welhan, J.A., 2016c, Geologic map of the Rexburg quadrangle, Bonneville county, Idaho: Idaho Geological Survey Digital Web Map 178, scale 1:24,000.

Phillips, W.M., Breedlovestrout, R.L, and Feeney, D.M., In Press, Geologic map of the Hawley Gulch quadrangle, Bonneville and Madison counties, Idaho: Idaho Geological Survey Digital Web

Map, scale 1:24,000.

Phillips, W.M. and Welhan, J.A, In Preparation, Geologic map of the Ammon quadrangle, Bonneville County, Idaho: Idaho Geological Survey Digital Web Map, scale 1:24,000.

Price, K.B., and Rodgers, D.W., 2010, Geologic Map of the North End of the Big Hole Mountains, Madison and Teton counties, Idaho: Idaho Geological Survey Technical Report 10-2, scale 1:24,000.

Prostka, H.J., and Hackman, R.J., 1974, Preliminary geologic map of the NW 1/4 Driggs 1 by 2 degree quadrangle, southeastern Idaho: U.S. Geological Survey, Open-File Report OF-74-105, scale 1:125,000.

Prostka, H.J., and Embree, G.F., 1978, Geology and geothermal resources of the Rexburg area, eastern Idaho: U.S. Geological Survey, Open-File Report OF-78-1009, scale 1:48,000.

Skipp, B., Prostka, H.J., and Schleicher, D.L., 1979, Preliminary geologic map of the Edie Ranch quadrangle, Clark County, Montana: U.S. Geological Survey Open-file Report 79-845, scale 1:62,500.

Staatz, M.H., and Albee, H.F., 1966, Geology of the Garns Mountain quadrangle, Bonneville, Madison, and Teton Counties, Idaho: U.S. Geological Survey Bulletin B-1205, scale 1:31,680.

Stearns, H.T., Crandall, L., Steward, W.G., 1938, Geology and ground-water resources of the Snake River plain in southeastern Idaho: U. S. Geological Survey Water-Supply Paper 774, 268 p. Available as: https://pubs.er.usgs.gov/publication/wsp774.

Szymanowski, Dawid, B.S. Ellis, Olivier Bachmann, Marcel Guillong, and W.M. Phillips, 2015, Bridging basalts and rhyolites in the Yellowstone–Snake River Plain volcanic province: The elusive intermediate step: Earth and Planetary Science Letters, v. 415, p. 80–89.

Watts, K.E., Leeman, W.P., Bindeman, I.N., and Larson P.B, 2010, Supereruptions of the Snake River plain; two-stage derivation of low-δ^{18}O rhyolites from normal-δ^{18}O crust as constrained by Archean xenoliths: Geology v. 38, no. 6., p. 503-506.

Watts, K.E., Bindeman, I.N., and Schmitt, A.K., 2011, Large-volume rhyolite genesis in caldera complexes of the Snake River Plain: Insights from the Kilgore Tuff of the Heise volcanic field, Idaho, with comparison to Yellowstone and Bruneau-Jarbidge rhyolites: Journal of Petrology v. 52, p. 8578-890.

Westgate, J.A., Pearce N.J.G., Perkins, W.T., Shane, P.A., and Preece, S.J., 2011, Lead isotope ratios of volcanic glass by laser ablation inductively-coupled plasma mass spectrometry: Application to Miocene tephra beds in Montana, USA and adjacent areas: Quaternary International, v. 246, p. 82-96.

Wotzlaw, J.F., Bindeman, I.N., Watts, K.E., Schmitt, A.K., Caricchi, L., Schaltegger, U., 2014, Linking rapid magma reservoir assembly and eruption trigger mechanisms at evolved Yellowstone-type supervolcanoes, Geology, v. 42 no. 9 p. 807-810.

U.S. Geological Survey, 1970, U.S. Geological Survey Chemical and Isotope Data Sites, Chemical and Isotope Data: Available at: http://hotspringchem.wr.usgs.gov/imgquery.php?rlon=-112&lat=44 (accessed 6 May 2015).

Spori Building. The Spori Building was built to house the Ricks Academy, which later became Ricks College and is now Brigham Young University–Idaho. Begun in September 1899, construction finished in 1903 (at a cost of $63,475). This photograph, taken in 1905, is the earliest known image of the building. Community members built the structure from hand-fashioned timber beams and hand-cut blocks of Huckleberry Ridge Tuff. The rock was likely quarried about 3 miles southeast of the building. The building was situated on the edge of the basalt of Rexburg at the edge of the Rexburg bench, overlooking the town of Rexburg. The original Spori Building was razed in 2000, partly due to concern about seismic risk. The building built to replace it retains some of its external characteristics, but is faced by Idaho travertine. (Photo courtesy of BYU-Idaho Library Special Collections.)

FIELD GUIDE TO LAVA BENCHES IN HENRYS FORK AND WARM RIVER CANYONS AND TO THE ORIGIN OF UPPER AND LOWER MESA FALLS, ISLAND PARK, IDAHO

Dan K. Moore,[1] Glenn F. Embree,[1] Duane E. Champion,[2] and Mel A. Kuntz[2]

[1]Brigham Young University, Rexburg, Idaho; [2]U.S. Geological Survey

Corresponding author: Dan K. Moore, moored@byui.edu

INTRODUCTION

The Henrys Fork (HF) of eastern Idaho, which flows from Henrys Lake and receives much input from springs, is one of the most famous trout streams of the United States. The headwaters of the river flow through Island Park, which lies in the southwest part of the Yellowstone I caldera and contains the entire Yellowstone II caldera (fig. 1). The HF enters the Yellowstone I caldera at Island Park dam, flows through Box Canyon, then meanders across a broad plain (fig. 1). Downstream of Riverside Campground, the river forms a deep canyon that contains cascades and falls, including Upper and Lower Mesa Falls (fig. 1). To the east, Warm River (WR) flows primarily from springs, including Warm River Spring. The headwaters of this river lie east and south of the Yellowstone II caldera in the southwest part of the Yellowstone I caldera. Between Warm River Spring and Bear Gulch, the WR also forms a deep canyon. Below Bear Gulch, both rivers traverse the southern flank of the Yellowstone I caldera, within one mile of each other. The confluence of WR and the HF lies near Warm River campground. From the confluence, the HF flows westward along the southern flank of the Yellowstone I caldera and onto the Snake River Plain (fig. 1).

The geologic foundations of Island Park developed in the Archean and Proterozoic when the Wyoming crustal province formed and developed. Paleozoic and Mesozoic sedimentary rocks deposited on this crystalline basement were thrust eastward during the Sevier Orogeny. Later, following the Laramide Orogeny, foundering of subducted lithosphere produced the Absaroka volcanic field. Block-faulted mountains and valleys developed in the area during Miocene-to-recent extension. The area rose in the Pliocene as the North American plate was carried over the Yellowstone hotspot. Pleistocene volcanic eruptions locally eliminated the surface expression of Basin and Range extension. The Island Park area developed as the Yellowstone I & II calderas formed and began filling—first with rhyolite lava domes and flows, and later with basalt flows, glacial outwash, alluvium, the Lava Creek Tuff, rhyolite lava flows from the Yellowstone III caldera to the east, and loess (fig. 1; Kuntz and others, in press; Christiansen, 2001; Christiansen and Embree, 1987).

These events and deposits influenced the development of both river canyons. Lava benches formed when locally sourced lava flows entered the HF and WR canyons, solidified, and were incised by the rivers. Moore and others (in press) correlate the remnants of these intracanyon lava benches with local basaltic lava fields, investigate the origin of Upper and Lower Mesa Falls, and explore the geologic history of the HF and WR canyons. This field guide introduces readers to localities in Island Park that are associated with the origin of lava benches and Upper and Lower Mesa Falls.

FIELD GUIDE

Figure 2 shows the field trip route, stops, and other notable locations. The geologic maps of Kuntz and others (in press) and Moore and others (in preparation) show the distribution of geologic units in the area of the field guide. Before beginning the trip, enter the coordinates from table 1 into a global positioning system (GPS) instrument. Use these coordinates to navigate to each spot. (We also provide road directions below.) The field guide begins ~2 mi north of Rexburg, Idaho at the intersection of 2nd East Street and Highway 20, near the northbound onramp.

En Route to Stop 1

From the onramp, drive north on Highway 20 for 25.0 mi, through Ashton, Idaho. As you do, familiarize yourself with the notable geologic features described below.

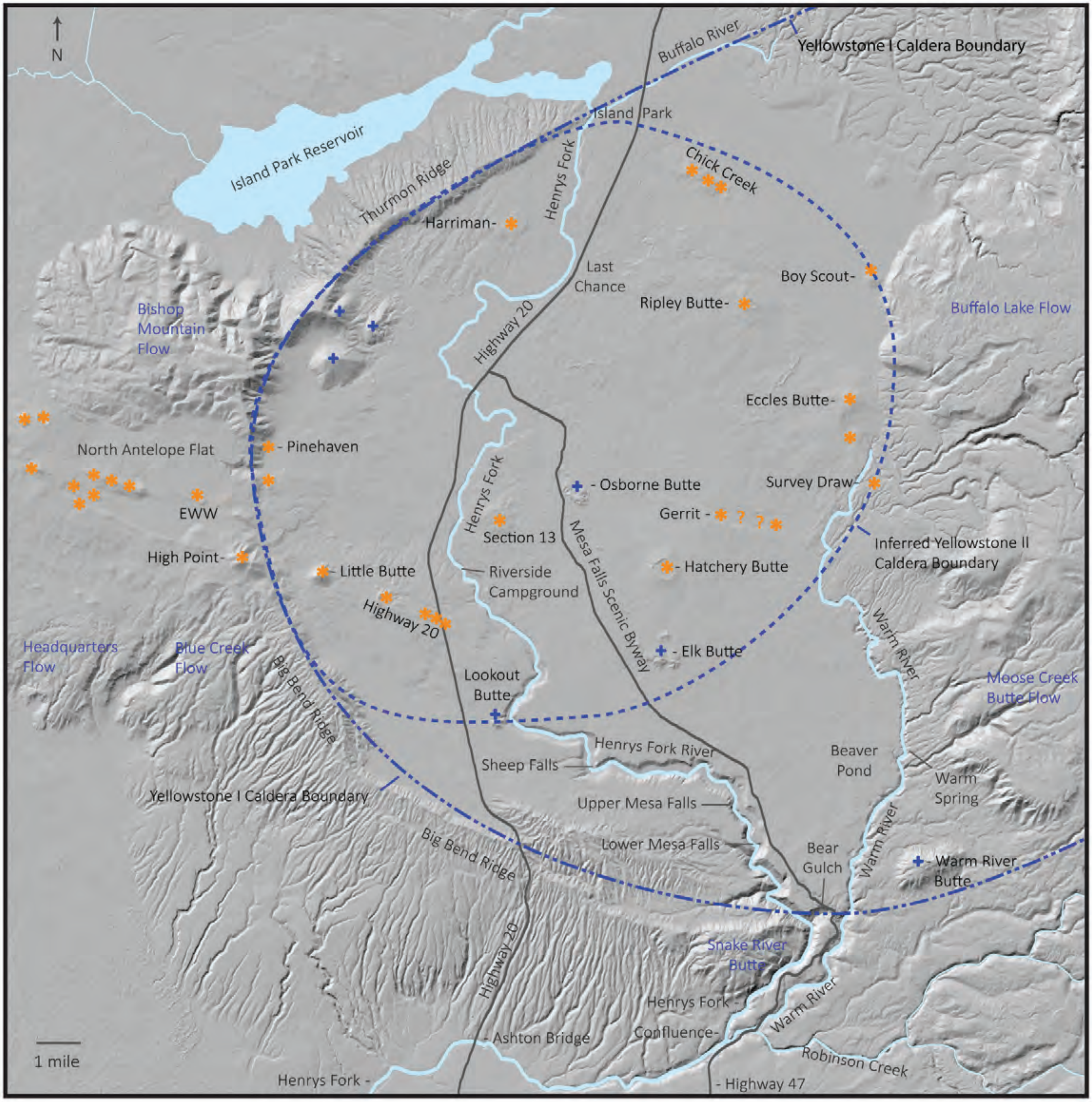

Figure 1. Notable geographic and geologic features near Island Park, Idaho (from Moore and others, in press). Labeled orange symbols (*) show vents for basalt lava fields; labeled blue symbols (+) show vents for rhyolite lava domes; blue lines show the Yellowstone I (—··) and II/Henry's Fork (···) caldera boundaries (Kuntz and others, in press; Christiansen, 2001); blue labels indicate rhyolite lava flows; and gray labels designate geographic features. The location of the Gerrit vent is uncertain; it may be a buried rift (see above).

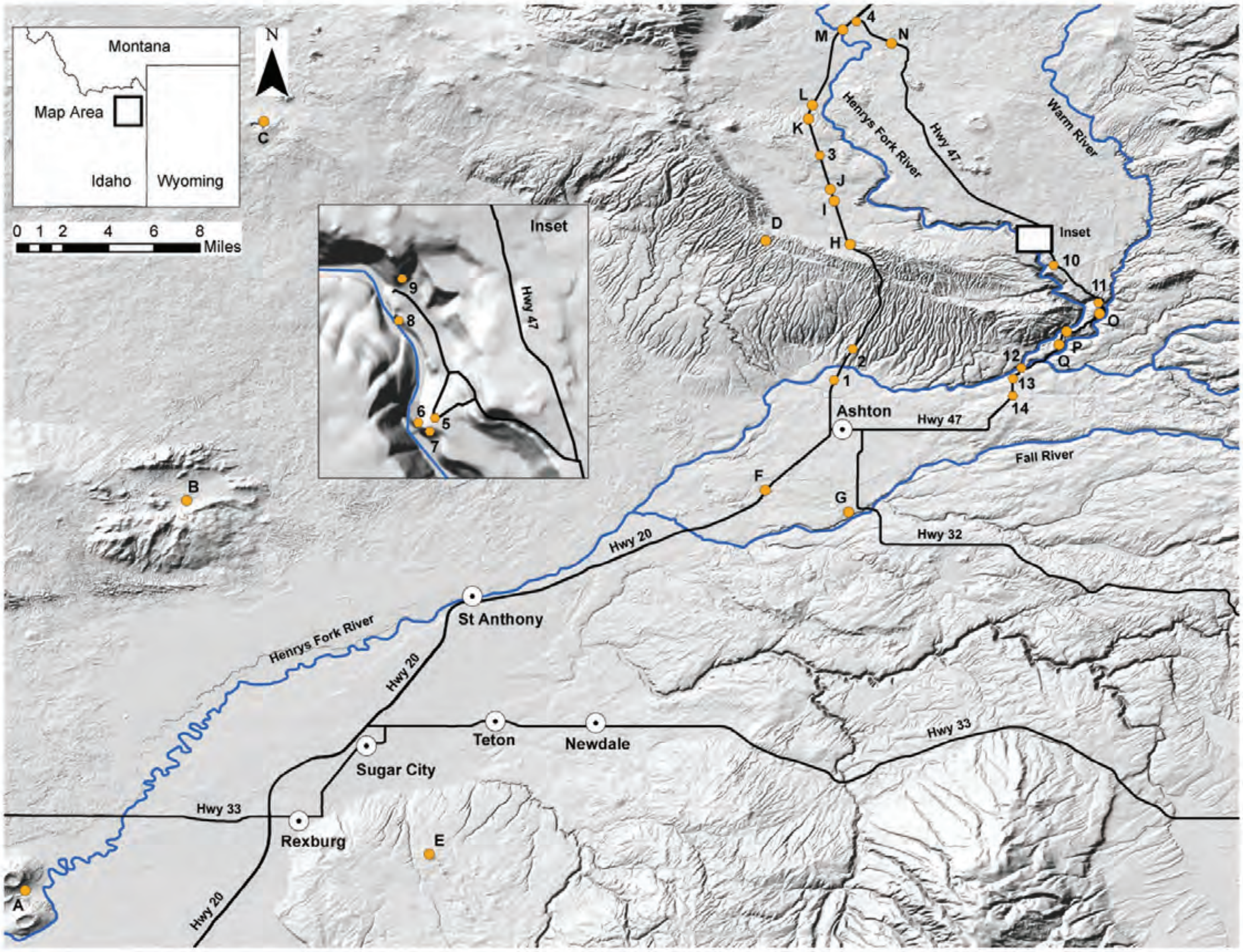

Figure 2. Field trip route and locations. Numbered locations are field trip stops; locations marked by letters are additional areas of interest. Table 1 lists location coordinates.

Location A.

The cone-shaped volcanic mounds to the southwest are the Menan Buttes, tuff cones that likely formed between 140 and 10 ka when a basaltic dike intersected water-saturated gravels deposited by the South Fork and Henrys Fork rivers (Phillips and Welhan, 2011).

Location B.

The hills in the foreground to the northwest are the Juniper Buttes. Here, a poorly exposed resurgent dome (3.3–3.7 Ma; Ar-Ar eruption age; Bindeman and others, 2007) uplifted and faulted the overlying Kilgore Tuff and basalt (Kuntz, 1979). Sand first deposited in glacial-period lakes to the southwest forms the dunes that surround the Buttes. A cinder cone lies on the eastern flank of the Buttes.

Location C.

The broad volcanic high to the north is the eastern part of the Spencer–High Point volcanic rift zone. This region trends east–west and consists of ~420 to 20 ka volcanic rift zones and lava fields, including the prominent, 126 ka Pine Butte Craters at ~12 o'clock (Kuntz and others, in press).

Location D.

The tree-covered slopes to the northeast are Big Bend Ridge, the western and southern flanks of the Yellowstone I caldera. The flat-topped portions mark the caldera rim; higher, mound-shaped segments are rhyolite lava domes.

Location E.

To the south lies the loess-covered Rexburg Bench. This elevated area consists of Heise caldera volcanic

Table 1. Field trip coordinates. Numbered locations are field trip stops; locations marked by letters are additional areas of interest. Datum: WGS84.

Location	Name	Latitude	Longitude
1	Overview	44.1028	111.4535
2	Ashton Hill	44.1225	111.4415
3	Highway 20 vent	44.2454	111.4625
4	Caldera overlook	44.3305	111.4393
5	Mesa Falls visitor's center	44.1878	111.3280
6	Upper Mesa Falls	44.1876	111.3294
7	Paleocanyon wall	44.1870	111.3284
8	Erosional features	44.1935	111.3310
9	Lava dam	44.1960	111.3307
10	Lower Mesa Falls	44.1757	111.3144
11	Bear Gulch	44.1519	111.2861
12	Confluence	44.1107	111.3348
13	Composite lava bench	44.1038	111.3399
14	Caldera rim overview	44.0929	111.3404
A	Menan Buttes	43.7793	111.9662
B	Juniper Buttes	44.0263	111.8637
C	Spencer - High Point area	44.2668	111.8149
D	Big Bend Ridge	44.1914	111.4969
E	Rexburg Bench	43.8022	111.7100
F	Huckleberry antiform	44.0330	111.4972
G	Ashton lava field vent	44.0192	111.4443
H	Edge of Elk Wallow Well lava field	44.1887	111.4434
I	Yellowstone II caldera boundary	44.2164	111.4534
J	Edge of Highway 20 lava field	44.2238	111.4558
K	Lava Creek Tuff	44.2686	111.4697
L	Edge of Pinehaven lava field	44.2772	111.4672
M	Edge of Ripley lava field	44.3250	111.4481
N	Edge of Hatchery Butte lava field	44.3163	111.4172
O	Composite lava bench	44.1450	111.2854
P	Glacial deposits	44.1337	111.3063
Q	Composite lava bench	44.1253	111.3108

rocks (6.6-4 Ma) overlain by the Huckleberry Ridge Tuff (Yellowstone I caldera; 2.1 Ma). On the west, the Rexburg basalt (3.59 ± 1.36 Ma; Embree and others, 2016) underlies the Huckleberry Ridge Tuff. The Rexburg Bench volcanic field, which consists of five flow fields, overlies the Huckleberry Ridge Tuff and includes the Sommer's Butte volcanic rift zone—seen as a northwest–southeast-trending alignment of cinder cones near the center of the Bench (Embree and others, this volume; Embree and others, 2016).

As you drive north, notice the rocks on both sides of the road. Between Rexburg and Saint Anthony, Highway 20 lies mostly on Pinedale-age glacial outwash and Holocene alluvial deposits (Phillips, 2012). North of St. Anthony, the road lies on basalt flows that moved down the Henrys Fork river drainage from the northeast, the Huckleberry Ridge Tuff, and glacial outwash and alluvial deposits (Kuntz and others, in press). Location F displays an antiform of Huckleberry Ridge Tuff, cored by alluvial deposits. Many such structures exist in the area. These antiforms are load structures produced by rapid deposition of the Huckleberry Ridge Tuff on water-saturated, unconsolidated sediments (Embree and Hoggan, 1999). The best examples of these structures are exposed in Teton Canyon and Hog Hollow (Embree and others, this volume). Near Ashton, the road lies mostly on the Ashton lava field (1.325 Ma; Kuntz and others, in press), which erupted from the vent at location G.

Pull into the Idaho Department of Transportation Historical Marker parking area, stop 1.

STOP 1

Overview of Yellowstone–Snake River Plain (YSRP) volcanism. The YSRP magmatic province encompasses the Yellowstone Plateau Volcanic Field to the northeast, the Eastern Snake River Plain to the southwest, and the area near the Idaho–Nevada–Oregon border. The province consists of voluminous deposits of rhyolite and basalt. Rhyolite magmatism began in the early Miocene and migrated northeast, as the North American plate moved southwest over the Yellowstone hotspot. Rhyolite is abundant on the Yellowstone plateau to the northeast; in Island Park and at this stop, basaltic lava flows have begun burying the rhyolite; to the southwest, up to several thousand feet of basalt covers the rhyolite.

The tree-covered slopes to the north are Big Bend Ridge, the southern flank of the Yellowstone I caldera. The flat-topped portions of Big Bend Ridge are the caldera rim; higher, mound-shaped segments are rhyolite lava domes. Snake River Butte, visible on the skyline at the east end of Big Bend Ridge, is a pre-collapse rhyolite lava flow that may have vented along the incipient ring fracture zone in the uplifted roof of the first cycle magma chamber.

Christiansen (2001) reports that the Yellowstone I caldera produced the voluminous (2,450 km^3) Huckleberry Ridge Tuff at 2 Ma, the Yellowstone II caldera produced the Mesa Falls Tuff (280 km^3) at 1.3 Ma, and the Yellowstone III caldera produced the Lava Creek Tuff (1,000 km^3) at 0.6 Ma (ages from Lanphere and others, 2002). Many smaller eruptions occurred during periods of relative quiescence between the climactic eruptions. Table 2 lists ages of selected volcanic units from the Island Park area.

Before leaving, note the Teton Mountains to the southeast. This range consists of Archean and Proterozoic metamorphic and igneous rocks, partly covered by west-dipping Paleozoic strata. The area of the present Teton Mountains experienced shortening and uplift during the Sevier and Laramide Orogenies; then, middle-Miocene-to-present (Basin and Range) extension in the area produced the current range (Love and others, 2003). Along the eastern front of the range, the Teton fault has displaced strata by more than 25,000 ft (Love and others, 2003). Pleistocene glacial erosion produced the prominent horns, U-shaped valleys, and moraines.

Drive north on Highway 20 for 1.5 mi, then pull into the parking area east of the highway, to stop 2.

STOP 2

Mesa Falls and Huckleberry Ridge Tuffs. The hills on both sides of the road contain the rhyolite tuffs deposited during the first two climactic eruptions of the Yellowstone volcanic field. The dark gray cliff at the base of the road to the west is the upper portion of the Huckleberry Ridge Tuff. Above this tuff lies a thin (<1 m) layer of loess and the volcanic deposits of the Mesa Falls Tuff, which grade upward from bedded pumaceous ash into welded tuff. Both tuffs contain phenocrysts of sanidine, quartz, plagioclase, and clinopyroxene. These tuffs dip subparallel to the present slope and cover Big Bend Ridge, indicating that the uplift that created this hill occurred during inflation of the Huckleberry magma chamber, before 2.1 Ma.

En Route to Stop 3

Drive north on Highway 20 for 18.5 mi. The Henrys Fork and Warm River canyons contain lava benches formed when local basalt lava flows entered the canyons, solidified, and were later incised by the rivers. There are remnants of at least six lava benches in Henrys Fork River canyon. They are from the Warm River, Elk Wallow Well, Highway 20, Gerrit, Hatchery Butte, and Pinehaven lava fields (table 2; Moore and others, in press). There are remnants of at least three lava benches in Warm River canyon. They are from the Warm River, Gerrit, and Hatchery Butte lava fields (table 2; Moore and others, in press). The Warm River lava field is the oldest basaltic lava flow found in Island Park, and the only one with reversed magnetic polarity. Lava from this field, which flowed from the east and south, formed the first lava bench in the canyon. Figure 3 contains profiles that show the distribu-

Table 2. $^{40/39}$Ar ages of selected volcanic units in Island Park. Basalt lava fields are shaded; those that entered the canyons and later formed lava benches are in italics. The ages of most lava fields are from Kuntz and others (in press); the age of Warm River lava field is from Abedini (2009); the ages of rhyolite units are from Christiansen (2001).

Volcanic Events	Ages (ka)
Pinehaven basalt lava field	*28 ± 8*
Ripley Butte basalt lava field	73 ± 24
Hatchery Butte basalt lava field	*81 ± 13*
Gerritt basalt lava field	*189 ± 32*
Section 13, Survey Draw, Harriman Ranch, Eccles Butte, and Boy Scout basalt lava fields	See Kuntz and others (in press)
Lava Creek Tuff	635 ± 2
Highway 20 basaltic andesite lava field	*737 ± 5*
Elk Wallow Well basalt lava field	*743 ± 5*
Warm River basalt lava field	*835 ± 17*
Elk Butte rhyolite lava dome Lookout Butte rhyolite lava dome	1200–1300?
Bishop Mountain rhyolite lava flow	1200 ± 10
Warm River Butte rhyolite lava dome	1240 ± 20
Osborn Butte rhyolite lava dome	1280 ± 10
Mesa Falls Tuff	1292 ± 50
Blue Creek rhyolite lava flow	1770 ± 20
Headquarters rhyolite lava flow	1820 ± 10
Huckleberry Ridge Tuff	2059 ± 4
Snake River Butte rhyolite lava flow	1990 ± 20

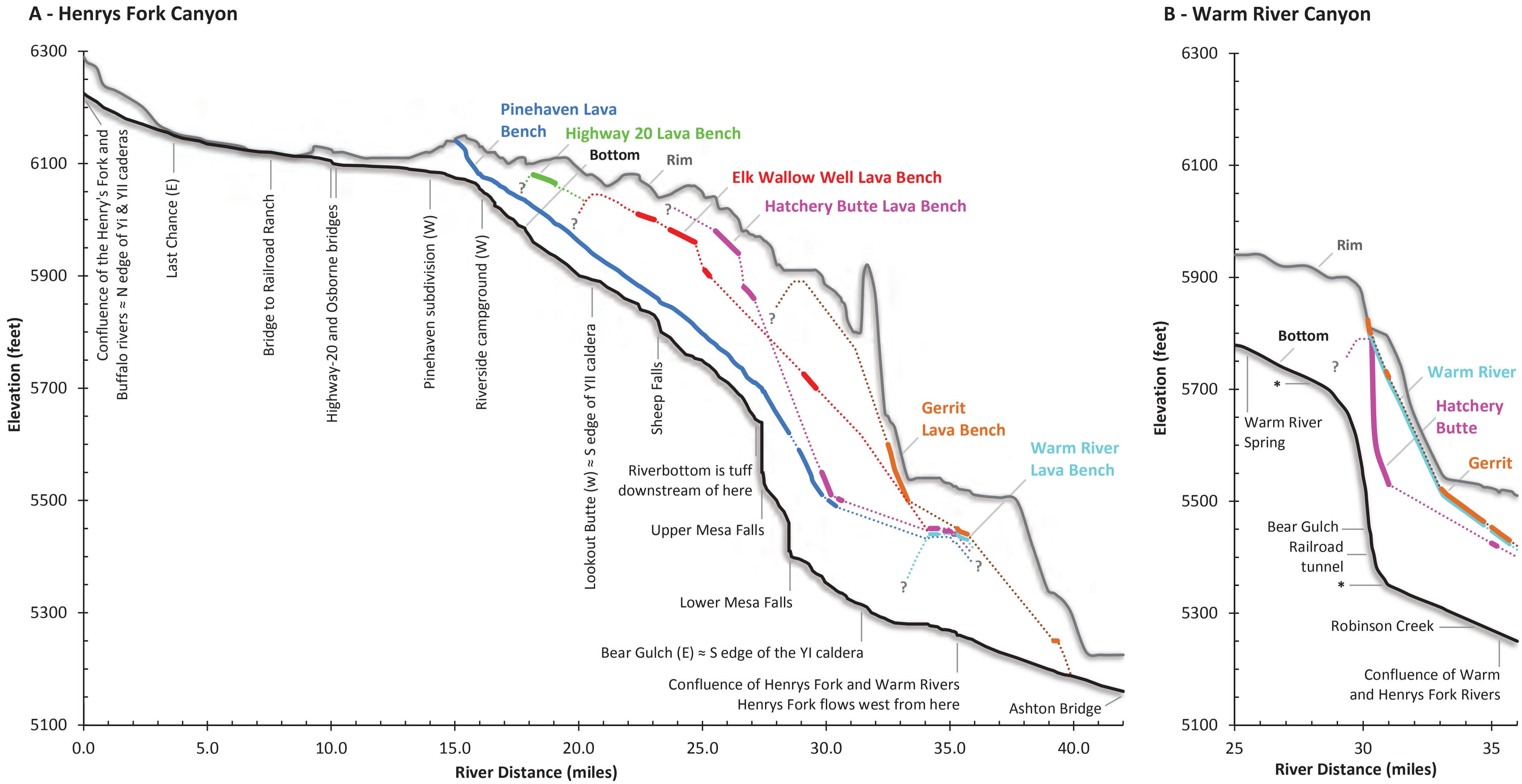

Figure 3. Longitudinal cross sections of Henrys Fork (A) and Warm River (B) canyons showing the distributions of the tops of lava benches (solid lines) and qualitative models of the inferred original distribution of lava benches (dotted lines), expressed as river distance (from north to south) versus elevation (from Moore and others, in press). Question marks indicate uncertainty inferred original distributions. Labels beneath the canyon bottom are locations along the river (cardinal directions abbreviated as N, S, E, and W). Lava flows that entered the HF and WR canyons would have formed lava dams. The possible locations of these dams are shown in these figures as dotted lines that dip upstream and end in question marks. The asterisks in (B) indicate changes in the rock type that forms the bottom of WR canyon. Basalt forms the bottom between the asterisks; elsewhere, rhyolite forms the bottom. Table 2 lists unit ages. Vertical exaggeration is about 110x.

tion of remnants of the Warm River lava bench along the walls of the HF and WR canyons; it also shows the inferred original distribution of the lava in the canyons. Figure 4 contains images of the lava benches. The younger benches formed from lava erupted from vents located in or near the Yellowstone II caldera to the north. Figure 1 shows the locations of vents for these lava fields, and table 2 shows their ages.

Location H.

This marks the southern boundary of the Elk Wallow Well lava field (table 2). The vent for this field lies in Antelope Flat, outside the caldera to the northwest, and is one of the easternmost vents in the Spencer–High Point volcanic rift zone (fig. 1; Kuntz and others, in press). This volcanic rift zone extends into Island Park and controls the location and orientation of several volcanic vents, including the Highway 20 vent (stop 3; Kuntz and others, in press). The Elk Wallow Well lava flows entered the Henrys Fork river canyon about a mile east of Highway 20. The lava flows produced the second lava bench in the HF canyon. Figure 3A is a profile of the canyon that shows the distribution of lava bench remnants and the inferred distribution of the lava flows that produced the benches. Most lava flows that entered the canyon dammed the river (upstream termination of dashed lines in fig. 3). Figure 4A shows a remnant of the Elk Wallow Well lava bench.

Location I.

This marks the approximate southern boundary of the Yellowstone II caldera, where it crosses the field trip route. Kuntz and others (in press) and Christiansen (2001) use Lookout Butte, a small rhyolite lava dome located 0.75 mi east, to infer the location of the boundary in this area.

Location J.

This marks the contact between the Elk Wallow Well and Highway 20 lava fields. The flow front of the Highway 20 flow to the north is steep because of the higher silica content/viscosity of this flow (Kuntz and others, in press; Moore and others, in press).

Pull off the road to the right, at the road cut that exposes oxidized cinders, stop 3.

STOP 3

Vent deposits of Highway 20 lava field. The Highway 20 flow field produced the next lava bench in HF canyon (table 2). This elongated vent erupted on trend with several other vents to the northwest and southeast, all of which are likely extensions of the Spencer–High Point volcanic rift zone into the caldera (fig. 1; Kuntz and others, in press). The vent deposits contain abundant oxidized cinders, rare bombs, large honey-colored plagioclase phenocrysts, and rare small pyroxene and olivine phenocrysts. This flow field formed shortly after the Elk Wallow Well lava field; its high viscosity and the Elk Wallow Well lava dam likely limited the distribution of Highway 20 lava flows from this field in the HF canyon (fig. 3A). Figure 4B shows a remnant of the Highway 20 lava bench.

En Route to Stop 4

Travel north on Highway 20 for 6.2 mi, and then turn right (east) onto Mesa Falls Scenic Byway (Highway 47).

Location K.

This marks Lava Creek Tuff, which likely lies on the Highway 20 lava field at this location.

Location L.

This marks the southern boundary of the Pinehaven lava field, which erupted from a vent to the west, along the edge of the caldera (fig. 1). This flow was the last to enter HF canyon (table 2). It forms a nearly continuous bench from Riverside Campground (where it entered the canyon) to Lower Mesa Falls (fig. 3A). The Mesa Falls Visitor's Center lies on this bench.

Location M.

This marks the boundary between the Pinehaven and Ripley Butte lava fields. Moore and others (in press) did not observe a Ripley Butte lava bench in either canyon. In fact, they did not observe lava benches in the canyons associated with the flow fields from any vents situated north of this location (fig. 1).

Turn right onto Highway 47 (Mesa Falls Scenic Byway), drive 0.2 mi, and then turn left (north) into the scenic overlook parking area, stop 4.

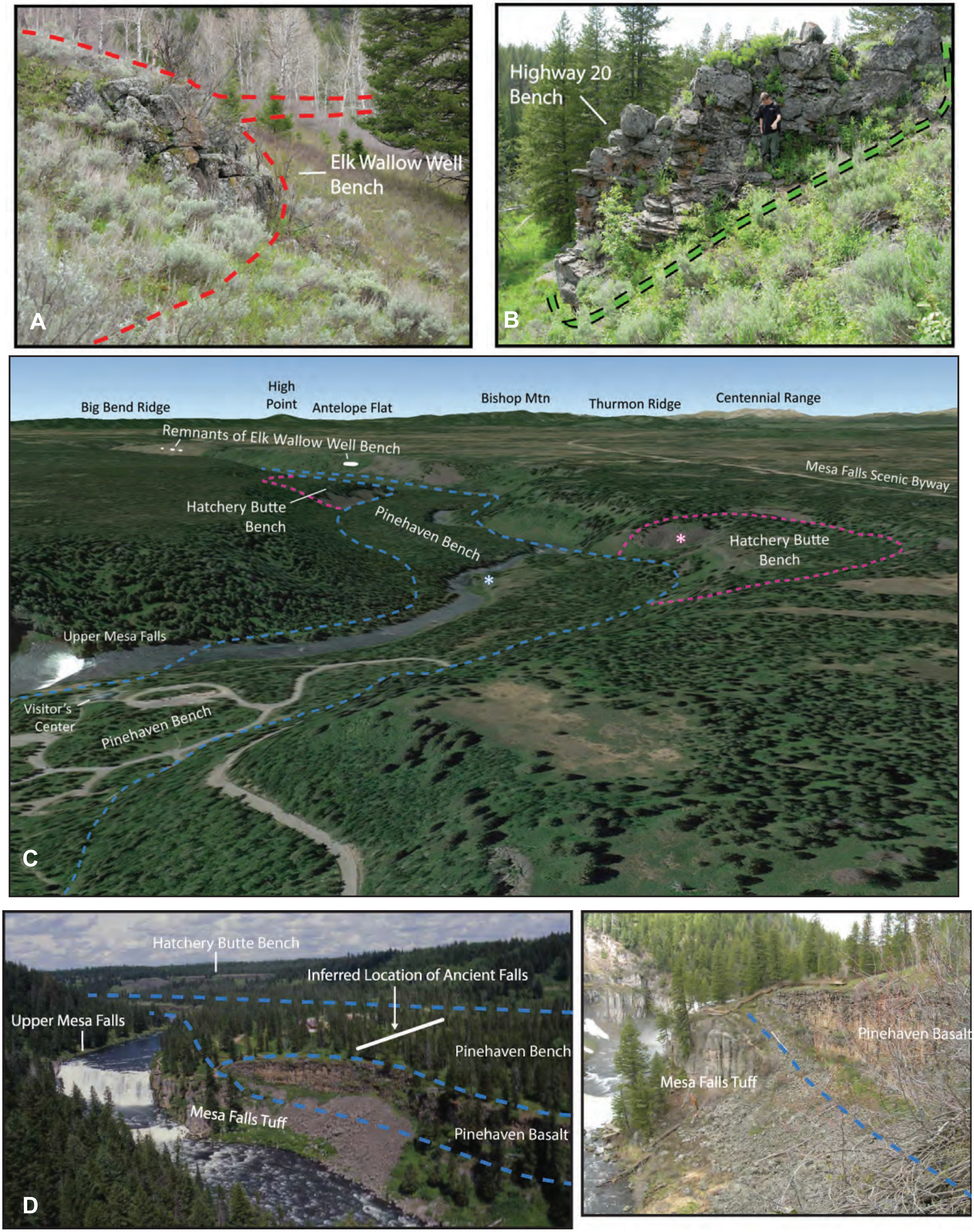
Elk Wallow Well Bench
A
Highway 20 Bench
B
Big Bend Ridge
High Point
Antelope Flat
Bishop Mtn
Thurmon Ridge
Centennial Range
Remnants of Elk Wallow Well Bench
Mesa Falls Scenic Byway
Hatchery Butte Bench
Pinehaven Bench
Hatchery Butte Bench
Upper Mesa Falls
Visitor's Center
Pinehaven Bench
C
Hatchery Butte Bench
Inferred Location of Ancient Falls
Upper Mesa Falls
Pinehaven Bench
Mesa Falls Tuff
Pinehaven Basalt
D
Pinehaven Basalt
Mesa Falls Tuff

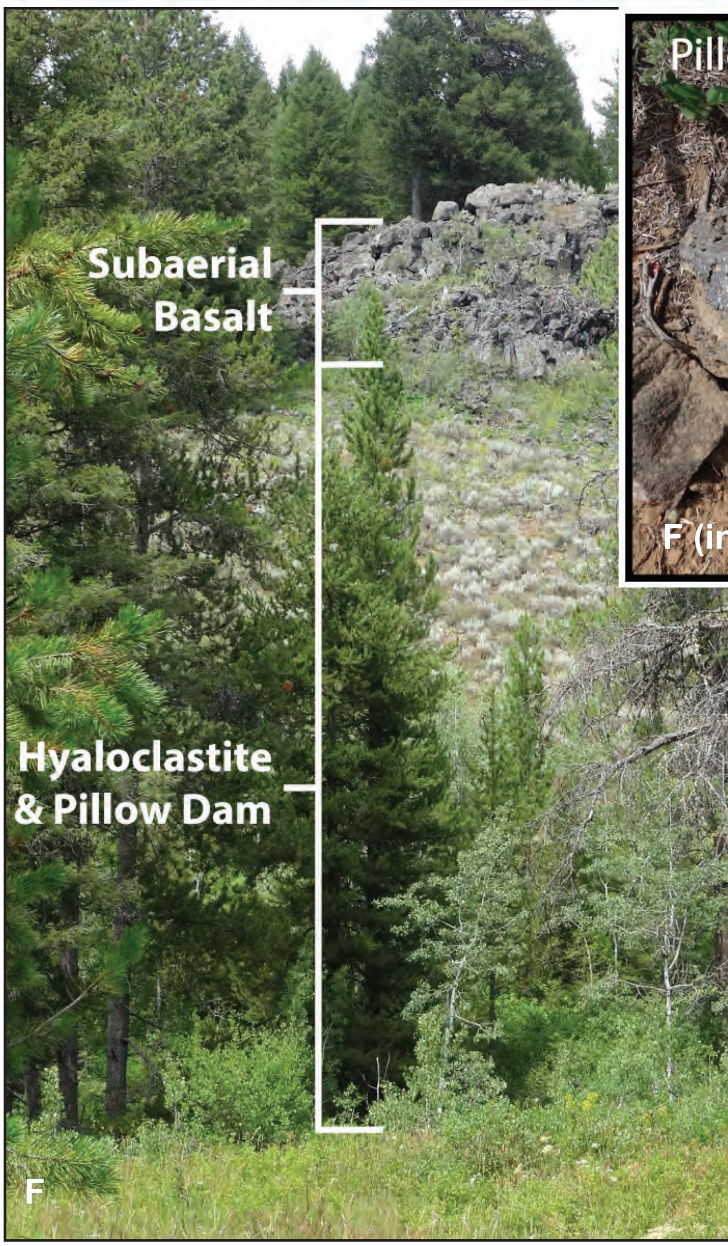

Figure 4. Annotated images of lava benches; the dashed lines show the distribution of lava benches (from Moore and others, in press) A. Annotated photo of a remnant of the Elk Wallow Well lava bench. B. Annotated photo of a remnant of the Highway 20 lava bench. C. Annotated, oblique Google Earth image of the area upstream from Upper Mesa Falls showing the distribution of the Pinehaven, Hatchery Butte, and Elk Wallow Well lava benches. The blue asterisk marks stop 8; the pink asterisk marks stop 9. D. Current river channel next to the Pinehaven paleochannel. The image on the left shows Upper Mesa Falls, the Pinehaven bench, and current channel in the HF canyon. Blue dashed lines mark the boundaries of the Pinehaven lava flows. The exposed edge of the Pinehaven bench shows the western wall and floor of the paleochannel. The white line marks the inferred location of ancient Upper Mesa Falls at the time it was buried by Pinehaven lava flows. The image on the right is a close-up of the western edge of the paleocanyon, which was cut into the Mesa Falls Tuff and partially filled by the Pinehaven lava flows. E. Photos of the scoured surface and potholes in the upper surface of the Pinehaven bench, at stop 8. F. Annotated photo of the Hatchery Butte lava dam/bench at stop 9, showing a hyaloclastite and pillow dam capped by a subaerial basalt flow; the inset photo is of pillow basalt fragments, on loess.

Figure 4 (continued). G. Annotated photo of the composite lava bench at location O, which consists of the normally polarized Gerrit bench in lateral contact with the reversely polarized Warm River bench. H. Annotated oblique Google Earth image of the area that includes the confluence of the Henrys Fork and Warm Rivers, showing the distribution of the Warm River, Gerrit, and Hatchery Butte lava benches. (No vertical exaggeration. For scale: the canyons upstream from the confluence are about 200 ft deep, and the distance between the left edge of the image and the confluence is 0.5 mi.)

STOP 4

Caldera overlook. This stop provides an overview of the region. We describe notable geographic and geologic features, starting to the north and moving counterclockwise. The Basin and Range mountains on the horizon between 1 and 11 o'clock—the Centennial and Henrys Mountains—consist of Precambrian metamorphic and Paleozoic sedimentary rocks, capped by Paleocene and Eocene volcanic rocks of the Absaroka volcanic field. Tuffs of the Yellowstone calderas lap onto the lower parts of these ranges and lie in the intervening basins. The surface expression of the Basin and Range province does not extend into Island Park, because these features were disrupted and buried by the Yellowstone supervolcanoes and associated deposits.

The tree-covered ridge in the foreground that extends counterclockwise from about 1 to 5 o'clock is the rim of the preserved Yellowstone I caldera (fig. 1). The northern part of the rim is Thurman Ridge; to the west and south, the rim is Big Bend Ridge, which we saw at Stop 1. To the north, the Buffalo River flows northeast along the caldera boundary (fig. 1). East of the river and west of Madison junction (in Yellowstone National Park), there is little geographic expression of the caldera rim. As mentioned earlier, the caldera rim is relatively flat; mound-shaped features on the rim indicate the presence of a silicic lava flow or dome. The mounds between about 10 and 9 o'clock are rhyolite lava domes and flows that erupted at nearly the same time as the Mesa Falls Tuff, e.g., the Bishop Mountain flow (fig. 1; table 2).

The topographic low south of Bishop Mountain, between about 9 and 8 o'clock, is Antelope Flat, a graben where the Spencer–High Point volcanic rift zone enters the caldera (Kuntz and others, in press). The vent for the Elk Wallow Well lava field lies just outside the caldera in Antelope Flat (fig. 1). This lava field flowed into the caldera, down the southwestern moat zone, and into the HF canyon (fig. 1). The southern boundary of Antelope Flat is High Point, a latite vent and flow field (Kuntz and others, in press). Between about 8 and 7 o'clock, the caldera rim is composed of the Blue Creek rhyolite lava flow, with the Headquarters rhyolite lava flow behind it (fig 1; table 2).

The Yellowstone I and II calderas share the same boundary from about 1 o'clock—near the Island Park Dam—westward to 7 o'clock—just south of the Blue Creek flow; east of these locations, the Yellowstone II caldera boundary leaves the Yellowstone I boundary and forms a circular feature marked by volcanic vents (fig. 1; Christiansen, 2001).

To the southeast at about 5:30 o'clock, Big Bend Ridge terminates at Snake River Butte (fig. 1), a rhyolite lava dome that erupted just before the Yellowstone I caldera formed (table 2). Rhyolite from this flow composes the core of the topographic high that separates the HF and WR canyons and extends into the eastern canyon wall of WR canyon (fig. 1). Warm River Butte lies at about 5 o'clock, just south of the Moose Creek Butte flow, which is mostly covered by the Lava Creek Tuff (fig. 1). Both of these features are associated with the eruption of the Mesa Falls Tuff (table 2). Rhyolite lava flows, including the Buffalo Lake flow located between 2 and 3 o'clock, form the tree-covered plateau to the east. These young flows erupted from the Yellowstone III caldera to the east and north, flowed west out of the caldera, and today form the eastern boundary of Island Park (fig. 1).

From here, the HF canyon deepens to the south. To the north, eruptions of basalt moved the river laterally. To the south, lava flows that reached the river partially filled the canyon and formed lava benches.

En Route to Stop 5

Drive south on Highway 47 for 12.8 mi.

Location N.

This marks the contact between the Ripley Butte and Hatchery Butte lava fields (Kuntz and others, in press). The Hatchery Butte lava field erupted from an edifice to the southeast and has the largest flow field in Island Park. Three lava fields entered, and later formed lava benches in WR canyon (fig. 3). First, Warm River lava flows entered both canyons from the south; they filled much of WR canyon below Bear Gulch (and the lowest reaches of HF canyon). Gerrit lava flows were the second to enter both canyons. They erupted from an unidentified vent to the east—possibly a buried rift, shown in fig. 1, flowed over the plateau between the rivers south of Lookout Butte, entered both canyons, and flowed past the confluence nearly to the Highway 20 bridge over the HF (fig. 1; Moore and others, in press). Hatchery Butte lava flows were the third to enter both canyons. They formed a hyaloclastite lava dam upstream from Upper Mesa Falls (at stop 9) in HF canyon and entered WR canyon mostly at Bear Gulch (Moore and others, in press). Figure 1 shows vent locations; table 2 shows the ages of these lava fields; and fig. 3 shows the distribution of lava bench remnants.

Turn right onto Upper Mesa Falls Road. The outcrops and float on the right as you descend into the canyon are from three units. The uppermost layers—the basalt of Hatchery Butte and the Lava Creek Tuff—are thin. The Mesa Falls Tuff forms the rest of the canyon wall. Travel ~1 mi to one of the parking lots, then walk to the Mesa Falls Visitor's Center, stop 5.

STOP 5

Mesa Falls Visitor's Center. Mesa Falls derives its name from its iconic falls and from the mesa, or table, formed by the lava bench created when Pinehaven lava flows entered and flowed down the canyon (figs. 1, 3A). At the visitor's center and parking lots, you are standing on the Pinehaven lava bench, which partly filled the paleocanyon. To the west, the river cut the present channel along the contact between the Pinehaven flows and the Mesa Falls Tuff. Figure 4C shows the distribution of the Pinehaven, Hatchery Butte, and Elk Wallow Well lava benches upstream from Upper Mesa Falls. If the visitor's center is open, take the opportunity to view the video that illustrates the volcanic history of Island Park, including the formation of the lava benches in HF and WR canyons.

As you leave the Visitor's Center, follow the trail directly in front of you downhill to the river, at the edge of the falls (stop 6).

STOP 6

Upper Mesa Falls. North of Upper Mesa Falls, the HF channel lies mostly on the Pinehaven flow. Between Upper and Lower Mesa Falls, the channel lies entirely to the side (west) of the Pinehaven lava bench, in the Mesa Falls Tuff. The Pinehaven bench is discontinuous below Lower Mesa Falls (fig. 3A).

The Mesa Falls Tuff erupted from the Yellowstone II caldera (fig. 1). Moore and others (this volume) show that this tuff, which formed as a single cooling unit, was emplaced as multiple sheets of ash. The erupted ash welded more intensely in the core of the thickest, hottest ash sheets, producing vertical density and hardness variations in the Mesa Falls Tuff. Figure 5 shows correlations between rock density (a proxy for rock hardness) and topographic profiles of the bottom and sides of the canyon. Moore and others (in press) suggest that the denser, more resistant layers in the tuff created Upper and Lower Mesa Falls; that the falls first formed near Bear Gulch, inside the Yellowstone I caldera boundary; and that the falls will continue to migrate upstream until they reach Lookout Butte, the southern edge of the Yellowstone II caldera boundary (fig. 1). They also suggest that Upper Mesa Falls migrates upstream by block collapse, as erosion of the underlying weaker rock undercuts the overlying stronger rock.

Walk downstream (south) along the boardwalk a short distance until you reach the southeastern-most portion of the boardwalk in the canyon, stop 7.

STOP 7

Ancient canyon wall. The basalt cliff face to the east exposes at least four of the flows that filled the ancient HF canyon. A typical flow package consists of a rubble zone at the base, upper and lower regions of vertical columnar joints (the upper and lower colonnade), a central region of nearly horizontal columnar joints (the entablature), and a pahoehoe flow top. At your feet to the east of the boardwalk platform lies the contact between the Pinehaven flow—east and above—and the Mesa Falls Tuff—west and below (fig. 4D). This contact marks the western side of the paleocanyon. After the Pinehaven lava flows partially filled the canyon, the river moved to the western edge of the basalt flows and cut the present canyon (fig. 4D).

Pinehaven flows downstream of Upper Mesa Falls are about twice as thick as they are upstream of the falls. Moore and others (in press) suggest this thickness change was produced when Pinehaven lava flows buried an ancient Upper Mesa Falls (now located beneath basalt, just south of the visitor's center).

Return to the visitor's center. Walk northwest from the visitor's center about 0.5 mi to stop 8.

STOP 8

Pinehaven lava bench. The HF has incised a channel into the Pinehaven lava flow at this location. The potholes and fluting at this stop (fig. 4E; located at white/blue asterisk in fig. 4C) record a time when the river flowed over the top of the Pinehaven basalt, before the river cut the current channel.

Walk northeast several hundred feet to stop 9.

STOP 9

Hatchery Butte lava dam. The basaltic rocks at this stop record the filling of the HF canyon by a lava dam produced by the Hatchery Butte lava flows. The lava dam consists of hyaloclastite, pillow lava, and subaerial lava. Figure 4F (located at white/pink asterisk in fig. 4C) is an annotated image of this outcrop, showing the lower hyaloclastite and pillow basalt portion of the dam, capped by a subaerial lava flow; it also contains a close-up of pillow fragments.

Walk back to the Visitor's Center, then to your vehicle. Drive out of the canyon on Upper Mesa Falls road. Turn right onto Highway 47 (Mesa Falls Scenic Byway). Drive 0.6 mi, and then pull into the Lower Mesa Falls Parking area. Walk south ~0.1 mi to the Lower Mesa Falls overlook along the canyon rim, stop 10.

STOP 10

Lower Mesa Falls. The HF at Lower Mesa Falls cascades over two closely spaced falls. On the left side of the falls is an abandoned channel and falls, where the river still occasionally flows during high runoff. Figure 5 shows the relationship between rock density—a proxy for rock hardness—and the elevation of Lower Mesa Falls. Moore and others (in press) suggest that these falls cannot migrate by block collapse because no exposed zone of weak rock lies beneath the falls. Instead, they suggest that these falls migrate upstream as the HF erodes its way through the resis-

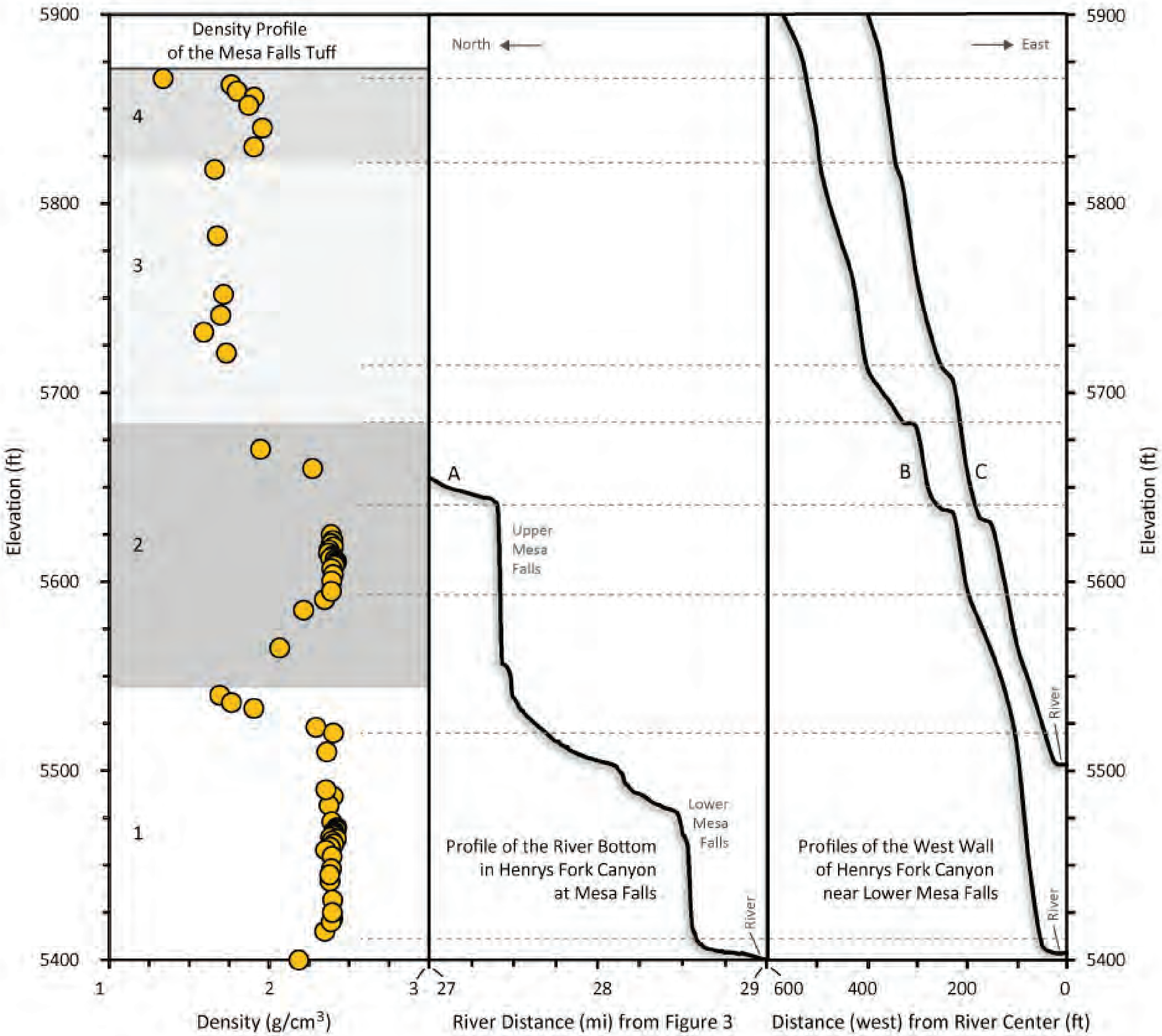

Figure 5. Plot of density versus elevation for the Mesa Falls Tuff in Henrys Fork canyon, relative to topographic profiles of the river bottom and west canyon wall (from Moore and others, in press). The density of the tuff (left panel) is a proxy for the degree of welding, which influences weathering and erosion rates. Profile A (middle panel) is the river profile, along the canyon bottom—from above Upper Mesa Falls to below Lower Mesa Falls; river distances correspond to those in figure 3. Profiles B and C (right panel) are of the west canyon wall and are oriented perpendicular to the river channel; distances are from the center of the river up the west canyon wall. (Profile B is from 1000 ft downstream of Lower Mesa Falls; profile C is from ~0.5 mi upstream of Lower Mesa Falls.) Horizontal dashed lines represent density changes in the Mesa Falls Tuff and changes in slope in the river bottom or along the canyon walls. Shaded, labeled zones in the density profile are our interpretation of distinct, erupted sheets of Mesa Falls Tuff. Vertical exaggeration is about 60x for the river profile and about 4x for the canyon wall profiles.

tant lowermost portion of the Mesa Falls Tuff (fig. 5).

Turn right (south) out of the Lower Mesa Falls parking area onto Highway 47 (Mesa Falls Scenic Byway). Drive 2.3 mi, then turn into the Bear Gulch Parking area, stop 11.

STOP 11

Bear Gulch Parking Lot. Bear Gulch marks the location of the Yellowstone I caldera boundary—defined here by a vertical contact between the Snake River Butte rhyolite lava dome to the south and the Mesa Falls Tuff to the north. To the west lies the deep HF canyon and Snake River Butte. North of Bear Gulch, the HF canyon walls consist of Mesa Falls Tuff; to the south, the canyon consists of the Snake River Butte rhyolite and the Huckleberry Ridge Tuff (Moore and others, in preparation). The presence of these units in the floor of the canyon suggest that there was a topographic low in the caldera rim in this area before the Huckleberry Ridge Tuff erupted (Moore and others, in press).

In the future, continued erosion of the deep tributary of the HF west of Bear Gulch will likely cause capture of WR by the HF; this may have happened at times in the past. Poor exposure on the walls of the tributary make unraveling the history of Bear Gulch challenging.

To the east lies the deep WR canyon. More than a mile north of Bear Gulch, the walls of WR canyon consist of Lava Creek Tuff (Moore and others, in preparation). From there to Bear Gulch, the walls consists mostly of the basalt of Warm River. Through this segment, the river gradient is steep (fig. 3B). South of Bear Gulch, the canyon incises the Snake River Butte rhyolite and then Huckleberry Ridge Tuff (Moore and others, in preparation).

WR canyon contains three lava benches—produced by lava flows from the Warm River, Gerrit, and Hatchery Butte lava fields (fig. 3B; Moore and others, in press). At ~835 ka, Warm River lava flows nearly filled WR canyon between Bear Gulch and the confluence with the HF. WR subsequently cut a new channel, leaving remnants of the Warm River basalt along the canyon wall (i.e., forming the Warm River lava bench). At ~189 ka, Gerrit lava flows entered WR canyon and filled it to the level of the Warm River lava bench. Later, the river cut a new channel, leaving a lava bench composed of both units. This composite lava bench consists of Gerrit flows juxtaposed against the older Warm River flows. Figure 4G, an annotated photo of location O, shows this composite bench. These units are petrographically indistinguishable, but can be distinguished magnetically: the basalt of Warm River is reversely polarized and the basalt of Gerrit is normally polarized. A subvertical contact separates these units; in places, erosion has removed the Gerrit lava bench, exposing the Warm River lava bench. At ~81 ka, Hatchery Butte lava flows entered and filled the bottom of WR canyon. Later, the river cut the current channel, forming the Hatchery Butte lava bench—which lies below the composite (Gerrit-Warm River) lava bench. Figures 3 and 4H show the distribution of lava benches (near the confluence of the Warm and Henrys Fork rivers, for fig. 4H).

The plateau north of Bear Gulch consists of the Gerrit lava field, partially covered by Hatchery Butte lava flows (Moore and others, in preparation). The road cut north of Bear Gulch shows Gerrit basalt flows overlain by tongues of Hatchery Butte basalt. These units can be distinguished by the relative abundance of olivine phenocrysts, which are rare in Gerrit basalt and conspicuous in Hatchery Butte basalt. Both units contain abundant pipe vesicles, suggesting that they may have erupted during winter (Embree and Hoggan, 1999).

The topographic high south of Bear Gulch is a remnant of the caldera flank. This remnant consists of Snake River Butte rhyolite, capped by Huckleberry Ridge Tuff, Lava Creek Tuff, and glacial gravels.

En Route to Stop 12

Turn right (south) out of the Bear Gulch Parking area onto Highway 47 (Mesa Falls Scenic Byway). Drive 4.1 mi.

Location O.

This marks the composite lava bench—formed by lava of the Warm River and Gerrit lava fields—shown in figure 4G. This lava bench continues downstream, along the canyon wall (fig. 3b, 4H).

Location P.

This marks a gravel pit dug in a deposit of glacial drift. This gravel also lies on the plateau just north of Bear Gulch. These deposits contain abundant clasts of basalt and rhyolite and sparse clasts of quartzite and andesite. Andesite clasts are from the Paleocene volcanic rocks exposed in Sawtell Peak and the Henrys Mountains east of Henrys Lake. Quartzite clasts are from the Henrys Mountains north of Henrys Lake. Deep canyons lie on both sides of this narrow remnant of the caldera flank. These deposits have implications for the glacial history of the area.

Location Q.

This marks another instance of the dual lava bench formed by lava of the Warm River and Gerrit lava fields. This lava bench continues downstream, on the canyon wall (figs. 3, 4H).

After crossing Warm River, turn right onto Howe Street, which becomes South River Road at the hairpin turn at the bottom of the hill. Drive west on South River Road for 0.4 mi to the bridge. Cross the bridge onto Fisherman's Drive. Turn into the parking area just west of the bridge, stop 12.

STOP 12

Confluence of the Henrys Fork and Warm Rivers. Here, the Henrys Fork and Warm Rivers converge along the bottom of the flank of the Yellowstone I caldera. The flank here is a dip slope of Huckleberry Ridge and Mesa Falls Tuff, as at stop 2. Figure 4H is an annotated image that shows the distribution of basalt mapped by Moore and others (in preparation). A remnant of the Hatchery Butte lava bench lies between the two rivers. (Lava from the Hatchery Butte flow field entered both canyons above Bear Gulch). Higher on the canyon wall lies the prominent composite lava bench, which consists of basalt from the Warm River and Gerrit lava fields. The Warm River basalt entered WR canyon from the east, then flowed up both canyons (Moore and others, in preparation). Gerrit lava flows, which entered both canyons near Bear Gulch, traveled more than 5 mi farther downstream, nearly to the Highway 20 bridge.

Return to Highway 47. Turn right (south). Drive 0.9 mi, and then turn into a small parking area on the left (east) side of the road, at the top of the hill near a basalt outcrop, stop 13.

STOP 13

Warm River and Gerrit composite lava bench. This stop presents the opportunity to examine an outcrop of the composite lava bench. The outcrop exposes the juxtaposed Warm River and Gerrit basalts.

Drive 1.0 mi south on Highway 47 (Mesa Falls Scenic Byway), and then turn left into a small parking area/farm road access, stop 14.

STOP 14

River canyons through the flank of the caldera. From here, the Big Bend Ridge skyline—west to east—consists of the caldera rim, Snake River Butte, HF & WR canyons, and Warm River Butte. Moore and others (in press) use the distribution and age of rock units in this area to infer the following history for this area of the canyon rim:

- Before 2.1 Ma, the area was a topographic low, eroded into and draining the hotspot highlands;
- Between 2.1 and about 1 Ma, the HF and WR canyons began forming by episodic glacial erosion, flow of water out of the caldera, and/or headward erosion; and
- Between ~1 Ma and present, the HF (below Riverside Campground) and the WR (below Bear Gulch) cut their current canyons through the flank of the caldera.

Drive south and west on Highway 47 to return to Highway 20 at Ashton, Idaho.

REFERENCES

Abedini, A.A., 2009, Basalt petrogenesis and evolution in the Yellowstone Plateau Volcanic Field [M.Sc. Thesis]: California State University, East Bay, 140 p.

Bindeman, I.N., Watts, K.E., Schmitt, A.K., Morgan, L.A., and Shanks, P.W.C., 2007, Voluminous low delta18O magmas in the late Miocene Heise volcanic field, Idaho: Implications for the fate of Yellowstone hotspot calderas: Geology, v. 35, p. 1019–1022.

Christiansen, R.L., 2001, The Quaternary and Pliocene Yellowstone Plateau Volcanic Field of Wyoming, Idaho, and Montana: United States Geological Survey Professional paper 729G, 145 p.

Christiansen, R.L., and Embree, G.F., 1987, Island Park, Idaho; transition from rhyolites of the Yellowstone Plateau to basalts of the Snake River plain Centennial field guide, in Beus, S.S. ed., Centennial field guide, Geol. Soc. Am.: Boulder, CO, United States, United States, p. 103–108.

Embree, G.F., Moore, D.K., Phillips, W.M., this volume, Field guide to the Rexburg Bench, Idaho, Northwest Geology, v. 45.

Embree, G.F., Moore, D.K., Phillips, W.M., Protska, H.J., 2016, Geologic maps of the Moody, White Owl Butte, and Wright Creek quadrangles, Madison and Teton counties, Idaho, Idaho Geological Survey Technical Report 16-2.

Embree, G.F., and Hoggan, R.D., 1999, Secondary deformation within the Huckleberry Ridge Tuff and subjacent Pliocene units near the Teton Dam; road log to the regional geology of the eastern margin of the Snake River plain, Idaho, in Hughes, S.S. and Thackray, G.D. eds., Guidebook to the geology of eastern Idaho, Idaho Museum of Natural History, Pocatello, ID, United States, p. 181–202.

Kuntz, M.A., Turrin, B.D., Champion, D.E., and Moore, D.K., in press, The Pleistocene volcanic and alluvial history of the Henrys Fork Caldera area, Fremont County, Idaho, in Kuntz, M.A., DeRito, J., and Van Kirk, R., eds., 2016, Geological, hydrological, and ecological Studies of the Henrys Fork of the Snake River, eastern Idaho, U.S. Geological Survey Professional Paper, U.S. Geological Survey.

Kuntz, M.A., 1979, Geologic map of the Juniper Buttes area, eastern Snake River plain, Idaho: U. S. Geological Survey Miscellaneous Investigation Series Map I-1115.

Lanphere, M.A., Champion, D.E., Christiansen, R.L., Izett, G.A., and Obradovich, J.D., 2002, Revised ages for tuffs of the Yellowstone Plateau volcanic field: Assignment of the Huckleberry Ridge Tuff to a new geomagnetic polarity event: Geological Society of America Bulletin, v. 114, no. 5, p. 559–568.

Love, J.D., Reed, J.C., Pierce, K.L., 2003, Creation of the Teton landscape : a geologic chronicle of Jackson Hole and the Teton Range: Grand Teton Natural History Association, Moose, Wyo.

Moore, D.K., Embree, G.F., Kuntz, M.A., Champion, D.E., Painter, Rasaka, B., and Lindsay, D., in preparation, Geologic map of the Henrys Fork canyon and Warm River canyons and surrounding areas, Island Park and Ashton areas, Idaho, U.S.A.: Idaho Geological Survey Technical Report.

Moore, D.K., Rothlisberger, B., Hartman, B., Phillips, W.M., and Melton, G., this volume, Depositional history of Yellowstone tuff members: insights from vertical density variations, southeast Idaho: Northwest Geology, v. 45.

Moore, D.K., Embree, G.F., Champion, D.E., Kuntz, M.A., Painter, C.S., Shenton, B., McGuire, K., Rasaka, B., Lindsey, D., George, A., Leishman, B., in press, Origin of lava benches and Upper and Lower Mesa Falls in the Henrys Fork and Warm River Canyons, Island Park, Idaho, in Kuntz, M.A., DeRito, J., and Van Kirk, R., eds., 2016, Geological, hydrological, and ecological studies of the Henrys Fork of the Snake River, eastern Idaho, U.S. Geological Survey Professional Paper, U.S. Geological Survey.

Phillips, W.M., 2012, Geologic map of the St. Anthony quadrangle, Fremont and Madison counties, Idaho, Idaho Geological Survey Digital Web Map 145.

Phillips, W.M., and Welhan, J.A., 2011, Geologic map of the Menan Buttes quadrangle, Jefferson and Madison Counties, Idaho, Idaho Geological Survey Digital Web Map 137.

FIELD GUIDE TO THE NEOGENE "DIVIDE UNIT" OF THE SOUTHERN BEAVERHEAD MOUNTAINS AND ASSOCIATED FEATURES, MONTANA AND IDAHO

Stuart D. Parker

University of Montana, Missoula, Montana 59812, USA

INTRODUCTION

This field guide to the southern Beaverhead Mountains focuses on the nature and tectonic significance of Neogene gravel and volcanic deposits formerly assigned to the "Divide unit" of the Cretaceous/Paleocene Beaverhead Group (Ryder and Scholten, 1973). The unit evidently represents the deposits of a major river system that was cross-cut by the Yellowstone hotspot about 4 Ma.

Figure 1. Field guide Stops 1-8, starting from Dubois, ID. Refer to "Motor Vehicle Use Map Caribou-Targhee National Forests" for detailed Forest Service road map.

The road log starts from Dubois, Idaho, along I-15. Field stops are located according to GPS measurements. See figures 1 and 2 for route and associated stops. From Dubois, exit onto Idaho Hwy 22 W. Take the immediate right onto Small Road, followed by a slight right on County Route 91 N. Follow this frontage road north and take a left onto Sky Line Road (FS road 323). Stop 1 is an overlook on the right side of the road, 1.8 mi from the frontage road.

STOP 1

Spencer–High Point volcanic rift zone overlook (GPS: 44.334028°N, 112.221845°W)

Visible to the southeast are the fissures, vents, and craters associated with the Spencer–High Point (SHP) volcanic rift zone (fig. 3). The SHP is a unique feature of the eastern Snake River Plain (ESRP) in that it contains the highest concentration of vents, has an E–W rather than NW–SE trend, and contains vents and fissures that do not parallel the trend (Kuntz and others, 1992). This fracture geometry has been compared to tension gashes, suggesting right-lateral shear (Kuntz and others, 1992). Features of the SHP are coincident with the Middle Creek Butte fault zone in the west and trend into the 1.3 Ma Henrys Fork caldera in the east (Kuntz and others, 1992; Morgan and McIntosh, 2005). The Middle Creek Butte fault exposes the Divide unit in its footwall. Volcanics of the SHP have been dated at 0.365 Ma and may be as young at <15 ka (Kuntz and others, 1992). These relationships may constrain initial exhumation of the Divide unit at only 0.365 Ma.

Figure 2. Detailed map showing off road access to sites 4 and 5.

Continue ascending on the main road. The road merges right, onto FS road 200. Two left merges follow, onto FS 801. The ultimate goal is the highest bald knoll to the NW. Staying on the largest, most well-worn road should get you there.

STOP 2

Divide unit gravel overlying the Kilgore Tuff (GPS: 44.401723°N, 112.335145°W)

This observation point lies on river gravel deposited on the 4.5 Ma Kilgore Tuff (Morgan and McIntosh, 2005). The steep cliff band of the Kilgore can be seen to the NW. Conifers are often observed in high densities around the Kilgore Tuff, where moisture is retained in the otherwise arid and well-drained gravel deposit. To the NW, the flat plateau of the Divide Creek area is visible, illustrating the nearly horizontal nature of the Kilgore Tuff at this location. River gravel caps the Kilgore Tuff, and is overlain by the angularly unconformable rhyolite of Indian Creek Butte (4.1 Ma), which has been eroded in this location (Morgan and McIntosh, 2005). This relationship constrains the end of deposition of the north-flowing drainage responsible for the 800 m of river cobbles observed in this location to between 4.5 and 4.1 Ma. Uplift associated with the ESRP and the Yellowstone volcanic system likely terminated this drainage. A broad volcanic plain persisted in the Pliocene until activation of the Middle Creek Butte fault uplifted and exposed the Divide deposit by 0.365 Ma (Barenek and others, 2006).

Continue west, down from the high point. Turn right onto FS 323 before entering a high plateau and a slight drainage. Stay right and travel north up the drainage towards the Continental Divide. The road will veer east to gain the divide.

STOP 3

Continental Divide overlook and Centennial shear zone boundary (GPS: 44.418819°N, 112.344126°W)

From this observation point, the Divide unit extends roughly 10 mi to the west (Ryder and Scholten, 1973). Geomorphic features west of this location contrast with those of the eastern deposit. In the east, drainages are dendritic and lack a preferred orientation. In the west, linear drainages trend NE–SW. Slide areas visible to the west typically correlate with highly

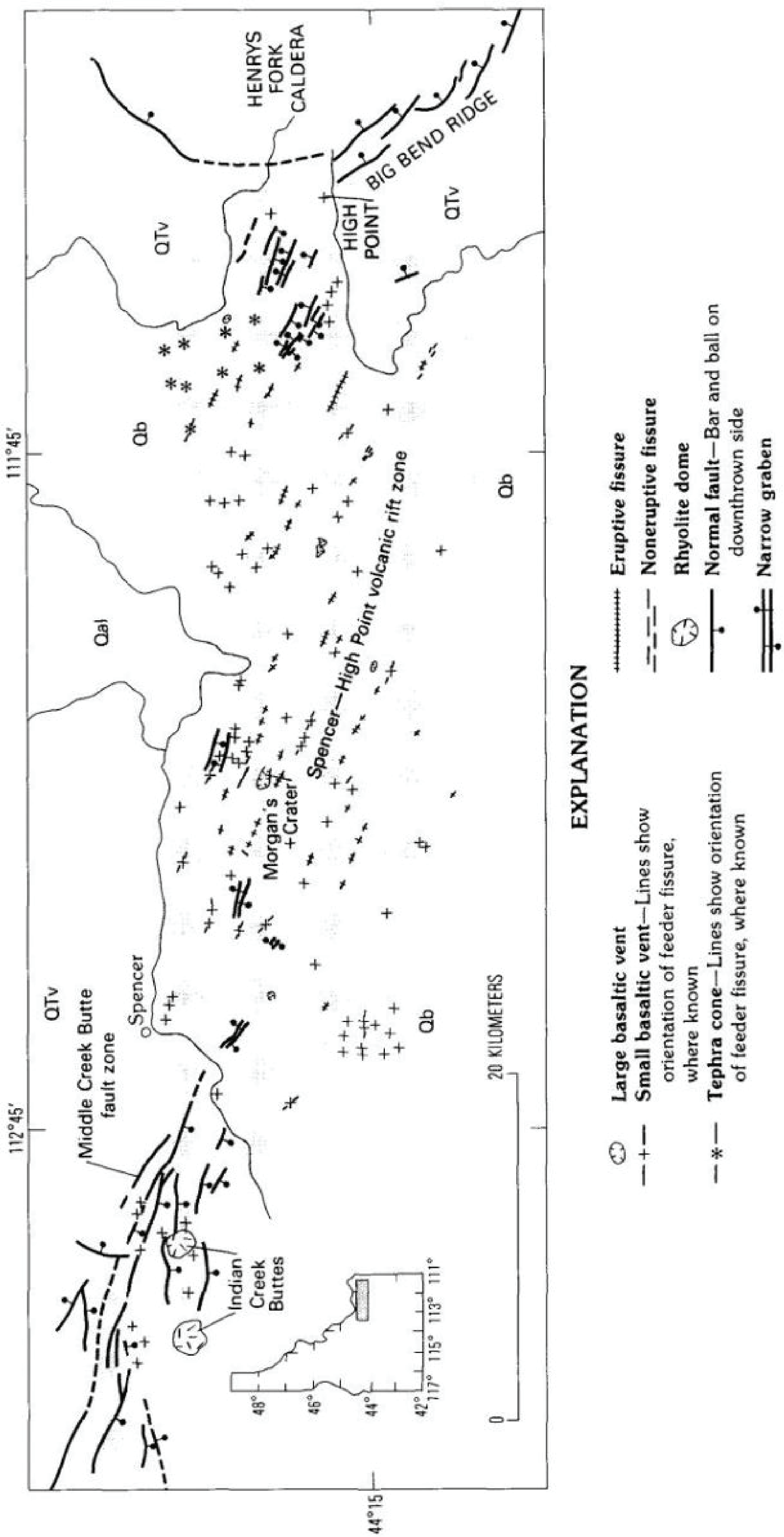

Figure 3. Structural and volcanic features of the Spencer–High Point (SHP) and Middle Creek Butte fault zone.

chaotic fault zones. Linear springs indicate surface expressions of groundwater flow intersecting impermeable calcite-cemented fault planes. High permeability and minimal surface water retention in the gravel deposit makes these linear springs a reliable method for identifying faults. Spring orientations are generally coincident with linear drainages. The Kilgore Tuff is absent in the west. The planar Kilgore Tuff projects above topography to the west, suggesting that increased erosion in the west has removed the tuff.

This drastic change in geomorphic habit marks the eastern boundary of the Centennial shear zone (CSZ). Right-lateral shear at a rate of 0.3–1.5 mm yr^{-1} is measured in GPS velocities of the region, which accommodates differential extension rates of the Centennial tectonic belt (CTB) and the ESRP (Payne and others, 2013). The main criticism with the CSZ hypothesis is that no strike-slip faults have been mapped within this proposed shear zone (Rodgers and others, 2002). The present study proposes that rotation and synthetic slip along preexisting faults suppresses the formation of a throughgoing strike-slip fault, allowing for dextral shear to be accommodated in the absence of major strike-slip faults. Instead, deformation in the CSZ is characterized by dense arrays (up to 580/km) of high-angle conjugate fractures with minimal vertical offset. These fractures subparallel shear sense in the CSZ. The dense fracture arrays observed throughout the western extent of the Divide unit overthicken the deposit to an apparent thickness of 2,000 m. Orientations of the largest pressure solution pits observed on quartzite cobbles throughout the deposit highlight a horizontal maximum principal stress orientation (σ_1) consistent with a simple shear tectonic setting and the CSZ hypothesis.

From the Divide (Stop 3), Stop 4 can be accessed by foot or ATV (fig. 2). Walk the ridgeline north until the ridgeline splits, then follow the northeast ridge. The outcrops are below the ridge on the east side in slide paths. Small stands of aspens lie just below the ridge. This outcrop is not spectacular and is located in fairly rugged terrain. One-way travel distance is 1.3 mi from the Divide stop. Navigate back to the Divide stop for continued directions.

STOP 4

Syndepositional faults of the Divide unit (GPS: 44.429490°N, 112.326884°W)

Poorly exposed outcrops below this ridge contain evidence for syntectonic deposition within the Divide unit. Parallel sets of oxidized fractures can be observed crossing numerous cobbles in clast support. These features parallel larger faults and provide a method of identification on the outcrop scale, since gullies draped by slope wash follow larger faults. Zones of fault breccia with extensive calcite cementation are also common, but poorly exposed. Fractures and normal faults at this location are highly organized and signify a major NNE-striking normal fault, typical of regional trends of Middle Miocene faults (Sears and Fritz, 1998). Joint sets cut bedding planes at oblique angles, suggesting that strata dipped to the east during the formation of joint sets. Bedding plane orientations show rotation coincident with the measured NE-striking normal fault, before subsequent rotation about the E–W-striking Middle Creek Butte fault. Large slide blocks, observable throughout the deposit, decrease in size from W to E and highlight an East-dipping slope during deposition. Fault strike also parallels the observed NNE-paleoflow as illustrated by clast-imbrication measurements. These observations strongly suggest syntectonic deposition in an active half-graben, likely during Middle Miocene time.

Stop 5 can also be accessed by foot or ATV (fig. 2). From the Divide stop (Stop 3), follow the ridge north. Follow the ridge as it wraps west for 1.3 mi, passing the ridge to Stop 4 and another NE-trending ridge. Follow the third ridge on the right (NNE); park here if on an ATV. Follow the ridge for 0.8 mi. The outcrops will be just below the ridge, on the west. Navigate back to the Divide stop when finished.

STOP 5

Typical sedimentary characteristics of the Divide unit (GPS: 44.444841°N, 112.342311°W)

This outcrop highlights typical clast assemblages and sedimentary structures of the Divide unit. Imbricated cobbles illustrate a consistent paleo-flow towards N 20° E. Armored beds can be observed, showing that the fluvial system was highly competent. Quartzite cobbles are most common, accounting for roughly 70% of clasts. Intermediate to felsic volcanic cobbles can be observed. Dacite cobbles containing smoky bi-pyramidal quartz phenocrysts were dated and found to have an eruptive age of 98.3 ± 1.7 Ma. Isotopic and mineralogical characteristics are highly similar to the Atlanta Lobe of the Idaho Batholith, suggesting the source was likely volcanic cover to the Idaho Batholith that has since been eroded or buried beneath the ESRP (van Middlesworth and Wood, 1998). Banded cobbles of limestone and chert can be observed throughout the deposit. These partially silicified crinoidal packstones and wackestones are sourced from the Mississippian Scott Peak and Middle Canyon Formations, which line the paleochannel to the SW (Buoniconti, 2008; Skipp and others, 1979). These distinct cobbles can be seen within the Neogene Sixmile Creek Formation to the NE, suggesting the two deposits are analogous, and likely components of the same fluvial system, sourced to the south. Angular chert and lithic grains dominate the sandstone matrix. Compositionally and texturally immature grains indicate first-order sources from proximal and distal normal faults, likely associated with onset of Basin and Range faulting in the area.

Follow FS 323 east, down from the Divide. Follow I-15 north to Modoc Rd. Take Modoc Rd SW towards Paul Reservoir. Stop 6 will be visible on the left, as the drainage wraps around to the SE. The powdery slopes are Cretaceous shale, with more competent ash layers visible throughout.

STOP 6

Underlying Cretaceous Aspen Shale (GPS: 44.491212°N, 112.343493°W)

Cretaceous shale lies unconformably beneath the Divide unit in this location. Ryder and Scholten (1973) assigned this unit to the Aspen Formation, while others (Skipp and Janecke, 2004) assign it to the Frontier Formation. The bentonitic shale contains numerous ash layers and terrestrial plant fossils in this location. Ash layers within the Aspen Formation and other local Cretaceous shales reveal Albian/Cenomanian ages, coincident with the dated dacite cobble interpreted as volcanic cover to the Idaho Batholith (Nichols and Jacobson, 1982). If these contemporaneous volcanics share a common source, the dacite cobbles must have traveled a large distance given the distal nature of the ash deposits of the shale unit.

To the west, the Divide unit overlies the Late Cretaceous/Paleocene Beaverhead Group and transitional conglomerates of unknown age, which likely represent recycling of the Beaverhead. The contact with the Aspen Shale represents an unconformity where the Beaverhead Group has been eroded and recycled into subsequent conglomerates such as the Divide unit. Given the nature of coarse quartzite conglomerates, analogous deposits resulting from progressive recycling of the Beaverhead Group would be difficult to discern. Near the next stop, notice the habit of hillslopes along Modoc Road. A change in hillslope characteristic marks the unconformable boundary between the Aspen Shale and the Divide unit.

Continue up Modoc Road towards Paul Reservoir. The lithological contact is just before the left fork in the road that bends towards Paul Reservoir. Take the left fork and park at the reservoir. The outcrops of interest will be visible to the east above the reservoir. The outcrops are 0.4 mi and 700 vertical feet away. The steep and somewhat loose slope is best climbed via one of the middle ridge lines.

STOP 7

Basal conglomerate of Paul Reservoir (GPS: 44.463073°N, 112.335667°W)

Perched above Paul Reservoir is perhaps the oldest outcrop of the Divide deposit. The lithologies present in this deposit are identical to those observed throughout the deposit. Characteristic pressure solution pits of the Divide unit are easily observed at this location. These pits formed when rounded quartzite cobbles in clast support concentrated applied force to a discrete contact. When alkaline pore water conditions exist, quartzite dissolves at such contacts. In the homogeneous gravel such as the Divide unit, the sizes of pressure solution pits correlate with the amount of applied force (Wiltschko and Sutton, 1982). The paleo-orientation of σ_1 can be estimated by measuring the common orientation of largest pits. In this location, pits do not tightly cluster to a common orientation and fractures radiate away from contacts. To the west, in the CSZ, pits and fractures lie parallel to the modern shear sense, indicating that tectonic stresses were responsible for the deformation.

Feldspathic cobbles are common in this outcrop and throughout the Divide unit, accounting for 32% of the total clast composition. This lithology has previously been assigned to the Belt Supergroup, although the observed northerly paleoflow is not consistent with this interpretation (Ryder and Scholten, 1973), since no Belt rocks occur to the south. To address this discrepancy, this project dated the detrital zircon as-

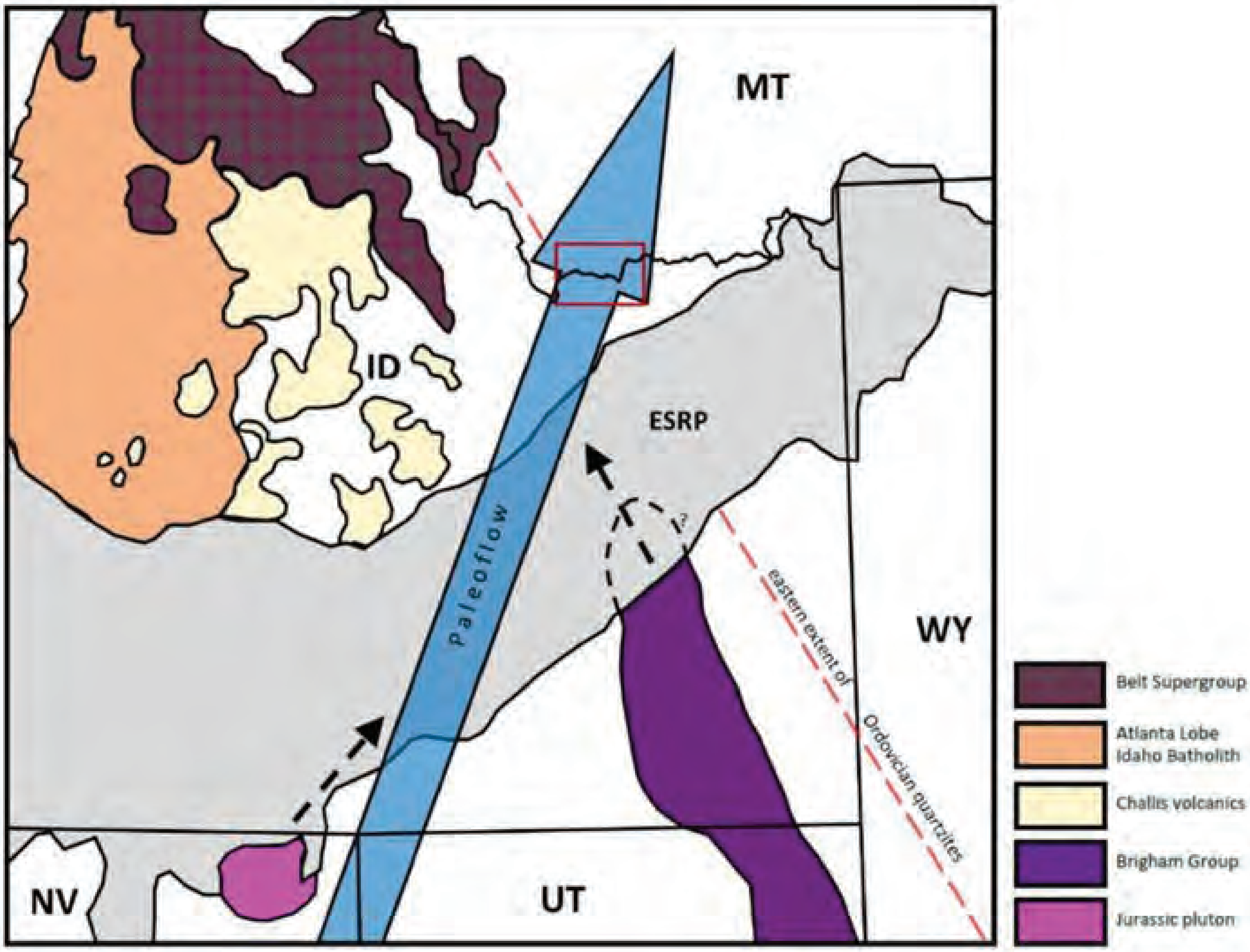

Figure 4. Simplified source map based on zircon analysis of *in situ* cobbles and sand grains. Field site highlighted in red box.

semblage from a feldspathic quartzite cobble. Detrital zircon analysis revealed an age signature matching the Brigham Group, which occurs roughly 120 mi to the upstream (south) where it is exposed beneath the Middle Miocene Bannock detachment (Carney and Janecke, 2005). This correlation constrains the maximum age of the deposit to Middle Miocene and illustrates that long-distance transport of large quartzite cobbles was common (fig. 4).

Detrital zircons within the sandstone matrix were also analyzed at this location. This analysis was used to assess the farthest extent of the drainage. If linkage to the Nevadian Basin and Range existed, as proposed by the Ancestral Colorado River hypothesis of Sears (2013), then Miocene-aged volcanic grains associated with extensive ignimbrites would likely be present in the sand matrix. Results show no such grains, and instead the system is flooded with Cretaceous-aged grains. These grains are likely recycled from the underlying Aspen Formation and volcanic cobbles within the deposit. Proximity to the basal contact skews the probability curve towards the Cretaceous and greatly reduces the odds of identifying far-traveled Miocene-aged zircons. Jurassic-aged grains were observed, and cannot be easily explained within the local stratigraphy. A Jurassic intrusion in northern Nevada is the most likely source and is consistent with paleoflow and age constraints (fig. 4) (Link and others, 2005). Detrital results of modern sands of the ESRP document Middle Miocene-aged grains which are unique to drainages linked to the Divide deposit and support a link to Nevada (Link and others, 2005).

CONCLUSION

In summary, field observations support reassigning the Divide unit of the Beaverhead Group of Ryder and Scholten (1973) to the Neogene Sixmile Creek Formation, which has been mapped 50 km northwest of the field area. The fluvial facies of the Sixmile Creek Formation, referred to as the Big Hole Member by Fritz and Sears (1993), exhibits similar clast compositions and paleo-flow indicators and contains similar interlayered Neogene volcanics. The sites are likely segments of a once-continuous, large river system with headwaters south of the present position of the eastern Snake River Plain. Tectonics associated with the Yellowstone hotspot and Snake River Plain evidently destroyed the river drainage at about 4 Ma.

REFERENCES

Buoniconti, M.R., 2008, The evolution of the carbonate shelf margins and fill of the Antler foreland basin by prograding Mississippian carbonates, northern US Rockies: University of Miami, PhD dissertation, 436 p.

Beranek, L.P., Link, P.K., and Fanning, C.M., 2006, Miocene to Holocene landscape evolution of the western Snake River Plain region, Idaho: Using the SHRIMP detrital zircon provenance record to track eastward migration of the Yellowstone hotspot: Geological Society of America Bulletin, v. 118, no. 9-10, p. 1027-1050.

Carney, S.M., and Janecke, S.U., 2005, Excision and the original low dip of the Miocene-Pliocene Bannock detachment system, SE Idaho: Northern cousin of the Sevier Desert detachment? Geological Society of America Bulletin, v. 117, no. 3-4, p. 334-353.

Fritz, W.J., and Sears, J.W., 1993, Tectonics of the Yellowstone hotspot wake in southwesternMontana: Geology, v. 21, no. 5, p. 427-430.

Kuntz, M.A., Covington, H.R., and Schorr, L.J., 1992, An overview of basaltic volcanism of the eastern Snake River Plain, Idaho, in Link, P.K, Kuntz, M.A., Platt, L.B., Regional geology of eastern Idaho and western Wyoming: Geological Society of America Memoir 179, p. 227-267.

Link, P.K., Fanning, C.M. and Beranek, L.P., 2005, Reliability and longitudinal change of detrital-zircon age spectra in the Snake River system, Idaho and Wyoming: An example ofreproducing the bumpy barcode: Sedimentary Geology, v. 182, no. 1, p. 101-142.

Morgan, L.A., and McIntosh, W.C., 2005, Timing and development of the Heise volcanic field, Snake River Plain, Idaho, western USA: Geological Society of America Bulletin, v. 117, no. 3-4, p. 288-306.

Nichols, D.J., and Jacobson, S.R., 1982, Palynostratigraphic framework for the Cretaceous (Albian□ Maestrichtian) of the overthrust belt of Utah and Wyoming: Palynology, v. 6, no.1, p. 119-147.

Nichols, D.J., Perry, W.J., and Johns, J.H., 1985, Reinterpretation of the palynology and age of Laramide syntectonic deposits, southwestern Montana, and revision of the Beaverhead Group: Geology, v. 13, no. 2, p. 149-153.

Payne, S., McCaffrey, R., and Kattenhorn, S., 2013, Extension-driven right-lateral shear in the Centennial shear zone adjacent to the eastern Snake River Plain, Idaho: Lithosphere, v. 5, p. 407-419.

Rodgers, D.W., Ore, H.T., Bobo, R.T., McQuarrie, N., and Zentner, N., 2002, Extension and subsidence of the eastern Snake River Plain, Idaho, in Bonnichsen, B., White, C.M, and McCurry, M.M., eds., Tectonic and Magmatic Evolution of the Snake River Plain Volcanic Province: Idaho Geological Survey Bulletin 30, p. 121-155.

Ryder, R.T., and Scholten, R., 1973, Syntectonic conglomerates in southwestern Montana: Their nature, origin, and tectonic significance: Geological Society of America Bulletin, v. 84, no.3, p. 773-796.

Sears, J.W., and Fritz, W.J., 1998, Cenozoic tilt domains in southwestern Montana; interference among three generations of extensional fault systems, in Faulds, J.E., and Stewart, J.H., eds., Accommodation zones and transfer zones; the regional segmentation of the Basin and Range Province, Geological Society of America Special Paper 323, p. 241-247.

Sears, J.W., 2013, Late Oligocene–early Miocene Grand Canyon: A Canadian connection? GSA Today, v. 23, no. 11, p. 4-10.

Skipp, B., and Janecke, S.U., 2004, Geologic map of the Montana part of the Dubois 30’ x 60’ quadrangle, southwest Montana: Montana Bureau of Mines and Geology MBMG 490, 12 p., scale 1:100,000.

Skipp, B., Prostka, H.J., and Schleicher, D.L., 1979, Preliminary geologic map of the Edie Ranch Quadrangle, Clark County, Idaho, and Beaverhead County, Montana: U.S. Geological Survey

Open-File Report 79- 845, scale 1:62,500.

van Middlesworth, P.E., and Wood, S.A., 1998, The aqueous geochemistry of the rare earth elements and yttrium; Part 7, REE, Th and U contents in thermal springs associated with the Idaho batholith: Applied Geochemistry, v. 13, no. 7, p. 861-884.

Wiltschko, D.V., and Sutton, S.J., 1982, Deformation by overburden of a coarse quartzite conglomerate: Journal of Geology, p. 725-733.